frontiers | Research Topics

The impacts of climate change and human activities on the structure and function of wetland/grassland ecosystems

Edited by
Zhongqing Yan, Kerou Zhang, Yunpeng Luo and Xiaodong Zhang

Published in
Frontiers in Ecology and Evolution

ISSN 1664-8714
ISBN 978-2-8325-3765-7
DOI 10.3389/978-2-8325-3765-7

About Frontiers

Frontiers is more than just an open access publisher of scholarly articles: it is a pioneering approach to the world of academia, radically improving the way scholarly research is managed. The grand vision of Frontiers is a world where all people have an equal opportunity to seek, share and generate knowledge. Frontiers provides immediate and permanent online open access to all its publications, but this alone is not enough to realize our grand goals.

Frontiers journal series

The Frontiers journal series is a multi-tier and interdisciplinary set of open-access, online journals, promising a paradigm shift from the current review, selection and dissemination processes in academic publishing. All Frontiers journals are driven by researchers for researchers; therefore, they constitute a service to the scholarly community. At the same time, the *Frontiers journal series* operates on a revolutionary invention, the tiered publishing system, initially addressing specific communities of scholars, and gradually climbing up to broader public understanding, thus serving the interests of the lay society, too.

Dedication to quality

Each Frontiers article is a landmark of the highest quality, thanks to genuinely collaborative interactions between authors and review editors, who include some of the world's best academicians. Research must be certified by peers before entering a stream of knowledge that may eventually reach the public - and shape society; therefore, Frontiers only applies the most rigorous and unbiased reviews. Frontiers revolutionizes research publishing by freely delivering the most outstanding research, evaluated with no bias from both the academic and social point of view. By applying the most advanced information technologies, Frontiers is catapulting scholarly publishing into a new generation.

What are Frontiers Research Topics?

Frontiers Research Topics are very popular trademarks of the *Frontiers journals series*: they are collections of at least ten articles, all centered on a particular subject. With their unique mix of varied contributions from Original Research to Review Articles, Frontiers Research Topics unify the most influential researchers, the latest key findings and historical advances in a hot research area.

Find out more on how to host your own Frontiers Research Topic or contribute to one as an author by contacting the Frontiers editorial office: frontiersin.org/about/contact

The impacts of climate change and human activities on the structure and function of wetland/grassland ecosystems

Topic editors

Zhongqing Yan — Beijing Key Laboratory of Wetland Ecological Function and Restoration, Chinese Academy of Forestry, China

Kerou Zhang — Chinese Academy of Forestry, China

Yunpeng Luo — Swiss Federal Institute for Forest, Snow and Landscape Research (WSL), Switzerland

Xiaodong Zhang — Chinese Academy of Forestry, China

Citation

Yan, Z., Zhang, K., Luo, Y., Zhang, X., eds. (2023). *The impacts of climate change and human activities on the structure and function of wetland/grassland ecosystems*. Lausanne: Frontiers Media SA. doi: 10.3389/978-2-8325-3765-7

Table of contents

frontiers | Frontiers in Ecology and Evolution

TYPE Editorial
PUBLISHED 09 October 2023
DOI 10.3389/fevo.2023.1296677

OPEN ACCESS

EDITED AND REVIEWED BY
Dennis Murray,
Trent University, Canada

*CORRESPONDENCE
Zhongqing Yan
yanzq@caf.ac.cn

RECEIVED 19 September 2023
ACCEPTED 02 October 2023
PUBLISHED 09 October 2023

CITATION
Zhang K and Yan Z (2023) Editorial: The impacts of climate change and human activities on the structure and function of wetland/grassland ecosystems.
Front. Ecol. Evol. 11:1296677.
doi: 10.3389/fevo.2023.1296677

Editorial: The impacts of climate change and human activities on the structure and function of wetland/grassland ecosystems

Kerou Zhang[1,2,3] and Zhongqing Yan[1,2,3]*

[1]Wetland Research Center, Institute of Ecological Conservation and Restoration, Chinese Academy of Forestry, Beijing, China, [2]Sichuan Zoige Wetland Ecosystem Research Station, Tibetan Autonomous Prefecture of Aba, China, [3]Beijing Key Laboratory of Wetland Services and Restoration, Beijing, China

KEYWORDS

climate change, human activities, structure and function, wetland ecosystems, grassland ecosystems

Editorial on the Research Topic
The impacts of climate change and human activities on the structure and function of wetland/grassland ecosystems

Wetland/grassland ecosystems play a crucial role in providing numerous ecosystem services, including water purification, flood prevention, carbon (C) sequestration, and habitat provision. However, these ecosystems are highly vulnerable to environmental changes. In recent years, climate change and human activities have put these ecosystems at risk of degradation or transformation (Cloern et al., 2016). This could lead to the release of C, exacerbating global warming and causing habitat loss, water pollution, and the introduction of invasive species (Gibbons et al., 2000; Jaureguiberry et al., 2022). As a result, there has been a decline in biodiversity and ecosystem service functions (Sharma and Singh, 2021; Martínez-Megías and Rico, 2022). On the one hand, wetland/grassland ecosystems support rich biodiversity, and studying their responses to climate change and human disturbances helps identify conservation priorities and provides information for implementing effective management practices. Conducting such research enables us to gain a deeper understanding of the ecological interactions and dependencies within these ecosystems. This knowledge empowers us to make well-informed decisions regarding their protection and restoration. On the other hand, wetland/grassland ecosystems are often interconnected with surrounding landscapes, making them susceptible to land use changes and habitat fragmentation caused by climate change and human activities. By studying the impacts of these disturbances, we can develop sustainable land-use practices, minimize negative effects, and promote their long-term viability. Therefore, the related research is crucial for understanding their vulnerability, protecting ecosystem services, preserving biodiversity, and providing information for sustainable management practices.

This Research Topic focuses on the impacts of climate change and human activities on various components, such as plants and soil, as well as ecological functions like C fixation and biodiversity maintenance, within wetland and grassland ecosystems including regional

or specific site scales. It utilizes a range of methods, such as manipulation experiments, remote sensing, ecological models, and machine learning techniques.

Climate change or human activities' effects on wetland/grassland plants

This thematic section contains eight papers on the study of climate change and human activities' effects on wetland/grassland plants. Based on a variety of research methods, these studies present several significant findings and new perspectives on vegetation coverage, aboveground biomass, plant stoichiometry and stable isotopes. Wang et al. based on the Global Database (CMCC-BioClimInd), identified the key bioclimatic indicators that indicate forage growth in the northeastern Qinghai-Tibet Plateau and revealed the physiological and ecological mechanisms behind forage growth in this region. In terms of stoichiometric ratios and stable isotope feature of plant issues, the findings of Wang et al. support the idea that shrubs in permafrost peatlands expand due to competition for nutrients under conditions of climate warming, which helps enhance our understanding of how various plant tissues in permafrost peatlands respond to climate change. Chen et al. utilized the Break for Additive Seasonal and Trend (BFAST) algorithm to detect abrupt changes in the monthly Normalized Difference Vegetation Index in wetlands and revealed a significant turning point in the greening of wetlands in the new century. The time-lag effect of alpine vegetation on climate variables is further discussed in the study. Based on the long-term altitude asymmetric warming experiment, Han et al. proposed that uneven warming at different altitudes could balance out plant α-diversity and aboveground net primary production in the northern alpine steppe of Qinghai-Tibetan Plateau. Lv et al. focused on Kobresia pygmaea, a dwarf sedge in the alpine meadow on the Qinghai-Tibet Plateau. They used the BIOMOD niche model to determine the potential distribution of its community and revealed the spatial distribution and driving factors from the perspectives of human activities and climate change. Feng et al. utilized the residual analysis method to simulate the potential net primary productivity (NPPp) of marsh wetland vegetation in the source region of the Yellow River. They employed the Zhou Guangsheng model to simulate NPPp and calculated the net primary production (NPP) influenced by human activities by comparing the results with the MOD17A3HGF product. The problem of quantifying the relative contribution of climate change and human activities to changes in NPPa in marsh wetland vegetation has been solved.

In addition, based on an investigation of vegetation communities in inland salt marsh wetlands, Kang et al. utilized meteorological, hydrological, and Landsat remote sensing image data, as well as a binary pixel model, to analyze the spatio-temporal distribution characteristics of vegetation coverage in inland salt marsh lake wetlands in Sugen. They also quantitatively analyzed the response of vegetation coverage to hydrometeorological factors, which is beneficial for preventing vegetation degradation in fragile ecosystems. Liu et al. utilized high-resolution remote sensing images from Sentinel-1 and Sentinel-2, as well as environmental and topographic data, along with remote sensing algorithms including traditional regression, machine learning, and deep learning models, to estimate the aboveground biomass (AGB) of mountain grasslands in southwest China. This method provides a high spatial resolution simulation solution for estimating the AGB of grassland with complex terrain, fragmented landscape, and interleaved vegetation distribution. Furthermore, Tao et al. conducted a study on the composition of the plankton community and its influencing factors. They found that an increase in biodiversity and improved resource use efficiency resulted in a more stable plankton community. Their research will contribute to the restoration of damaged wetlands and provide a valuable reference for the protection of urban wetland ecosystems.

Climate change or human activities' effects on wetland/grassland soil biogeochemical cycles

In this thematic issue, the main factors considered to affect soil element cycling in wetland/grassland are warming, precipitation changes (including timing and intensity), and external nitrogen (N) input. Ma et al. conducted a laboratory experiment to investigate the changes in carbon dioxide emissions and soil enzyme activity under warming in a boreal peatland. They also examined the litter positions in the soil and the response mechanism of climate warming on litter decomposition. Tong et al. conducted a greenhouse experiment to investigate the effects of warming and drought on the C, N, and phosphorus cycles in the soil of alpine meadows. The study proposed an interesting finding that microorganisms did not directly benefit significantly from the increased nutrient availability under the prevailing conditions. Furthermore, in the Inner Mongolia steppe, Chen et al. investigated the biotic and abiotic factors that influence methane (CH_4) uptake through a manipulated experiment involving warming and precipitation addition. Zheng et al. investigated the co-regulatory effects of timing and plant composition on CH_4 uptake under heavy rainfall using a manipulative experiment and a mixed-effect model. At the same time, the study highlights that climate-driven changes in dominant species are highly likely to alter ecosystem feedback. Based on field investigations, Cong et al. conducted an in-depth study on the stability of C pools under climate change and human activities. They assessed the effects of climate factors and human activities on C pools in natural and degraded peatlands, and highlighted the sensitivity and vulnerability of C pools in shrub peatlands under anthropogenic interference. Through a field N input experiment and high-throughput sequencing technology, Huang et al. found that the response of the soil bacterial phylogenetic community to short-term N input was more sensitive than that of the species community. This finding emphasizes the importance of considering the phylogenetic level in research on the response of soil bacterial communities to short-term N input. Song et al. monitored the long-

term net ecosystem exchange (NEE) flux using an open-path eddy covariance system and identified a pattern in which NEE responds to the size of rainfall events. This study contributes to a deeper understanding of the C cycle and its regulatory mechanisms in the temperate desert steppe. More significantly, it also provides valuable long-term continuous field monitoring data for the validation of ecological models.

In addition, there is one paper that mainly focuses on wetland degradation. Sun et al. utilized an expert scoring method and analytic hierarchy process, along with networks and administrative units, to examine wetland degradation at a regional scale in Northeast China. Their findings clearly indicate that human activities, such as construction, overgrazing, deforestation, and reclamation, were the primary causes of wetland degradation, which could provide a new perspective for the index selection and model construction of comprehensive evaluation of wetland degradation in other cold areas.

In summary, this Research Topic explores a range of wetland and grassland ecosystems, with a specific focus on the impact of climate change and human activities on their vegetation and soil biogeochemical cycles. These papers can provide valuable insights for addressing the challenges brought about by environmental changes and ensuring the continued health and functionality of these vital ecosystems.

Author contributions

KZ: Writing – original draft. ZY: Writing – review & editing.

Funding

This work was supported by the National Natural Science Foundation of China (Nos. 32201410) and the Fundamental Research Funds of the Chinese Academy of Forestry (Nos. CAFYBB2022SY041).

Acknowledgments

We deeply thank all the authors and reviewers who have participated in this Research Topic.

Conflict of interest

The authors declare that the research was conducted in the absence of any commercial or financial relationships that could be construed as a potential conflict of interest.

Publisher's note

References

Cloern, J. E., Abreu, P. C., Carstensen, J., Chauvaud, L., Elmgren, R., Grall, J., et al. (2016). Human activities and climate variability drive fast-paced change across the world's estuarine-coastal ecosystems. *Glob. Change Biol.* 22 (2), 513–529. doi: 10.1111/gcb.13059

Gibbons, J. W., Scott, D. E., Ryan, T. J., Buhlmann, K. A., Tuberville, T. D., Metts, B. S., et al. (2000). The Global Decline of Reptiles, Déjà Vu Amphibians: Reptile species are declining on a global scale. Six significant threats to reptile populations are habitat loss and degradation, introduced invasive species, environmental pollution, disease, unsustainable use, and global climate change. *BioScience* 50 (8), 653–666. doi: 10.1641/0006-3568(2000)050[0653:TGDORD]2.0.CO;2

Jaureguiberry, P., Titeux, N., Wiemers, M., Bowler, D. E., Coscieme, L., Golden, A. S., et al. (2022). The direct drivers of recent global anthropogenic biodiversity loss. *Sci. Adv.* 8 (45), eabm9982. doi: 10.1126/sciadv.abm9982

Martínez-Megías, C., and Rico, A. (2022). Biodiversity impacts by multiple anthropogenic stressors in Mediterranean coastal wetlands. *Sci. Total Environ.* 818, 151712. doi: 10.1016/j.scitotenv.2021.151712

S. Sharma and P. Singh (Eds.) (2021). *Wetlands conservation: Current challenges and future strategies* (United States of America: John Wiley & Sons).

frontiers | Frontiers in Ecology and Evolution

TYPE Original Research
PUBLISHED 24 November 2022
DOI 10.3389/fevo.2022.1073177

OPEN ACCESS

EDITED BY
Zhongqing Yan,
Chinese Academy of Forestry,
China

REVIEWED BY
Zheng Gang Guo,
Lanzhou University,
China
Jingxue Zhao,
Lanzhou University,
China

*CORRESPONDENCE
Chengqun Yu
yucq@igsnrr.ac.cn

SPECIALTY SECTION
This article was submitted to Population, Community, and Ecosystem Dynamics, a section of the journal Frontiers in Ecology and Evolution

RECEIVED 18 October 2022
ACCEPTED 28 October 2022
PUBLISHED 24 November 2022

CITATION
Huang S, Yu C, Fu G, Sun W, Li S and Xiao J (2022) Different responses of soil bacterial species diversity and phylogenetic diversity to short-term nitrogen input in an alpine steppe at the source of Brahmaputra.
Front. Ecol. Evol. 10:1073177.
doi: 10.3389/fevo.2022.1073177

Different responses of soil bacterial species diversity and phylogenetic diversity to short-term nitrogen input in an alpine steppe at the source of Brahmaputra

Shaolin Huang[1,2], Chengqun Yu[1]*, Gang Fu[1], Wei Sun[1], Shaowei Li[1] and Jianyu Xiao[1,2]

[1]Lhasa Plateau Ecosystem Research Station, Key Laboratory of Ecosystem Network Observation and Modeling, Institute of Geographic Sciences and Natural Resources Research, Chinese Academy of Sciences, Beijing, China, [2]University of Chinese Academy of Sciences, Beijing, China

The Qinghai-Tibet Plateau has experienced an increase in N deposition/input due to global change. However, it remains unclear how the responses and whether the responses of soil bacterial diversity to short-term N input are consistent at different levels. Here, we investigated soil bacterial species and phylogenetic α-diversity and community composition based on a short-term nitrogen input experiment (five levels: 0, 2.5, 5, 10, and 20gNm^{-2} y^{-1}) in an alpine steppe at the source of Brahmaputra, using high-throughput sequencing technology. Short-term nitrogen input did not affect the species α-diversity and β-diversity of soil bacteria. However, soil bacterial phylogenetic α-diversity and dissimilarity increased with increasing nitrogen input. Different relative contributions and correlations of primary factors to species and phylogenetic diversity under short-term nitrogen input may result in different responses, in which ecological processes also play a role. Therefore, studying the response of soil bacteria to short-term nitrogen input should take into account not only the species level but also the phylogenetic level. We should pay close attention to the potential influence of short-term nitrogen deposition/fertilization on the soil bacterial community in the alpine steppe on the Tibetan Plateau.

KEYWORDS

nitrogen deposition, soil bacteria, species diversity, phylogenetic diversity, community structure, alpine steppe, Brahmaputra

Introduction

Nitrogen (N) is a vital factor that controls species composition and diversity in terrestrial ecosystems (Zechmeister-Boltenstern et al., 2011). In the last century, human activities have dramatically increased nitrogen deposition globally (Galloway et al., 2004; Bobbink et al., 2010). On the one hand, in a nitrogen-deficient ecosystem, elevated nitrogen

deposition can relieve nitrogen limitation in the system. On the other hand, excessive nitrogen would result in nitrogen pollution due to fossil combustion and deliberate N fertilization (Gruber and Galloway, 2008), which would greatly affect the biogeochemical cycles of C and N in terrestrial ecosystems. One of the most plentiful soil microbes in terrestrial ecosystems is bacteria, which play vital roles in promoting vital biogeochemical procedures in soils (Bardgett and van der Putten, 2014; Delgado-Baquerizo et al., 2019; Zhang et al., 2020). Thus, understanding how the soil bacterial community responds to N enrichment is of great value for predicting the effects of nitrogen deposition on subterranean terrestrial ecosystems.

With the development of high-throughput sequencing technology, a growing number of studies have studied the response of the soil bacterial community to nitrogen input in wetland (Li et al., 2019a), forests (Nie et al., 2018; Wang et al., 2021), grasslands (Zhang and Han, 2012; Ling et al., 2017), and alpine regions on the Tibetan Plateau (Li et al., 2020a, 2021; Mu et al., 2021; Yang et al., 2021). However, how different nitrogen input rates affect the response of soil bacterial species diversity to short-term nitrogen input still remains controversial (Li et al., 2020a; Zhang et al., 2022). Although Zhang et al. (2022) reported that different nitrogen input rates increased soil bacterial α-diversity on the Loess Plateau, Li et al. (2020a) found that different nitrogen input rates decreased soil bacterial α-diversity on the Qinghai-Tibetan Plateau. In addition, Bradley et al. (2006) found that short-term (1–2 months) N application (0, 5.44, and 27.2 g N m^{-2} y^{-1}) had insignificant effects on soil bacterial α-diversity in a grassland at the Cedar Creek LTER in Minnesota, USA. These inconsistent results may have been caused by different nitrogen input rates, durations, climatic conditions, vegetation conditions, and land-use types among these studies. In addition to the unclear response of soil bacterial species diversity to short-term nitrogen input, as well as soil bacterial phylogenetic diversity. Soil bacterial diversity contains not only species diversity but also phylogenetic diversity, which can all deduce community assembly mechanisms (Zhou and Ning, 2017). Some previous studies have reported that phylogenetic diversity reveals more information about community construction than taxonomic diversity (Jia and Du, 2014) and has a strong connection with stability (Zhang et al., 2019), which is an important index. Although Turlapati et al. (2013) have reported that chronic N-amended can increase the phylogenetic diversity of soil bacteria, as well as species diversity. However, little attention has been given to the effects of phylogenetic diversity during changes in soil bacterial communities in response to short-term nitrogen input, and whether the effects on species diversity and phylogenetic diversity are consistent.

The Qinghai-Tibet Plateau is known as the "Roof of the World" and the "Third Pole of the Earth," which is an important barrier to the ecological security of China and Asia (Sun et al., 2012). The high altitude and low temperature of the Qinghai-Tibet Plateau make it very sensitive to global change. From the 1980s to the 2000s, the dose of N deposition increased significantly, ranging from 4 to 13.8 kg N ha^{-1} y^{-1} on the Tibetan Plateau (Liu et al., 2013). At the same time, nitrogen fertilizer application is used to manage degraded grasslands, improve soil fertility and increase plant productivity on the Tibetan Plateau (Zhao and Zhou, 1999; Wang et al., 2020; Li et al., 2020b). However, few studies have examined the effect of different nitrogen input rates on soil bacterial phylogenetic diversity, particularly in the alpine steppe in the western Tibetan Plateau. The Brahmaputra River basin originates west of the Tibetan Plateau, which links Bangladesh, Bhutan, China, and India and is an important international river (Barua, 2018). Therefore, it is important to study the effect of different nitrogen input rates on the alpine steppe at the source of Brahmaputra.

In this study, we investigated the responses of soil bacterial species and phylogenetic diversity to short-term (<1 year) N input based on a field nitrogen input experiment with five levels (i.e., 0, 2.5, 5, 10, and 20 g N m^{-2} y^{-1}) in an alpine steppe at the source of Brahmaputra, using the high-throughput Illumina sequencing technology. Specifically, we mainly aimed to investigate how the responses of soil bacterial species and phylogenetic diversity to short-term (<1 year) nitrogen input and whether the effects were consistent in the alpine steppe at the source of Brahmaputra.

Materials and methods

Study sites

This study was conducted in an alpine steppe of Zhongba County (29° 37′ N, 82° 21′ E, 4,763 m above sea level), Tibet Autonomous Region, China. The mean annual temperature is approximately 5.1°C, and the mean annual precipitation is approximately 320 mm. The dominant species in this steppe is *Potentilla bifurca*, accompanied by *Microula sikkimensis*, *Chenopodium glaucum*, *Heteropappus semiprostratus*, *Carex atrofusca,* and *Carex thibetica Franch*. The soil texture type is sandy loam belonging to alpine steppe soil. The soil organic carbon, soil moisture, soil bulk density, and pH values are 0.57%–0.81%, 5.44%–6.13%, 1.49–1.66 g/cm^3, and 8.27–8.47, respectively.

Experimental design

We designed a one-way factorial design (nitrogen application) with five treatments: 0 (control), 2.5, 5, 10, and 20 g N m^{-2} y^{-1} and were characterized by N0 (control), N2.5, N5, N10, and N20, respectively. In August 2021, a total of 25 5 × 5 m plots were laid out based on a randomized design, and each treatment had five replicates. The distance between any two neighboring plots was approximately 3 m. Nitrogen was applied in the form of urea, which was applied in the afternoon on a cloudy day.

Plant community investigation, soil sampling, and high-throughput sequencing

In September 2021, we recorded the number of plant species, height, and coverage of each plant species within a 0.5 m × 0.5 m quadrat in the middle of each plot (Zhang and Fu, 2021; Tian and Fu, 2022). In each plot, five 3.8 cm diameter soil cores (0–10 cm and 10–20 cm) were collected from the four corners and the middle of each quadrat in cross diagonals after plant community investigation. We mixed and sieved the soil samples through a 2-mm mesh to remove roots and stones. Some of the soil samples were promptly placed in a nitrogen canister and brought back to the laboratory to measure the soil bacterial community, and some of the soil samples retained freshness in the refrigerator to measure the soil physicochemical properties.

High-throughput sequencing procedures are described at length in the Supplementary material. Through analysis, there were 20,850 operational taxonomic units in the surface soil and 19,624 operational taxonomic units in the subsurface soil of the soil bacterial community across the 50 samples.

Statistical analysis

We calculated the response ratio to assess the effect size of N addition for a specific variable (Fu and Shen, 2016; Fu and Shen, 2017).

$$R = \frac{Ni}{N0} \quad (1)$$

where *Ni* is the *N* addition rate, and *N*0 is the control treatment.

One-way ANOVA was used to measure the effects of N input on the soil properties, plant α-diversity, and species α-diversity of the soil bacterial community. The microeco package was used to obtain the α-diversity (OTUs, ACE, Chao1, Shannon, and Simpson) and β-diversity of the soil bacterial species (Yu et al., 2019; Zong and Fu, 2021). The picante package was used to calculate soil bacterial phylogenetic α-diversity (PD, MPD, MNTD, NRI, and NTI) and β-diversity (Sun et al., 2021). The linear discriminant analysis (LDA) effect size (LEfSe) method in microeco package was used to recognize significant differences in soil bacteria, and then Duncan's multiple comparison test was used to calculate the differential species of soil bacteria. RandomForest package was used to calculate the relative contribution to soil bacterial species and phylogenetic α-diversity of each concerned variable. We calculated the correlations between species and phylogenetic α-diversity of the soil bacterial community and environmental characteristics. The microeco package was used to perform the Mantel test between species and the phylogenetic community composition of soil bacteria and environmental variables. The iCAMP package was used to calculate the community assembly processes of the soil bacterial community (Zhou and Ning, 2017; Han et al., 2022; Zhong and Fu, 2022). When the βNTI was < −2, the community turnover was Homogeneous Selection. When the βNTI was >2, the community turnover was Heterogeneous Selection. When the βNTI was between −2 and 2, and the RC_{Bray} was < −0.95, the community turnover was Homogenizing Dispersal. When the βNTI was between −2 and 2, and the RC_{Bray} was >0.95, the community turnover was Dispersal Limitation. When the βNTI was between −2 and 2, and the RC_{Bray} was between −0.95 and 0.95, the community turnover may be weak selection, weak dispersal, diversification, and drift. The software used in this study was R4.0.2, SPSS 25, and Origin 2022.

Results

Variations in abiotic and biotic characteristics along the N input gradient

Nitrogen input significantly increased soil available nitrogen (NH_4^+-N, NO_3^--N, AN:AP, and NH_4^+-N:NO_3^--N) in both surface and subsurface soils (Supplementary Table S1). Compared to N0, the soil NH_4^+-N contents of the surface and subsurface soils under N20 all increased by 16.42-and 6.57-fold, respectively. Compared to N0, the soil NO_3^--N contents of the surface and subsurface soils under N20 all increased by 19.27-and 12.67-fold, respectively. Compared to N0, the soil AN:AP of the surface and subsurface soils under N20 all increased by 22.39- and 8.24-fold, respectively. Soil NH_4^+-N:NO_3^--N was also significantly changed by N input in both surface and subsurface soils. However, plant α-diversity, soil pH, SM, SOC, TN, TP, AP, and soil enzymes did not significantly change along the N input gradient (Supplementary Tables S1, S2).

Variations in soil bacterial species and phylogenetic α-diversity along the N input gradient and their relationships with abiotic and biotic characteristics

The effect size of soil bacterial species α-diversity showed no relationships with the nitrogen input rate in either the surface or subsurface soil (Supplementary Figure S1). The effect size of soil bacterial phylogenetic α-diversity, including MPD in surface soil and NRI in subsurface soil, increased with the nitrogen input rate (Figures 1A,B). However, the effect size of soil bacterial phylogenetic α-diversity, including PD, MNTD, NRI, and NTI in surface soil and PD, MPD, MNTD, and NTI in subsurface soil, showed no relationships with the nitrogen input rate (Supplementary Figure S2).

The relative contributions of environmental variables to the R_{OTUs} variation in surface soil were listed in the following order: R_{TN}, R_{TP}, $R_{C:N}$, R_{SM}, etc., and they together explained 69.41% of the R_{OTUs} variation along the N input gradient (Supplementary Figure S3a). The relative contributions of

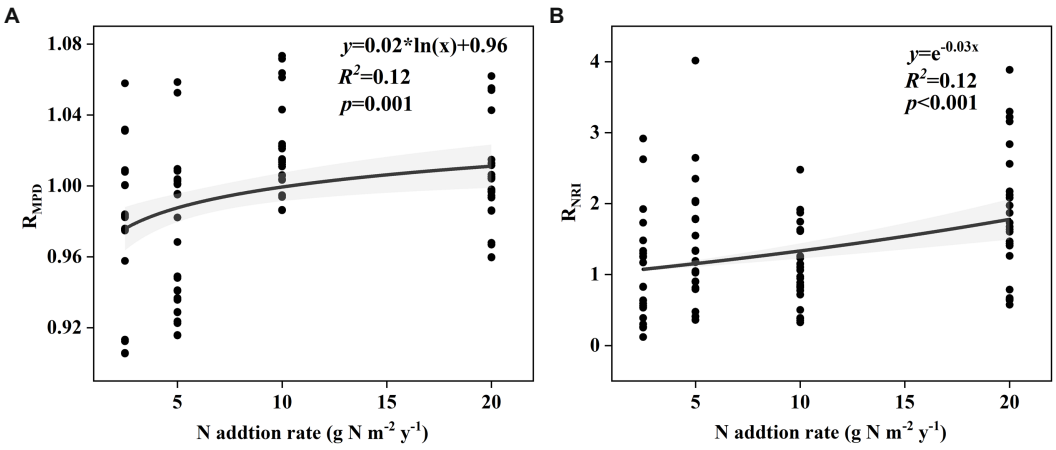

FIGURE 1
Relationships between nitrogen input rate and the effect size of nitrogen input on phylogenetic α-diversity of soil bacteria **(A)** MPD in surface soil and **(B)** NRI in subsurface soil in an alpine steppe.

environmental variables to the R_{ACE} variation in surface soil were listed in the following order: R_{TN}, R_{UA}, $R_{C:N}$, R_{SM}, R_{CL}, etc., and they together explained 72.8% of the R_{ACE} variation along the N input gradient (Supplementary Figure S3b). The relative contributions of environmental variables to the R_{Chao1} variation in surface soil were listed in the following order: R_{UA}, $R_{C:N}$, R_{TN}, $R_{C:P}$, etc., and they together explained 72.68% of the R_{Chao1} variation along the N input gradient (Supplementary Figure S3c). The relative contributions of environmental variables to the $R_{Shannon}$ variation in surface soil were listed in the following order: R_{SM}, $R_{SRplant}$, R_{SOC}, $R_{C:N}$, R_{UA}, etc., and they together explained 81.14% of the $R_{Shannon}$ variation along the N input gradient (Supplementary Figure S3d). The relative contributions of environmental variables to the $R_{Simpson}$ variation in surface soil were listed in the following order: R_{SM}, $R_{C:N}$, $R_{C:P}$, $R_{SRplant}$, R_{SC}, R_{SOC}, R_{ALP}, etc., and they together explained 84.59% of the $R_{Simpson}$ variation along the N input gradient (Supplementary Figure S3e).

The relative contributions of environmental variables to the R_{OTUs} variation in subsurface soil were listed in the following order: R_{SM}, R_{NO3--N}, $R_{Shannonplant}$, R_{ALP}, etc., and they together explained 68.75% of the R_{OTUs} variation along the N input gradient (Supplementary Figure S4a). The relative contributions of environmental variables to the R_{ACE} variation in subsurface soil were listed in the following order: R_{SM}, R_{TP}, R_{UA}, $R_{C:N}$, R_{TN}, etc., and they together explained 66.73% of the R_{ACE} variation along the N input gradient (Supplementary Figure S4b). The relative contributions of environmental variables to the R_{Chao1} variation in subsurface soil were listed in the following order: R_{UA}, R_{TP}, R_{SM}, $R_{C:N}$, R_{AP}, R_{pH}, R_{NH4+-N}, R_{NO3--N}, etc., and they together explained 64.5% of the R_{Chao1} variation along the N input gradient (Supplementary Figure S4c). The relative contributions of environmental variables to the $R_{Shannon}$ variation in subsurface soil were listed in the following order: R_{CL}, $R_{C:N}$, R_{SM}, R_{AP}, R_{TP}, etc., and they together explained 58.48% of the $R_{Shannon}$ variation along the N input gradient (Supplementary Figure S4d). The relative contributions of environmental variables to the $R_{Simpson}$ variation in subsurface soil were listed in the following order: R_{NO3--N}, R_{CT}, R_{CL}, etc., and they together explained 90.25% of the $R_{Simpson}$ variation along the N input gradient (Supplementary Figure S4e).

The relative contributions of environmental variables to the R_{MPD} variation in surface soil were listed in the following order: R_{SM}, R_{TP}, R_{SC}, etc., and they together explained 66% of the variation in the R_{MPD} along the N input gradient (Figure 2A). The relative contributions of environmental variables to the R_{NRI} variation in surface soil were listed in the following order: R_{SM}, R_{TP}, R_{TN}, R_{SOC}, $R_{pielouplant}$, $R_{C:N}$, R_{NO3--N}, R_{ALP}, $R_{C:N}$, etc., and they together explained 73.48% of the variation in the R_{NRI} along the N input gradient (Supplementary Figure S5a). The relative contributions of environmental variables to the R_{PD} variation in surface soil were listed in the following order: R_{TP}, R_{SM}, R_{TN}, $R_{C:N}$, etc., and they together explained 79.36% of the variation in the R_{PD} along the N input gradient (Supplementary Figure S5b). The relative contributions of environmental variables to the R_{MNTD} variation in surface soil were listed in the following order: R_{SM}, R_{CL}, $R_{NH4+-N:NO3--N}$, R_{CT}, etc., and they together explained 73.26% of the variation in the R_{MNTD} along the N input gradient (Supplementary Figure S5c). The relative contributions of environmental variables to the R_{NTI} variation in surface soil were listed in the following order: R_{TN}, R_{ALP}, R_{TP}, R_{NH4+-N}, R_{SM}, etc., and they together explained 88.17% of the variation in the R_{NTI} along the N input gradient (Supplementary Figure S5d).

The relative contributions of environmental variables to the R_{MPD} variation in subsurface soil were listed in the following order: R_{CL}, R_{TP}, $R_{C:N}$, R_{AP}, R_{CT}, R_{NH4+-N}, etc., and they together explained 65.36% of the variation in the R_{MPD} along the N input gradient (Supplementary Figure S5e). The relative contributions of environmental variables to the R_{NRI} variation in subsurface soil were listed in the following order: $R_{pielouplant}$, R_{SC}, R_{ALP}, R_{NH4+-N}, R_{TP},

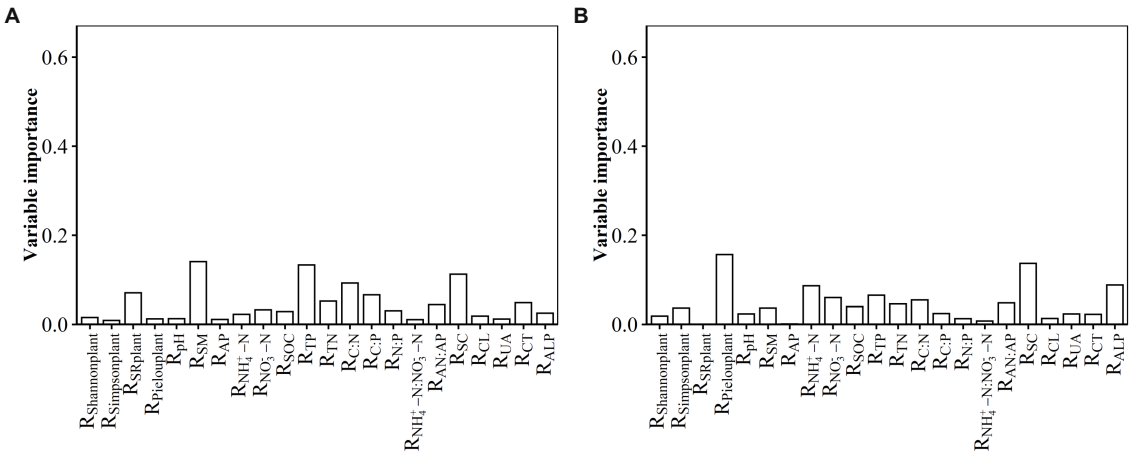

FIGURE 2
Relative contribution of observed soil and plant variables to the effect size of nitrogen input on **(A)** MPD in surface soil and **(B)** NRI in subsurface soil along the N input gradient in an alpine steppe. $R_{shannonplant}$: effect size of nitrogen input on Shannon index of plant community; $R_{simpsonplant}$: effect size of nitrogen input on Simpson index of plant community; $R_{SRplant}$: effect size of nitrogen input on species richness of plant community; $R_{pielouplant}$: effect size of nitrogen input on Pielou index of plant community; R_{SM}: effect size of nitrogen input on soil moisture; R_{AP}: effect size of nitrogen input on available phosphorus; R_{NH4+-N}: effect size of nitrogen input on ammonium nitrogen; R_{NO3--N}: effect size of nitrogen input on nitrate nitrogen; R_{SOC}: effect size of nitrogen input on soil organic carbon; R_{TP}: effect size of nitrogen input on total phosphorus; R_{TN}: effect size of nitrogen input on total nitrogen; $R_{C:N}$: effect size of nitrogen input on ratio of carbon to nitrogen; $R_{C:P}$: effect size of nitrogen input on ratio of carbon to phosphorus; $R_{N:P}$: effect size of nitrogen input on ratio of nitrogen to phosphorus; $R_{NH4+-N:NO3--N}$: effect size of nitrogen input on ratio of ammonium nitrogen to nitrate nitrogen; $R_{AN:AP}$: effect size of nitrogen input on ratio of available nitrogen to available phosphorus; R_{SC}: effect size of nitrogen input on soil sucrase; R_{CL}: effect size of nitrogen input on soil cellulase; R_{UA}: effect size of nitrogen input on soil urease; R_{CT}: effect size of nitrogen input on soil catalase; R_{ALP}: effect size of nitrogen input on soil alkaline phosphatase.

R_{NO3--N}, etc., and they together explained 42.8% of the variation in the R_{NRI} along the N input gradient (Figure 2B). The relative contributions of environmental variables to the R_{PD} variation in subsurface soil were listed in the following order: R_{TP}, R_{SM}, R_{TN}, R_{UA}, $R_{C:N}$, etc., and they together explained 68.08% of the variation in the R_{PD} along the N input gradient (Supplementary Figure S5f). The relative contributions of environmental variables to the R_{MNTD} variation in subsurface soil were listed in the following order: R_{CL}, $R_{C:N}$, R_{TP}, R_{UA}, etc., and they together explained 70.63% of the variation in the R_{MNTD} along the N input gradient (Supplementary Figure S5g). The relative contributions of environmental variables to the R_{NTI} variation in subsurface soil were listed in the following order: R_{UA}, R_{SM}, R_{TN}, R_{ALP}, R_{CL}, $R_{C:N}$, etc., and they together explained 64.22% of the variation in the R_{NTI} along the N input gradient (Supplementary Figure S5h).

Variations in soil bacterial species and phylogenetic community composition along the N input gradient and their relationships with abiotic and biotic characteristics

For the soil bacterial species community, soil bacterial species β-diversity had no relationships with nitrogen input dose in either surface or subsurface soil (Supplementary Figure S6). There were 28 differential groups of soil bacterial communities in the surface soil, including 4 classes, 4 orders, 6 families, and 14 genus, and they displayed dissimilar variation tendencies with the N input gradient (Figure 3A; Supplementary Table S3). There were 26 differential groups of soil bacterial communities in the subsurface soil, including 4 classes, 6 orders, 4 families, 11 genus, and 1 species, and they displayed dissimilar variation tendencies with the N input gradient (Figure 3B; Supplementary Table S4). Duncan multiple comparison showed that c__Chthonomonadetes, c__Lineage_IIa, and c__Lineage_IIb under the control treatment were significantly higher than those under the N20 treatment, and c__S0134_terrestrial_group under the N20 treatment was significantly higher than that under the control treatment in surface soil (Supplementary Table S3). According to the results of the Mantel test, the soil bacterial species community composition was significantly correlated with SOC, TP, TN, C: N, and SC ($p < 0.05$) and marginally significantly correlated with C:P, and ALP in the surface soil ($p < 0.1$). The soil bacterial species community composition was significantly correlated with SM, TP, and TN ($p < 0.05$) and marginally significantly interrelated with SOC and SC in subsurface soil (Table 1, $p < 0.1$).

The soil bacterial phylogenetic β-diversity between the control and nitrogen addition treatments significantly increased with increasing nitrogen addition rates in both the surface and subsurface soils (Figure 4, $p < 0.05$). According to the results of the Mantel test, the soil bacterial phylogenetic community composition was significantly interrelated with TP, NH_4^+-N:NO_3^--N, and SC ($p < 0.05$) and marginally significantly interrelated with pH, NO_3^--N, and C:P in the surface soil ($p < 0.1$). The soil bacterial phylogenetic

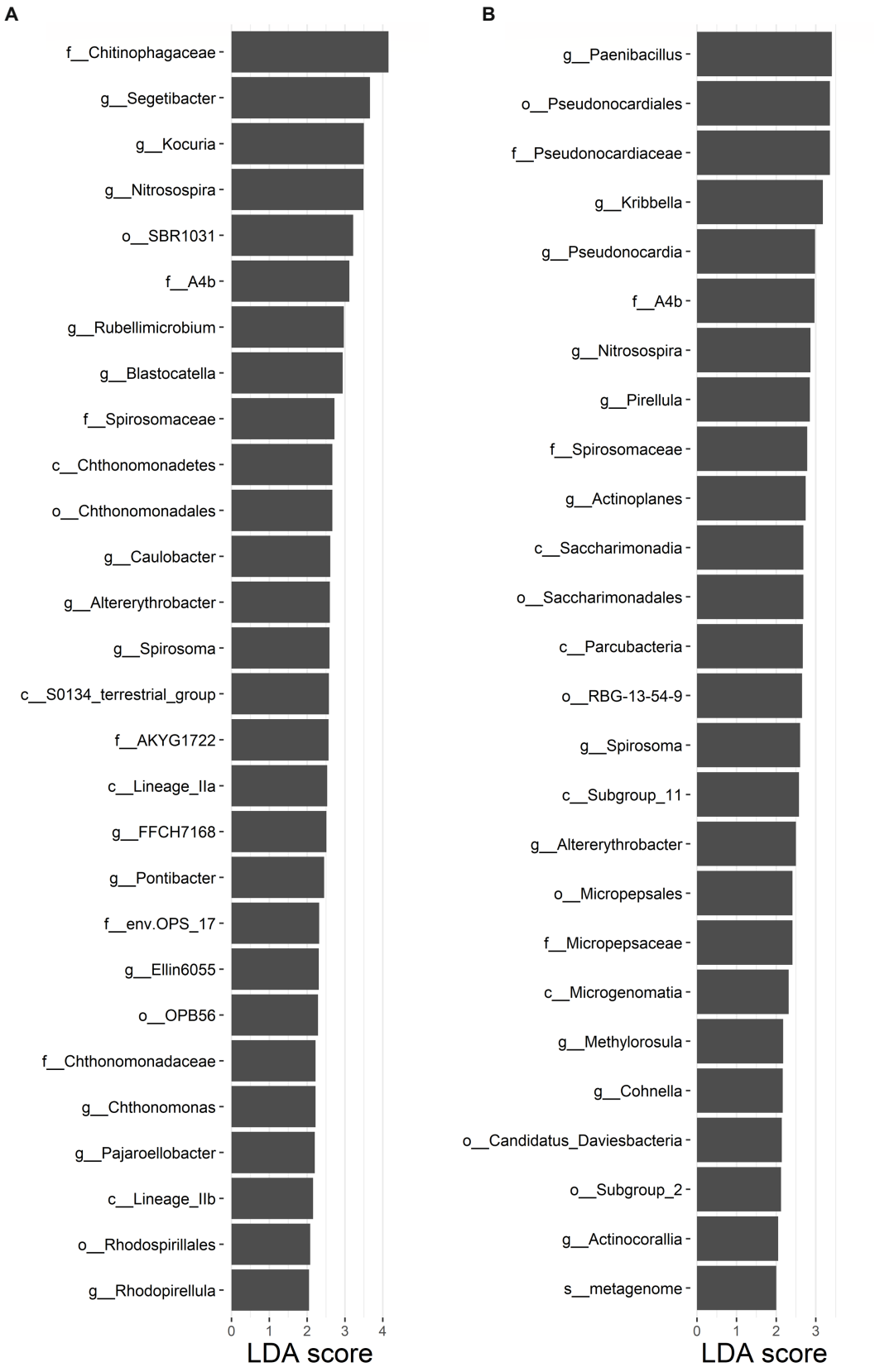

FIGURE 3
Soil bacterial community with linear discriminant analysis (LDA) scores >2 in **(A)** surface soil and **(B)** subsurface soil in an alpine steppe.

community composition was significantly interrelated with NO_3^--N and AN:AP and marginally significantly correlated with NH_4^+-N, CT, and ALP in the subsurface soil (Table 1, $p < 0.1$).

Response of the community assembly of the soil bacterial community to nitrogen input

Changes in the effect size of nitrogen input on "Heterogeneous Selection," "Homogeneous Selection," "Dispersal Limitation," "Homogenizing Dispersal," and "Drift and Others" in both surface and subsurface soil are shown in Figure 5 and Supplementary Figure S7. 'Homogenizing Dispersal' significantly decreased and "Drift and Others" marginally significantly increased with the nitrogen input rates in surface soil (Figures 5A,B), while others showed no relationships with the nitrogen input rates (Supplementary Figure S7).

TABLE 1 Mantel test between soil bacterial species and phylogenetic community composition and soil and plant variables based on the Bray–Curtis and βMNTD dissimilarity matrix.

Variables	Species		Phylogenetic	
	Surface	Subsurface	Surface	Subsurface
$Shannon_{plant}$	−0.04	−0.12	−0.22	−0.17
$Simpson_{plant}$	−0.07	−0.14	−0.16	−0.12
SR_{plant}	0.03	−0.03	−0.30	−0.23
$Pielou_{plant}$	−0.11	−0.14	−0.19	−0.11
pH	−0.02	0.07	**0.22+**	0.14
SM	0.09	**0.41****	0.02	0.12
AP (mg kg^{-1})	−0.20	0.07	−0.26	0.14
NH_4^+-N	−0.05	−0.03	0.11	**0.19+**
NO_3^--N	−0.01	0.02	**0.12+**	**0.33****
SOC	**0.39****	**0.16+**	0.05	0.07
TP	**0.42****	**0.41****	**0.37****	0.08
TN	**0.45****	**0.20***	0.05	0.10
C: N	**0.26***	0.14	0.13	0.11
C:P	**0.24+**	0.13	**0.19+**	0.00
N:P	0.13	0.12	0.18	0.05
NH_4^+-N:NO_3^--N	−0.11	−0.07	**0.30****	0.20
AN:AP	−0.05	0.02	0.12	**0.30***
SC (mg g^{-1} d^{-1})	**0.47****	**0.12+**	**0.22***	−0.01
CL (mgg^{-1} 3 d^{-1})	−0.16	−0.01	−0.15	0.08
UA (mg g^{-1} d^{-1})	0.11	0.13	0.12	−0.01
CT (ml g^{-1} 20 min^{-1})	0.12	−0.01	−0.10	**0.15+**
ALP (mg g^{-1} 2 h^{-1})	**0.18+**	0.07	0.08	**0.20+**

+,* and ** indicated the correlations were significant at $p < 0.1$, $p < 0.05$ and $p < 0.01$, respectively. The bold values indicated significant correlations.

Discussion

Variations in species and phylogenetic α-diversity of the soil bacterial community along the N input gradient

We found that the species α-diversity and phylogenetic α-diversity of the soil bacterial community had different responses to nitrogen input in the alpine steppe at the Brahmaputra site, which was likely a result of one or more of the following reasons. First, soil moisture is an important factor in determining the species and phylogenetic α-diversity of the soil bacterial community (Li et al., 2021; Liu et al., 2022). However, there were no significant changes in soil moisture along the nitrogen input gradient (Supplementary Table S1). Second, plant α-diversity can still affect soil bacterial richness and α-diversity (Bakker et al., 2010; Zhang and Han, 2012; Ren et al., 2018). The response ratio of nitrogen input to the plant Pielou index increased with increasing nitrogen input dose (Supplementary Figure S8a), and had a significant positive correlation with phylogenetic α-diversity (Supplementary Table S5), but had no significant relationship with species α-diversity (Supplementary Table S6). Third, TP is also correlated with soil bacterial α-diversity (Feng et al., 2017; Zhang et al., 2017; Yang et al., 2020). The response ratio of nitrogen input to total phosphorus decreased with increasing nitrogen input dose (Supplementary Figure S8b), and had a significant negative correlation with phylogenetic and species α-diversity (Supplementary Tables S5, S6). Furthermore, the relative contribution of total phosphorus to phylogenetic α-diversity was higher than that to species α-diversity in this study. Fourth, the soil bacterial community correlated with soil enzyme activities (Li et al., 2019b). The response ratio of nitrogen input to soil sucrase decreased with increasing nitrogen input dose (Supplementary Figure S8c), and had a significant negative correlation with phylogenetic and species α-diversity (Supplementary Tables S5, S6). In this study, soil sucrase had great importance on phylogenetic α-diversity rather than species α-diversity. Fifth, the relative contributions of other environmental factors to the species and phylogenetic α-diversity of the soil bacterial community in both the surface and subsurface soils were negligible. The different relative contributions of dominant factors to species and phylogenetic α-diversity may led to different responses.

Variations in species and phylogenetic community composition of soil bacteria along the N input gradient

In this study, we also found that the responses of phylogenetic β-diversity and species β-diversity to short-term nitrogen input were different in the alpine steppe at the Brahmaputra site. This phenomenon was likely caused by the following several reasons. First, the diversity in the different dimensions of the soil microbial

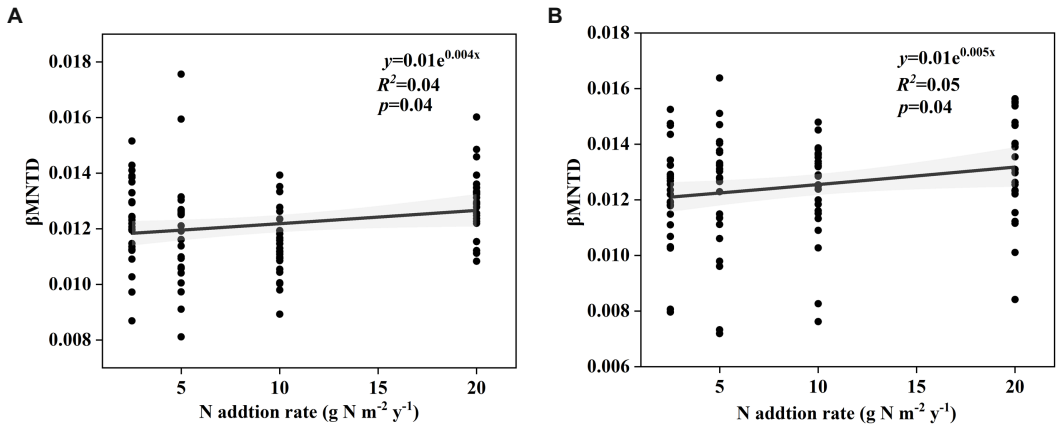

FIGURE 4
Change in the effect size of nitrogen input on soil bacterial phylogenetic βMNTD in surface soil **(A)** and subsurface soil **(B)** along the N input gradient in an alpine steppe.

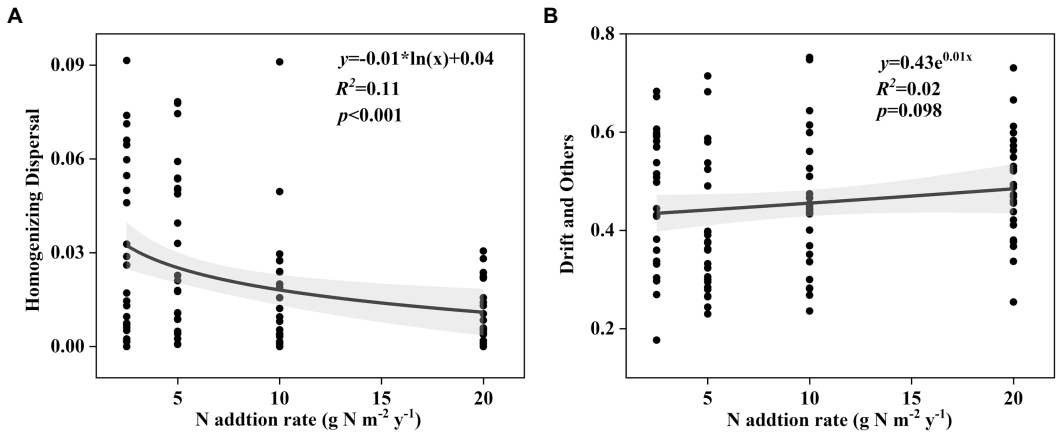

FIGURE 5
Change in the effect size of nitrogen input on **(A)** Homogenizing Dispersal, **(B)** Drift and Others in surface soil along the N input gradient in an alpine steppe.

community may be related to environmental factors in different ways (Zong and Fu, 2021; Zhong and Fu, 2022). In this study, soil NH_4^+-N and NO_3^--N contents increased with increasing nitrogen input (Supplementary Table S1). Furthermore, the soil NH_4^+-N and NO_3^--N contents were marginally significantly and significantly correlated with phylogenetic community composition, but had no correlation with species community composition (Table 1). Second, phylogenetic information is better than taxonomic information in identifying some ecological processes during community assembly (Zhou and Ning, 2017). That is, ecological processes are more closely linked to phylogenetic diversity than taxonomic diversity. Some previous studies have shown that the "Homogenizing Dispersal" process leads to more similarity in communities, while the "Drift" process results in relatively low similarity in communities (Zhou and Ning, 2017). In this study, the "Homogenizing Dispersal" process decreased and the "Drift" process increased with increasing nitrogen input (Figures 4A,B), thus leading to an increase in phylogenetic β-diversity with increasing nitrogen input. The different correlations of environmental factors and ecological processes with species and phylogenetic β-diversity perhaps resulted in different responses.

Conclusion

Based on a short-term (<1 year) field nitrogen input experiment in an alpine steppe at the source of Brahmaputra, we found that short-term nitrogen input did not change the species diversity of soil bacteria, but greatly affected phylogenetic diversity. The increased

magnitude of soil bacterial phylogenetic α-diversity and β-diversity increased with increasing nitrogen input dose. The different responses of soil bacterial species and phylogenetic diversity to short-term nitrogen input were likely due to differences in their relative contributions to major factors and relationships with primary factors, in which ecological processes also play a role. This study proved that the responses of the soil bacterial phylogenetic community were more sensitive than those of the species community to short-term nitrogen input. It also highlighted the importance of taking into account the phylogenetic level when studying the response of short-term nitrogen input to the soil bacterial community. Given that grasslands on the Tibetan Plateau are receiving increased N input, it is critical to understand the response of soil bacterial diversity to N-enriched conditions. Considering that prolonged nitrogen deposition may have different and more profound effects on soil bacterial communities in different dimensions, future studies are needed.

Data availability statement

The datasets generated for this study can be found online at: Bacterial https://kdocs.cn/l/cp7HHdCzj9N7. Further inquiries should be directed to the corresponding author.

Author contributions

CY, GF, and HS planned and designed the study. WS, SL, and JX performed the experiments and conducted fieldwork. HS analyzed the data and wrote the manuscript. All authors contributed to the article and approved the submitted version.

Funding

This research was supported by the Effects of short-term fertilization on soil microbial community structure in degraded alpine steppe at the source of Brahmaputra (XZ202201ZR0064G), Youth Innovation Promotion Association of Chinese Academy of Sciences (2020054), the National Natural Science Foundation of China (31600432), Bingwei Outstanding Young Talents Program of Institute of Geographic Sciences and Natural Resources Research, Chinese Academy of Sciences (2018RC202), Tibet Science and Technology Major Projects of the Pratacultural Industry (XZ202101ZD0003N), and Construction Project of Fixed Observation and Experimental Station of Support System for Agricultural Green Development in Zhongba County.

Acknowledgments

I would like to give my heartfelt thanks to Zhongba County People's Government and Zhongba County Agriculture and Rural Bureau for the help of selection of study areas.

Conflict of interest

The authors declare that the research was conducted in the absence of any commercial or financial relationships that could be construed as a potential conflict of interest.

Publisher's note

Supplementary material

The Supplementary material for this article can be found online at: https://www.frontiersin.org/articles/10.3389/fevo.2022.1073177/full#supplementary-material

References

Bakker, M. G., Glover, J. D., Mai, J. G., and Kinkel, L. L. (2010). Plant community effects on the diversity and pathogen suppressive activity of soil streptomycetes. *Appl. Soil Ecol.* 46, 35–42. doi: 10.1016/j.apsoil.2010.06.003

Bardgett, R. D., and van der Putten, W. H. (2014). Belowground biodiversity and ecosystem functioning. *Nature* 515, 505–511. doi: 10.1038/nature13855

Barua, A. (2018). Water diplomacy as an approach to regional cooperation in South Asia: a case from the Brahmaputra basin. *J. Hydrol.* 567, 60–70. doi: 10.1016/j.jhydrol.2018.09.056

Bobbink, R., Hicks, K., Galloway, J., Spranger, T., Alkemade, R., Ashmore, M., et al. (2010). Global assessment of nitrogen deposition effects on terrestrial plant diversity: a synthesis. *Ecol. Appl.* 20, 30–59. doi: 10.1890/08-1140.1

Bradley, K., Drijber, R. A., and Knops, J. (2006). Increased N availability in grassland soils modifies their microbial communities and decreases the abundance of arbuscular mycorrhizal fungi. *Soil Biol. Biochem.* 38, 1583–1595. doi: 10.1016/j.soilbio.2005.11.011

Delgado-Baquerizo, M., Bardgett, R. D., Vitousek, P. M., Maestre, F. T., Williams, M. A., Eldridge, D. J., et al. (2019). Changes in belowground biodiversity during ecosystem development. *Proc. Natl. Acad. Sci. U. S. A.* 116, 6891–6896. doi: 10.1073/pnas.1818400116

Feng, Y., Guo, Z., Zhong, L., Zhao, F., Zhang, J., and Lin, X. (2017). Balanced fertilization decreases environmental filtering on soil bacterial community assemblage in North China. *Front. Microbiol.* 8:2376. doi: 10.3389/fmicb.2017.02376

Fu, G., and Shen, Z. X. (2016). Response of alpine plants to nitrogen addition on the Tibetan plateau: a meta-analysis. *J. Plant Growth Regul.* 35, 974–979. doi: 10.1007/s00344-016-9595-0

Fu, G., and Shen, Z. X. (2017). Response of alpine soils to nitrogen addition on the Tibetan plateau: a meta-analysis. *Appl. Soil Ecol.* 114, 99–104. doi: 10.1016/j.apsoil.2017.03.008

Galloway, J. N., Dentener, F. J., Capone, D. G., Boyer, E. W., Howarth, R. W., Seitzinger, S. P., et al. (2004). Nitrogen cycles: past, present, and future. *Biogeochemistry* 70, 153–226. doi: 10.1007/s10533-004-0370-0

Gruber, N., and Galloway, J. N. (2008). An earth-system perspective of the global nitrogen cycle. *Nature* 451, 293–296. doi: 10.1038/nature06592

Han, F. S., Yu, C. Q., and Fu, G. (2022). Warming alters elevation distributions of soil bacterial and fungal communities in alpine grasslands. *Glob. Ecol. Conserv.* 39:e02306. doi: 10.1016/j.gecco.2022.e02306

Jia, P., and Du, G. (2014). Measuring functional and phylogenetic diversity in community ecology. *Chinese Bull. Life Sci.* 26, 153–157.

Li, Y., He, J.-S., Wang, H., Zhou, J., Yang, Y., and Chu, H. (2021). Lowered water table causes species substitution while nitrogen amendment causes species loss in alpine wetland microbial communities. *Pedosphere* 31, 912–922. doi: 10.1016/s1002-0160(21)60023-1

Li, Y., Nie, C., Liu, Y. H., Du, W., and He, P. (2019b). Soil microbial community composition closely associates with specific enzyme activities and soil carbon chemistry in a long-term nitrogen fertilized grassland. *Sci. Total Environ.* 654, 264–274. doi: 10.1016/j.scitotenv.2018.11.031

Li, J. S., Shao, X. Q., Huang, D., Shang, J. Y., Liu, K. S., Zhang, Q., et al. (2020b). The addition of organic carbon and nitrogen accelerates the restoration of soil system of degraded alpine grassland in Qinghai-Tibet plateau. *Ecol. Eng.* 158:106084. doi: 10.1016/j.ecoleng.2020.106084

Li, W., Sheng, H., Ekawati, D., Jiang, Y., and Yang, H. (2019a). Variations in the compositions of soil bacterial and fungal communities due to microhabitat effects induced by simulated nitrogen deposition of a bamboo Forest in wetland. *Forests* 10:1098. doi: 10.3390/f10121098

Li, J. J., Yang, C., Zhou, H. K., and Shao, X. Q. (2020a). Responses of plant diversity and soil microorganism diversity to water and nitrogen additions in the Qinghai-Tibetan plateau. *Glob. Ecol. Conserv.* 22:e1003. doi: 10.1016/j.gecco.2020.e01003

Ling, N., Chen, D., Guo, H., Wei, J., Bai, Y., Shen, Q., et al. (2017). Differential responses of soil bacterial communities to long-term N and P inputs in a semi-arid steppe. *Geoderma* 292, 25–33. doi: 10.1016/j.geoderma.2017.01.013

Liu, J. J., Jin, L., Shan, Y. X., Burgess, K. S., and Ge, X. J. (2022). Elevation explains variation in soil microbial diversity and community composition under experimental warming and fertilization treatments in mountain meadows. *Appl. Soil Ecol.* 171:104311. doi: 10.1016/j.apsoil.2021.104311

Liu, X., Zhang, Y., Han, W., Tang, A., Shen, J., Cui, Z., et al. (2013). Enhanced nitrogen deposition over China. *Nature* 494, 459–462. doi: 10.1038/nature11917

Mu, Z., Dong, S., Li, Y., Li, S., Shen, H., Zhang, J., et al. (2021). Soil bacterial community responses to N application and warming in a Qinghai-Tibetan plateau alpine steppe. *Front. Ecol. Evol.* 9:709518. doi: 10.3389/fevo.2021.709518

Nie, Y. X., Wang, M. C., Zhang, W., Ni, Z., Hashidoko, Y., and Shen, W. J. (2018). Ammonium nitrogen content is a dominant predictor of bacterial community composition in an acidic forest soil with exogenous nitrogen enrichment. *Sci. Total Environ.* 624, 407–415. doi: 10.1016/j.scitotenv.2017.12.142

Ren, B., Hu, Y., Chen, B., Zhang, Y., Thiele, J., Shi, R., et al. (2018). Soil pH and plant diversity shape soil bacterial community structure in the active layer across the latitudinal gradients in continuous permafrost region of northeastern China. *Sci. Rep.* 8:5619. doi: 10.1038/s41598-018-24040-8

Sun, W., Li, S. W., Wang, J. H., and Fu, G. (2021). Effects of grazing on plant species and phylogenetic diversity in alpine grasslands. *Northern Tibet. Ecol. Eng.* 170:106331. doi: 10.1016/j.ecoleng.2021.106331

Sun, H., Zheng, D., Yao, T., and Zhang, Y. (2012). Protection and construction of the National Ecological Security Shelter Zone on Tibetan plateau. *Acta Geograph. Sin.* 67, 3–12.

Tian, Y., and Fu, G. (2022). Quantifying plant species α-diversity using normalized difference vegetation index and climate data in alpine grasslands. *Remote Sens.* 14:5007. doi: 10.3390/rs14195007

Turlapati, S. A., Minocha, R., Bhiravarasa, P. S., Tisa, L. S., Thomas, W. K., and Minocha, S. C. (2013). Chronic N-amended soils exhibit an altered bacterial community structure in Harvard Forest, MA, USA. *FEMS Microbiol. Ecol.* 83, 478–493. doi: 10.1111/1574-6941.12009

Wang, J. Q., Shi, X. Z., Zheng, C. Y., Suter, H., and Huang, Z. Q. (2021). Different responses of soil bacterial and fungal communities to nitrogen deposition in a subtropical forest. *Sci. Total Environ.* 755:142449. doi: 10.1016/j.scitotenv.2020.142449

Wang, D., Zhou, H., Yao, B., Wang, W., Dong, S., Shang, Z., et al. (2020). Effects of nutrient addition on degraded alpine grasslands of the Qinghai-Tibetan plateau: a meta-analysis. *Agric. Ecosyst. Environ.* 301:106970. doi: 10.1016/j.agee.2020.106970

Yang, P., Luo, Y., Gao, Y., Gao, X. L., Gao, J. F., Wang, P. K., et al. (2020). Soil properties, bacterial and fungal community compositions and the key factors after 5-year continuous monocropping of three minor crops. *PLoS One* 15:e0237164. doi: 10.1371/journal.pone.0237164

Yang, F., Zhang, Z., Barberan, A., Yang, Y., Hu, S., and Guo, H. (2021). Nitrogen-induced acidification plays a vital role driving ecosystem functions: insights from a 6-year nitrogen enrichment experiment in a Tibetan alpine meadow. *Soil Biol. Biochem.* 153:108107. doi: 10.1016/j.soilbio.2020.108107

Yu, C. Q., Han, F. S., and Fu, G. (2019). Effects of 7 years experimental warming on soil bacterial and fungal community structure in the northern Tibet alpine meadow at three elevations. *Sci. Total Environ.* 655, 814–822. doi: 10.1016/j.scitotenv.2018.11.309

Zechmeister-Boltenstern, S., Michel, K., and Pfeffer, M. (2011). Soil microbial community structure in European forests in relation to forest type and atmospheric nitrogen deposition. *Plant Soil* 343, 37–50. doi: 10.1007/s11104-010-0528-6

Zhang, J., Ai, Z., Liang, C., Wang, G., and Xue, S. (2017). Response of soil microbial communities and nitrogen thresholds of Bothriochloa ischaemum to short-term nitrogen addition on the loess plateau. *Geoderma* 308, 112–119. doi: 10.1016/j.geoderma.2017.08.034

Zhang, J., Ai, Z., Liu, H., Tang, D. W. S., Yang, X., Wang, G., et al. (2022). Short-term N addition in a Pinus tabuliformis plantation: microbial community composition and interactions show different linkages with ecological stoichiometry. *Appl. Soil Ecol.* 174:104422. doi: 10.1016/j.apsoil.2022.104422

Zhang, H. R., and Fu, G. (2021). Responses of plant, soil bacterial and fungal communities to grazing vary with pasture seasons and grassland types. *Northern Tibet. Land Degrad. Dev.* 32, 1821–1832. doi: 10.1002/ldr.3835

Zhang, X., and Han, X. (2012). Nitrogen deposition alters soil chemical properties and bacterial communities in the Inner Mongolia grassland. *J. Environ. Sci.* 24, 1483–1491. doi: 10.1016/s1001-0742(11)60900-5

Zhang, X., Huang, Y., Liu, S., Fu, S., Ming, A., Li, X., et al. (2019). Mixture of tree species enhances stability of the soil bacterial community through phylogenetic diversity. *Eur. J. Soil Sci.* 70, 644–654. doi: 10.1111/ejss.12780

Zhang, H. R., Li, S. W., Zhang, G. Y., and Fu, G. (2020). Response of soil microbial communities to warming and clipping in alpine meadows in northern Tibet. *Sustainability* 12:5617. doi: 10.3390/su12145617

Zhao, X. Q., and Zhou, X. M. (1999). Ecological basis of alpine meadow ecosystem management in Tibet: Haibei alpine meadow ecosystem Research Station. *Ambio* 28, 642–647.

Zhong, Z., and Fu, G. (2022). Response of soil fungal species, phylogenetic and functional diversity to diurnal asymmetric warming in an alpine agricultural ecosystem. *Agric. Ecosyst. Environ.* 335:107993. doi: 10.1016/j.agee.2022.107993

Zhou, J. Z., and Ning, D. L. (2017). Stochastic community assembly: does it matter in microbial ecology? *Microbiol. Mol. Biol. Rev.* 81:81. doi: 10.1128/MMBR.00002-17

Zong, N., and Fu, G. (2021). Variations in species and function diversity of soil fungal community along a desertification gradient in an alpine steppe. *Ecol. Indic.* 131:108197. doi: 10.1016/j.ecolind.2021.108197

frontiers | Frontiers in Ecology and Evolution

TYPE Original Research
PUBLISHED 13 December 2022
DOI 10.3389/fevo.2022.1071947

OPEN ACCESS

EDITED BY
Ben Niu,
Institute of Geographic Sciences and Natural Resources Research (CAS), China

REVIEWED BY
Jiang Peipei,
Shandong Normal University, China
Tao Zhang,
Shenyang Agricultural University, China

*CORRESPONDENCE
Xianwei Wang
wangxianwei@iga.ac.cn
Xiaoxin Sun
sunxiaoxin@nefu.edu.cn

SPECIALTY SECTION
This article was submitted to Population, Community, and Ecosystem Dynamics, a section of the journal Frontiers in Ecology and Evolution

RECEIVED 17 October 2022
ACCEPTED 24 November 2022
PUBLISHED 13 December 2022

CITATION
Wang S, Wang X, Sun X, Ma G, Du Y and Jiang J (2022) Stoichiometry and stable isotopes of plants and their response to environmental factors in boreal peatland, Northeast China.
Front. Ecol. Evol. 10:1071947.
doi: 10.3389/fevo.2022.1071947

Stoichiometry and stable isotopes of plants and their response to environmental factors in boreal peatland, Northeast China

Shujie Wang[1,2], Xianwei Wang[2]*, Xiaoxin Sun[1,3]*, Guobao Ma[1,2], Yu Du[2] and Jingyi Jiang[1,2]

[1]Key Laboratory of Sustainable Forest Ecosystem Management-Ministry of Education, School of Forestry, Northeast Forestry University, Harbin, China, [2]Key Laboratory of Wetland Ecology and Environment, Northeast Institute of Geography and Agroecology, Chinese Academy of Sciences, Changchun, China, [3]Heilongjiang Sanjiang Plain Wetland Ecosystem Research Station, Fuyuan, China

The alterations of plant composition and diversity pose a threat to the stability of the carbon pool in boreal peatland under climate change. We collected the samples of three plant functional types (deciduous shrubs, evergreen shrubs, and sedge) in seven permafrost peatlands of the Great Hing'an Mountains, China, and measured the properties of total carbon (TC), nitrogen (TN), and phosphorus (TP), their stoichiometric ratios (C:N, C:P, and N:P), and the stable isotope values ($\delta^{13}C$ and $\delta^{15}N$) of six tissues (ranging from leaves to roots). For TC, TN, and TP, the contents had an average of 470.69±1.56, 8.03±0.23, and 1.71±0.61mg·g^{-1}, respectively. TC contents of sedge were lower than those of shrubs for the whole plant. The allocations of N and P to shrub leaves were higher than to stems and roots. There was a similar trend of TN and TP contents, and stoichiometric ratios from leaves to roots between deciduous shrubs and evergreen shrubs. Shrubs and sedge have similar C: N in leaves and fine roots, while leaves of sedge C:P and N:P ratios were higher than shrubs, mainly showed that sedge is N and P co-limitation and shrubs are N limitation. The values of $\delta^{13}C$ and $\delta^{15}N$ were significantly higher in leaves and roots of sedge than those of shrubs, which means shrubs have higher nutrient acquisition strategies. These results support the shrubs are expanding in the boreal peatland under climate warming through nutrient competition. TC contents of all deciduous shrubs and sedge tissues were positively linear correlated to MAT and the values of $\delta^{13}C$ and $\delta^{15}N$ in sedge had significant relationships with MAT and MAP. Our results imply warming can increase plant photosynthesis in boreal peatland, and sedge was more sensitive to climate change. These findings would be helpful to understanding the responses of different plant tissues to climate changes in permafrost peatland.

KEYWORDS

boreal peatland, ecological stoichiometry, plant functional types, stable carbon isotopic, ^{15}N natural abundance

Introduction

The global peatland area only accounts for 3% of the land area (Yu et al., 2010), but with the highest carbon content among all terrestrial ecosystems (Dise, 2009). It was an important global carbon sink and played a key role in mitigating climate change (Gorham, 1991; Beaulne et al., 2021). Plants are an important part of peatland systems, which fix carbon through photosynthesis (Bubier et al., 1999). However, peatland plants have been great changes under climate change (Sun et al., 2010a; Bragazza et al., 2013). Some studies find that shrubs have been expanded in the peatland with warming (Meier and Bowman, 2008; Lyons et al., 2020), while other studies show that graminoids are more sensitive to climate change (Sun et al., 2010b, 2011). These different feedbacks are dependent on vegetation types and research scales (Gao et al., 2006). Nevertheless, more studies focus on aboveground plant dynamics, few studies investigate the changes in plants belowground under climate change (Lyons and Lindo, 2020; Malhotra et al., 2020).

Plant functional types (PFTs) in peatland, which are deciduous shrubs (DS), evergreen shrubs (ES), and sedge, have different carbon cycle pathways and nutrient acquisition strategies (Aerts et al., 2009). Plant stoichiometric characteristics can reflect the utilization of nutrients among different plant species (Liu and Hu, 2020). The higher C: N and C: P ratios can show the higher utilization efficiency of N and P by plants (Herbert et al., 2003; Xu et al., 2022); the lower C: N ratio can characterize that plants have a shorter life span (especially for roots Yu et al., 2022), higher growth rate (Gusewell and Koerselman, 2002; Liu and Hu, 2020), and a fast decomposition rate (Liu et al., 2022); the N:P ratio is closely related to nutrient availability, and can act as an indicator of types of nutrient limitation (Gusewell, 2004). However, it is still few studies that present stoichiometry extent ranging from leaves to roots in peatland PFTs. It is essential to understand the relationships between belowground changes and nutrient cycling.

The stable carbon and nitrogen isotopes in plant different tissues can provide information on plant response to present environmental conditions (Dawson et al., 2002). Climate warming and environmental change can influence the stable isotope abundance of plants. More ^{13}C could be consumed with increasing temperature (Smith et al., 1973; Welker et al., 2003; Rao et al., 2017) and humidity (Amesbury et al., 2015). On the one hand, higher temperature increases enzymatic activity in photosynthesis, thereby affecting carbon isotope fractionation (Farquhar et al., 1989). On the other hand, the opening of plant stomata in a humid environment results in increased stomatal conductance (Smith et al., 1973), leading to a decreased CO_2 concentration gradient between the inside and outside of plants (Su et al., 2000), which ultimately reduces $\delta^{13}C$. There was a study found that plant $\delta^{15}N$ values have been negatively correlated with temperature, which thought that lower temperature enhanced the viscosity of soil solution, leading to water stress of plants, thus increasing the $\delta^{15}N$ value of plants (Liu et al., 2018). There are some research indicates that carbon and nitrogen stable isotopes can also reflect limiting nutrients for plant growth (Piao et al., 2004; Clarkson et al., 2005) and the sources of nutrient elements to a certain extent (Welker et al., 2003; Hobbie et al., 2009). However, carbon and nitrogen isotopes just have been conducted in peatland plant leaves. The belowground biomass of plants was much higher than aboveground in boreal peatland (Wang et al., 2016). Therefore, the relative study of plant roots would be helpful to understand the responses of plants to climate change.

In this study, we collected samples of different plant tissues (i.e., leaves and roots of sedge, leaves, green stems, brown stems, fine roots, medium roots, and coarse roots of shrubs) in five species falling into three plant functional types, namely deciduous shrubs, evergreen shrubs, and sedge in seven typical permafrost peatlands, and analyzed the total carbon (TC), nitrogen (TN), and phosphorus (TP) contents, $\delta^{13}C$, and $\delta^{15}N$ values. This study aimed to clarify the different contents of TC, TN, and TP, and carbon and nitrogen isotopes among three PFTs and tissues (leaves, stems, and roots), and to explore the relationships between these plant properties and environmental factors. As mentioned above, a lower C: N ratio can be used as an indicator of a higher plant growth rate, so we hypothesized that the C: N ratio would be significantly negatively correlated with mean annual temperature (MAT). In addition, we hypothesized that the carbon and nitrogen isotopes of deciduous plants would be negatively correlated with MAT and mean annual precipitation (MAP).

Study area, materials, and methods

Study area and a description of plant species

The study area of the current study is in northern Great Hing'an Mountains, Northeast China (50°07′02″–53°33′42″N, 121°10′53″–127°01′21″E) and represents a typical permafrost peatland. This area has an average altitude, mean annual temperature, and mean annual precipitation of 573 m, −3°C, and 400 mm, respectively. The study area shows seasonal rainfall, with over 80% falling between June and August (Sun et al., 2011). Shrubs constitute the dominant vegetation type in the study area. Deciduous shrubs mainly include *Betula fruticosa*, *Vaccinium uliginosum*, and *Salix myrtilloides*. Evergreen shrubs include *Ledum palustre*, *Chamaedaphne calyculata*, and *Rhododendron lapponicum*. Sedges include *Carex globularis* and *Eriophorum vaginatum*, and forbs include *Saussurea amurensis* and *Polygonatum odoratum*. Bryophytes mainly include *Sphagnum palustre* and *Bryum argenteum*. Therefore, the peatland plant community in the study area consists of a shrub-sedge-moss structure, with an obvious and simple vertical structure.

Seven typical permafrost peatlands were examined in the present study (Figure 1; from north to south: Beijicun (BJC), Tuqiang (TQ), Amuer (AME), Pangu (PG), Tahe (TH), Huzhong (HZ), and Xinlin (XL)). A handheld global positioning system

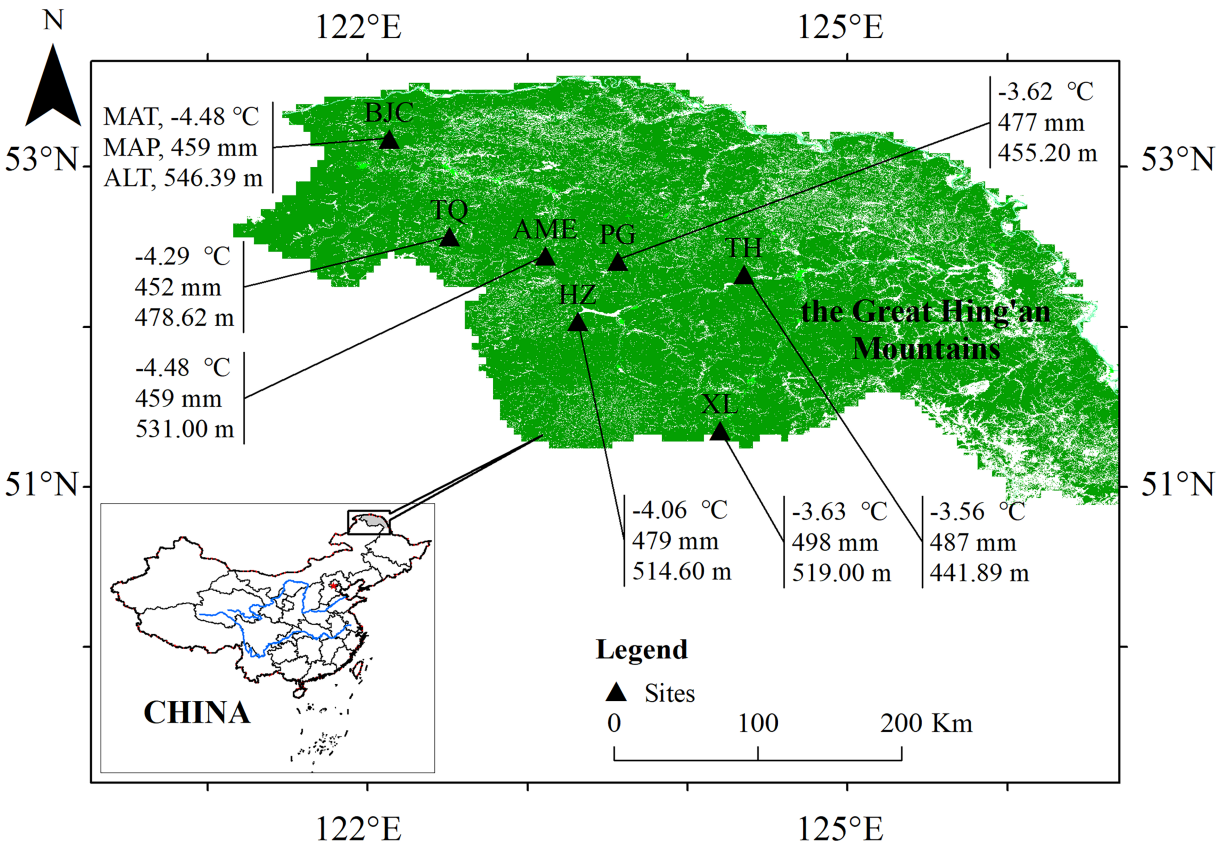

FIGURE 1
Seven typical boreal peatland sites in the study area of the present study. MAT, mean annual temperature; MAP, mean annual precipitation; ALT, altitude. Sites: BJC, Beijicun; TQ, Tuqiang; AME, Amuer; PG, Pangu; TH, Tahe; HZ, Huzhong; XL, Xinlin. The same below.

(GPS) was used to record the longitude, latitude, and altitude of each site. This study collected samples from common dominant plant species (i.e., *C. globularis*, *B. fruticosa*, *V. uliginosum*, *L. palustre*, and *C. calyculata*) in these sites.

Sampling and chemical analyses

During the sampling of sedge tissues, leaves and roots samples were collected, with three replicates of each sample taken from 1 × 1 m plots and 21 plots in total. During the sampling of shrub tissues, samples of leaves, green stems, brown stems, fine roots (0–2 mm), medium roots (2–5 mm), and coarse roots (>5 mm) were collected in triplicate in the above 21 plots. Each final sample was expressed as the mean of the three replicates ± standard error (SE). Leaf and stem samples were placed into kraft paper bags, marked, and dried in an oven at 65°C to a constant weight. Impurities (roots of other plants and peat soil) were removed from roots samples, after which the samples were placed in bags and dried. A ball mill was used to fully crush plant samples to be tested. The present study implemented a dispersed sampling regime to avoid as far as possible plants affected by pests and diseases.

Properties of C, N, and P

The total carbon (TC) content of plants was determined by the combustion method. Here, glucose (400 mg $C \cdot g^{-1}$) was used as the standard, 15 ± 2 mg of each plant to be tested was extracted, and a total organic carbon analyzer (TOC-Lcph SSM-5000A, Shimadzu, Japan) was used to determine the TC content.

A continuous flow analyzer (Seal AA3, Seal, Germany) was used to determine total nitrogen (TN) and total phosphorus (TP) contents. A 100 mg subsample of each plant to be analyzed was placed into a 50-mL digestion tube, three blank controls were set, and a catalyst was added along with 98% concentrated sulfuric acid. After 8 hours, the solution was boiled until achieving transparency and then allowed to cool to room temperature. Deionized water was then added to the sample to a volume of 50 ml to form the sample solution to be tested. From the sample solution to be tested, 2 ml was extracted and diluted five times using deionized water. Ammonium sulfate solution was then used as a standard to determine the sample N content. A sub-sample of the sample solution to be tested was mixed with 7.2 M sodium hydroxide at a ratio of 3:1, following which potassium dihydrogen

phosphate solution was used as the standard to determine the content of P.

Stable isotopes of ^{13}C and ^{15}N

A 100 mg subsample of the sample to be tested was extracted for the measurement of ^{13}C: ^{12}C and ^{15}N: ^{14}N ratios of CO_2 and N_2 using an elemental analyzer gas stable isotope mass spectrometer (EA-IRMS, Thermo Fisher; Farquhar et al., 1989). Isotope ratios were converted to "δ" unit: $\delta\ (‰) = [(R_{sample} / R_{standard}) - 1] \times 1{,}000$, where R_{sample} and $R_{standard}$ are the ^{13}C: ^{12}C or ^{15}N: ^{14}N molar abundance ratios of the sample and standard (PDB or atmospheric; Farquhar et al., 1982; Spasojevic and Weber, 2021).

Data analysis

One way analysis of variance (ANOVA) was used to test the differences in plant properties, stoichiometric ratios, and $\delta^{13}C$ and $\delta^{15}N$ among sites, PFTs, and tissues of plants. Pearson correlation analysis was used to analyze the correlation between C, N, and P contents, $\delta^{13}C$ and $\delta^{15}N$, and environmental factors. The MAT and MAP data for each site were downloaded from the National Meteorological Science Data Center[1]. Dataanalysis and mapping tools used in the present study included ArcGIS 10.2, Excel 2010, Origin 2022, and SPSS 28.0.

All data at each site were expressed as the mean ± SE when analyzing the differences among sites, whereas the mean ± SE of all data of each category in each site was used when analyzing the differences among PFTs or tissues. Leaves and roots of sedge correspond to leaves and fine roots of shrubs, respectively, when the results were analyzed.

Results

Stoichiometry, $\delta^{13}C$ and $\delta^{15}N$ among all sites

The TC of boreal peatland plants in the Great Hing'an Mountains ranged from 381.28 to 547.40 $mg \cdot g^{-1}$, with an average of 470.69 ± 1.56 $mg \cdot g^{-1}$; TN ranged from 1.12 to 30.15 $mg \cdot g^{-1}$, with an average of 8.03 ± 0.23 $mg \cdot g^{-1}$; TP ranged from 0.36 to 12.98 $mg \cdot g^{-1}$, with an average of 1.71 ± 0.61 $mg \cdot g^{-1}$; C: N ranged from 16.49 to 382.57, with an average of 79.41 ± 1.92; C: P ranged from 39.37 to 1323.04, with an average of 388.89 ± 9.84; N: P ranged from 0.56 to 33.82, with an average of 5.89 ± 0.17; the $\delta^{13}C$ value ranged from −31.62 to −25.19‰, with an average of −29.16 ± 0.05‰, and the $\delta^{15}N$ value ranged from −7.66 to 2.83‰, with an average of −4.39 ± 0.08‰.

There were differences in plant properties, stoichiometric ratios, and isotope values among the different permafrost peatlands (Table 1). The TC and TN contents of plants in XL and TH sites exceeded those of other sites, whereas plants in XL and BJC sites had the highest TP content. The highest C:N ratio was found in TQ, whereas the highest C:P and N:P ratios were found in plants in PG and TH. The highest $\delta^{13}C$ value was found in BJC, whereas the $\delta^{15}N$ value in TH was significantly higher than those of other sites ($p < 0.05$).

Plant properties and stoichiometric ratios among PFTs

Sedge showed the smallest TC content both in leaves and roots ($p < 0.05$; Figure 2A), its TN content in leaves was significantly lower than that of DS ($p < 0.05$), and similar to that of ES (Figure 2B). The TP content of sedge was significantly lower than that of shrubs in leaves ($p < 0.05$), but slightly higher than that of shrubs in roots (Figure 2C). The C:P and N:P ratios of sedge were significantly higher than that of shrubs in leaves ($p < 0.05$), but lower in roots (Figures 2E,F).

There was a similar change trend of different functional shrubs in properties and stoichiometric ratios among leaves, stems, and roots, but there were differences in quantity (Figure 2). The TC, TN, and TP contents and N: P ratio decreased from leaves to roots, except fine roots (Figures 2A–C,F). On the contrary, the C: N and C: P ratios of shrubs increased from leaves to roots, but appeared low values at fine roots, obviously (Figures 2D,E). In addition, the TC content of ES was significantly higher than that of DS, especially in leaves, except for green stems and fine roots ($p > 0.05$; Figure 2A). The TN content of DS was higher than that of ES from the whole plant ($p < 0.05$; Figure 2B). The C: N ratio of DS was lower than that of ES ($p < 0.05$), and the difference was larger at the roots (Figure 2D), indicating that deciduous shrubs had faster root growth. ES had a higher C: P ratio than DS in medium and coarse roots ($p < 0.05$; Figure 2E), while had a lower N: P ratio in green stems, brown stems, and fine roots ($p < 0.05$; Figure 2F).

$\delta^{13}C$ and $\delta^{15}N$ among PFTs

There were differences in $\delta^{13}C$ and $\delta^{15}N$ among different PFTs, especially the values of sedge were significantly higher than those of shrubs ($p < 0.05$; Figure 3).

The $\delta^{13}C$ value of ES was lower than that of DS, except for coarse roots (Figure 3A). For sedge, the $\delta^{15}N$ values in leaves were significantly higher than those of roots ($p < 0.05$), while the values of shrubs gradually increased from leaves to roots, with the largest value in fine roots (Figure 3B). The $\delta^{15}N$ value of DS was higher than ES, but it decreased from fine roots to coarse roots, and the values were lower than that of ES in coarse roots eventually (Figure 3B).

1 http://www.nmic.cn/

TABLE 1 Mean properties, stoichiometric ratios, and isotope values of plants at each site.

Sites	TC/mg·g^{-1}	TN/mg·g^{-1}	TP/mg·g^{-1}	C:N ratio	C:P ratio	N:P ratio	δ^{13}C/‰	δ^{15}N/‰
BJC	455.14 ± 4.65d	7.47 ± 0.55abc	2.20 ± 0.20ab	75.58 ± 4.67bc	293.16 ± 21.52c	4.30 ± 0.33c	−28.62 ± 0.15a	−4.67 ± 0.22b
TQ	456.17 ± 4.39d	6.62 ± 0.48c	1.84 ± 0.14bc	94.01 ± 5.52a	360.75 ± 25.19bc	4.69 ± 0.37bc	−29.35 ± 0.12c	−4.46 ± 0.17b
AME	457.67 ± 3.71d	8.04 ± 0.53abc	1.64 ± 0.10c	79.03 ± 6.03bc	365.36 ± 24.29b	5.63 ± 0.34b	−28.96 ± 0.13ab	−4.50 ± 0.18b
PG	478.78 ± 2.89bc	8.64 ± 0.58ab	1.17 ± 0.08d	74.01 ± 4.75bc	496.80 ± 22.83a	8.42 ± 0.65a	−29.52 ± 0.16c	−4.54 ± 0.21b
TH	487.77 ± 2.67ab	9.25 ± 0.79a	1.15 ± 0.43d	69.90 ± 4.27c	488.14 ± 27.53a	7.77 ± 0.37a	−29.39 ± 0.12c	−3.12 ± 0.24a
HZ	468.79 ± 3.87c	7.02 ± 0.52bc	1.57 ± 0.08 cd	85.37 ± 4.76ab	341.13 ± 16.98bc	4.73 ± 0.36bc	−28.89 ± 0.16ab	−4.75 ± 0.29b
XL	491.57 ± 3.53a	9.19 ± 0.77a	2.32 ± 0.27a	74.36 ± 4.01bc	370.23 ± 29.56b	5.56 ± 0.35b	−29.23 ± 0.11bc	−4.39 ± 0.21b
Mean	470.69 ± 1.56	8.03 ± 0.23	1.71 ± 0.61	79.41 ± 1.92	388.89 ± 9.84	5.89 ± 0.17	−29.16 ± 0.05	−4.39 ± 0.08

Mean, mean value of each site. Different letters indicate significant differences between the same column, $p < 0.05$. Data displayed in the table are mean value ± standard error (SE) of all data (including leaves, stems, and roots) in each site.

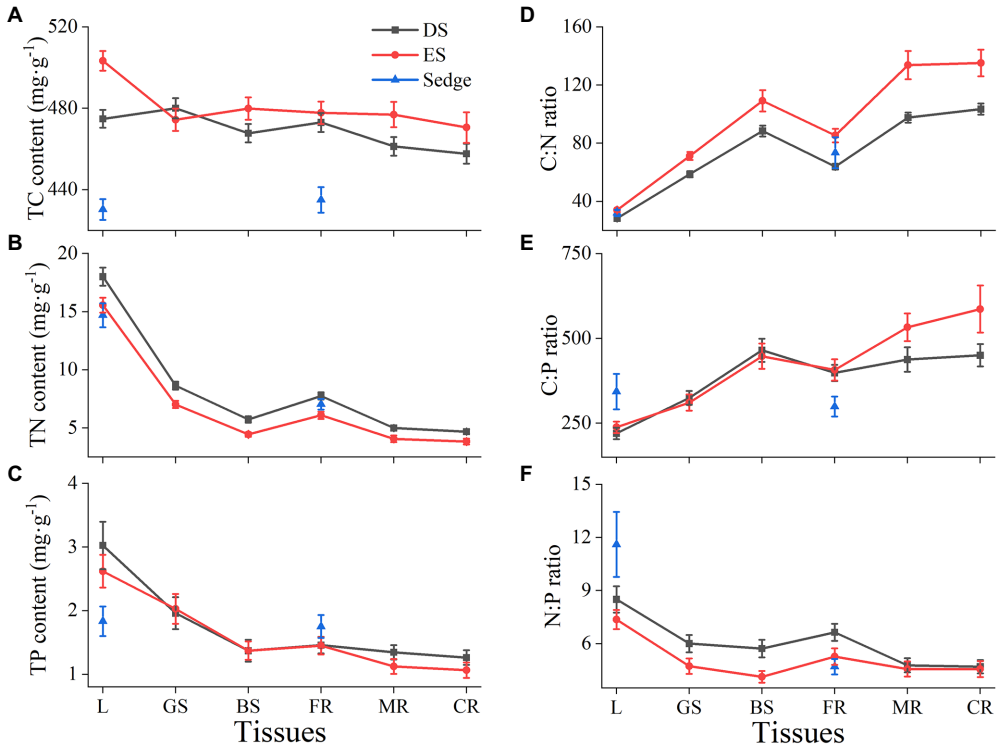

FIGURE 2
The TC **(A)**, TN **(B)**, and TP **(C)** content, C:N **(D)**, C: P **(E)** and N: P **(F)** ratios among different plant functional types (PFTs) and tissues. Ds, deciduous shrubs; Es, evergreen shrubs; L, leaves; GS, green stems; BS, brown stems; FR, fine roots (0–2mm); MR, medium roots (2–5mm); CR, coarse roots (> 5mm). Data shown are the mean value ± standard error (SE) of all same tissues within PFTs. The same below.

Relationships between values of properties, stoichiometric ratios, and isotopes and environmental factors

The TC contents from the whole plants of DS and sedge were significantly positively correlated with MAT ($p < 0.01$), but these contents of leaves, green stems, and coarse roots were significantly positively correlated with MAT in ES ($p < 0.05$; Supplementary Table S1). The TN contents of leaves, fine roots, and medium roots in DS, brown stems and fine roots in ES, and leaves in sedge were significantly positively correlated with MAT ($p < 0.05$). There were negative correlations between TP contents of fine roots in DS and roots in sedge and MAT ($p < 0.05$). The MAP also has an effect on the plant properties (Supplementary Table S2), especially the TC content of DS was significantly positively correlated with MAP ($p < 0.05$).

There were no significant relationships between MAT and MAP and δ^{13}C values of all tissues for DS ($p > 0.05$). The δ^{13}C values of leaves, green stems, and fine roots in ES were significantly more negative with increasing MAT ($p < 0.05$; Figure 4). There were significant correlations between the δ^{13}C values in leaves of sedge and MAT, but not in roots ($p < 0.05$; Figures 4A,C). δ^{15}N

values of leaves and roots in sedge, green stems and brown stems in deciduous shrubs were significantly positively correlated with MAT ($p < 0.05$; Figures 5A-D). $\delta^{13}C$ values of leaves in sedge and medium roots in evergreen shrubs were significantly negatively correlated with MAP ($p < 0.05$; Figures 6A,B). $\delta^{15}N$ values of leaves and roots in sedge, green stems and brown stems in deciduous shrubs were significantly positively correlated with MAP ($p < 0.05$; Figures 6C-F).

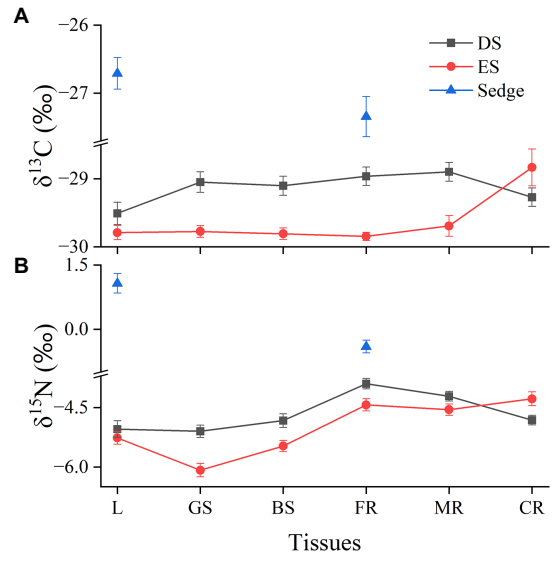

FIGURE 3
$\delta^{13}C$ **(A)** and $\delta^{15}N$ **(B)** values among different plant functional types (PFTs) and tissues.

Discussion

Properties and stoichiometric ratios in peatland plants

In this study, the TC contents of sedge tissues were lower than those of shrubs. A similar result was found in the ombrotrophic peatland of Switzerland (Gavazov et al., 2016). Shrubs have more lignin, which may result in higher TC content than sedge (Kastovska et al., 2018; Yu et al., 2022). All tissues of deciduous shrubs showed higher TN content and lower C: N ratio than evergreen shrubs, which means that deciduous shrubs have high resource acquisition strategies and growth rates (Liu and Hu, 2020), especially for the roots. TP content was not changed greatly for whole plants between deciduous and evergreen shrubs, but the C:P ratio of evergreen shrubs was significantly higher than that of deciduous shrubs in the medium and coarse roots. This was also confirmed that deciduous roots grow faster. In our study, the TN,

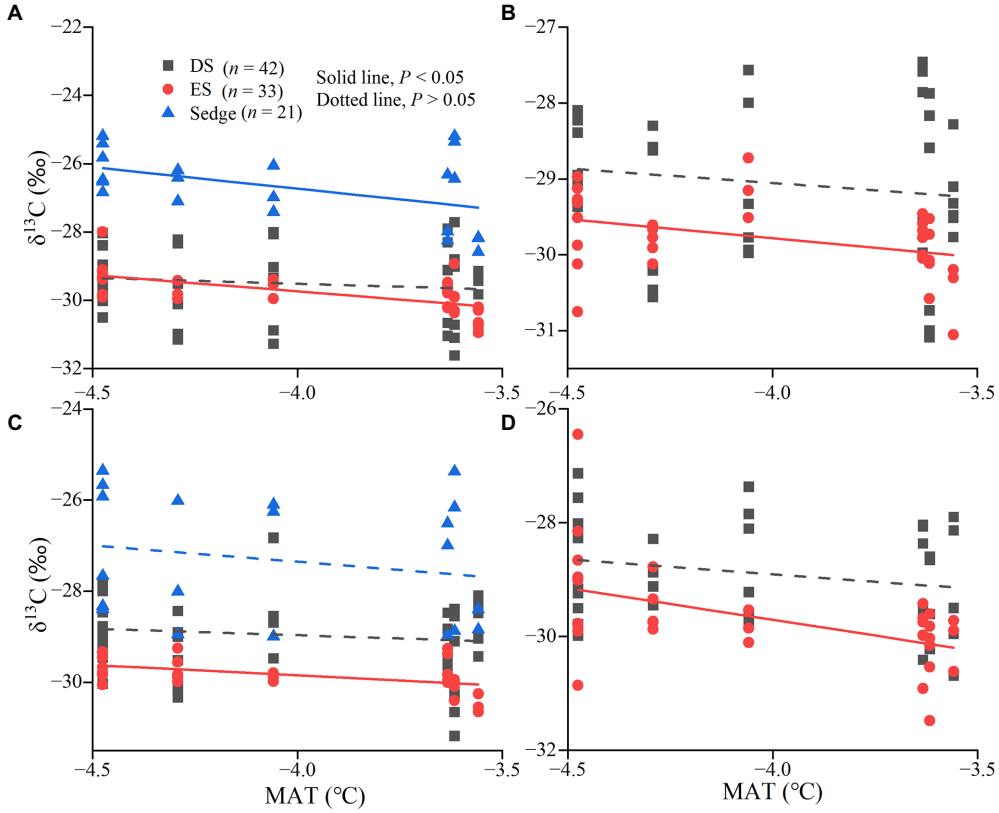

FIGURE 4
Linear fitting between $\delta^{13}C$ values and mean annual temperature (MAT). The relationship between $\delta^{13}C$ values of leaves **(A)**, green stems **(B)**, fine roots **(C)**, and medium roots **(D)** and MAT.

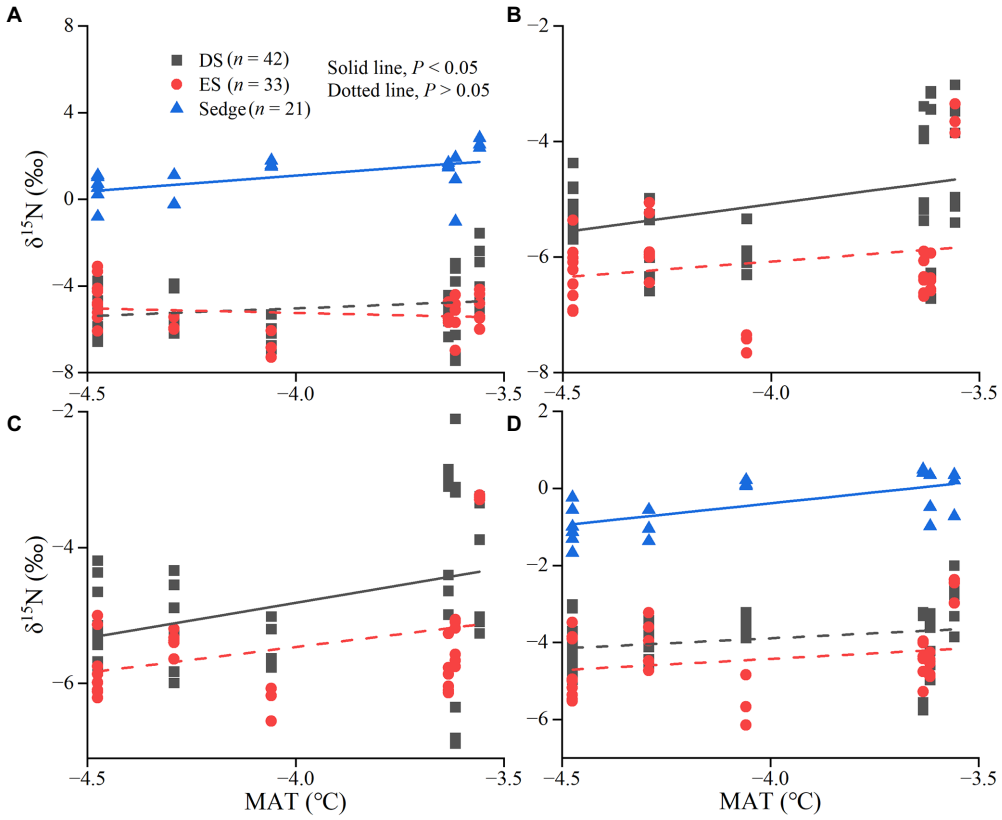

FIGURE 5
Linear fitting between $\delta^{15}N$ value and mean annual temperature (MAT). The relationship between $\delta^{15}N$ values of leaves **(A)**, green stems **(B)**, brown stems **(C)**, and fine roots **(D)** and MAT.

and TP contents decreased from leaves to roots, except for fine roots. It means that the fine roots have a high metabolic rate, which needs higher N and P to maintain normal physiological activities (Yu et al., 2022). Fine roots are the main tissues that absorb mineral nutrients from soil, so the TN and TP contents are higher than those of coarse roots (Nadelhoffer, 2000; Xu et al., 2012; Yu et al., 2022). Fine roots absorb nutrients from soil, then most nutrients are transported to aboveground tissues and accumulated in the stems and leaves (Piao et al., 2004; Wang and Moore, 2014). This causes higher TN and TP contents in leaves.

The plant TN contents of the study area were lower than those of plants in forest peatlands of the Great Hing'an Mountains (Liu and Hu, 2020), in marsh of Sanjiang Plain (Lou et al., 2012), and in wetlands of Europe (Gusewell and Koerselman, 2002). Nitrogen was in general the nutrient limiting the growth of peat plants in permafrost of the Great Hing'an Mountains (Liu et al., 2022), as shown by the plant stoichiometric ratios of peatlands in Canada (Wang and Moore, 2014). It is generally believed that an N: P ratio < 10 or > 20 represents N or P limitation respectively, whereas a ratio of between 10 and 20 represents co-limitation of N and P (Gusewell, 2004). Our study showed a mean N: P ratio for all plants and tissues was 5.86 (<10), representing a strong N limitation. Furthermore, the N: P ratio in leaves of sedge (11.61 ± 1.83) was much higher than that of deciduous and evergreen shrubs (8.50 ± 0.74 and 7.36 ± 0.55, respectively), indicating that the growth of sedge was limited by N and P, while shrubs were limited by N. Shrubs have been expended in boreal peatland under climate warming and permafrost degradation by increasing N availability (Bragazza et al., 2013; Lyons et al., 2020; McCabe, 2020; Song et al., 2021). Only N limitation of shrubs could be one of the reasons that climate change promotes shrub growth, while sedges would continue to be limited by P.

$\delta^{13}C$ And $\delta^{15}N$ in peatland plants

There was little difference in $\delta^{13}C$ values among tissues but varies greatly among different PFTs in our study. The $\delta^{13}C$ values of leaves and roots were the highest in sedge ($p < 0.05$), which might be due to the low content of lignin and lipid (Hobbie and Werner, 2004). The $\delta^{13}C$ values of all shrubs tissues were lower than those of sedge tissues, especially for roots, which indicated that shrubs had higher internal water use efficiency and lower stomatal conductance (Brooks et al., 1997). In addition, the high nutrient contents in plants could also improve the photosynthetic capacity of plants (Li and Huang, 2009), thus making the $\delta^{13}C$ value more negative. Those indicated that the nutrient flow in shrubs was faster, and could also support that shrubs in peatlands

have higher nutrient acquisition strategies (Li, 2015). Furthermore, variations in the carbon isotope composition of CO_2 available for photosynthesis may have an impact on this disparity between species (Galimov, 2000). Some studies have found that differences in growth morphology among species, such as plant stature and canopy density of vegetation, will cause changes in $\delta^{13}C$ value (Brooks et al., 1997; Amesbury et al., 2015). We found that C: N ratios were negatively correlated with $\delta^{13}C$ in deciduous leaves ($p < 0.01$; Supplementary Table S3), which may be explained by the hardly decomposable compounds (cellulose, etc.) in shrubs (Werth and Kuzyakov, 2010). There was also a significant positive correlation between $\delta^{13}C$ and TN of deciduous leaves (Supplementary Table S3), which may be partly related to the photosynthetic process (Welker et al., 2003; Moore and Bubier, 2020).

In our study, the $\delta^{15}N$ values of sedge were significantly higher than those of shrubs ($p < 0.05$). The sedge has long roots which could absorb stable organic nitrogen (Makarov et al., 2014; Feng et al., 2016) or inorganic nitrogen in deep soil (Hobbie and Hobbie, 2006). This led to higher $\delta^{15}N$ values for the whole plant in sedge. Furthermore, it may be that sedges use ammonium salts in a larger proportion than nitrate, which will also cause a slight enrichment of plant $\delta^{15}N$ values (Welker et al., 2003). Shrub in peatland is the mycorrhizal plant. ^{15}N could be consumed by mycorrhizal fungi during plant nitrogen transport and depleted by mycorrhizal fungi, resulting in lower ^{15}N in the shrubs (Michelsen et al., 1998; Asada et al., 2005; Clarkson et al., 2005). Our results showed that $\delta^{15}N$ values of fine roots were higher than the other tissues for shrubs. Mycelium is surrounded in the tips of fine roots with rich ^{15}N (Michelsen et al., 1998; Welker et al., 2003), which leads to high $\delta^{15}N$ values in the roots (especially in fine roots) of shrubs. In deciduous brown stems, the $\delta^{15}N$ was positively correlated with TN ($p < 0.01$), but negatively correlated with C: N ratio ($p < 0.01$; Supplementary Table S4). Skrzypek et al. (2008) showed a similar result, indicating that $\delta^{15}N$ reflects the isotopic composition of nitrate assimilated from water. Gavazov et al. (2016) reported that the content of exchangeable nitrogen in soil can affect $\delta^{15}N$ abundance. Future studies should combine soil properties and PFTs.

In brief, different PFTs and tissues had different ways of obtaining and using nutrients. For both $\delta^{13}C$ and $\delta^{15}N$ values, there was a clear change in the trend at the coarse roots (Figure 3), which may be due to root depth (Nadelhoffer et al., 1996; Kohzu et al., 2003) or other reasons. The belowground studies are still limited in peatland and relative studies would be helpful to assess the N cycling and C dynamics in boreal peatlands.

Response to the environment

Our study indicated that all tissues of deciduous shrubs and sedge showed positive linear correlations between TC contents and MAT ($p < 0.01$), whereas the TC contents of leaves, green stems, and coarse roots in evergreen shrubs were significantly positively correlated with MAT ($p < 0.05$). This means that warming can increase plant photosynthesis, thereby promoting plant growth (Wu et al., 2019; Zhang et al., 2019), especially for deciduous plants. In addition, we found that the TN content and N:P ratios of deciduous shrubs and sedge were more positively correlated with MAT than evergreen shrubs. This indicated that deciduous plants might become the dominant species of the community, fundamentally altering the peatland ecosystem function (Moore and Bubier, 2020), and even affecting the carbon pool balance of peatland. There was a negative correlation between C: N ratio and temperature in a warming experiment (Liu et al., 2022). But in our study, with the increase in temperature, the C:N ratio has a downward trend but has not reached a significant level, which was different from our first hypothesis. The plant growth in peatlands would be more complex under climate warming. The TC contents of all tissues in deciduous plants were also positively correlated with MAP ($p < 0.01$). While other properties and stoichiometric ratios did not respond as sensitively to MAP, it means precipitation mainly influenced the plant C fixation in the peatlands.

The $\delta^{13}C$ of leaves and green stems in evergreen shrubs, and leaves in sedge showed a negative correlation with MAT in our study. One direct explanation for this observation was that plants close their stoma to avoid excessive evaporation due to a temperature rise, resulting in a decrease in $\delta^{13}C$ (Rao et al., 2017). Another explanation was that temperature indirectly affects $\delta^{13}C$ by using N (Welker et al., 2003). Previous studies had shown that the melting of permafrost would release a large amount of available nitrogen for plants and increased the nutrient circulation rate (Keuper et al., 2012). These changes could influence stomatal density and leaf thickness, thereby reducing ^{13}C of plant tissue (Piao et al., 2004). Rao et al. (2017) showed that more negative ^{13}C values occurred in wetter environments, whereas some studies believed that there was no correlation between ^{13}C and humidity (Skrzypek et al., 2007; Amesbury et al., 2015). The latter point was similar to our study, there was no significant correlation between $\delta^{13}C$ of leaves in shrubs and MAP. It is probably because the permafrost peatland may have sufficient water conditions and shrubs have higher absorption capacity. MAP did not significantly influence the $\delta^{13}C$ of aboveground tissues in shrubs.

Most previous studies focused on the influence of mycorrhizal types on $\delta^{15}N$ values (Michelsen et al., 1998; Clarkson et al., 2005; Moore and Bubier, 2020), but only a few studies had shown the relationship between $\delta^{15}N$ values and environmental factors. We found that $\delta^{15}N$ of deciduous stems and sedge were significantly positively correlated with MAT, which was contrary to our second hypothesis. The activity of nitrifying bacteria increased with warming (Kang et al., 2011), and the higher temperature increased the net nitrification potential of soil or increased the soil nitrogen cycle, and finally lead to ^{15}N enrichment in plants (Liu et al., 2007). In our study, the $\delta^{15}N$ value of leaves and roots in sedge was positively correlated with MAP. Fewer ammonium ions (NH_4^+) will be created in humid soil, and more dissolved organic nitrogen will be absorbed by the action of ectomycorrhiza, promoting ^{15}N enrichment in plants (Kang et al., 2011).

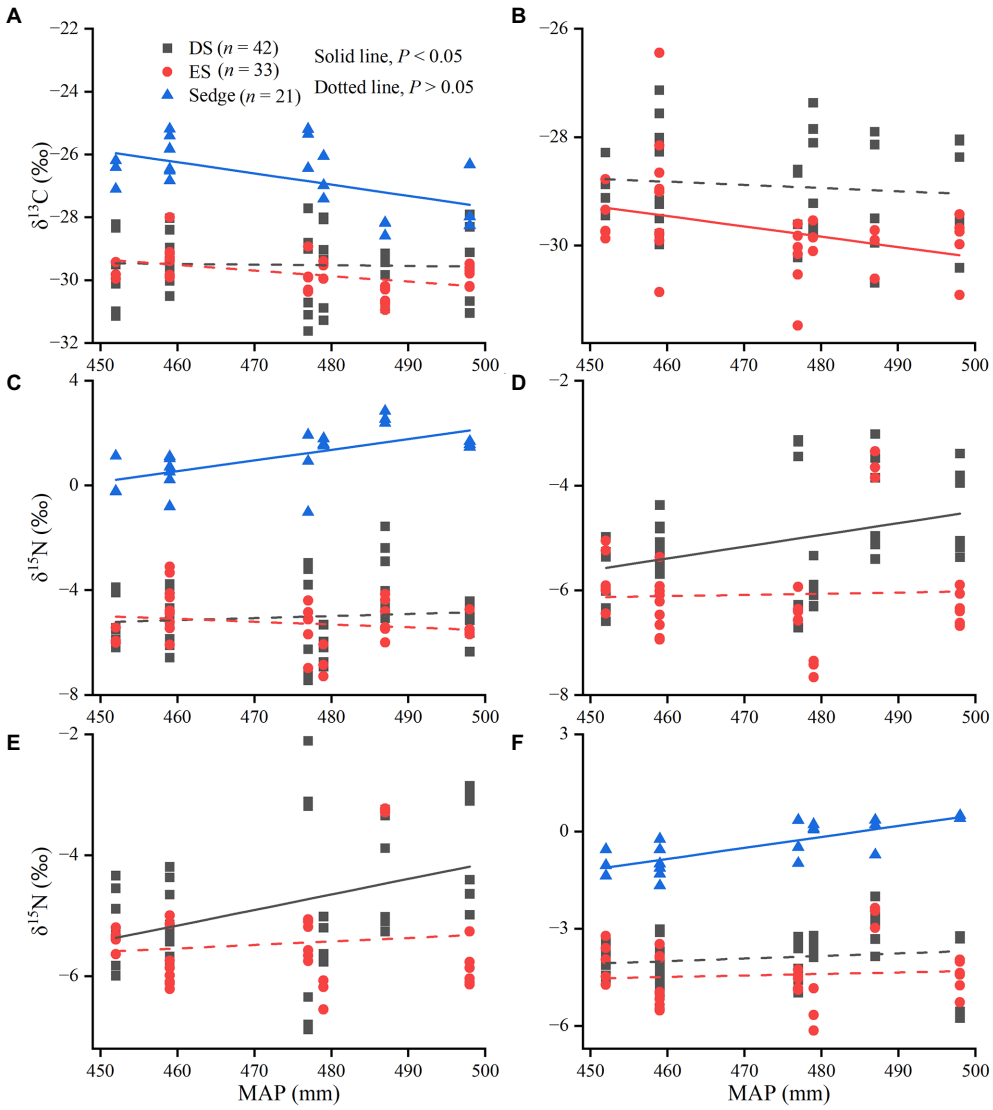

FIGURE 6
Linear fitting between $\delta^{13}C$ and $\delta^{15}N$ values and mean annual precipitation (MAP). The relationship between $\delta^{13}C$ values of leaves **(A)** and medium roots **(B)**, $\delta^{15}C$ values of leaves **(C)**, green stems **(D)**, brown stems **(E)**, and fine roots **(F)** and MAP.

Conclusion

Climate warming has changed plant distribution and community structure, which will threaten the carbon pool balance of boreal peatland. We explore the nutrient utilization of different plant functional types and allocation among different tissues (ranging from leaves to roots), and reveal the adaptive survival strategies of different functional plants in boreal peatland to the environment comprehensively. Compared with sedge, shrubs have higher TC contents, and shrubs have a large allocation of nutrients to leaves. Deciduous shrubs have high resource acquisition strategies and growth rates than evergreen shrubs, especially in roots. The growth of sedge is limited by N and P whereas shrubs are limited by N. And shrubs have been proven to have a higher nutrient acquisition strategy in our study, which also explains the shrub expansion of boreal peatland. The rising temperature can increase plant photosynthesis in boreal peatland, and sedge is more responsive to climate change. To better understand the effects of climate change on the carbon pool of boreal peatland, however, future research still needs to incorporate plant properties with litter, soil, and even surface water research.

Data availability statement

The original contributions presented in the study are included in the article/Supplementary material, further inquiries can be directed to the corresponding authors.

Author contributions

SW: writing-original draft preparation. XW and XS: funding acquisition. XW: conceptualization. XS: methodology. GM and YD: investigation. JJ: data curation. All authors contributed to the article and approved the submitted version.

Funding

The work was supported by National Natural Science Foundation of China No. 41971143 and 42271111, and National Science & Technology Fundamental Resources Investigation Program of China No. 2019FY100600.

Acknowledgments

We wish to acknowledge Zhenling Gao for the field work and Jinli Gao for the laboratory analyses.

Conflict of interest

The authors declare that the research was conducted in the absence of any commercial or financial relationships that could be construed as a potential conflict of interest.

The AE BN declared a shared affiliation with the authors XW, NC, and YD at the time of review.

Publisher's note

All claims expressed in this article are solely those of the authors and do not necessarily represent those of their affiliated organizations, or those of the publisher, the editors and the reviewers. Any product that may be evaluated in this article, or claim that may be made by its manufacturer, is not guaranteed or endorsed by the publisher.

Supplementary material

The Supplementary material for this article can be found online at: https://www.frontiersin.org/articles/10.3389/fevo.2022.1071947/full#supplementary-material

References

Aerts, R., Callaghan, T. V., Dorrepaal, E., van Logtestijn, R. S. P., and Cornelissen, J. H. C. (2009). Seasonal climate manipulations result in species-specific changes in leaf nutrient levels and isotopic composition in a sub-arctic bog. *Funct. Ecol.* 23, 680–688. doi: 10.1111/j.1365-2435.2009.01566.x

Amesbury, M. J., Charman, D. J., Newnham, R. M., Loader, N. J., Goodrich, J. P., Royles, J., et al. (2015). Carbon stable isotopes as a palaeoclimate proxy in vascular plant dominated peatlands. *Geochim. Cosmochim. Acta* 164, 161–174. doi: 10.1016/j.gca.2015.05.011

Asada, T., Warner, B. G., and Aravena, R. (2005). Nitrogen isotope signature variability in plant species from open peatland. *Aquat. Bot.* 82, 297–307. doi: 10.1016/j.aquabot.2005.05.005

Beaulne, J., Garneau, M., Magnan, G., and Boucher, E. (2021). Peat deposits store more carbon than trees in forested peatlands of the boreal biome. *Sci. Rep.* 11:2657. doi: 10.1038/s41598-021-82004-x

Bragazza, L., Parisod, J., Buttler, A., and Bardgett, R. D. (2013). Biogeochemical plant-soil microbe feedback in response to climate warming in peatlands. *Nat. Clim. Chang.* 3, 273–277. doi: 10.1038/nclimate1781

Brooks, J. R., Flanagan, L. B., Buchmann, N., and Ehleringer, J. R. (1997). Carbon isotope composition of boreal plants: functional grouping of life forms. *Oecologia* 110, 301–311. doi: 10.1007/s004420050163

Bubier, J. L., Frolking, S., Crill, P. M., and Linder, E. (1999). Net ecosystem productivity and its uncertainty in a diverse boreal peatland. *J. Geophys. Res.-Atmos.* 104, 27683–27692. doi: 10.1029/1999jd900219

Clarkson, B. R., Schipper, L. A., Moyersoen, B., and Silvester, W. B. (2005). Foliar N-15 natural abundance indicates phosphorus limitation of bog species. *Oecologia* 144, 550–557. doi: 10.1007/s00442-005-0033-4

Dawson, T. E., Mambelli, S., Plamboeck, A. H., Templer, P. H., and Tu, K. P. (2002). Stable isotopes in plant ecology. *Annu. Rev. Ecol. Syst.* 33, 507–559. doi: 10.1146/annurev.ecolsys.33.020602.095451

Dise, N. B. (2009). Peatland response to global change. *Science* 326, 810–811. doi: 10.1126/science.1174268

Farquhar, G. D., Ehleringer, J. R., and Hubick, K. T. (1989). Carbon isotope discrimination and photosynthesis. *Annu. Rev. Plant Physiol. Plant Mol. Biol.* 40, 503–537. doi: 10.1146/annurev.pp.40.060189.002443

Farquhar, G. D., Oleary, M. H., and Berry, J. A. (1982). On the relationship between carbon isotope discrimination and the inter-cellular carbon-dioxide concentration in leaves. *Aust. J. Plant Physiol.* 9, 121–137. doi: 10.1071/pp9820121

Feng, W., Xu, L., Wang, X., Li, H., and Jiang, J. (2016). Response of *Carex cinerascens* populations to groundwater level gradients in the Poyang Lake wetland. *Acta Ecol. Sin.* 36, 5109–5115. doi: 10.5846/stxb201501220180

Galimov, E. M. (2000). Carbon isotope composition of Antarctic plants. *Geochim. Cosmochim. Acta* 64, 1737–1739. doi: 10.1016/s0016-7037(99)00328-2

Gao, J., Ma, K., and Feng, Z. (2006). Effects of landscape composition, structure and gradient pattern on plant diversity. *Chin. J. Ecol.* 25, 1087–1094. doi: 10.1016/S1872-2032(06)60052-8

Gavazov, K., Hagedorn, F., Buttler, A., Siegwolf, R., and Bragazza, L. (2016). Environmental drivers of carbon and nitrogen isotopic signatures in peatland vascular plants along an altitude gradient. *Oecologia* 180, 257–264. doi: 10.1007/s00442-015-3458-4

Gorham, E. (1991). Northern peatlands-role in the carbon-cycle and probable responses to climatic warming. *Ecol. Appl.* 1, 182–195. doi: 10.2307/1941811

Gusewell, S. (2004). N: P ratios in terrestrial plants: variation and functional significance. *New Phytol.* 164, 243–266. doi: 10.1111/j.1469-8137.2004.01192.x

Gusewell, S., and Koerselman, M. (2002). Variation in nitrogen and phosphorus concentrations of wetland plants. *Perspect. Plant Ecol. Evol. Syst.* 5, 37–61. doi: 10.1078/1433-8319-0000022

Herbert, D. A., Williams, M., and Rastetter, E. B. (2003). A model analysis of N and P limitation on carbon accumulation in Amazonian secondary forest after alternate land-use abandonment. *Biogeochemistry* 65, 121–150. doi: 10.1023/a:1026020210887

Hobbie, J. E., and Hobbie, E. A. (2006). N-15 in symbiotic fungi and plants estimates nitrogen and carbon flux rates in Arctic tundra. *Ecology* 87, 816–822. doi: 10.1890/0012-9658(2006)87[816,Nisfap]2.0.Co;2

Hobbie, J. E., Hobbie, E. A., Drossman, H., Conte, M., Weber, J. C., Shamhart, J., et al. (2009). Mycorrhizal fungi supply nitrogen to host plants in Arctic tundra and boreal forests: N-15 is the key signal. *Can. J. Microbiol.* 55, 84–94. doi: 10.1139/w08-127

Hobbie, E. A., and Werner, R. A. (2004). Intramolecular, compound-specific, and bulk carbon isotope patterns in C-3 and C-4 plants: a review and synthesis. *New Phytol.* 161, 371–385. doi: 10.1111/j.1469-8137.2004.00970.x

Kang, H., Liu, C., Yu, W., Wu, L., Chen, D., Sun, X., et al. (2011). Variation in foliar delta N-15 among oriental oak (Quercus variabilis) stands over eastern China: patterns and interactions. *J. Geochem. Explor.* 110, 8–14. doi: 10.1016/j.gexplo.2011.02.002

Kastovska, E., Strakova, P., Edwards, K., Urbanova, Z., Barta, J., Mastny, J., et al. (2018). Cotton-grass and blueberry have opposite effect on peat characteristics and nutrient transformation in peatland. *Ecosystems* 21, 443–458. doi: 10.1007/s10021-017-0159-3

Keuper, F., van Bodegom, P. M., Dorrepaal, E., Weedon, J. T., van Hal, J., van Logtestijn, R. S. P., et al. (2012). A frozen feast: thawing permafrost increases plant-available nitrogen in subarctic peatlands. *Glob. Chang. Biol.* 18, 1998–2007. doi: 10.1111/j.1365-2486.2012.02663.x

Kohzu, A., Matsui, K., Yamada, T., Sugimoto, A., and Fujita, N. (2003). Significance of rooting depth in mire plants: evidence from natural (15) N abundance. *Ecol. Res.* 18, 257–266. doi: 10.1046/j.1440-1703.2003.00552.x

Li, S. (2015). *Mutual Influence Between Santalum Album and Its Host on Water and Nutrient*. Bejing, China: Chinese Academy of Forestry.

Li, Y., and Huang, J. (2009). Photosynthetic physiological responses of glycyrrhiza uralensis under different water and nutrient supplies in kubuqi desert, China. *Acta Phytoecol. Sin.* 33, 1112–1124. doi: 10.3773/i.issn.1005-264x.2009.06.011

Liu, X., and Hu, Y. (2020). C:N:P stoichiometry of leaves and fine roots in typical forest swamps of the greater Hinggan Mountains, China. *J. Appl. Ecol.* 31, 3385–3394. doi: 10.13287/j.1001-9332.202010.007

Liu, Z., Song, Y., Wang, X., Tan, W., Zhang, H., Gao, J., et al. (2022). Effects of simulated warming on plant growth and carbon and nitrogen characteristics in permafrost peatland. *Ecol. Environ. Sci.* 31, 1765–1772. doi: 10.16258/j.cnki.1674-5906.2022.09.006

Liu, X., Zhang, Y., Su, Q., Li, Z., Feng, T., and Song, Y. (2018). Gradient variation of delta~(15) N values in herbs and its indication to environmental information in the agro-pastoral ecotone in the north of China. *J. Univ. Chin. Acad. Sci.* 35, 749–760. doi: 10.7523/i.issn.2095-6134.2018.06.006

Liu, X., Zhao, L., Gasaw, M., Gao, D., Qin, D., and Ren, J. (2007). Foliar delta C-13 and delta N-15 values of C-3 plants in the Ethiopia Rift Valley and their environmental controls. *Chin. Sci. Bull.* 52, 1265–1273. doi: 10.1007/s11434-007-0165-5

Lou, Y., Wang, G., Lu, X., and Jiang, M. (2012). Nitrogen and phosphorus content of vascular plant species in herbaceous marshes in the SANJIANG PLAIN, Northeast China. *Fresenius Environ. Bull.* 21, 3766–3772.

Lyons, C. L., Branfireun, B. A., McLaughlin, J., and Lindo, Z. (2020). Simulated climate warming increases plant community heterogeneity in two types of boreal peatlands in north-Central Canada. *J. Veg. Sci.* 31, 908–919. doi: 10.1111/jvs.12912

Lyons, C. L., and Lindo, Z. (2020). Above- and belowground community linkages in boreal peatlands. *Plant Ecol.* 221, 615–632. doi: 10.1007/s11258-020-01037-w

Makarov, M. I., Onipchenko, V. G., Malysheva, T. I., van Logtestijn, R. S. P., Soudzilovskaia, N. A., and Comelissen, J. H. C. (2014). Determinants of N-15 natural abundance in leaves of co-occurring plant species and types within an alpine lichen heath in the northern Caucasus. *Arct. Antarct. Alp. Res.* 46, 581–590. doi: 10.1657/1938-4246-46.3.581

Malhotra, A., Brice, D. J., Childs, J., Graham, J. D., Hobbie, E. A., Stel, H. V., et al. (2020). Peatland warming strongly increases fine-root growth. *Proc. Natl. Acad. Sci. U. S. A.* 117, 17627–17634. doi: 10.1073/pnas.2003361117

McCabe, S.J. (2020). *Permafrost Thaw Drives Changes in Plant Community Characteristics and Nutrient Stoichiometry, with Increases in the Magnitude of c-cycling in an Arctic Peatland*. Columbus, OH: The Ohio State University.

Meier, C. L., and Bowman, W. D. (2008). Links between plant litter chemistry, species diversity, and below-ground ecosystem function. *Proc. Natl. Acad. Sci. U. S. A.* 105, 19780–19785. doi: 10.1073/pnas.0805600105

Michelsen, A., Quarmby, C., Sleep, D., and Jonasson, S. (1998). Vascular plant N-15 natural abundance in heath and forest tundra ecosystems is closely correlated with presence and type of mycorrhizal fungi in roots. *Oecologia* 115, 406–418. doi: 10.1007/s004420050535

Moore, T. R., and Bubier, J. L. (2020). Plant and soil nitrogen in an Ombrotrophic peatland, southern Canada. *Ecosystems* 23, 98–110. doi: 10.1007/s10021-019-00390-w

Nadelhoffer, K. J. (2000). The potential effects of nitrogen deposition on fine-root production in forest ecosystems. *New Phytol.* 147, 131–139. doi: 10.1046/j.1469-8137.2000.00677.x

Nadelhoffer, K., Shaver, G., Fry, B., Giblin, A., Johnson, L., and McKane, R. (1996). N-15 natural abundances and N use by tundra plants. *Oecologia* 107, 386–394. doi: 10.1007/bf00328456

Piao, H. C., Zhu, J. M., Zhu, S. F., Yu, D. L., and Ran, J. C. (2004). Altitudinal variations of nutrient concentrations and carbon isotope compositions in a C_3 plant and the effects of nutrient interactions on carbon isotope discrimination in limestone areas of Southwest China. *Advance in Earth Sciences* 19, 412–418.

Rao, Z., Guo, W., Cao, J., Shi, F., Jiang, H., and Li, C. (2017). Relationship between the stable carbon isotopic composition of modern plants and surface soils and climate: a global review. *Earth Sci. Rev.* 165, 110–119. doi: 10.1016/j.earscirev.2016.12.007

Skrzypek, G., Kaluzny, A., Wojtun, B., and Jedrysek, M.-O. (2007). The carbon stable isotopic composition of mosses: a record of temperature variation. *Org. Geochem.* 38, 1770–1781. doi: 10.1016/j.orggeochem.2007.05.002

Skrzypek, G., Paul, D., and Wojtun, B. (2008). Stable isotope composition of plants and peat from Arctic mire and geothermal area in Iceland. *Polish Polar Res.* 29, 365–376. doi: 10.1007/s11104-007-9321-6

Smith, B. N., Herath, H. M. W., and Chase, J. B. (1973). Effect of growth temperature on carbon isotopic ratios in barley, pea and rape. *Plant Cell Physiol.* 14, 177–178. doi: 10.1104/pp.14.1.177

Song, Y., Jiang, L., Song, C., Wang, X., Ma, X., Zhang, H., et al. (2021). Microbial abundance and enzymatic activity from tussock and shrub soil in permafrost peatland after 6-year warming. *Ecol. Indic.* 126:107589. doi: 10.1016/j.ecolind.2021.107589

Spasojevic, M. J., and Weber, S. (2021). Variation in delta C-13 and delta N-15 within and among plant species in the alpine tundra. *Arct. Antarct. Alp. Res.* 53, 340–351. doi: 10.1080/15230430.2021.2000567

Su, B., Han, X. G., Li, L. H., Huang, J. H., Bai, Y. F., and Qu, C. M. (2000). Responses of δ13C value and water use efficiency of plant species to environmental gradients along the grassland zone of Northeast China transect. *Chin. J. Plant Ecol.* 24, 648–655.

Sun, J., Li, X., Wang, X., Lv, J., and Li, Z. (2010a). Plant species distribution in permafrost wetlands of the great Hing'an mountain valleys and its response to global climate change. *J. Earth Sci.* 21, 266–270. doi: 10.1007/s12583-010-0232-8

Sun, J., Li, X., Wang, X., Lv, J., Li, Z., and Hu, Y. (2010b). Analysis of structures of permafrost wetland plant communities along environmental gradients in the Da Hinggan Mountains, China. *Acta Phytoecol. Sin.* 34, 1165–1173. doi: 10.3724/SP.J.1088.2010.00432

Sun, J., Li, X., Wang, X., Lv, J., Li, Z., and Hu, Y. (2011). Latitudinal pattern in species diversity and its response to global warming in permafrost wetlands in the great Hing'an mountains, China. *Russ. J. Ecol.* 42, 123–132. doi: 10.1134/s1067413611020111

Wang, P., Heijmans, M. M. P. D., Mommer, L., van Ruijven, J., Maximov, T. C., and Berendse, F. (2016). Belowground plant biomass allocation in tundra ecosystems and its relationship with temperature. *Environ. Res. Lett.* 11:055003. doi: 10.1088/1748-9326/11/5/055003

Wang, M., and Moore, T. R. (2014). Carbon, nitrogen, phosphorus, and potassium stoichiometry in an Ombrotrophic peatland reflects plant functional type. *Ecosystems* 17, 673–684. doi: 10.1007/s10021-014-9752-x

Welker, J. M., Jonsdottir, I. S., and Fahnestock, J. T. (2003). Leaf isotopic (delta C-13 and delta N-15) and nitrogen contents of Carex plants along the Eurasian coastal Arctic: results from the Northeast passage expedition. *Polar Biol.* 27, 29–37. doi: 10.1007/s00300-003-0562-4

Werth, M., and Kuzyakov, Y. (2010). C-13 fractionation at the root-microorganisms-soil interface: a review and outlook for partitioning studies. *Soil Biol. Biochem.* 42, 1372–1384. doi: 10.1016/j.soilbio.2010.04.009

Wu, H., Gao, Q., Ganjurjav, H., Li, Y., Yan, Y., Hu, G., et al. (2019). Effects of grazing and simulated warming on plant community structure and productivity of alpine grassland in northern Xizang, China. *Chin. J. Plant Ecol.* 43, 853–862. doi: 10.17521/cjpe.2018.0288

Xu, G., Fan, X., and Miller, A. J. (2012). "Plant nitrogen assimilation and use efficiency" in *Annual review of plant biology*. ed. S. S. Merchant, PALO ALTO, CA :ANNUAL REVIEWS vol. 63, 153–182.

Xu, R., Liu, J., Wang, L., Yan, Y., Ma, X., and Li, M. (2022). Analysis of root and leaf functional traits and C, N, P stoichiometry of *Cunninghamia lanceolate* from different provenances. *Acta Ecol. Sin.* 42, 6298–6310. doi: 10.5846/stxb202103230765

Yu, H., Gao, R., Yang, W., Yang, L., Li, S., Lin, Y., et al. (2022). Carbon, nitrogen, and phosphorus contents of leaf, root, and soil and their relationships in dominant herbaceous plants in dry-hot valley. *Chin. J. Appl. Environ. Biol.* 28, 727–735. doi: 10.19675/.cnki.1006-687x.2021.01008

Yu, Z., Loisel, J., Brosseau, D. P., Beilman, D. W., and Hunt, S. J. (2010). Global peatland dynamics since the last glacial maximum. *Geophys. Res. Lett.* 37:L13402. doi: 10.1029/2010gl043584

Zhang, Q., Zhou, J., Li, X., Yang, Z., Zheng, Y., Wang, J., et al. (2019). Are the combined effects of warming and drought on foliar C:N:P: K stoichiometry in a subtropical forest greater than their individual effects? *For. Ecol. Manag.* 448, 256–266. doi: 10.1016/j.foreco.2019.06.021

frontiers | Frontiers in Ecology and Evolution

TYPE Original Research
PUBLISHED 15 December 2022
DOI 10.3389/fevo.2022.1078104

OPEN ACCESS

EDITED BY
Ben Niu,
Institute of Geographic Sciences and Natural Resources Research (CAS), China

REVIEWED BY
Guang Zhao,
Institute of Geographic Sciences and Natural Resources Research (CAS), China
Feng Li,
Institute of Subtropical Agriculture (CAS), China

*CORRESPONDENCE
Xianwei Wang
wangxianwei@iga.ac.cn
Xiaoxin Sun
sunxiaoxin@nefu.edu.cn

SPECIALTY SECTION
This article was submitted to Population, Community, and Ecosystem Dynamics, a section of the journal Frontiers in Ecology and Evolution

RECEIVED 24 October 2022
ACCEPTED 28 November 2022
PUBLISHED 15 December 2022

CITATION
Ma G, Wang X, Sun X, Wang S, Du Y and Jiang J (2022) Effects of warming and litter positions on litter decomposition in a boreal peatland.
Front. Ecol. Evol. 10:1078104.
doi: 10.3389/fevo.2022.1078104

Effects of warming and litter positions on litter decomposition in a boreal peatland

Guobao Ma[1,2], Xianwei Wang[1]*, Xiaoxin Sun[2,3]*, Shujie Wang[1,2], Yu Du[1] and Jingyi Jiang[1,2]

[1]Key Laboratory of Wetland Ecology and Environment, Northeast Institute of Geography and Agroecology, Chinese Academy of Sciences, Changchun, China, [2]Key Laboratory of Sustainable Forest Ecosystem Management-Ministry of Education, School of Forestry, Northeast Forestry University, Harbin, China, [3]Heilongjiang Sanjiang Plain Wetland Ecosystem Research Station, Fuyuan, China

Litter decomposition is an important source of carbon accumulation in the permafrost peatlands. Climate warming has led to shrub expansions and accelerated litter mixing with soils and fluctuations in the water table. However, little is known about how changes in the position of the litter will affect litter decomposition under climate warming. To reveal the mechanisms of response of the location of litter in the soil and climate warming to litter decomposition in permafrost peatlands. Here, we selected the evergreen shrub, *Chamaedaphne calyculata*, and the deciduous shrub, *Vaccinium uliginosum*, from the permafrost peatlands of the Greater Hing'an Mountains, China. The leaf litter was placed on the soil surface (no-mixing) and mixed with the soil (soil-litter mixing), and then it was incubated for 124 days at 15°C (control) and 20°C (warming). Our results showed that warming significantly increased the CO_2 emission rates of *C. calyculata* and *V. uliginosum* by 19.9 and 17.4%, respectively. When compared to no-mixing, the CO_2 emission rates were reduced (not significantly) by 1.5 (*C. calyculata*) and increased 13.6% (*V. uliginosum*) with soil-litter mixing. Interestingly, soil-litter mixing suppressed the positive effect of warming on the CO_2 emission rates relative to no-mixing, and the suppressing effects in the *V. uliginosum* subplot were stronger than those in the *C. calyculata* subplot. Specifically, warming significantly increased the CO_2 emissions of *C. calyculata* by 27.4% under no-mixing but the increase decreased to 13.1% under soil-litter mixing. Similarly, warming induced significant increases in the CO_2 emissions of *V. uliginosum*, with an increase of 38.8% under no-mixing but non-significant increases (1.9%) were observed under soil-litter mixing. The combination of the enzyme activities of β-1,4-glucosidase, β-1,4-xylosidase and β-D-1,4-cellobiosidase and laccase and phenolics explained more than 60.0% of the variability in the CO_2 emissions of *C. calyculata* and *V. uliginosum*, respectively. Our study highlights the importance of litter positions in mediating the responses of litter decomposition to climate warming and shrub expansions in the northern peatlands.

KEYWORDS

boreal peatland, litter decomposition, soil-litter incubation, CO_2 fluxes, enzyme activity

Introduction

Around 400–500 Pg of C has been stored in the peatlands since the beginning of the Holocene (Yu et al., 2010). The distribution of the peat soil organic carbon is uneven and widespread across the northern peatlands. This occurs mainly because organic matter decomposition is limited due to the low temperature in this ecosystem, resulting in an imbalance between plant production and organic matter decomposition (Freeman et al., 2001; Moore and Basiliko, 2006). The consequence is a large accumulation of peat, composed of dead plant litter (Clymo, 1984). Thus, litter decomposition is one of the key factors affecting soil organic carbon storage in the northern peatlands (Strakova et al., 2012). Climate warming has been identified as an essential driver of litter decomposition. Warming accelerates changes in the community compositions (Zhang, Y. et al., 2022), such as vascular plant expansions (Luan et al., 2019), and the mixture of the soils and litter (Song et al., 2017). However, there is very limited knowledge about the interactive effects of warming and changes in the plant community structure and litter positions on litter decomposition in the northern peatlands. Therefore, to accurately assess and predict the carbon balance of the boreal peatlands, it is crucial to re-examine litter decomposition and its response to climate warming.

The effect of climate warming on litter decomposition could be regulated by functional groups in the northern peatlands. It is commonly accepted that climate warming effectively increases microbial activities, and, thus, stimulates litter decomposition (Ferreira et al., 2015; Liu et al., 2017). In contrast, the neutral and negative effects of warming on litter decomposition have also been emphasized in the northern peatlands (Aerts, 2006; Boyero et al., 2011; Butenschoen et al., 2011). These discrepancies suggest that climate warming alone is not enough to explain the complex variability in litter decomposition and, therefore, it might also be regulated by functional groups. With climate warming, there is growing evidence that the northern peatlands will experience greater vascular plant expansions (Elmendorf et al., 2012; Sistla et al., 2013; Dieleman et al., 2015). Additionally, due to the differences in the litter chemistries of vascular plants, it has been found that the decomposition rate of leaf litter from the deciduous shrub *Betula nana* is higher than that of the evergreen shrubs *Vaccinium vitis-idaea* and *Rhododendron palustre* (McLaren et al., 2017). However, studies on the differences in the responses of the decomposition of different vascular plants to climate warming in the northern peatlands are still limited.

The uncertainties of the effects of warming on decomposition might also be attributed to the litter positions. Strong winds and fluctuations in the water table could lead to the topsoil mixing with the litter under climate warming (Hewins et al., 2017). Soil-litter mixing could influence litter decomposition through two different but equally important ways, including (1) acting as a microbial colonization vehicle on the surface of the litter and (2) insulating the litter from temperature or moisture, thus, extending the time window for microbially mediated decomposition opportunities (Throop and Archer, 2007). Recent incubation experiments (Gao et al., 2022; Zhang, X. H. et al., 2022) and *in situ* litter decomposition in arid ecosystems (Siegenthaler et al., 2010; Corteselli et al., 2017) have well documented the differences in the litter decomposition rates among litter positions. Nevertheless, current studies have mostly focused on the litter decomposition rates in the surface soils but have not considered soil-litter mixing. Considering the important role that soil-litter mixing plays in affecting the litter decomposition, lacking related studies of soil-litter mixing in the northern peatlands potentially amplifies the critical uncertainties regarding the response of CO_2 emissions that are induced by litter decomposition due to climate warming.

Peatlands are widespread in the Greater Hing'an Mountains, which is experiencing rapid climate warming and, consequently, permafrost degradation, leading to shrub expansion and changes in the water table, which may induce changes in the litter position. Therefore, the boreal peatlands of the Greater Hing'an Mountains provide a rare opportunity to investigate the linkages between climate warming, species change, litter position, and litter decomposition. Here, we collected fresh litter from the evergreen shrub *Chamaedaphne calyculata* and the deciduous shrub *Vaccinium uliginosum* in the Greater Hing'an Mountains. The litter was located on the soil surface or mixed with the soil, and they were incubated at 15 and 20°C for a period of 124 days to evaluate the response of the CO_2 emission rates to warming, the functional group, litter positions, and their interactions. Therefore, the aims of the study were (1) to estimate the impacts of warming on the CO_2 emission rates of litter decomposition and differentiate whether the warming impacts varied due to the functional groups and litter positions; and (2) to identify the driving factors of the response of the CO_2 emission rates from litter decomposition to the different treatments.

Materials and methods

Study region

Plant litter and soil samples were collected from a site in the Greater Hing'an Mountains permafrost peatlands in northeastern China (52.56 °N, 122.51 °E, 467 m a.s.l.). The region has a cool temperate continental monsoon climate. The mean annual temperature and precipitation at the study site over the last 30 years were −3.9°C and 452 mm (Song et al., 2018), respectively. The vegetation of the study site is relatively simple, including the shrubs *Betula fruticosa*, *C. calyculata*, and *V. uliginosum*, Cyperaceae *Eriophorum vaginatum,* and bryophyte *Sphagnum palustre* (Zhang, X. H. et al., 2022). In this study, we selected the litter of the evergreen shrub *C. calyculata* and deciduous shrub *V. uliginosum* to study the effects of different temperatures and different locations on the early decomposition of peatland litter in permafrost regions.

Sample collection and incubation

Six 20 × 20 m plots were randomly selected in the peatland. Within each sample plot, five peat cores (10 cm inner diameter) were randomly collected in the 0–10 cm soil layer in early September 2021. The soil samples were air-dried after removing the plant roots, and all the samples were mixed evenly and passed through a 2 mm sieve. The fresh litter was collected by gently shaking the shrubs. For each species, the plant litter that was sampled from the different plots was mixed well, oven-dried at 65°C, and divided into two subsamples. One subsample was used for the incubation experiments, and the other subsample was oven dried to a constant weight at 65°C to determine the moisture content and milled to pass through a 0.15 mm sieve for chemical analysis (the C, N, P, and phenolic initial content) (Table 1).

The litter decomposition C emission rate was determined by a laboratory incubation experiment (Gao et al., 2022). For each litter treatment, a cylindrical culture bottle (12 cm in diameter and 16 cm in height) was filled with 80 g of dry soil at the bottom, and the dry soil was adjusted to 60.0% of the maximum water-holding capacity in the field with 0–10 cm of pore water from the peatlands. The location of the litter (5 g) in the soil was divided into two treatments: at the soil surface (no-mixing) and fully mixed with the soil (soil-litter mixing). To prevent the litter from absorbing soil water, the litter was soaked with pore water in advance until it was saturated. Then, it was cultivated in the dark at 15°C (control) and 20°C (warming) for 124 days, which represents the average temperature of the growing season from May to September (13°C) and July (18°C) at the sampling sites, respectively. In total, there were 40 microcosm samples (2 litter treatments × 2 incubation temperatures × 2 litter locations × 4 replicates). During the incubation period, to maintain a constant microcosm sample moisture, water supplementation was carried out by weighing the samples every 7 days. The frequency of the sampling was increased at the beginning of the incubation period because the high C content that was available at the beginning of the decomposition of the litter contributed to a high respiration rate for the microorganisms (Mao et al., 2018; Gao et al., 2022). Additionally, a gas-tight syringe was used to collect 30 ml of the sample gas on days 1, 2, 4, 7, 11, 17, 24, 34, 44, 64, 84, 104, and 124 of the incubation. The bottles were closed tightly, the plastic cap was fitted with the pumping port for 24 h before pumping, and they were open for the rest of the incubation time. The analysis of the sample CO_2 concentration in the syringes was conducted within 24 h using an Agilent 7820A gas chromatograph (Agilent Technologies, Carpinteria, CA, United States). The CO_2 release rate was calculated as described by Robertson et al. (1999). After the incubation, the litter was collected and its C, N, P, and phenolic compound contents were measured.

TABLE 1 The initial quality of the *Chamaedaphne calyculata* and *Vaccinium uliginosum* litter.

Parameter	*C. calyculata*	*V. uliginosum*
C content (mg g^{-1})	533.14 ± 1.16a	492.00 ± 1.75b
N content (mg g^{-1})	3.80 ± 0.15b	5.30 ± 0.16a
P content (mg g^{-1})	0.49 ± 0.01b	1.42 ± 0.02a
C/N ratio	140.21 ± 5.90a	92.88 ± 2.50b
C/P ratio	1076.57 ± 26.98a	344.29 ± 3.98b
N/P ratio	7.69 ± 0.46a	3.70 ± 0.05b
Phenolics content (mg g^{-1})	21.02 ± 1.49b	25.81 ± 0.53a

The numbers are the mean ± standard deviation ($n = 4$). The letters represent different means ($p < 0.05$).

Sample analysis

We used 5 g of fresh soil to determine the potential activity of four hydrolytic enzymes β-1,4-glucosidase (βG, EC 3.2.1.21), β-1,4-xylosidase (βX, EC 3.2.1.37), β-D-1,4-cellobiosidase (CBH, EC 3.2.1.91), and β-1,4-N-ace-tylglucosaminidase (NAG, EC 3.2.1.14) and the oxidative enzyme laccase (EC 1.10.3.2). The enzymes, βG, βX, CBH, and NAG were assayed using 4-methylumbelliferone (MUB)-β-D-glucoside, 4-MUB-β-D-xyloside, 4-MUB-β-D-cellobioside, and 4-MUB-N-acetyl-β-D-glucosaminide, respectively, as the specific substrates. The hydrolases were analyzed using a black 96-well microtiter plate. Briefly, under the different treatments, 5 g of soil was mixed with 150 ml of 50 mM sodium acetate buffer (pH 5.5) in a high-speed stirrer for 10 min. Then, 4-MUB (10 mM) was used as a standard solution. Next, using an 8-channel electronic pipette, we added 200 µl of the soil suspension and 50 µl of sodium acetate buffer (blank control), 200 µl of the soil suspension and 50 µl of the standard solution (quench standard), 200 µl of sodium acetate buffer and 50 µl of the standard solution (reference standard), 200 µl of sodium acetate buffer and 50 µl of enzyme substrate (negative control), and 200 µl of the soil suspension and 50 µl of enzyme substrate (sample controls). After completion, the microplates were incubated in the dark at 25°C for 4 h. Subsequently, 10 µl of 0.5 mol L^{-1} NaOH solution was added to each well to stop the reaction. The fluorescence values of each well were measured using a Multi-Detection Microplate Reader (CYTATION 5, BioTek, United States) with excitation and emission wavelengths of 365 mm and 450 mm, respectively. The activity of phenol oxidase was estimated using 2,2-azino-bis (3-ethylbenzthiazoline-6-sulfonic acid) as a substrate. Furthermore, estimation of the potential laccase activity for promoting polyphenol degradation was conducted on 96-well transparent microtiter plates. Each assay microplate also contained a sample well (50 µl of the substrate solution and 200 µl of the soil suspension), blank well (200 µl of the soil suspension and 50 µl of the sodium acetate buffer), and negative control (200 µl of sodium acetate buffer and 50 µl of the substrate solution). The plates were incubated at 20°C in darkness for at least 2 h (Rinkes et al., 2013). Also, the activity was quantified by measuring the absorbance at 420 nm using a Multi-Detection Microplate Reader (BioTek; Eichlerova et al., 2012), and the enzyme activities were expressed in nmol h^{-1} g^{-1}.

To measure the extractable phenolic content of each plant litter sample, the Folin–Ciocalteu method was used to determine the phenolic concentration (Bärlocher et al., 2020). We put 0.2 g of the litter into a 50 ml centrifuge tube, added 30 ml of 95% methanol solution, and sonicated it at 540 W and 40–50°C for 30 min, three times. The extracts were combined, and they were centrifuged at 5000 r/min for 15 min, 0.2 ml of supernatant was transferred to a 10 ml centrifuge tube, 4.8 ml of deionized water was added and it was shaken well, 0.5 ml of Folin-Ciocalteau's reagent and 1.5 ml of Na_2CO_3 were added, and the sample was mixed thoroughly and incubated at 30°C for 2 h. The same procedure was applied to 10 mg/ml of gallic acid standard to produce a standard curve. The absorbance values were measured at 760 nm.

The total carbon (TC) and nitrogen (TN) were measured on a TC-TN analyzer (Shimadzu, Tokyo, Japan). To determine the concentration of Phosphorus (TP), the litter samples were digested at 365°C in concentrated H_2SO_4 and an AA3 continuous flow autoanalyzer (Seal AA3 Analytical, Norderstedt, Germany) was used.

Statistical analysis

The effects of the experimental warming, different vegetation litter, different locations, and their interaction effects, were analyzed using a repeated measures analysis of variance and IBM SPSS Statistics 20, with the sampling date as a random effect. This was followed by Tukey's comparison test, which was used to compare the difference in the means of the litter's chemical properties. Additionally, a new method, relative weights, was used to quantify the relative contributions of the NAG, litter stoichiometry, phenolics, laccase, and carbon cycle enzymes to the CO_2 emission rate. This approach approximates the average increase in R^2 (coefficient of determination), which is obtained by adding a predictor variable to allthe possible submodels (LeBreton and Tonidandel, 2008), and it has been used in recent analyses (Chen et al., 2021). In this study, a principal component analysis (PCA) was used to reduce the number of variables that were tested (Cardenas et al., 2015). The PCA was performed on the βG, CBH, and βX enzyme activities and the litter C, N, P, C/N, C/P, and N/P, and their final scores were used as variables for the relative weight analysis of the carbon cycle enzymes and litter stoichiometry, respectively.

Results

Effects of warming and the litter positions on the CO_2 emissions

The warming and litter positions and their interactions significantly affected the CO_2 emission rates ($p < 0.05$; Figure 1; Table 2). Warming induced significant increases in the CO_2 emissions of *C. calyculata* and *V. uliginosum*, which were 19.9 and 17.4% ($p < 0.05$), respectively, relative to the control treatment (Figure 1; $p < 0.05$). When compared to the soil-litter mixing treatment, the CO_2 emission rates of *C. calyculata* and *V. uliginosum* were reduced (not significantly) by 1.5% ($p > 0.05$) and increased by 13.6% ($p > 0.05$), respectively (Figure 1). It was also observed that warming-induced positive effects on the CO_2 emission rates were significantly negatively regulated by the litter positions of the observed species (Figure 1; Table 2; $p < 0.05$). The CO_2 emission rate of *C. calyculata* under the warming treatment was significantly 27.4 and 13.1% higher than that of the control in the no-mixing and soil-litter mixing treatments, respectively ($p < 0.05$; Figure 1). Then, in the no-mixing treatment, the CO_2 emission rate of *V. uliginosum* under the warming treatment was, on average, 2.99 ± 0.16 C kg^{-1} h^{-1} mg higher than that of the control ($p < 0.05$) but this significant difference, which was induced by warming, disappeared in the soil-litter mixing treatment ($p > 0.05$; Figure 1). Overall, compared with no-mixing, soil-litter mixing decreased the sensitivity of the litter CO_2 emission rate to warming but the decreases for *V. uliginosum* were higher than those for *C. calyculata*.

Treatment effects on the control factors of the CO_2 emission rate

Enzyme activities

Warming increased the enzyme activities of βG, βX, CBH, and NAG for *C. calyculata* by 69.1 ($p < 0.05$), 26.9 ($p > 0.05$), 164.5 ($p < 0.05$), and 66.2% ($p < 0.05$) relative to the control but laccase decreased by 20.0% ($p > 0.05$; Figure 2). The responses of the enzyme activities to warming were regulated by the litter positions. In the no-mixing treatment, warming significantly increased the activities of βG and CBH for *C. calyculata* ($p < 0.05$; Figure 2). The increase in the βG and CBH activities due to warming under the soil-litter mixing treatment was less than that of the no-mixing treatment (Figure 2). In contrast to βG and CBH, which warmed slightly, and NAG which increased in the no-mixing treatment ($p > 0.05$), significant increases were observed in the soil-litter mixing treatment ($p < 0.05$; Figure 2). Additionally, the activities of laccase and βX for *C. calyculata* showed non-significant changes with warming under the no-mixing and soil-litter mixing treatments ($p > 0.05$; Figure 2).

The enzyme activities of βG, CBH, and NAG for *V. uliginosum* were, on average, 24.5 ($p < 0.05$), 57.9 ($p < 0.05$), and 16.3% ($p > 0.05$) lower, respectively, in the warmed treatment than in the control treatment but increases were observed for βX and laccase, which increased by 10.8 ($p > 0.05$) and 25.6%, respectively ($p < 0.05$; Figure 3). The sensitivity of the enzyme activities to warming varied with the litter positions. Warming

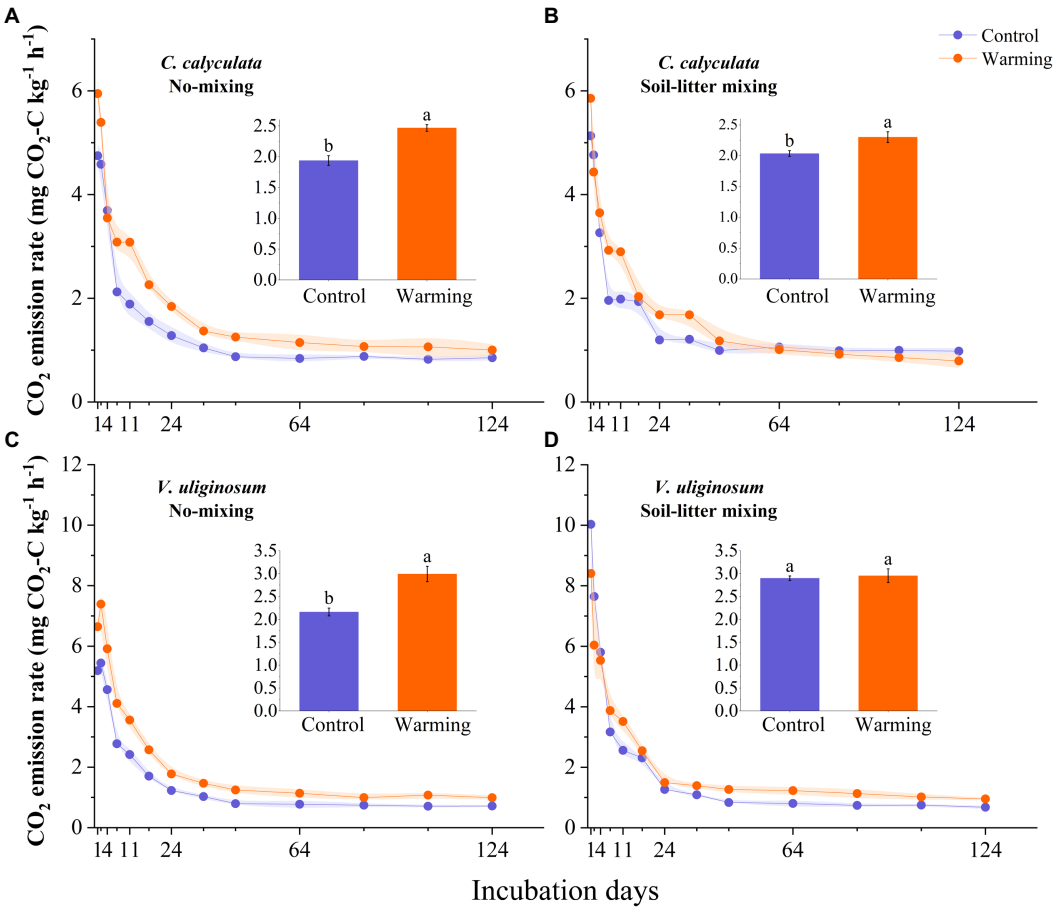

FIGURE 1
The dynamic CO_2 emissions rate for the *C. calyculata* (**A,B**) and *V. uliginosum* (**C,D**) litter decomposition under warming and treatments with different positions. On each solid line, the shading around the points represents the mean±standard deviation (n=4 replicates). The panel inset shows the average CO_2 emission rate throughout the incubation period, under the different treatments (the different letters in the insets represent statistical differences (p<0.05) based on a Tukey's multiple comparison test).

TABLE 2 A repeated measures analysis of variance shows the effects of climate warming and litter location and the interactions between them on the CO_2 emission rates from the different plant litter (*C. calyculata* and *V. uliginosum*).

	C. calyculata			*V. uliginosum*		
	DF	***F*-value**	***P***	***DF***	***F*-value**	***P***
Position	1	0.93	0.352	1	32.56	**<0.001**
Warming	1	134.44	**<0.001**	1	51.88	**<0.001**
Position × Warming	1	14.76	**0.002**	1	39.81	**<0.001**

DF, Degrees of freedom. Significant (p < 0.05) values are presented in bold.

induced significant increases (and insignificant reductions) in laccase (βG and CBH) for *V. uliginosum* in the no-mixing treatment but this significant difference was not detected in the soil-litter mixing treatment (Figure 3; p > 0.05). Both NAG and βX showed insignificant (p > 0.05) changes in response to warming under either the no-mixing or soil-litter mixing treatments (Figure 3).

Chemical properties of the litter

Compared with the control treatment, warming decreased the C concentrations, C/N, C/P, N/P, and phenolics of *C. calyculata* by 2.9 (p > 0.05), 16.6 (p > 0.05), 18.2 (p > 0.05), 1.0 (p > 0.05), and 22.1% (p > 0.05), respectively, and increased the N and P concentrations by 10.8 (p > 0.05) and 11.9% (p > 0.05), respectively (Table 3). The warming effects on the chemical properties differed under the different litter positions. Warming significantly increased the N and P concentrations of *C. calyculata* (p < 0.05) and significantly decreased the C/N, C/P, and phenolics of *C. calyculata* in the no-mixing treatment (p < 0.05), whereas significant responses were not observed in the soil-litter mixing treatment (Table 3). Additionally, warming did not significantly alter the C concentrations of *C. calyculata* in the no-mixing treatment (p > 0.05) but significant decreases were found in the soil-litter mixing treatment (p < 0.05; Table 3). Also, N/P did not show significant changes in response to warming in comparison

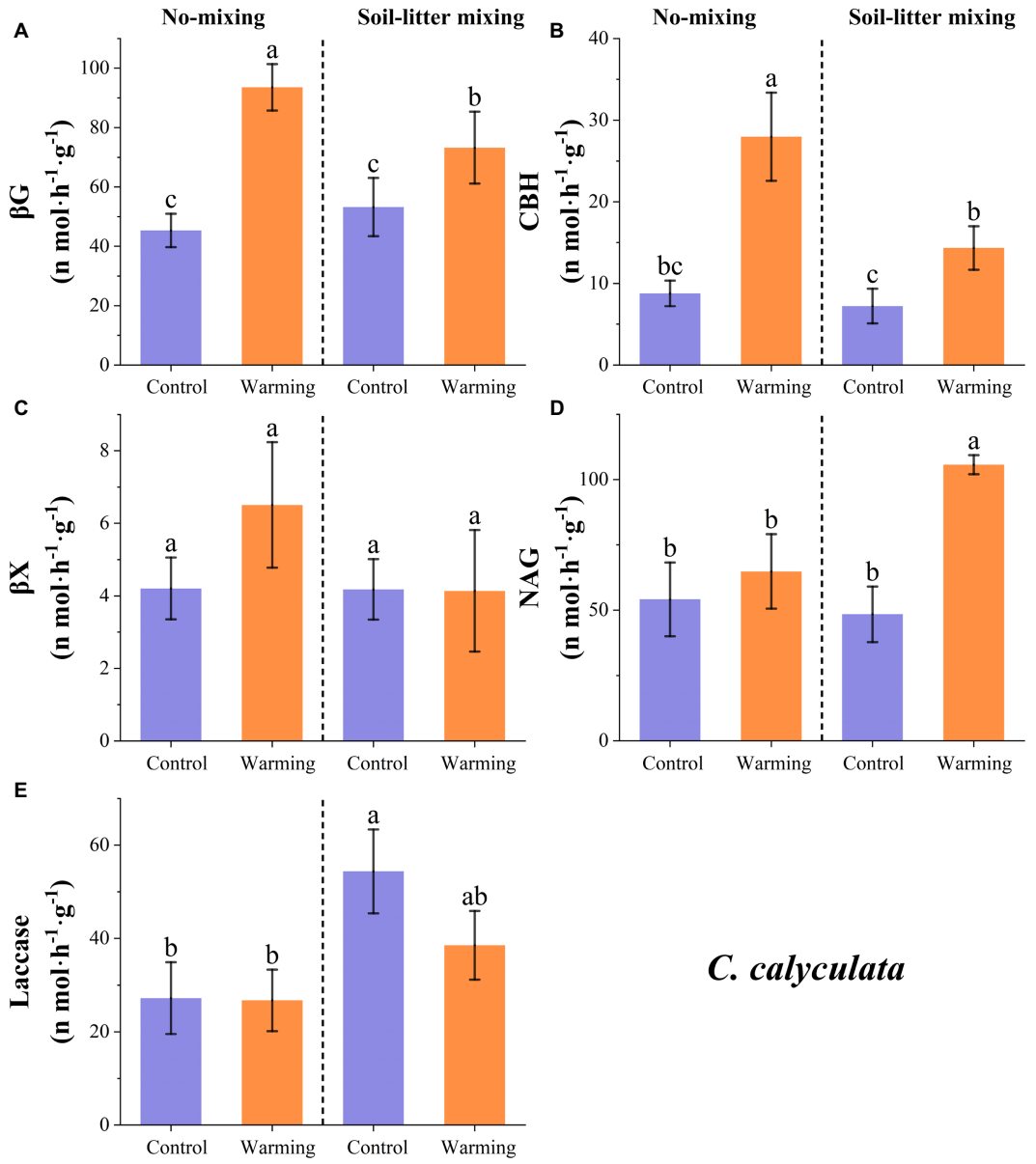

FIGURE 2
The responses of the potential enzyme activities of *C. calyculata* to warming under the no-mixing and soil-litter mixing treatments. The enzymes are **(A)** β-glucosidase (βG), **(B)** Cellobiohydrolase (CBH), **(C)** β-xylosidase (βX), **(D)** N-acetyl-glucosaminidase (NAG), and **(E)** Laccase. The values are the mean±standard deviation of each treatment (n=4). The different letters indicate significant differences (p<0.05) in the enzyme activities under the different treatments.

to the control under both the no-mixing and soil-litter mixing treatments ($p > 0.05$; Table 3).

The C concentrations, C/N, C/P, and phenolics of *V. uliginosum* were, on average, 5.1 ($p > 0.05$), 15.8 ($p > 0.05$), 9.0 ($p > 0.05$), and 48.6% lower ($p > 0.05$), and the N concentrations, P concentrations, and N/P were 13.5 ($p > 0.05$), 5.2 ($p > 0.05$), and 7.5% ($p > 0.05$) higher, respectively, in the warmed subplots than those in the control subplots (Table 3). Overall, the responses of the C and N concentrations and phenolics to warming varied with the litter positions. Additionally, warming did not induce significant changes in the P, C/P, and N/P values when compared to those of the control in both the no-mixing and soil-litter mixing treatments ($p > 0.05$), whereas warming significantly decreased C/N relative to that of the control under both litter positions ($p < 0.05$; Table 3).

Impacts of the enzyme activities and litter chemistries on the CO_2 emission rate

We used a PCA and relative weight analysis to explore the correlation between the CO_2 emission rate and soil enzymes and

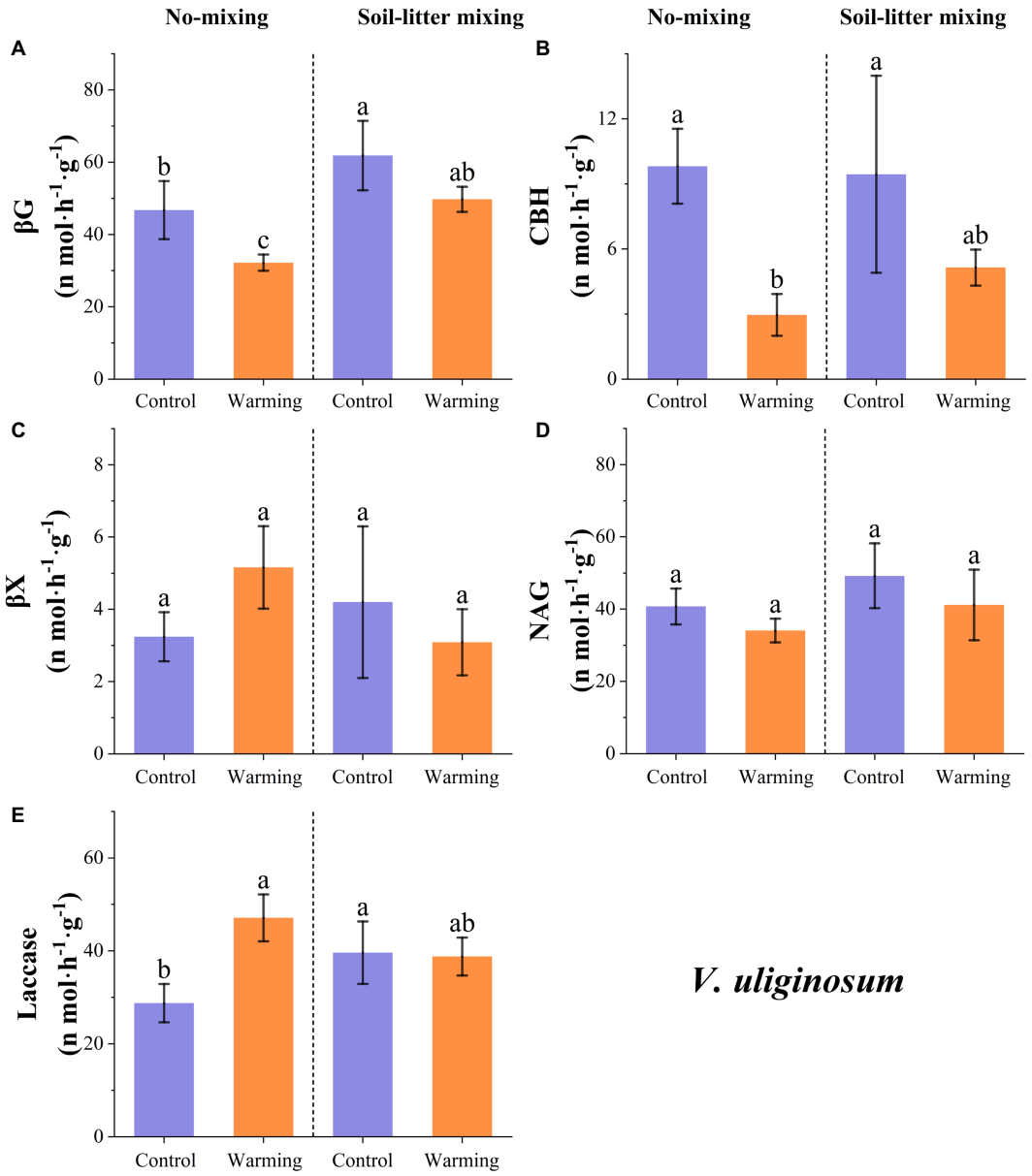

FIGURE 3
The responses of the potential enzyme activities of *V. uliginosum* to warming under the no-mixing and soil-litter mixing treatments. The enzymes are **(A)** β-glucosidase (βG), **(B)** Cellobiohydrolase (CBH), **(C)** β-xylosidase (βX), **(D)** N-acetyl-glucosaminidase (NAG), and **(E)** Laccase. The values are the mean±standard deviation of each treatment (n=4). The different letters indicate significant differences (p<0.05) in the enzyme activities under the different treatments.

litter chemistries. Our analyses showed that the enzyme activities of βG, βX, and CBH were positively and significantly correlated with the average rate of CO_2 emission from *C. calyculata* but these significant correlations were not observed for the other variables (Figure 4). More than 60.0% of the variability in the CO_2 emissions from *C. calyculata* can be explained by the enzyme activities of βG and CBH when using the relative weight analysis (Figure 4). In contrast to *C. calyculata*, laccase and the phenolic compounds exerted significant negative effects on the CO_2 emission rate of *V. uliginosum*, and the remaining chemical indicators were not significant (Figure 4). The relative contributions of laccase and the phenolic compounds to the CO_2 emissions of *V. uliginosum* were 35.2 and 38.8%, respectively (Figure 4).

Discussion

It is commonly reported that litter decomposition responds to climate warming and its underlying mechanisms when litter is located on the soil surface (Hough et al., 2022; Yang et al., 2022;

TABLE 3 The effects of warming and the litter positions on the TC, TN, TP, and phenolics contents of the *C. calyculata* and *V. uliginosum* litter.

			TC (mg g^{-1})	TN (mg g^{-1})	TP (mg g^{-1})	C/N ratio	C/P ratio	N/P ratio	Phenolics (mg g^{-1})
C. calyculata	No-mixing	Control	523.50 ± 1.66a	6.82 ± 0.60c	0.63 ± 0.04c	77.12 ± 7.04a	832.30 ± 58.90a	10.90 ± 1.73b	6.27 ± 0.45a
		Warming	515.67 ± 6.58a	8.36 ± 0.71b	0.81 ± 0.02b	62.05 ± 6.15b	633.56 ± 18.25b	10.26 ± 0.82b	4.71 ± 0.13b
	Soil-litter mixing	Control	482.47 ± 2.28b	15.35 ± 0.39a	1.15 ± 0.06a	31.43 ± 0.89c	418.71 ± 23.52c	13.31 ± 0.39a	2.20 ± 0.17c
		Warming	460.42 ± 4.35c	16.22 ± 0.58a	1.18 ± 0.03a	28.40 ± 0.99c	388.62 ± 14.34c	13.69 ± 0.71a	1.88 ± 0.17c
V. uliginosum	No-mixing	Control	501.08 ± 7.79a	8.93 ± 0.67c	1.04 ± 0.02b	56.30 ± 3.82a	478.19 ± 7.83a	8.51 ± 0.49b	9.21 ± 0.70a
		Warming	463.67 ± 7.25b	9.76 ± 0.37c	1.05 ± 0.04b	47.50 ± 1.61b	439.44 ± 16.89ab	9.25 ± 0.23b	4.02 ± 0.59b
	Soil-litter mixing	Control	464.52 ± 2.75b	15.85 ± 0.67b	1.15 ± 0.07ab	29.34 ± 1.38c	404.10 ± 24.95bc	13.80 ± 1.25a	1.91 ± 0.15c
		Warming	451.80 ± 14.66b	18.36 ± 0.51a	1.26 ± 0.14a	24.60 ± 0.57d	363.06 ± 52.72c	14.75 ± 2.08a	1.68 ± 0.15c

The TC, TN, and TP are the contents of the total carbon, total nitrogen, and total phosphorus, respectively. The values in the column with different superscripted letters indicate that significant differences exist among the litter species at $p < 0.05$.

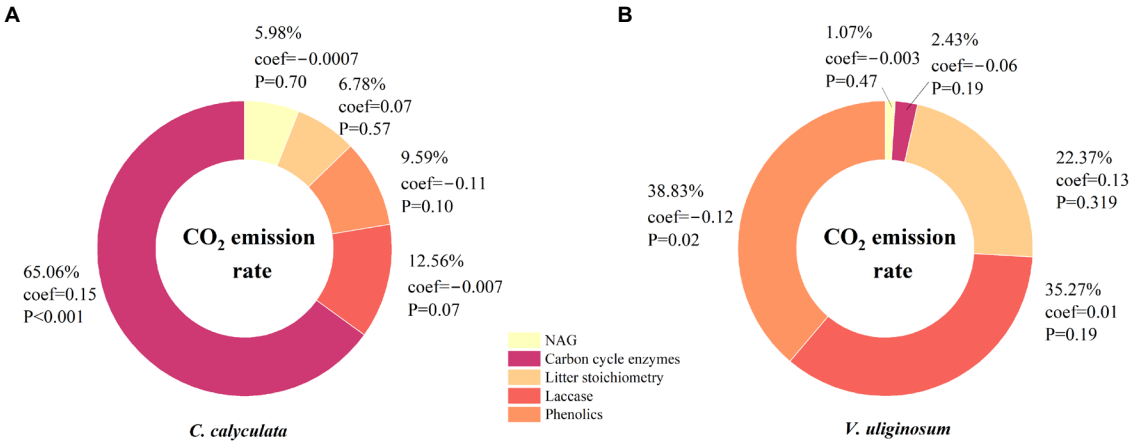

FIGURE 4
The relative weights of the effects of the soil enzyme activity and litter chemistry on the rate of CO_2 emissions from the *C. calyculata* **(A)** and *V. uliginosum* **(B)** litter under the different treatments. A principal component analysis (PCA) was used, resulting in five explanatory variables: the litter stoichiometry, soil carbon cycle enzymes, soil nitrogen cycle enzymes, laccase, and phenolics. The percentages show the relative weight of these variables, and coef refers to the standardized regression coefficient. The *p*-values represent the effects of the explanatory variables on the CO_2 emission rates.

Zhang, X. H. et al., 2022). However, this is not always the case. The litter can be mixed into the soil due to wind and water movement with changes in the peat soil porosity under a warming climate (Kechavarzi et al., 2010; Lee et al., 2014). Studies have shown that the response of CO_2 emissions to soil-litter mixing differs from no-mixing (Hewins et al., 2013; Erdenebileg et al., 2018). However, in the northern peatland ecosystem, these differences were previously unobserved. Our study found that warming and litter positions greatly altered the CO_2 emission rates of *C. calyculata* and *V. uliginosum*. More importantly, soil-litter mixing significantly restrained the warming-induced positive effects on the CO_2 emission rates of *C. calyculata* and *V. uliginosum* when compared to no-mixing. The observed negative effects of the litter positions of *C. calyculata* were stronger than those of *V. uliginosum*. These response processes are mainly attributed to the chemical properties of the litter and microcosm soil enzyme activities (Figure 5).

Evergreen shrub litter in response to warming and the litter positions

The variability in the CO_2 emission rates of *C. calyculata* depended on the enzymatic activities. It has been commonly observed that warming significantly accelerates litter decomposition (Mao et al., 2018; Zhang et al., 2019) and increases CO_2 release (Gao et al., 2022). Similarly, we found that the CO_2 emission rate of the evergreen shrub was significantly increased by warming under the same litter positions. Increases in the CO_2 emission rates in response to warming could be attributed to the increased microbial abundance and enzymatic activities of CBH and βG (Meyer et al., 2022). Warming can influence enzymatic activities in two different ways. First, higher temperatures can enhance soil microbial activity and biomass by accelerating the rate of microbial metabolism (Chen et al., 2015). Second, decreasing labile C with time at higher temperatures leads to increasing C

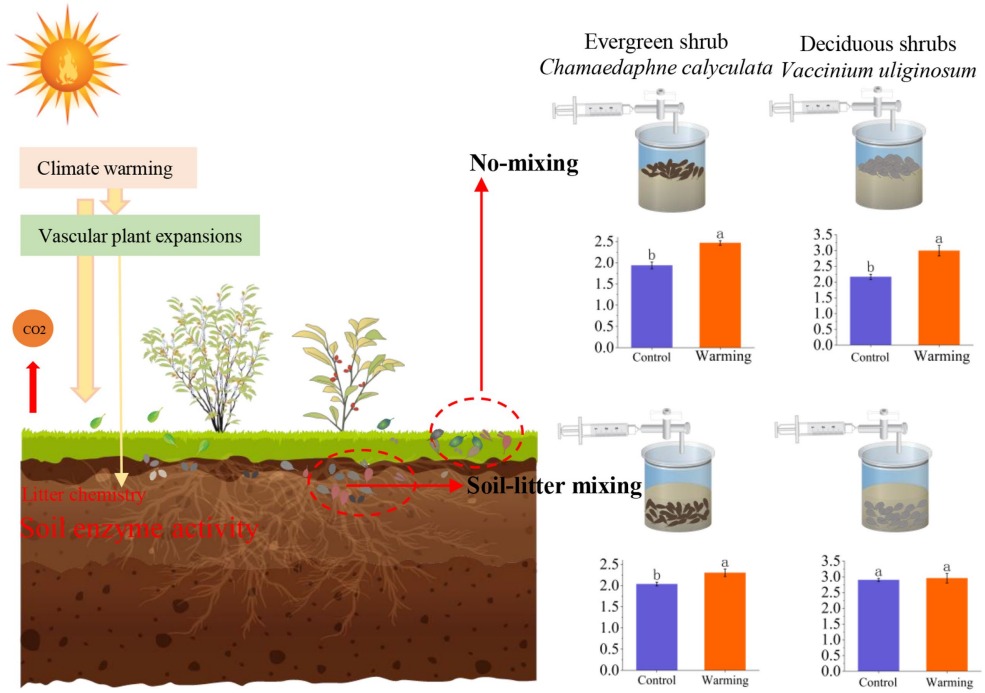

FIGURE 5
A mechanism framework for the response of leaf litter decomposition to warming at different positions. The two plants in the left half of the figure represent plants *C. calyculata* and *V. uliginosum*. The two red dashed boxes, from left to right, represent litter mixed with soil (Soil-litter mixing) and litter on the soil surface (No-mixing), respectively. The bar graphs in the right half of the figure shows the average CO_2 emission rate throughout the incubation period, under the different treatments (the different letters in the insets represent statistical differences (p<0.05) based on a Tukey's multiple comparison test).

limitations for the microorganisms, resulting in the production of more C-acquiring enzymes at later stages of initiation.

When compared to the no-mixing treatment, soil-litter mixing significantly decreased the sensitivity of the CO_2 emission rate of *C. calyculata*'s litter to warming. This negative effect could be because of decreased enzymatic activities driven by the litter water content under soil-litter mixing (Zhao et al., 2021). Our study showed that warming significantly reduced the moisture content of the litter by 28.3% when compared to that of the control in the no-mixing treatment but no significant changes were observed in the soil-litter mixing treatment (Figure 6). This could lead to decreases in the sensitivity of βG and CBH to warming with soil-litter mixing relative to no-mixing, supporting the findings of previous studies. Microorganisms in relatively dry litter need to excrete more enzymes to obtain sufficient resources to compensate for the moisture-limiting effects of warming (Allison et al., 2010). Furthermore, water limitations can increase the fungal biomass and, in turn, exert strong impacts on enzyme activities, especially in terms of degrading more complex polymers (e.g., cellulose; Schneider et al., 2012). Thus, when compared to no-mixing, soil-litter mixing decreased the response of βG and CBH to warming, and, thus, the sensitivity of the rates of the CO_2 emissions to warming under no-mixing was higher than that under soil-litter mixing.

Deciduous shrub litter in response to warming and the litter positions

The response of the litter decomposition of *V. uliginosum* to warming was attributable to changes in the soluble phenolic compounds. In the peatlands, the concept of "enzyme latch" is believed to be the main constraint of carbon decomposition. The lack of oxygen in water-saturated peat inhibits phenol oxidase activity, and, thus, leads to the accumulation of soluble phenolic compounds in the peatland, which, in turn, interact with proteins and inhibit microbial activity (Freeman et al., 2001, 2004). In this study, the relative weight was used to determine that the soluble phenolic compounds play an important role in driving changes in the CO_2 emission rate. Further, a significant negative correlation was found between the phenolic compound concentrations and CO_2 emission rates, which is consistent with the findings of Fenner and Freeman (2011) in peatland ecosystems. The results show that warming significantly reduces the phenolic concentration of *V. uliginosum*'s litter, resulting in higher CO_2 emissions.

The response of *V. uliginosum*'s litter decomposition to warming varied with the litter positions. Under the no-mixing treatment, warming significantly decreased the CO_2 emissions rate by 38.8% but an insignificant decrease of 1.9% was observed

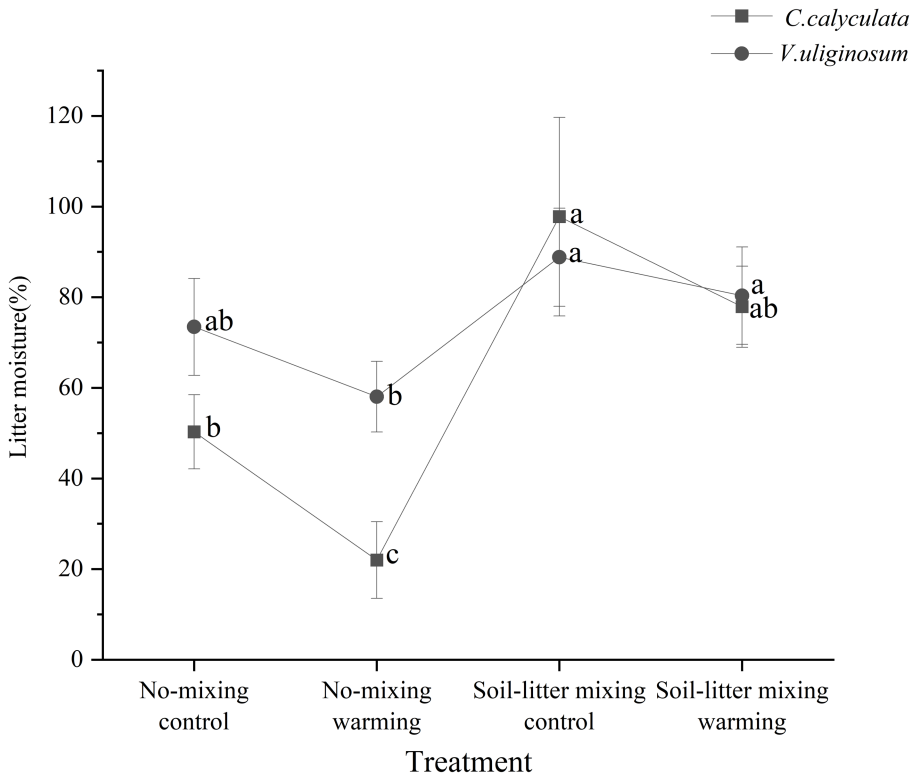

FIGURE 6
The moisture content of *C. calyculata* (square) and *V. uliginosum* (circle) litter at the end of the incubation. The letters represent significant differences among the four treatments (Bonferroni multiple comparison tests, $p<0.05$). The error bars indicate the standard deviation.

under-litter mixing. Laccase and the phenolic compounds were important factors influencing the decomposition of *V. uliginosum*'s litter (Zhao et al., 2019; Fenner and Freeman, 2020). The oxidase activities are limited by oxygen under soil-litter mixing (Ellis et al., 2009), partly counteracting the positive response of laccase activity to warming. Thus, compared with no-mixing, warming did not significantly increase laccase activities under the soil-litter mixing treatment, in turn, leading to a stronger response of the phenolic compounds to warming in the no-mixing treatment than that in the soil-litter mixing treatment.

Differences in the CO_2 emission rates between the species

Litter quality is considered to be an important factor that directly affects the decomposition rate at the regional and global scales (Aerts, 1997). It is commonly accepted that litter with high N concentrations and low C/N is easily decomposed (Hong et al., 2021). The tissue N content is a major factor that controls the rate of litter decomposition on a global scale, and the rate of decay of the soil organic matter is usually positively correlated with the effectiveness of N (Zhang et al., 2008). Decomposers tend to increase following relatively strict stoichiometric requirements (Cleveland and Liptzin, 2007), and higher litter quality (low C/N) will support a higher total microbial biomass and, correspondingly, have more bacteria (Bray et al., 2012). In high N litter, more resources may be allocated to C-acquiring enzymes such as cellulases, resulting in higher C decomposition rates in low C/N litter (Tan et al., 2020). In this study, we found that the deciduous shrub of *V. uliginosum* had higher N content and lower C/N than those of the evergreen shrub *C. calyculata*. These differences resulted in the CO_2 emission rate of *V. uliginosum* being significantly higher than that of *C. calyculata*. Similarly, the observations of the decomposition of two dominant plants in a typical alpine tundra ecosystem showed that low N content and high C/N resulted in lower decomposition rates and soil respiration (Zhang, Y. J. et al., 2022).

Conclusion

Based on a 124-day incubation experiment, this study focused on the differences in the response of evergreen and deciduous shrub litter to warming, litter positions, and their interactions. Warming and litter positions significantly altered

the CO_2 emission rates of *C. calyculata* and *V. uliginosum*. More importantly, soil-litter mixing significantly restrained the warming-induced positive effects on the CO_2 emission rates of *C. calyculata* and *V. uliginosum* when compared to no-mixing. The observed negative effects of *C. calyculata* were stronger than those of *V. uliginosum*. Exploring different plant leaf litter in peatland ecosystems in response to warming and decomposition positions may help broaden our understanding of the contribution of peatland ecosystems to terrestrial C sinks. There is also a need to expand this work from the laboratory to the field to confirm these laboratory-based findings in future research.

Data availability statement

The original contributions presented in the study are included in the article/supplementary material, further inquiries can be directed to the corresponding authors.

Author contributions

XW developed the theoretical consideration and planned the study. YD and JJ were responsible for the sample collection. XW and XS provides funding. GM wrote the manuscript. All authors contributed to reviewing the analyses and the final text.

Funding

The work was supported by the National Natural Science Foundation of China no. 41971143, 42271111 and 41861134029.

Acknowledgments

We wish to acknowledge Zhenling Gao for the field work and Jinli Gao for the laboratory analyses.

Conflict of interest

The authors declare that the research was conducted in the absence of any commercial or financial relationships that could be construed as a potential conflict of interest.

The AE IBN and RE1 GZ declared a shared affiliation with the authors XW and YD at the time of review.

Publisher's note

All claims expressed in this article are solely those of the authors and do not necessarily represent those of their affiliated organizations, or those of the publisher, the editors and the reviewers. Any product that may be evaluated in this article, or claim that may be made by its manufacturer, is not guaranteed or endorsed by the publisher.

References

Aerts, R. J. O. (1997). Climate, leaf litter chemistry and leaf litter decomposition in terrestrial ecosystems: A triangular relationship. *Oikos* 79, 439–449. doi: 10.2307/3546886

Aerts, R. (2006). The freezer defrosting: Global warming and litter decomposition rates in cold biomes. *J. Ecol.* 94, 713–724. doi: 10.1111/j.1365-2745.2006.01142.x

Allison, S. D., Wallenstein, M. D., and Bradford, M. A. (2010). Soil-carbon response to warming dependent on microbial physiology. *Nat. Geosci.* 3, 336–340. doi: 10.1038/ngeo846

Bärlocher, F., Gessner, M. O., and Garca, M. (2020). *Methods to study litter decomposition: A practical guide*. Dordrecht: Springer.

Boyero, L., Pearson, R. G., Gessner, M. O., Barmuta, L. A., Ferreira, V., Graça, M. A., et al. (2011). A global experiment suggests climate warming will not accelerate litter decomposition in streams but might reduce carbon sequestration. *Ecol. Lett.* 14, 289–294. doi: 10.1111/j.1461-0248.2010.01578.x

Bray, S. R., Kitajima, K., and Mack, M. C. (2012). Temporal dynamics of microbial communities on decomposing leaf litter of 10 plant species in relation to decomposition rate. *Soil Biol. Biochem.* 49, 30–37. doi: 10.1016/j.soilbio.2012.02.009

Butenschoen, O., Scheu, S., and Eisenhauer, N. (2011). Interactive effects of warming, soil humidity and plant diversity on litter decomposition and microbial activity. *Soil Biol. Biochem.* 43, 1902–1907. doi: 10.1016/j.soilbio.2011.05.011

Cardenas, R. E., Hattenschwiler, S., Valencia, R., Argoti, A., and Dangles, O. (2015). Plant herbivory responses through changes in leaf quality have no effect on subsequent leaf-litter decomposition in a neotropical rain forest tree community. *New Phytol.* 207, 817–829. doi: 10.1111/nph.13368

Chen, J., Luo, Y. Q., Xia, J. Y., Jiang, L. F., Zhou, X. H., Lu, M., et al. (2015). Stronger warming effects on microbial abundances in colder regions. *Sci. Rep.* 5:18032. doi: 10.1038/srep18032

Chen, N., Song, C. C., Xu, X. F., Wang, X. W., Cong, N., Jiang, P. P., et al. (2021). Divergent impacts of atmospheric water demand on gross primary productivity in three typical ecosystems in China. *Agric. For. Meteorol.* 307:108527. doi: 10.1016/j.agrformet.2021.108527

Cleveland, C. C., and Liptzin, D. (2007). C: N: P stoichiometry in soil: is there a "Redfield ratio" for the microbial biomass? *Biogeochemistry* 85, 235–252. doi: 10.1007/s10533-007-9132-0

Clymo, R. (1984). The limits to peat bog growth. *Biol. Sci.* 303, 605–654.

Corteselli, E. M., Burtis, J. C., Heinz, A. K., and Yavitt, J. B. (2017). Leaf litter fuels Methanogenesis throughout decomposition in a forested peatland. *Ecosystems* 20, 1217–1232. doi: 10.1007/s10021-016-0105-9

Dieleman, C. M., Branfireun, B. A., McLaughlin, J. W., and Lindo, Z. (2015). Climate change drives a shift in peatland ecosystem plant community: Implications for ecosystem function and stability. *Globl. Change Biol.* 21, 388–395. doi: 10.1111/gcb.12643

Eichlerova, I., Snajdr, J., and Baldrian, P. (2012). Laccase activity in soils: Considerations for the measurement of enzyme activity. *Chemosphere* 88, 1154–1160. doi: 10.1016/j.chemosphere.2012.03.019

Ellis, T., Hill, P. W., Fenner, N., Williams, G. G., Godbold, D., and Freeman, C. (2009). The interactive effects of elevated carbon dioxide and water table draw-down on carbon cycling in a Welsh ombrotrophic bog. *Ecol. Eng.* 35, 978–986. doi: 10.1016/j.ecoleng.2008.10.011

Elmendorf, S. C., Henry, G. H. R., Hollister, R. D., Bjork, R. G., Boulanger-Lapointe, N., Cooper, E. J., et al. (2012). Plot-scale evidence of tundra vegetation change and links to recent summer warming. *Nat. Clim. Chang.* 2, 453–457. doi: 10.1038/nclimate1465

Erdenebileg, E., Ye, X. H., Wang, C. W., Huang, Z. Y., Liu, G. F., and Cornelissen, J. H. C. (2018). Positive and negative effects of UV irradiance explain interaction of litter position and UV exposure on litter decomposition and nutrient dynamics in a semi-arid dune ecosystem. *Soil Biol. Biochem.* 124, 245–254. doi: 10.1016/j.soilbio.2018.06.013

Fenner, N., and Freeman, C. (2011). Drought-induced carbon loss in peatlands. *Nat. Geosci.* 4, 895–900. doi: 10.1038/ngeo1323

Fenner, N., and Freeman, C. (2020). Woody litter protects peat carbon stocks during drought. Nature. *Climate Change* 10:363. doi: 10.1038/s41558-020-0727-y

Ferreira, V., Chauvet, E., and Canhoto, C. (2015). Effects of experimental warming, litter species, and presence of macroinvertebrates on litter decomposition and associated decomposers in a temperate mountain stream. *Can. J. Fish. Aquat. Sci.* 72, 206–216. doi: 10.1139/cjfas-2014-0119

Freeman, C., Fenner, N., Ostle, N. J., Kang, H., Dowrick, D. J., Reynolds, B., et al. (2004). Export of dissolved organic carbon from peatlands under elevated carbon dioxide levels. *Nature* 430, 195–198. doi: 10.1038/nature02707

Freeman, C., Ostle, N., and Kang, H. (2001). An enzymic 'latch' on a global carbon store - a shortage of oxygen locks up carbon in peatlands by restraining a single enzyme. *Nature* 409:149. doi: 10.1038/35051650

Gao, S. Q., Song, Y. Y., Song, C. C., Wang, X. W., Ma, X. Y., Gao, J. L., et al. (2022). Effects of temperature increase and nitrogen addition on the early litter decomposition in permafrost peatlands. *Catena* 209:105801. doi: 10.1016/j.catena.2021.105801

Hewins, D. B., Archer, S. R., Okin, G. S., McCulley, R. L., and Throop, H. L. (2013). Soil-litter mixing accelerates decomposition in a Chihuahuan Desert grassland. *Ecosystems* 16, 183–195. doi: 10.1007/s10021-012-9604-5

Hewins, D. B., Sinsabaugh, R. L., Archer, S. R., and Throop, H. L. (2017). Soil-litter mixing and microbial activity mediate decomposition and soil aggregate formation in a sandy shrub-invaded Chihuahuan Desert grassland. *Plant Ecol.* 218, 459–474. doi: 10.1007/s11258-017-0703-4

Hong, J. T., Lu, X. Y., Ma, X. X., and Wang, X. D. (2021). Five-year study on the effects of warming and plant litter quality on litter decomposition rate in a Tibetan alpine grassland. *Sci. Total Environ.* 750:142306. doi: 10.1016/j.scitotenv.2020.142306

Hough, M., McCabe, S., Vining, S. R., Pedersen, E. P., Wilson, R. M., Lawrence, R., et al. (2022). Coupling plant litter quantity to a novel metric for litter quality explains C storage changes in a thawing permafrost peatland. *Globl. Change Biol.* 28, 950–968. doi: 10.1111/gcb.15970

Kechavarzi, C., Dawson, Q., and Leeds-Harrison, P. B. (2010). Physical properties of low-lying agricultural peat soils in England. *Geoderma* 154, 196–202. doi: 10.1016/j.geoderma.2009.08.018

LeBreton, J. M., and Tonidandel, S. (2008). Multivariate relative importance: extending relative weight analysis to multivariate criterion spaces. *J. Appl. Psychol.* 93, 329–345. doi: 10.1037/0021-9010.93.2.329

Lee, H., Fitzgerald, J., Hewins, D. B., McCulley, R. L., Archer, S. R., Rahn, T., et al. (2014). Soil moisture and soil-litter mixing effects on surface litter decomposition: A controlled environment assessment. *Soil Biol. Biochem.* 72, 123–132. doi: 10.1016/j.soilbio.2014.01.027

Liu, G. D., Sun, J. F., Tian, K., Xiao, D. R., and Yuan, X. Z. (2017). Long-term responses of leaf litter decomposition to temperature, litter quality and litter mixing in plateau wetlands. *Freshw. Biol.* 62, 178–190. doi: 10.1111/fwb.12860

Luan, J. W., Wu, J. H., Liu, S. R., Roulet, N., and Wang, M. (2019). Soil nitrogen determines greenhouse gas emissions from northern peatlands under concurrent warming and vegetation shifting. *Commun. Biol.* 2:132. doi: 10.1038/s42003-019-0370-1

Mao, R., Zhang, X. H., Song, C. C., Wang, X. W., and Finnegan, P. M. (2018). Plant functional group controls litter decomposition rate and its temperature sensitivity: An incubation experiment on litters from a boreal peatland in Northeast China. *Sci. Total Environ.* 626, 678–683. doi: 10.1016/j.scitotenv.2018.01.162

McLaren, J. R., Buckeridge, K. M., van de Weg, M. J., Shaver, G. R., Schimel, J. P., and Gough, L. (2017). Shrub encroachment in Arctic tundra: Betula nana effects on above- and belowground litter decomposition. *Ecology* 98, 1361–1376. doi: 10.1002/ecy.1790

Meyer, N., Xu, Y., Karjalainen, K., Adamczyk, S., Biasi, C., van Delden, L., et al. (2022). Living, dead, and absent trees-how do moth outbreaks shape small-scale patterns of soil organic matter stocks and dynamics at the subarctic mountain birch treeline? *Globl. Change Biol.* 28, 441–462. doi: 10.1111/gcb.15951

Moore, T., and Basiliko, N. (2006). "Decomposition in boreal peatlands," in *Boreal Peatland Ecosystems* (Berlin: Springer-Verlag), 125–143.

Rinkes, Z. L., Sinsabaugh, R. L., Moorhead, D. L., Grandy, A. S., and Weintraub, M. N. (2013). Field and lab conditions alter microbial enzyme and biomass dynamics driving decomposition of the same leaf litter. *Front. Microbiol.* 4:260. doi: 10.3389/fmicb.2013.00260

Robertson, G. P., Wedin, D., Groffman, P., Blair, J., Holland, E., Nedelhoffer, K., et al. (1999). "Soil carbon and nitrogen availability. Nitrogen mineralization, nitrification and soil respiration potentials," in *Standard Soil Methods for Long-Term Ecological Research*. eds. G. P. Robertson, C. S. Bledsoe, D. C. Coleman and P. Sollins (New York: Oxford University Press Oxford University Press), 258–271.

Schneider, T., Keiblinger, K. M., Schmid, E., Sterflinger-Gleixner, K., Ellersdorfer, G., Roschitzki, B., et al. (2012). Who is who in litter decomposition? Metaproteomics reveals major microbial players and their biogeochemical functions. *ISME J.* 6, 1749–1762. doi: 10.1038/ismej.2012.11

Siegenthaler, A., Buttler, A., Bragazza, L., van der Heijden, E., Grosvernier, P., Gobat, J. M., et al. (2010). Litter- and ecosystem-driven decomposition under elevated CO2 and enhanced N deposition in a sphagnum peatland. *Soil Biol. Biochem.* 42, 968–977. doi: 10.1016/j.soilbio.2010.02.016

Sistla, S. A., Moore, J. C., Simpson, R. T., Gough, L., Shaver, G. R., and Schimel, J. P. (2013). Long-term warming restructures Arctic tundra without changing net soil carbon storage. *Nature* 497:615. doi: 10.1038/nature12129

Song, Y. Y., Song, C. C., Hou, A. X., Ren, J. S., Wang, X. W., Cui, Q., et al. (2018). Effects of temperature and root additions on soil carbon and nitrogen mineralization in a predominantly permafrost peatland. *Catena* 165, 381–389. doi: 10.1016/j.catena.2018.02.026

Song, Y., Zou, Y. C., Wang, G. P., and Yu, X. F. (2017). Altered soil carbon and nitrogen cycles due to the freeze-thaw effect: A meta-analysis. *Soil Biol. Biochem.* 109, 35–49. doi: 10.1016/j.soilbio.2017.01.020

Strakova, P., Penttila, T., Laine, J., and Laiho, R. (2012). Disentangling direct and indirect effects of water table drawdown on above- and belowground plant litter decomposition: Consequences for accumulation of organic matter in boreal peatlands. *Globl. Change Biol.* 18, 322–335. doi: 10.1111/j.1365-2486.2011.02503.x

Tan, X. P., Machmuller, M. B., Huang, F., He, J. H., Chen, J., Cotrufo, M. F., et al. (2020). Temperature sensitivity of ecoenzyme kinetics driving litter decomposition: the effects of nitrogen enrichment, litter chemistry, and decomposer community. *Soil Biol. Biochem.* 148:107878. doi: 10.1016/j.soilbio.2020.107878

Throop, H. L., and Archer, S. R. (2007). Interrelationships among shrub encroachment, land management, and litter decomposition in a semidesert grassland. *Ecol. Appl.* 17, 1809–1823. doi: 10.1890/06-0889.1

Yang, K., Zhu, J. J., Zhang, W. W., Zhang, Q., Lu, D. L., Zhang, Y. K., et al. (2022). Litter decomposition and nutrient release from monospecific and mixed litters: Comparisons of litter quality, fauna and decomposition site effects. *J. Ecol.* 110, 1673–1686. doi: 10.1111/1365-2745.13902

Yu, Z. C., Loisel, J., Brosseau, D. P., Beilman, D. W., and Hunt, S. J. (2010). Global peatland dynamics since the last glacial maximum. *Geophys. Res. Lett.* 37:L13402. doi: 10.1029/2010gl043584

Zhang, D. Q., Hui, D. F., Luo, Y. Q., and Zhou, G. Y. (2008). Rates of litter decomposition in terrestrial ecosystems: global patterns and controlling factors. *J. Plant Ecol.* 1, 85–93. doi: 10.1093/jpe/rtn002

Zhang, Y. J., Jin, Y. H., Xu, J. W., He, H. S., Tao, Y., Yang, Z. P., et al. (2022). Effects of exogenous N and endogenous nutrients on alpine tundra litter decomposition in an area of high nitrogen deposition. *Sci. Total Environ.* 805:150388. doi: 10.1016/j.scitotenv.2021.150388

Zhang, Y., Song, C., Wang, X., Chen, N., Zhang, H., Du, Y., et al. (2022). Warming effects on the flux of CH4 from peatland mesocosms are regulated by plant species composition: Richness and functional types. *Sci. Total Environ.* 806:150831. doi: 10.1016/j.scitotenv.2021.150831

Zhang, X. H., Wang, X. W., Finnegan, P. M., Tan, W. W., and Mao, R. (2019). Effects of litter mixtures on aerobic decomposition rate and its temperature sensitivity in a boreal peatland. *Geoderma* 354:113890. doi: 10.1016/j.geoderma.2019.113890

Zhang, X. H., Zhang, Y. H., Jiang, S. S., Song, C. C., Zhang, J. B., and Mao, R. (2022). Dominant species and evenness level co-regulate litter mixture decomposition in a boreal peatland. *Plant Soil* 474, 423–436. doi: 10.1007/s11104-022-05346-z

Zhao, Y. P., Xiang, W., Yan, S., Huang, Y. B., and Fan, W. G. (2019). Laccase activity in sphagnum-dominated peatland: A study based on a novel measurement of delay dynamics (MDD) for determining laccase activity. *Soil Biol. Biochem.* 133, 108–115. doi: 10.1016/j.soilbio.2019.03.003

Zhao, L., Yebra, M., van Dijk, A., Cary, G. J., Matthews, S., and Sheridan, G. (2021). The influence of soil moisture on surface and sub-surface litter fuel moisture simulation at five Australian sites. *Agric. For. Meteorol.* 298–299:108282. doi: 10.1016/j.agrformet.2020.108282

frontiers | Frontiers in Ecology and Evolution

TYPE Original Research
PUBLISHED 19 January 2023
DOI 10.3389/fevo.2023.1113802

OPEN ACCESS

EDITED BY
Zhongqing Yan,
Chinese Academy of Forestry, China

REVIEWED BY
Dehua Mao,
Northeast Institute of Geography and Agroecology (CAS), China
Lie Yang,
Wuhan University of Technology, China

*CORRESPONDENCE
Jia Wang
✉ wangjia2009@bjfu.edu.cn

SPECIALTY SECTION
This article was submitted to Population, Community, and Ecosystem Dynamics, a section of the journal Frontiers in Ecology and Evolution

RECEIVED 01 December 2022
ACCEPTED 04 January 2023
PUBLISHED 19 January 2023

CITATION
Chen Y, Sun L, Xu J, Liang B, Wang J and Xiong N (2023) Wetland vegetation changes in response to climate change and human activities on the Tibetan Plateau during 2000–2015.
Front. Ecol. Evol. 11:1113802.
doi: 10.3389/fevo.2023.1113802

Wetland vegetation changes in response to climate change and human activities on the Tibetan Plateau during 2000–2015

Yuhan Chen[1,2], Lu Sun[1,2], Jiangqi Xu[1,2], Boyi Liang[1,2], Jia Wang[1,2]* and Nina Xiong[1,2]

[1]Institute of Geographic Information System (GIS), Remote Sensing (RS), and Global Positioning System (GPS), Beijing Forestry University, Beijing, China, [2]Beijing Key Laboratory of Precise Forestry, Beijing Forestry University, Beijing, China

The Tibetan Plateau (TP), known as the third pole, is the highest plateau in the world. It has numerous wetlands, which are important ecological security barriers and plays an important role in mitigating global climate change. This paper employed breaks for additive seasonal and trend (BFAST) algorithm for the mutation detection of the monthly normalized difference vegetation index (NDVI) in wetlands. In addition, correlation analysis and residual analysis were used to study the response of climate change and human activities to NDVI of alpine wetland vegetation in the TP during 2000–2015. The results indicate that the NDVI showed a weak upward trend of 0.009/10a ($P < 0.05$) with the climate presenting a trend of dry heat development. The NDVI of the growing season was greatly affected by temperature factors with the highest correlation coefficient of 0.686 ($P < 0.01$). The temperature in the month before and solar radiation in the 3 months before also presented a time lag effect on NDVI, and their correlation coefficients were 0.574 ($P < 0.05$) and 0.636 ($P < 0.05$), respectively. Additionally, human activities may have a positive impact on the wetland after 2008. This study explored, for the first time, the NDVI variations of the dynamic wetland and their correlations with temperature, precipitation and solar radiation.

KEYWORDS

NDVI, climate change, human activities, the Tibetan Plateau, BFAST, correlation analysis

1. Introduction

With the process of global warming, ecosystems are affected by more and more natural and human factors. Studies have shown that climate variation can change vegetation coverage (Timoney et al., 2019; Wen et al., 2019; Rezaei and Gurdak, 2020; Goodwin et al., 2021). The Tibetan Plateau (TP) is an eco-sensitive area to climate change (Wei and Wu, 2021). Wetlands provide immense storage of carbon that, if released with climate shifts, could accelerate those changes (Mitsch et al., 2009). Climate change threatens terrestrial water storage and Himalayan plant species over the TP (Salick et al., 2014; Li et al., 2022). As the third pole, the TP has the largest wetland area in China, which may significantly affect the TP's vegetation (Yuan et al., 2014; Wang et al., 2020). The threat of climate change is considered to be a major factor that can affect the function and biogeochemistry of wetlands (Salimi et al., 2021). In the case of the Alpine wetland, it is vulnerable to low temperatures, strong evapotranspiration, large direct radiation and special ecological environments (including glaciers, frozen soils, deserts, meadows, etc.) (Kraaijenbrink et al., 2017; Dakhil et al., 2019; Wei and Wu, 2021).

Although the response of vegetation to climate change has become a hot topic of the research of the TP, most of them focus on grassland or forest ecosystems (Ding et al., 2013; Yi et al., 2014; Sun et al., 2016; Wang et al., 2016; Dakhil et al., 2019; Xiong et al., 2019). Therefore, in the context of climate variation, clarifying the response of wetland vegetation to climatic change in the TP is crucial.

For the study of wetland vegetation on the TP, Shen et al. (2022) (Kun et al., 2020) found that vegetation growth was influenced by temperature and precipitation, but the limitation is that the wetland extent in their research was fixed. A study (Xue et al., 2018) revealed that the wetlands on the TP have started to deteriorate. About 6.4% of their area has been lost from the 1970s to 2010s. In fact, wetland space is dynamic and changing. With this in mind, we discussed the vegetation cover status of the changing wetlands year by year.

For meteorological research, we not only discussed temperature and precipitation like others (Wang et al., 2011; Guo et al., 2014; Jiang et al., 2017; Shen et al., 2022), but also added solar radiation. The TP has abundant solar energy resources because of its high elevation (Wang and Qiu, 2009). Solar radiation plays a critical role in hydrological cycling, vegetation growth, climate, weather change, and so on (Yaghoubi and Sabzevari, 1996; Zhou et al., 2010; Yue and Huang, 2011; Colak et al., 2013). What's more, scholars have studied the time-lag effect of climate (Bao et al., 2014; Diao et al., 2021; Zuo et al., 2021). Richard and Poccard (1998) and Zhe and Zhang (2021) used correlation coefficients to investigate the relationship between climate and the Normalized Difference Vegetation Index (NDVI), attesting a time response of the current and previous months. Guo et al. (2014) also found the time-lag effect of NDVI response to climate change, while the study area was in the semiarid region of the TP. Currently, the time-lag effects are still poorly understood in alpine wetland vegetation.

The alpine wetland vegetation is facing more severe and variable climatic conditions as well as complex ecosystems. In this study, monthly NDVI data and various meteorological data from 2000 to 2015 were used to analyze the vegetation greenness of the wetlands in the TP for a long time series by the breaks for additive seasonal and trend (BFAST) model and other methods. The main objective of our investigation has been to reveal the tipping points (Lenton, 2013) of wetland greenness and climate in the new century, and to explain the extent of climate change and human activities on alpine vegetation. In addition, the time-lag effects of alpine vegetation on climate variables can be further discussed by investigating the temporal pattern in NDVI of the vegetation growing season. This research is expected to provide scientific reference for vegetation protection, ecological management and rational development in this area under the background of climate change.

2. Materials and methods

2.1. Study area

The Tibetan Plateau (26° 00′ 12″ N∼39° 46′ 50″ N, 73° 18′ 52″ E∼104° 46′ 59″ E) is located in the southwest of China (**Figure 1**), about 2,945 km long from east to west and 1,532 km long from north to south (Chen et al., 2021). Due to its high elevation, this region has quite cold winters, mild summers and large diurnal temperature variations (Xiong et al., 2019) and the solar radiation of the TP is relatively high (Zhou et al., 2010). The annual average temperature is approximately between −5 and 8°C (Xin et al., 2008; Wang and Han, 2012). The inter-annual variation in temperature on the TP is small but the diurnal variation is large (Kirillin et al., 2021; Zhang et al., 2021). Known as the water towers of Asia (Yao et al., 2022), however, most of the TP is an arid and semi-arid region with not much precipitation (Zhang et al., 2000). The annual precipitation on the TP is about 400 mm, and there are significant seasonal differences in precipitation (Wang and Han, 2012; Wang et al., 2021). Spring and winter are the driest seasons on the annual scale. The main land use type in the area is grassland, followed by forest (Tang et al., 2018).

2.2. Data

Land use data (Xu et al., 2021) were obtained through Google Earth Engine (GEE) platform with a spatial resolution of 30 m. The User's Accuracy (UA) of wetland for this data set is higher, with UA of 71.06%, compared with datasets like Globeland30, FROM-GLC, and GLC-FCS30 (UA of 52.23, 29.25, and 47.17%, respectively). What's more, the kappa coefficient for Asian reached 0.72 and the UA for the land use type of wetland reached 76.09%. In this paper, we yearly extracted the wetland and water body data from 2000 to 2015 as a mask for analyzing NDVI changes.

The vegetation index can reflect the vegetation cover, among which, NDVI is the best indicator to reflect the vegetation growth condition and vegetation cover. In this paper, the continuous time series SPOT/VEGETATION NDVI satellite remote sensing data were used to synthesize the 10 days NDVI data into monthly data by using the maximum-value composition (MVC) (Holben, 1986) technique, and was free downloaded from the Resource and Environment Data Cloud Platform, Chinese Academy of Sciences[1] with a 1 km resolution from 2000 to 2015 (Xu, 2018). In order to avoid the interference of non-vegetation information on the alpine wetland vegetation NDVI with reference (Yu et al., 2012; Ding et al., 2013; Kun et al., 2020) to the previous vegetation NDVI thresholds on the TP, the data in this research must meet certain requirements as follows: (1) the average value of NDVI in April-September shall be more than 0.10; (2) the value of NDVI shall exceed than 0; (3) the average value of NDVI in winter shall be less than 0.4; (4) June to October was selected as the length of growth season (LOG) for analyzing whether there is a hysteresis response of NDVI to climate.

The meteorological data used were monthly precipitation (Peng, 2020), temperature (Peng, 2019), and solar radiation (Feng and Wang, 2020) data from 2000 to 2015 from the National Tibetan Plateau/Third Pole Environment Data Center.[2] The spatial resolution of precipitation data and average temperature data is 1 km, and the resolution of solar radiation data is 10 km. For further comparing the impacts of seasonal climate factors on NDVI, we calculated the average values of climate factors during spring (March, April, and May), summer (June, July, and August), autumn (September, October, and November), and winter (December, January, and February).

1 http://www.resdc.cn

2 http://data.tpdc.ac.cn/zh-hans/

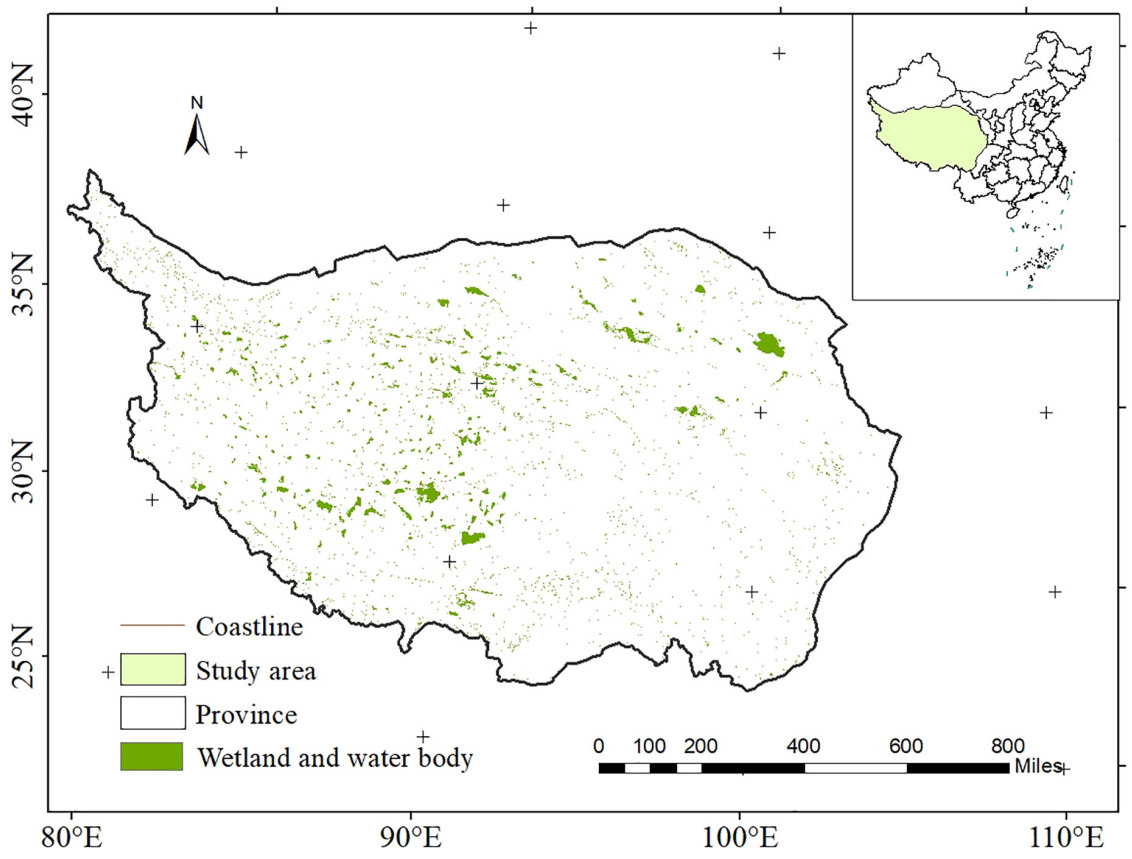

FIGURE 1
Location of the study area.

2.3. Methodology

2.3.1. Mutation detection

For this study, the BFAST algorithm was used to analyze the abrupt change characteristics of vegetation greenness in alpine wetlands between 2000 and 2015. BFAST was first proposed in 2010 to make vegetation disturbance identification well in remote sensing data identification (Verbesselt et al., 2010b), and now the algorithm is used in several fields (Wang et al., 2014; Fang et al., 2018; Gholamnia et al., 2019), including climate analysis, hydrological analysis, and economic analysis. In this study, the BFAST package in R statistical software is used to obtain the tipping points of monthly NDVI of wetlands on the TP from 2000 to 2015, which can provide an analysis of the effect of climate anomalies on vegetation greenness and also help to research whether there is a lag period in the effect of climate on vegetation greenness. Formula is as follows (Verbesselt et al., 2010a):

$$Y_t = T_t + S_t + e_t \, (t = 1, \ldots, n) \tag{1}$$

where Y_t is the observed data at time t; T_t is the fitted trend component; $S_t$is the fitted seasonal component; e_t is the remainder component; n is the total number of observed data. The BFAST procedures (Watts and Laffan, 2014) use a parameter known as h to determine the maximum number of breaks in the data set. This parameter can help in detecting trend changes. Following their work and the recommendations by Verbesselt et al. (2010b) and Fang et al. (2018), we hypothesized that the minimum interval between adjacent abrupt changes was approximately 2 years within a 16-year time series (2000–2015) in this study, therefore, h = 0.13 was used. Besides, the "harmonic" seasonal model was chosen for natural vegetation, while the "dummy" model is often used for cropland (Verbesselt et al., 2010a).

What's more, based on the correlation between climate and NDVI, we used the Mann–Kendall mutation test (Kendall, 1938; Shadmani et al., 2012) to calculate the tipping points in meteorology and verify the wetland vegetation changes in response to climate change.

2.3.2. Correlation analysis

Pearson's correlation coefficients were calculated for examining the relationship between NDVI (during vegetation growing season, from June to October) and precipitation, average temperature, solar radiation in the current month, the first month before, the first 2 months before and the first 3 months before. This research used this common method of testing correlation to analyze the time lag effect of vegetation response to climate. The calculation steps are as follows (Xiong et al., 2019):

$$r = \frac{cov(x, y)}{\sqrt{cov(x, x)cov(y, y)}} \tag{2}$$

where r is the linear correlation coefficient; cov is the covariance; x is the NDVI value; y is the precipitation (mm), temperature (°C), or solar radiation (W/m^2). The value of r ranges from −1 to l, and the larger the absolute value, the higher the degree of correlation.

If $r < 0$, it indicates that the index promotes NDVI; otherwise, it inhibits NDVI.

2.3.3. Residual analysis

One of the most important factors that can affect the vegetation of a region is climate change. The residual analysis method can also separate the effects of human activities from those caused by environmental changes (Evans and Geerken, 2004). The predicted value of NDVI is fitted by meteorological factors, which is the amount of climate change impact. The difference between the calculated value and the true value of NDVI can be considered as the influence of human factors. This method is called residual analysis and has been widely used (Herrmann et al., 2005; Higginbottom and Symeonakis, 2014; Fernández-Giménez et al., 2017; Jiang et al., 2017; Chu et al., 2019). It can be presented using the following equation:

$$\varepsilon = NDVI_{real} - NDVI_{pre} \quad (3)$$

where ε is the NDVI residual; $NDVI_{real}$ is the true value of NDVI; $NDVI_{pre}$ is the predicted value of NDVI. If $\varepsilon > 0$, it indicates that human activities have a positive impact; If $\varepsilon < 0$, it indicates human activities produce negative effects; if $\varepsilon = 0$, indicating that the impact of human activities is relatively weak. If the residuals trend is significant, the NDVI variations can be explained by human activities (Jiang et al., 2017; Chu et al., 2019).

3. Results

3.1. Analysis of vegetation greenness changes in alpine wetlands

As shown in **Figure 2**, the NDVI of wetland vegetation in the TP was relatively small and changed gently until May, generally between 0.1 and 0.2. After May, the surface vegetation in the region increased rapidly, reaching a maximum in July and August. Then, it gradually decreased and dropped below 0.2. It can be seen that the growing season of wetland vegetation in the TP was more consistent with the description of vegetation in this region starting to germinate and grow in May and dying off by mid-late October in other article (Ding et al., 2013), indicating that the NDVI reflection of plant growth is consistent with other observations. Comparing **Figures 2A**, **B** the month-by-month trend of NDVI was approximately the same, but during the vegetation growing season, the values of NDVI in the wetland were significantly higher than the overall regional NDVI values. This may be due to the fact that a large area of the TP is covered with grassland vegetation, and wetlands have relatively sufficient water compared to arid grassland ecosystems, which promotes the growth of vegetation in wetland (Piao et al., 2007).

For interannual variability, the study found that the area of wetlands was constantly undergoing changes, from 1,069.16 in 2000 to 1,100.49 km^2 in 2015, increasing year by year. Not only the increase in wetland area, but also the increase of NDVI within the wetland area. The monthly NDVI values of wetlands in the TP from 2000 to 2015 were examined according to the BFAST model method, and in the overall time series analysis, the NDVI values showed an overall increasing trend. The trend was detected in the trend term, in which a tipping point was observed between 2013 and 2014 (**Figure 3**). Original time series (Y_t) and seasonal component (S_t) showed cyclic regular changes, indicating that vegetation is suitable for long-term monitoring and research. The dashed line in Tt represents the times of abrupt change in NDVI in the trend components. There was one break, which was in 2013 with the largest magnitude (−0.013). Time of the biggest change detected in the trend component was 165th data, corresponding to September in 2013, and the broad time range was from February 2013 to January 2014.

It can be seen from **Figure 4** that the annual mean NDVI of alpine wetland vegetation also showed a weak upward trend of 0.009/10a ($P < 0.05$). The mean NDVI in spring, summer and autumn also increased, on the contrary, the mean NDVI in winter showed a downward trend. This is also consistent with the NDVI change of the entire TP (Sun and Qin, 2016). The mean NDVI in autumn and winter varied greatly with R squared values of 0.01573 and 0.07625, respectively, and p values of 0.6435 and 0.3005, respectively. The mean NDVI values in spring ($P < 0.01$) were smaller than those in summer ($P < 0.01$), implying that the response of vegetation to climate may not be as pronounced. Summer is in the vegetation growing season, therefore, the reliability of this paper in studying the relationship between climatic factors and NDVI by using the vegetation growing season is further verified.

3.2. Analysis of climate change characteristics

There is no doubt that the climate in the TP has changed under the condition of global warming. The interannual and seasonal trends of temperature, precipitation and solar radiation in the wetlands of the TP from 2000 to 2015 are shown in **Figure 5**, and **Table 1** shows the statistical interannual and seasonal climate tendency rates of these meteorological elements.

The annual mean temperature of the wetlands was similar to the spring and autumn mean temperatures (all of them were around 0°C), displaying an increasing trend with a climatic tendency rate of 0.04, 0.27, and 0.13°C/10a, respectively. In contrast, the mean temperature in summer and winter showed a decreasing trend with a faster decrease in winter (−0.52°C/10a). In general, the warming in spring and autumn contributed more to the annual mean temperature change, giving a slightly increasing trend.

Precipitation was less in 2002, 2006, and 2015, not exceeding 130 mm, with more pronounced fluctuations. In general, it represented a decreasing trend with a climatic tendency rate of about −1.83 mm/10a. Except for summer, seasonal changes in precipitation could be seen as an overall decreasing trend, only with slightly different magnitudes, with the fastest decrease in spring (−1.67 mm/10a) and the slowest decrease in autumn (−0.14 mm/10a). Rainfall in winter was scarce, with a multi-year average of 4.75 mm, and also showed a decreasing trend (−0.3 mm/10a). Summer showed a slightly increasing trend with a climatic tendency rate of 0.27 mm/10a. Although precipitation in summer was an increasing trend, the increase was small and much less than the decrease in precipitation in other seasons. It is worth mentioning that the variation in precipitation was greater than the variation in temperature in each season, which may be due to changes in the monsoon system in East Asia (Wang et al., 2011).

Solar radiation displayed an increasing trend with a climatic tendency rate of about 2.27 W/m^2/10a. Unlike the seasonal overall

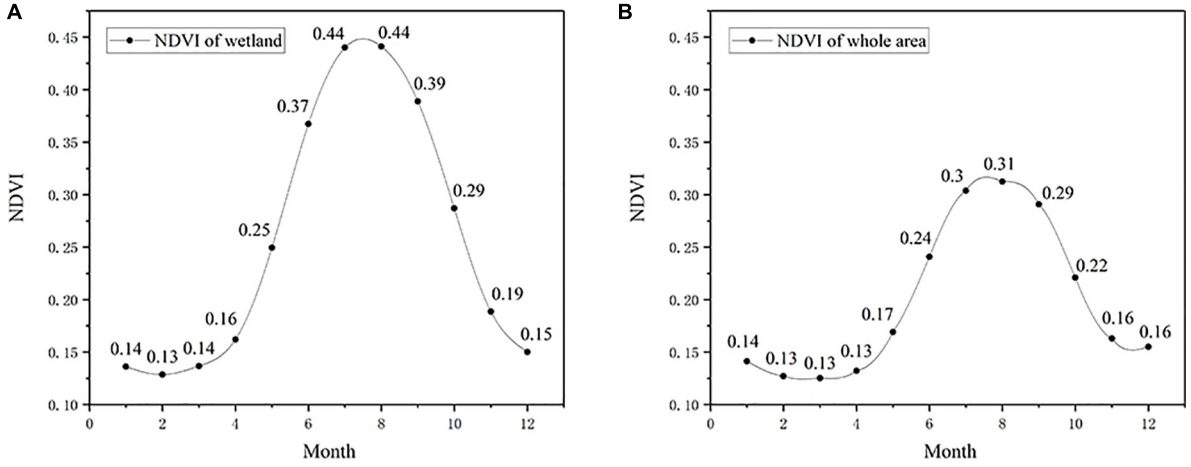

FIGURE 2
The multi-yearly seasonal variation for **(A)** averaged normalized difference vegetation index (NDVI) of wetland and **(B)** averaged NDVI in the TP.

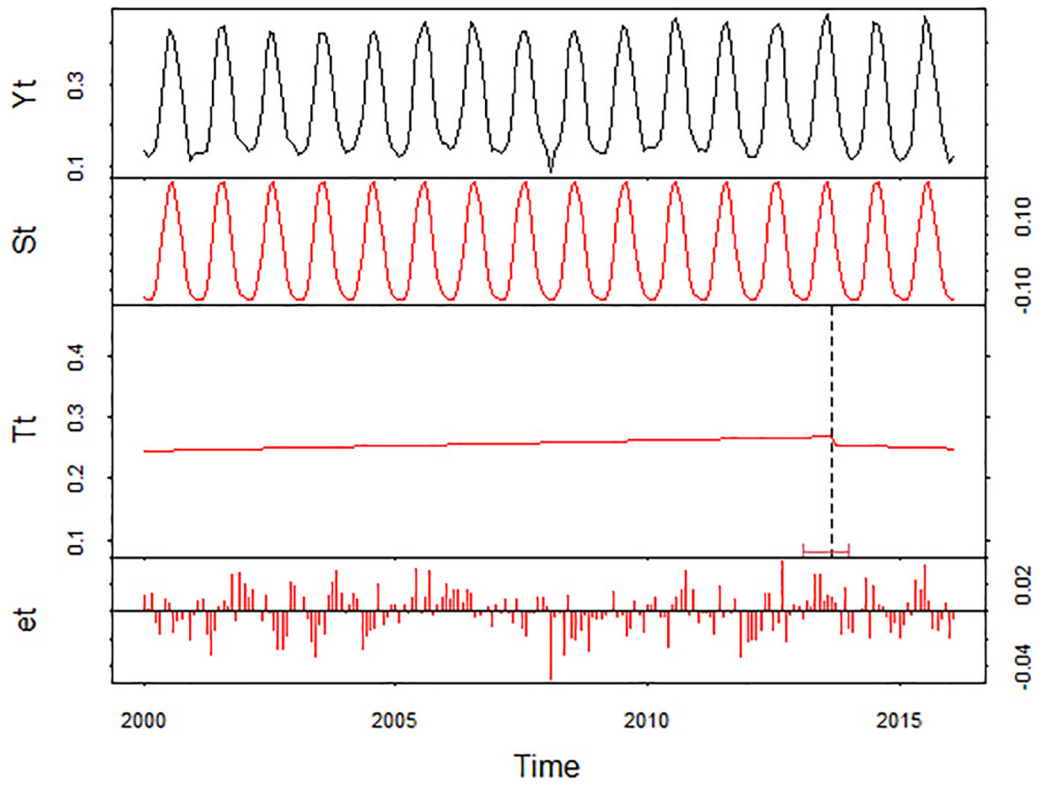

FIGURE 3
Breaks for additive seasonal and trend (BFAST) breakdown of normalized difference vegetation index (NDVI) time series for the 2000–2015 period for alpine wetland vegetation in TP.

decreasing trend in precipitation, the seasonal differences in solar radiation were more pronounced. There was a decreasing trend in autumn (−0.68 W/m^2/10a) and winter (−0.99 W/m^2/10a). Solar radiation exceeded 250 W/m^2 in both spring (1.51 W/m^2/10a) and summer (2.42 W/m^2/10a), and contributed more to the annual solar radiation variation.

In summary, the trends of the three meteorological elements show that climate change in the alpine wetlands of the TP had a tendency to develop toward dryness and heat.

3.3. Correlation analysis of NDVI and climatic factors

There is a correlation between climate and NDVI, which may be due to a certain degree of lag of vegetation growth on climate environment. For example, in case of heavy snowfall in winter or extreme drought in summer, the climate change in 1 month might affect the vegetation growth in the next month. The study found that the monthly average temperature, precipitation, and solar radiation

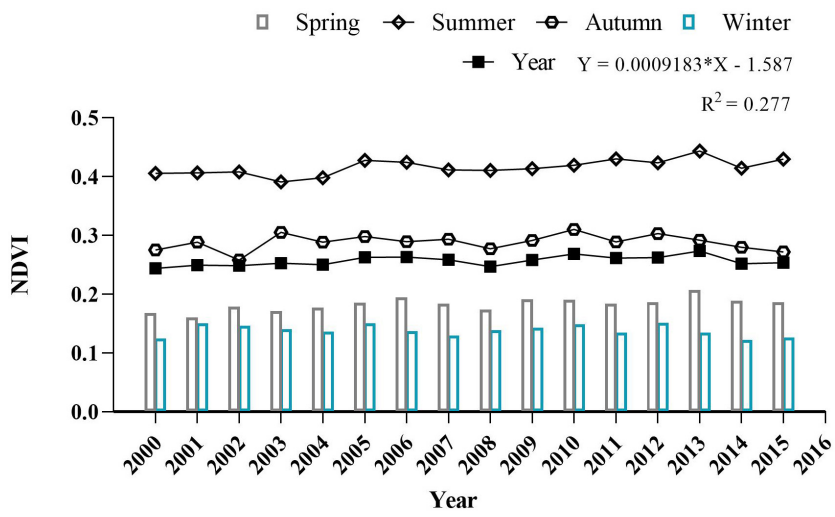

FIGURE 4
The change trend of normalized difference vegetation index (NDVI) of alpine wetland vegetation from 2000 to 2015.

of the wetlands in the TP from 2000 to 2015 were correlated with the monthly NDVI, and the results are shown in **Table 2**.

As seen in **Table 2**, the NDVI of alpine wetland vegetation in the TP was more influenced by the temperature factor, with the highest correlation coefficient of 0.686 ($P < 0.01$). The temperature of the current month and the temperature of the previous month were both strongly correlated with the NDVI of the growing season month. For correlation coefficients ranging from 0.6 to 0.8, it indicated that the recent temperature factor of the vegetation growing season positively influenced the NDVI. And from **Figure 6**, we can get that the value of the real NDVI was higher than the value of linear regression when the temperature of the month before the growing season is higher than 10°C or lower than 8°C.

In contrast to the temperature factor which was greatly affected by the current month, the effect of solar radiation on vegetation was greater as time goes forward. The effect of solar radiation on NDVI was greater in the third month ahead than in the other times, reaching 0.636 ($P < 0.01$), which was a positive correlation (**Figure 6C**). The effect of solar radiation on NDVI was weaker or even uncorrelated at other times.

Precipitation in the month prior to the growing season had a greater effect on NDVI than precipitation in the current month, but the influence was not as strong as temperature and solar radiation, reaching only 0.574 ($P < 0.01$), which is a moderate correlation. This is consistent with Wang et al.'s (2011) study, where the correlation of mean temperature influenced the variation of NDVI on a long time scale. It can be seen from the relationship between NDVI in the growing season and the precipitation of the previous month (**Figure 6B**) that the higher the precipitation, the better the vegetation growth.

The relationship between precipitation, temperature, solar radiation factors, and wetland NDVI on the TP shows that all three climatic factors have a positive effect on NDVI, and there is a degree of lag between vegetation growth and changes in the climatic environment. The tipping points in vegetation NDVI between 2013 and 2014 may be due to abnormal weather in the first few months of the vegetation growing season.

3.4. Analysis of the impact of human activities on NDVI

Residual analysis calculated the trend of human activities by the difference between the real NDVI and the regression-predicted NDVI. **Figure 7** plots the distribution of the residuals sorted by time. The statistical results demonstrate that there is an unclear positive trend. Before 2008, the residuals were mostly negative, indicating that human activities might have a negative impact on vegetation. Conversely, human activities gradually had a positive impact on vegetation after this period, but this impact was relatively minor. In general, the anthropogenic influence showed a continuing positive trend, while the wetland vegetation on the TP might still be mainly influenced by climate.

4. Discussion

4.1. Responses of vegetation to climate

It was found that the annual mean NDVI increased from 2000 to 2015, and the mean NDVI in spring, summer and autumn also showed an increasing trend (**Figure 4**). The annual average temperature increased, precipitation decreased, and solar radiation increased (**Table 1**). Based on the analysis, the ecological environment of the TP developed toward a favorable direction under the positive impact of climate change, which is in accordance with the previous study (Wang and Han, 2012).

Surprisingly, we found that various scholars had different findings about the trend of precipitation on the TP. Some scholars found that the average annual precipitation had a decreasing trend (Wang and Han, 2012; Zhang et al., 2016; Tang et al., 2018; Zhe and Zhang, 2021) while others believed that the TP was showing warm and humid development (Sun and Qin, 2016; Shen et al., 2022). There may be three possible reasons for this phenomenon: (1) Spatial differences. The whole TP was warm and humid overall (Sun and Qin, 2016), but there were rainfall differences in different

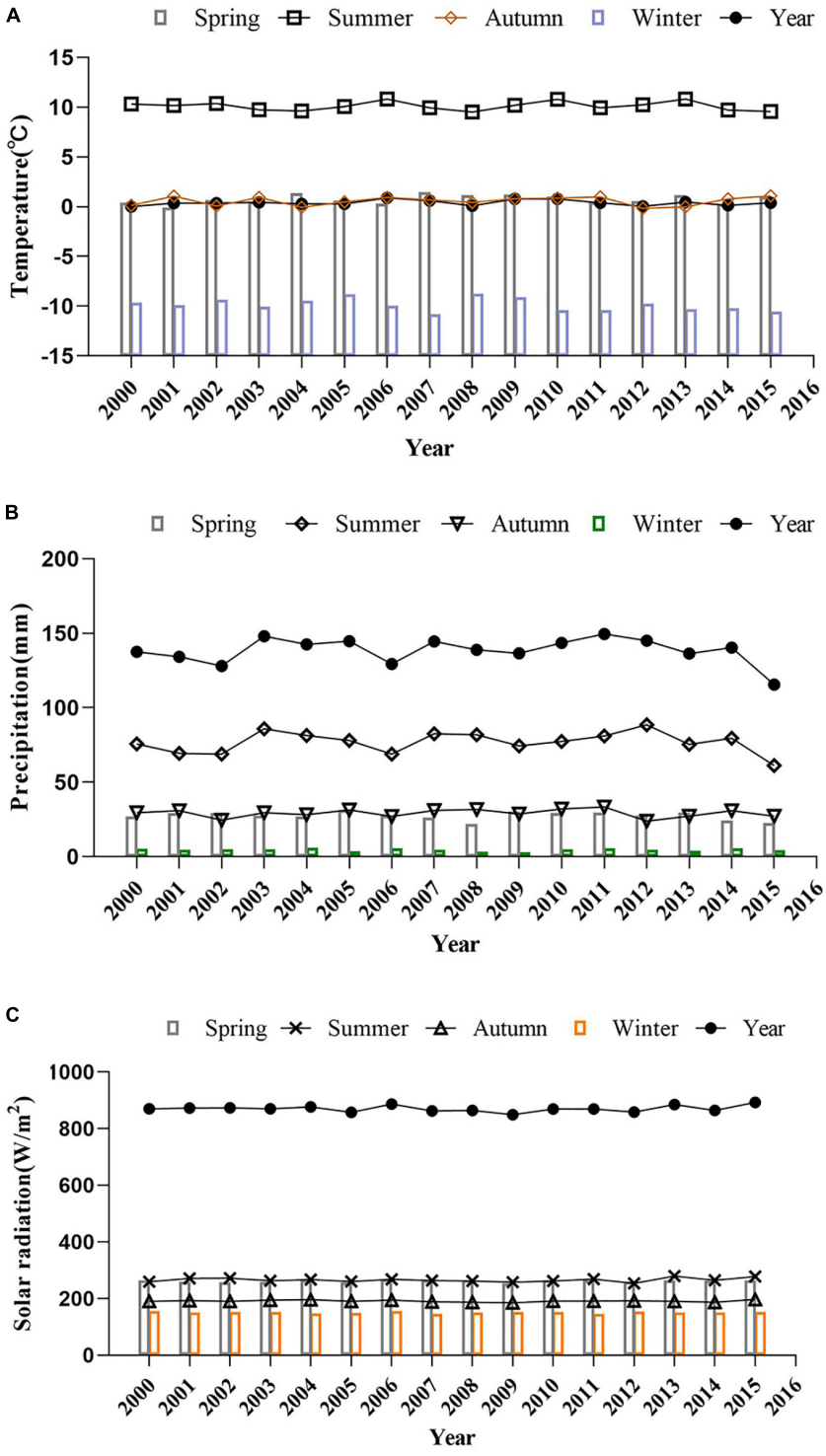

FIGURE 5
The change trend of **(A)** temperature, **(B)** precipitation, and **(C)** solar radiation from 2000 to 2015.

regions. (2) Temporal differences. Some scholars revealed a decline in precipitation by 2008 (Wang and Han, 2012; Zhang et al., 2016), while others found an increase by 2020 (Shen et al., 2022). (3) Vegetation species differences. Different types of vegetation may produce different sensitivities to climatic change. For example, from 2000 to 2017, the growing season precipitation of herbaceous marshes and seasonal brackish marshes on the TP showed an overall upward trend, while marshy meadows and inland salt marshes had a downward trend (Kun et al., 2020). Therefore, the present study area is the wetland area of the TP with a trend of dry heat development from 2000 to 2015.

Mutations may be associated with phenology, long term changes and a "remainder" component related to irregular short-term variations or noise (e.g., clouds or atmospheric scatter) (Lambert et al., 2015). The annual as well as the spring, the summer average NDVI reached the highest value within 16 years in 2013 (**Figure 4**).

TABLE 1 The climate tendency rate statistical results of climate factor from 2000 to 2015.

Time scale	Temperature		Precipitation		Solar radiation	
	Linear equation	R	Linear equation	R	Linear equation	R
Spring	$y = 0.027 \times x - 52.94$	0.28	$y = -0.167 \times x + 362.2$	0.30	$y = 0.151 \times x - 42.12$	0.19
Summer	$y = -0.005 \times x + 20.79$	0.06	$y = 0.027 \times x + 22.58$	0.02	$y = 0.242 \times x - 220.9$	0.17
Autumn	$y = 0.013 \times x - 24.97$	0.14	$y = -0.014 \times x + 57.08$	0.02	$y = -0.068 \times x + 327.6$	0.10
Winter	$y = -0.052 \times x + 95.10$	0.40	$y = -0.030 \times x + 64.72$	0.16	$y = -0.099 \times x + 350.3$	0.15
Year	$y = 0.004 \times x - 8.011$	0.07	$y = -0.183 \times x + 506.6$	0.10	$y = 0.227 \times x + 414.8$	0.10

TABLE 2 Lag analysis of climate factors in different months on normalized difference vegetation index (NDVI).

	Correlation coefficient			
	Current month	The month before	Two months before	Three months before
Temperature	0.686**	0.610**	0.274*	0.246
Precipitation	0.326**	0.574**	0.306*	0.003
Solar radiation	0.138	−0.054	0.286*	0.636**

Significant at $^{**}P < 0.01$ and $^{*}P < 0.05$ levels.

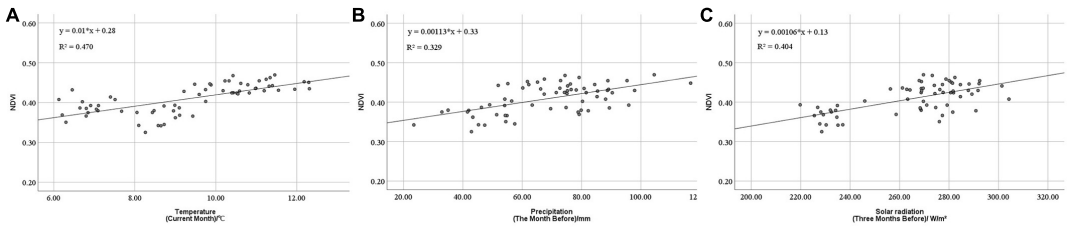

FIGURE 6
Relationship between the growing season normalized difference vegetation index (NDVI) of wetlands and climate in the TP from 2000 to 2015: **(A)** normalized difference vegetation index (NDVI) and temperature (the current month); **(B)** NDVI and precipitation (the month before); **(C)** NDVI and solar radiation (the 3 months before).

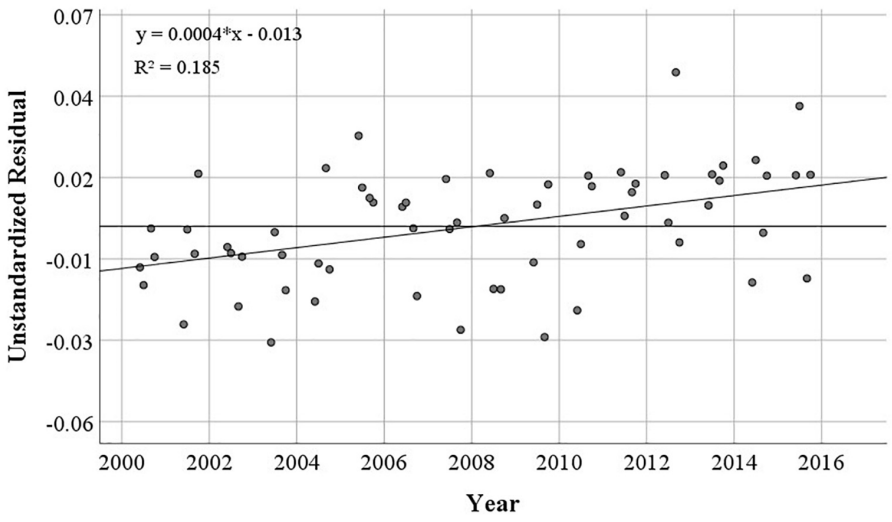

FIGURE 7
The temporal trend of unstandardized residuals.

The tipping point of NDVI was at this time. In 2013, the temperature was at a high value at the corresponding time and the vegetation growth was good due to the positive correlation between temperature and vegetation growth. The precipitation in spring was also at a high value, providing a good base for vegetation growth. The average monthly solar radiation in spring reached the second highest value within 15 years (264.77 W/m^2) and the highest value in summer (279.34 W/m^2). Adequate light ensured lush vegetation growth. In

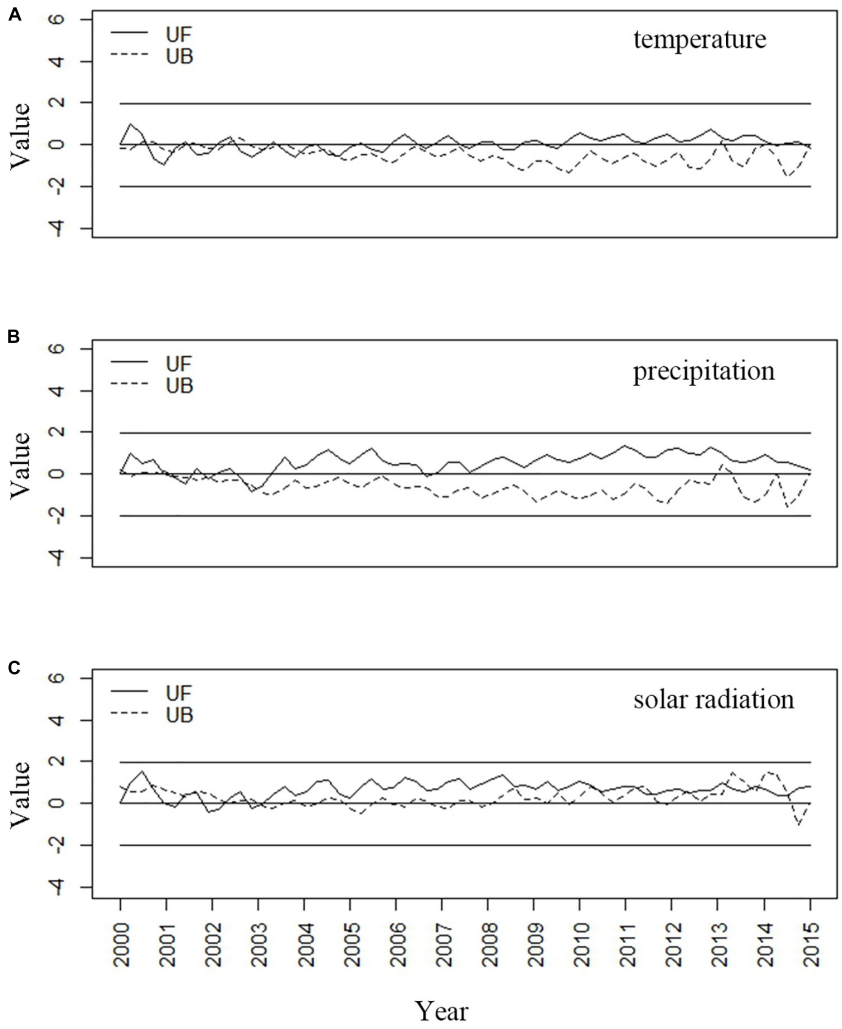

FIGURE 8
Mann–Kendall statistic curve of climate in vegetation growing season: **(A)** temperature (the current month); **(B)** precipitation (the month before); **(C)** solar radiation (the 3 months before).

the following 2 years, the precipitation and temperature decreased to a certain extent (**Figures 5A**, **B**), which may also lead to the vegetation growth being worse than that in 2013. Therefore, in BFAST detection, NDVI after 2013 has a downward trend.

The results of Mann–Kendall mutation test (**Figure 8**) showed that the changes in vegetation were approximately in line with the changes in meteorology. All three meteorological statistics had changes in 2013 (abrupt changes occurred when the UF and UB curves intersected). Among them, temperature and precipitation showed an increasing trend after a period of stability, with a trend of change after 2013, which was able to verify the abrupt change point of vegetation in 2013. For solar radiation, the UF and UB curves clearly intersected after 2013. Thus, the vegetation growth status changed equally when meteorological changes occurred, further proving that vegetation responds to climate.

4.2. Effect on vegetation greenness

The time lag effects of the vegetation responses to climates (**Table 2**) show significantly different lag effects of vegetation responses to different climatic factors. Consequently, there was a significant correlation ($P < 0.01$) between the temperature and the growing season NDVI of the wetland. The inapparent time lag effect of air temperature may be due to a fact: it is a natural law that air temperature varies seasonally. During the plant growing season, air temperature is a key trigger for certain vegetation growth periods, and vegetation follows the change of air temperature into different growth periods (Duo et al., 2017). Thus, there is an inconspicuous time lag effect of air temperature on plant growth at the monthly scale. At the same time, we found that NDVI of wetland on the TP was more sensitive to temperature, which is consistent with the findings of Shen et al. (2014), Sun and Qin (2016), and Wang et al. (2020). Without water shortage, the temperature was the primary factor limiting vegetation growth, and the influence of precipitation on vegetation growth was less important.

Precipitation and solar radiation have a time-lag effect on NDVI. The time lag of the vegetation responses to precipitation in wetlands is approximately 1 month. In line with the findings of Zhe and Zhang (2021), NDVI values were most correlated with the cumulative climate values of the current and previous months. The difference is that we found that the precipitation of the previous month has a

higher correlation with NDVI. For solar radiation, the more forward the time is, the higher the correlation is. The time lag to solar radiation is 3 months which matches the observed in earlier studies (Wu et al., 2015). Possibly because the solar radiation in spring and summer is relatively consistent, so compared with other regions, vegetation on the TP is exposed to sufficient solar radiation earlier for photosynthesis.

The NDVI of wetland vegetation on the TP shows an overall upward trend, indicating that the vegetation is growing more luxuriantly. The major climate-driven factors for vegetation growth are diverse and are closely related to vegetation characteristics and climatic conditions. For the wetland areas of the Tibetan Plateau, the temperature is the primary factor that drives vegetation growth. Within a certain temperature range, the higher the temperature, the better the vegetation growth condition. Higher temperatures and more rain can promote photosynthesis, maintaining the role of wetlands as carbon sinks (Salimi et al., 2021). It should be noted that enhanced evapotranspiration and permafrost degradation might create an imbalance in soil temperature, moisture, and nutrients, limiting the growth of alpine vegetation (Yi et al., 2014; Wang et al., 2016).

Meanwhile, The result of NDVI residual (**Figure 7**) indicates that human activities have little positive impact. This study confirms that the TP is relatively undisturbed by human activities (Li et al., 2022). Wetlands were degraded and reduced in size from 1967 to 2004 (Zhang et al., 2011), however, they have since grown in size, which may be caused by human activities. In terms of vegetation growth, we believe that it is mainly affected by climate.

Overall, this study provides a theoretical basis for revealing the time-lag effects of alpine wetland vegetation responses to climate, and the results hold significant value for the climate-based prediction of variations in vegetation growth in the future.

4.3. Limitations and future work

The current study in this paper may have certain uncertainties and shortcomings. Firstly, the remote sensing data used in this study may be affected by clouds, atmosphere, solar altitude angle, and other factors, so the uncertainty of the data itself may affect the research results of this paper. Secondly, the climate of the TP is complex. It is a debatable issue whether the wetlands on the TP are developing warm and humid or dry and hot. Our next plan anticipates expanding the study time to discuss climate change over a longer time scale. In addition, wetland vegetation species are diverse and the growth periods are not identical, and the meteorological effects on different wetland vegetation need to be further revealed. In order to more accurately reveal wetland vegetation changes and their mechanisms on the TP, future studies need to be further supported by more precise data and research methods.

5. Conclusion

Taking alpine wetlands in the TP as an example, this research used mutation detection, correlation analysis and residual analysis to study the relationship between climate change, human activities and vegetation. The conclusion are divided into four specific sections.

(1) The NDVI of wetlands on the TP showed a slight upward trend from 2000 to 2015, indicating an increase in vegetation greenness. The abrupt change in NDVI occurred between 2013 and 2014, and the NDVI values increased before the abrupt change and decreased after the abrupt change.
(2) Temperature (0.04°C/10a) and solar radiation (2.27 W/m2/10a) increased and precipitation (−1.83 mm/10a) decreased, which means the wetlands of the TP showed a trend of dry-heating. Climate change varies widely from season to season.
(3) NDVI of alpine wetland vegetation on the TP was strongly influenced by temperature factors. Precipitation in the first month before and solar radiation in the 3 months before were higher correlated with the NDVI of the vegetation growing season, reflecting the time-lag effect.
(4) NDVI residual values were both positive and negative, with an overall slight upward trend with time. Human activities may have little positive impact on wetland vegetation in the TP.

Data availability statement

Publicly available datasets were analyzed in this study. This data can be found here: http://www.resdc.cn and http://data.tpdc.ac.cn/zh-hans/.

Author contributions

YC and JW: conceptualization. YC, LS, and JX: methodology, formal analysis, and investigation. YC and JX: software. YC: validation, data curation, writing—original draft preparation, and visualization. YC and LS: resources. BL, LS, and JW: writing—review and editing. JW, BL, and NX: supervision. JW: project administration and funding acquisition. All authors have read and agreed to the published version of the manuscript.

Funding

This research was funded by The Second Tibetan Plateau Scientific Exploration (grant no. 2019QZKK0608) and National Natural Science Foundation of China (grant nos. 42171329 and 42077454).

Acknowledgments

This is a short text to acknowledge the contributions of specific colleagues, institutions, or agencies that aided the efforts of the authors.

Conflict of interest

The authors declare that the research was conducted in the absence of any commercial or financial relationships that could be construed as a potential conflict of interest.

Publisher's note

References

Bao, G., Qin, Z., Bao, Y., Zhou, Y., Li, W., and Sanjjav, A. (2014). NDVI-based long-term vegetation dynamics and its response to climatic change in the Mongolian Plateau. *Remote Sens.* 6, 8337–8358. doi: 10.3390/rs6098337

Chen, X., Wang, X., Feng, X., Zhang, X., and Luo, G. (2021). Ecosystem service trade-off and synergy on Qinghai-Tibet Plateau. *Geogr. Res* 40, 18–34. doi: 10.1016/j.jenvman.2021.112447

Chu, H., Venevsky, S., Wu, C., and Wang, M. (2019). NDVI-based vegetation dynamics and its response to climate changes at Amur-Heilongjiang River Basin from 1982 to 2015. *Sci. Total Environ.* 650, 2051–2062. doi: 10.1016/j.scitotenv.2018.09.115

Colak, I., Sagiroglu, S., Demirtas, M., and Yesilbudak, M. (2013). A data mining approach: Analyzing wind speed and insolation period data in Turkey for installations of wind and solar power plants. *Energy Conv. Manag.* 65, 185–197. doi: 10.1016/j.enconman.2012.07.011

Dakhil, M. A., Xiong, Q., Farahat, E. A., Zhang, L., Pan, K., Pandey, B., et al. (2019). Past and future climatic indicators for distribution patterns and conservation planning of temperate coniferous forests in southwestern China. *Ecol. Indic.* 107:105559. doi: 10.1016/j.ecolind.2019.105559

Diao, C., Liu, Y., Zhao, L., Zhuo, G., and Zhang, Y. (2021). Regional-scale vegetation-climate interactions on the Qinghai-Tibet Plateau. *Ecol. Inform.* 65:101413. doi: 10.1016/j.ecoinf.2021.101413

Ding, M., Zhang, Y., Sun, X., Liu, L., Wang, Z., and Bai, W. (2013). Spatiotemporal variation in alpine grassland phenology in the Qinghai-Tibetan Plateau from 1999 to 2009. *Chin. Sci. Bull.* 58, 396–405. doi: 10.1007/s11434-012-5407-5

Duo, A., Zhao, W., Gong, Z., Zhang, M., and Fan, Y. (2017). Temporal analysis of climate change and its relationship with vegetation cover on the north china plain from 1981 to 2013. *Acta Ecol. Sin.* 37, 576–592. doi: 10.5846/stxb201507301600

Evans, J., and Geerken, R. (2004). Discrimination between climate and human-induced dryland degradation. *J. Arid Environ.* 57, 535–554. doi: 10.3390/s18113676

Fang, X., Zhu, Q., Ren, L., Chen, H., Wang, K., and Peng, C. (2018). Large-scale detection of vegetation dynamics and their potential drivers using MODIS images and BFAST: A case study in Quebec, Canada. *Remote Sens. Environ.* 206, 391–402. doi: 10.1016/j.rse.2017.11.017

Feng, F., and Wang, K. (2020). *High spatial resolution (10km) surface solar radiation dataset with by merging sunshine hours over China China (1983-2017)*. Beijing: National Tibetan Plateau Data Center.

Fernández-Giménez, M. E., Venable, N. H., Angerer, J., Fassnacht, S. R., Reid, R. S., and Khishigbayar, J. (2017). Exploring linked ecological and cultural tipping points in Mongolia. *Anthropocene* 17, 46–69. doi: 10.1016/j.ancene.2017.01.003

Gholamnia, M., Khandan, R., Bonafoni, S., and Sadeghi, A. (2019). Spatiotemporal analysis of MODIS NDVI in the semi-arid region of Kurdistan (Iran). *Remote Sens.* 11:1723. doi: 10.3390/rs11141723

Goodwin, M. J., Zald, H. S., North, M. P., and Hurteau, M. D. (2021). Climate-driven tree mortality and fuel aridity increase wildfire's potential heat flux. *Geophys. Res. Lett.* 48:e2021GL094954. doi: 10.1029/2021GL094954

Guo, B., Zhou, Y., Wang, S.-X., and Tao, H.-P. (2014). The relationship between normalized difference vegetation index (NDVI) and climate factors in the semiarid region: A case study in Yalu Tsangpo River basin of Qinghai-Tibet Plateau. *J. Mountain Sci.* 11, 926–940. doi: 10.1007/s11629-013-2902-3

Herrmann, S. M., Anyamba, A., and Tucker, C. J. (2005). Recent trends in vegetation dynamics in the African Sahel and their relationship to climate. *Glob. Environ. Change* 15, 394–404. doi: 10.1016/j.gloenvcha.2005.08.004

Higginbottom, T. P., and Symeonakis, E. (2014). Assessing land degradation and desertification using vegetation index data: Current frameworks and future directions. *Remote Sens.* 6, 9552–9575. doi: 10.3390/rs6109552

Holben, B. N. (1986). Characteristics of maximum-value composite images from temporal AVHRR data. *Int. J. Remote Sens.* 7, 1417–1434. doi: 10.1080/01431168608948945

Jiang, L., Bao, A., Guo, H., and Ndayisaba, F. (2017). Vegetation dynamics and responses to climate change and human activities in Central Asia. *Sci. Total Environ.* 599, 967–980. doi: 10.1016/j.scitotenv.2017.05.012

Kendall, M. G. (1938). A new measure of rank correlation. *Biometrika* 30, 81–93. doi: 10.1093/biomet/30.1-2.81

Kirillin, G. B., Shatwell, T., and Wen, L. (2021). Ice-Covered lakes of tibetan plateau as solar heat collectors. *Geophys. Res. Lett.* 48:e2021GL093429. doi: 10.1029/2021GL093429

Kraaijenbrink, P. D., Bierkens, M., Lutz, A., and Immerzeel, W. (2017). Impact of a global temperature rise of 1.5 degrees Celsius on Asia's glaciers. *Nature* 549, 257–260. doi: 10.1038/nature23878

Kun, X., Zhang, J., and Lv, X. (2020). Spatio-temporal change ofmarshes NDVI and its response to climate change in the Qinghai-Tibet Plateau. *Acta Ecol. Sin.* 40, 6259–6268.

Lambert, J., Denux, J.-P., Verbesselt, J., Balent, G., and Cheret, V. (2015). Detecting clear-cuts and decreases in forest vitality using MODIS NDVI time series. *Remote Sens.* 7, 3588–3612. doi: 10.3390/rs70403588

Lenton, T. M. (2013). Environmental tipping points. *Ann. Rev. Environ. Resour.* 38, 1–29. doi: 10.1146/annurev-environ-102511-084654

Li, X., Long, D., Scanlon, B. R., Mann, M. E., Li, X., Tian, F., et al. (2022). Climate change threatens terrestrial water storage over the Tibetan Plateau. *Nat. Clim. Change* 12, 801–807. doi: 10.1038/s41558-022-01443-0

Mitsch, W. J., Gosselink, J. G., Zhang, L., and Anderson, C. J. (2009). *Wetland ecosystems*. New York, NY: John Wiley & Sons.

Peng, S. (2019). *1-km Monthly Mean Temperature Dataset for China (1901–2017)*. Beijing: National Tibetan Plateau Data Center.

Peng, S. (2020). *1-km Monthly Precipitation Dataset for China (1901–2017)*. Beijing: National Tibetan Plateau Data Center. doi: 10.5194/essd-2019-145

Piao, S., Friedlingstein, P., Ciais, P., Viovy, N., and Demarty, J. (2007). Growing season extension and its impact on terrestrial carbon cycle in the Northern Hemisphere over the past 2 decades. *Glob. Biogeochem. Cycles* 21:B3018. doi: 10.1029/2006GB002888

Xu, X. C., Li, B. J., Liu, X. P., Li, X., and Shi, Q. (2021). Mapping annual global land cover changes at a 30 m resolution from 2000 to 2015. *Natl. Remote Sens. Bull.* 25, 1896–1916. doi: 10.11834/jrs.20211261

Rezaei, A., and Gurdak, J. J. (2020). Large-scale climate variability controls on climate, vegetation coverage, lake and groundwater storage in the Lake Urmia watershed using SSA and wavelet analysis. *Sci. Total Environ.* 724:138273. doi: 10.1016/j.scitotenv.2020.138273

Richard, Y., and Poccard, I. (1998). A statistical study of NDVI sensitivity to seasonal and interannual rainfall variations in Southern Africa. *Int. J. Remote Sens.* 19, 2907–2920. doi: 10.1080/014311698214343

Salick, J., Ghimire, S. K., Fang, Z., Dema, S., and Konchar, K. M. (2014). Himalayan alpine vegetation, climate change and mitigation. *J. Ethnobiol.* 34, 276–293. doi: 10.2993/0278-0771-34.3.276

Salimi, S., Almuktar, S. A., and Scholz, M. (2021). Impact of climate change on wetland ecosystems: A critical review of experimental wetlands. *J. Environ. Manag.* 286:112160. doi: 10.1016/j.jenvman.2021.112160

Shadmani, M., Marofi, S., and Roknian, M. (2012). Trend analysis in reference evapotranspiration using Mann-Kendall and Spearman's Rho tests in arid regions of Iran. *Water Resour. Manag.* 26, 211–224. doi: 10.1007/s11269-011-9913-z

Shen, X., Liu, Y., Zhang, J., Wang, Y., Ma, R., Liu, B., et al. (2022). Asymmetric impacts of diurnal warming on vegetation carbon sequestration of marshes in the Qinghai Tibet Plateau. *Glob. Biogeochem. Cycles* 36:e2022GB007396. doi: 10.1029/2022GB007396

Shen, Z., Fu, G., Yu, C., Sun, W., and Zhang, X. (2014). Relationship between the growing season maximum enhanced vegetation index and climatic factors on the Tibetan Plateau. *Remote Sens.* 6, 6765–6789. doi: 10.3390/rs6086765

Sun, J., and Qin, X. (2016). Precipitation and temperature regulate the seasonal changes of NDVI across the Tibetan Plateau. *Environ. Earth Sci.* 75, 1–9. doi: 10.1111/gcb.13081

Sun, J., Qin, X., and Yang, J. (2016). The response of vegetation dynamics of the different alpine grassland types to temperature and precipitation on the Tibetan Plateau. *Environ. Monit. Assess.* 188, 1–11. doi: 10.1007/s10661-015-5014-4

Tang, Z., Sun, G., Zhang, N., He, J., and Wu, N. (2018). Impacts of land-use and climate change on ecosystem service in Eastern Tibetan Plateau, China. *Sustainability* 10:467. doi: 10.3390/su10020467

Timoney, K. P., Mamet, S. D., Cheng, R., Lee, P., Robinson, A. L., Downing, D., et al. (2019). Tree cover response to climate change in the forest-tundra of north-central Canada: fire-driven decline, not northward advance. *Écoscience* 26, 133–148. doi: 10.1080/11956860.2018.1532868

Verbesselt, J., Hyndman, R., Newnham, G., and Culvenor, D. (2010a). Detecting trend and seasonal changes in satellite image time series. *Remote Sens. Environ.* 114, 106–115. doi: 10.1016/j.rse.2009.08.014

Verbesselt, J., Hyndman, R., Zeileis, A., and Culvenor, D. (2010b). Phenological change detection while accounting for abrupt and gradual trends in satellite image time series. *Remote Sens. Environ.* 114, 2970–2980. doi: 10.1016/j.rse.2010.08.003

Wang, F., Zhao, G., Mu, X., Gao, P., and Sun, W. (2014). Regime shift identification of runoff and sediment loads in the Yellow River Basin, China. *Water* 6, 3012–3032. doi: 10.3390/w6103012

Wang, G., Bai, W., Li, N., and Hu, H. (2011). Climate changes and its impact on tundra ecosystem in Qinghai-Tibet Plateau, China. *Clim. Change* 106, 463–482. doi: 10.1007/s10584-010-9952-0

Wang, G., and Han, L. (2012). "The vegetation NDVI variation trend in Qinghai-Tibet Plateau and its response to climate change," in *Proceedings of the 2012 2nd International Conference on Remote Sensing, Environment and Transportation Engineering*, (Manhattan, NY: IEEE), 1–4.

Wang, Q., and Qiu, H.-N. (2009). Situation and outlook of solar energy utilization in Tibet, China. *Renew. Sustain. Energy Rev.* 13, 2181–2186. doi: 10.1016/j.rser.2009.03.011

Wang, R., He, M., and Niu, Z. (2020). Responses of alpine wetlands to climate changes on the Qinghai-Tibetan Plateau based on remote sensing. *Chin. Geograph. Sci.* 30, 189–201. doi: 10.1007/s11769-020-1107-2

Wang, X., Yi, S., Wu, Q., Yang, K., and Ding, Y. (2016). The role of permafrost and soil water in distribution of alpine grassland and its NDVI dynamics on the Qinghai-Tibetan Plateau. *Glob. Planet. Change* 147, 40–53. doi: 10.1016/j.gloplacha.2016.10.014

Wang, Y., Shen, X., Jiang, M., Tong, S., and Lu, X. (2021). Spatiotemporal change of aboveground biomass and its response to climate change in marshes of the Tibetan Plateau. *Int. J. Appl. Earth Observ. Geoinform.* 102:102385. doi: 10.1016/j.jag.2021.102385

Watts, L. M., and Laffan, S. W. (2014). Effectiveness of the BFAST algorithm for detecting vegetation response patterns in a semi-arid region. *Remote Sens. Environ.* 154, 234–245. doi: 10.1016/j.rse.2014.08.023

Wei, X., and Wu, P. (2021). Responses of soil insect communities to alpine wetland degradation on the eastern Qinghai-Tibetan Plateau, China. *Eur. J. Soil Biol.* 103:103276. doi: 10.1016/j.ejsobi.2020.103276

Wen, Y., Liu, X., Yang, J., Lin, K., and Du, G. (2019). NDVI indicated inter-seasonal non-uniform time-lag responses of terrestrial vegetation growth to daily maximum and minimum temperature. *Glob. Planet. Change* 177, 27–38. doi: 10.1016/j.gloplacha.2019.03.010

Wu, D., Zhao, X., Liang, S., Zhou, T., Huang, K., Tang, B., et al. (2015). Time-lag effects of global vegetation responses to climate change. *Glob. Change Biol.* 21, 3520–3531. doi: 10.1111/gcb.12945

Xin, Z., Xu, J., and Zheng, W. (2008). Spatiotemporal variations of vegetation cover on the Chinese Loess Plateau (1981–2006): Impacts of climate changes and human activities. *Sci. China Ser. D* 51, 67–78. doi: 10.1007/s11430-007-0137-2

Xiong, Q., Xiao, Y., Halmy, M. W. A., Dakhil, M. A., Liang, P., Liu, C., et al. (2019). Monitoring the impact of climate change and human activities on grassland vegetation dynamics in the northeastern Qinghai-Tibet Plateau of China during 2000–2015. *J. Arid Land* 11, 637–651. doi: 10.1007/s40333-019-0061-2

Xu, X. (2018). China annual vegetation index (NDVI) spatial distribution dataset. *Chin. Acad. Sci.* 10:2018060601.

Xue, Z., Lyu, X., Chen, Z., Zhang, Z., Jiang, M., Zhang, K., et al. (2018). Spatial and temporal changes of wetlands on the Qinghai-Tibetan Plateau from the 1970s to 2010s. *Chin. Geograph. Sci.* 28, 935–945. doi: 10.1007/s11769-018-1003-1

Yaghoubi, M., and Sabzevari, A. (1996). Further data on solar radiation in Shiraz, Iran. *Renew. Energy* 7, 393–399.

Yao, T., Bolch, T., Chen, D., Gao, J., Immerzeel, W., Piao, S., et al. (2022). The imbalance of the Asian water tower. *Nat. Rev. Earth Environ.* 3, 618–632. doi: 10.1038/s43017-022-00299-4

Yi, S., Wang, X., Qin, Y., Xiang, B., and Ding, Y. (2014). Responses of alpine grassland on Qinghai–Tibetan plateau to climate warming and permafrost degradation: a modeling perspective. *Environ. Res. Lett.* 9:074014. doi: 10.1088/1748-9326/9/7/074014

Yu, H., Xu, J., Okuto, E., and Luedeling, E. (2012). Seasonal response of grasslands to climate change on the Tibetan Plateau. *PLoS One* 7:e49230. doi: 10.1371/journal.pone.0049230

Yuan, Y., Si, G., Wang, J., Luo, T., and Zhang, G. (2014). Bacterial community in alpine grasslands along an altitudinal gradient on the Tibetan Plateau. *FEMS Microbiol. Ecol.* 87, 121–132. doi: 10.1111/1574-6941.12197

Yue, C.-D., and Huang, G.-R. (2011). An evaluation of domestic solar energy potential in Taiwan incorporating land use analysis. *Energy Policy* 39, 7988–8002. doi: 10.1016/j.enpol.2011.09.054

Zhang, D., Fengquan, L., and Jianmin, B. (2000). Eco-environmental effects of the Qinghai-Tibet Plateau uplift during the Quaternary in China. *Environ. Geol.* 39, 1352–1358. doi: 10.1007/s002540000174

Zhang, G., Nan, Z., Yin, Z., and Zhao, L. (2021). Isolating the contributions of seasonal climate warming to permafrost thermal responses over the Qinghai-Tibet Plateau. *J. Geophys. Res.* 126:e2021JD035218. doi: 10.1029/2021JD035218

Zhang, W., Yi, Y., Song, K., Kimball, J. S., and Lu, Q. (2016). Hydrological response of alpine wetlands to climate warming in the eastern Tibetan Plateau. *Remote Sens.* 8:336. doi: 10.3390/rs8040336

Zhang, Y., Wang, G., and Wang, Y. (2011). Changes in alpine wetland ecosystems of the Qinghai–Tibetan plateau from 1967 to 2004. *Environ. Monit. Assess.* 180, 189–199. doi: 10.1007/s10661-010-1781-0

Zhe, M., and Zhang, X. (2021). Time-lag effects of NDVI responses to climate change in the Yamzhog Yumco Basin, South Tibet. *Ecol. Indic.* 124:107431. doi: 10.1016/j.ecolind.2021.107431

Zhou, X., Wang, F., Fan, J., and Ochieng, R. M. (2010). Performance of solar chimney power plant in Qinghai-Tibet Plateau. *Renew. Sustain. Energy Rev.* 14, 2249–2255. doi: 10.1016/j.rser.2010.04.017

Zuo, D., Han, Y., Xu, Z., Li, P., Ban, C., Sun, W., et al. (2021). Time-lag effects of climatic change and drought on vegetation dynamics in an alpine river basin of the Tibet Plateau, China. *J. Hydrol.* 600:126532. doi: 10.1016/j.jhydrol.2021.126532

frontiers | Frontiers in Ecology and Evolution

TYPE Methods
PUBLISHED 26 January 2023
DOI 10.3389/fevo.2022.1076005

OPEN ACCESS

EDITED BY
Zhongqing Yan,
Chinese Academy of Forestry, China

REVIEWED BY
Zhenming Zhang,
Beijing Forestry University, China
Ji-Zhong Wan,
Qinghai University, China

*CORRESPONDENCE
Wenmei Ma
✉ maxiaolu0607@126.com

SPECIALTY SECTION
This article was submitted to Population, Community, and Ecosystem Dynamics, a section of the journal Frontiers in Ecology and Evolution

RECEIVED 21 October 2022
ACCEPTED 06 December 2022
PUBLISHED 26 January 2023

CITATION
Wang L, Ma W, Zhou D, Chen Q, Liu L and Li L (2023) Bioclimatic drivers of forage growth and cover in alpine rangelands. *Front. Ecol. Evol.* 10:1076005. doi: 10.3389/fevo.2022.1076005

Bioclimatic drivers of forage growth and cover in alpine rangelands

Li Wang[1], Wenmei Ma[2]*, Dan Zhou[2], Qi Chen[1], Lu Liu[2] and Long Li[3,4]

[1]Meteorological Bureau of Qinghai Province, Institute of Meteorological Science Research of Qinghai Province, Xining, China, [2]Meteorological Bureau of Qinghai Province, Meteorological Service Center of Qinghai Province, Xining, China, [3]School of Geographical Science, Qinghai Normal University, Xining, China, [4]QingHai Remote Sensing Center for Nature Resources, Xining, China

Context: Climate change and human activities have significant impacts on the Qinghai–Tibetan Plateau; the alpine ecosystem in this region has been degraded. A decline in forage yield reduces the livestock carrying capacity, but an unmitigated increase may lead to overfeeding and damage to vegetation. These changes have eventually led to grassland degradation and a series of ecological problems. Therefore, it is essential to examine bioclimatic factors that affect forage growth in grasslands.

Objective: To identify bioclimatic factors associated with forage growth and coverage in the Qinghai–Tibetan Plateau.

Methods: We examined how forage growth and coverage are affected by 35 bioclimatic indicators published in a global database (CMCC-BioClimInd).

Results and conclusions: We comprehensively considered the relationship between 35 indicators and forage yield and coverage and found that the combination of temperature and precipitation indicators had a very high correlation with yield and coverage. When we evaluated the relationship between each index and forage yield, forage yield was found to be significantly correlated with 16 bioclimatic indices. Forage yield was positively correlated with yearly positive precipitation (R^2=0.49, p<0.05), annual precipitation (R^2=0.48, p<0.05), and precipitation of driest quarter (R^2=0.47, p<0.05), and negatively correlated with temperature seasonality (R^2=0.52, p<0.05), precipitation seasonality (R^2=0.39, p<0.05), and simplified continentality index (R^2=0.48). Forage coverage was significantly correlated with 15 bioclimatic indicators. It showed positive correlations with precipitation of driest quarter (R^2=0.36, p<0.05), precipitation of driest month (R^2=0.33, p<0.05), and annual precipitation (R^2=0.31, p<0.05), and negative correlations with temperature seasonality (R^2=0.415, p<0.05), annual temperature range, precipitation seasonality, and simplified continentality index (R^2=0.37, p<0.05).

Significance: We identified bioclimatic indicators that affect forage growth in the northeastern Qinghai–Tibetan Plateau, and explored the physiological and ecological mechanisms underlying forage growth. Our results provide a scientific basis for future forage management, early determination of livestock carrying capacity, rational management of animal husbandry practices, and ecological protection and restoration efforts.

KEYWORDS

Qinghai–Tibetan plateau, Forage, output, coverage, bioclimatic index

1. Introduction

Rangelands account for more than 30% of global land area and provide biodiversity and wildlife habitats as well as a broad range of ecosystem services, including production of food and forage material and protection of soil and water resources (Parton et al., 2012; Schohr, 2014; Liu et al., 2021). However, climate change has had a considerable impact on global water and heat resources, resulting in significant changes in forage yield and coverage (Walther et al., 2002; Parmesan, 2006; Chen et al., 2011). Growing-season precipitation is generally recognized as the primary factor driving annual grassland forage production (Le Houérou, 1984). Accordingly, several studies have developed regression models linking precipitation and temperature to peak annual forage production (Murphy, 1970; Pitt and Heady, 1978; Chaplin-Kramer and George, 2013). These studies have reported a positive relationship between peak forage production, precipitation, and air temperature (Liu et al., 2021). A recent study on the link between microclimate and forage growth found that wetter topographic locations were more productive in a dry year (water limitation), whereas warmer topographic locations were more productive in a wet year (energy limitation; Devine et al., 2019). Guo et al. (2010) found that the combination of precipitation and temperature was the main factor affecting forage yield. Li (2014) showed that the forage growth period was accompanied by a prominent discrepancy between heat and water conditions; low levels of precipitation and higher temperatures led to higher levels of evapotranspiration, resulting in low forage yield.

The Qinghai–Tibetan Plateau has a unique climate, hydrological features, and soil development background, and hosts a typical alpine ecosystem. Alpine ecosystems are fragile and exhibit complex and sensitive responses to global climate change (Yao et al., 2017). Climate change directly affects the spatiotemporal patterns of environmental factors, such as light, temperature, and water, all of which are highly predictive of forage yield and coverage (Qin et al., 2014). Under conditions of relatively stable forage distribution and crop rotation, warmer temperatures may cause early flowering, change crop phenology, shorten the maturity, and growth periods of crops, affect the accumulation of dry matter, and reduce crop yield (Zhang, 2016). Climate change affects forage yields in alpine ecosystems, forcing farmers and herders to change crop planting structures, grazing intensity, and rotational grazing modes (Ding et al., 2013). As alpine ecosystems are more sensitive to global climate change than other ecosystems (Grabherr et al., 1994), it is important to identify the main climatic factors that affect alpine pastures.

The Qinghai Province is a typical alpine pasture region in China. Grasslands account for 47% of the land area in this region and are mainly concentrated in the southern region of the Qinghai Plateau, Qilian Mountains, and mountains on the southeast edge of the Qaidam Basin. There has been little research regarding the impact of climatic factors on forage in the northeastern Qinghai–Tibetan Plateau (Wang et al., 2013; Shen et al., 2015). Current research on the impact of climate on forage yield, coverage, and height mainly focuses on using annual or seasonal indices such as precipitation or temperature. These indices are used to express the characteristics of climate, examine its variations, and predict future changes in climate and its effects on forage yield. However, recent research suggests that it is important to utilize additional bioclimatic indicators with clearer ecological significance, such as factors related to seasonal precipitation in the wettest and coldest seasons. Utilizing more comprehensive climatic indicators that integrate hydrothermal conditions can improve our understanding of the relationship between forage availability and climate. Vegetation-climate relationships determined using simple climatic indices have some significance; however, it is important to comprehensively evaluate the responses of vegetation to climatic and other environmental factors (Ni, 1998).

With increasing availability of climate information, several global datasets of bioclimatic indicators have become popular scientific references. These include WorldClim (Hijmans et al., 2010; Fick and Hijmans, 2017), CHELSA (Karger et al., 2017), CliMond (Kriticos et al., 2012, 2014), EcoClimate (Matheus and Lima-Ribeiro, 2015), ENVIREM (Title and Bemmels, 2018), and MERRAclim (Vega et al., 2018). Among these datasets, WorldClim was the most frequently cited. The recently updated version 2.1 (January, 2020) provides 19 bioclimatic indicators. Recently, Noce et al. (2020) presented CMCC-BioClimInd, a global gridded dataset that provides 35 bioclimatic indicators (Noce et al., 2020; including 16 indicators added on the basis of the WorldClim dataset).

In the present study, we used 35 bioclimatic indicators to investigate how bioclimatic factors affect forage output and cover. We screened out the bioclimatic indicators that have significant impacts on forage grass growth, clarified how these indicators affected growth, and accounted for the vacancy by only including precipitation and temperature in the forage grass growth analysis in the northeastern Qinghai–Tibetan Plateau. In addition, we clarified the ecological significance of the latest bioclimatic indicators for forage grass growth in the northeast of the Qinghai–Tibetan plateau. Our results are useful for future forage management, early determination of livestock carrying capacity, rational arrangement of animal husbandry, and implementation of ecological protection and restoration actions.

2. Materials and methods

2.1. Study area

The study area was located in Qinghai Province, China (Figure 1), which occupies the northeast region of the Qinghai–Tibetan Plateau (geographical location 31°9′–39°9′ N and

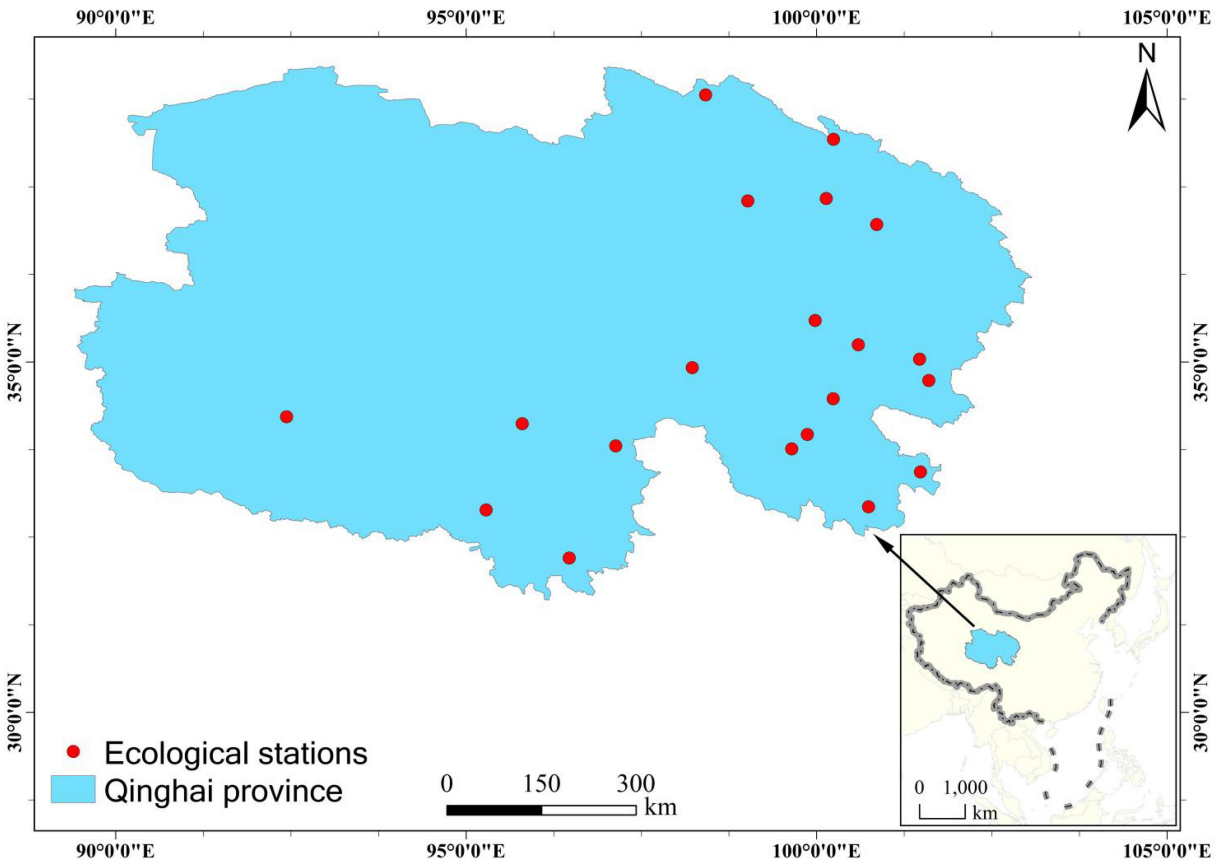

FIGURE 1
Geographical location and distribution of 20 ecological stations in the northeast region of the Qinghai–Tibetan Plateau.

89°35′–103°04′ E). The total land area is 7.2×10^5 km^2, and most of the area lies at an elevation of 3,000–5,000 m above sea level. The higher elevations lie to the west and northwest, and the lower elevations lie in the east and center of the region. Qinghai Province is connected to Gansu Province in the north and east, and lies adjacent to the Xinjiang Uygur Autonomous Region in the northwest, Tibet Autonomous Region in the south and southwest, and Sichuan Province in the southeast. The plateau has a continental climate characterized by low temperatures, large temperature differences between day and night, low levels of concentrated precipitation, high numbers of sunshine hours, and strong solar radiation.

The natural grassland in the northeastern region of the Qinghai–Tibetan Plateau covers a large land area, has a wide distribution, exhibits significant differences in natural conditions, and hosts rich and diverse grassland types. These include mountain dry grasslands, alpine dry grasslands, mountain meadows, alpine meadows, mountains, plains, deserts, alpine deserts, humid swamp meadows, moist shrubs, and sparse forests. Alpine meadows and alpine grasslands account for 44.2224 million mu, which is 80.88% of the total grassland area in the province.

2.2. Bioclimatic indices

The complete CMCC-BioClimInd dataset is available from PANGAEA.[1] It consists of 805 files in NetCDF4 format with a $0.5 \times 0.5°$grid resolution and global coverage (except Antarctica) (Noce et al., 2020). We used the spatial analysis function in ArcGIS 10.2 to extract the simulated values of 35 bioclimatic indicators from 20 stations in the northeast region of the Qinghai–Tibetan Plateau (Table 1). Based on these data, we calculated the average values for each station; we propose that the bioclimate index data are based on the fitted value of climate data from historical periods. In future work, we will use the definitions and calculation methods to calculate the bioclimatic indicators with the measured meteorological data. Grass growth is affected by a variety of bioclimatic indicators; a single indicator cannot describe the overall situation. First, we defined the contribution percentage of each indicator through principal component analysis. It can be seen from Table 1 that the contribution of the first principal component

1 https://doi.org/10.1594/PANGAEA.904278

TABLE 1 Principal component analysis of 35 bioclimatic indexes.

Code	Full name	F1	F2
Bio1	Annual mean temperature	0.937	0.347
Bio2	Mean diurnal range	0.496	−0.275
Bio3	Isothermalit	0.621	−0.577
Bio4	Temperature seasonality	−0.723	0.59
Bio5	Max temperature of warmest month	0.662	0.712
Bio6	Min temperature of coldest month	0.837	0.374
Bio7	Temperature annual range	−0.245	0.529
Bio8	Mean temperature of wettest quarter	0.808	0.578
Bio9	Mean temperature of driest quarter	0.971	0.176
Bio10	Mean temperature of warmest quarter	0.809	0.579
Bio11	Mean temperature of coldest quarter	0.984	0.141
Bio12	Annual precipitation	0.764	−0.621
Bio13	Precipitation of wettest month	0.718	−0.652
Bio14	Precipitation of driest month	0.485	−0.738
Bio15	Precipitation seasonality	−0.799	0.332
Bio16	Precipitation of wettest quarter	0.75	−0.636
Bio17	Precipitation of driest quarter	0.644	−0.714
Bio18	Precipitation of warmest quarter	0.763	−0.616
Bio19	Precipitation of coldest quarter	0.619	−0.705
Bio20	Ellenberg quotient	−0.24	0.907
Bio21	Yearly positive temperature	0.827	0.531
Bio22	Sum of annual temperature	0.937	0.346
Bio23	Ombrotermic index	−0.135	−0.943
Bio24	Yearly positive precipitation	0.856	−0.482
Bio25	Modified Kira coldness index	0.961	0.265
Bio26	Modified Kira warmth index	0.574	0.16
Bio27	Simplified continentality index	−0.721	0.616
Bio28	Mean temperature of warmest month	0.771	0.627
Bio29	Mean temperature of coldest month	0.988	0.092
Bio30	Mean temperature of driest month	0.919	0.275
Bio31	Mean temperature of wettest month	0.767	0.63
Bio32	Modified Thermicity index	0.857	0.499
Bio33	Ombrothermic index of summer and the previous month	0.758	−0.62
Bio34	Potential Evapotranspiration Hargreaves	0.948	0.28
Bio35	Potential Evapotranspiration Thornthwaite	0.858	0.482
Proper value/%		20.45	10.42
Variance contribution rate/%		58.45	29.77
Cumulative contribution rate%		58.45	88.22

(F1) is 58.45%, and factors such as mean temperature of the cold quarter (Bio11) and annual mean temperature (Bio1) also play a major role, mainly reflecting the role of heat on pasture growth. The second principal component (F2) mainly reflects the effect of the combination of precipitation and temperature, such as the Ellenberg quotien (Bio20) and Omboremic index (Bio23), on forage growth. The load values of Bio20 and Bio23 were 0.907 and − 0.943, respectively, including 29% of the contribution percentage.

2.3. Forage output and coverage

Forage data and basic meteorological variables were obtained from the ecological meteorological station built by the Qinghai Meteorological Bureau in 2002, which has recorded observations since 2003 with high-level management. Most grasslands in the study area are alpine meadows. The grasslands around Tianjun, Tongde, Tuole, and Tuotuohe stations are alpine grasslands, and those around Gangcha and Xinghai stations are temperate grasslands. Representative vegetation, terrain, soil types, and microclimatic factors were considered when selecting study sites for measuring forage cover. The observation sites covered an area of no more than $10 \times 10\,km^2$ and were located on pastures with flat terrain, no more than 20 km away from the meteorological station. The sites were enclosed by a net fence and surrounded by pile driving (height, 50 cm above the ground; the top 10 cm was painted red). A $50 \times 50\,m^2$ area in the observation field was surrounded by a 1.5-m-tall fence, and the local maximum forage yield was measured through continuous monitoring. During the forage growth period, foraging by herd animals is prohibited in this area. The parameters measured included forage growth period, yield, height, and coverage. Data collected between 2003 and 2019 were used in this study. Observations were recorded in strict accordance with the guidelines for agrometeorological observations, and data were recorded continuously.

2.4. Data analysis

To extract the simulated values of the 35 bioclimatic indicators, we used the spatial analysis function in ArcGIS 10.2. We then used simple regression models and Pearson's correlation analyses to explore the relationships between forage output and bioclimatic indices. Finally, we selected the indicators that were significantly related to forage yield and coverage ($p < 0.05$) for analysis, which was performed using SigmaPlot 12.5 (Systat Software, United States) and SPSS (version 22, IBM Corp., United States).

3. Results

3.1. Relationship between forage output and bioclimatic indices

First, we analyzed the correlation between the three principal components and forage yield from an overall perspective. The correlations between principal components 1 and 3 and forage yield were not significant ($p > 0.05$). As shown in Figure 2, there was a strong positive correlation between forage yield and principal component 2, the combined indicators of precipitation and temperature ($R^2 = 0.40$; $p < 0.001$).

We analyzed the correlation between forage yield and 35 bioclimatic indicators (Figure 3) and found significant correlations between forage yield and 16 bioclimatic indicators. Bio3 (isothermality), Bio9 (mean temperature of the driest quarter), Bio11 (mean temperature of the cold quarter), Bio12 (annual precipitation), Bio13 (precipitation in the wettest month), Bio14 (precipitation in the driest month), Bio16 (precipitation in the wettest quarter), Bio17 (precipitation in the driest quarter), Bio18 (precipitation in the winter quarter), Bio19 (precipitation in the cold quarter), Bio24 (annual positive precipitation), Bio29 (mean temperature of the coldest month), and Bio33 (ombrothermic indices of summer and the previous month) were positively correlated with forage yield, with correlation coefficients (R^2) ranging from 0.23 0.49 (Figure 2). The magnitude of the correlation was in the following order: Bio24, Bio12, Bio17, Bio16, Bio33, Bio13, Bio18, Bio14, Bio19, Bio11, Bio3, and Bio9. The forage yield was most highly correlated with Bio24 ($R^2 = 0.49$), Bio12 ($R^2 = 0.48$), and Bio17 ($R^2 = 0.47$). Yield was negatively correlated with Bio4 (temperature seasonality), Bio15 (precipitation seasonality), and Bio27 (simplified continuity index), with R^2 values of 0.39–0.52. The forage yield was most strongly negatively correlated with Bio4 ($R^2 = 0.52$), followed by Bio27 ($R^2 = 0.48$).

3.1. Relationship between forage cover and bioclimatic indices

First, we conducted a correlation analysis of the three principal components and grass coverage from an overall perspective. The correlation between principal components 1 and 3 and grass coverage was not significant ($p > 0.05$). As shown in Figure 4, there was a strong positive correlation between grass coverage and principal component 2, the combined index of precipitation and temperature ($R^2 = 0.30$, $p < 0.001$).

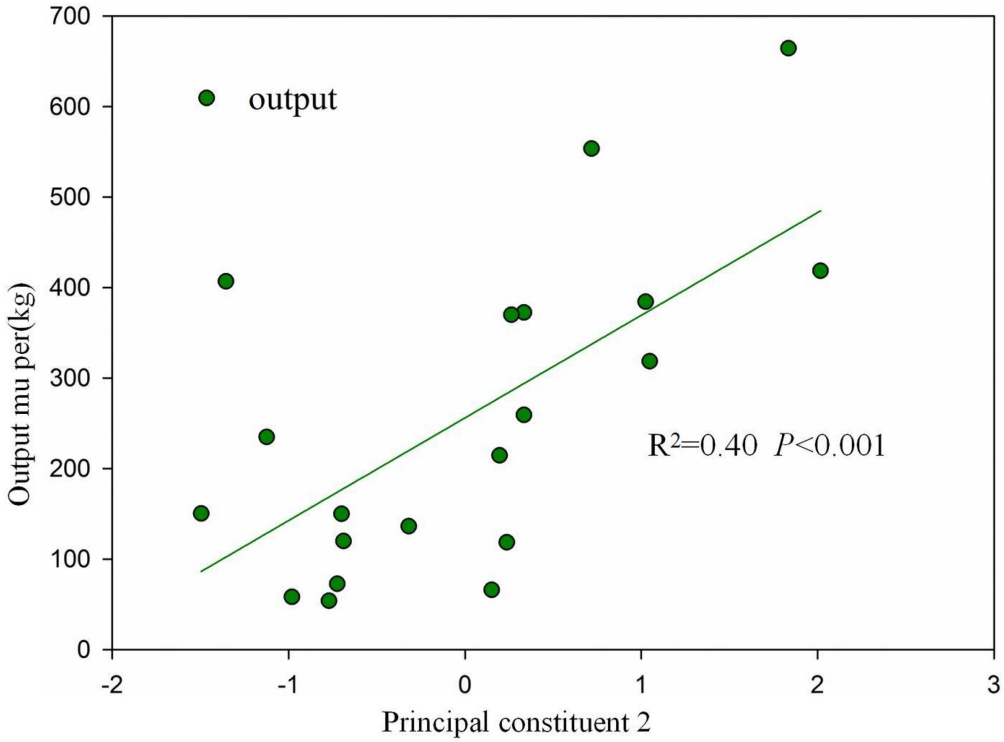

FIGURE 2
Relationships between forage output and Principal component 2.

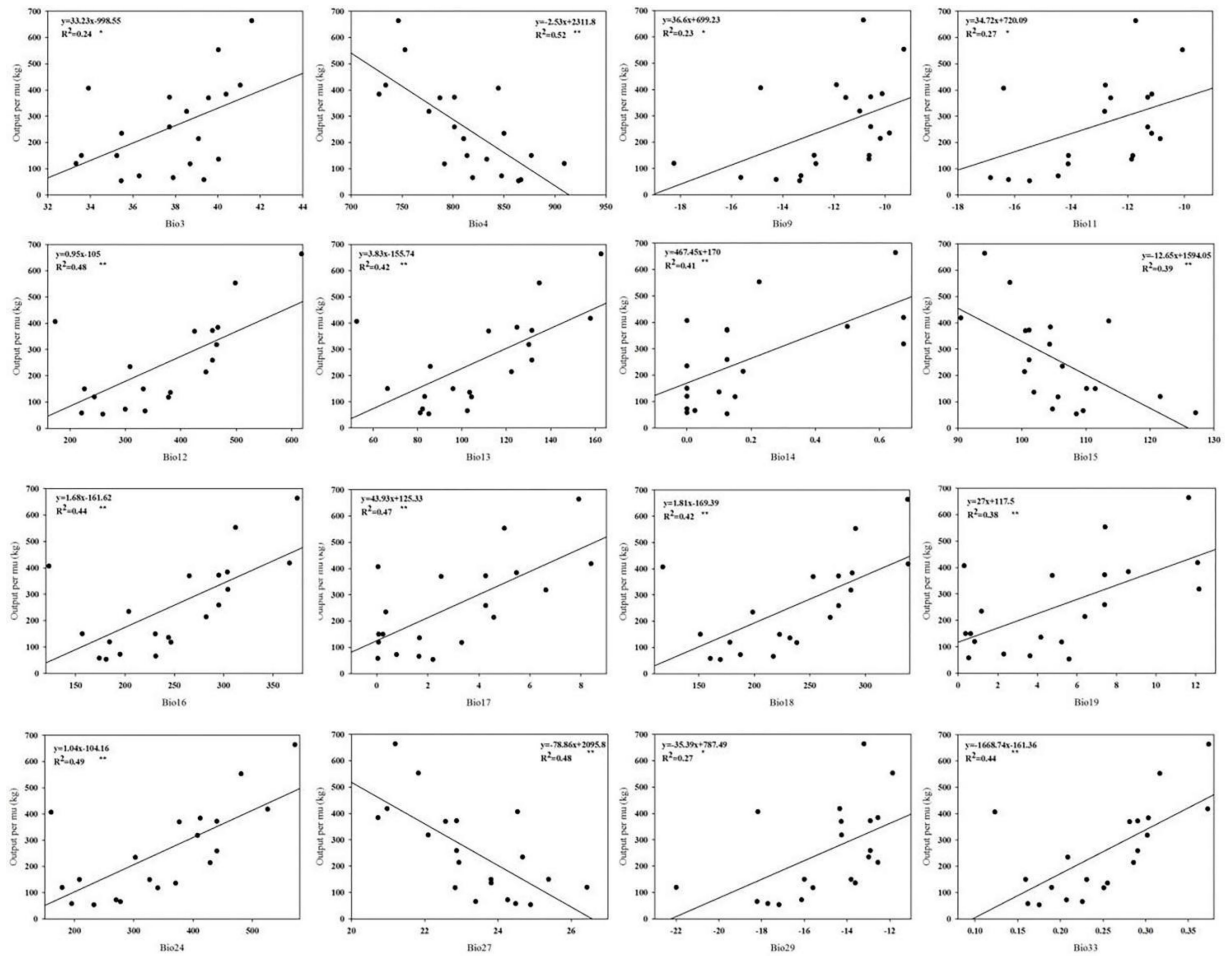

FIGURE 3
Relationships between forage output and 16 bioclimatic indices.

We analyzed the correlation between forage cover and 35 bioclimatic indicators (Figure 5) and found that coverage was significantly correlated with 15 bioclimatic indicators. Bio11 (mean temperature of the cold quarter), Bio12 (annual precipitation), Bio13 (precipitation in the wettest month), Bio14 (precipitation in the driest month), Bio16 (precipitation in the wettest quarter), Bio17 (precipitation in the driest quarter), Bio18 (precipitation in the winter quarter), Bio19 (precipitation in the cold quarter), Bio24 (annual positive precipitation), Bio29 (mean temperature of the cold month), and Bio33 (ombrothermic index of summer and previous month) were positively correlated with forage output, with R^2 values between 0.20 and 0.36. The magnitude of the correlation was in the following order: Bio17, Bio14, Bio12, Bio24, Bio18, Bio16, Bio19, Bio33, Bio13, Bio29, and Bio11. Forage cover was most highly correlated with Bio17 ($R^2 = 0.36$), Bio14 ($R^2 = 0.33$), and Bio12 ($R^2 = 0.31$). Coverage was negatively correlated with Bio4 (temperature seasonality), Bio7 (annual temperature range), Bio15 (precipitation seasonality), and Bio27 (simplified continuity index), with R^2 values of 0.25–0.415. The coverage showed the highest correlation with Bio4 ($R^2 = 0.415$), followed by Bio27 ($R^2 = 0.37$).

4. Discussion

4.1. Relationship between forage output and bioclimatic indices

We found that forage yield was significantly correlated with 16 bioclimatic indicators, and had the strongest correlations with Bio24, Bio12, and Bio17. Thus, forage yield is closely associated with annual precipitation, followed by temperature. This is consistent with the findings of previous studies (Bai et al., 2008). However, unlike previous studies, we performed a more detailed analysis and found that forage yield was more closely related to annual positive precipitation than to annual precipitation. Annual positive precipitation reflects the summed long-term averages of total precipitation (cumulative daily precipitation) for months with long-term average daily temperatures (Tg) exceeding 0°C (Rivas-Martínez et al., 2011); therefore, annual positive precipitation incorporates temperature data to some extent. The growth potential of plants is highest when favorable precipitation and temperature conditions coincide (Liu et al., 2021), and this

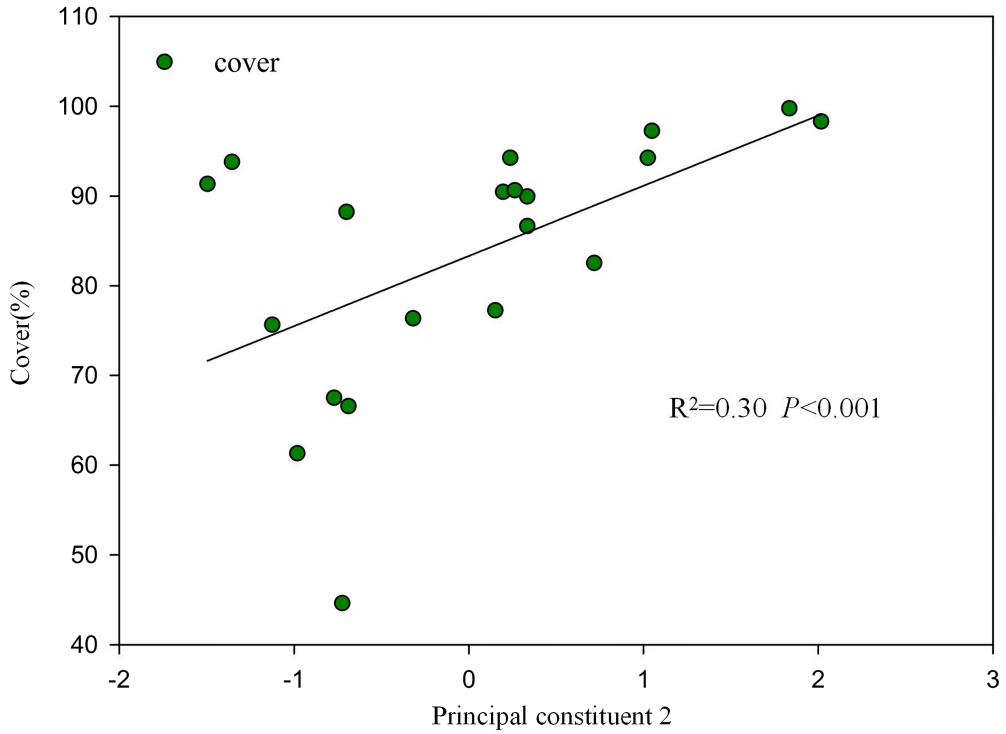

FIGURE 4
Relationships between forage cover and Principal component 2.

may explain why forage yield was more closely related to positive annual precipitation in this study.

Our results also revealed a strong correlation between forage yield and precipitation during the driest season. During the driest seasons in the study region, autumn and winter, soil movement, and snow formation caused by precipitation increase the soil water content, which is conducive to plant re-emergence in spring and growth in summer (Nandintsetseg and Shinoda, 2011; Richardson et al., 2013). Schenk and Jackson (2010) analyzed plant root systems on a global scale and found that higher precipitation in winter led to deeper plant roots. This improves the water absorption capacity of roots, allowing them to meet the transpiration needs of plants.

In the present study, forage yield was negatively correlated with Bio4 (temperature seasonality), Bio15 (precipitation seasonality), and Bio27 (simplified continuity index). The high values of Bio4 and Bio27 indicated a large range of temperature variations in this region. The northeast region of the Qinghai–Tibetan Plateau is an arid area; some studies have shown that under drought conditions, exposure to intense cold and heat can aggravate water stress in plants, which depletes the available energy reserves required for rooting, transpiration, and defense responses (Harper et al., 2009). The precipitation seasonality index, which reflects the degree of change in precipitation over a given period, was negatively correlated with forage yield, indicating that greater degrees of change in precipitation were associated with lower forage yields. This is consistent with the findings of previous studies that showed that low but continuous precipitation is favorable for forage growth, while uneven precipitation is unfavorable (Liu et al., 2021). Under global change, the frequency of observed and predicted extreme weather events (temperature and precipitation) increases. Extreme temperature and extreme precipitation can indicate an increase in the temperature seasonal, precipitation seasonal, and simplified continuity indices. The results of this study showed that higher indicator values are associated with greater adverse impacts on pasture growth. In future pasture management, we can take preventive measures using extreme predictions.

According to the relationship between bioclimatic indicators and forage yield, we suggest that during the drought period, artificial rainfall and other methods should be used to supplement water availability, taking temperature into account, to achieve matching between precipitation and temperature and increase the forage yield. In addition, cold- and drought-resistant and high-yield grass species should be selected to improve grass yield and achieve a balance between grass and livestock; this would promote modernization of animal husbandry and achieve sustainable grassland ecological protection.

4.2. Relationship between forage cover and bioclimatic indices

Forage coverage was significantly correlated with 15 bioclimatic indicators and was most highly correlated with

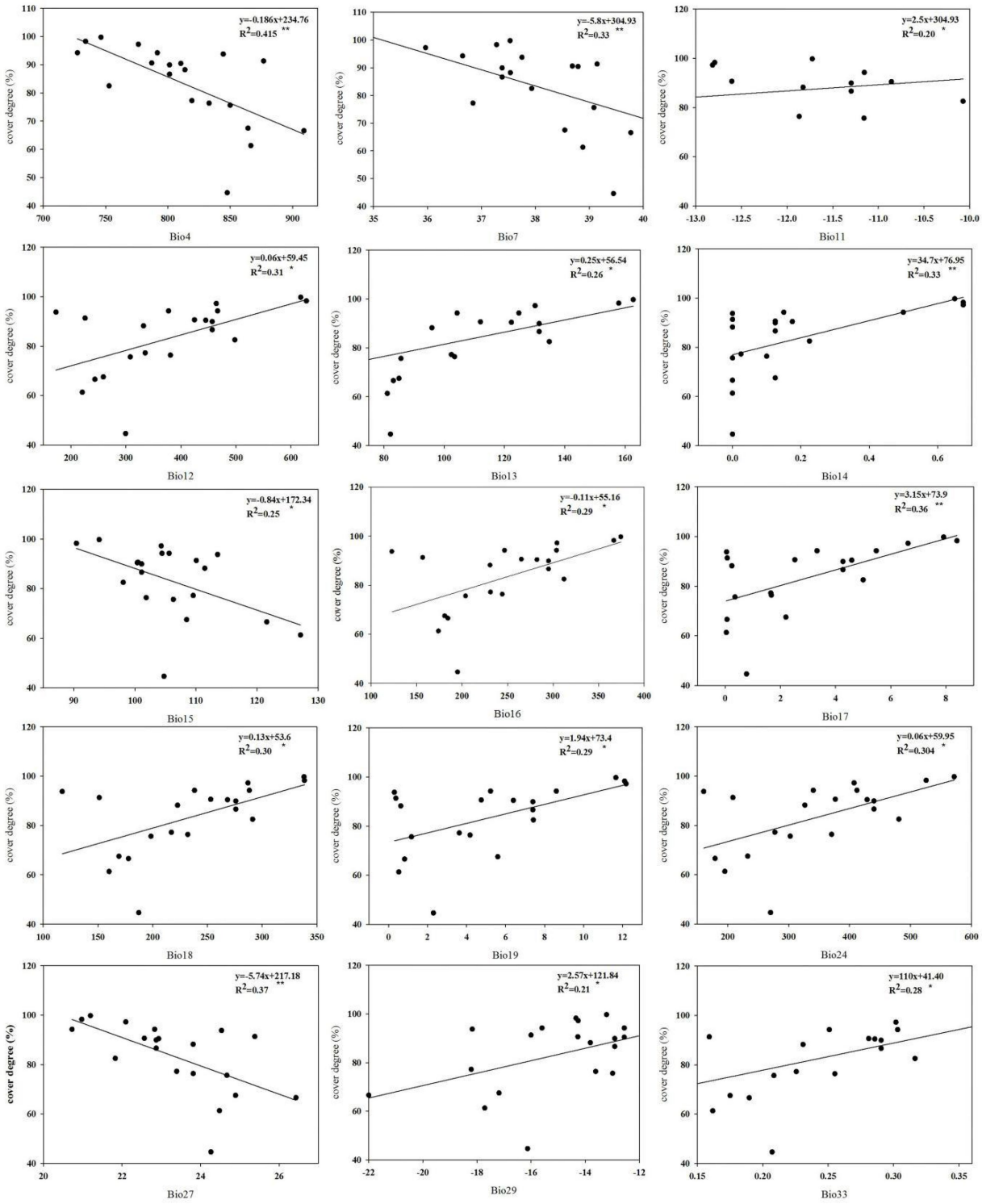

FIGURE 5
Relationship between forage coverage and 15 bioclimatic indices.

Bio17 (precipitation in the driest quarter), Bio14 (precipitation in the driest month), and Bio12 (annual precipitation). Forage coverage reflects the proportion of the study area covered by vertically projected vegetation and is the most direct representation of biomass (Wang, 2020). Several studies have reported a positive correlation between annual precipitation and aboveground biomass (Ma et al., 2008; Hu, 2010; Guo et al., 2012). In this study, forage cover was closely related to

precipitation of driest month and driest quarter. This may be because precipitation during these seasons increases soil water content, which promotes plant growth in spring and summer (Nandintsetseg and Shinoda, 2011; Richardson et al., 2013). Moreover, adequate water storage before germination is beneficial for early forage growth and can increase the surface area of roots and leaves. When external temperatures become more favorable in later growth stages, plants with larger leaves, and roots can capture solar radiation and soil water more effectively (Becchetti et al., 2016). Good growth and development during the early stages also increase grass coverage, which may promote the infiltration of rainfall into the soil and increase soil water storage for subsequent use. We found a relatively weak correlation between forage cover and indicators of adequate precipitation (precipitation during the wettest season and wettest month).

Forage coverage was negatively correlated with Bio4, Bio7, Bio15, and Bio27. The magnitude of the correlation was highest for Bio4, followed by Bio27, which is consistent with the results for forage yield. This is likely because the seasonal index of temperature, annual range of temperature, and simplified continental index indicate the degree of change in temperature. Higher indices represent greater changes in temperature. When the severity of temperature change exceeds the adaptability of plants to new environmental conditions, the internal balance and stability of plants may decline, leading to serious, and irreparable damage (Siegmund et al., 2016).

The seasonal precipitation index reflects the change in precipitation within a given period. This index was negatively correlated with forage cover, indicating that a greater degree of change in precipitation is associated with lower forage cover. Duncan and Woodmansee (1975) showed that low but continuous precipitation occurs throughout the growing season and is conducive to forage growth (Duncan and Woodmansee, 1975). Liu et al. (2021) showed that in dry years, uniform rainfall promotes forage growth. In contrast, when the soil moisture is sufficient (as in wet years), areas with uniform precipitation are less favorable to forage growth than those with variable precipitation (Liu et al., 2021). These reports confirm the findings of the present study. The northeast region of the Qinghai–Tibetan Plateau experiences low precipitation; our results indicate that low levels of continuous precipitation promote forage growth, whereas uneven distribution of precipitation reduces forage growth.

Based on the relationship between bioclimatic indicators and coverage, we suggest increasing the diversity of pastures. Pasture diversity increases coverage and prevents soil erosion. When encountering extreme precipitation, the soil maintains its water storage capacity; however, herbage maintains diversity. Under certain conditions, the relationship between temperature and water can be adjusted to achieve the maximum growth rate and increase coverage through adaptation to the local environment. According to the prediction of extreme weather conditions, we also suggest changing the community structure of pastures. Some studies have found that extreme drought significantly inhibits the growth of perennial plants, but promotes the growth of annual plants.

5. Conclusion

We comprehensively considered the relationship between 35 bioclimatic indicators and forage yield and coverage, and found that the combination of temperature and precipitation indicators had a very high correlation with yield and coverage. Forage yield was significantly correlated with 16 bioclimatic indices; yearly positive precipitation, annual precipitation, and precipitation in the driest quarter showed the highest positive correlations with forage yield. Temperature seasonality, precipitation seasonality, and the simplified continentality index were negatively correlated with forage yield; temperature seasonality had the greatest negative correlation. Forage cover was correlated with 15 bioclimatic indicators, including positive correlations with precipitation in the driest quarter, precipitation in the driest month, and annual precipitation, and negative correlations with temperature seasonality, temperature annual range, precipitation seasonality, and the simplified continentality index. Temperature seasonality had the highest negative correlation with forage cover, followed by the simplified continentality index. These results reflect the complex responses of forage growth to multiple climatic and environmental factors. By establishing the relationships between 35 bioclimatic indicators and forage yield and coverage, this study screened the bioclimatic indicators that are important for forage growth in the northeast region of the Qinghai–Tibetan Plateau. We discuss the physiological and ecological mechanisms underlying the response of forage growth to the latest bioclimatic indicators. In future studies, we will build a bioclimatic index system specifically for forage growth, detail the associated principles and calculation methods, and establish a climate model for pasture growth in the northeast region of the Qinghai–Tibetan Plateau. This will provide a scientific basis for the early determination of livestock carrying capacity and reasonable animal husbandry. These results may contribute to the ecological protection and restoration of this region.

Data availability statement

The original contributions presented in the study are included in the article/supplementary material, further inquiries can be directed to the corresponding author.

Author contributions

LW and WM: designed the study and completed the manuscript. DZ: revised the manuscript. QC, LuL, and LoL

contributed to the data collection and processing. All authors have read and agreed to the published version of the manuscript.

Funding

This research was supported by the Natural Science Foundation of China (grant no. 42165014).

Acknowledgments

This is a short text to acknowledge the contributions of specific colleagues, institutions, or agencies that aided the efforts of the authors.

Conflict of interest

The authors declare that the research was conducted in the absence of any commercial or financial relationships that could be construed as a potential conflict of interest.

Publisher's note

All claims expressed in this article are solely those of the authors and do not necessarily represent those of their affiliated organizations, or those of the publisher, the editors and the reviewers. Any product that may be evaluated in this article, or claim that may be made by its manufacturer, is not guaranteed or endorsed by the publisher.

References

Bai, Y., Wu, J., Xing, Q., Pan, J., Huang, D., and Han, X. (2008). Primary production and rain use efficiency across a precipitation gradient on the Mongolia plateau. *Ecol. Lett.* 89, 2140–2153. doi: 10.1890/07-0992.1

Becchetti, T., George, M., McDougald, N., Dudley, D., Connor, M., Flavel, D., et al. (2016). Rangeland management series: annual range forage production. doi: 10.3733/ucanr.8018,

Chaplin-Kramer, R., and George, M. (2013). Effects of climate change on range forage production in the San Francisco Bay area. *PLoS One* 8:e57723. doi: 10.1371/journal.pone.0057723

Chen, I.-C., Hill, J. K., Ohlemuller, R., Roy, D. B., and Thomas, C. D. (2011). Rapid range shifts of species associated with high levels of climate warming. *Science* 333, 1024–1026. doi: 10.1126/science.1206432

Devine, S. M., O'Geen, A. T., O'Geen, , Larsen, R. E., Dahlke, H. E., Liu, H., et al. (2019). Microclimate–forage growth linkages across two strongly contrasting precipitation years in a Mediterranean catchment. *Ecohydrology* 12:12e2156. doi: 10.1002/eco.2156

Ding, M., Zhang, Y., Sun, X., Liu, L., Wang, Z., and Bai, W. (2013). Spatiotemporal variation in alpine grassland phenology in the Qinghai-Tibetan plateau from 1999 to 2009. *Chin. Sci. Bull.* 58, 396–405. doi: 10.1007/s11434-012-5407-5

Duncan, D. A., and Woodmansee, R. G. (1975). Forecasting forage yield from precipitation in California's annual rangeland. *J. Range Manag.* 28, 327–329. doi: 10.2307/3897788

Fick, S., and Hijmans, R. (2017). WorldClim 2: new1-km spatial resolution climate surfaces for global land areas. *Int. J. Climatol.* 37, 4302–4315. doi: 10.1002/joc.5086

Grabherr, G., Gottfried, M., and Pauli, H. (1994). Climate effects on mountain plants. *Nature* 369, 449–450. doi: 10.1038/369449a0

Guo, Q., Hu, Z., Li, S., Li, X., Sun, X., and Yu, G. (2012). Spatial variations in aboveground net primary productivity along a climate gradient in Eurasian temperate grassland: effects of mean annual precipitation and its seasonal distribution. *Glob. Chang. Biol.* 18, 3624–3631. doi: 10.1111/gcb.12009

Guo, L., Zhao, H., and Ji, S. (2010). Effects of climates on primary production of alpine stipa krylovii grassland. *J. Northwest Agric. Forest. Univ.* 38, 189–196. doi: 10.13207/j.cnki.jnwafu.2010.08.012

Hijmans, R., Cameron, S., Parra, L., Jones, P., and Jarvis, A. (2010). Very high resolution interpolated climate surfaces for global land areas. *Int. J. Climatol.* 20, 1965–1978. doi: 10.3390/s20051316

Harper, R. J., Smettem, K. R. J., and Carter, J. O. (2009). Drought deaths in eucalyptus globulus (labill.) plantations in relation to soils, geomorphology and climate. *Plant & Soil.* 324, 199–207. doi: 10.1007/s11104-009-9944-x

Hu, Z., Yu, G., Fan, J., Zhong, H., Wang, S. (2010). Precipitation-use efficiency along a 4500-km grassland transect. *Global ecology and biogeography* 19, 842–851. doi: 10.1111/j.1466-8238.2010.00564.x

Karger, D. N., Conrad, J., Böhner, T., Kawohl, H., Kreft, R., Soria-Auza, N., et al. (2017). Climatologies at high resolution for the earth's land surface areas. *Sci. Data* 4:170122. doi: 10.1038/sdata.2017.122

Kriticos, D. J., Jaroik, V., and Ota, N. (2014). Extending the suite of bioclim variables: a proposed registry system and case study using principal components analysis. *Methods Ecol. Evol.* 5, 956–960. doi: 10.1111/2041-210X.12244

Kriticos, D. J., Webber, B. L., Leriche, A., Ota, N., Macadam, I., Bathols, J., et al. (2012). Climond: global high-resolution historical and future scenario climate surfaces for bioclimatic modelling. *Methods Ecol. Evol.* 3, 53–64. doi: 10.1111/j.2041-210X.2011.00134.x

Le Houérou, H. N. (1984). Rain use efficiency: a unifying concept in arid-land ecology. *J. Arid Environ.* 7, 213–247. doi: 10.1016/S0140-1963(18)31362-4

Li, X. (2014). Influence of climate change on the growth and development of dominant forages in Inner Mongolia grassland. Dissertation/master's thesis. [China (IL)]: Inner Mongolia Agricultural University.

Liu, H., Jin, L., Roche, M., O'Geen, A., and Dahlgren, R. A. (2021). Understanding spatial variability of forage production in California grasslands: delineating climate, topography and soil controls. *Environ. Res. Lett.* 16:014043. doi: 10.1088/1748-9326/abc64d

Ma, W., Yang, Y., He, J., Zeng, H., and Fang, J. (2008). Above-and belowground biomass in relation to environmental factors in temperate grasslands, Inner Mongolia. *Sci China C Life Sci* 51, 263–270. doi: 10.1007/s11427-008-0029-5

Matheus, S., and Lima-Ribeiro, (2015). Ecoclimate: a database of climate data from multiple models for past, present, and future for macroecologists and biogeographers. *Biodiver. Inform.* 10, 1–21. doi: 10.17161/bi.v10i0.4955

Murphy, A. H. (1970). Predicted forage yield based on fall precipitation in California annual grasslands. *J. Range Manag.* 23:363. doi: 10.2307/3896168

Nandintsetseg, B., and Shinoda, M. (2011). Seasonal change of soil moisture in Mongolia: its climatology and modelling. *Int. J. Climatol.* 31, 1143–1152. doi: 10.1002/joc.2134

Ni, J. (1998). Indexes of vegetation-climate Classificateon and its applications. *Chin. J. Ecol.* 17, 34–45. doi: 10.13292/j.1000-4890.1998.0071

Noce, S., Caporaso, L., and Santini, M. (2020). A new global dataset of bioclimatic indicators. *Sci. Data* 7:398. doi: 10.1038/s41597-020-00726-5

Parmesan, C. (2006). Ecological and evolutionary responses to recent climate change. *Annu. Rev. Ecol. Evol. Syst.* 37, 637–669. doi: 10.1146/annurev.ecolsys.37.091305.110100

Parton, W., Morgan, J., Smith, D., Grosso, S. D., Prihodko, L., Dan, L. C., et al. (2012). Impact of precipitation dynamics on net ecosystem productivity. *Glob. Chang. Biol.* 18, 915–927. doi: 10.1111/j.1365-2486.2011.02611.x

Pitt, M. D., and Heady, H. F. (1978). Responses of annual vegetation to temperature and rainfall patterns in northern California. *Ecology* 59, 336–350. doi: 10.2307/1936378

Qin, D., Zhou, B., and Xiao, C. (2014). Progress in studies of cryospheric changes and their impacts on climate of China. *J. Meteorol. Res.* 28, 732–746. doi: 10.1007/s13351-014-4029-z

Richardson, A. D., Keenan, T. F., Migliavacca, M., Ryu, Y., Sonnentag, O., and Toomey, M. (2013). Climate change, phenology, and phenological control of vegetation feedbacks to the climate system. *Agric. For. Meteorol.* 169, 156–173. doi: 10.1016/j.agrformet.2012.09.012

Rivas-Martínez, S., Rivas Sáenz, S., and Penas, A. (2011). Worldwide bioclimatic classification system. *Glob. Geob.* 1, 1–638. doi: 10.5616/gg110001

Schenk, H. J., and Jackson, R. B. (2010). Rooting depths, lateral root spreads and below-ground/above-ground allometries of plants in water-limited ecosystems. *J. Ecol.* 90, 480–494. doi: 10.1046/j.1365-2745.2002.00682.x

Schohr, T. K. (2014). Sustaining multifunctional working rangelands: Social, economic, and ecological insights into rancher decision-making. [dissertation/master's thesis]. [California (IL)]: University of California

Shen, M., Piao, S., Dorji, T., Qiang, L., Nan, C., Chen, X., et al. (2015). Plant phenological responses to climate change on the Tibetan plateau: research status and challenges. *Natl. Sci. Rev.* 2, 454–467. doi: 10.1093/nsr/nwv058

Siegmund, J., Wiedermann, M., Donges, J., and Donner, R. (2016). Impact of climate extremes on flowering dates of four shrub species. *Biogeosciences* 13, 5541–5555. doi: 10.5194/bg-13-5541-2016

Title, P. O., and Bemmels, J. B. (2018). ENVIREM: an expanded set of bioclimatic and topographic variables increases flexibility and improves performance of ecological niche modeling. *Ecography* 41, 291–307. doi: 10.1111/ecog.02880

Vega, G. C., Pertierra, L. R., and Olalla-Tárraga, M. Á. (2018). Erratum: MERRAclim, a high-resolution global dataset of remotely sensed bioclimatic variables for ecological modelling. *Sci. Data* 5:180070. doi: 10.1038/sdata.2018.70

Walther, G. R., Post, E., Convey, P., Menzel, A., Parmesan, C., Beebee, T. J. C., et al. (2002). Ecological responses to recent climate change. *Nature* 416, 389–395. doi: 10.1038/416389a

Wang, C., Meng, F., Li, X., Jiang, L., Bai, L., and Wang, S. (2013). Responses of alpine grassland ecosystem on Tibetan plateau to climate change: A mini review. *Chin. J. Ecol.* 32, 1587–1595. doi: 10.13292/j.1000-4890.2013.0255

Wang, B. (2020). Study on ecological evaluation, monitoring and protection of meadow steppe in Inner Mongolia. [dissertation/master's thesis] [China (IL)]: Inner Mongolia Agricultural University.

Yao, T., Piao, S., Shen, M., Gao, J., Yang, W., Zhang, G., et al. (2017). Chained impacts on modern environment of interaction between westerlies and Indian monsoon on Tibetan plateau. *Bull. Chin. Acad. Sci.* 32, 976–984. doi: 10.16418/J.ISSN.1000-3045.2017.09.007

Zhang, X. (2016). Phase relationship and driving mechanism of humidity change in Holocene Asian monsoon region and inland region. [dissertation/master's thesis] [China (IL)]: Lanzhou University.

frontiers | Frontiers in Ecology and Evolution

TYPE Original Research
PUBLISHED 02 February 2023
DOI 10.3389/fevo.2023.1127973

OPEN ACCESS

EDITED BY
Ben Niu,
Institute of Geographic Sciences and Natural Resources Research (CAS), China

REVIEWED BY
Gang Fu,
Institute of Geographic Sciences and Natural Resources Research (CAS), China
Yanan Cao,
Hebei University of Engineering, China

*CORRESPONDENCE
Baoping Meng
✉ mengbp18@ntu.edu.cn

SPECIALTY SECTION
This article was submitted to Population, Community, and Ecosystem Dynamics, a section of the journal Frontiers in Ecology and Evolution

RECEIVED 20 December 2022
ACCEPTED 16 January 2023
PUBLISHED 02 February 2023

CITATION
Lv Y, Sun Y, Yi S and Meng B (2023) Human activities dominant the distribution of *Kobresia pygmaea* community in alpine meadow grassland in the east source region of Yellow River, China.
Front. Ecol. Evol. 11:1127973.
doi: 10.3389/fevo.2023.1127973

Human activities dominant the distribution of *Kobresia pygmaea* community in alpine meadow grassland in the east source region of Yellow River, China

Yanyan Lv[1,2], Yi Sun[1,2], Shuhua Yi[1,2] and Baoping Meng[1,2]*

[1]Institute of Fragile Eco-Environment, Nantong University, Nantong, Jiangsu, China, [2]School of Geographic Science, Nantong University, Nantong, Jiangsu, China

Kobresia pygmaea is the endemic and one of the most important species in the alpine meadow in the Qinghai-Tibet Plateau. It is the key stage in the management of degraded grassland, and irreversible degradation will take place after the degradation succession phases of the *Kobresia pygmaea* community. However, knowledge about the spatial distribution and driving factors were still unknown. In this study, the potential distribution of the *Kobresia pygmaea* community was determined using the BIOMOD niche model. Combine with the reality distribution based on remote sensing classification, the driving factors of climate and human activities were identified. The findings revealed that: (1) among all environmental factors, the maximum radiation, monthly temperature difference, driest period precipitation were the main climate influencing factors for the *Kobresia pygmaea* community distribution, and random forest model achieved the highest prediction accuracy and best stability of any niche model. (2) The potential distribution area of *Kobresia pygmaea* community was 653.25km^2 (account for 3.28% of the study area), and mostly located in northern and central of Zeku County, northeast of Henan County, and northeast, central, and eastern parts of Maqu County. (3) Climate factors driven 21.12% of *Kobresia pygmaea* community reality distribution, while human activities driven for 79.98%. Our results revealed that human activities dominant the reality distribution of *Kobresia pygmaea* community in alpine meadow grassland in the east source region of Yellow River, China.

KEYWORDS

***Kobresia pygmaea* community, BIOMOD, potential distribution, alpine meadow, driving factors**

1. Introduction

Kobresia pygmaea is an endemic and one of the most prominent plants on the Qinghai-Tibet Plateau's (QTP) alpine meadow (Zhang and Noltie, 2010; Miehe et al., 2011). Since the 1980s, alpine meadow grassland has degraded to varying degrees owing to the cumulative impacts of climate change and human activity, particularly in the Yellow River's source region (Wang et al., 2015). This might limit the sustainable growth of animal husbandry and endanger local ecological security (Liu et al., 2018). The degradation succession phases of the alpine meadow grassland community are (I) *Stipa silena* + *Festuca ovina* + *Kobresia humilis*, (II) *Kobresia humilis*, (III) *Kobresia pygmaea*, and (IV) black soil type. The *Kobresia pygmaea* community, in particular, is a critical stage in the management of degraded grassland (Cao and Long, 2009). The original community structure may be swiftly

restored in the first two stages by removing any disruption or artificial measures (Lin, 2017). Generally, the *Kobresia pygmaea* community builds almost closed, non-specific, golf-course like the lawn with a felty root mat (Miehe et al., 2019). This characteristic of mat is benefit for against external disturbance, increasing nutrient storage and grassland productivity (Miehe et al., 2008). However, with the fragmentation of *Kobresia pygmaea* community turf, the water budget, carbon cycle, and soil nutrition have been significantly lost (Miehe et al., 2019). Further degradation of the *Kobresia pygmaea* community will result in permanent degradation till the severest stage of black soil type (Li et al., 2013). Hence, mapping the existing distribution and driving factors of *Kobresia pygmaea* meadow, are crucial for taking mitigation and adaptation measures.

Currently, however, the majority of *Kobresia pygmaea* community researches are conducted at the plot scale using manipulative studies (Ma et al., 2017; Li et al., 2018). The geographical distribution and driving factors in the QTP are largely unknown (Zhang and Noltie, 2010; Miehe et al., 2011, 2019). With the development of remote sensing classification methods, satellite images and machine learning were successfully applied at the community level (Chen et al., 2018; Su et al., 2020; Wen et al., 2010). Meng et al. (2021) mapped the *Kobresia pygmaea* community through the random forest (RF) method based on the combination of remote sensing, texture and topographic indices (Meng et al., 2021). However, the driving factors of climate and human activities for its reality distribution are not distinguished. Similar to the Residuals-Trend model (Wessels et al., 2004, 2007), the potential distribution of vegetation community is only controlled by climate factors. Thus, the human-induced vegetation variation could be detected after removing the climate factors (Li et al., 2018).

The niche model is also known as the species distribution model or the habitat model. The model associates species with information on environmental factors and geographical attributes of sites where the species was present or absent (Elith and Leathwick, 2009). These models can be used to forecast or better understand species distribution (Halvorsen, 2012; Xu et al., 2015; Petitpierre et al., 2017; Citores et al., 2020). In the last 20 to 30 years, niche models have grown fast due to the development of empirical models based on statistics or theoretical derivation. There are now about 20 species distribution models in use (Zhu et al., 2013; Xu et al., 2015). Most specialized models are supported by software, such as GARP and Maxent (Stockwell and Peters, 1999; Phillips et al., 2006). Furthermore, various multi-model integrated systems, such as openModeller, BIOMOD, dismo, and others, have been created in recent years (Thuiller et al., 2009; Muoz et al., 2011). The advancement considerably encourages the use of this model in ecology and geography. BIOMOD (BIOdiversity MODeling) has been merged with hundreds of empirical statistical models, including the maximum entropy model (ME), generalized linear model (GLM), and generalized additive model (GAM), and its influence on species niche prediction has been successfully studied (Thuiller et al., 2009).

To evaluate the species' prospective range, a large number of observation samples of fundamental niche are required (Li and Guo, 2013). With the advancement of airborne remote sensing technology in recent years, unmanned aerial vehicle (UAV) technology has provided a novel and practical method for grassland resource monitoring. This approach compensates for the shortcomings of satellite remote sensing and other traditional monitoring techniques (Yi, 2017). UAVs have been widely used in the treatment and analysis of vegetation coverage, patches, gravel, pika holes, and grassland plant species and communities in a large area of the QTP due to their advantages of efficient mobility, ease of operation, and high photo resolution (Yi et al., 2016; Meng et al., 2018; Sun et al., 2018). At the same time, Yi (2017) created a series of UAV aerial photography systems based on the climatic and environment features of the QTP. The repeated observation of a large number of working sites may be accomplished, providing assistance for the *Kobresia pygmaea* community's field observation in the research region.

In this study, a UAV is utilized to observe the *Kobresia pygmaea* community, and a portion of alpine meadow in the Yellow River's source region is employed to conduct the following investigations: (1) The main climate driving factors and potential distribution of *Kobresia pygmaea* community; (2) Identify the driving factors of climate and human activities for *Kobresia pygmaea* community reality distribution.

2. Data and methods

2.1. Study area

The research area is located on the eastern side of the QTP, east of the Yellow River's source region, and includes Zeku County and Henan County in Qinghai Province, as well as Maqu County in Gansu Province (Figure 1). It is one of the most significant animal husbandry bases in the QTP, as well as an important water supply conservation region in China. The coordinates are 33°03′35°33' N, 100°33′102°33′ E, with elevations ranging from 2,871 to 4,850 m. The average annual precipitation is 400 ~ 600 mm, the average annual temperature is −2.4°C ~ 2.1°C, and it belongs to the continental plateau temperate monsoon. The major grassland type in this area is alpine meadow, which accounts for 79.67% of the total study area, followed by mountain meadow, marsh meadow, and alpine grassland, which account for 13.22, 1.78, and 1.69%, respectively (Figure 2). The main grassland vegetation is Poaceae community and *kobresia humilis* community in the study area, with the dominant species *Elymus nutans, Stipa silena, Festuca*

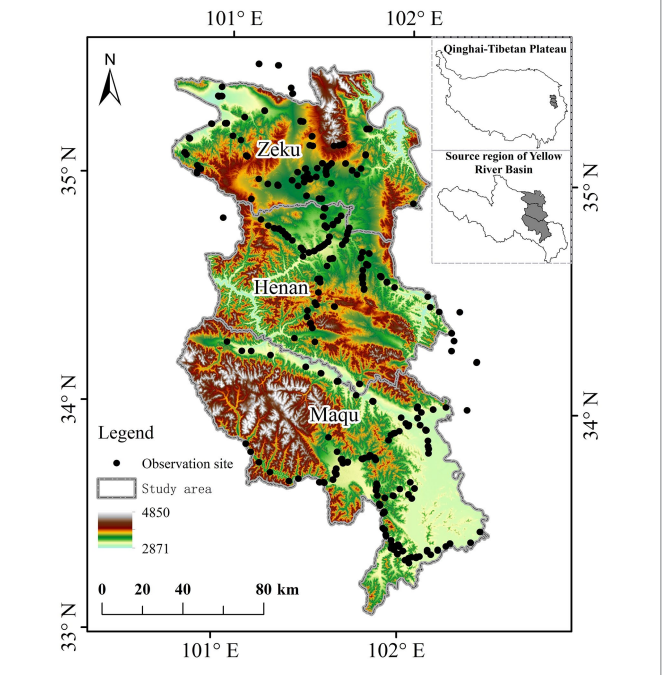

FIGURE 1
Location of study area.

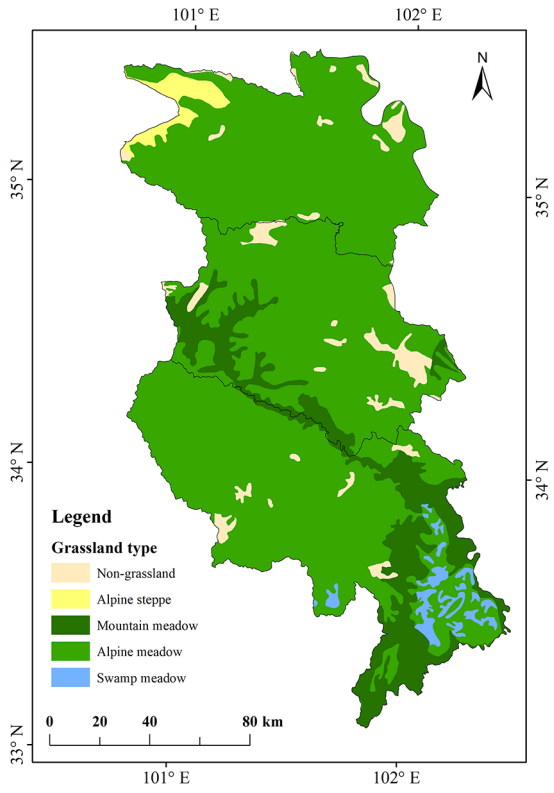

FIGURE 2
Grassland types of study area.

ovina, and *Kobresia humilis*. The *Kobresia pygmaea* is the dominant species in *Kobresia pygmaea* community, with a lower species richness than other vegetation communities in alpine meadow grassland. Weeds are the dominant species in the black soil type vegetation community. Grassland plants have a relatively short growing season, lasting just around 150 days from May to September. Grazing is the most common technique of grassland usage, while yak and sheep are the most common animals.

2.2. Materials and methods

2.2.1. Field observation and preprocess of aerial photos

The field observations of the *Kobresia pygmaea* community in this study were obtained from photographs collected by UAVs (Phantom 3 professional and Mavic 2 zoom Quad-Rotor intelligent UAVs). The observation sites were selected based on grassland growth state and spatial representativeness, and the flight path was developed with four paths in each site. One Grid flight mode and three Belt types are included (Figure 3A). The flight paths of UAVs were designed using FragMAP (Yi et al., 2016). A Phantom 3 professional was used to perform the Grid mode (within the 200 m × 200 m area) at a height of 20 m (red dot in Figures 3A,B), and a Mavic 2 zoom was used to perform the Belt mode (within the 40 m × 40 m area) at a height of 2 m (yellow dot in Figures 3A,C). Sixteen grassland images were then shot vertically downhill in each mode; the photograph resolution of Grid and Belt is 1 cm and 0.09 cm, respectively, and their coverage is 26 m × 35 m and 3.43 m × 2.57 m.

The photographs were verified individually and assigned to the presence or absence of *Kobresia pygmaea* community sites based on the primary species of grass flora, grassland coverage, textural aspects of plant development, and plateau pika activity (Figure 4). In comparison to other grass communities, the *Kobresia pygmaea* community displays distinct morphological and textural features, including closed and monospecific structures (Figure 4A), polygonal crack patterns (Figure 4B), and a felty root mat (Figure 4C; Cao and Long, 2009). Furthermore, when cracking and collapse intensified, pika and noxious plants proliferate. From 2015 to 2019, 751 sample plots were observed in the pinnacle of grassland expansion (Figure 1). All observation locations were labeled as having or not having a *Kobresia pygmaea* community, which was subsequently utilized in the BIOMOD prediction input.

2.2.2. Acquisition and processing of remote sensing and environmental data

The MOD13Q1 NDVI remote sensing data utilized in this investigation was obtained from the National Aeronautics and Space Administration in the United States (USGS). The total number of photos downloaded was 23, the spatial resolution is 250 m, and the orbit number is H26V05. The primary preprocessing steps are: (1) picture projection was changed using MODIS Projection Tool (MRT) and defined as WGS1984; (2) resampling of the image resolution into 250 m in ArcMap and defined projection as Albers; (3) cell statistics tool was used to determine the maximum, minimum, average, and variation range of NDVI in 2019. Climate, soil, and terrain are the three most critical environmental factors. Climate data were obtained from the Institute of Tibetan Plateau, Chinese Academy of Sciences (Yang et al., 2010; Chen et al., 2011). These datasets include yearly average temperatures, precipitation, and humidity, as well as seasonal indices such as wettest season, driest season, hottest season, and coldest season, with a total of 33 grid layers. The soil dataset was obtained from the cold and dry regions science data center, Northwest institute of ecological environment and resources, Chinese Academy of Science.[1] Including the sand and clay concentrations of the surface soil (0–30 cm; represented as clay1 and sand1) and the bottom soil (30–60 cm; represented as clay2 and sand2); The DEM data used in this study were 90 m shuttle radar topography mission (SRTM) images (version V004) in Geo-TIFF format[2] resampled to 250 m. Based on the DEM, the slope, topographic position index (TPI), and aspect were determined. All of the above environmental parameters were evenly projected as Albers with a spatial resolution of 250 m and utilized as input to BIOMOD.

2.3. Biodiversity modeling niche model simulation

2.3.1. Biodiversity modeling contrustion

In this study, BIOMOD2 was utilized to simulate the possible distribution of the *Kobresia pygmaea* community, which was then used to reflect the prospective dispersion of the community (Thuiller et al., 2009). There are 10 niche models available, including the generalized linear model (GLM), generalized enhanced regression model (GBM),

1 http://westdc.Westgis.ac.cn/data/
2 http://srtm.csi.cgiar.org/

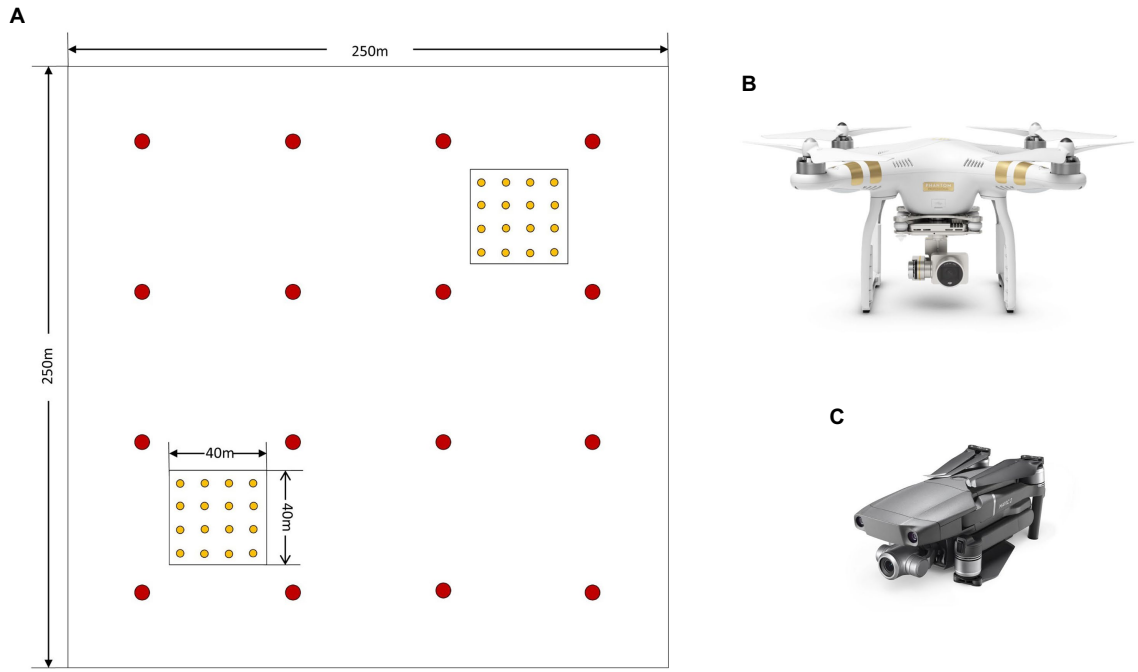

FIGURE 3
Strategy of field observation and data collection, **(A)** is the strategy of observation sites, **(B)** and **(C)** are Phantom 3 professional and Mavic 2 zoom Quad-Rotor intelligent UAVs.

FIGURE 4
Aerial photographs of *Kobresia pygmaea* community, **(A)** the patch characteristics of *Kobresia pygmaea* community observed at height of 20m, **(B)** the phenomenon of cracking and collapse in *Kobresia pygmaea* community observed at height of 2m, and **(C)** the felty root mat of *Kobresia pygmaea* community observed at height of 2m with double wide-angle zoom lenses.

generalized additive model (GAM), classification tree analysis (CAT), artificial neural network (ANN), surface range envelope (SRE), flexible discriminant analysis (FDA), multiple Adaptive regression Splines (MARS), random forest (RF), and maximum entropy model (MaxEnt). The presence and absence of *Kobresia pygmaea* community data, as well as the corresponding environmental parameters, are fed into the niche model, and the output is the likelihood of *Kobresia pygmaea* community presence in space. To limit the impact of information redundancy on niche model performance, the "Importance index" and cumulative contribution were utilized to select the primary impacting elements. To examine the importance of each environmental factor, the leave-one-out cross-validation (LOOCV) approach (Meng et al., 2020) was utilized. The correlation coefficient (CV) between the predicted results based on variables of total environment factors and one deleted environment factor was determined for each occasion. The Importance values are then derived by subtracting 1 from this correlation coefficient. The Importance Index formula is as follows:

$$\text{Importance} = 1 - \text{cor}\left(\text{pred\_ref}, \text{pred\_shuffled}\right) \quad (1)$$

where all gathered environmental factors are defined as the reference dataset, and elements deleted from all are defined as the shuffled dataset. Prediction results based on all environmental factors are represented by pred ref., whereas prediction results based on factors removed from all are represented by pred shuffled. The results are used to compute the correlation (cor). Then, using equation (2), the primary influencing elements were chosen based on the cumulative contribution (more than 85%), determined according to Importance value from high to low. The contribution formula is:

$$\text{Contribution}_i = \text{Importance}_i / \sum_{i=1}^{n} \text{Importance}_i \quad (2)$$

Contribution_i represent contribution for i-th factor, Importance_i represent Importance for i-th factor, and $\sum_{i=1}^{n} \text{Importance}_i$ represent total of all factors Importance value.

2.3.2. The accuracy evaluation of niche model

True skill statistics (TSS) and AUC [area under the operating characteristic curve (ROC)] were employed in this study to assess the accuracy of niche model prediction. The TSS considers the likelihood of success of the random conjecture by taking omission average error into account. TSS has a value between 0 and 1, and the closer the number is to 1, the better the model's performance. The ROC curve is a composite indicator that measures the sensitivity and specificity of continuous variables, with each point on the curve representing the sensitivity to signal stimuli. AUC values vary from 0.5 to 1. The closer to one, the better the model forecast; conversely, the closer to 0.5, the closer the model prediction is to a random guess.

$$\text{TSS} = \text{Sensitivity} + \text{Specificity} - 1 = \text{TRP} - \text{FRP} \quad (3)$$

where TPR represent true positive rate, FPR represent false positive rate.

2.4. The driving factors of *Kobresia pygmaea* community

In this study, the reality distribution of *Kobresia pygmaea* community was obtained from remote sensing classification, produced by Meng et al. (2021) at the same space and time range (Meng et al., 2021). We predicted these potential distribution by transforming the probabilities of presence into binary data (suitable/unsuitable; Liu et al., 2013; Ma et al., 2021). The potential distribution of *Kobresia pygmaea* community was calculated by the optimal niche model (region with existence probability higher than 50%). The spatial overlay analysis was used to distinguish the driving factors of *Kobresia pygmaea* community distribution in ArcMap 10.2 software. For example, the overlap between potential and reality distribution is believed to be driven by climate factors, otherwise, driven by human activities.

3. Results

3.1. Spatial heterogeneity of observed *Kobresia pygmaea* community

The spatial distribution of observation sites for *Kobresia pygmaea* community presence/absence was shown in Figure 5. Maqu County has the largest percentage of *Kobresia pygmaea* community presence sites among the 751 observed sites, with 68 observed sites accounting for 19.82% of total observed sites. Zeku and Henan County come next, with 37 and 22 presence observation sites, respectively, accounting for 16.74 and 11.76% of total observed sites. Overall, the number of *Kobresia pygmaea* community presence sites among all observed sites is limited, representing only 16.91% of total observed sites.

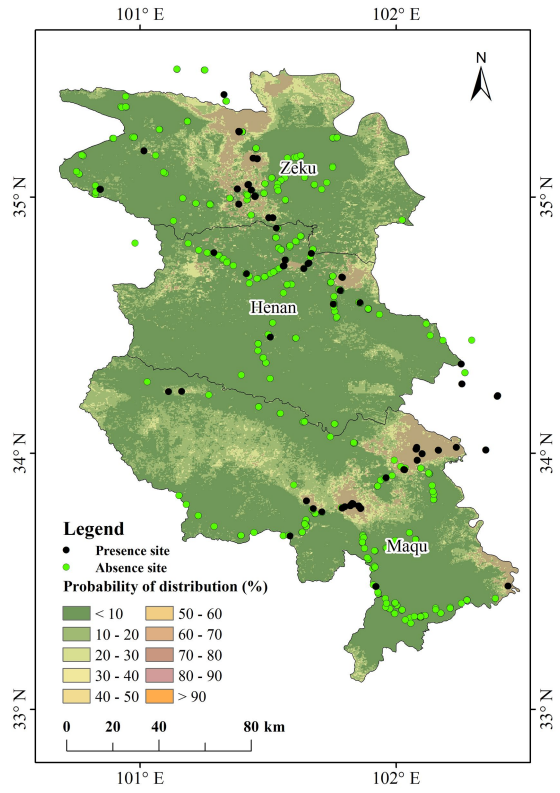

FIGURE 5
Distribution of presence probability of *Kobresia pygmaea* community.

3.2. Model construction and accuracy evaluation

Table 1 showed the Importance and Contribution value results based on LOOCV and 9 specialized models (except for GAM, test run failed). The maximum radiation, monthly temperature range, precipitation in the driest period, warmest season radiation, precipitation in the driest season, maximum NDVI in the growing season, and annual mean radiation all had higher Importance values than others, with values more than 0.20. Furthermore, the maximal radiation had the greatest Importance, with a value of 0.30. Temperature seasonality, average humidity, maximum humidity, humidity in the wettest, driest, warmest and coolest season had a poor influence on the *Kobresia pygmaea* community, with Importance values close to zero. There are 22 environmental factors with a cumulative contribution of more than 85% (Table 1).

Table 2 displays the TSS and AUC of nine models obtained by taking the average of multiple runs. Among all models, the RF model had the best predictive performance, with an average TSS and AUC of 0.74 and 0.92, respectively. Because the model's SD and CV values for TSS and AUC are minimal (TSS, 0.09 and 0.12; AUC, 0.03 and 0.03), it had excellent prediction accuracy and stability. The GBM model came in second place, with average TSS and AUC values of 0.72 and 0.90, respectively. SD and CV of TSS are 0.08 and 0.12, respectively, whereas the SD and CV of the AUC are 0.03 and 0.04, respectively. The SRE and MAENT models performed poorly in terms of accuracy and stability, with average TSS of 0.25 and 0.29, and AUC of 0.63 and 0.68, respectively. The models' prediction results were closest to random (AUC = 0.5). As a result, it could be stated that the prediction accuracy

TABLE 1 Influencing factors for *Kobresia pygmaea* community.

No.	Environmental factors	Important value	Cumulative contribution (%)
1	Maximum radiation	0.3004	6.61
2	Monthly temperature range	0.2726	12.61
3	Precipitation in the driest period	0.2616	18.37
4	Warmest season radiation	0.2329	23.50
5	Precipitation in the driest season	0.2304	28.57
6	Maximum NDVI in growth season	0.2151	33.30
7	Annual mean radiation	0.2010	37.72
8	Annual precipitation	0.1831	41.75
9	Average of driest season	0.1810	45.74
10	Precipitation in the wettest period	0.1782	49.66
11	Annual temperature range	0.1733	53.47
12	Minimum temperature	0.1718	57.25
13	Precipitation in the coldest season	0.1673	60.94
14	Minimum NDVI in growth season	0.1579	64.41
15	Precipitation in the warmest season	0.1488	67.69
16	Mean NDVI in growth season	0.1453	70.88
17	Range of NDVI in growth season	0.1375	73.91
18	Precipitation in the wettest season	0.1270	76.70
19	Average of warmest season	0.1141	79.22
20	Average of wettest season	0.1108	81.65
21	Wettest season radiation	0.1057	83.98
22	Elevation	0.1042	86.27

of these two models for the presence of the *Kobresia pygmaea* population in the studied region is poor.

3.3. The presence probability of *Kobresia pygmaea* community in the study area

The RF model with the best accuracy in numerous runs (TSS and AUC are 0.86 and 0.97, respectively) was selected to estimate the possible geographical distribution of the *Kobresia pygmaea* community in the research region, based on the results of the niche model accuracy evaluation in 2.3. The results revealed that the probability of *Kobresia pygmaea* community existence in most of the research region is less than 10% (accounting for 72.45% of the whole study area). The probability range of 10%~50% accounted for 24.28% of the whole study area. Only 3.07% of the total research area had a probability of more than 50%, whereas 0.75% had a probability greater than 80%. The regions with a high probability of *Kobresia pygmaea* community existence are mostly located in Zeku County's northern and central regions, Henan County's northeast, and Maqu County's northeast, central, and eastern parts (Figure 5).

3.4. Driving factors of *Kobresia pygmaea* community

According to the reality distribution of *Kobresia pygmaea* community acquired by remote sensing classification (Meng et al., 2021), the driving force of climate and human activities was identified. As Figure 6 shows, The potential distribution of *Kobresia pygmaea* community was mainly located in the north and around the county urban area of Zeku County (around the town of Zequ and Qiakeri), with an area of 262.44 km^2 (2.78% of Zeku County); the northeast of Henan County (east of county urban area and towns of Tuoyema), with an area of 62 km^2 (0.95% Henan County); the part of county urban area, towns of Awancang, and east of Manrima in Maqu County, with an area of 328.81 km^2 (8.33% of Maqu County). As a whole, the potential distribution of *Kobresia pygmaea* community reached 653.25 km^2, and accounted for 3.28% of the study area.

The results of driving factors were shown in Figure 6. The region where the *Kobresia pygmaea* community potential distribution and reality distribution overlapped, was located in the north and around the county urban area in Zeku County, east of county urban area in Henna, and the part of county urban area, towns of Awancang in Maqu. The area of overlapping region was 302.94 km^2 (1.52% of the study area), accounting for 45.55% of potential distribution and 21.12% of reality distribution. In other words, about 21.12% of *Kobresia pygmaea* community was derived by climate factors, and human activities are the main factor leading to the formation of *Kobresia pygmaea* community in the study area.

4. Discussion

4.1. The influencing factors on the distribution of *Kobresia pygmaea* community

In general, grassland *Kobresia pygmaea* communities could be found in the northwest of the QTP at altitudes ranging from 4,400–4,800 m. The

TABLE 2 Performance of each niche model.

Index		Model								
		GLM	GBM	CTA	ANN	SRE	FDA	MARS	RF	MAXENT
TSS	Mean	0.62	0.72	0.47	0.39	0.25	0.65	0.63	**0.74**	0.29
	SD	0.09	0.08	0.14	0.15	0.08	0.22	0.07	**0.09**	0.05
	CV	0.15	0.12	0.30	0.38	0.32	0.33	0.11	**0.12**	0.19
AUC	Mean	0.86	0.90	0.75	0.72	0.63	0.87	0.86	**0.92**	0.68
	SD	0.05	0.03	0.08	0.23	0.04	0.28	0.04	**0.03**	0.04
	CV	0.06	0.04	0.11	0.32	0.06	0.32	0.05	**0.03**	0.07

GLM is the generalized linear model, GBM is the generalized enhanced regression model, GAM is the generalized additive model, CAT is the classification tree analysis, ANN is the artificial neural network, SRE is the surface range envelope, FDA is the flexible discriminant analysis, MARS is the multiple Adaptive regression Splines, RF is the random forest and MaxEnt is the maximum entropy model, TSS is the true skill statistics, AUC is the area under the operating characteristic curve, SD depicts standard deviation, and CV depicts coefficient of variation. Bold values means the best accuracy.

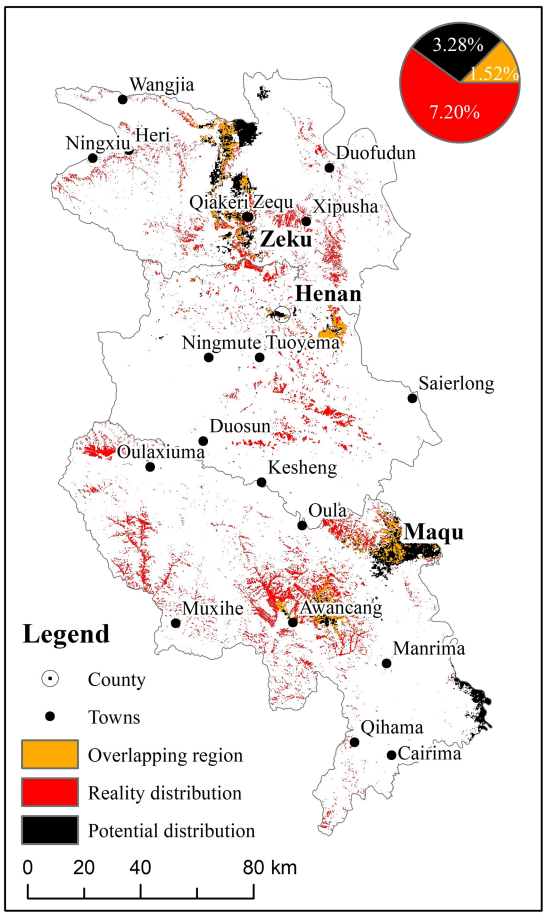

FIGURE 6
Reality and potential spatial distribution of *Kobresia pygmaea* community.

primary limiting factors for their growth are precipitation and nutrition (the soil quality is poor, and the annual precipitation is less than 450 mm with frequent seasonal drought; Li J. M. et al., 2016; Li R. et al., 2016). During the long process of natural selection, the *Kobresia pygmaea* community formed a compact and well-developed root system that not only protects soils from grazer trampling but also helps to cope with nutrient limitations by enabling medium-term nutrient storage and increasing productivity and competitive ability of roots against leaching and other losses (Miehe et al., 2019). Aside from climatic conditions, human activities have an impact on the *Kobresia pygmaea* community. Although the intensity of human activity on the Tibetan Plateau is low, the growth during the last two decades has been significantly greater than in other parts of the world (Li et al., 2017, 2018). Since 1960, with the shift of management strategies such as pastures, destocking, sedentarization, privatization, and fencing, overgrazing has been the key factor influencing the spatial distribution of the *Kobresia pygmaea* community (Gao and Li, 2016; Qiu, 2016). Overgrazing is another major cause of grassland deterioration in the QTP (Bai et al., 2002; Zhou et al., 2005; Li et al., 2010; Wang et al., 2012; Zhang et al., 2015).

In this study, precipitation in the driest period was discovered to be critically important in the east of the Yellow River's source region, in addition to the hottest season, the yearly average and maximum radiation, and the monthly temperature range (Table 1, with Importance values greater than 0.20). The growth season for alpine grassland in the Yellow River's source region is from May to September, with rain and high-temperature dominating (Meng et al., 2018). Extreme weather conditions (such as drought and high temperatures) hinder plant development during this time period (Miehe and Miehe, 2005). However, the distinctive structure of the *Kobresia pygmaea* community root may successfully withstand these occurrences (Li J. M. et al., 2016; Li R. et al., 2016; Miehe et al., 2019), which is also consistent with the results of environmental variables in our study.

The mean elevation of eastern edge of this study area is lower than 4,000 m, and mean annual precipitation is ≥450 mm. Poaceae community (*Elymus nutans* + *Stipa silena* + *Festuca ovina*) is widely distributed, overgrazing is the main inducing factor for grassland vegetation community variation (Zhou et al., 2005; Cao and Long, 2009; Miehe et al., 2019). Our result showed that the area of *Kobresia pygmaea* community potential distribution was 302.94 km^2, accounting for 21.12% of reality distribution in study area. Results of this study have shown that nearly 80% of the reality *Kobresia pygmaea* community is without climate driving (Figure 6). In other words, we demonstrate that the existence of *Kobresia pygmaea* community is mainly generated by human activities (for example, grazing) in the east source region of Yellow River. The *Kobresia pygmaea* community is the key stage in the management of degraded grassland. Further degradation of *Kobresia pygmaea* community will cause irreversible degradation (Cao and Long, 2009; Li et al., 2013). Our study might offer a scientific foundation for managing alpine meadow erosion in the Yellow River's source region.

4.2. Limitation for optimal niche model

Ten niche models were evaluated and examined in this study for their application to predict the spatial distribution of the *Kobresia*

pygmaea community. GLM, GBM, GAM, CTA, MARS, MaxEnt, SRE, and FDA were statistically or rules-based models, whereas ANN and RF were machine-learning algorithm-based models (Breiman, 1996; Phillips et al., 2006; Zhu et al., 2013). In this study, the RF model had superior prediction accuracy (with TSS and AUC of 0.74 and 0.92) and stability (CV of TSS and AUC of 0.12 and 0.03). There are, however, inevitable variables that impact model accuracy. Firstly, as compared to other models, the RF model is data-driven, which can automatically obtain and understand data, and has a flexible methodology. Expectedly, as the size of the input data set grows, so the model's estimation will be improved correspondingly (Han, 2001; He, 2008; Verrelst et al., 2015). It is made up of a big sample decision tree that is developed using high-dimensional data and has a high tolerance for data inaccuracy (Breiman, 1996, 2001). However, training an RF model with a limited sample size is complex, as it needs a substantial amount of tagged data and ground observed data (Verrelst et al., 2015; Ali et al., 2016). Furthermore, this type of model contains numerous elements, some of which (such as the climate) have high spatial quantization errors. As a result, the model continues to have some limits and uncertainties (Lehnert et al., 2015; Gao et al., 2013; Meng et al., 2020).

4.3. Unmanned aerial vehicle technology enables large-scale monitoring on the *Kobresia pygmaea* community

Kobresia pygmaea community distribution has received increasing attention in recent years as a key species of alpine meadow grassland on the QTP. However, its geographical distribution on the plateau is unknown (Zhang and Noltie, 2010; Miehe et al., 2011), and only a few scattered investigations at the sample plot level have been conducted (Dickore, 1995; Zhang and Noltie, 2010; Cao and Long, 2009). A large number of observation sites should be supplied before predicting the possible geographical distribution of the *Kobresia pygmaea* community (Li and Guo, 2013). However, utilizing the standard artificial observation approach makes large-scale observation impossible (Miehe et al., 2019).

In this work, the UAV aerial photography system FragMap was employed to acquire grass community observations, resulting in large-scale, fixed point, and repetitive observation of the *Kobresia pygmaea* community (Yi, 2017; Meng et al., 2018). The images taken by the UAV's Grid and Belt modes have a high resolution (1 cm and 0.09 cm for Grid and Belt mode, respectively) and a vast spatial representative range (1 photograph can represent a traditional observation site). And the resolution is sufficient to discern the *Kobresia pygmaea* community in the alpine meadow (Figure 4; Sun et al., 2018).

As a result, it is a remarkable novelty for this study to successfully employ a UAV aerial photography system to acquire observation sites for the existence or absence of the *Kobresia pygmaea community* in the Yellow River's source region. On the one hand, it saves a significant amount of people and material resources as well as economic input; on the other hand, it improves observation efficiency and enables large-scale fixed repetitive observation (Yi et al., 2016). However, the vegetation pieces and grassland communities were acquired by visual interpretation, and it requires good knowledge of plant taxonomy and time-consuming. Hence, the automatic identification of vegetation pieces and grassland communities based on aerial photographs and the deep-learning algorithm requires further exploration (Lv et al., 2022).

5. Conclusion

The forecast accuracy of 10 niche models was assessed in BIOMOD based on UAV observations of the *Kobresia pygmaea* community and its associated environmental parameters in the eastern section of the Yellow River's Source basin. The preliminary distribution of the *Kobresia pygmaea* community was predicted, and the following findings were reached: (1) Six of the 44 tested environmental factors (maximum radiation, monthly temperature difference, precipitation in the driest period, radiation in the warmest season, precipitation in the driest season, and annual average radiation) have high Importance values (>0.20), and there are 22 influencing factors in the study area with a cumulative contribution of more than 85%. (2) The RF model had the highest accuracy and stability in predicting the spatial distribution of the *Kobresia pygmaea* community, with TSS, AUC of 0.74 and 0.92, respectively; (3) the regions with a probability of *Kobresia pygmaea* community presence greater than 50% are primarily located in northern and central areas of Zeku County, northeastern and central areas of Henan County, and northeast, central, and eastern areas of Maqu County; (4) About 21.12% of *Kobresia pygmaea* community was derived by climate factors, and nearly 80% was derived by human activities. Human activities are the main factor leading to the formation of *Kobresia pygmaea* community in the east source region of Yellow River.

Data availability statement

The original contributions presented in the study are included in the article/supplementary material, further inquiries can be directed to the corresponding author.

Author contributions

YL and YS collected the data and write the manuscript. SY revised the manuscript. BM collected the data and revised the manuscript. All authors contributed to the article and approved the submitted version.

Funding

This study was supported by National Natural Science Foundation (nos. 42071056 and 31901393).

Acknowledgments

We thank the National Park of Qilian Mountain for helping in the field observation.

Conflict of interest

The authors declare that the research was conducted in the absence of any commercial or financial relationships that could be construed as a potential conflict of interest.

Publisher's note

References

Ali, I., Cawkwell, F., Dwyer, E., Barrett, B., and Green, S. (2016). Satellite remote sensing of grasslands: from observation to management-a review. *J. Plant Ecol.* 9, 649–671. doi: 10.1093/jpe/rtw005

Bai, W., Zhang, Y., Xie, G., and Shen, Z. (2002). Analysis of formation causes of grassland degradation in maduo county in the source region of yellow river. *J. Appl. Ecol.* 13, 823–826.

Breiman, L. (1996). Bagging predictors. *Mach. Learn.* 24, 123–140. doi: 10.1007/BF00058655

Breiman, L. (2001). Random forests. *Mach. Learn.* 45, 5–32. doi: 10.1023/A:1010933404324

Cao, G. M., and Long, R. J. (2009). System stability and its self-maintaining mechanism by grazing in alpine Kobresia meadow. *Chin. J. Agrometeorol.* 30, 553–559.

Chen, Y. Y., Yang, K., He, J., Qin, J., Jshi, J. C., Du, J. Y., et al. (2011). Improving land surface temperature modeling for dry land of China. *J. Geophys. Res.* 116:D20104. doi: 10.1029/2011JD015921

Chen, Q., Yu, R., Hao, Y., Wu, L., Zhang, W., Zhang, Q., et al. (2018). A new method for mapping aquatic vegetation especially un-derwater vegetation in lake ulansuhai using GF-1 satellite data. *Remote Sens.* 10:1279. doi: 10.3390/rs10081279

Citores, L., Ibaibarriaga, L., Lee, D. J., Brewer, M. J., Santo, M., and Chust, G. (2020). Modelling species presence - absence in the ecological niche theory framework using shape-constrained generalized additive models. *Ecol. Model.* 418:108926. doi: 10.1016/j.ecolmodel.2019.108926

Dickore, B. W. (1995). Revision and chorology of monocotyledonae of the Karakorum. Flora Karakorumensis I. *Angiospermac, Monocotyledonae. Stapfia (Linz)* 39:298. b App. (in German).

Elith, J., and Leathwick, J. R. (2009). Species distribution models: ecological explanation and prediction across space and time. *Ann. Rev. Ecol. Evol. Syst.* 40, 677–697. doi: 10.1146/annurev.ecolsys.110308.120159

Gao, S., Liu, Z. G., Xu, J. F., Mutz, S. G., He, S. Y., and Gao, S. B. (2013). Research on fault diagnosis for traction transformer on the basis of model-based diagnosis and expert system. *J. China Railw. Soc.* 35, 42–49.

Gao, J., and Li, X. (2016). Degradation of frigid swampy meadows on the Qinghai-Tibet plateau: current status and future directions of research. *Prog. Phys. Geogr.* 40, 794–810. doi: 10.1177/0309133316659283

Halvorsen, K., Arndt, A., Rosdahl, H., and Thorstensson, A. (2012). Evaluation of three different models of the shoulder kinematics: application to kayak paddling.

Han, L. C. A. (2001). Method of modifying error for non-synchronicity of grass yield remote sensing estimation and measurement. *Int. J. Remote Sens.* 22, 3363–3372. doi: 10.1080/01431160010006421

He, Q. (2008). *Neural Network and Its Application in IR*. Graduate School of Library and Information Science. Champaign, IL, USA: University of Illinois at Urbana-Champaign Spring.

Lehnert, L. W., Meyer, H., Wang, Y., Miehe, G., Thies, B., Reudenbach, C., et al. (2015). Retrieval of grassland plant coverage on the Tibetan plateau based on a multi-scale, multi-sensor and multi-method approach. *Remote Sens. Environ.* 164, 197–207. doi: 10.1016/j.rse.2015.04.020

Li, J. M., Ehlers, T. A., Werner, M., Mutz, S. G., Steger, C., and Paeth, H. (2016). Late quaternary climate, precipitation δ18O, and Indian monsoon variations over the Tibetan plateau. *Earth Planet. Sci. Lett.* 457, 412–422. doi: 10.1016/j.epsl.2016.09.031

Li, X., Gao, J., Brierley, G., Qiao, Y., Zhang, J., and Yang, Y. (2013). Rangeland degradation on the Qinghai-Tibet plateau: implications for rehabilitation. *Land Degrad. Dev.* 24, 72–80. doi: 10.1002/ldr.1108

Li, W. K., and Guo, Q. H. (2013). How to assess the prediction accuracy of species presence-absence models without absence data? *Ecography* 6, 788–799. doi: 10.1111/j.1600-0587.2013.07585.x

Li, L., Hang, Y., Liu, L., Wu, J., Li, S., Zhang, H., et al. (2018). Current challenges in distinguishing climatic and anthropogenic contributions to alpine grassland variation on the Tibetan plateau. *Ecol. Evol.* 8, 5949–5963. doi: 10.1002/ece3.4099

Li, R., Luo, T., Mölg, T., Zhao, J., Li, X., Cui, X., et al. (2016). Leaf unfolding of Tibetan alpine meadows captures the arrival of monsoon rainfall. *Sci. Rep.* 6:20985. doi: 10.1038/srep20985

Li, S., Wu, J., Gong, J., and Li, S. (2017). Human footprint in Tibet: assessing the spatial layout and effectiveness of nature reserves. *Sci. Total Environ.* 621, 18–29. doi: 10.1016/j.scitotenv.2017.11.216

Li, W., Xue, Z., Guo, S., Xu, D., Fan, C., and Zhang, J. (2010). Vegetation coverage changes and analysis of the driving forces in Maqu county based on 3S technology. *J. Lanzhou Univ.* 46, 85–95.

Lin, L. (2017). Response and Adaptation of Plant-Soil System of Alpine Meadows in Different Successional Stages to Grazing Intensity. PHD thesis, Gansu Agricultural University, Lanzhou, China

Liu, C., White, M., and Newell, G. (2013). Selecting thresholds for the prediction of species occurrence with presence-only data. *J. Biogeogr.* 40, 778–789. doi: 10.1111/jbi.12058

Liu, S., Zamanian, K., Schleuss, P., Zarebanadkouki, M., and Kuzyakov, Y. (2018). Degradation of Tibetan grasslands: consequences for carbon and nutrient cycles. *Agric. Ecosyst. Environ.* 252, 93–104. doi: 10.1016/j.agee.2017.10.011

Lv, Y., Zhao, X. Q., Zhang, S. R., Zhang, J. G., Yue, K. T., Meng, B. P., et al. (2022). Herbaceous dominant the changes of normalized difference vegetation index in the transition zone between desert and typical steppe in Inner Mongolia, China. *Front. Plant Sci.* 12:2044. doi: 10.3389/fpls.2021.832044

Ma, Z., Liu, H., Mi, Z., Zhang, Z., Wang, Y., Xu, W., et al. (2017). Climate warming reduces the temporal stability of plant community biomass production. *Nat. Commun.* 8:15378. doi: 10.1038/ncomms15378

Ma, L., Mi, C., Qu, J., Ge, D., Yang, Q., and Wilcove, D. S. (2021). Predicting range shifts of pikas (Mammalia, Ochotonidae) in China under scenarios incorporating land use change, climate change and dispersal limitations. *Divers. Distrib.* 27, 2384–2396. doi: 10.1111/ddi.13408

Meng, B. P., Gao, J. L., Liang, T. G., Cui, X., Yin, J. P., Feng, Q. S., et al. (2018). Modeling of alpine grassland cover based on unmanned aerial vehicle technology and multi-factor methods: a case study in the east of Tibetan plateau. *China. Remote Sens.* 10:320. doi: 10.3390/rs10020320

Meng, B. P., Liang, T. G., Yi, S. H., Yin, J. P., Cui, X., Ge, J., et al. (2020). Modeling alpine grassland above ground biomass based on remote sensing data and machine learning algorithm: a case study in the east of Tibetan plateau, China. *IEEE J. Sel. Top. Appl. Earth Observ.* 13, 2986–2995. doi: 10.1109/JSTARS.2020.2999348

Meng, B., Yang, Z., Yu, H., Qin, Y., Sun, Y., Zhang, J., et al. (2021). Mapping of *Kobresia pygmaea* community based on unmanned aerial vehicle technology and gaofen remote sensing data in alpine meadow grassland: a case study in eastern of Qinghai-Tibetan plateau. *Remote Sens.* 13:2483. doi: 10.3390/rs13132483

Miehe, G., Miehe, S., Kaiser, K., Jianquan, L., and Zhao, X. (2008). Status and dynamics of the Kobresia pygmaea ecosystem on the Tibetan plateau. *Ambio: J. Hum. Environ.* 4:37.

Miehe, G., Bach, K., Miehe, S., Kluge, J., Yang, Y., Duo, L., et al. (2011). Alpine steppe plant communities of the Tibetan highlands. *Appl. Veg. Sci.* 14, 547–560. doi: 10.1111/j.1654-109X.2011.01147.x

Miehe, G., and Miehe, S. (2005). Environmental changes in the pastures of Xizang. *Marburger Geographische Schriften.* 135, 282–311.

Miehe, G., Schleuss, P., Seeber, E., Babel, W., Biermann, T., Braendle, M., et al. (2019). The *Kobresia pygmaea* ecosystem of the Tibetan highlands - origin, functioning and degradation of the world's largest pastoral alpine ecosystem Kobresia pastures of Tibet. *Sci. Total Environ.* 648, 754–771. doi: 10.1016/j.scitotenv.2018.08.164

Muoz, M. E. D. S., Giovanni, R. D., Siqueira, M. F. D., Sutton, T., Brewer, P., Pereira, R. S., et al. (2011). Open Modeller: a generic approach to species' potential distribution modelling. *Geo Informatica.* 15, 111–135.

Petitpierre, B., Broennimann, O., Kueffer, C., Daehler, C., and Guisan, A. (2017). Selecting predictors to maximize the transferability of species distribution models: lessons from cross-continental plant invasions. *Glob. Ecol. Biogeogr.* 26, 275–287. doi: 10.1111/geb.12530

Phillips, S., Anderson, R., and Schapire, R. (2006). Maximum entropy modeling of species geographic distribution. *Ecol. Model.* 190, 231–259. doi: 10.1016/j.ecolmodel.2005.03.026

Qiu, J. (2016). Trouble in Tibet. *Nature* 529, 142–145. doi: 10.1038/529142a

Stockwell, D., and Peters, D. (1999). The GARP modelling system: problem and solution to automated spatial prediction. *Int. J. Geogr. Inf. Sci.* 13, 143–158. doi: 10.1080/136588199241391

Su, Y., Guo, Q., Hu, T., Guan, H., Jin, S., An, S., et al. (2020). An updated vegetation map of China (1:1000000). *Sci. Bull.* 65, 1125–1136. doi: 10.1016/j.scib.2020.04.004

Sun, Y., Yi, S., and Hou, F. (2018). Unmanned aerial vehicle methods makes species composition monitoring easier in grasslands. *Ecol. Indic.* 95, 825–830. doi: 10.1016/j.ecolind.2018.08.042

Thuiller, W., Lafourcade, B., Engler, R., and Araújo, M. B. (2009). BIOMOD – a platform for ensemble forecasting of species distributions. *Ecography* 32, 369–373. doi: 10.1111/j.1600-0587.2008.05742.x

Verrelst, J., Camps-Valls, G., Muñoz-Marí, J., Rivera, J. P., Veroustraete, F., Clevers, J. G. P. W., et al. (2015). Optical remote sensing and the retrieval of terrestrial vegetation bio-

geophysical properties – a review. *ISPRS J. Photogramm. Remote Sens.* 108, 273–290. doi: 10.1016/j.isprsjprs.2015.05.005

Wang, S., Duan, J., Xu, G., Wang, Y., Zhang, Z., Rui, Y., et al. (2012). Effects of warming and grazing on soil n availability, species composition, and ANPP in an alpine meadow. *Ecology* 93, 2365–2376. doi: 10.1890/11-1408.1

Wang, P., Lassoie, J., Morreale, S., and Dong, S. (2015). A critical review of socioeconomic and natural factors in ecological degradation on the Qinghai-Tibetan plateau, China. *Rangeland J.* 37:1. doi: 10.1071/RJ14094

Wen, Q., Zhang, Z., Liu, S., Wang, X., and Wang, C. (2010). Classification of grassland types by modis time-series images in Tibet, China. *IEEE J. Sel. Top. Appl. Earth Observ. Remote Sens.* 3, 404–409. doi: 10.1109/JSTARS.2010.2049001

Wessels, K. J., Prince, S. D., Frost, P. E., and van Zyl, D. (2004). Assessing the effects of human-induced land degradation in the former homelands of northern South Africa with a 1 km AVHRR NDVI time-series. *Remote Sens. Environ.* 91, 47–67. doi: 10.1016/j.rse.2004.02.005

Wessels, K. J., Prince, S. D., Malherbe, J., Small, J., Frost, P. E., and Van Zyl, D. (2007). Can human-induced land degradation be distinguished from the effects of rainfall variability? A case study in South Africa. *J. Arid Environ.* 68, 271–297. doi: 10.1016/j.jaridenv.2006.05.015

Xu, Z. L., Peng, H. H., and Peng, S. Z. (2015). The development and evaluation of species distribution models. *Acta Ecol. Sin.* 35:5846. doi: 10.5846/stxb201304030600

Yang, K., He, J., Tang, W. J., Qin, J., and Cheng, C. C. (2010). On downward shortwave and longwave radiations over high altitude regions: observation and modeling in the Tibetan plateau. *Agric. For. Meteorol.* 150, 38–46. doi: 10.1016/j.agrformet.2009.08.004

Yi, S. (2017). Frag MAP: a tool for long-term and cooperative monitoring and analysis of small-scale habitat fragmentation using an unmanned aerial vehicle. *Int. J. Remote Sens.* 38, 1–12. doi: 10.1080/01431161.2016.1253898

Yi, S., Chen, J., Qin, Y., and Xu, G. W. (2016). The burying and grazing effects of plateau pika on alpine grassland are small: a pilot study in a semiarid basin on the Qinghai-Tibet plateau. *Biogeosciences* 13, 6273–6284. doi: 10.5194/bg-13-6273-2016

Zhang, Y., Gao, Q., Dong, S., Liu, S., Wang, X., Su, X., et al. (2015). Effects of grazing and climate warming on plant diversity, productivity and living state in the alpine rangelands and cultivated grasslands of the Qinghai-Tibetan plateau. *Rangel. J.* 37, 57–65. doi: 10.1071/RJ14080

Zhang, S. R., and Noltie, H. J. (2010). "Kobresia Willd," in *Flora of China*. eds. Z. Y. Wu, P. H. Raven and D. Y. Hong (St. Louis: Science Press, Beijing, and Missouri Botanical Garden Press), 23, 269–285.

Zhou, H., Zhao, X., Zhou, L., Tang, Y., Liu, W., and Shi, Y. (2005). Application of analytic hierarchy process on the alpine grassland degradation in the source region of the Yangtze and yellow rivers. *Resour. Sci.* 27, 63–70.

Zhu, G. P., Liu, G. Q., Bu, W. J., and Gao, Y. B. (2013). Ecological niche modeling and its applications in biodiversity conservation. *Biodivers. Sci.* 21, 90–98. doi: 10.3724/SP.J.1003.2013.09106

frontiers | Frontiers in Ecology and Evolution

TYPE Original Research
PUBLISHED 08 March 2023
DOI 10.3389/fevo.2023.1149595

OPEN ACCESS

EDITED BY
Kerou Zhang,
Chinese Academy of Forestry, China

REVIEWED BY
Gang Fu,
Institute of Geographic Sciences and Natural Resources Research (CAS), China
Xiaolong Huang,
Nanjing Institute of Geography and Limnology (CAS), China

*CORRESPONDENCE
Linfeng Li
✉ lilinfeng@ucas.ac.cn

SPECIALTY SECTION
This article was submitted to Population, Community, and Ecosystem Dynamics, a section of the journal Frontiers in Ecology and Evolution

RECEIVED 22 January 2023
ACCEPTED 17 February 2023
PUBLISHED 08 March 2023

CITATION
Zheng Z, Wen F, Li C, Guan S, Xiong Y, Liu Y, Qian R, Lv M, Xu S, Cui X, Wang Y, Hao Y and Li L (2023) Methane uptake responses to heavy rainfalls co-regulated by seasonal timing and plant composition in a semiarid grassland. *Front. Ecol. Evol.* 11:1149595. doi: 10.3389/fevo.2023.1149595

Methane uptake responses to heavy rainfalls co-regulated by seasonal timing and plant composition in a semiarid grassland

Zhenzhen Zheng[1], Fuqi Wen[1], Congjia Li[1], Shuntian Guan[1], Yunqi Xiong[1], Yuan Liu[1], Ruyan Qian[1], Mengbo Lv[1], Shaorui Xu[1], Xiaoyong Cui[1], Yanfen Wang[2,3], Yanbin Hao[1,2] and Linfeng Li[3]*

[1]College of Life Sciences, University of Chinese Academy of Sciences, Beijing, China, [2]Beijing Yanshan Earth Critical Zone National Research Station, University of Chinese Academy of Sciences, Beijing, China, [3]College of Resources and Environment, University of Chinese Academy of Sciences, Beijing, China

Heavy rainfalls caused by global warming are increasing widespread in the future. As the second greenhouse gas, the biological processes of methane (CH_4) uptake would be strongly affected by heavy rainfalls. However, how seasonal timing and plant composition affect CH_4 uptake in response to heavy rainfalls is largely unknown. Here, we conducted a manipulative experiment to explore the effects of heavy rainfall imposed on middle and late growing season stage on CH_4 uptake of constructed steppe communities including graminoid, shrub and their mixture in Inner Mongolia, China. The results of mixed effect model showed that both heavy rainfalls decreased CH_4 uptake. Nevertheless, the effect magnitude and the pathways were varied with seasonal timing. Relatively, the late heavy rainfall had larger negative effects. Structural equation model suggested that late heavy rainfall decreased CH_4 uptake through decreased diffusivity, *pmoA* abundance, and NH_4^+-N content, as products of high soil water content (SWC). However, middle heavy rainfall decreased CH_4 uptake only by increasing SWC. Additionally, aboveground biomass (AGB) had negative effects on CH_4 uptake under both heavy rainfalls. Additionally, plant composition not only affected CH_4 uptake but also regulated CH_4 uptake in response to heavy rainfalls. Late heavy rainfall had less negative effect on CH_4 uptake in graminoid community than in other two communities, in coincidence with less reduction in NH_4^+-N content and less increase in SWC and AGB. In contrast, we did not observe obvious difference in effects of middle heavy rainfall on CH_4 uptake across three communities. Our findings demonstrated that magnitude and pathways of heavy rainfall effects on CH_4 uptake were strongly co-regulated by seasonal timing and plant composition.

KEYWORDS

CH_4, climate extremes, greenhouse gasses, methanotrophs, community composition, precipitation

Introduction

Methane (CH_4) is a powerful greenhouse gas and strongly contributes to global warming and resultant changes in precipitation, as the global warming potential is 28–36 times than that of carbon dioxide (CO_2) at 100-y timescale (Jiang et al., 2012; Fischer and Knutti, 2016; Otto et al., 2018; IPCC, 2021). Aerobic soils are important CH_4 sink, in which 9–47 Tg CH_4 $year^{-1}$ from the atmosphere was oxidated by methanotroph through methane monooxygenase (MMO) (Elango et al., 1997; Fest et al., 2015; Yue et al., 2019, 2022). The subunit genes of MMOs, specifically *pmoA,* are used as biomarker genes for the presence and abundance of bacterial methanotrophs (Fest et al., 2015; Tentori and Richardson, 2020). Therefore, understanding effects of changes in precipitation on CH_4 uptake in drylands and underlying microbial mechanisms have great implications for prediction of future carbon cycling and its feedback to climate changes.

It has been confirmed that precipitation changes are expected to significantly influence the intensity of CH_4 sinks (Aronson et al., 2019; Martins et al., 2021). For example, increased precipitation by 30% significantly increased CH_4 uptake in temperate deserts (Yue et al., 2019). In contrast, CH_4 uptake was decreased and unchanged by increased precipitation in alpine meadows and in degraded steppe grasslands, respectively (Chen W. W. et al., 2013; Wu et al., 2020). Meta-analysis studies suggested that increased precipitation can decrease CH_4 uptake in terrestrial ecosystems at the global scale (Chen H. et al., 2013; Yan et al., 2018). Although these results highlighted the important role of increased precipitation in regulating CH_4 uptake in aerobic soils, to date, there is great uncertainty about the effects of extreme precipitation with several days (e.g., heavy rainfall events), rather than chronic increases in precipitation at seasonal timescale, on CH_4 uptake.

Effects of chronic increases in precipitation and heavy rainfall on CH_4 uptake may be largely different. Soil moisture controlled CH_4 uptake through affecting the methanotroph community and altering air-soil diffusion (Wei et al., 2015). A bell-shaped relationship was observed between soil moisture and CH_4 uptake with CH_4 uptake reached the peak at intermediate soil moisture (Dijkstra et al., 2013; Li et al., 2016; Zhang et al., 2021). Above the optimum soil moisture, soil moisture would limit oxygen (O_2) diffusion in soils and depress the activity of methanotroph communities, inhibiting CH_4 uptake (Curry, 2007; Liptzin et al., 2011; Zhuang et al., 2013). Hence, slight increases in precipitation may promote methanotroph community and thereby increase CH_4 uptake while heavy rainfall caused saturation soil moisture and thereby would reduce CH_4 uptake. Additionally, CH_4 uptake is sensitive to soil ammonium (NH_4^+-N) and nitrate (NO_3^--N). NH_4^+-N had an inhibiting effect on CH_4 uptake mainly through replacing CH_4 to be oxidized by methanotroph (Schnell and King, 1994; Yue et al., 2022), while NO_3^--N had an inhibiting effect on CH_4 uptake through changing methanotroph activity and composition or enhancing soil oxidation potential and environment (Le Mer and Roger, 2001; Yue et al., 2022). Increased precipitation is likely to enhance soil inorganic nitrogen by accelerating mineralization (Cabrera and Kissel, 1988; Bai et al., 2012). In contrast, soil inorganic nitrogen may decline through leaching and runoff under heavy rainfalls (Borken and Matzner, 2009; Cregger et al., 2014). Thus, slight increases in precipitation and heavy rainfall are likely to induce opposite impacts on CH_4 uptake through the pathway of NH_4^+-N and NO_3^--N content.

Furthermore, seasonal timing and plant composition potentially modulate CH_4 uptake in response to heavy rainfalls. Previous studies suggested that seasonal timing strongly regulates effects of heavy rainfall on multiple ecosystem attributes such as soil water, carbon, and nitrogen availability, as well as plant biomass and phenology (Li et al., 2019; Post and Knapp, 2020; Li et al., 2022). Therefore, we except that impacts of heavy rainfall on CH_4 uptake may be also regulated by seasonal timing. Indeed, Zhao et al. (2017) found that CH_4 uptake was reduced by 62% and 45% during the period of middle and late heavy rainfall, respectively. Besides, there were significant differences in the composition and abundance of methanogens in soil with different plant species, resulting in different potential of CH_4 uptake (Dai et al., 2015). For example, CH_4 uptake capacity was stronger in soil of oat than that in native vegetation (Hüppi et al., 2022). Moreover, plant communities with higher-diversity were less negatively affected by floods and mature plants can withstand flooding better than seedlings (Gattringer et al., 2017; Wright et al., 2017). Although several studies had reported that plant community composition and seasonal timing could moderate heavy rainfall effects on CH_4 uptake capacity (Liebner et al., 2015; Tong et al., 2017; Zhao et al., 2017; Yue et al., 2022), it is unknown the interactions on CH_4 uptake in the face of heavy rainfall.

To explore the individual and especially interactive effects of heavy rainfall timing and species composition on CH_4 uptake in response to heavy rainfall, we conducted a field experiment in which heavy rainfall occurring in middle and late growing season were imposed on plots with three experimental plant communities of graminoids, shrubs and their combination, respectively. We hypothesized that: (1) Heavy rainfalls would suppress CH_4 uptake due to reduced diffusivity and methanotrophs activity, regardless of seasonal timing, (2) Heavy rainfall occurring in middle growing season with high air temperatures may cause less saturated soil conditions, thus CH_4 uptake is likely to be less decreased by middle heavy rainfall than late heavy rainfall, and (3) Plant community composition would adjust CH_4 uptake in response to heavy rainfalls though soil moisture, inorganic content, aboveground biomass and methanotrophs activities.

Materials and methods

Study site

We carried out the study at the Research Station of Animal Ecology (44°18′ N, 116°45′ E 1079 m.a.s.l) in a semiarid grassland of Inner Mongolia Autonomous Region, China. The study site has a temperate continental semi-arid climate, of which the mean annual precipitation (1953 to 2017) is 281 mm and the mean annual temperature is 2.5°C. The plant species in the study region is mainly dominated by xeric rhizomatous grasses, needle grasses and perennial forbs such as *Leymus chinensis, Stipa grandis* and *Medicago falcata*. The soil type in this experimental region is classified as chestnut soil consisting of 60% sand, 18% clay and 17% silt.

Experiment design

The experiment was began in 2012. In this study, we reported the data measured in 2021. According to the statistical analysis of

~60-year (1953–2012) historical meteorological data provided by The Xilin Gol League Meteorological Administration, the longest continuous rainfall period of daily precipitation (≥ 3 mm) was 20 days during the growing season. The total effective precipitation was calculated over all 20 days periods, which was 250 mm. Thus, heavy rainfall was defined as 250 mm rainfall over 20 d in this study (12.5 mm d^{-1}) (Hao et al., 2017). We used a two-way split-plot experiment design to study the effect of heavy rainfall on CH_4 uptake joint control of seasonal timing and plant composition. The main treatment had 9 plots and each main plot was made up of 3 sub-plots, thus there were total 27 sub-plots in heavy rainfall treatments experiment (Supplementary Figure S1). Specifically, three heavy rainfall treatments were set up in the main plots with three replicates: ambient control, mid-stage heavy rainfall (HR-mid, 15 July-5 August) and late-stage heavy rainfall (HR-late, 15 August-5 September), respectively. Three plant community compositions were set up in the sub-plots: graminoid (*Leymus chinensis* and *Stipa grandis*), shrub (*Caragana microphylla* and *Artemisia frigida*) and their mixture. Plant seeds of dominant local species were cultivated at the start of the study in early May 2012. The total coverage of graminoids, shrub and mixture community were 70, 80, and 75%, respectively.

Twenty-seven 2 m × 2 m sub-plots were established with 1-m intervals between sub-plots. The ambient control sub-plots remained uncovered year-round. Heavy rainfall treatment sub-plots were covered with 27 m^2 rainout shelters (4.5 m × 6 m, height 3 m) to prevent natural rainfall and greenhouse effect during the treatment periods. The rainout shelters were made of transparent polyester fiber material to ensure no significant shading. Non-target plant seedlings in each subplot were weekly removed to maintain fixed plant community composition during the entire growing season.

CH_4 flux and soil water content measurements

Soil water content (SWC) and CH_4 fluxes were measured three times monthly during the growing season in 2021. Time domain reflectometry (TDR 300 Soil Moisture Meter) with 20 cm probe was used to record SWC. CH_4 fluxes were measured by laser-based fast greenhouse gas analyzer with an in-house closed chamber. The data collection frequency of 1 Hz was utilized to measure CH_4 fluxes (Kang et al., 2018). The volume of cube chamber is 1.25×10^5 cm^3, which was equipped with two electric fans in the center of the chamber ceiling to mix air concentration. Laser-based fast greenhouse gas analyzer has two 20-m rubber internal pipes, which were used to connect with the closed chamber through two 2-cm diameter holes on top of the chamber. Two pipes were used to transport gas from the greenhouse gas analyzer to the chamber and return from the chamber to the analyzer. Each subplot had a stainless frame (length × width × height = 50 cm × 50 cm × 10 cm) with 2 cm wide water groove. Each frame was installed and inserted 7 cm deep in soil and retained 3 cm above ground. Enough water should be put into the grooves of frames to guarantee gas tightness before mounting the chamber on the frame. Gas sampling area in each sub-plot was measured between 9:00 am and 10:00 am local time. In each sampling area, the gas in chamber was measured for 10 min, and the chamber should be opened for 2 min before the next measurement. We calculated CH_4 flux from the linear slope.

$$Fc = \frac{dc}{dt} \times \frac{M}{V_0} \times \frac{P}{P_0} \times \frac{T_0}{T} \times H$$

where F is the CH_4 flux rate [mg/(m^2·h)]; dc / dt is the cumulative growth rate of CH_4; M and P represent the molar mass of CH_4 (g/mol) and the air pressure (Pa), respectively; V_0 and P_0 represent the standard molar volume (22.41 m^3/mol) and standard air pressure (101,325 Pa), respectively; T and T_0 represent the absolute temperature inside the chamber (oK) and absolute temperature (oK), respectively; and H is the effective height of the chamber (m).

Above-ground biomass measurement

Harvest method was used to measure above-ground biomass (AGB). We harvested all aboveground living plant tissues in a 50 cm × 50 cm quadrat of each sub-plot on September 21st, 2021. All plant tissues of each quadrat were put in the oven and dried at 65°C until they had constant weight.

Soil property measurement

Three soil cores were taken in 20 cm deep in each plot using an auger (2.5 cm in diameter) on September 21st, 2021. Roots and stones of soil were removed from three core sets and homogenized by 2 mm sieves. The extract was a mixture solution of 10 g fresh soil sample and 40 ml 0.5 M K_2SO_4 solution, which were shaken for 30 min in shaker. After mixing well, NH_4^+-N and NO_3^--N concentration of soil sample were detected by a continuous flow automatic ion analyzer (SEAL Analytical GmbH, Norderstedt, Germany) (Wachendorf et al., 2008).

DNA extraction and qPCR

DNA were extracted from fresh soil of 0.5 g by Power Soil DNA Isolation Kit (MOBIO Laboratories, United States) according to the specification information. DNA quality of soil was assessed by NanoDrop 2000 UV–Vis spectrophotometer (Thermo Scientific, Wilmington, Delaware, USA). The methanotrophic *pmoA* gene abundance was determined by quantitative polymerase chain reaction (qPCR) using Eppendorf Masterpiece realplex sequence detection system (Applied Biosystems 7500/7600). Standard curves were created with plasmid DNA in ten-fold serial dilutions. The primer sets were used for *pmoA*: 5′-GGNGACTGGGACTTCTGG-3′ and 5′-CCGGMGCAACGTCYTTACC-3′. The 20 μL qPCR reaction consisted of 1 μL DNA template, 0.2 μL of front and back primer, 10.4 μL mixture solution of ROX and Takara SYBR®Premix Ex Taq ™ (Perfect RealTime) and 8.4 μL sterile water. After the reaction solution has been thoroughly mixed, the hole in the 96-well plate was filled with 20 μL qPCR reaction solution. Additionally, the contamination was detected by adding 19 μL qPCR reaction solution into the hole of 96-well plate without DNA template during the experiment. The sequential reaction conditions for the *pmoA* gene were set as: an initial denaturation at 95°C for 30 s, followed by 40 cycles at 95°C for 30 s, 60°C for 45 s, and 68°C for 45 s, with a final extension at 80°C for 30 s.

Statistical analyses

We conducted Duncan's multiple comparison to test differences of heavy rainfall with seasonal timing, plant composition and their interaction effects on variables including CH_4 uptake, soil water content, aboveground biomass, *pmoA* abundance, NH_4^+-N and NO_3^--N content. Mixed-effects models were conducted using the NLME package in R v.3.4.4 (R Core Team, 2018) to compare the effects of middle and late growing season heavy rainfall, plant composition, and the interaction effects of plant composition and heavy rainfall on the above variables, respectively. Structural equation model (SEM) analyzes were performed using the piecewise SEM package to explore direct and indirect impacts of heavy rainfall on CH_4 uptake (Domeignoz-Horta et al., 2020). The most variation can explain by this model, including low Akaike Information Criterion (AIC), a nonsignificant Chi-squared test ($p > 0.05$) and high Comparative Fit Index (CFI > 0.9).

Result

Seasonal dynamics and response of soil moisture content to heavy rainfalls

Total growing season precipitation (GSP) of control, HR-mid and HR-late were 351 mm, 513.16 mm, and 559.02 mm, respectively. Regardless of seasonal timing, SWC was significantly increased by heavy rainfalls in all three communities ($p = 0.01$ and <0.0001 for HR-mid and HR-late, respectively; Figure 1 and Table 1). Overall, SWC in HR-late seems slightly higher than that in HR-mid (Figures 1E,F; Supplementary Figure S2). Plant community composition had no significant effects on SWC ($p = 0.54$ for composition, Table 1). However, the SWC in graminoid community was slightly less increased by heavy rainfalls compared with shrub and mixture communities (Supplementary Figure S2).

Response of CH_4 uptake to heavy rainfalls

Over the growing season, averaged CH_4 uptake significantly decreased by HR-mid ($p = 0.03$) and HR-late ($p < 0.0001$) in all three communities (Figures 2E,F). The reductions were mainly occurred during the period of the heavy rainfalls. Relatively, HR-late had larger negatively effects on CH_4 uptake than HR-mid. There were significant differences of CH_4 uptake among three communities with the least CH_4 uptake in shrub community ($p < 0.0001$, Table 1; Supplementary Figure S3). HR-late effects on CH_4 uptake depended on plant composition ($p = 0.03$ for HR-late × Composition), with the least decreased CH_4 uptake in graminoid community than that in other two communities. There was also a marginally significant interaction between HR-mid × Composition ($p = 0.08$) on CH_4 uptake, but the effects of HR-mid on CH_4 uptake were similar across three communities. Collectively, negative effects of heavy rainfalls on CH_4 uptake modulated by seasonal timing and plant community composition.

Response of *pmoA* abundance, AGB, NH_4^+-N and NO_3^--N to heavy rainfalls

Similarly, heavy rainfalls effects on soil inorganic N content and *pmoA* abundance were changed with seasonal timing and plant community composition. Both two heavy rainfalls significantly declined *pmoA* abundance for three communities but the effects were larger in mixture community than in other two communities ($p = 0.01$ and 0.0001 for HR-mid × Composition and HR-late × Composition) (Figure 3A; Table 1). Regardless of plant composition, HR-mid and HR-late unchanged and significantly increased AGB, respectively (Figure 3B; Table 1), NH_4^+-N was significantly increased by HR-mid but significantly declined by HR-late in three communities (Figure 3C). Similarly, HR-mid significantly increased NO_3^--N content (Figure 3D; Table 1), mainly in graminoid and mixture communities. In contrast, HR-late had little effects on NO_3^--N content.

The influence of abiotic and biotic factors on CH_4 uptake

Structural equation model showed that SWC had directly negative impacts on CH_4 uptake and *pmoA* abundance under two heavy rainfalls. Additionally, CH_4 uptake negatively correlated with AGB under two heavy rainfalls. However, CH_4 uptake positively correlated with *pmoA* abundance in HR-late but not in HR-mid. SWC had significantly positive impact on NH_4^+ under HR-mid, while opposite impact between SWC and NH_4^+ was found in HR-late. Moreover, NH_4^+ positively correlated with *pmoA* abundance only in HR-late. NO_3^- had no significant relationships with CH_4 uptake (Figure 4). In short, heavy rainfalls with different seasonal timing decreased CH_4 uptake through different pathways.

Discussion

Understanding extreme precipitation scenario on CH_4 uptake has important implications for predicting future global climate changes and terrestrial C cycling. To explore how seasonal timing and plant composition affected CH_4 uptake in response to heavy rainfalls, we conducted a manipulative experiment in a semiarid grassland of Inner Mongolia, China. In this study, we identified CH_4 uptake in response to heavy rainfall are regulated by independent and especially interactive effects of heavy rainfall timing and plant composition. Our results demonstrate that seasonal timing strongly controls size and pathway of negative effects of heavy rainfall on CH_4 uptake and importantly the regulating effects of plant composition on CH_4 uptake response to heavy rainfall via soil water content, *pmoA* abundance, NH_4^+-N content and AGB.

Heavy rainfalls decrease CH_4 uptake

CH_4 uptake was significantly decreased by heavy rainfalls, regardless of seasonal timing and plant community composition in our study (Figure 2). Previous study showed that soil moisture and CH_4 uptake had a hump-shaped relationship, where the optimum

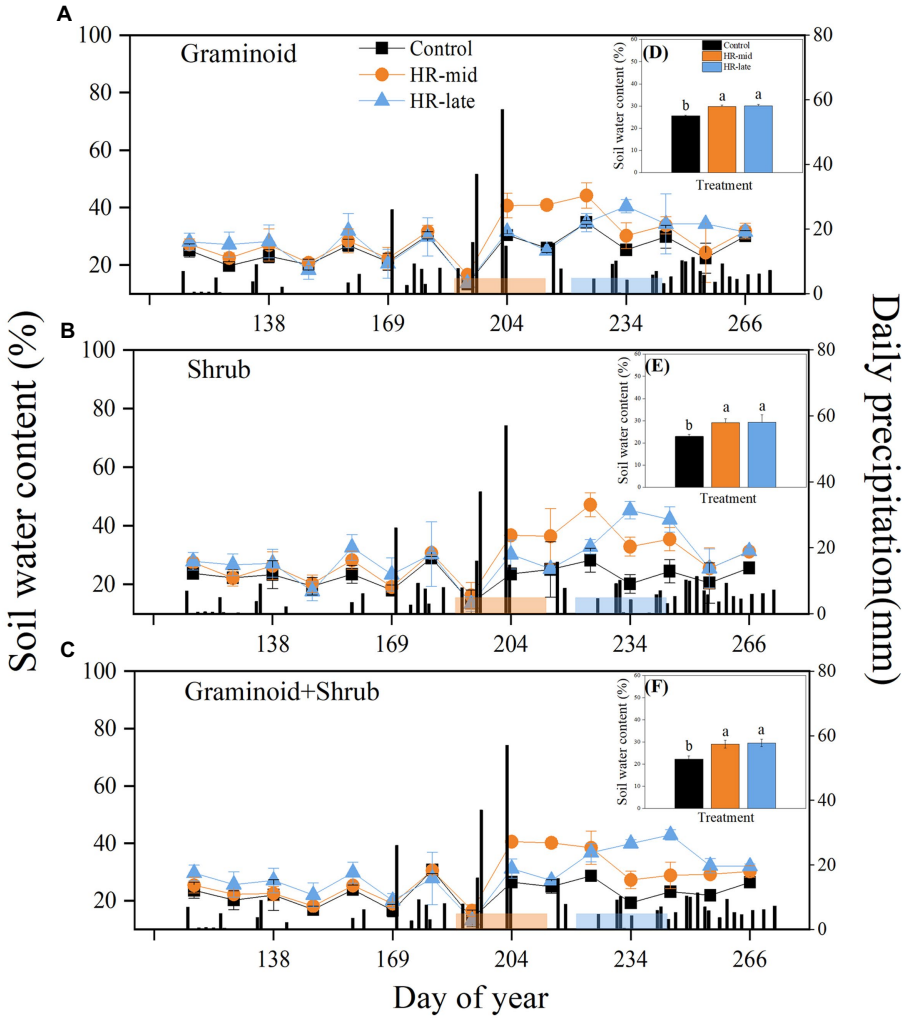

FIGURE 1
Seasonal dynamic and mean of soil water content under heavy rainfall treatments in graminoid **(A,D)**, shrub **(B,E)**, and graminoid +shrub **(C,F)** plots. Different letters above bars in d, e and f indicate significant difference among treatments at $p \leq 0.05$. The orange and blue shaded regions in a–c indicate the periods of the HR-mid (heavy rain imposed in middle of the growing season, orange line) and HR-late (heavy rainfall imposed late in the growing season, blue line) treatments, respectively. Error bars show one standard error of the mean.

TABLE 1 ***p*-Value from mixed-effect model analyzes of HR-mid and HR-late, community composition and their interactions on soil water content (SWC), aboveground biomass (AGB), CH_4 uptake, abundance of *pmoA*, and content of NH_4^+-N and NO_3^--N.**

Fixed effect	DF		SWC	AGB	CH_4 uptake	*pmoA*	NH_4^+-N	NO_3^--N
	Num	Den						
HR-mid	1	24	**0.01**	0.44	**0.04**	**<0.0001**	**<0.0001**	**0.04**
HR-late	1	24	**<0.0001**	**0.05**	**<0.0001**	**<0.0001**	**0.004**	0.77
Composition	2	24	0.27	**<0.0001**	**<0.0001**	**0.001**	**0.03**	0.21
HR-mid × Composition	2	24	0.85	0.85	0.08	**0.01**	0.22	0.10
HR-late × Composition	2	24	0.49	0.95	**0.03**	**0.0001**	0.58	0.96

p-Values in bold are statistically significant to an alpha value of 0.05.

moisture is 10 % -12 % for highest CH_4 uptake in a semiarid and arid soils (Dijkstra et al., 2011; Li et al., 2016; Yue et al., 2022). Moderate soil moisture could significantly promote CH_4 uptake, which could be significantly inhibited by too- low or too- high soil moisture (Van den Pol-van Dasselaar et al., 1998; Dijkstra et al., 2011). In our study, SWC were above 12% in all treatments throughout the growing season. High soil moisture induced by heavy rainfalls would cause anaerobic soil conditions, low soil oxygen (O_2) concentrations and CH_4 diffusion (Figure 1). Additionally, *pmoA* abundance decreased in both two heavy rainfalls (Figure 3A). Taken together, these results

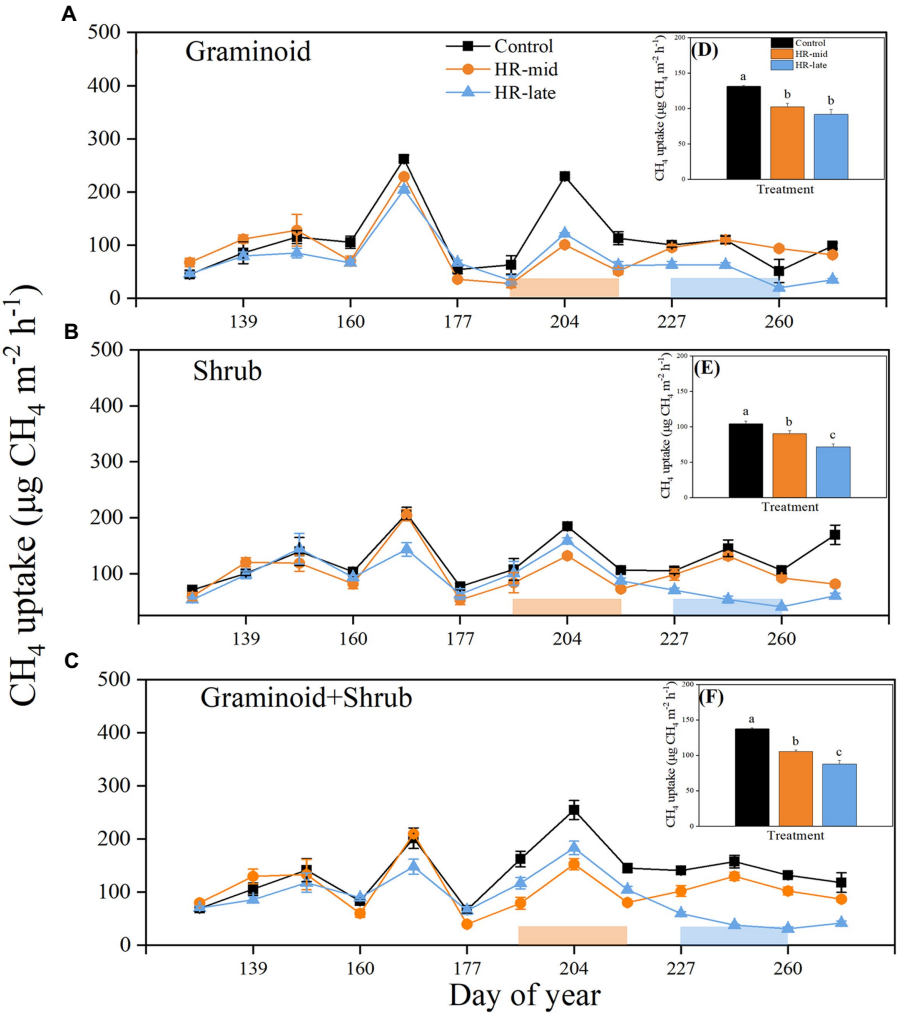

FIGURE 2
Seasonal dynamic and mean of CH_4 uptake under heavy rainfall treatments in graminoid **(A,D)**, shrub **(B,E)**, and graminoid +shrub **(C,F)** plots. Different letters above bars in d, e and f indicate significant difference among treatments at $p \leq 0.05$. The orange and blue shaded regions in a–c indicate the periods of the HR-mid (heavy rain imposed in middle of the growing season, orange line) and HR-late (heavy rainfall imposed late in the growing season, blue line) treatments, respectively. Error bars show one standard error of the mean.

suggested that experimental heavy rainfalls continuously decreased CH_4 diffusivity and O_2 availability and thus inhibited the activity of methanotrophs, supporting our first hypothesis. As a result, SWC showed negatively relationship with CH_4 uptake under two heavy rainfalls in our study (Figure 4).

Magnitude and pathways of heavy rainfall effects on CH_4 uptake depend on seasonal timing

Although two heavy rainfalls had negative effects on CH_4 uptake, the effect magnitude varied with seasonal timing. Consistent with the second hypothesis, CH_4 uptake is less decreased by HR-mid than HR-late in all three communities (Figure 2). This may be because HR-mid received less precipitation than HR-late (513.16 mm vs. 559.02 mm, Figure 1). In addition, higher air temperatures during the period of HR-mid would induce larger evapotranspiration. As a result, HR-mid caused less saturated soil conditions than HR-mid, which was reflected by slightly lower SWC in HR-mid than in HR-late (Figure 1F). As discussed above, SWC had negative impacts on CH_4 uptake in our study. Thus, lower SWC and corresponding less saturated soil conditions under HR-mid induced less reduction in CH_4 uptake.

Structural equation model showed that SWC and resultant anaerobic conditions were main controller of CH_4 uptake (Wei et al., 2015; Zhou et al., 2021). AGB also had direct negative effects on CH_4 uptake under both heavy rainfalls (Figure 4B). Previous studies showed similar trends that increased AGB may contribute to increasing soil water-holding capacity, maintaining high soil moisture and inhibiting soil substrate availability. As a result, methanotrophs activities and CH_4 oxidation in soil were inhibited (Robson et al., 2007; Zhang et al., 2012; Tang et al., 2018). Besides, high SWC directly and indirectly inhibited *pmoA* abundance through decreasing NH_4^+-N content, ultimately, suppressing CH_4 uptake in HR-late. CH_4 was oxidated by methanotroph, thus, it is not surprising that low *pmoA*

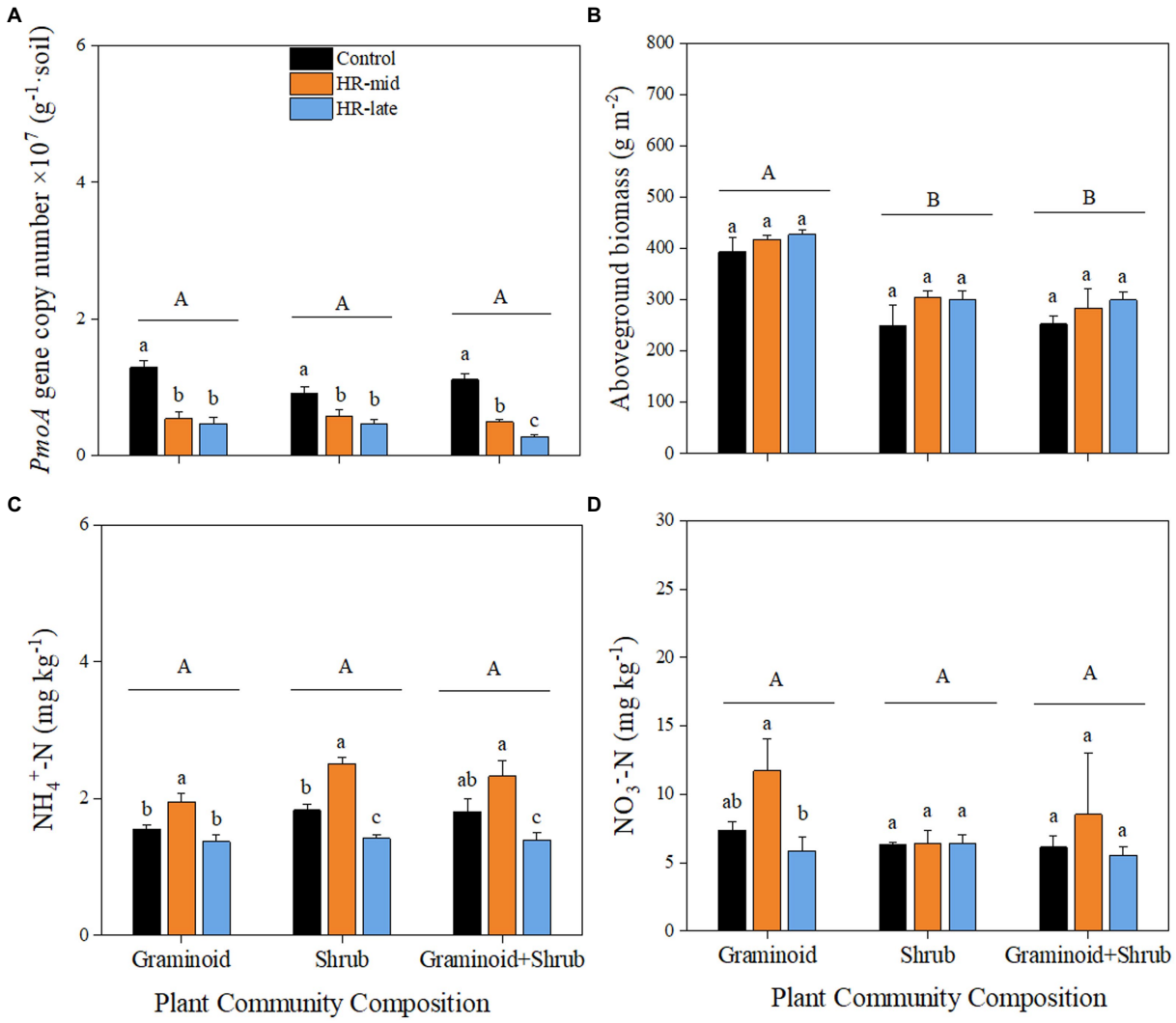

FIGURE 3
Responses of *pmoA* abundance **(A)**, above-ground biomass (AGB) **(B)**, NH_4^+-N **(C)** and NO_3^--N **(D)** to heavy rainfall treatments in three plant communities. Different letters above bars indicate significant difference among treatments at $p \leq 0.05$.

abundance would limit CH_4 uptake (Degelmann et al., 2010; Zhang et al., 2019; Kaupper et al., 2021;). Previous studies have found that the process of methanotrophs using CH_4 as both an energy and carbon source generally requires soil NH_4^+-N as N source (Rigler and Zechmeister-Boltenstern, 1999; Schimel and Weintraub, 2003; Bürgmann, 2011), resulting in decreased soil NH_4^+-N content can inhibit methanotrophs activities and *pmoA* abundance (Le Mer and Roger, 2001; Xu and Inubushi, 2007; Yue et al., 2016, 2022). However, some findings of other studies suggest that decreased NH_4^+-N availability in soils can promote CH_4 oxidation as higher NH_4^+-N can replace CH_4 to be oxidized by methanotroph (Song et al., 2020; Yue et al., 2022). Therefore, the net effects of NH_4^+-N on CH_4 uptake depend on the relative size of the two processes. Nevertheless, the mechanism was not suitable for HR-mid. Similar to HR-late, HR-mid declined *pmoA* abundance, however, it had no significant correlation with CH_4 uptake. This may be because increased NH_4^+-N content under HR-mid leaded to the oxidation of NH_4^+-N instead of CH_4 by methanotrophs, thus resulting in the most decreased CH_4 uptake in mixture community, although the largest reduction of *pmoA* abundance were found in graminoid community. As NO_3^--N content was little impacted by heavy rainfalls, it had no effects on CH_4 uptake in this study. Our results are consistent with the finding that soil NO_3^--N concentrations and CH_4 uptake had no correlation in a subtropical plantation forest ecosystem (Wang et al., 2014). Taken together, our study proved that the pathways underlying CH_4 uptake in response to heavy rainfall depend on seasonal timing.

Plant composition regulates responses of CH_4 uptake to heavy rainfalls

Multiple lines of evidence proved that plant composition is a controlling factor in regulation of soil CH_4 oxidation. CH_4 uptake would increase with enhanced plant diversity as high plant biodiversity promoted microbial activities (Altor and Mitsch, 2006; Bouchard et al., 2007; Schultz et al., 2011; Hassan et al., 2019). Niklaus et al. (2016) showed that the presence of legume plants inhibited soil CH_4 oxidation capacity due to decline in plant N acquisition. Likewise, CH_4

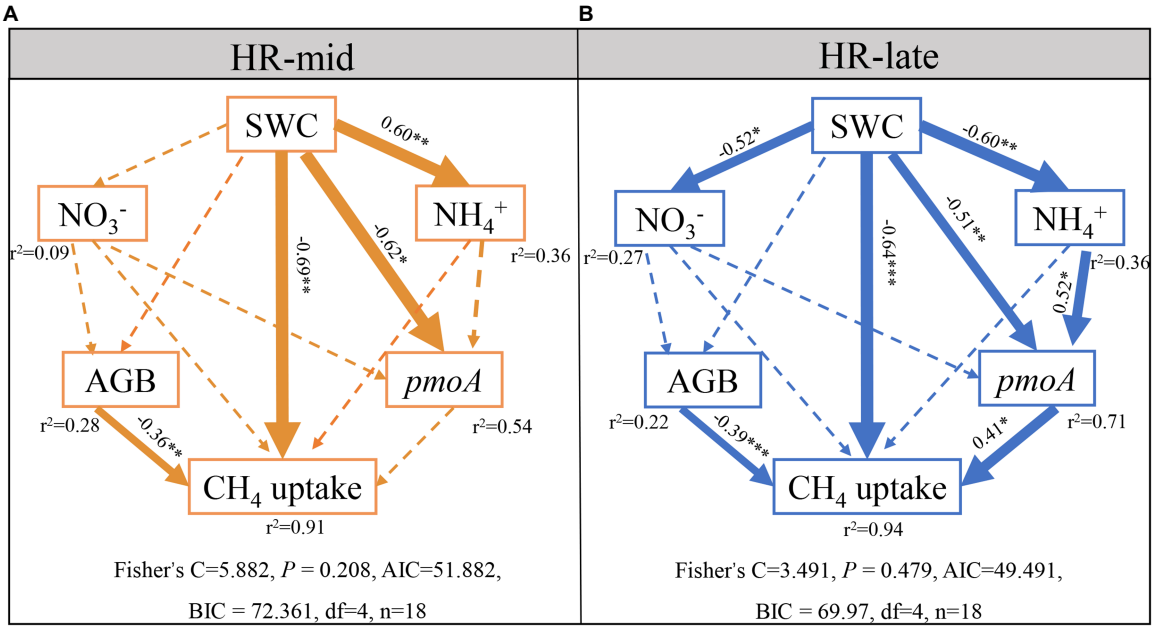

FIGURE 4
Structural equation models analysis of the direct and indirect effects of soil, microbe and plant variables on CH_4 uptakes under HR-mid **(A)** and HR-late **(B)** treatment. SWC: soil water content; AGB: aboveground, biomass; NH_4^+ and NO_3^-: soil ammonium and nitrate content. Solid and dashed lines indicate significant ($p \leq 0.05$) and nonsignificant ($p > 0.05$) relationships, respectively. Width of the line is proportional to the strength of path coefficients expressed by the numbers adjacent on lines. r^2 values denote the proportion of variance explained for each variable.

uptake had significant differences among three communities, where CH_4 uptake was less in shrub community than in graminoid and mixture communities in our study (Supplementary Figure S3; Table 1). It may be because shrubs had harmful effects on methanotrophs activities and CH_4 uptake through the chemistry of root exudates and N competition among plants and microbes (Zak et al., 2003; Hassan et al., 2019).

Importantly, plant composition regulated CH_4 uptake to heavy rainfalls, reflected by significant interactions between plant composition and heavy rainfalls (Table 1). Negative effects of HR-late on CH_4 uptake was the least in graminoid community than in other two communities. The potential explanation may be that HR-late had larger positive effects on SWC and AGB and larger negative effects on *pmoA* abundance and NH_4^+-N content in shrub and mixture communities (Figures 1F, 3A), although the interactions were only significant on SWC and *pmoA* abundance. This finding supports the third hypothesis that plant composition would regulate CH_4 uptake in response to heavy rainfalls though soil moisture, inorganic content, aboveground biomass and methanotrophs activities. Although previous studies proved that plant communities with higher-diversity are less negatively affected by floods (Gattringer et al., 2017; Wright et al., 2017), the least increase in SWC, AGB and the least decrease NH_4^+-N content were observed in graminoid community under HR-late. Previous studies have reported that precipitation infiltration and evaporation rate vary with plant species composition. Evaporation and transpiration can remove water from shallow soil layers after rainfall and thus decrease soil moisture (Coughenour, 1984; Weltzin et al., 2003; Springer et al., 2006; MacIvor and Lundholm, 2011; Moore et al., 2022). Graminoids are shallower rooting with deeper and faster infiltration and faster evaporation rate, leading to lower soil moisture and the duration of soil saturation in graminoid community (Springer et al., 2006). Therefore, HR-late had the least negative effect on CH_4 uptake in graminoid community under HR-late. Overall, SWC, *pmoA* abundance and NH_4^+-N content had the least reduction in graminoid, leading to the least decreased CH_4 uptake in HR-late. However, HR-mid had similar negative effects on CH_4 uptake across three communities although the interaction between HR-mid and plant composition on CH_4 uptake was statistically significant ($p = 0.08$). Therefore, we concluded that CH_4 uptake in response to climate extremes jointly controlled by interaction of seasonal timing and plant composition.

Conclusion

Our results highlight the vital role of seasonal timing and plant composition in regulating heavy rainfall effects on CH_4 uptake. Specifically, although both heavy rainfalls reduced CH_4 sink, late heavy rainfall had larger negative effects than middle heavy rainfall. This is because decreased NH_4^+-N induced by late heavy rainfall had negative effects on *pomA* abundance and further suppressing CH_4 sink, in addition to directly negative effects of high soil moisture induced by heavy rainfall. Besides, shrub community had lower CH_4 uptake than graminoid and mixture communities. Moreover, late heavy rainfall had the least negative effects on CH_4 uptake in graminoid communities than in other two communities, indicating that climate extremes-driven shifts in dominant species would in turn alter ecosystem feedbacks. Therefore, to improve prediction accuracy of terrestrial ecosystems feedbacks to climate changes, we encourage future studies to further quantify the interactive effects between seasonal timing and plant on regulating carbon cycling in response to climate extremes.

Data availability statement

The original contributions presented in the study are included in the article/Supplementary material, further inquiries can be directed to the corresponding author.

Author contributions

LL designed the experiments. ZZ and FW performed the experiments. ZZ and LL analyzed the data. ZZ wrote the manuscript. ZZ, FW, CL, SG, YX, YL, RQ, ML, SX, XC, YW, YH, and LL provided the editorial advice. All authors contributed to the article and approved the submitted version.

Funding

This project was funded by the funds for the National Natural Science Foundation of China (42041005 and 32101313), China Postdoctoral Science Foundation (2021M693138), and the Fundamental Research Funds for the Central Universities (E1E40607 and E1E40511).

Conflict of interest

The authors declare that the research was conducted in the absence of any commercial or financial relationships that could be construed as a potential conflict of interest.

Publisher's note

Supplementary material

The Supplementary material for this article can be found online at: https://www.frontiersin.org/articles/10.3389/fevo.2023.1149595/full#supplementary-material

References

Altor, A., and Mitsch, W. (2006). Methane flux from created riparian marshes: relationship to intermittent versus continuous inundation and emergent macrophytes. *Ecol. Eng.* 28, 224–234. doi: 10.1016/j.ecoleng.2006.06.006

Aronson, E. L., Goulden, M. L., and Allison, S. D. (2019). Greenhouse gas fluxes under drought and nitrogen addition in a Southern California grassland. *Soil Biol. Biochem.* 131, 19–27. doi: 10.1016/j.soilbio.2018.12.010

Bai, J., Gao, H., Xiao, R., Wang, J., and Huang, C. (2012). A review of soil nitrogen mineralization as affected by water and salt in coastal wetlands: issues and methods. *CLEAN–Soil Air Water* 40, 1099–1105. doi: 10.1002/clen.201200055

Borken, W., and Matzner, E. (2009). Reappraisal of drying and wetting effects on C and N mineralization and fluxes in soils. *Glob. Chang. Biol.* 15, 808–824. doi: 10.1111/j.1365-2486.2008.01681.x

Bouchard, V., Frey, S., Gilbert, J., and Reed, S. (2007). Effects of macrophyte functional group richness on emergent freshwater functions. *Ecology* 88, 2903–2914. doi: 10.1890/06-1144.1

Bürgmann, H. (2011). "Methane oxidation (aerobic)" in *Encyclopedia of Geobiology*. eds. J. Reitner and V. Thiel (Amsterdam: Springer)

Cabrera, M. L., and Kissel, D. E. (1988). Evaluation of a method to predict nitrogen mineralized from soil organic matter under field conditions. *Soil Sci. Soc. Am. J.* 52, 1027–1031. doi: 10.2136/sssaj1988.03615995005200040024x

Chen, W. W., Zheng, X. H., Chen, Q., Wolf', B., Butterbach-Bahl, K., Bruggemann, N., et al. (2013). Effects of increasing precipitation and nitrogen deposition on CH_4 and N_2O fluxes and ecosystem respiration in a degraded steppe in Inner Mongolia, China. *Geoderma* 192, 335–340. doi: 10.1016/j.geoderma.2012.08.018

Chen, H., Zhu, Q., Peng, C., Wu, N., Wang, Y., Fang, X., et al. (2013). The impacts of climate change and human activities on biogeochemical cycles on the Qinghai-tibetan plateau. *Glob. Chang. Biol.* 19, 2940–2955. doi: 10.1111/gcb.12277

Coughenour, M. B. (1984). A mechanistic simulation analysis of water use, leaf angles, and grazing in east African graminoids. *Ecol. Model.* 26, 203–230. doi: 10.1016/0304-3800(84)90070-X

Cregger, M. A., McDowell, N. G., Pangle, R. E., Pockman, W. T., and Classen, A. T. (2014). The impact of precipitation change on nitrogen cycling in a semi-arid ecosystem. *Funct. Ecol.* 28, 1534–1544. doi: 10.1111/1365-2435.12282

Curry, C. L. (2007). Modeling the soil consumption of atmospheric methane at the global scale. *Glob. Biogeochem. Cycles* 21:GB4012. doi: 10.1029/2006GB002818

Dai, Y., Zhen, W., Xie, S., and Liu, Y. (2015). Methanotrophic community abundance and composition in plateau soils with different plant species and plantation ways. *Appl. Microbiol. Biotechnol.* 99, 9237–9244. doi: 10.1007/s00253-015-6782-z

Degelmann, D. M., Borken, W., Drake, H. L., and Kolb, S. (2010). Different atmospheric methane-oxidizing communities in European beech and Norway spruce soils. *Appl. Environ. Microbiol.* 76, 3228–3235. doi: 10.1128/AEM.02730-09

Dijkstra, F. A., Morgan, J. A., Follett, R. F., and Lecain, D. R. (2013). Climate change reduces the net sink of CH_4 and N_2O in a semiarid grassland. *Glob. Chang. Biol.* 19, 1816–1826. doi: 10.1111/gcb.12182

Dijkstra, F. A., Morgan, J. A., Von Fischer, J. C., and Follett, R. F. (2011). Elevated CO_2 and warming effects on CH_4 uptake in a semiarid grassland below optimum soil moisture. *J. Geophys. Res. Atmos.* 116, 79–89. doi: 10.1029/2010JG001288

Domeignoz-Horta, L. A., Pold, G., Liu, X. J. A., Frey, S. D., Melillo, J. M., and DeAngelis, K. M. (2020). Microbial diversity drives carbon use efficiency in a model soil. *Nat. Commun.* 11, 3684–3610. doi: 10.1038/s41467-020-17502-z

Elango, N. A., Radhakrishnan, R., Froland, W. A., Wallar, B. J., Earhart, C. A., Lipscomb, J. D., et al. (1997). Crystal structure of the hydroxylase component of methane monooxygenase from Methylosinus trichosporium OB3b. *Protein Sci.* 6, 556–568. doi: 10.1002/pro.5560060305

Fest, B., Wardlaw, T., Livesley, S. J., Duff, T. J., and Arndt, S. K. (2015). Changes in soil moisture drive soil methane uptake along a fire regeneration chronosequence in a eucalypt forest landscape. *Glob. Chang. Biol.* 21, 4250–4264. doi: 10.1111/gcb.13003

Fischer, E. M., and Knutti, R. (2016). Observed heavy precipitation increase confirms theory and early models. *Nat. Clim. Change* 6, 986–991. doi: 10.1038/NCLIMATE3110

Gattringer, J. P., Donath, T. W., Eckstein, R. L., Ludewig, K., Otte, A., and Harvolk-Schoning, S. (2017). Flooding tolerance of four floodplain meadow species depends on age. *PLoS One* 12:e0176869. doi: 10.1371/journal.pone.0176869

Hao, Y. B., Zhou, C. T., Liu, W. J., Li, L. F., Kang, X. M., Jiang, L. L., et al. (2017). Aboveground net primary productivity and carbon balance remain stable under extreme precipitation events in a semiarid steppe ecosystem. *Agric. For. Meteorol.* 240-241, 1–9. doi: 10.1016/j.agrformet.2017.03.006

Hassan, M. K., McInroy, J. A., and Kloepper, J. W. (2019). The interactions of rhizodeposits with plant growth-promoting rhizobacteria in the rhizosphere: a review. *Agriculture* 9:142. doi: 10.3390/agriculture9070142

Hüppi, R., Horváth, L., Dezső, J., Puhl-Rezsek, M., and Six, J. (2022). Soil nitrous oxide emission and methane exchange from diversified cropping Systems in Pannonian Region. *Front. Environ. Sci.* 10:857625. doi: 10.3389/fenvs.2022.857625

IPCC, (2021). *Climate Change 2021: The Physical Science Basis. Contribution of Working Group I to the Sixth Assessment Report of the Intergovernmental Panel on Climate Change*. Cambridge University Press, England pp. 3–32.

Jiang, Z., Song, J., Li, L., Chen, W., Wang, Z., and Wang, J. (2012). Extreme climate events in China: IPCC-AR4 model evaluation and projection [J]. *Clim. Chang.* 110, 385–401. doi: 10.1007/s10584-011-0090-0

Kang, X., Yan, L., Cui, L., Zhang, X., Hao, Y., Wu, H., et al. (2018). Reduced carbon dioxide sink and methane source under extreme drought condition in an alpine peatland. *Sustainability* 10:4285. doi: 10.3390/su10114285

Kaupper, T., Mendes, L. W., Lee, H. J., Mo, Y., Poehlein, A., and Jia, Z. (2021). When the going gets tough: emergence of a complex methane-driven interaction network during recovery from desiccation-rewetting. *Soil Biol. Biochem.* 153:108109. doi: 10.1016/j.soilbio.2020.108109

Le Mer, J., and Roger, P. (2001). Production, oxidation, emission and consumption of methane by soils: a review. *Eur. J. Soil Biol.* 37, 25–50. doi: 10.1016/S1164-5563(01)01067-6

Li, L., Fan, W., Kang, X., Wang, Y., Cui, X., Xu, C., et al. (2016). Responses of greenhouse gas fluxes to climate extremes in a semiarid grassland. *Atmos. Environ.* 142, 32–42. doi: 10.1016/j.atmosenv.2016.07.039

Li, L., Hao, Y., Zheng, Z., Wang, W., Biederman, J. A., Wang, Y., et al. (2022). Heavy rainfall in peak growing season had larger effects on soil nitrogen flux and pool than in the late season in a semiarid grassland. *Agric. Ecosyst. Environ.* 326:107785. doi: 10.1016/j.agee.2021.107785

Li, L., Zheng, Z., Biederman, J. A., Xu, C., Xu, Z., Che, R., et al. (2019). Ecological responses to heavy rainfall depend on seasonal timing and multi-year recurrence. *New Phytol.* 223, 647–660. doi: 10.1111/nph.15832

Liebner, S., Ganzert, L., Kiss, A., Yang, S., Wagner, D., and Svenning, M. M. (2015). Shifts in methanogenic community composition and methane fluxes along the degradation of discontinuous permafrost. *Front. Microbiol.* 6:356. doi: 10.3389/fmicb.2015.00356

Liptzin, D., Silver, W. L., and Detto, M. (2011). Temporal dynamics in soil oxygen and greenhouse gases in two humid tropical forests. *Ecosystems* 14, 171–182. doi: 10.1007/s10021-010-9402-x

MacIvor, J. S., and Lundholm, J. (2011). Performance evaluation of native plants suited to extensive green roof conditions in a maritime climate. *Ecol. Eng.* 37, 407–417. doi: 10.1016/j.ecoleng.2010.10.004

Martins, C. S., Nazaries, L., Delgado-Baquerizo, M., Macdonald, C. A., Anderson, I. C., and Singh, B. K. (2021). Rainfall frequency and soil water availability regulate soil methane and nitrous oxide fluxes from a native forest exposed to elevated carbon dioxide. *Funct. Ecol.* 35, 1833–1847.

Moore, P. A., Pypker, T. G., Hribljan, J. A., Chimner, R. A., and Waddington, J. M. (2022). Examining the peatland shrubification-evapotranspiration feedback following multi-decadal water table manipulation. *Hydrol. Process.* 36:e14719. doi: 10.1002/hyp.14719

Niklaus, P. A., Le Roux, X., Poly, F., Buchmann, N., Scherer-Lorenzen, M., Weigelt, A., et al. (2016). Plant species diversity affects soil–atmosphere fluxes of methane and nitrous oxide. *Oecologia* 181, 919–930. doi: 10.1007/s00442-016-3611-8

Otto, F. E., van der Wiel, K., van Oldenborgh, G. J., Philip, S., Kew, S. F., and Uhe, P. (2018). Climate change increases the probability of heavy rains in northern England/southern Scotland like those of storm Desmond-a real-time event attribution revisited [J]. *Environ. Res. Lett.* 13:024006. doi: 10.1088/1748-9326/aa9663

Post, A. K., and Knapp, A. K. (2020). The importance of extreme rainfall events and their timing in a semi-arid grassland. *J. Ecol.* 108, 2431–2443. doi: 10.1111/1365-2745.13478

Rigler, E., and Zechmeister-Boltenstern, S. (1999). Oxidation of ethylene and methane in forest soils-effect of CO_2 and mineral nitrogen. *Geoderma* 90, 147–159. doi: 10.1016/S0016-7061(98)00099-8

Robson, T. M., Lavorel, S., Clement, J. C., and Rouxc, X. L. (2007). Neglect of mowing and manuring leads to slower nitrogen cycling in subalpine grasslands. *Soil Biol. Biochem.* 39, 930–941. doi: 10.1016/j.soilbio.2006.11.004

R Core Team. (2018). R: a language and environment for statistical computing. Vienna, Austria: R Foundation for Statistical Computing. [WWW document] URL https://www.r-project.org/

Schimel, J. P., and Weintraub, M. N. (2003). The implications of exoenzyme activity on microbial carbon and nitrogen limitation in soil: a theoretical model. *Soil Biol. Biochem.* 35, 549–563. doi: 10.1016/S0016-7061(98)00099-8

Schnell, S., and King, G. M. (1994). Mechanistic analysis of ammonium inhibition of atmospheric methane consumption in Forest soils. *Appl. Environ. Microbiol.* 60, 3514–3521. doi: 10.1128/aem.60.10.3514-3521.1994

Schultz, R., Andrews, S., O'Reilly, L., Bouchard, V., and Frey, S. (2011). Plant community composition more predictive than diversity of carbon cycling in freshwater wetlands. *Wetlands* 31, 965–977. doi: 10.1007/s13157-011-0211-6

Song, W. M., Chen, S. P., Zhou, Y. D., and Lin, G. H. (2020). Rainfall amount and timing jointly regulate the responses of soil nitrogen transformation processes to rainfall increase in an arid desert ecosystem. *Geoderma* 364:114197. doi: 10.1016/j.geoderma.2020.114197

Springer, A. E., Amentt, M. A., Kolb, T. E., and Mullen, R. M. (2006). Evapotranspiration of two vegetation communities in a high-elevation riparian meadow at hart prairie, Arizona. *Water Resour. Res.* 42:3. doi: 10.1029/2004WR003863

Tang, S., Zhang, Y., Zhai, X., Wilkes, A., Wang, C., and Wang, K. (2018). Effect of grazing on methane uptake from Eurasian steppe of China. *BMC Ecol.* 18, 11–17. doi: 10.1186/s12898-018-0168-x

Tentori, E. F., and Richardson, R. E. (2020). Methane monooxygenase gene transcripts as quantitative biomarkers of methanotrophic activity in Methylosinus trichosporium OB3b. *Appl. Environ. Microbiol.* 86, e01048–e01020. doi: 10.1128/AEM.01048-20

Tong, C., Cadillo-Quiroz, H., Zeng, Z. H., She, C. X., Yang, P., and Huang, J. F. (2017). Changes of community structure and abundance of methanogens in soils along a freshwater–brackish water gradient in subtropical estuarine marshes. *Geoderma* 299, 101–110. doi: 10.1016/j.geoderma.2017.03.026

Van den Pol-van Dasselaar, A., Van Beusichem, M. L., and Oenema, O. (1998). Effects of soil moisture content and temperature on methane uptake by grasslands on sandy soils. *Plant Soil* 204, 213–222. doi: 10.1023/A:1004371309361

Wachendorf, C., Lampe, C., Taube, F., and Dittert, K. (2008). Nitrous oxide emissions and dynamics of soil nitrogen under 15N-labeled cow urine and dung patches on a sandy grassland soil. *J. Plant Nutr. Soil Sci.* 171, 171–180. doi: 10.1002/jpln.200625217

Wang, Y., Cheng, S., Fang, H., Yu, G., Xu, M., Dang, X., et al. (2014). Simulated nitrogen deposition reduces CH_4 uptake and increases N_2O emission from a subtropical plantation forest soil in southern China. *PLoS One* 9:e93571. doi: 10.1371/journal.pone.0093571

Wei, D., Xu-Ri, T.-T., Wang, Y. S., and Wang, Y. H. (2015). Considerable methane uptake by alpine grasslands despite the cold climate: in situ measurements on the central Tibetan plateau, 2008–2013. *Glob. Chang. Biol.* 21, 777–788. doi: 10.1111/gcb.12690

Weltzin, J. F., Loik, M. E., Schwinning, S., Williams, D. G., Fay, P. A., Haddad, B. M., et al. (2003). Assessing the response of terrestrial ecosystems to potential changes in precipitation. *Bioscience* 53, 941–952. doi: 10.1641/0006-3568(2003)053

Wright, A. J., de Kroon, H., Visser, E. J., Buchmann, T., Ebeling, A., Eisenhauer, N., et al. (2017). Plants are less negatively affected by flooding when growing in species-rich plant communities. *New Phytol.* 213, 645–656. doi: 10.1111/nph.14185

Wu, H., Wang, X., Ganjurjav, H., Hu, G., Qin, X., and Gao, Q. (2020). Effects of increased precipitation combined with nitrogen addition and increased temperature on methane fluxes in alpine meadows of the Tibetan plateau. *Sci. Total Environ.* 705:135818. doi: 10.1016/j.scitotenv.2019.135818

Xu, X., and Inubushi, K. (2007). Effects of nitrogen sources and glucose on the consumption of ethylene and methane by temperate volcanic forest surface soils. *Chin. Sci. Bull.* 52, 3281–3291. doi: 10.1007/s11434-007-0499-z

Yan, G. Y., Mu, C. C., Xing, Y. J., and Wang, Q. G. (2018). Responses and mechanisms of soil greenhouse gas fluxes to changes in precipitation intensity and duration: a meta-analysis for a global perspective. *Can. J. Soil Sci.* 98, 591–603. doi: 10.1139/cjss-2018-0002

Yue, P., Cui, X., Wu, W., Gong, Y., Li, K., Goulding, K., et al. (2019). Impacts of precipitation, warming and nitrogen deposition on methane uptake in a temperate desert. *Biogeochemistry* 146, 17–29. doi: 10.1007/s10533-019-00606-0

Yue, P., Li, K., Gong, Y., Hu, Y., Mohammat, A., Christie, P., et al. (2016). A five-year study of the impact of nitrogen addition on methane uptake in alpine grassland. *Sci. Rep.* 6:32064. doi: 10.1038/srep32064

Yue, P., Zuo, X., Li, K., Li, X., Wang, S., and Misselbrook, T. (2022). Precipitation changes regulate the annual methane uptake in a temperate desert steppe. *Sci. Total Environ.* 804:150172. doi: 10.1016/j.scitotenv.2021.150172

Zak, D. R., Holmes, W. E., White, D. C., Peacock, A. D., and Tilman, D. (2003). Plant diversity, soil microbial community, and ecosystem function: are there any links? *Ecology* 84, 2042–2050. doi: 10.1890/02-0433

Zhang, L., Adams, J. M., Dumont, M. G., Li, Y., Shi, Y., He, D., et al. (2019). Distinct methanotrophic communities exist in habitats with different soil water contents. *Soil Biol. Biochem.* 132, 143–152. doi: 10.1016/j.soilbio.2019.02.007

Zhang, L., Guo, D., Niu, S., Wang, C., Shao, C., and Li, L. (2012). Effects of mowing on methane uptake in a semiarid grassland in northern China. *PLoS One* 7:e35952. doi: 10.1371/journal.pone.0035952

Zhang, Z., Wang, G., Wang, H., Qi, Q., Yang, Y., and He, J. S. (2021). Warming and drought increase but wetness reduces the net sink of CH_4 in alpine meadow on the Tibetan plateau. *Appl. Soil Ecol.* 167:104061. doi: 10.1016/j.apsoil.2021.104061

Zhao, H., Li, T., Li, L., and Hao, Y. (2017). A stable CH_4 sink responding to extreme precipitation events in a fenced semiarid steppe. *J. Soils Sediments* 17, 2731–2741. doi: 10.1007/s11368-017-1798-x

Zhou, X., Smaill, S. J., Gu, X., and Clinton, P. W. (2021). Manipulation of soil methane oxidation under drought stress. *Sci. Total Environ.* 757:144089. doi: 10.1016/j.scitotenv.2020.144089

Zhuang, Q., Chen, M., Xu, K., Tang, J., Saikawa, E., Lu, Y., et al. (2013). Response of global soil consumption of atmospheric methane to changes in atmospheric climate and nitrogen deposition. *Glob. Biogeochem. Cycles* 27, 650–663. doi: 10.1002/gbc.20057

frontiers | Frontiers in Ecology and Evolution

TYPE Original Research
PUBLISHED 09 March 2023
DOI 10.3389/fevo.2023.1146850

OPEN ACCESS

EDITED BY
Zhongqing Yan,
Chinese Academy of Forestry, China

REVIEWED BY
Guangbin Lei,
Institute of Mountain Hazards and Environment (CAS), China
Chang Huang,
Northwest University, China
Shen Tan,
Peking University, China

*CORRESPONDENCE
Can Xu
✉ xucan@mail.cgs.gov.cn

SPECIALTY SECTION
This article was submitted to Population, Community, and Ecosystem Dynamics, a section of the journal Frontiers in Ecology and Evolution

RECEIVED 18 January 2023
ACCEPTED 13 February 2023
PUBLISHED 09 March 2023

CITATION
Liu W, Xu C, Zhang Z, De Boeck H, Wang Y, Zhang L, Xu X, Zhang C, Chen G and Xu C (2023) Machine learning-based grassland aboveground biomass estimation and its response to climate variation in Southwest China.
Front. Ecol. Evol. 11:1146850.
doi: 10.3389/fevo.2023.1146850

Machine learning-based grassland aboveground biomass estimation and its response to climate variation in Southwest China

Wenjun Liu[1], Cong Xu[2], Zhiming Zhang[1], Hans De Boeck[1,3], Yanfen Wang[4,5], Liankai Zhang[6,7], Xiongwei Xu[6,7], Chen Zhang[6,7], Guiren Chen[6,7] and Can Xu[6,7]*

[1]School of Ecology and Environmental Sciences, Yunnan University, Kunming, China, [2]State Key Laboratory of Remote Sensing Science, Aerospace Information Research Institute, Chinese Academy of Sciences, Beijing, China, [3]Research Group Plants and Ecosystems (PLECO), University of Antwerp, Antwerp, Belgium, [4]College of Resources and Environment, University of Chinese Academy of Sciences, Beijing, China, [5]Beijing Yanshan Earth Critical Zone National Research Station, University of Chinese Academy of Sciences, Beijing, China, [6]Kunming General Survey of Natural Resources Center, China Geological Survey, Kunming, China, [7]Technology Innovation Center for Natural Ecosystem Carbon Sink, Ministry of Natural Resources, Kunming, China

The demand for accurate estimation of aboveground biomass (AGB) at high spatial resolution is increasing in grassland-related research and management, especially for those regions with complex topography and fragmented landscapes, where grass and shrub are interspersed. In this study, based on 519 field AGB observations, integrating Synthetic Aperture Radar (SAR; Sentinel-1) and high-resolution (Sentinel-2) remote sensing images, environmental and topographical data, we estimated the AGB of mountain grassland in Southwest China (Yunnan Province and Guizhou Province) by using remote sensing algorithms ranging from traditional regression to cutting edge machine learning (ML) and deep learning (DL) models. Four models (i.e., multiple stepwise regression (MSR), random forest (RF), support vector machine (SVM) and convolutional neural network (CNN)) were developed and compared for AGB simulation purposes. The results indicated that the RF model performed the best among the four models (testing dataset: decision co-efficient (R^2) was 0.80 for shrubland and 0.75 for grassland, respectively). Among all input variables in the RF model, the vegetation indices played the most important role in grassland AGB estimation, with 6 vegetation indices (EVI, EVI2, NDVI, NIRv, MSR and DVI) in the top 10 of input variables. For shrubland, however, topographical factors (elevation, 12.7% IncMSE (increase in mean squared error)) and SAR data (VH band, 11.3% IncMSE) were the variables which contributed the most in the AGB estimation model. By comparing the input variables to the RF model, we found that integrating SAR data has the potential to improve grassland AGB estimation, especially for shrubland (26.7% improvement in the estimation of shrubland AGB). Regional grassland AGB estimation showed a lower mean AGB in Yunnan Province (443.6g/m^2) than that in Guizhou Province (687.6g/m^2) in 2021. Moreover, the correlation between five consecutive years (2018–2022) of AGB data and climatic factors calculated by partial correlation analysis showed that regional AGB was positively related with mean annual precipitation in more than 70% of the grassland and 60% of the shrubland area, respectively. Also, we found a positive relationship with mean annual temperature in 62.8% of the grassland and 55.6% of the shrubland area, respectively. This study demonstrated that integrating SAR into grassland AGB estimation led to a remote sensing estimation model that greatly improved the accuracy of modeled

mountain grassland AGB in southwest China, where the grassland consists of a complex mix of grass and shrubs.

KEYWORDS

aboveground biomass, grassland, shrubland, machine learning, SAR, climate

1. Introduction

Grassland is one of the most widely distributed terrestrial ecosystems, accounting for more than 40% of the world's land surface (Scurlock and Hall, 2002). It plays an important role in providing human livelihood through the livestock production of grazing animals and additional ecosystem services such as regulating the terrestrial carbon cycling, maintaining biodiversity and preventing soil erosion (Flombaum and Sala, 2007; Wang et al., 2010; Niu et al., 2014; Mu et al., 2016). Grassland aboveground biomass (AGB) is one of the key indicators for evaluating in grassland growth status, utilization, and related environment assessment (Ali et al., 2016). Therefore, the accurate and timely estimation of grassland AGB is crucial for research and optimizing management.

Traditional surveys of grassland AGB is directly measured by harvesting the aboveground materials, drying, and weighing in laboratories, which has high estimation accuracy but is limited to small areas due to its time-consuming nature and the labor involved (Sinha et al., 2015). With continuous launches of advanced satellites, leading to images with various spatial extent and temporal scales, coupled with the development of computing technology, remote sensing has become an efficient and low-cost approach which is widely applied in grassland monitoring at regional levels or global scales (Jin et al., 2014; Quan et al., 2017; Yang et al., 2018). The main principle of remote sensing based AGB estimation is to model the relationship between remote sensing parameters and field AGB observations, and subsequently apply the model to extrapolate AGB estimates to a regional scale. More specifically, there are three main categories of remote sensing-based grassland AGB estimation models or methods: empirical relationships with VIs, machine learning (ML) models and process-based model.

Establishing relationships between VIs and recorded AGB is the most common and direct approach for regional grassland AGB assessment. Many studies have reported that there is a strong correlation between the VIs, including normalized difference vegetation index (NDVI; Wei et al., 2021), enhanced vegetation index (EVI; Ge et al., 2018), soil adjusted vegetation index (SAVI; Ren et al., 2018), ratio vegetation index (RVI; Guerschman et al., 2009) and biomass in varies satellite images. However, VIs are subjected to the influence of environmental condition and the capability of characterizing vegetation status in certain circumstance, which can introduce errors and uncertainties into AGB estimation (Ali et al., 2016). In recent years, efforts have been made to improve the estimation accuracy by constructing estimation model with multiple VIs or introducing specific VIs transformation to enhance the sensitivity of VIs to AGB or decrease the influences by environmental factors such as soil and other background factors (Li et al., 2013, 2016). ML methods, the non-parametric models constructed by both remote sensing images and environment data, are to find solutions that optimize performance metrics for a certain parameter from multiple sources based on a "learning process" (Jordan and Mitchell, 2015). These methods can integrate multiple factors, learn from complicated nonlinear data, and provide better simulations than empirical regression models (Powell et al., 2010). Moreover, ML models could provide accurate estimations of nonlinear relationship from various data, which help increase understanding of the driving forces in the ecosystem research (Ramoelo et al., 2015). Over the last decades, AGB assessment methods have been developed ranging from traditional multiple linear regression (MLR) to ML models such as support vector machine (SVM), random forests (RF) and artificial neural network (ANN). Nowadays, ML models have been widely applied in remote sensing grassland AGB estimation (Morais et al., 2021). A recent literature review on ML methods used for grassland AGB estimation pointed out that the RF model was the most frequently used algorithm, followed by partial least squares regression (PLSR), but there was no significant difference between the accuracy of ML models (Morais et al., 2021). Various conclusions have been reported in ML model comparison studies, for examples, Zeng et al. (2019, 2021) used four ML model in grassland AGB simulations and found that the RF model performed the best, explaining 86% of the observed data variation on the Tibetan Plateau, while Zhang et al. (2018) reported ANN was better in a sawgrass marsh AGB prediction. In addition, considering there is no evidence that the performance of the ML algorithms themselves has been improving over time, and since the training process and the equations of the ML models cannot be observed, the applicability of ML models still needs to be analyzed to select suitable models in specific studies (Ali et al., 2016; Yang et al., 2018). Besides the above mentioned classical ML models, the use of deep learning, an advanced ML technique which can automatically extract high dimensional 'hidden' features through a deeper neural network with hierarchical structure, has increased in recent years (LeCun et al., 2015). Convolutional neural network (CNN) is considered as the most representative among them, which has been widely used in image classification (Wang et al., 2021). CNN model usually includes input layer, convolutional layer, pooling layer, fully connected layer and output layer. Unlike image classification, the last layer of CNN model for regression prediction accumulates the previous layer directly without adding *soft*-max function. However, AGB estimation usually lacks enough samples for CNN model training, and thus the potential of using CNN for AGB estimation is not well established yet (Dong et al., 2020).

Besides the ML algorithms selection, input variables are another relevant factor affecting grassland AGB estimation accuracy. Independent variables (or explanatory variables) such as meteorological, topographical, and geographic variables are the most common environmental variables, while the abundance of VIs provided by optical remote sensors are the main remote sensing input parameters. However, the use of optical data for estimating grassland

AGB has several limitations including that the acquisition of high quality images is restricted by weather conditions, spectral information and VIs saturation occurring in dense vegetation areas, while it also lacks the ability to provide vegetation structure information (Lu, 2007). Synthetic aperture radar (SAR) sensors can penetrate through clouds without illumination conditions limitations, and the SAR system can provide valuable information about vegetation structure though a series of algorithms (Barrett et al., 2014). Therefore, integration of optical and SAR data could overcome several limitations and thus could improve the performance of grassland AGB estimations (Naidoo et al., 2019). The potential of this integration has been proven in a grazed grassland (Wang et al., 2019), and thus it is worth to apply the concept in a more complex vegetation, such as shrubby grassland.

Located at the intersection of South and East Asia, the Yunnan-Guizhou plateau including Yunnan and Guizhou provinces is the dominant feature of Southwest China. Influenced by South and East Asian Monsoons and complex topography, the vegetation of Yunnan-Guizhou plateau is highly varied, ranging from subtropical forest to open grasslands (Chu et al., 2021). The plateau is the main distribution area of China's thermal shrub grassland, which consists of patches of grass hills, grass slopes, scrub grassland, dry savanna, and alpine meadows, which all are relevant for developing animal husbandry (Shen et al., 2016). However, grassland ecosystems in Southwest China are relatively understudied in the earth observation field. There is still a knowledge gap with respect to the estimation of regional aboveground biomass for grassland with complex topography and high small-scale heterogeneity.

In this study, our primary objectives were to (1) develop and compare the capability of four models including a traditional regression model [i.e., multiple stepwise regression (MSR)], two classical ML models (i.e., RF, SVM) and a deep learning model (i.e., CNN) in grassland AGB estimation in Southwest China. (2) explore the potential of integrating SAR (Sentinel-1) and high resolution optical remote sensing (Sentinel-2) with gridded environmental and topographic data to develop regional grassland AGB estimation model to derive the spatial patterns of AGB for the Southwest China grassland of 2021, and (3) analyze the spatial and temporal variation of grassland AGB in Southwest China and its response to climatic factors, by mapping the grassland AGB from 2018 to 2022.

2. Materials and methods

2.1. Study area

The study area includes Yunnan and Guizhou provinces (21°8′–29°15′N, 97°31′–109°35′E), in which the Yunnan-Guizhou plateau is located (Figure 1). These two provinces cover about 570,000 km^2 with a large elevational span, ranging from less than 100 m to over 6,000 m a.s.l., with much of the region being mountainous or dotted with karst landscapes. The climate belongs to highland monsoon climate, with small annual but large daily temperature differences, and abundant radiation and rainfall. The mean annual temperature in the study area is 24°C, and the mean annual precipitation is approximately 1,100 mm, with around 80% concentrated in summer and autumn based on the data from 22 meteorological stations over the past 20 years. A highly variable climate and edaphic space provides suitable light, soil and climate for diverse vegetation development and creates a rich diversity of biological resources. Grassland and shrubland are important vegetation types in the region accounting for over 14% of the area, with about 40% of Southern China's grassland area is located in Yunnan based on data derived from a national grassland survey (Wu et al., 2017). The mainly grassland types include alpine meadows, temperate grassland, and mountain grassland, while warm shrubland, dry and hot sparse tree shrubland and thermal shrubland are the main shrubland types. Grassland and shrubland are distributed over almost the entire area except for the southwestern part of the study area, but the complex topographic conditions of the area determine the fragmented distribution of grassland and shrubland.

2.2. Data acquisition

2.2.1. Field data

Field data surveys were conducted during the growing season of 2021. In order to match the ground samples with the satellite data, we regularly set five sample plots of 1 m × 1 m at each sample points for grassland and set one sample plots of 5 m × 5 m for shrubland with an interval distance of over 1 km between the plots so as to assure the representativeness of the samples. AGB of grassland and shrubland were acquired by harvesting all aboveground portions of vegetation within the sample plots, and weighing dried biomass. Moreover, the geographic coordinate pairs of each sample plot were also accurately recorded by a Trimble GeoXH 3,000 handheld GPS with decimeter-level position accuracy for acquiring the corresponding features of satellite data. A total of 519 samples including 298 samples for pure grassland and 221 samples for shrubland were collected across the study area, covering cover all the typical types of the grassland and shrubland (Figure 1).

2.2.2. Remote sensing data

Sentinel-2 (S2) images covering the study area were acquired and processed through Google Earth Engine (https://code.earthengine.google.com/, GEE). In order to maintain consistency with ground measured data, all available imageries of S2A in the July and August, 2021 were collected, as well as supplemental images in May, June, September, and October whenever the region was not covered by clouds. Sentinel-2 covers 13 spectral bands from visible and near-infrared to short-wave infrared with a revisit period of 5 days and a spatial resolution from 10 to 60 m. It also contains three bands in the red-edge range, which is effective for monitoring vegetation information. We obtained the reflectance of 11 raw bands and calculated 11 vegetation indices based on the 11 bands as the input variables.

Sentinel-1 (S1) consists of two satellites, A and B, carrying a C-band synthetic aperture radar (SAR) that provides continuous imagery during day, night, and all types of weather. The polarization mode of S1 includes the single polarization mode (HH or VV) and the dual polarization mode (HH + HV or VV + VH). VH and VV are commonly used for the estimation of vertical parameters. Moreover, to match with the data from field measurements, we used data of S1 with 10 m spatial resolution in early August for AGB estimation.

Topography factors were obtained from digital elevation model (DEM) data with 12.5 m spatial resolution, which is the elevation data collected by ALOS (Advanced Land Observing Satellite)

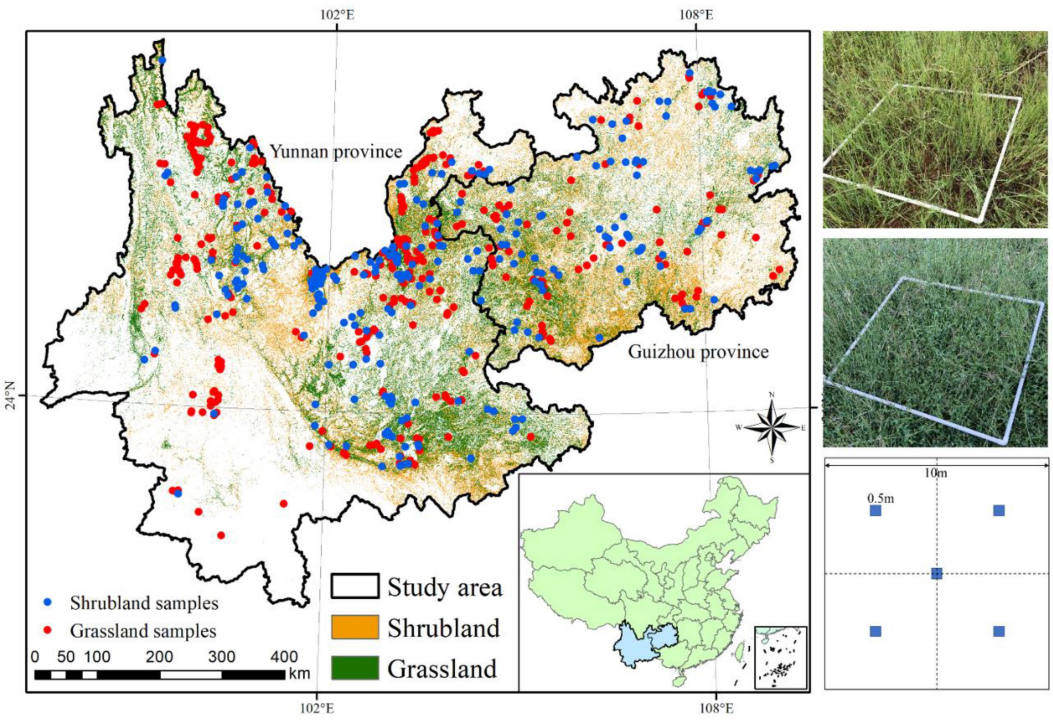

FIGURE 1
The location of the study area and the distribution of shrubland and grassland, as well as field data sample points.

phased array type L-band synthetic aperture radar (PALSAR). ALOS DEM elevation data has a horizontal and vertical accuracy of 12.5 m, which can be downloaded on https://search.asf.alaska.edu/. Based on the elevation data, slope and aspect were calculated for each pixel.

Environmental data was collected from three sources: the derived products of MODIS (MOD11A2.006) provides the terra land surface temperature with 1 km spatial resolution; A downscaled precipitation product with 1 km spatial resolution developed by Elnashar et al. (2020) was used to extract the annual mean precipitation; Water Vapor Pressure (Water VP) was from S2.

Landcover types data was obtained from the latest ChinaCover dataset with 10 m spatial resolution (provided by the State Key Laboratory of Remote Sensing Science, Aerospace Information Research Institute, Chinese Academy of Sciences, China. The data was updated in 2020, but not released yet; Wu et al., 2017), from which we extracted the grassland and shrubland to represent the great definition of grassland in this study.

2.3. Feature selection

Five types of features were used as input variables for machine learning models for the estimation of shrubland and grassland AGB (Table 1), including remote sensing spectral bands (Blue, Green, Red, Edge 1, Edge 2, Edge 3, Near Infrared (NIR), Edge 4, Water vapor, short-wave infrared 1 (SWIR 1) and SWIR 2) and VIs calculated by spectral bands (SR, NDVI, MSR, DVI, SAVI, EVI, NIRv, kNDVI, EVI2, GCC, and Clred Edge) from Sentinel-2, C-band SAR (VV and VH) from Sentinel-1; three topography factors (elevation, aspect and slope) from ALOS, and three environmental factors [Water VP, annual mean precipitation (Precipitation) and land surface temperature (LST)] from MODIS and downscaling algorithms. All the features corresponding to each sample points were extracted and then used in the model training and validation combined with ground measured AGB of grassland and shrubland.

2.4. Grassland aboveground biomass estimation models

Four models for predicting the aboveground biomass are used in our study: multiple stepwise regression (MSR), random forest (RF), support vector machine (SVM), and convolutional neural network (CNN).

MSR is a statistical analysis method used to determine the quantitative relationship of interdependence between two or more variables. It understands and interprets the relationships between AGB and the features from satellite data intuitively, and is sensitive to the abnormal values as well (Wu et al., 2016).

RF is a compositional supervised learning method that can be considered as an extension of decision trees. The RF regression model builds multiple unrelated decision trees by randomly drawing the input features to obtain prediction in a parallel manner. It is the most-used method for grassland AGB prediction (Wang et al., 2019; Zeng et al., 2019). Each decision tree yields a prediction result from the extracted samples and features, and the regression prediction result of the whole forest is obtained by

TABLE 1 Features from remote sensing data as inputs of machine learning models for aboveground biomass estimation of grassland and shrubland.

Type	Name	Equation or description	Source
Spectral band	Blue	Central band:497 nm	Sentinel-2
	Green	Central band:560 nm	Sentinel-2
	Red	Central band:665 nm	Sentinel-2
	Edge 1	Central band:704 nm	Sentinel-2
	Edge 2	Central band:740 nm	Sentinel-2
	Edge 3	Central band:783 nm	Sentinel-2
	NIR	Central band:835 nm	Sentinel-2
	Edge 4	Central band:865 nm	Sentinel-2
	Water vapor	Central band:945 nm	Sentinel-2
	SWIR 1	Central band:1614 nm	Sentinel-2
	SWIR 2	Central band:2202 nm	Sentinel-2
C-band SAR	VH	Dual-band cross-polarization, vertical transmit/horizontal receive	Sentinel-1
	VV	Single co-polarization, vertical transmit/vertical receive	Sentinel-1
Topography factor	Aspect	The direction in which the slope is projected on a horizontal plane	ALOS
	Elevation	The vertical distance above sea level	ALOS
	Slope	The ratio of the vertical height to the horizontal distance	ALOS
Vegetation index	SR	NIR / red	Sentinel-2
	NDVI	$(NIR - Red) / (NIR + Red)$	Sentinel-2
	MSR	$\frac{NIR / Red - 1}{\sqrt{NIR / Red + 1}}$	Sentinel-2
	DVI	$NIR - red$	Sentinel-2
	SAVI	$(1 + L) * (NIR - red) / (NIR + Red + L)$	Sentinel-2
	EVI	$2.5 * (NIR - Red) / (NIR + 6 * Red - 7.5 * Blue + 1)$	Sentinel-2
	NIRv	$NDVI * NIR$	Sentinel-2
	kNDVI	$\tanh NDVI^2$	Sentinel-2
	EVI2	$2.5 * (NIR - Red) / (NIR + 2.4 * Red + 1)$	Sentinel-2
	GCC	$Green / (Red + Green + Blue)$	Sentinel-2
	Clred Edge	$NIR / Edge1$	Sentinel-2
Environmental factor	Water VP	Water Vapor Pressure.	Sentinel-2
	Precipitation	Annual mean precipitation	Downscaled product
	LST	Land surface temperature	MOD11A2

All features are at 10 m spatial resolution, except the Edge 1–4, SWIR 1, 2 (20 m), Water vapor (60 m), elevation and derived aspect and slope (12.5 m) and LST and Precipitation are at 1 km spatial resolution.

combining the results of all trees and taking the average, to reduce the risk of overfitting. A Bayesian optimization procedure is applied to determine the number of trees and the number of selected predictors for each tree.

SVM maps input features to a high-dimensional space through functions and uses kernel functions to effectively overcome the dimensional catastrophe caused by mapping. It is based on the principle of finding a regression plane such that all the data of a set are closest to that plane. The method is suitable for small-sample, nonlinear prediction problems and has good generalization ability (Zhang et al., 2015).

CNN is a deep learning method that deduces features of the next layer by using convolution kernel with shared weights, which greatly reduces the number of parameters that need to be trained.

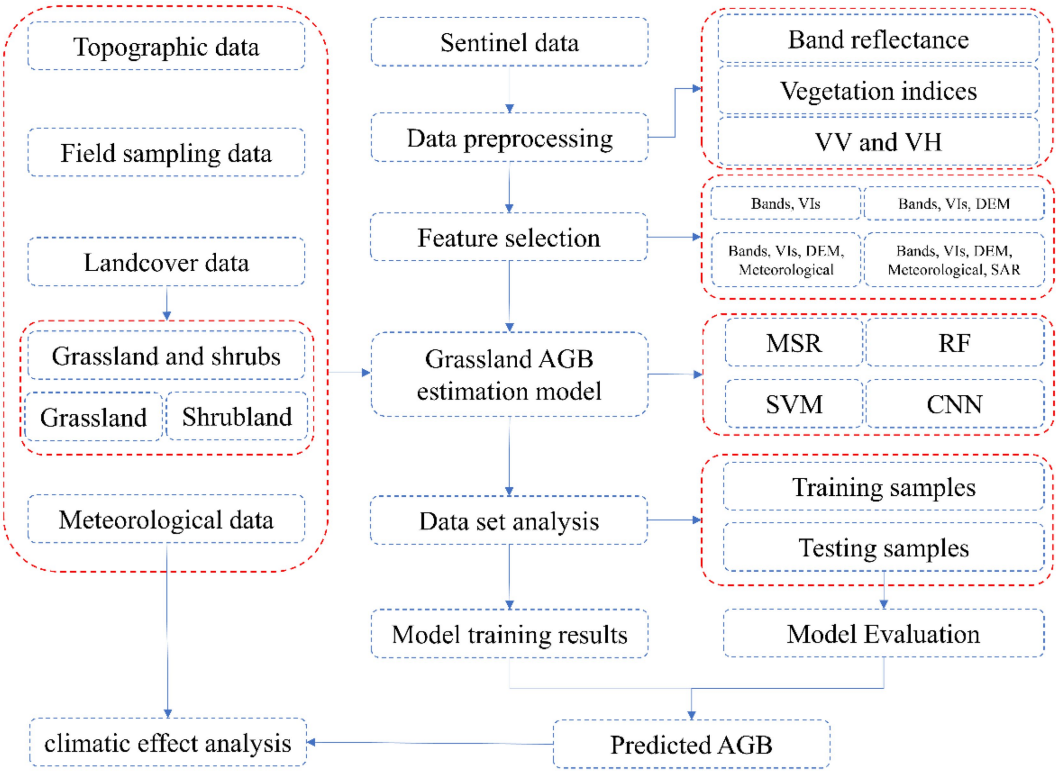

FIGURE 2
The technical flowchart of grassland AGB estimation in this study.

Based on the AGB of samples and their corresponding remote sensing features, we built a simplified CNN model and added a one-dimensional convolution layer. The input shape was defined by our independent variables. We added flatten and dense layers and optimized them using the Adam algorithm. *ReLU* (Krizhevsky et al., 2017) and root mean square error (RMSE) were used as the activation and function.

The workflow to establish the best AGB estimation model in this study is shown in Figure 2. Specifically, firstly, considering grassland is a mix grassy vegetation and shrubs in the study area, we developed and compared the performance of four models (MSR, RF, SVM and CNN) in two scenarios: directly modelling AGB of grassland and shrubland together, or modelling them separately. Secondly, we tested the best feature selection for AGB estimation, especially the potential application of Sentinel-1 SAR data. Moreover, a timeseries of grassland AGB was calculated to analyze how climatic factors impact grassland AGB variation in Southwest China.

2.5. Prediction accuracy

The field sample plots were divided into two subsets with approximately three-fourths of the plots used for model training (*N* is 214 and 158 in grassland and shrubland, respectively) and the others used for model validation ($N=84$ in grassland and $N=63$ in shrubland). In this study, the coefficient of determination (R^2), root mean square error (RMSE) and mean absolute percentage error (MAPE) were calculated for evaluating the performance of prediction models. In addition, the 1:1 line was used to measure how far the ground-measured AGB values deviated from the predicted AGB values. A detailed description of the assessment indicators is shown as follows:

$$R^2 = 1 - \frac{\sum_{i=1}^{n}\left(\hat{y}_i - y_i\right)^2}{\sum_{i=1}^{n}\left(\overline{y_i} - y_i\right)^2} \quad (1)$$

$$RMSE = \sqrt{\frac{1}{n}\sum_{i=1}^{n}\left(\hat{y}_i - y_i\right)^2} \quad (2)$$

$$MAPE = \frac{100\%}{n}\sum_{i=1}^{n}\left|\frac{\hat{y}_i - y_i}{y_i}\right| \quad (3)$$

where n is the number of sample plots, y_i and $\hat{y}_i$ are the field measured and predicted AGB of plots *i*. $\overline{y_i}$ is the mean measured AGB of all plots.

TABLE 2 The statistical descriptions of the measured AGB for the training set, validation set and all data of grassland and shrubland.

Types	Datasets	Number	Max (g/m^2)	Min (g/m^2)	Mean (g/m^2)	STD (g/m^2)	CV (%)
Shrubland	Training	158	3742.9	650.9	1879.43	774.87	41
	Validation	63	3186.86	648.9	1703.14	677.08	40
	All	221	3742.9	648.9	1829.17	751.03	41
Grassland	Training	214	1289.63	202.35	681.88	278.77	40
	Validation	84	1269.3	217.00	663.27	252.96	38
	All	298	1289.63	202.35	672.50	265.80	40

Max, Min, Mean, STD, and CV represent the maximum, minimum, mean, standard deviation and coefficient of variation for AGB of different datasets.

2.6. Partial correlation analysis

Partial correlation analysis is a process of eliminating the effect of the third variable when two variables are simultaneously correlated with the third variable and only analyzing the linear correlation between the two variables, which is commonly applied to assess the influences of climate change to the variation of grassland AGB (Guo et al., 2021; Xu et al., 2022). We applied it to determine the respective effects of temperature and precipitation on the differences of AGB distribution, with the indicator calculated as follows:

$$r_{xy(z)} = \frac{r_{xy} - r_{xz}r_{yz}}{\sqrt{1-r_{xz}^2}\sqrt{1-r_{yz}^2}} \quad (4)$$

where $r_{xy(z)}$ is the partial correlation coefficient between variable x and variable y after excluding the influence of variable z. r_{xy} , r_{yz} and r_{xz} represent the Pearson correlation coefficients between each pair of AGB, temperature and precipitation, respectively, which is calculated as follows:

$$r_{xy} = \frac{\sum_{i=1}^{n}(x_i - \bar{x})(y_i - \bar{y})}{\sqrt{\sum_{i=1}^{n}(x_i - \bar{x})^2}\sqrt{\sum_{i=1}^{n}(y_i - \bar{y})^2}} \quad (5)$$

where x_i and y_i are the value of variable x and y in the year i; $\bar{x}$ and $\bar{y}$ represent the mean value of variable x and y from 2018 to 2022;

Additionally, a t-test is applied to test the significance of the partial correlation coefficient at a significance level of 0.05.

3. Results

3.1. The differences of ground survey of grassland and shrubland AGB

Overall, the biomass of shrubland was about 3 times higher than that of grassland, but the variation was large. According to ground sample plots, the measured AGB of shrubland had a wider range (from 648.9 to 3742.9 g/m^2), with a mean AGB of 1829.2 g/m^2, while the grassland AGB ranged from 202.4 to 1289.6 g/m^2 with an average of 672.5 g/m^2 (Table 2). Meanwhile, the AGB of shrubland also showed a larger standard deviation (751 g/m^2) than that in grassland (265.8 g/m^2), but their coefficient of variation (CV) was similar; 41 and 40% in shrubland and grassland, respectively. The high STD and CV were indicative of the high spatial heterogeneity in the study area.

3.2. Performance of grassland AGB estimation models

The four grassland AGB estimation models (MSR, RF, SVM and CNN) showed comparable results in the two modelling scenarios (Scenario 1: modelling all samples of grassland and shrubland together or Scenario 2: separately modelling them; Figure 3). We chose best model and better modelling scenarios through the following steps. (1) In general, the performance of CNN (testing R^2 ranging from 0.7 to 0.82) and RF (testing R^2 ranging from 0.64 to 0.8) models were significantly better than MSR (testing R^2 ranging from 0.33 to 0.42) and SVM (testing R^2 ranging from 0.45 to 0.64). (2) As compared to Scenario 1 (R^2 was 0.7 and 0.64 for CNN and RF, respectively), both CNN (R^2 was 0.72 and 0.82 for grassland and shrubland, respectively) and RF (R^2 was 0.75 and 0.8 for grassland and shrubland, respectively) algorithms performed better in Scenario 2. (3) Since the R^2 were very close for CNN and RF in Scenario 2, the comparisons of RMSE suggested that RF (131.2 and 267.8 g/m^2 for grassland and shrubland, respectively) was superior over CNN (152.4 and 315.4 g/m^2 for grassland and shrubland, respectively), reducing RMSE 14 and 15% for modeling AGB of grassland and shrubs, respectively. In summary, separately modelling grassland and shrubland by RF model was the best approach for AGB estimations in this study.

Since the RF was the most suitable model in this study, the importance of input variables for RF was calculated (Figure 4). Some differences between grassland and shrubland for the top 10 most important factors were found. Compared with shrubland, the VIs were more important for monitoring grassland AGB using RF. There were 6 indices (EVI, EVI2, NDVI, NIRv, MSR, and DVI) in the top 10 factors, with EVI being the most important factor for predicting grassland AGB. Short-wavelength infrared bands (SWIR1 and SWIR2) were more important than the visible and near-infrared bands. Furthermore, Water VP and LST were also important in RF model for estimating grassland AGB. For shrubland, elevation was the most important biogeographical parameter affecting AGB (12.7% IncMSE), while VH was the least important variable (11.3% IncMSE), which was not reflected in the estimate of grassland AGB. The important VIs in shrubland were GCC, SR, DVI, EVI2, kNDVI, which was distinct from grassland. Additionally, Edge 3 was the most important spectral band for shrubland AGB estimation.

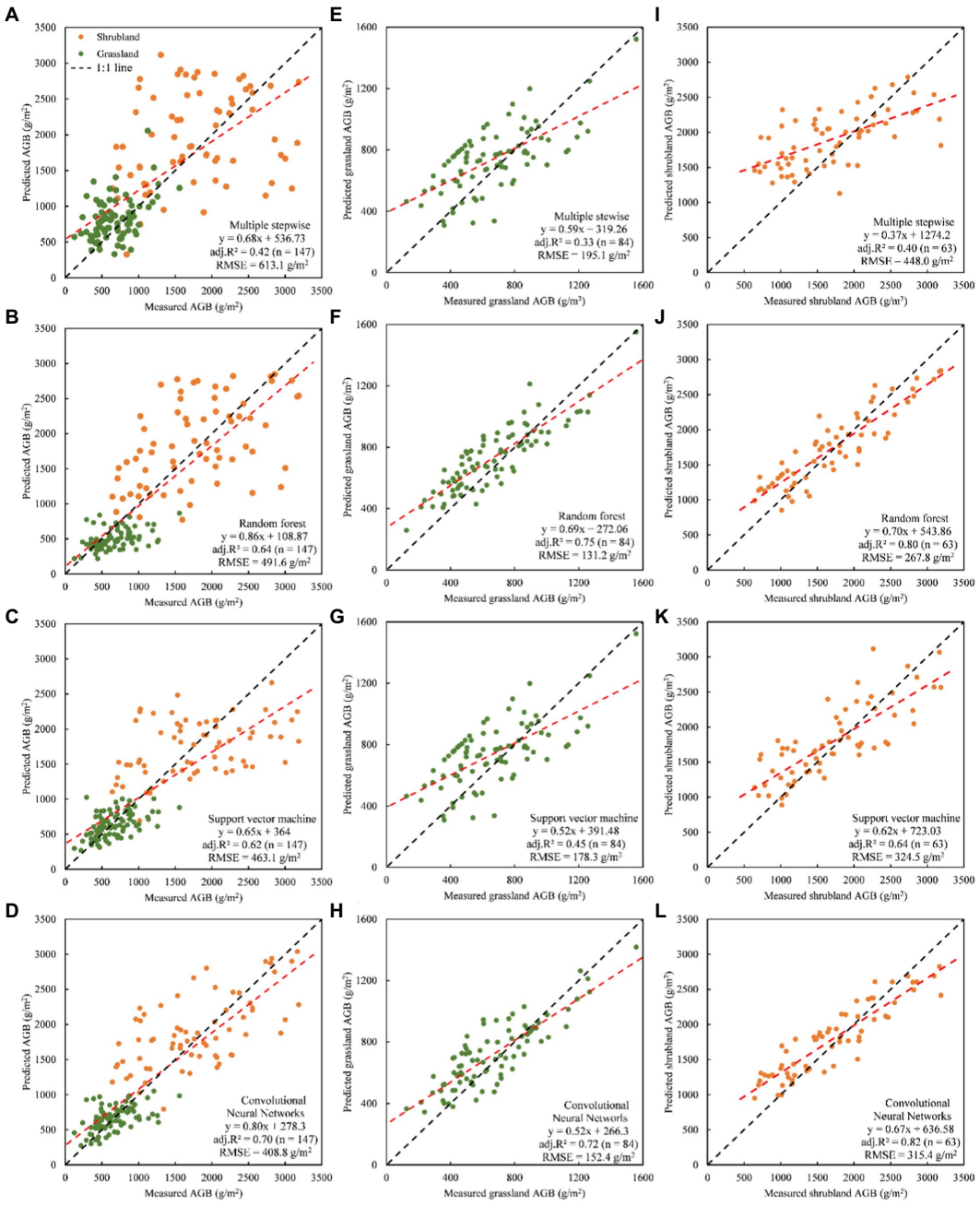

FIGURE 3
Scatter plot between measured and predicted AGB using the various prediction models in two modelling scenarios [Scenario 1: modelling all samples of grassland and shrubland together **(A–D)**; Scenario 2: separately modelling grassland **(E–H)** and shrubland **(I–L)**].

3.3. Selection of input variables

High resolution optical images (Sentinel-2), SAR images (Sentinel-1), environmental and topographic data were major features to predict AGB of grassland by using the ML model. Since the RF model was superior among all eight ML models, the testing of the best combinations of input variables was carried out for regional AGB estimation. As shown in Table 3, all feature groups correlated strongly with validation AGB of grassland and shrubland, with R^2 ranging from 0.60 to 0.75 and 0.54 to 0.8 for grassland and shrubland, respectively. Although it was obvious that the AGB model performed the best when all features were used as input variables, with the addition of SAR data into the AGB model of shrubland leading to the greatest improvement, increasing the accuracy expressed by the value of R^2 from 0.57 to 0.68, while RMSE decreased from 454.1 to 332.7 g/m^2.

Other than the remote sensing images of the Sentinel series, we also explored effects of spatial resolution variation on AGB estimation accuracy. MODIS data with 250 m resolution was used to instead of Sentinel without any other modifications to the RF model. This resulted in R^2 values sustainably decreasing from 0.75 to 0.47 and 0.8 to 0.53 for grassland and shrubland, respectively (Figure 5; Table 3), demonstrating that the remote sensing source with

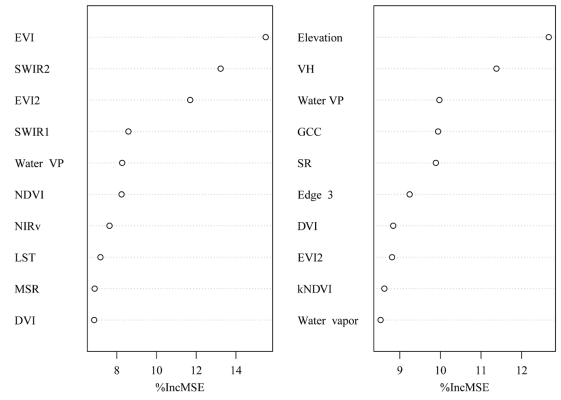

FIGURE 4
Importance (increase in mean squared error, %IncMSE) of input variables for random forest model in AGB estimation for grassland and shrubland.

TABLE 3 Performance of various feature groups for AGB estimation using random forest.

Feature groups	Shrubland			Grassland		
	R^2	RMSE (g/m^2)	MAPE (%)	R^2	RMSE (g/m^2)	MAPE (%)
Optical bands	0.54	469.3	18.7	0.60	170.4	22.5
Optical bands and VIs	0.57	454.1	17.0	0.67	156.2	19.4
All bands and VIs	0.68	332.7	13.3	0.70	148.7	16.9
All bands, VIs and DEM	0.77	273.4	10.9	0.72	138.3	13.1
All bands, VIs, DEM and environmental	0.80	267.8	10.2	0.75	131.2	11.3

Optical Bands represents the bands reflectance of Sentinel-2; VIs represents the vegetation indices calculated based on Sentinel-2; All Bands are the group of Optical Bands and Sentinel-1 bands; DEM is a topography factor including aspect, elevation and slope; Environmental includes the environmental factors Water VP, Precipitation and LST.

better-detailed imaging was much more suitable for AGB estimation in this mountain grassland.

3.4. Spatial distribution of grassland and shrubland AGB

The AGB of grassland and shrubland across our study area in 2021 was predicted by best by the RF model (Figure 6). AGB of grassland and shrubland showed a similar spatial distribution with lower values distributed in the northwest and higher AGB in the central region, especially in the west of Guizhou province. The predicted mean grassland AGB was 596.1 g/m^2 (STD was 209.5 g/m^2) and most AGB values were concentrated in the ranges between 400 g/m^2 and 900 g/m^2 (as shown by the pixel frequency in the figure), which covered over half of the grassland area. The mean AGB was lower in Yunnan province (mean ± STD = 443.6 g/m^2 ± 224.8 g/m^2) than in Guizhou province (mean ± STD = 687.6 g/m^2 ± 258.5 g/m^2). The shrubland had higher mean AGB (1728.3 g/m^2) and STD (470.8 g/m^2) than grassland. The range of the predicted AGB for shrubland was 107.3–3473.6 g/m^2 with over 70% of the shrubland area having AGB between 900 and 2,100 g/m^2. The mean shrubland AGB in Guizhou province (mean ± STD = 1244.2 ± 466.8 g/m^2) was also higher than that in Yunnan province (mean ± STD = 2303.9 ± 502.7 g/m^2).

We further analyzed the influences of topography (elevation and slope) on the spatial patter of AGB in the southwest mountainous area (Figure 7). The mean AGB of grassland and shrubland tended to decrease with increasing elevation. However, a lower mean AGB was found in the grassland elevation below 1,000 m, which might be affected by human activities like grazing and mowing. There were different influences of slope for the distribution of grassland and shrubland AGB. Slope barely affected the distribution of grassland AGB and the mean AGB was almost uniform (714.5 g/m^2 in the slope range of 30–35 degrees and 850.7 g/m^2 in the slope range of 20–25 degrees) across all ranges. By comparison, mean AGB of shrubland was highest in the flat area (2768.6 g/m^2 in the slope less than 5 degree) and tended to decrease as the slope gets steeper (1755.9 g/m^2 in the slope more than 35 degree).

3.5. Effects of precipitation and temperature on spatial AGB distribution

Precipitation and temperature are the most important climate factors affecting grassland growth. By using the RF model, we estimated AGB for five consecutive years (2018–2022) and then applied partial correlation analysis to calculate spatial correlations of AGB with mean annual temperature (MAT) and mean annual precipitation (MAP) in grassland and shrubland of this area. The results suggested a large spatial distribution variation regarding the influence of climatic factors on AGB (Figure 8). Generally, the positive relationship between AGB and MAP existed in a large proportion (70.3%) of the grassland, and 62.8% of which showed positive response to MAT (Table 4). In terms of spatial distribution, grasslands with significant positive correlation between two climate factors (MAP and MAT) and AGB were mainly concentrated in the central part of the study area (the boundary region of these two provinces), which accounted for over 29.4 and 29.5% area, respectively. Opposite effects of MAT and MAP on AGB were detected mainly in the southern and western regions. For shrubland, AGB showed a positive or significant positive correlation with MAP and MAT across 60.1 and 55.6% of the shrubland area, respectively, mainly in the central region.

Moreover, we calculated the AGB responses to climatic factors along the temperature and precipitation gradient along 2°C (MAT) and 200 mm (MAP) steps. The results shown in Figure 9 indicated that there was a parabolical correlation between MAT and AGB of both grassland and shrubland ($R^2 = 0.86$, $p < 0.05$ and $R^2 = 0.97$, $p < 0.05$ for grassland and shrubland, respectively). More specifically, AGB of grassland and shrubland showed significant increasing trends below 19 and 18°C, respectively, (purple line in Figure 8A,C), and gradually decreased when temperature above 19 and 24°C, respectively (green line). Meanwhile, generally positive linear correlations between MAP and AGB of grassland and shrubland were observed ($R^2 = 0.55$, $p < 0.05$ and $R^2 = 0.57$, $p < 0.05$ for grassland and shrubland, respectively); however, turning points were observed in the relationships. Below MAP of 1,300 and 1,200 mm for grassland and shrubland, respectively,

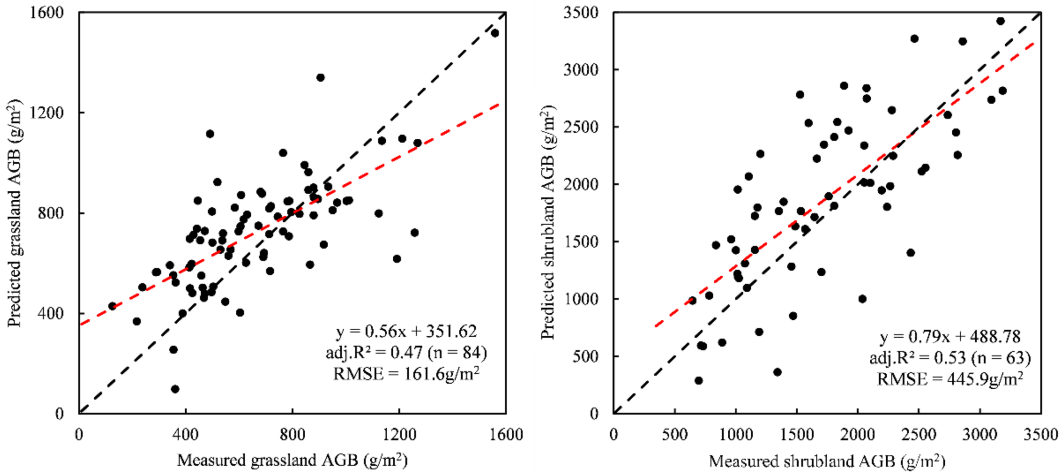

FIGURE 5
Scatter plot between measured and predicted AGB for grassland and shrubland using the RF based on the MODIS data with 250m spatial resolution.

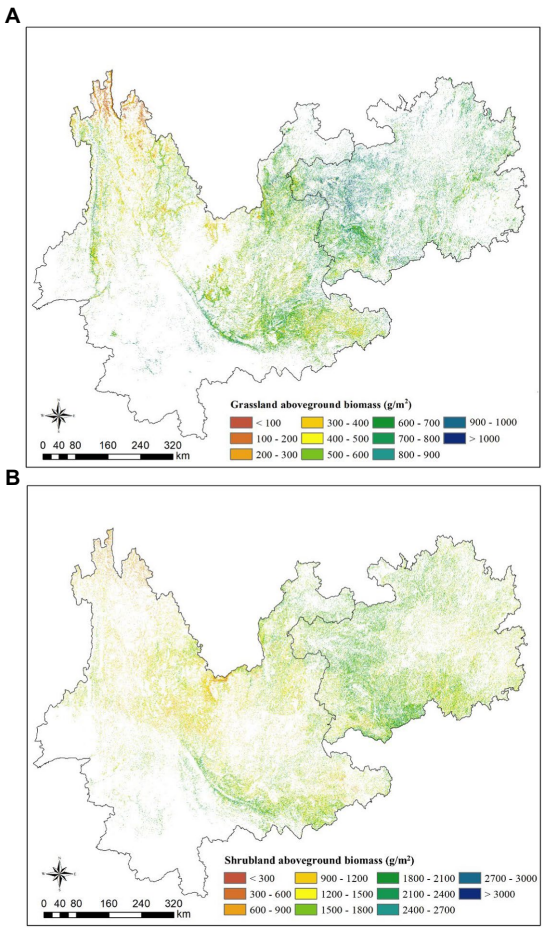

FIGURE 6
Spatial distribution of AGB of grassland **(A)** and shrubland **(B)** in Yunnan and Guizhou provinces in 2021.

AGB significantly increased with MAP; when MAP was above these values, AGB exhibited slightly decreasing trends with precipitation (Figures 8B,D).

4. Discussion

4.1. Model performances and variables selection

Numerous studies have demonstrated that ML models are a reliable tool in grassland AGB prediction due to their powerful interpretation ability and high efficiency (Zhang et al., 2015; Cheng et al., 2022). However, few studies have been conducted in mountain grassland due to its complex vegetation structure and topography (Cheng et al., 2022). In this study, four models were developed and tested for grassland AGB estimation on the Yunnan-Guizhou plateau. We found that due to the high landscape heterogeneity in this mountain grassland, separately modelling the pure grassland and shrubland yielded the best results. Among all AGB estimation algorithms, the ML and DL models had better accuracy than the traditional regression model. In this study, RF and CNN both produced encouraging results for grassland (R^2 was 0.75 and 0.7 for RF and CNN, respectively) and shrubland (R^2 was 0.8 and 0.82 for RF and CNN, respectively; Figure 3), with RF and its lower RMSE than CNN (14 and 15% lower in grassland and shrubland, respectively) achieving the best performance in grassland AGB estimation in Southwest China overall. These results were consistent with previous studies, suggesting that ML models, which have the advantage of accurately estimating complex non-linear relationship across variables, were more effective in dealing with multiple factors than ordinary regression models (Idowu et al., 2016; Lyu et al., 2021). Among ML models, some case studies have indicated that RF model performed better than other ML models in AGB estimation of grassland. Wang et al. (2017) simulated grassland AGB in a semiarid grassland and found that the RF model had a higher accuracy as compared to SVM model. Tang et al. (2021) also showed the RF model was superior to SVM, PLSR and back-propagation artificial neural network (BP-ANN) in AGB monitoring of the headwater of the Yellow River grasslands. Some recent comparison studies on AGB estimation performance of DL and ML models suggested CNN algorithm was found to perform better than classical ML models (i.e., RF, SVM), due to CNN was more sensitive to

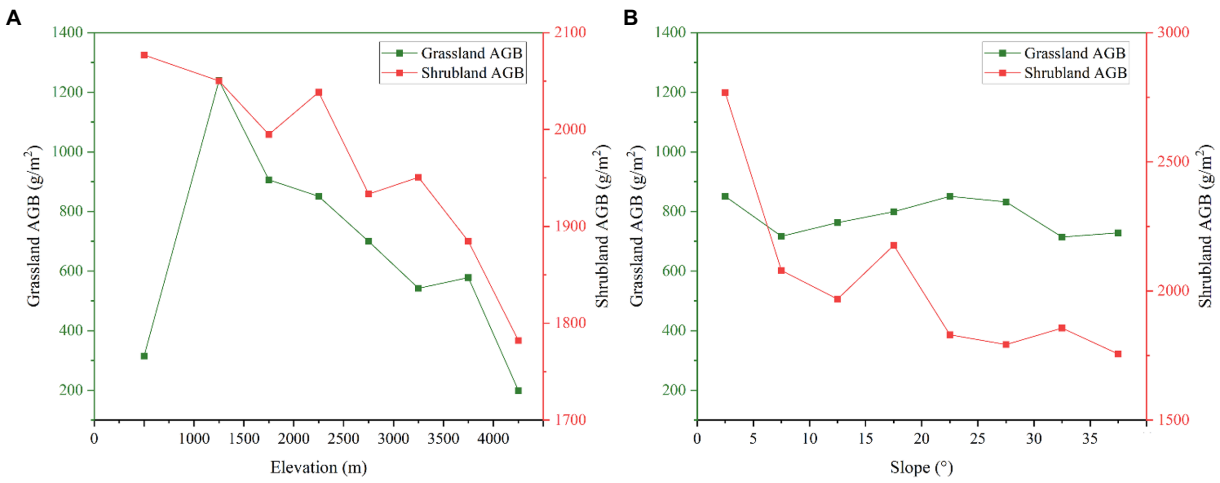

FIGURE 7
The variation of grassland and shrubland AGB along the elevation **(A)** and slope **(B)**.

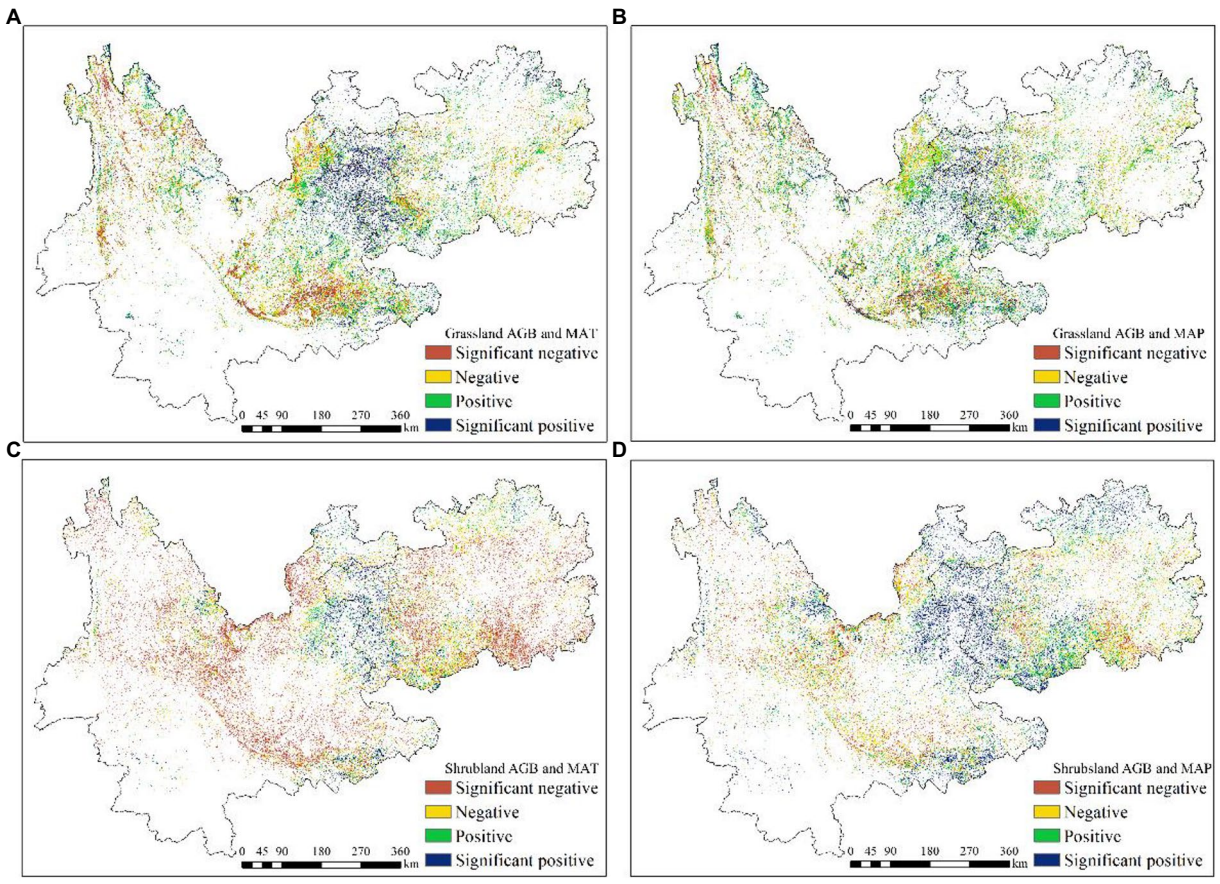

FIGURE 8
Partial correlation between grassland AGB and mean annual temperature **(A)**, grassland AGB and mean annual precipitation **(B)**, shrubland AGB and mean annual temperature **(C)**, shrubland AGB and mean annual precipitation **(D)** at the significance level of 0.05 from 2018 to 2022.

changes in features (Du et al., 2021; Zhang et al., 2022). While another case study showed RF would obtain slightly better accuracy than CNN if the data was elaborately designed (Dong et al., 2020). In our study, attribute to the designed modelling strategy and RF model's strong robust to noise and outliers of heterogeneous ecosystems (Anaya et al., 2009; Xu et al., 2019), RF was found to be the most suitable model in AGB estimation of the mountain grassland in Southwest China.

TABLE 4 Statistics of area percentage with different Influence of climate factors on AGB for grassland and shrubland: different relationships in different areas.

Area percentage (%)	Grassland AGB and MAT	Grassland AGB and MAP	Shrubland AGB and MAT	Shrubland AGB and MAP
Significant negative	16.5	11.8	15.3	15.5
Negative	20.7	17.9	29.1	24.4
Positive	33.3	40.9	37.0	36.8
Significant positive	29.5	29.4	18.6	23.3

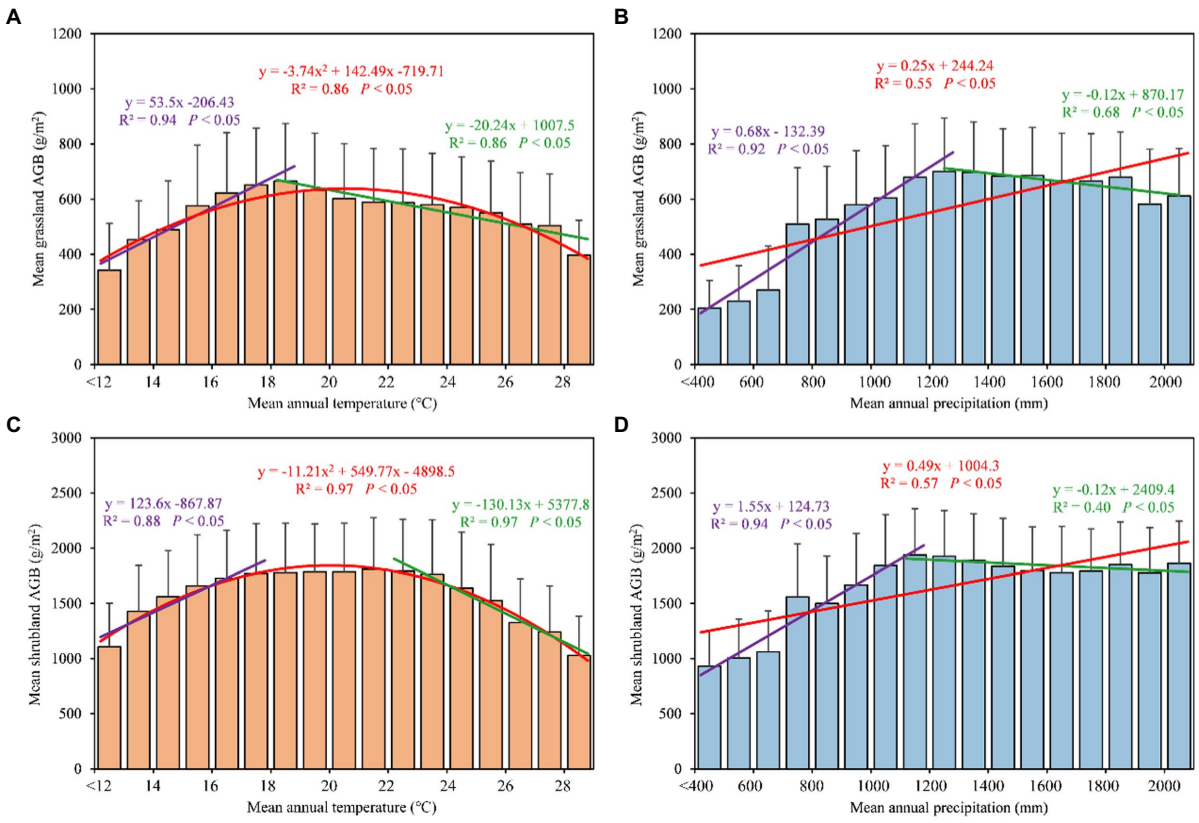

FIGURE 9
Relationship of average AGB of grassland **(A and B)** and shrubland **(C and D)** with MAT (2°C) and MAP (200 mm) gradients data from 2018 to 2022.

Varies environmental factors affecting grassland growth including climate, soil and topography are common input variables to ML models in grassland related studies (Meng et al., 2020; Wang et al., 2022). However, most of these studies used only a single remote sensing data source. Since SAR has advantages in obtaining vegetation structure information, we introduced Sentinel-1 SAR images in our study area, where the grassland is highly mixed with shrubs. In this study, VIs played a more important role in pure grassland estimation, and the EVI and SWIR contributed the most among VIs in the RF model (Figure 4). Some previous research suggested that although EVI did not inevitably outperform NDVI in grassland mapping and AGB estimation, EVI was still an improvement with regards to obtaining more reasonable values in different vegetation density situation (Liu et al., 2014), and SWIR was the most relevant index for grassland extraction in mountain grassland (Cheng et al., 2022). In contrast, elevation and backscatter values from vertical and horizontal (VH) polarization were the two most important input variables for the shrubland AGB estimation model, which suggested shrubland biomass was greatly influenced by topography and vegetation structure in Southwest China. Some studies also reported that VH polarization data from Sentinel-1 SAR image had a higher accuracy than VV polarization data in biomass estimation (Liu et al., 2019). Moreover, the AGB estimation accuracy (R^2) of shrubland significantly improved from 0.57 to 0.68 while reducing RMSE by 26.7% when Sentinel-1 SAR was introduced to the RF model. However, recent case studies have reported conflicting outcomes regarding the performance of combining SAR in grassland AGB estimation. For example, Wang et al. (2019) indicated that the integration of Sentinel-1, Landsat 8, and Sentinel-2 improved the estimation of AGB by more than 30% compared to using only Sentinel-1 in a native pasture of Oklahoma, USA; However, study by Chiarito et al. (2021) showed there was

only a slight improvement when Sentinel-1 SAR was included in alpine meadows in Italy. Finally, While Raab et al. (2020) even reported no positive effect on the model performance by combining Sentinel-1 and Sentinel-2 data in semi-natural grasslands of Germany. Nevertheless, our research demonstrated the potential of combining SAR and high-resolution optical data to provide accurate AGB estimation in shrubs mixed mountain grassland.

4.2. Response of grassland AGB to climatic variables

Climate factors including precipitation and temperature are main drivers of biophysical processes and growth in grassland ecosystems. There is a strong positive linear relationship between AGB and MAP based on long-term observations in almost all grassland ecosystems (Bai et al., 2004; Knapp et al., 2017). However, increasing studies have suggested that the response of AGB to MAP would saturate under extreme wet conditions and the AGB-MAP linear relationship would be modified (Wilcox et al., 2016; Flombaum et al., 2017). For example, Hao et al. (2017) presented that AGB did not show a significant increase when growing season precipitation increased to extremely high values based on near 40 years long-term inventory data in a semiarid grassland. In this study, a general positive linear correlation between MAP and AGB was found for both grassland and shrubland. However, when MAP exceeded 1,300 and 1,200 mm for grassland and shrubland, respectively, AGB showed a slight decreasing trend rather than increasing further with MAP. Zeng et al. (2019) reported a similar relationship between MAP and AGB on the Tibetan Plateau. The spatial distribution of the MAP-AGB relationship indicated that the AGB of grassland (70%) and shrubs (60%) responded generally positively to MAP. Shrubland were less sensitive to climate factors than grassland, as evidenced by the lower proportion of areas where significant responses were found. According to a recent field study in central Yunnan province, MAP and MAT did not directly affect shrubland biomass and the ratio of root and shoot, but changed the relationship between the stoichiometric characteristics and environmental factors (Guo et al., 2022).

Clear parabolical correlations between AGB and MAT were observed for both grassland and shrubland. The turning point of grassland AGB along the temperature gradient was around 19°C, while shrubland AGB would gradually decrease when temperatures exceeded 24°C, which confirmed that shrubland were more tolerant to higher temperatures than grassland. Around 63% of grassland and 56% of shrubland showed a positive correlation with MAT, which for both was lower than the area positively correlated with MAP. This suggests that MAP played a more positive role for grass and shrub growth than MAT. Since extreme temperatures are occurring more frequently in this region under climate change (Yan et al., 2021), increasing drought risks to be amplified by heatwaves and thus threaten ecosystem functioning and human welfare.

4.3. Limitations and future optimization

Our study demonstrated that the integration of SAR and high-resolution optical remote sensing data into the random forest model can yield better performance in mountain grassland AGB estimation in Southwest China. The combination of multi-source remote sensing data provided an opportunity to monitor AGB from a multi-dimensional perspective. Additional satellite data, such as satellite-based hyperspectral and LiDAR data from multi-platforms, can further improve the correct inclusion of vegetation biochemical and structural features, which would lead to further increases in accuracy of grassland AGB estimation in the future. Furthermore, soil percentage in each pixel due to land fragmentation should also be noted, as this causes the uncertainty of the band reflectance and vegetation indices. The use of multi-temporal data could be considered as an approach by acquiring the soil information in the pre-growing season and eliminating or reducing its effects based on pixel unmixing (Li et al., 2016). Additionally, Sentinel series images were fully available in our study area after 2018, and the 5 years of data were able to use in this study is still too short for thorough climate related analyses, and may thus introduce some uncertainty. In fact, the spatial resolution of climate data is relatively coarse (1 km) and it is worth considering the fusion of high precision data (Sentinel) and long time series data such as MODIS data to produce long time series AGB spatial distribution dataset with high precision for a more accurate analysis of the influence of climate variables on AGB in the past time. This could enable refined management and sustainable development strategies for grassland.

5. Conclusion

AGB is one of the key indicators for grassland ecosystem research and management. In this study, we constructed and compared four remote sensing estimation model including a traditional regression model (multiple stepwise regression, MSR), two classical machine learning models (random forest, RF and supporting vector machine, SVM) and a deep learning model (convolutional neural network, CNN) to estimate grassland AGB in Yunnan and Guizhou Provinces, Southwest China. Our study suggests that separately modelling AGB of pure grassland and shrubland achieved better results than modelling them together. Among all test models, the RF model with input variables from field survey, high-resolution optical data (Sentinel-2), SAR data (Sentinel-1), environmental data and topographic data led to the best performance for AGB estimation of both grassland and shrubland. Among all input variables in the RF model, the vegetation indices (i.e., EVI, EVI2, and NDVI) were the most important for grassland AGB estimation, while topographical factor (i.e., elevation) and SAR data (i.e., VH band) contributed the most to the shrubland AGB estimation model. We also demonstrated that integrating the SAR data into input variables had great potential to improve the accuracy of AGB estimation, especially for shrubland, improving AGB estimation by 21%. Regional grassland AGB mapping showed high spatial heterogeneity, with lower values distributed in the Northwest and higher AGB in the central region. The mean AGB of grassland was lower in Yunnan Province (443.6 g/m^2) than that in Guizhou Province (687.6 g/m^2) in 2021. The climatic effects on AGB variation showed that there was a positive linear correlation with MAP, but a parabolical correlation with MAT for both grassland and shrubland AGB based on the estimation of grassland AGB in Southwest China from 2018 to 2022. This study provides an effective and accurate method to estimate mountain grassland AGB and offers a new insight to better understanding spatial variation in

grassland AGB and its response to climatic factors in Southwest China.

Data availability statement

The original contributions presented in the study are included in the article/supplementary material, further inquiries can be directed to the corresponding author.

Author contributions

All authors listed have made a substantial, direct, and intellectual contribution to the work and approved it for publication.

Funding

This research was funded by the China Geological Survey Project (ZD20220133), the National Natural Science Foundation of China (32260300), and the Project for Talent and Platform of Science and Technology in Yunnan Province Science and Technology Department (202205AM070005).

Acknowledgments

Authors would like to thank the support of provincial for Bama Snow Mountain vertical complex ecosystem research station during the field sample, contributions of Rongxiao Che for language editing, Hongwei Zeng's advice for manuscript revising and the reviewers for their very helpful comments, suggestions that substantially improved the paper.

Conflict of interest

The authors declare that the research was conducted in the absence of any commercial or financial relationships that could be construed as a potential conflict of interest.

Publisher's note

All claims expressed in this article are solely those of the authors and do not necessarily represent those of their affiliated organizations, or those of the publisher, the editors and the reviewers. Any product that may be evaluated in this article, or claim that may be made by its manufacturer, is not guaranteed or endorsed by the publisher.

References

Ali, I., Cawkwell, F., Dwyer, E., Barrett, B., and Green, S. (2016). Satellite remote sensing of grasslands: from observation to management. *J. Plant Ecol.* 9, 649–671. doi: 10.1093/jpe/rtw005

Anaya, J. A., Chuvieco, E., and Palacios-Orueta, A. (2009). Aboveground biomass assessment in Colombia: a remote sensing approach. *For. Ecol. Manag.* 257, 1237–1246. doi: 10.1016/j.foreco.2008.11.016

Bai, Y. F., Han, X. G., Wu, J. G., Chen, Z. Z., and Li, L. H. (2004). Ecosystem stability and compensatory effects in the Inner Mongolia grassland. *Nature* 431, 181–184. doi: 10.1038/nature02850

Barrett, B., Nitze, I., Green, S., and Cawkwell, F. (2014). Assessment of multi-temporal, multi-sensor radar and ancillary spatial data for grasslands monitoring in Ireland using machine learning approaches. *Remote Sens. Environ.* 152, 109–124. doi: 10.1016/j.rse.2014.05.018

Cheng, X., Liu, W., Zhou, J., Wang, Z., Zhang, S., and Liao, S. (2022). Extraction of mountain grasslands in Yunnan, China, from sentinel-2 data during the optimal phenological period using feature optimization. *Agronomy* 12:1948. doi: 10.3390/agronomy12081948

Chiarito, E., Cigna, F., Cuozzo, G., Fontanelli, G., Mejia Aguilar, A., Paloscia, S., et al. (2021). Biomass retrieval based on genetic algorithm feature selection and support vector regression in Alpine grassland using ground-based hyperspectral and Sentinel-1 Sar data. *Eur. J. Remote Sens.* 54, 209–225. doi: 10.1080/22797254.2021.1901063

Chu, Y., Wee, A. K. S., Lapuz, R. S., and Tomlinson, K. W. (2021). Phylogeography of two widespread C4 grass species suggest that tableland and valley grassy biome in southwestern China pre-date human modification. *Glob. Ecol. Conserv.* 31:e01835. doi: 10.1016/j.gecco.2021.e01835

Dong, L., Du, H., Han, N., Li, X., Zhu, D. E., Mao, F., et al. (2020). Application of convolutional neural network on lei bamboo above-ground-biomass (Agb) estimation using Worldview-2. *Remote Sens.* 12:958. doi: 10.3390/rs12060958

Du, C., Fan, W., Ma, Y., Jin, H. I., and Zhen, Z. (2021). The effect of synergistic approaches of features and ensemble learning Algorith on aboveground biomass estimation of natural secondary forests based on Als and Landsat 8. *Sensors* 21, 5974–6002. doi: 10.3390/s21175974

Elnashar, A., Zeng, H., Wu, B., Zhang, N., Tian, F., Zhang, M., et al. (2020). Downscaling Trmm monthly precipitation using Google earth engine and Google cloud computing. *Remote Sens.* 12:3860. doi: 10.3390/rs12233860

Flombaum, P., and Sala, O. E. (2007). A non-destructive and rapid method to estimate biomass and aboveground net primary production in arid environments. *J. Arid Environ.* 69, 352–358. doi: 10.1016/j.jaridenv.2006.09.008

Flombaum, P., Yahdjian, L., and Sala, O. E. (2017). Global-change drivers of ecosystem functioning modulated by natural variability and saturating responses. *Glob. Chang. Biol.* 23, 503–511. doi: 10.1111/gcb.13441

Ge, J., Meng, B., Liang, T., Feng, Q., Gao, J., Yang, S., et al. (2018). Modeling alpine grassland cover based on Modis data and support vector machine regression in the headwater region of the Huanghe River, China. *Remote Sens. Environ.* 218, 162–173. doi: 10.1016/j.rse.2018.09.019

Guerschman, J. P., Hill, M. J., Renzullo, L. J., Barrett, D. J., Marks, A. S., and Botha, E. J. (2009). Estimating fractional cover of photosynthetic vegetation, non-photosynthetic vegetation and bare soil in the Australian tropical savanna region upscaling the Eo-1 Hyperion and Modis sensors. *Remote Sens. Environ.* 113, 928–945. doi: 10.1016/j.rse.2009.01.006

Guo, Z., Chen, W., Chen, Q., Liu, X., Hong, S., Zhu, X., et al. (2022). Biomass distribution pattern and stoichiometric characteristics in main shrub ecosystems in Central Yunnan, China. *PeerJ* 10:e13005. doi: 10.7717/peerj.13005

Guo, D., Song, X., Hu, R., Cai, S., Zhu, X., and Hao, Y. (2021). Grassland type-dependent spatiotemporal characteristics of productivity in Inner Mongolia and its response to climate factors. *Sci. Total Environ.* 775:145644. doi: 10.1016/j.scitotenv.2021.145644

Hao, Y. B., Zhou, C. T., Liu, W. J., Li, L. F., Kang, X. M., Jiang, L. L., et al. (2017). Aboveground net primary productivity and carbon balance remain stable under extreme precipitation events in a semiarid steppe ecosystem. *Agric. For. Meteorol.* 240-241, 1–9. doi: 10.1016/j.agrformet.2017.03.006

Idowu, S., Saguna, S., Åhlund, C., and Schelén, O. (2016). Applied machine learning: forecasting heat load in district heating system. *Energ. Buildings* 133, 478–488. doi: 10.1016/j.enbuild.2016.09.068

Jin, Y., Yang, X., Qiu, J., Li, J., Gao, T., Wu, Q., et al. (2014). Remote sensing-based biomass estimation and its spatio-temporal variations in temperate grassland, Northern China. *Remote Sens.* 6, 1496–1513. doi: 10.3390/rs6021496

Jordan, M. I., and Mitchell, T. M. (2015). Machine learning: trends, perspectives, and prospects. *Science* 349, 255–260. doi: 10.1126/science.aaa8415

Knapp, A. K., Ciais, P., and Smith, M. D. (2017). Reconciling inconsistencies in precipitation-productivity relationships: implications for climate change. *New Phytol.* 214, 41–47. doi: 10.1111/nph.14381

Krizhevsky, A., Sutskever, I., and Hinton, G. E. (2017). ImageNet classification with deep convolutional neural networks. *Commun. ACM* 60, 84–90. doi: 10.1145/3065386

Lecun, Y., Bengio, Y., and Hinton, G. (2015). Deep learning. *Nature* 521, 436–444. doi: 10.1038/nature14539

Li, F., Jiang, L., Wang, X., Zhang, X., Zheng, J., and Zhao, Q. (2013). Estimating grassland aboveground biomass using multitemporal Modis data in the West Songnen Plain, China. *J. Appl. Remote. Sens.* 7:073546. doi: 10.1117/1.Jrs.7.073546

Li, F., Zeng, Y., Luo, J., Ma, R., and Wu, B. (2016). Modeling grassland aboveground biomass using a pure vegetation index. *Ecol. Indic.* 62, 279–288. doi: 10.1016/j.ecolind.2015.11.005

Liu, Y., Gong, W., Xing, Y., Hu, X., and Gong, J. (2019). Estimation of the forest stand mean height and aboveground biomass in Northeast China using Sar sentinel-1B, multispectral sentinel-2A, and Dem imagery. *ISPRS J. Photogramm. Remote Sens.* 151, 277–289. doi: 10.1016/j.isprsjprs.2019.03.016

Liu, X., Zhang, J., Zhu, X., Pan, Y., Liu, Y., Zhang, D., et al. (2014). Spatiotemporal changes in vegetation coverage and its driving factors in the Three-River headwaters region during 2000–2011. *J. Geogr. Sci.* 24, 288–302. doi: 10.1007/s11442-014-1088-0

Lu, D. (2007). The potential and challenge of remote sensing-based biomass estimation. *Int. J. Remote Sens.* 27, 1297–1328. doi: 10.1080/01431160500486732

Lyu, X., Li, X., Gong, J., Li, S., Dou, H., Dang, D., et al. (2021). Remote-sensing inversion method for aboveground biomass of typical steppe in Inner Mongolia, China. *Ecol. Indic.* 120:106883. doi: 10.1016/j.ecolind.2020.106883

Meng, B., Liang, T., Yi, S., Yin, J., Cui, X., Ge, J., et al. (2020). Modeling alpine grassland above ground biomass based on remote sensing data and machine learning algorithm: a case study in east of the Tibetan Plateau, China. *IEEE J. Sel. Top. Appl. Earth Observ. Remote Sens.* 13, 2986–2995. doi: 10.1109/JSTARS.2020.2999348

Morais, T. G., Teixeira, R. F. M., Figueiredo, M., and Domingos, T. (2021). The use of machine learning methods to estimate aboveground biomass of grasslands: a review. *Ecol. Indic.* 130:108081. doi: 10.1016/j.ecolind.2021.108081

Mu, J., Zeng, Y., Wu, Q., Niklas, K. J., and Niu, K. (2016). Traditional grazing regimes promote biodiversity and increase nectar production in Tibetan alpine meadows. *Agric. Ecosyst. Environ.* 233, 336–342. doi: 10.1016/j.agee.2016.09.030

Naidoo, L., Van Deventer, H., Ramoelo, A., Mathieu, R., Nondlazi, B., and Gangat, R. (2019). Estimating above ground biomass as an indicator of carbon storage in vegetated wetlands of the grassland biome of South Africa. *Int. J. Appl. Earth Obs. Geoinf.* 78, 118–129. doi: 10.1016/j.jag.2019.01.021

Niu, K., Choler, P., De Bello, F., Mirotchnick, N., Du, G., and Sun, S. (2014). Fertilization decreases species diversity but increases functional diversity: a three-year experiment in a Tibetan alpine meadow. *Agric. Ecosyst. Environ.* 182, 106–112. doi: 10.1016/j.agee.2013.07.015

Powell, S. L., Cohen, W. B., Healey, S. P., Kennedy, R. E., Moisen, G. G., Pierce, K. B., et al. (2010). Quantification of live aboveground forest biomass dynamics with Landsat time-series and field inventory data: a comparison of empirical modeling approaches. *Remote Sens. Environ.* 114, 1053–1068. doi: 10.1016/j.rse.2009.12.018

Quan, X., He, B., Yebra, M., Yin, C., Liao, Z., Zhang, X., et al. (2017). A radiative transfer model-based method for the estimation of grassland aboveground biomass. *Int. J. Appl. Earth Obs. Geoinf.* 54, 159–168. doi: 10.1016/j.jag.2016.10.002

Raab, C., Riesch, F., Tonn, B., Barrett, B., Meißner, M., Balkenhol, N., et al. (2020). Target-oriented habitat and wildlife management: estimating forage quantity and quality of semi-natural grasslands with Sentinel-1 and Sentinel-2 data. *Remote Sens. Ecol. Conserv.* 6, 381–398. doi: 10.1002/rse2.149

Ramoelo, A., Cho, M. A., Mathieu, R., Madonsela, S., Van De Kerchove, R., Kaszta, Z., et al. (2015). Monitoring grass nutrients and biomass as indicators of rangeland quality and quantity using random forest modelling and WorldView-2 data. *Int. J. Appl. Earth Obs. Geoinf.* 43, 43–54. doi: 10.1016/j.jag.2014.12.010

Ren, H., Zhou, G., and Zhang, F. (2018). Using negative soil adjustment factor in soil-adjusted vegetation index (Savi) for aboveground living biomass estimation in arid grasslands. *Remote Sens. Environ.* 209, 439–445. doi: 10.1016/j.rse.2018.02.068

Scurlock, J. M. O., and Hall, D. O. (2002). The global carbon sink: a grassland perspective. *Glob. Chang. Biol.* 4, 229–233. doi: 10.1046/j.1365-2486.1998.00151.x

Shen, H. H., Zhu, Y. K., Zhao, X., Geng, X. Q., and Gao, S. Q. (2016). Analysis of current grassland resources in China. *Chin. Sci. Bull.* 61, 139–154. doi: 10.1360/N972015-00732

Sinha, S., Jeganathan, C., Sharma, L. K., and Nathawat, M. S. (2015). A review of radar remote sensing for biomass estimation. *Int. J. Environ. Sci. Technol.* 12, 1779–1792. doi: 10.1007/s13762-015-0750-0

Tang, R., Zhao, Y., and Lin, H. (2021). Spatio-temporal variation characteristics of aboveground biomass in the headwater of the Yellow River based on machine learning. *Remote Sens.* 13:3404. doi: 10.3390/rs13173404

Wang, P., Fan, E., and Wang, P. (2021). Comparative analysis of image classification algorithms based on traditional machine learning and deep learning. *Pattern Recogn. Lett.* 141, 61–67. doi: 10.1016/j.patrec.2020.07.042

Wang, Y., Qin, R., Cheng, H., Liang, T., Zhang, K., Chai, N., et al. (2022). Can machine learning algorithms successfully predict grassland aboveground biomass? *Remote Sens.* 14:3843. doi: 10.3390/rs14163843

Wang, Y., Wang, G., Wu, Q., Niu, F., and Cheng, H. (2010). The impact of vegetation degeneration on hydrology features of alpine soil. *J. Glaciol. Geocryol.* 32, 989–998. doi: 10.1080/00949651003724790

Wang, Y., Wu, G., Deng, L., Tang, Z., Wang, K., Sun, W., et al. (2017). Prediction of aboveground grassland biomass on the loess plateau, China, using a random forest algorithm. *Sci. Rep.* 7:6940. doi: 10.1038/s41598-017-07197-6

Wang, J., Xiao, X., Bajgain, R., Starks, P., Steiner, J., Doughty, R. B., et al. (2019). Estimating leaf area index and aboveground biomass of grazing pastures using Sentinel-1, Sentinel-2 and Landsat images. *ISPRS J. Photogramm. Remote Sens.* 154, 189–201. doi: 10.1016/j.isprsjprs.2019.06.007

Wei, P., Chen, S., Wu, M., Jia, Y., Xu, H., and Liu, D. (2021). Increased ecosystem carbon storage between 2001 and 2019 in the northeastern margin of the Qinghai-Tibet plateau. *Remote Sens.* 13:3986. doi: 10.3390/rs13193986

Wilcox, K. R., Blair, J. M., Smith, M. D., and Knapp, A. K. (2016). Does ecosystem sensitivity to precipitation at the site-level conform to regional-scale predictions? *Ecology* 97, 561–568. doi: 10.1890/15-1437.1

Wu, B. F., Qian, J., and Zeng, Y. (2017). *Land cover atlas of the People's republic of China (1:1,000,000)*. Beijing, Sinomaps Press.

Wu, C., Shen, H., Shen, A., Deng, J., Gan, M., Zhu, J., et al. (2016). Comparison of machine-learning methods for above-ground biomass estimation based on Landsat imagery. *J. Appl. Remote. Sens.* 10:035010. doi: 10.1117/1.JRS.10.035010

Xu, D., Chen, B., Shen, B., Wang, X., Yan, Y., Xu, L., et al. (2019). The classification of grassland types based on object-based image analysis with multisource data. *Rangel. Ecol. Manag.* 72, 318–326. doi: 10.1016/j.rama.2018.11.007

Xu, C., Liu, W., Zhao, D., Hao, Y., Xia, A., Yan, N., et al. (2022). Remote sensing-based spatiotemporal distribution of grassland aboveground biomass and its response to climate change in the Hindu Kush Himalayan Region. *Chin. Geogr. Sci.* 32, 759–775. doi: 10.1007/s11769-022-1299-8

Yan, W., He, Y., Cai, Y., Qu, X., and Cui, X. (2021). Relationship between extreme climate indices and spatiotemporal changes of vegetation on Yunnan Plateau from 1982 to 2019. *Glob. Ecol. Conserv.* 31:e01813. doi: 10.1016/j.gecco.2021.e01813

Yang, S., Feng, Q., Liang, T., Liu, B., Zhang, W., and Xie, H. (2018). Modeling grassland above-ground biomass based on artificial neural network and remote sensing in the Three-River headwaters region. *Remote Sens. Environ.* 204, 448–455. doi: 10.1016/j.rse.2017.10.011

Zeng, N., Ren, X., He, H., Zhang, L., Li, P., and Niu, Z. (2021). Estimating the grassland aboveground biomass in the Three-River Headwater Region of China using machine learning and Bayesian model averaging. *Environ. Res. Lett.* 16:16. doi: 10.1088/1748-9326/ac2e85

Zeng, N., Ren, X., He, H., Zhang, L., Zhao, D., Ge, R., et al. (2019). Estimating grassland aboveground biomass on the Tibetan plateau using a random forest algorithm. *Ecol. Indic.* 102, 479–487. doi: 10.1016/j.ecolind.2019.02.023

Zhang, C., Denka, S., Cooper, H., and Mishra, D. R. (2018). Quantification of sawgrass marsh aboveground biomass in the coastal Everglades using object-based ensemble analysis and Landsat data. *Remote Sens. Environ.* 204, 366–379. doi: 10.1016/j.rse.2017.10.018

Zhang, F., Tian, X., Zhang, H., and Jiang, M. (2022). Estimation of aboveground carbon density of forests using deep learning and multisource remote sensing. *Remote Sens.* 14:3022. doi: 10.3390/rs14133022

Zhang, B., Zhang, L., Xie, D., Yin, X., Liu, C., and Liu, G. (2015). Application of synthetic Ndvi time series blended from Landsat and Modis data for grassland biomass estimation. *Remote Sens.* 8:10. doi: 10.3390/rs8010010

frontiers | Frontiers in Ecology and Evolution

TYPE Original Research
PUBLISHED 14 March 2023
DOI 10.3389/fevo.2023.1149240

OPEN ACCESS

EDITED BY
Zhongqing Yan,
Chinese Academy of Forestry,
China

REVIEWED BY
Lie Yang,
Wuhan University of Technology,
China
Yongheng Gao,
Chengdu Institute of Biology (CAS),
China

*CORRESPONDENCE
Zhen'an Yang
✉ yza2765@126.com

SPECIALTY SECTION
This article was submitted to Population, Community, and Ecosystem Dynamics, a section of the journal Frontiers in Ecology and Evolution

RECEIVED 21 January 2023
ACCEPTED 23 February 2023
PUBLISHED 14 March 2023

CITATION
Tong Y, Long Y and Yang Z (2023) Effects of warming and isolation from precipitation on the soil carbon, nitrogen, and phosphorus, and their stoichiometries in an alpine meadow in the Qinghai–Tibet Plateau: A greenhouse warming study.
Front. Ecol. Evol. 11:1149240.
doi: 10.3389/fevo.2023.1149240

Effects of warming and isolation from precipitation on the soil carbon, nitrogen, and phosphorus, and their stoichiometries in an alpine meadow in the Qinghai–Tibet Plateau: A greenhouse warming study

Yongpeng Tong[1], Yanjun Long[2] and Zhen'an Yang[1]*

[1]College of Science, Shihezi University, Shihezi, Xinjiang, China, [2]College of Life Science, China West Normal University, Nanchong, Sichuan, China

Introduction: In the Qinghai–Tibet Plateau (QTP), alpine meadows are among the most noticeable reflection of global climate change. However, effects of global warming on soils hosting alpine meadows in the QTP, such as reduced moisture because of low precipitation, remain unclear.

Methods: Here, the soil moisture content (SMC), pH, dissolved organic carbon (DOC), ammonium nitrogen (NH_4^+–N), nitrate nitrogen (NO_3^-–N) and available phosphorus (AP) contents in the QTP were analyzed. The changes in and stoichiometries of total carbon, nitrogen, and phosphorus (TC, TN, and TP), microbial biomass carbon, nitrogen, and phosphorus (MBC, MBN, and MBP), β-1,4-glucosidase (BG), β-1,4-N-acetylglucoaminosidase (NAG), leucine aminopeptidase (LAP), and acid phosphatase (ACP) in the 0–30cm layer of soils associated with warming in a greenhouse in the QTP from 2015 to 2020 were characterized.

Results: We found that warming in the greenhouse significantly decreased the SMC, NO_3^-–N, MBC, MBN, MBP, BG, LAP, ACP, and enzymatic C:N ratio. The warming increased the DOC, NH_4^+–N, AP, MBC:MBN, and enzymatic N:P ratios noticeably. The pH, TC, TN, TP, C:N, C:P, N:P, MBC:MBP, MBN:MBP, and enzymatic C:P ratios were minimally affected.

Conclusion: The results showed that warming and isolation from precipitation promoted mineralization of N and P in the soil but did not significantly alter the cycling of elements in soils in an alpine meadow.

KEYWORDS

ecological stoichiometric characteristics, extracellular enzyme activities, warming, isolation from precipitation, soil moisture content

1. Introduction

Worldwide, warming and precipitation variability is the most important manifestation of global climate change (Zhang W. X. et al., 2021), and these events will become more frequent in the future (IPCC, 2021). According to climate models, the global average temperature of the atmosphere will increase by 2–5°C relative to the pre-industrial revolution level before the end of the 21st century (Wieder et al., 2013; Meng et al., 2020). Temperature is a major driver of biogeochemical processes and thus warming alters the cycling of carbon (C), nitrogen (N), and phosphorus (P) in terrestrial ecosystems (Zhou et al., 2013a,b). Global warming increases the release of C from plants (leaves and roots) during photosynthesis (Zhao et al., 2016; Wang et al., 2021), the decomposition of soil organic C, and the flux of C from soils because of the enhanced activation of these processes (Fang et al., 2015). To improve the prediction of consequences linked to global warming, numerous simulation studies have been conducted (Fu et al., 2012; Wang et al., 2014; Meng et al., 2020). However, these studies have produced conflicting result. For example, the responses of microbial communities in soils to global warming differ according to the duration of experiments. Short-term (<3 years) warming studies show no significant impact on the microbial biomass in soils, whereas, warming that exceeds 3 years either increased or decreased the microbial biomass (Fu et al., 2012). Moreover, numerous studies have demonstrated that global warming is worsening phenomena such as droughts (Hu et al., 2020) because high temperatures stimulate evaporation and plant transpiration and increase soil water loss (Harte et al., 1995; Wan et al., 2002). Additionally, these studies commonly focused on one factor (Hu et al., 2020), such as warming (Fu et al., 2012; Wang et al., 2014; Meng et al., 2020), precipitation variability (Hu et al., 2020), and N deposition (Yang et al., 2021). Therefore, studies to evaluate the response of terrestrial ecosystems (grassland, forest, cropland) to climate change based on multiple components (Zhou et al., 2013a), such as vegetation and soil, as well as their interrelationships, are needed.

Soil is a crucial component of terrestrial ecosystems. It is the primary source of nutrients and water for plant growth, and thus, regulates the proliferation of plants (Yang et al., 2018; Tan et al., 2021). In soils, C, N, and P affect the metabolism and growth of plants, and therefore, a better understanding of relationships and the dynamics between elements can improve the management of terrestrial ecosystems (Tan et al., 2021). In addition to its utility for predicting the retention of nutrients and biomass production at varying scales (subcellular to ecosystem scales), the ecological stoichiometric approach enables the exploration of material circulation, energy balance, and the relationship between vegetation and the environment in terrestrial ecosystems (Sinsabaugh et al., 2009; Li et al., 2013; Yang et al., 2018). Thus, the ecological stoichiometric was used to reveal climate change (e.g., warming and precipitation variability) in the turnover of soil elements is very credible.

In soils, microorganisms cause decay of organic matter (Zhou et al., 2013a), maintain the balance between C, N, and P in terrestrial ecosystems (Gong et al., 2019), and ensure the availability of nutrients to plant through the provision of extracellular enzymes (Zhou et al., 2013a; Zhu et al., 2020). Therefore, the microbial biomass and elemental composition of secreted enzymes can be severely affected by the C:N:P ratio of the soil (Zhou et al., 2013a; Gong et al., 2019; Zhu et al., 2020). For, example, strong correlations were reported between the soil C:N and C:P ratios in high mountains, low mountains, and lowlands (Li et al., 2012; Gong et al., 2019). However, according to other studies, the stoichiometry of elements in soils and microbial biomass exhibit a weak or no correlation (Ehlers et al., 2010). In these studies, the ratios of elements in the microbial biomass were considered homeostatic and independent of the soil environment (Li et al., 2012). The relationships between elements in biomass and soils remain unclear. Therefore, to improve adaptation to climate change, further studies elucidating relationships between the stoichiometry of elements in soils and microbial biomass are needed.

The Qinghai–Tibet Plateau (QTP) is an area extremely sensitive to global climate change, and its ecosystems are quite fragile (Wang et al., 2014; Yang et al., 2018, 2021; Zhu et al., 2020). In particular, the average temperature rise in the region is ~40% higher than the global average (Luo et al., 2009; Zi et al., 2018). Therefore, it represents an ideal region for characterization of the response of terrestrial ecosystems to global climate change, such as warming (Luo et al., 2009; Fu et al., 2012; Zhao et al., 2016; Zi et al., 2018), warming and N fertilization (Zhao et al., 2014), increasing precipitation and warming (Niu et al., 2010). In addition, annual precipitation in the central part of the QTP exhibits an increasing trend, whereas a decreasing trend is displayed outside the region (Yang et al., 2011). Considering that vegetation covers more than 40% of the QTP, many studies on effects of global warming and other factor on plants and soils have been conducted in the region (Luo et al., 2009; Niu et al., 2010; Fu et al., 2012; Zhao et al., 2014, 2016; Zi et al., 2018). For example, warming can alter species of plant communities because of the enhanced availability of nutrients to competitive species, thereby inhibiting the growth of less competitive species (Zhao et al., 2016). Therefore, the growth and production of plants can be changed because of variations in the growing season and phenology of plants (Zi et al., 2018). Nevertheless, few studies on interactions between climatic factors and soils in alpine steppe ecosystems are available. Altitude, soil temperature and C/N ratio have the greatest impact on the diversity and composition of soil microbial communities in alpine ecosystems. Altitude is the most important environmental factor. It can not only adjust the availability of microclimate and nutrients, but also affect microbial communities by adjusting geographical distance (Cui et al., 2019). Due to the steep environmental gradient, different climatic zones may occur over a very short geographical distance. Therefore, we also need to carry out long-term multi-gradient warming research to explore the adaptation of the QTP to climate change.

Thus, here, a greenhouse experiment was conducted in an alpine meadow in the northeastern margin of the QTP, China. The hypothesis was that isolation from precipitation and warming can significantly alter the cycling of elements in soils in an alpine meadow. This study had three objectives: (1) determine if ecological stoichiometric characteristics, such as extracellular enzyme activities, were significantly altered, (2) determine changes in the cycling of elements in the soils, and (3) highlight mechanisms of the alterations caused by warming and decreased precipitation. We studied the relationship between soil physical and chemical properties and soil EEAs, which may provide insights on the mechanism of the interaction between climate factors and soil in alpine grassland ecosystem.

2. Materials and methods

2.1. Site description

The alpine meadow that was studied is in Hongyuan County, Sichuan Province, in the northeastern margin of the QTP, China (32°58′N, 102°37′E, 3475 m a.s.l.). The area is characterized by a cold plateau climate, with a mean annual temperature of 1.57°C and mean annual precipitation (1961–2015) of 752.21 mm (data from Chinese Meteorological Data Service Centre, http://data.cma.cn//). The coldest and hottest months are January and July, with mean temperatures of −9.66 and 11.12°C (Yang et al., 2021).

Soil in the study area is typical of an alpine meadow according to the soil classification standard of China. The meadow that was studied has served as a winter pasture (November–May) for yaks since 1996, and thus, it was fenced in July 2013. Vegetation in the region is dominated by the following species: *Elymus nutans* Griseb., *Deschampisa caespitosa* (L.) Beauv., *Koeleria litwinowii* Dom., *Kobresia setchwanensis* Hand.-Mazz., *Festaca ovina* L., *Saussurea nigrescens* Maxim., *Trollius farreri stapf*, *Anemone rivularis* Buch.-Ham. ex DC. var. flore-minore Maxim., and *Astragalus polycladus* Bur. et Franch (Yang et al., 2021).

2.2. Experimental design and sampling

One greenhouse (27 × 7.2 × 3.5 m) that was constructed in September 2015 was unperturbed prior to sampling. Temperature data loggers (WatchDog B101) were installed inside and outside the greenhouse on April 19, 2020, to collect data that were utilized for analyzing effects of warming. A data logger (A1) was installed at a height of 1.5 m in the center of the greenhouse to measure the air temperature, while another (A2) was buried at a depth of 10 cm at the same location as A1 to collect temperature data in the soil. Two data loggers (A3 and A4) were installed similar to A1 and A2, ~10 m from the edge of the greenhouse, to measure the air and soil temperature outside. The data loggers were retrieved and taken to the laboratory on May 11, 2021, and the collected data were downloaded.

In July 2020 (~5 years following the commencement of the greenhouse experiment), five 1 × 1 m quadrats (W, warming) along the principal axis of the greenhouse that were ~3 m apart were selected for sampling. In addition, five 1 m × 1 m quadrats (CK) ~10 m from the edges of the greenhouse were sampled. In each quadrant, the soil surface was cleaned and five cores (evenly distributed along a diagonal) were collected from the 0–30 cm (0–10, 10–20, and 20–30 cm intervals) layer using an auger (4 cm in diameter), and these were used for determination of properties of the soils.

2.3. Laboratory analysis

2.3.1. Sample preparation

Soil samples from each quadrant were mixed to produce a composite, which was sieved through a 2-mm mesh. Part of the sieved sample was used subsequently to determine the soil moisture content (SMC), pH, dissolved organic carbon (DOC), ammonium nitrogen (NH_4^+–N), nitrate nitrogen (NO_3^-–N), microbial biomass carbon (MBC), microbial biomass nitrogen (MBN), microbial biomass phosphorus (MBP), β-1,4-glucosidase (BG), β-1,4-N-acetylglucoaminosidase (NAG), leucine aminopeptidase (LAP), and acid phosphatase (ACP) contents. Another portion was air-dried, and a split was ground to <0.25 mm in diameter and used to determine the concentration of available phosphorus (AP), whereas another split was ground to <0.15 mm and utilized to measure the concentrations of TC, TN, and TP.

2.3.2. Determination of soil properties

Approximately 5 g of fresh soil was used to determine the pH of each sample using an acidimeter (PHS-3C, Shengke, China) following extraction for 30 min (200 r min^{-1}) with distilled water (m:v = 1:5) at the ambient temperature. Relatedly, ~10 g of fresh soil was used to measure the SMC of each sample by drying to a constant weight at 105°C (Jiao et al., 2020). Further, another 5 g of fresh soil was extracted with 2 M KCl (m:v = 1:10) and filtered through a 0.45 μm filter membrane, and the DOC was determined from this sample using an automated total organic C analyzer (Shimadzu, TOC-Vwp, Japan; Zhang et al., 2018). A continuous flow analytical system (Auto Analyzer Bran + Luebbe, Germany) was used to determine the concentrations of NH_4^+–N and NO_3^-–N in the samples following the extraction of ~5 g of fresh soil with 2 M KCL (m:v = 1:10) on a shaker (200 r min^{-1}) at the ambient temperature for 1 h. The concentrations of AP in the soil samples were determined using a spectrophotometer (Shimadzu, UV2450, Japan) at 880 nm after extraction with 0.2 M $NaHCO_3$ (m:v = 1:10) on a shaker (200 r min^{-1}) at the ambient temperature for 1 h, whereas those of TC and TN were measured using an elemental analyzer (Elementar Vario MACRO, Elementar, Germany). The concentration of TP was determined colorimetrically using a spectrophotometer (Shimadzu, UV2450, Japan) at 880 nm after the digestion of each sample with H_2SO_4 and H_2O_2 followed by H_2SO_4 and $HClO_4$ (Yang et al., 2018). The stoichiometric ratios of C, N, and P are based on the mass of each element.

2.3.3. Measurement of the soil microbial biomass

The concentrations of MBC, MBN, and MBP were determined based on the chloroform-fumigation extraction method. Approximately 10 g of fresh soil was fumigated with chloroform in the dark for 24 h (fumigated soil), while another 10 g was cultivated without chloroform in the dark for 24 h (nonfumigated soil). Subsequently, ~5 g each of fumigated and nonfumigated soil samples were extracted using 0.5 M K_2SO_4 (m:v = 1:5) on a shaker at the ambient temperature for 1 h (200 r min^{-1}). The concentrations of MBC and MBN were then determined correspondingly using an automated total organic C analyzer (Shimadzu, TOC-Vwp, Japan) and an auto analyzer (Bran + Luebbe, Germany). The other 5 g each of fumigated and nonfumigated soil samples were extracted using 0.5 M $NaHCO_3$ (m:v = 1:10, pH = 8.5) on a shaker at the ambient temperature for 30 min (200 r min^{-1}). The concentration of MBP in each soil sample was then determined using a spectrophotometer (Shimadzu, UV2450, Japan) at 880 nm. The soil microbial biomass element (MBE) was determined using the following expression:

$$MBE = (CF - CUF) / K \quad (1)$$

where CF is the concentration of an element in the fumigated soil, CUF is the concentration of an element in the nonfumigated soil, and

K is the correction factor. In the present study, the K values that were used for calculation of the MBC, MBN, and MBP were 0.45, 0.54, and 0.4, respectively (Zederer et al., 2017). The stoichiometric ratios of the MBC, MBN, and MBP are expressed based on the mass of each element.

2.3.4. Measurement of extracellular enzyme activities

A slightly modified 4-methyl-umbelliferyl substrate conjugate was used to determine extracellular enzyme activities (EEAs) (Saiya-Corka et al., 2002). Approximately 1 g of fresh soil (diameter < 0.15 mm) was mixed with 125 ml of an acetate buffer (50 mM, pH = 5.0) on a shaker (200 r min^{-1}) at room temperature for 20 min to produce soil suspensions. Black 96-well microplates were then divided into six parts and eight replicate wells for each part. These included the following: sample assay (SA), sample control (SC), quench control (QC), reference standard (RS), negative control (NC), and blank (B) wells. First, 200 μL of the buffer was added to each of the B, RS, and NC wells. Second, 50 μL of the buffer was added into each of the B and SC wells to eliminate the natural fluorescence interference of the buffer and soil in the well plate. Third, 200 μL of the soil suspension was added to each of the SC, SA, and QC wells, and then 50 μL of a 10-μM MUB solution was poured into each of the RS and QC wells. Finally, 50 μL of a 200-μM MUB-linked substrate was added to each of the NC and SA wells, and the time was noted. The microplates were covered and incubated in the dark at 25°C for 4 h, and 10 μL of 1.0 M NaOH was added to each well to stop the reaction. The fluorescence intensities of samples were then measured at excitation wavelength of 365 nm and 450 nm emission filters. The substrates for the BG, NAG, LAP, and ACP were 4-methylumbelliferyl-β-D-glucopyranoside, 4-Methylumbelliferyl, N-acetyl-β-D-glucosaminide, L-Leucine-7-amino-4-methylcoumarin hydrochloride, and 4-Methylumbelliferyl phosphate, respectively. The EEAs were calculated according to the method described in a previous study (DeForest, 2009) and expressed in mmol h^{-1} g^{-1}. The C:N, C:P, and N:P ratios of extracellular enzymes were correspondingly expressed as Ln(BG):Ln(LAP + NAG), Ln(BG):LN(ACP), and Ln(LAP + NAG):Ln(ACP) (Zhu et al., 2020).

2.4. Data analysis

The Statgraphics3.0 software (STN, St Louis, MO, United States) was used to perform all statistical analyses. The two-way ANOVA was used for data analysis following normality testing. The treatment (CK and W) and soil depth (0–10, 10–20, and 20–30 cm) served as independent variables. The Tukey-HSD was used to correct *p*-values associated with the multi-comparisons, and the difference between means was considered significant if the *p*-value of the ANOVA F-test was ≤0.05. All data are expressed as the mean ± the standard error (SE).

3. Results

3.1. Microclimate analysis

The results show that compared with the control, the greenhouse increased the air and soil temperatures by average values of 8.32 and 7.52°C, respectively (Figure 1; Supplementary Table S1, $p < 0.001$) between April 20, 2020 and October 10, 2021.

3.2. Variations in soil properties and the concentrations of carbon, nitrogen, and phosphorus

Compared with the control, the greenhouse significantly decreased the SMC (Figure 2A, $p < 0.001$) and concentration of NO_3^-–N (Figure 2E, $p < 0.001$) in the soil. In contrast, the greenhouse increased the concentrations of DOC (Figure 2C, $p < 0.001$), NH_4^+–N (Figure 2D, $p < 0.001$), and AP (Figure 2D, $p < 0.001$) in the soil. Interestingly, the greenhouse minimally affected the pH (Figure 2B, $p = 0.410$), and concentrations of TC (Figure 3A, $p = 0.827$), TN (Figure 3B, $p = 0.713$), and TP (Figure 3C, $p = 0.860$) in the soil. Moreover, the C:N (Figure 3D, $p = 0.615$), C:P (Figure 3E, $p = 0.781$), and N:P (Figure 3F, $p = 0.605$) ratios for samples from inside and outside the greenhouse were comparable.

3.3. Variations in soil microbial biomass and enzymes

The concentrations of MBC (Figure 4A, $p < 0.001$), MBN (Figure 4B, $p < 0.001$), and MBP (Figure 4C, $p < 0.001$), and activities of BG (Figure 5C, $p < 0.001$), LAP (Figure 5C, $p < 0.001$), NAG (Figure 5C, $p = 0.001$), and ACP (Figure 5D, $p < 0.001$), as well as the enzymatic C:N ratio (Figure 5E, $p < 0.001$) for samples from the greenhouse were considerably lower than those for samples from outside. In contrast, compared with control samples, the greenhouse increased the MBC:MBN (Figure 4D, $p < 0.001$) and enzymatic N:P (Figure 5G, $p < 0.001$) ratios. Notably, the MBC:MBP (Figure 4E, $p = 0.267$), MBN:MBP (Figure 4F, $p = 0.159$), and enzymatic C:P (Figure 5F, $p = 0.064$) ratios for soils inside and outside the greenhouse were comparable.

4. Discussion

4.1. Variations in soil properties

According to previous studies, warming can increase evaporation from soils and transpiration of plants, and these processes decrease the availability of water, and thus, the SMC (Zhou et al., 2013a,b). In the present study, the SMC was significantly decreased (Figure 2A) compared with the control. However, in addition to the warming, the greenhouse shielded the soil from precipitation during the period from September 2015 to July 2021 (prior to sampling). Therefore, the SMC was dependent on soil osmosis and capillary pore conditions in the greenhouse (Xiao et al., 2011), and the weakened soil capillary action caused by the increased evaporation exacerbated the decrease in the SMC (Wu et al., 2019).

In a previous study, warming was reported to exert no significant effect on the pH of soils in alpine meadows in the QTP (Zheng et al., 2012), and results in the present study are consistent with this observation (Figure 2B). However, the 5 years duration of warming was probably short to significantly influence the soil pH. According to another study on alpine meadows, warming starts to considerably

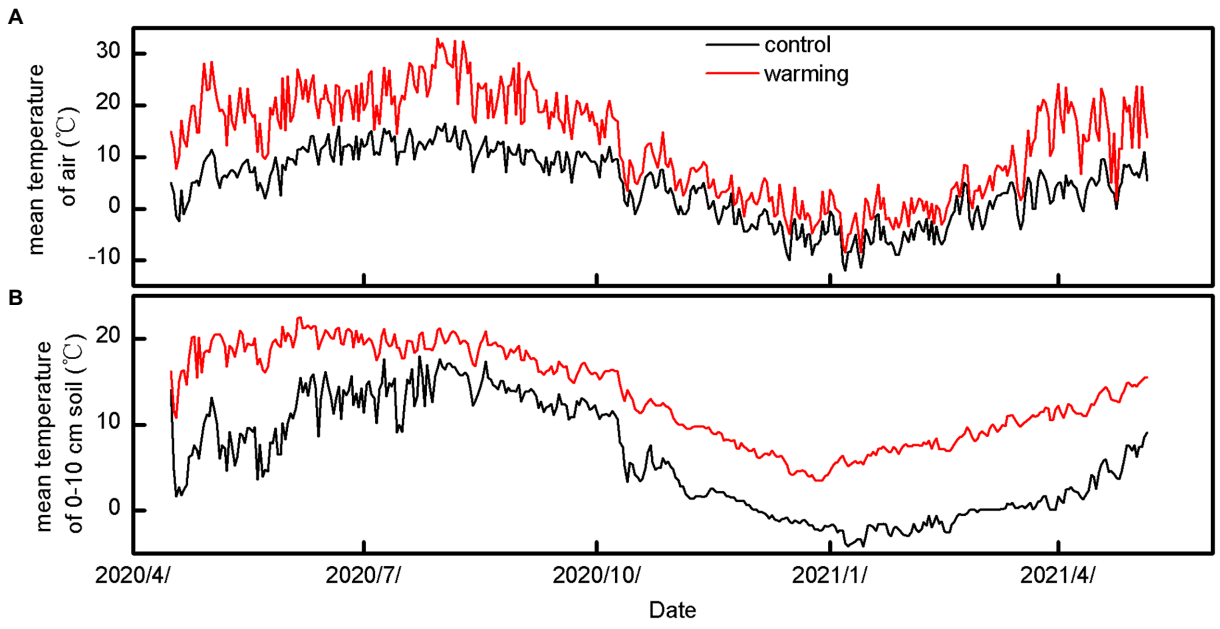

FIGURE 1
The mean temperature of air **(A)** and 10 cm soil **(B)** under control and warming during 20/4/2020–10/5/2021.

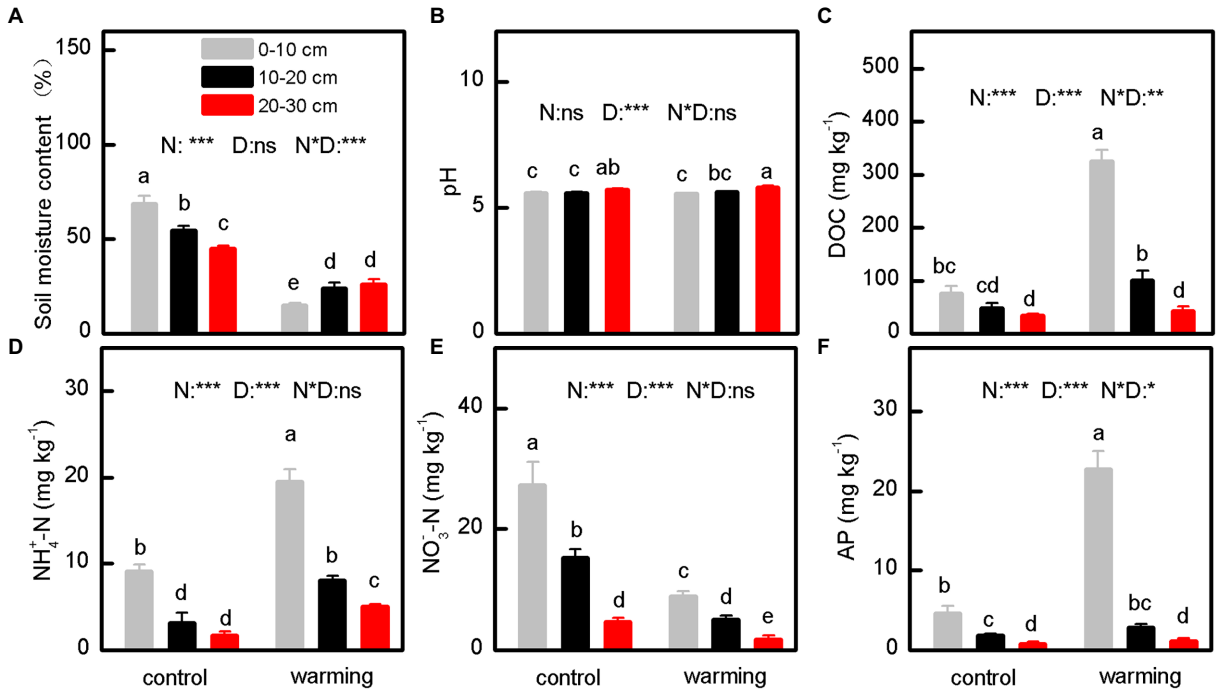

FIGURE 2
The SMC (soil moisture content) **(A)**, pH **(B)**, DOC (dissolved organic carbon) **(C)**, NH_4^+-N (ammonium nitrogen) **(D)**, NO_3^--N (nitrate nitrogen) **(E)** and AP (available phosphorus) **(F)** of soil under control and warming. *p*-value of the ANOVA of treatments (control and warming, N), soil depths (0–10, 10–20 and 20–30 cm, D) and interactive of treatments and soil depths (N*D) is indicated: $*p \leq 0.05$; $**p \leq 0.01$; $***p \leq 0.001$; ns, not significant.

impact the soil pH after at least 20 years (Zhang X. et al., 2021). Considering that fungi are tolerant to low pH conditions and high pH conditions are favorable for the growth of bacteria (Zhang et al., 2016). Therefore, the slight increase of the soil pH in the greenhouse (Figure 2B) probably increased the population of bacteria. However, a high MBC:MBN ratio (Figure 4D) is attributed to an increase in fungi (Yang et al., 2018), and thus, the impact of a high pH in the present study appears inconsistent with previous observations. Therefore, the effect of warming in alpine meadows on the soil pH requires further investigation.

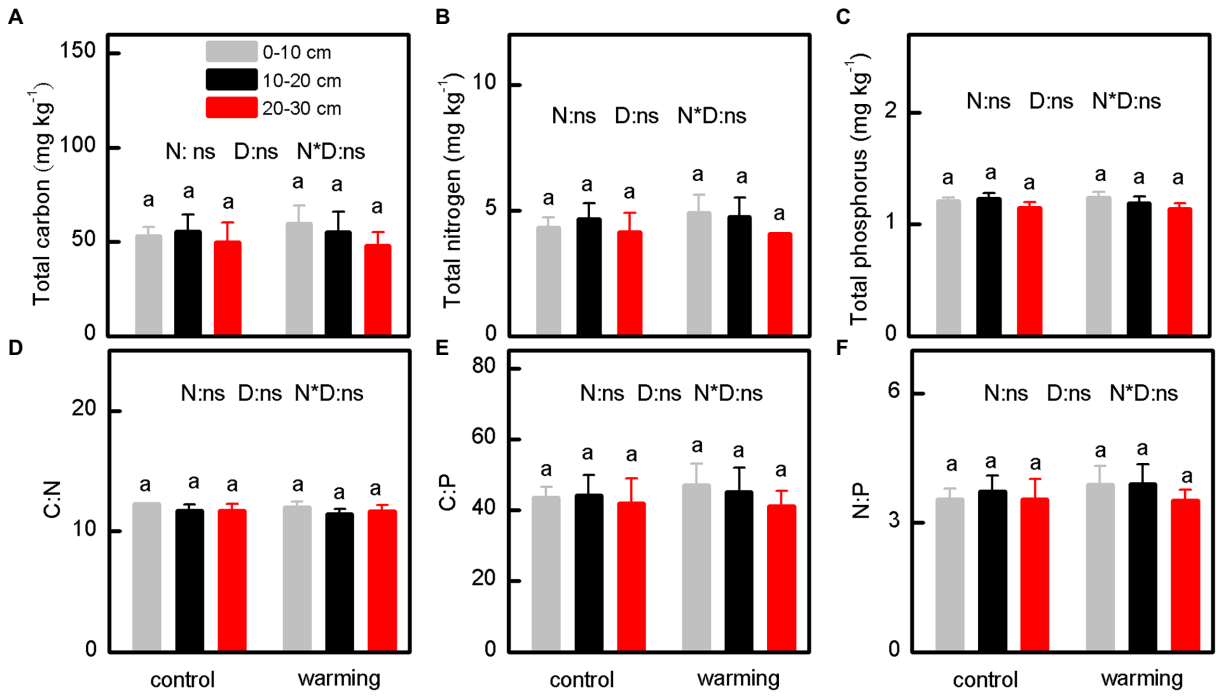

FIGURE 3
The concentration of total carbon **(A)**, total nitrogen **(B)**, total phosphorus **(C)**, and the ratio of C:N **(D)**, C:P **(E)** and N:P **(F)** of soil under control and warming. *p*-value of the ANOVA of treatments (control and warming, N), soil depths (0–10, 10–20 and 20–30 cm, D) and interactive of treatments and soil depths (N*D) is indicated: $*p \leq 0.05$; $**p \leq 0.01$; $***p \leq 0.001$; ns, not significant.

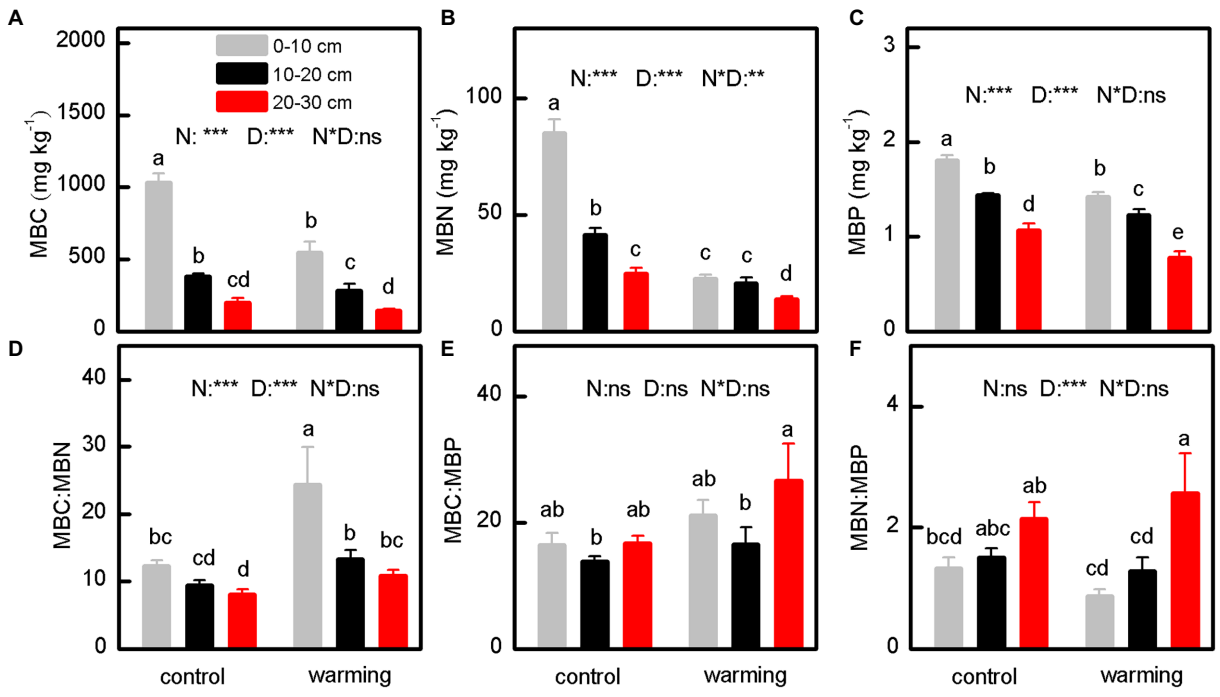

FIGURE 4
The microbial biomass carbon **(A)**, microbial biomass nitrogen **(B)**, microbial biomass phosphorus **(C)**, and their stoichiometric ratios **(D–F)** of soil under control and warming. *p*-value of the ANOVA of treatments (control and warming, N), soil depths (0–10, 10–20 and 20–30 cm, D) and interactive of treatments and soil depths (N*D) is indicated: $*p \leq 0.05$; $**p \leq 0.01$; $***p \leq 0.001$; ns, not significant.

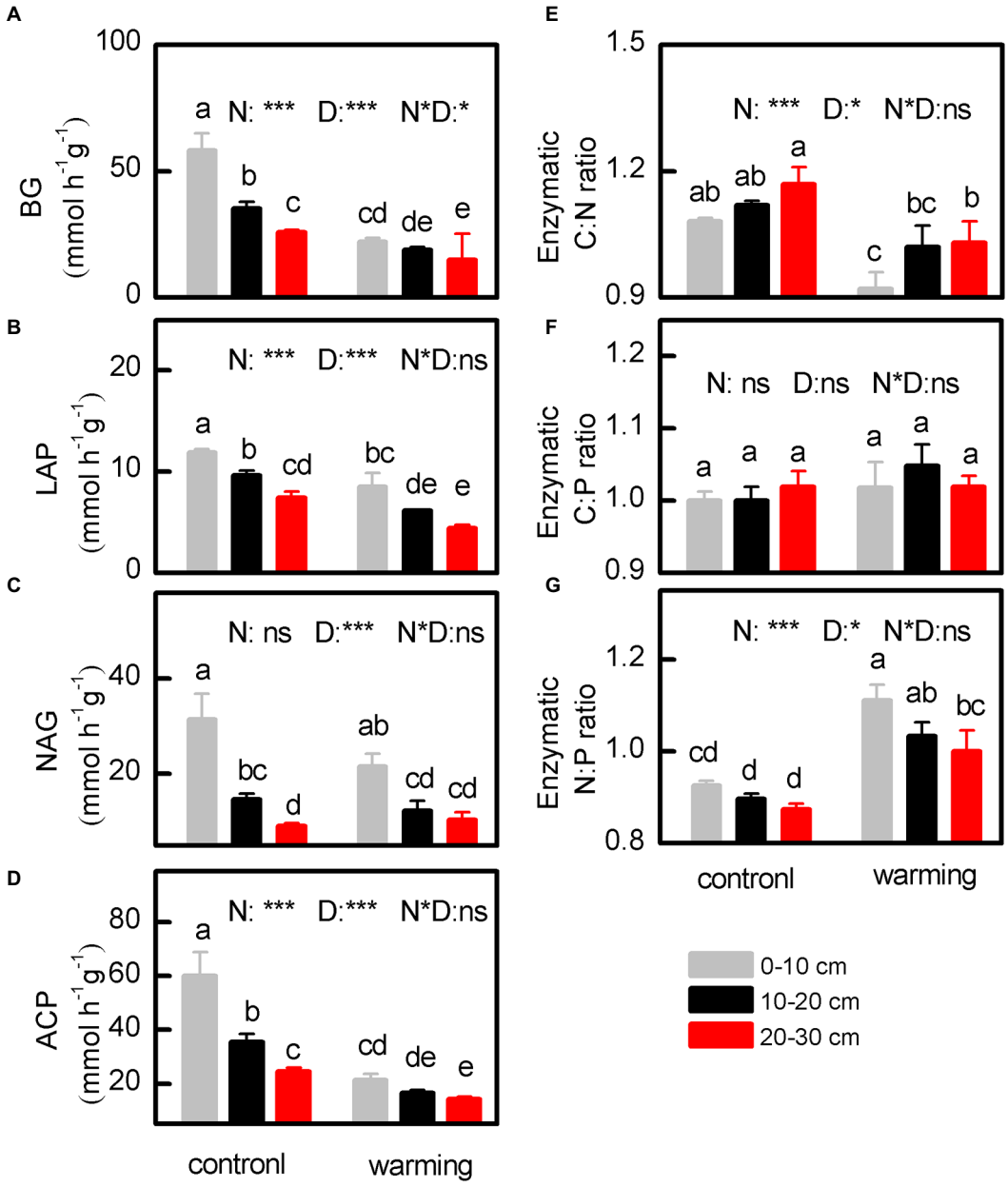

FIGURE 5
The activity of BG (β-1,4-glucosidase) **(A)**, LAP (leucine aminopeptidase) **(B)**, NAG (β-1,4-N-acetylglucoaminosidase) **(C)** and ACP (acid phosphatase) **(D)** and the stoichiometric ratios of C-, N- and P-degrading enzymes **(E–G)** of soil under control and warming. *p*-value of the ANOVA of treatments (control and warming, N), soil depths (0–10, 10–20 and 20–30 cm, D) and interactive of treatments and soil depths (N*D) is indicated: $*p \leq 0.05$; $**p \leq 0.01$; $***P \leq 0.001$; ns, not significant.

The soil DOC exerts an important influence on the biochemical cycle. According to a previous study, warming significantly increased the DOC concentration in soil solutions (Luo et al., 2009), and this observation is consistent with results in the present study (Figure 2C). Warming enhances biological activity, including the decomposition of organic matter in soils (Luo et al., 2009). Moreover, warming and drying promote the production of dissolved organic matter (Luo et al., 2009). The decrease of soil moisture enhances the release of soil organic matter from roots (Kuzyakov and Domanski, 2000), and the amount of soil leached impacts the concentration of DOC (Zhang Q. Y. et al., 2019; Zhang S. S. et al., 2019). Owing to the lower leaching associated with drying, the released DOC was low, and thus, the soil DOC increased (Figure 2C).

The results in the present study reveal that warming and drying significantly increase the concentration of NH_4^+–N (Figure 2D) and decrease the concentration of NO_3^-–N (Figure 2E) in soils. These results show that even though the N mineralization rate increased, the nitrification rate in the soil decreased. In all ecosystems, a decrease in the availability of water limits the growth of plants (Hartmann et al., 2013; Schaeffer et al., 2017). This in turn reduces the production of roots and litter, which are the principal sources of N for plant growth (Hartmann et al., 2013; Schaeffer et al., 2017). According to previous

studies, the accumulation of NH_4^+–N begins during a drought period, and the rate is higher than that of NO_3^-–N because of the lower nitrification in dry soils (Manzoni et al., 2014). Cells from dead microorganisms promote mineralization of N by drought-surviving microorganisms (Schaeffer et al., 2017), and this increased the concentration of NH_4^+–N in the soil (Figure 2D). In contrast, the concentration of NO_3^-–N in the soil decreased (Figure 2E). This is attributed to the low microbial activity in the soil that is associated with the loss of soil moisture (Figure 2A), which inhibited nitrification (Khan et al., 2016). Moreover, the N uptake preference of plants will also change at different growth stages (Cui et al., 2017). At the same time, a large amount of nitrate absorbed by plants may be assimilated into ammonium roots and amino acids in roots, resulting in the reduction of NO_3^-–N content (Liu et al., 2017). Alternatively, 16S rRNA gene abundance data suggest that the nitrifying activity of bacteria and archaea in the soil decreased under drought conditions, and the reduced nitrification rate accounts for the low NO^{3-}–N concentration (Hartmann et al., 2013; Figure 2E). While, low MBN (Figure 4B), and high MBC/MBN ratio (Figure 4D) reflect a decrease in nitrifiers in the greenhouse soil (Khan et al., 2016). Therefore, as the SMC decreased (Figure 2A), the NO_3^--N concentration also decreased (Figure 3E). Concurrently, the increasing temperature and decreasing water content promoted mineralization of organophosphorus in the soil (Zuccarini et al., 2020). The associated improved availability of P in the soil is manifested by the elevated concentration of AP (Figure 3F).

4.2. Variations in soil carbon, nitrogen, and phosphorus, and their stoichiometries

Warming alters the activities of enzymes in soils, and this subsequently affects the cycling of C and N (Gong et al., 2015). In the present study, the concentrations of TC (Figure 3A), TN (Figure 3B), and TP (Figure 3C) and the C:N (Figure 3D), C:P (Figure 3E), and N:P (Figure 3F) ratios of the soil were high. These results suggest that changes in the DOC, NH_4^+–N, NO_3^-–N, and AP were probably insufficient to alter the stability of their coupled relationships. This implies that the warming and isolation from precipitation in the present study minimally altered the cycling of C, N, and P in the alpine meadow.

In terrestrial ecosystems, the soil is an important pool for C and N, and their inputs (plant photosynthesis) and outputs (microbial decomposition, N absorption, and inter-cycling) control the balance of these elements (Tang et al., 2021). In the warming experiment, the net primary production and plant C absorption as total primary production increased (Deng et al., 2021; Tang et al., 2021). However, the increase was offset by the rise in C emissions to the atmosphere, and thus, no significant change occurred in the TC content of the soil (Figure 4A). Alternatively, the effect of warming on the soil respiration continued to decline, and thus, no significant change was observed as the duration of warming increased (Frey et al., 2008). This indirectly demonstrates that soil carbon minimally changed, and this was likely because the effect of decreased precipitation and warming in the meadow attained a stable state.

Relatedly, the net N mineralization rate increased because of the warming, whereas the soil TN was unaffected, and this is probably linked to the limited microbial carbon source (Tang et al., 2021). Even though the decomposition of organic matter can alter the soil TP, this change is limited, because it largely depends on the weathering of rocks (Yang et al., 2015; Jiao et al., 2016). Therefore, in the present study, the concentration of TP in the soil was unaffected by warming (Figure 4C). Moreover, the C:N:P stoichiometric ratio of soil directly influences the genetic resistance of the microbial population (Luo et al., 2020). In the present study, the C:N (Figure 4D), C:P (Figure 4E), and N:P (Figure 4F) ratios exhibited no significant change, and this is possibly because the microbial community can maintain a stoichiometric steady-state as an adaptation to changes in the status of nutrients.

4.3. Variation in soil microbial biomass

Microbes can decrease the production of enzymes, for example, by limiting substrates and other resources, including water (Nannipieri et al., 2012; Stark et al., 2014). This observation is consistent with results obtained in the present study (Figures 4A–C). The microbial biomass in soil is closely correlated to the type of vegetation (Baldrian et al., 2008). Deep-rooted species, such as grasses, can increase the storage of carbon *via* inputs of root material, microbial processing, and matrix stabilization, whereas forbs are associated with the opposite (Liu et al., 2018). In fact, if the proportion of grass decreases while that of forbs increases (unpublished data), soil root exudates and the MBC decrease (Figure 4A). In addition, bacteria need more N for assimilation than fungi (Högberg et al., 2007), and an increase in temperature is favorable for fungi in the soil microbial community (Zhao et al., 2014). This is consistent with the decrease in MBN that was obtained in the present study (Figure 4B). The increase in fungi explains the high MBC:MBN ratio (Figure 4D), considering that the C:N ratio of fungi (4.5–15) is significantly higher than that of bacteria (3–5) (Yang et al., 2018). The warming also increased the availability of N, which limited the phosphorus from microorganisms, which explains the decline in the concentration of MBP (Gong et al., 2019). In the present study, the MBC:MBN ratio (Figure 4D) in the soil increased, whereas the MBC:MBP (Figure 4E) and MBN:MBP (Figure 4F) ratios exhibited minor changes under the warming and decreased precipitation conditions. These changes mainly depended on the sampling period, and the level is the main factor that affects both the MBN and MBP concentrations (Li et al., 2016).

According to a previous simulation study, warming significantly increased the availability of nutrients, but the soil microbial biomass was essentially unchanged. These observations suggest that microorganisms in the soil did not directly benefit from higher availability of nutrients (Xu et al., 2010). While, in this study, warming and isolation from precipitation in the greenhouse significantly increased the concentrations of DOC (Figure 2C), NH_4^+–N (Figure 2D) and AP (Figure 2F), whereas the concentrations of MBC (Figure 4A), MBN (Figure 4B), and MBP (Figure 4C) decreased. These results also suggest that microorganisms in the soil failed to benefit directly from the higher availability of nutrients under the warming conditions.

4.4. Variations in activities of soil enzymes

The effects of warming on soil EEA that have been reported in previous studies vary (Zhou et al., 2013a; Wang et al., 2014). However,

in this study, the BG (Figure 5A), LAP (Figure 5B), and ACP (Figure 5D) significantly decreased, whereas the NAG (Figure 5C) slightly decreased (mean = 15.32% for the 0–30 cm soil layer). In general, warming can enhance the efficiency of extracellular enzymes, thereby decreasing the production of such enzymes by microbes involved in the cycling of C and nutrients (Zhou et al., 2013a). This observation is supported by the strong positive correlations between the soil EEA and MBC ($r = 0.693–0.809$, $p < 0.01$), MBN ($r = 0.717–0.907$, $p < 0.01$), and MBP ($r = 0.785–0.911$, $p < 0.01$) (Supplementary Table S2). In addition, the strong positive correlation between the soil EEA and SWC ($r = 0.439–0.869$, $p < 0.01$; Supplementary Table S2) indicates that the soil EEA mainly depends on the soil moisture (Carlyle et al., 2011; Zhou et al., 2013a). Excluding the BG, the hydraulic isolation in soils caused by drought exerts direct physiological and indirect (reduction of substrate diffusion) pressures on the microbial community (Schaeffer et al., 2017). These pressures decrease microbial activities, and thus, accelerate the decomposition of organic carbon in soil, thereby decreasing the soil SOC (Schindlbacher et al., 2011; Schaeffer et al., 2017). The BG is closely related to the decomposition of cellulose, and its activity was also decreased by the warming (Zhou et al., 2013a; Figure 5A). The significant decrease in the N-acquisition enzyme LAP (Figure 5B) and slight decrease in the NAG (Figure 5C) under the warming conditions in this work may be linked to decreased oxidation of NH_4^+–N and an increase in the concentration of NH_4^+–N (Hartmann et al., 2013).

Therefore, the synthesis of N-acquisition enzymes (NAG and LAP) appears to be closely related to the fungal biomass, whereas some C-acquisition enzymes (e.g., BG) are more associated with bacteria (Fanin et al., 2016). Therefore, the decrease in the enzymatic C:N ratio (Figure 5E) was likely caused by an increase in fungi/bacteria in the microbial community owing to the warming. In the present study, the decrease in the enzymatic C:N ratio (Figure 5E) is primarily associated with the decrease in the BG (Figure 5A), which is more than those of the total LAP (Figure 5B) and NAG (Figure 5C). This is because the temperature sensitivities of N-acquisition enzymes are lower than those of C-acquisition enzymes (Steinweg et al., 2013). Therefore, the N-acquisition enzymes slightly decreased in response to the N limitation under warming conditions (Steinweg et al., 2013). However, considering that the activities of the BG and ACP decreased comparably, the enzymatic C:P ratio exhibits no significant change (Figure 5F). This is probably because the soil microbial community can attain a stoichiometric homeostasis in response to changes in the status of nutrients. To reach the elemental homeostasis, microorganisms can alternatingly adjust their production of extracellular enzymes by maximizing the mobilization of substrates that are rich in limiting elements (Mooshammer et al., 2014).

A field experiment in a temperate grassland region revealed significant differences in the response of soil EEA at different depths to climate change (Zhou et al., 2013a). In particular, changes in the 0–10 and 10–20 cm soil layers were mainly driven by the pH, NH_4^+–N, and NO_3^-–N, and NH_4^+–N, and the microbial biomass, respectively (Zhou et al., 2013a). However, results obtained in this study (Figure 5) differed from those of this previous study (Zhou et al., 2013a). The differences are mainly attributed to direct effects of warming on the soil temperature and SWC, instead of changes in the quantity of organic matter and the quality of nutrients in the soil (Sardans et al., 2008). Therefore, the SMC and activities of extracellular enzymes decrease as the depth of the soil layer increases (Figure 5A). Meanwhile, the strong positive correlations between the WSC and MBC ($r = 0.537$, $p < 0.01$), MBN ($r = 0.801$, $p < 0.01$), MBP ($r = 0.681$, $p < 0.01$), BG ($r = 0.869$, $p < 0.01$), LAP ($r = 0.628$, $p < 0.01$), NAG ($r = 0.439$, $p < 0.01$), and ACP ($r = 0.845$, $p < 0.01$; Supplementary Table S2) in this study are probably because of the isolation of soil in the greenhouse from precipitation for ~5 years, and thus, the soil in the greenhouse was severely short of water. Alternatively, the EEA data in the present study may be controlled primarily by the WSC in the 0–30 cm soil layer.

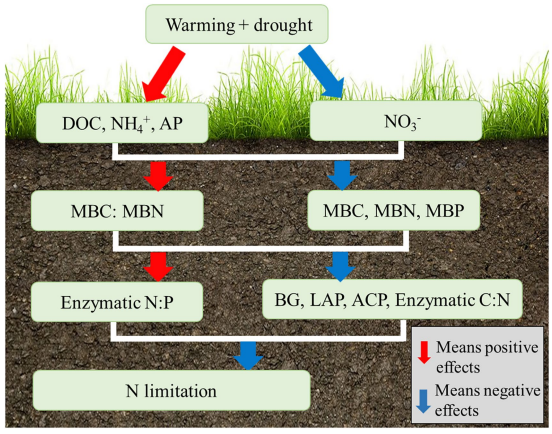

FIGURE 6
The conceptual map of warming and drought affecting the alpine meadow on the QTP.

4.5. Effects of warming and isolation from precipitation on the availability of nitrogen

In alpine meadows, soil N is usually limited (Yang et al., 2021), and this can be accentuated as other components change because of warming and isolation from precipitation (Figure 6). First, the decrease in the concentration of NO_3^-–N surpassed the increase in the concentration of NH_4^+–N (Figures 2D,E). This was because the mineralization of N was promoted (Schaeffer et al., 2017), nitrification of N was inhibited (Hartmann et al., 2013; Khan et al., 2016), and a large amount of N absorbed by plants (Liu et al., 2017). Alternatively, the concentration of available N decreased (Supplementary Table S2). Second, the concentrations of MBC, MBN, and MBP significantly decreased because of the warming and drought, and the decrease in the concentration of MBN was higher than that of the MBC (Figures 3A–C), and thus, the MBC:MBN ratio increased (Figure 3E), which indicates a severe MBN deficiency. This may be because that soil microorganisms failed to benefit directly from the higher availability of nutrients under the warming conditions. Third, with the help of decreasing oxidation of NH_4^+–N and an increasing in the concentration of NH_4^+–N (Hartmann et al., 2013) under the warming conditions, the activity of the LAP (Figure 5B) and NAG (Figure 5C) were all decreased in response to the warming and isolation from precipitation. In conclusion, warming and isolation from precipitation enhance the limitation of N in alpine meadows.

4.6. Limitations

There were some limitations in this work. Firstly, the greenhouse increases the soil temperature, which is likely to be the realistic impact of future climate change (Carlyle et al., 2011). However, the atmospheric temperature was increased by 8.32°C in the greenhouse in this work (Figure 1A), which is higher than the predicted increase relative to the pre-industrial revolution level before the end of the 21st century (Wieder et al., 2013; Meng et al., 2020). Secondly, the high temperature can stimulate evaporation and plant transpiration and increase soil water loss (Harte et al., 1995; Wan et al., 2002) but the soil water loss caused by global warming is not as same as the isolation from precipitation studies in this work, and the SMC was dependent on soil osmosis and capillary pore conditions in the greenhouse (Xiao et al., 2011). Therefore, we are still far from explaining the impact of global climate change on the soil of the QTP. Additionally, warming and precipitation variability will become more frequent in the future (IPCC, 2021). Therefore, to consider the change of water grid under the influence of climate warming and drought in many aspects, it is necessary to carry out long-term continuous monitoring.

5. Conclusion

In the present study, a greenhouse experiment was conducted in an alpine meadow in the QTP to simulate the response of soils in the area to global warming. Data were generated for the SWC, pH, and changes in the DOC, NH_4^+–N, NO_3^-–N, and AP concentrations, as well as the stoichiometries of TC, TN, TP, MBC, MBN, MBP, BG, NAG, LAP, and ACP using samples that were collected from the 0–30 cm soil layer, over a duration of ~5 years (2015–2020). Evidently, the greenhouse warming significantly decreased the SMC, NO_3^-–N, MBC, MBN, MBP, BG, LAP, ACP, and enzymatic C:N ratio. Conversely, it considerably increased the DOC, NH_4^+–N, AP, MBC:MBN, and enzymatic N:P ratio. Interestingly, it minimally affected the soil pH, TC, TN, TP, C:N, C:P, N:P, MBC:MBP, MBN:MBP, and enzymatic C:P ratios. These results indicated that warming and isolation from precipitation promoted the mineralization of N and P in the soils. However, microorganisms in the soils minimally benefited directly from the higher availability of nutrients associated with the warming and isolation from precipitation. The warming and isolation from precipitation also significantly altered the microbial biomass, EEA, and their stoichiometric ratios, but the concentrations of C, N, and P in the soils exhibited limited changes. Therefore, to adequately understand the response of terrestrial ecosystems to the cycling of C and N under warming conditions, continuous monitoring over an extended duration is required.

Data availability statement

The datasets used and/or analyzed during the current study are available from the corresponding author upon reasonable request—ZY (yza2765@126.com).

Author contributions

YT: data curation and writing—original draft preparation. YL: methodology, investigation, and formal analysis. ZY: conceptualization, investigation, formal analysis, data curation, and writing—review and editing. All authors contributed to the article and approved the submitted version.

Acknowledgments

We would like to thank Editage (www.editage.cn) for English language editing.

Conflict of interest

The authors declare that the research was conducted in the absence of any commercial or financial relationships that could be construed as a potential conflict of interest.

Publisher's note

Supplementary material

The Supplementary material for this article can be found online at: https://www.frontiersin.org/articles/10.3389/fevo.2023.1149240/full#supplementary-material

References

Baldrian, P., Trögl, J., Frouz, J., Snajdr, J., Valàšková, V., Merhautvá, V., et al. (2008). Enzyme activities and microbial biomass in topsoil layer during spontaneous succesion in spoil heaps after brown coal mining. *Soil Biol. Biochem.* 40, 2107–2115. doi: 10.1016/j.soilbio.2008.02.019

Carlyle, C. N., Fraser, L. H., and Turkington, R. (2011). Tracking soil temperature and moisture in a multi-factor climate experiment in temperate grassland: do climate manipulation methods produce their intended effects? *Ecosystems* 14, 489–502. doi: 10.1007/s10021-011-9425-y

Cui, Y. X., Bing, H. J., Fang, L. C., Wu, Y. H., Yu, J. L., Shen, G. T., et al. (2019). Diversity patterns of the rhizosphere and bulk soil microbial communities along an altitudinal gradient in an alpine ecosystem of the eastern Tibetan plateau. *Geoderma* 338, 118–127. doi: 10.1016/j.geoderma.2018.11.047

Cui, J. H., Yu, C. Q., Qiao, N., Xu, X. L., Tian, Y. Q., and Ouyang, H. (2017). Plant preference for NH_4^+ versus NO_3^- at different growth stages in an alpine agroecosystem. *Field Crop Res.* 201, 192–199. doi: 10.1016/j.fcr.2016.11.009

DeForest, J. L. (2009). The influence of time, storage temperature, and substrate age on potential soil enzyme activity in acidic forest soils using MUB-linked substrates and L-DOPA. *Soil Biol. Biochem.* 41, 1180–1186. doi: 10.1016/j.soilbio.2009.02.029

Deng, L., Peng, C. H., Kim, D. G., Li, J. W., Liu, Y. L., Hai, X. Y., et al. (2021). Drought effects on soil carbon and nitrogen dynamics in global natural ecosystems. *Earth-Sci. Rev.* 214:103501. doi: 10.1016/j.earscirev.2020.103501

Ehlers, K., Bakken, L. R., Frostegård, Å., Frossard, E., and Bünemann, E. K. (2010). Phosphorus limitation in a Ferralsol: impact on microbial activity and cell internal P pools. *Soil Biol. Biochem.* 42, 558–566. doi: 10.1016/j.soilbio.2009.11.025

Fang, X., Zhou, G., Li, Y., Liu, S., Chu, G., Xu, Z., et al. (2015). Warming effects on biomass and composition of microbial communities and enzyme activities within soil aggregates in subtropical forest. *Biol. Fert. Soils* 52, 353–365. doi: 10.1007/s00374-015-1081-5

Fanin, N., Moorhead, D., and Bertrand, I. (2016). Eco-enzymatic stoichiometry and enzymatic vectors reveal differential C, N, P dynamics in decaying litter along a land-use gradient. *Biogeochemistry* 129, 21–36. doi: 10.1007/s10533-016-0217-5

Frey, S., Drijber, R., Smith, H., and Melillo, J. (2008). Microbial biomass, functional capacity, and community structure after 12 years of soil warming. *Soil Biol. Biochem.* 40, 2904–2907. doi: 10.1016/j.soilbio.2008.07.020

Fu, G., Shen, Z. X., Zhang, X. Z., and Zhou, Y. T. (2012). Response of soil microbial biomass to short-term experimental warming in alpine meadow on the Tibetan plateau. *Appl. Soil Ecol.* 61, 158–160. doi: 10.1016/j.apsoil.2012.05.002

Gong, S. W., Zhang, T., and Guo, J. X. (2019). Warming and nitrogen addition change the soil and soil microbial biomass C:N:P stoichiometry of a meadow steppe. *Int. J. Env. Res. Pub. He.* 16:2705. doi: 10.3390/ijerph16152705

Gong, S. W., Zhang, T., Guo, R., Cao, H. B., Shi, L. X., Guo, J. X., et al. (2015). Response of soil enzyme activity to warming and nitrogen addition in a meadow steppe. *Soil Res.* 53, 242–252. doi: 10.1071/SR14140

Harte, J., Torn, M. S., Chang, F. R., Feifarek, B., Kinzig, A. P., Shaw, R., et al. (1995). Climate warming and soil microclimate: results from a meadow-warming experiment. *Eco. Appl* 5, 132–150. doi: 10.2307/1942058

Hartmann, A. A., Barnard, R. L., Marhan, S., and Niklaus, P. A. (2013). Effects of drought and N-fertilization on N cycling in two grassland soils. *Oecologia* 171, 705–717. doi: 10.1007/s00442-012-2578

Högberg, M. N., Chen, Y., and Högberg, P. (2007). Gross nitrogen mineralisation and fungi-to-bacteria ratios are negatively correlated in boreal forests. *Biol. Fertil. Soils* 44, 363–366. doi: 10.1007/s00374-007-0215-9

Hu, Y. L., Wang, S., Niu, B., Chen, Q. Y., Wang, J., Zhao, J. X., et al. (2020). Effect of increasing precipitation and warming on microbial community in Tibetan alpine steppe. *Environ. Res.* 189:109917. doi: 10.1016/j.envres.2020.109917

IPCC. (2021). *Climate change 2021: The physical science basis. Contribution of working group I to the sixth assessment report of the intergovernmental panel on climate change*. Cambridge, United Kingdom and New York, NY: Cambridge University Press, 2021.

Jiao, Y. L., Chu, G. M., Yang, Z. A., Wang, Y., and Wang, M. (2020). Bacterial diversity in the rhizosphere of *anabasis aphylla* in the Gurbantunggut Desert, China. *Curr. Microbiol.* 77, 3750–3759. doi: 10.1007/s00284-020-02177-y

Jiao, F., Shi, X. R., Han, F. P., and Yuan, Z. Y. (2016). Increasing aridity, temperature and soil pH induce soil C-N-P imbalance in grasslands. *Sci. Rep.* 6:19601. doi: 10.1038/srep19601

Khan, K. S., Mike, R., Castillo, X., Kaiser, M., and Joergensen, R. G. (2016). Microbial biomology, fungi and bacteria residues and their relationship to the C/N/P/S rate of soil organics. *Geoderma* 271, 115–123. doi: 10.1016/j.geoderma.2016.02.019

Kuzyakov, Y., and Domanski, G. (2000). Carbon input by plants into the soil. *Review. J. Plant Nutr. Soil Sci.* 163, 421–431. doi: 10.1002/1522-2624(200008)163:4<421::AID-JPLN421>3.0.CO;2-R

Li, H., Li, J., He, Y. L., Li, S. J., Liang, Z. S., Peng, C. H., et al. (2013). Changes in carbon, nutrients and stoichiometric relations under different soil depths, plant tissues and ages in black locust plantations. *Acta Physiol. Plant.* 35, 2951–2964. doi: 10.1007/s11738-013-1326-6

Li, H. J., Liu, J. W., Yang, L., Zheng, H. F., Liu, Y., Yang, W. Q., et al. (2016). Effects of simulated climate warming on soil microbial biomass carbon, nitrogen and phosphorus of alpine forest. *Chin. J. Appl. Environ. Biol.* 22, 599–605. doi: 10.3724/SP.J.1145.2015.12022 (in Chinese with English Abstract)

Li, Y., Wu, J., Liu, S., Shen, J., Huang, D., Su, Y., et al. (2012). Is the C:N:P stoichiometry in soil and soil microbial biomass related to the landscape and landuse in southern subtropical China? *Global Biogeochem. Cycle* 26, 1–14. doi: 10.1029/2012GB004399

Liu, M., Li, C. C., Xu, X. L., Wanek, W. G., Jiang, N., Wang, H. M., et al. (2017). Organic and inorganic nitrogen uptake by 21 dominant tree species in temperate and tropical forests. *Tree Physiol.* 37, 1515–1526. doi: 10.1093/treephys/tpx046

Liu, H. Y., Mi, Z. R., Lin, L., Wang, Y. H., Zhang, Z. H., Zhang, F. W., et al. (2018). Shifting plant species composition in response to climate change stabilizes grassland primary production. *Proc. Natl. Acad. Sci. U. S. A.* 115, 4051–4056. doi: 10.1073/pnas.1700299114

Luo, C. Y., Xu, G. P., Wang, Y. F., Wang, S. P., Lin, X. W., Hu, Y. G., et al. (2009). Effects of grazing and experimental warming on DOC concentrations in the soil solution on the Qinghai-Tibet plateau. *Soil Biol. Biochem.* 41, 2493–2500. doi: 10.1016/j.soilbio.2009.09.006

Luo, G. W., Xue, C., Jiang, Q. H., Xiao, Y., Zhang, F. G., Guo, S. W., et al. (2020). Soil carbon, nitrogen, and phosphorus cycling microbial populations and their resistance to global change depend on soil C:N:P stoichiometry. *mSystems.* 5, e00162–e00120. doi: 10.1128/mSystems.00162-20

Manzoni, S., Schaeffer, S. M., Katul, G., Porporato, A., and Schimel, J. P. (2014). A theoretical analysis of microbial eco-physiological and diffusion limitations to carbon cycling in drying soils. *Soil Biol. Biochem.* 73, 69–83. doi: 10.1016/j.soilbio.2014.02.008

Meng, C., Tian, D. S., Zeng, H., Li, Z. L., Chen, H. Y. H., and Niu, S. L. (2020). Global meta-analysis on the responses of soil extracellular enzyme activities to warming. *Sci. Total Environ.* 705:135992. doi: 10.1016/j.scitotenv.2019.135992

Mooshammer, M., Wanek, W., Zechmeister-Boltenstern, S., and Richter, A. (2014). Stoichiometric imbalances between terrestrial decomposer communities and their resources: mechanisms and implications of microbial adaptations to their resources. *Front. Microbiol.* 5, 22–32. doi: 10.3389/fmicb.2014.00022

Nannipieri, P., Giagnoni, L., Renella, G., Puglisi, E., Ceccanti, B., Masciandaro, G., et al. (2012). Soil enzymology: classical and molecular approaches. *Biol. Fertil. Soils* 48, 743–762. doi: 10.1007/s00374-012-0723-0

Niu, S. L., Wu, M. Y., Han, Y., Xia, J., Li, L., and Wan, S. (2010). Water-mediated responses of ecosystem carbon fluxes to climatic change in a temperate steppe. *New Phytol.* 177, 209–219. doi: 10.1111/j.1469-8137.2007.02237.x

Saiya-Corka, K. R., Sinsabaugha, R. L., and Zakb, D. R. (2002). The effects of long term nitrogen deposition on extracellular enzyme activity in an Acer saccharum forest soil. *Soil Biol. Biochem.* 34, 1309–1315. doi: 10.1016/S0038-0717(02)00074-3

Sardans, J., Peñuelas, J., and Estiarte, M. (2008). Changes in soil enzymes related to C and N cycle and in soil C and N content under prolonged warming and drought in a Mediterranean shrubland. *Appl. Soil Ecol.* 39, 223–235. doi: 10.1016/j.apsoil.2007.12.011

Schaeffer, S. M., Homyak, P. M., Boot, C. M., Roux-Michollet, D., and Schimel, J. P. (2017). Soil carbon and nitrogen dynamics throughout the summer drought in a California annual grassland. *Soil Biol. Biochem.* 115, 54–62. doi: 10.1016/j.soilbio.2017.08.009

Schindlbacher, A., Rodler, A., Kuffner, M., Kitzler, B., Sessitsch, A., and Zechmeister-Boltenstern, S. (2011). Experimental warming effects on the microbial community of a temperate mountain forest soil. *Soil Biol. Biochem.* 43, 1417–1425. doi: 10.1016/j.soilbio.2011.03.005

Sinsabaugh, R. L., Hill, B. H., and Follstad, S. J. (2009). Ecoenzymatic stoichiometry of microbial organic nutrient acquisition in soil and sediment. *Nature* 462, 795–798. doi: 10.1038/nature08632

Stark, S., Männistö, M. K., and Eskelinen, A. (2014). Nutrient availability and pH jointly constrain microbial extracellular enzyme activities in nutrient-poor tundra soils. *Plant Soil* 383, 373–385. doi: 10.1007/s11104-014-2181-y

Steinweg, J. M., Dukes, J. S., Paul, E. A., and Wallenstein, M. D. (2013). Microbial responses to multi-factor climate change: effects on soil enzymes. *Front. Microbiol.* 4:146. doi: 10.3389/fmicb.2013.00146

Tan, Q. Q., Wang, G. A., Smith, M. D., Chen, Y. Z., and Yu, Q. (2021). Temperature patterns of soil carbon: nitrogen: phosphorus stoichiometry along the 400 mm isohyet in China. *Catena* 203:105338. doi: 10.1016/j.catena.2021.105338

Tang, S. R., Cheng, W. G., Hu, R. G., Guigue, J. L., Hattori, S., Tawaraya, K., et al. (2021). Five-year soil warming changes soil C and N dynamics in a single rice paddy field in Japan. *Sci. Total Environ.* 756:143845. doi: 10.1016/j.scitotenv.2020.143845

Wan, S. Q., Luo, Y. Q., and Wallace, L. L. (2002). Changes in microclimate induced by experimental warming and clipping in tallgrass prairie. *Glob. Chang. Biol.* 8, 754–768. doi: 10.1046/j.1365-2486.2002.00510.x

Wang, X. X., Dong, S. K., Gao, Q. Z., Zhou, H. K., Liu, S. L., Su, X. K., et al. (2014). Effects of short-term and long-term warming on soil nutrients, microbial biomass and enzyme activities in an alpine meadow on the Qinghai-Tibet plateau of China. *Soil Biol. Biochem.* 76, 140–142. doi: 10.1016/j.soilbio.2014.05.014

Wang, S., Quan, Q., Meng, C., Chen, W. N., Luo, Y. Q., and Niu, S. L. (2021). Experimental warming shifts coupling of carbon and nitrogen cycles in an alpine meadow. *J. Plant Ecol.* 14, 541–554. doi: 10.1093/jpe/rtab008

Wieder, W. R., Bonan, G. B., and Allison, S. D. (2013). Global soil carbon projections are improved by modelling microbial processes. *Nat. Clim. Chang.* 3, 909–912. doi: 10.1038/NCLIMATE1951

Wu, G. L., Huang, Z., Liu, Y. F., Cui, Z., Liu, Y., Chang, X. F., et al. (2019). Soil water response of plant functional groups along an artificial legume grassland succession under semi-arid conditions. *Agric. For. Meteorol.* 278:107670. doi: 10.1016/j.agrformet.2019.107670

Xiao, G. J., Zhang, Q., Li, Y., Zhang, F. J., and Luo, C. K. (2011). Effect of winter warming on soil moisture and salinization. *Trans. CSAE* 27, 46–51. doi: 10.3969/j.issn.1002-6819.2011.08.008, (in Chinese with English Abstract)

Xu, Z. F., Wan, C., Xiong, P., Tang, Z., Hu, R., Cao, X. K., et al. (2010). Initial responses of soil CO2 efflux and C, N pools to experimental warming in two contrasting forest ecosystems, Eastern Tibetan Plateau. *Plant Soil*, 336, 183–195. doi: 10.1007/s11104-010-0461-8

Yang, X. J., Huang, Z. Y., Zhang, K. L., and Cornelissen, J. H. C. (2015). C:N:P stoichiometry of Artemisia species and close relatives across northern China: unraveling effects of climate, soil and taxonomy. *J. Ecol.* 103, 1020–1031. doi: 10.1111/1365-2745.12409

Yang, K., Ye, B. S., Zhou, D. G., Wu, B. Y., Foken, T., Qin, J., et al. (2011). Response of hydrological cycle to recent climate changes in the Tibetan plateau. *Clim. Chang.* 109, 517–534. doi: 10.1007/s10584-011-0099-4

Yang, Z. A., Zhan, W., Jiang, L., and Chen, H. (2021). Effect of short-term low-nitrogen addition on carbon, nitrogen and phosphorus of vegetation-soil in alpine meadow. *Int. J. Environ. Res. Public Health* 18:10998. doi: 10.3390/ijerph182010998

Yang, Z. A., Zhu, Q. A., Zhan, W., Xu, Y. Y., Zhu, E. X., Gao, Y. H., et al. (2018). The linkage between vegetation and soil nutrients and their variation under different grazing intensities in an alpine meadow on the eastern Qinghai-Tibetan plateau. *Ecol. Eng.* 110, 128–136. doi: 10.1016/j.ecoleng.2017.11.001

Zederer, D. P., Talkner, U., Spohn, M., and Joergensen, R. G. (2017). Microbial biomass phosphorus and C/N/P stoichiometry in forest floor and a horizons as affected by tree species. *Soil Biol. Biochem.* 111, 166–175. doi: 10.1016/j.soilbio.2017.04.009

Zhang, W. X., Furtado, K., Wu, P. L., Zhou, T. J., Chadwick, R., Marzin, C., et al. (2021). Increasing precipitation variability on daily-to-multiyear time scales in a warmer world. *Sci. Adv.* 7:eabf8021. doi: 10.1126/sciadv.abf8021

Zhang, J. J., Peng, C. H., Xue, W., Yang, Z. A., Yang, B., Li, P., et al. (2018). Soil CH_4 and CO_2 dynamics and nitrogen transformation with incubation in mountain forest and meadow ecosystems. *Catena* 163, 24–32. doi: 10.1016/j.catena.2017.12.005

Zhang, X., Ren, H. Y., Kang, J., Zhu, Y., Li, D. H., and Han, G. D. (2021). Effects of warming and nitrogen addition on soil physical and chemical properties in desert steppe of Inner Mongolia. *Chin. J. Grassl.* 43, 17–24. doi: 10.16742/j.zgcdxb.20190225, (in Chinese with English Abstract)

Zhang, Q. Y., Shao, M. A., Jia, X. X., and Wei, X. R. (2019). Changes in soil physical and chemical properties after short drought stress in semi-humid forest. *Geoderma* 338, 170–177. doi: 10.1016/j.geoderma.2018.11.051

Zhang, Q., Wu, J. J., Yang, F., Lei, Y., Zhang, Q. F., and Cheng, X. L. (2016). Alterations in soil microbial commuity composition and biomass following agricultural land use change. *Sci. Rep.* 6:36587. doi: 10.1038/srep36587

Zhang, S. S., Zheng, Q., Noll, L., Hu, Y. T., and Wanek, W. (2019). Environmental effects on soil microbial nitrogen use efficiency are controlled by allocation of organic nitrogen to microbial growth and regulate gross N mineralization. *Soil Biol. Biochem.* 135, 304–315. doi: 10.1016/j.soilbio.2019.05.019

Zhao, Y. Y., Xu, L. H., Yao, B. Q., Ma, Z., Zhang, C. H., Wang, F. P., et al. (2016). Influence of simulated warming to the carbon, nitrogen and their stability isotope-(δ13C, δ15N) contents in alpine meadow plant leaves. Acta bot. *Boreal.-Occident. Sin.* 36, 777–783. doi: 10.7606/j.issn.1000-4025.2016.04.0777

Zhao, C. Z., Zhu, L. Y., Liang, J., Yin, H. J., Yin, C. Y., Li, D. D., et al. (2014). Effects of experimental warming and nitrogen fertilization on soil microbial communities and processes of two subalpine coniferous species in eastern Tibetan plateau. *Plant Soil* 382, 189–201. doi: 10.1007/s11104-014-2153-2

Zheng, Y., Yang, W., Sun, X., Wang, S. P., Rui, Y. C., Luo, C. Y., et al. (2012). Methanotrophic community structure and activity under warming and grazing of alpine meadow on the Tibetan plateau. *Appl. Microbiol. Biotechnol.* 93, 2193–2203. doi: 10.1007/s00253-011-3535-5

Zhou, X. Q., Chen, C. R., Wang, Y. F., Xu, Z. H., Duan, J. C., Hao, Y. B., et al. (2013b). Soil extractable carbon and nitrogen, microbial biomass and microbial metabolic activity in response to warming and increased precipitation in a semiarid inner Mongolian grassland. *Geoderma* 206, 24–31. doi: 10.1016/j.geoderma.2013.04.020

Zhou, X. Q., Chen, C. R., Wang, Y. F., Xu, Z. H., Han, H. Y., Li, L. H., et al. (2013a). Warming and increased precipitation have differential effects on soil extracellular enzyme activities in a temperate grassland. *Sci. Total Environ.* 444, 552–558. doi: 10.1016/j.scitotenv.2012.12.023

Zhu, X. M., Liu, M., Kou, Y. P., Liu, D. Y., Liu, Q., Zhang, Z. L., et al. (2020). Differential effects of N addition on the stoichiometry of microbes and extracellular enzymes in the rhizosphere and bulk soils of an alpine shrubland. *Plant Soil* 449, 285–301. doi: 10.1007/s11104-020-04468-6

Zi, H. B., Hua, L., Wang, C. T., Wang, G. X., Wu, P. F., Lerdauca, M., et al. (2018). Responses of soil bacterial community and enzyme activity to experimental warming of an alpine meadow. *Eur. J. Soil Sci.* 69, 429–438. doi: 10.1111/ejss.12547

Zuccarini, P., Asensio, D., Ogaya, R., Sardans, J., and Peñuelas, J. (2020). Effects of seasonal and decadal warming on soil enzymatic activity in a P-deficient Mediterranean shrubland. *Glob. Chang. Biol.* 26, 3698–3714. doi: 10.1111/gcb.15077

frontiers | Frontiers in Ecology and Evolution

TYPE Original Research
PUBLISHED 14 March 2023
DOI 10.3389/fevo.2023.1148580

OPEN ACCESS

EDITED BY
Xiaodong Zhang,
Chinese Academy of Forestry,
China

REVIEWED BY
Lijuan Ren,
Jinan University,
China
Tan Lu,
Institute of Hydrobiology (CAS),
China

*CORRESPONDENCE
Xinxin Lu
✉ luxinxinchina@163.com
Yawen Fan
✉ fanyaw_hrbnu@163.com

†These authors have contributed equally to this work

SPECIALTY SECTION
This article was submitted to Population, Community, and Ecosystem Dynamics, a section of the journal Frontiers in Ecology and Evolution

RECEIVED 20 January 2023
ACCEPTED 23 February 2023
PUBLISHED 14 March 2023

CITATION
Tao T, Wang H, Na X, Liu Y, Zhang N, Lu X and Fan Y (2023) Temperate urban wetland plankton community stability driven by environmental variables, biodiversity, and resource use efficiency: A case of Hulanhe Wetland.
Front. Ecol. Evol. 11:1148580.
doi: 10.3389/fevo.2023.1148580

Temperate urban wetland plankton community stability driven by environmental variables, biodiversity, and resource use efficiency: A case of Hulanhe Wetland

Tao Tao[1†], Hao Wang[1†], Xinyuan Na[1], Yan Liu[1,2], Nannan Zhang[3], Xinxin Lu[1,2*] and Yawen Fan[1,2*]

[1]College of Life Sciences and Technology, Harbin Normal University, Harbin, China, [2]Key Laboratory of Biodiversity of Aquatic Organisms, Harbin Normal University, Harbin, China, [3]Modern Educational Technology and Experiment Center, Harbin Normal University, Harbin, China

In this study, we explored the driving factors behind plankton community structure. Due to the rapid development of cities, the occupation and development of wetland resources have increased lately, making the urban wetland ecosystems unstable and degrading the ecological functions gradually. Understanding the driving factors behind plankton community structure has certain theoretical and guiding significance for the protection, sustainable development, and ecological restoration of aquatic biodiversity in urban wetland ecosystems. We set up 12 sampling points in the Hulanhe Wetland, with the continuous monitoring of plankton from April to August and October 2021. The eco-environmental factors, plankton community structure, biodiversity index, resource use efficiency (RUE), and Bray–Curtis community turnover value were analyzed. A total of 209 species of 91 genera, 42 families, 11 classes, 22 orders of phytoplankton, and 90 species of four classes of zooplankton were identified. The community structure was mainly composed of Bacillariophyta, Chlorophyta, Cyanophyta, Protozoa, and Rotifera. To explore the correlation between phytoplankton and zooplankton, a correlation study was performed. We found a stable feeding preference between phytoplankton and zooplankton. The key influencing factors were identified by ordinary least squares regression, and the main driving factors of plankton community structure were discussed. The results showed that the stability of the Increased biodiversity and resource utilization efficiency have led to more stable plankton communities. This stability pattern is also strongly affected by water temperature, pH and total nitrogen in the external environment. This study will be helpful in the restoration of damaged wetlands, which would be beneficial for the protection of urban wetland ecosystems.

KEYWORDS

Hulanhe Wetland, plankton, grazing, community stability, resource use efficiency, diversity indicators

1. Introduction

Plankton is an important part of the aquatic ecosystem (MacArthur, 1955; Liu et al., 2021). It has a short life cycle and responds quickly to anthropogenic effects and natural changes. They are also considered good biological indicators for assessing wetland ecological health (Seilheimer et al., 2009; Easson and Lopez, 2019; Jonkers et al., 2019; Liu et al., 2021). Therefore, studying the plankton community structure is beneficial for wetland ecological environmental protection.

Community stability refers to the ability of a community to maintain its original structural and functional state, resist disturbance, or return to its original state after disturbance (Holling, 1973; Boucot, 1985; Sennhauser, 1991). It is an important manifestation of ecosystem function (Tilman, 1999; Pennekamp et al., 2018). Community structure is affected by the combined effects of biotic and abiotic factors, such as resource use efficiency (RUE) (Tian et al., 2017), biodiversity (Zhang H. et al., 2016), and water environmental factors (Schaum et al., 2016; Tian et al., 2016; Amorim and Moura, 2021). In the same natural aquatic ecosystem, different habitats often cause differences in plankton community structure partly due to different nutrient concentrations (Zheng et al., 2020). The application of RUE can eliminate community differences caused by different nutrient concentrations; therefore, it is widely used in the study of plankton community structure. Anthropogenic disturbance can destroy ecosystem function and brings challenges to ecological restoration. The correlation between RUE and community stability depends on the degree of disturbance to the ecosystem. In other words, with the aggravation of human disturbance, such as water pollution and fishery, RUE will decrease with the decrease in plankton species abundance (Norberg et al., 2001; Filstrup et al., 2014). In recent years, the correlation between plankton diversity and community stability has become one of the ecological hotspots in conservation biology. Communities with more species or complex interspecies associations are more stable than single-species communities (Mougi, 2022). Communities with high biodiversity have less competition among species, which makes the community more stable and the ecological function guarantee insure higher (MacArthur, 1955; Elton, 2020). In addition, prior studies have shown that total phosphorus (TP), total nitrogen (TN), water temperature (WT), and dissolved oxygen (DO) have also been confirmed to relate to plankton community stability (Tian et al., 2016; He et al., 2021).

Global climate changes and anthropogenic activities lead to a rapid decrease in urban wetland areas and threaten the habitat integrity and stability of the urban wetland ecosystems (Matchett and Fleskes, 2017; Zhang et al., 2020). The overall ecological condition of urban wetlands has shown a declining pattern over the years (Hui et al., 2011). The Hulanhe Wetland Reserve is located on the north bank of Songhua River, Heilongjiang Province. It is the largest natural urban wetland in China (Xing, 2016). The community structure of diverse animals (Gao et al., 2015), diverse plants (Cheng, 2013), hydrozoan (Liu, 2012), and phytoplankton in the Hulanhe Wetland and surrounding waters has received much attention(Hui et al., 2011; Lu et al., 2014; Jia et al., 2021). To date, most research on the water ecology of the Hulanhe Wetland has mainly focused on the effects of plankton, plant community composition, abundance changes, and environmental factors (Hui et al., 2011; Lu et al., 2014; Jia et al., 2021). However, the research on the stability of plankton community is still insufficient.

Our study focused on the Hulanhe Wetland Reserve and the Hulan River, a tributary of the Songhua River that flows through the wetland, in 2021. We aimed to describe the plankton community structures and the correlations between them in the Hulanhe Wetland, to screen and identify the main factors driving plankton community structure, and to provide a theoretical basis for the protection of wetland biodiversity in the Hulanhe Estuary for the restoration of the damaged wetland ecosystems. Therefore, we put forward the following hypotheses: (1) there was a specific corresponding tendency to a predatory relationship between phytoplankton and zooplankton in the Hulanhe Wetland and (2) the stability of the plankton community in the Hulanhe Wetland is driven and regulated by both biotic and abiotic factors. The validation of these hypotheses would provide a theoretical basis for the water environment management of the Hulanhe Wetland from the perspective of plankton stability, which is beneficial for local water quality management and makes specific contributions to the further research and development of the restoration of other damaged wetland ecosystems.

2. Materials and methods

2.1. Research area, sampling point layout, and sampling time

The Hulan River, a tributary of the Songhua River, is located in the central part of Heilongjiang Province, between N 45°09′-46°10′, E 126°76′-127°31′. The reserve extends in the east–west belt along the north bank of the Songhua River. The length of the reserve is 63.5 km from east to west, 21.3 km from north to south, and 179.5 km in circumference. According to the habitat characteristics of the Hulanhe Wetland, it is divided into 12 sampling points: water inlet areas (S1, S2, S3, and S12), water outlet areas (S9, S10, and S11), wetland protection areas (S4, S5, S6, S7, and S8), an area affected by agriculture (S2), and an area affected by fisheries (S10) (Figure 1). In this study, phytoplankton and zooplankton specimens were collected in spring (April, May), summer (June, July, August), and autumn (October) in 2021, and the physicochemical indicators of the water body were analyzed. The longitude and latitude data of the sampling points were collected *via* GPS, and ArcGIS 10.2 (ESRI, Redlands, CA, United States) was used to draw the sampling points map.

2.2. Environmental data collection and sampling

2.2.1. Environmental variables

At each sampling site, surface water samples (0–0.5 m) were collected in triplicate for physicochemical analyses. The collection of water quality samples and plankton samples from the Hulanhe Wetland was carried out simultaneously. The WT, pH, conductivity (Cond.), DO, and turbidity (Tur) were measured with a multi-parameter water quality analyzer (YSI ProPlus, YSI, United States). TP, TN, chemical oxygen demand (COD_{Mn}), and biochemical oxygen demand (BOD_5) were the environmental factors analyzed in the laboratory within 24 h of sampling (GB 3838–2002).

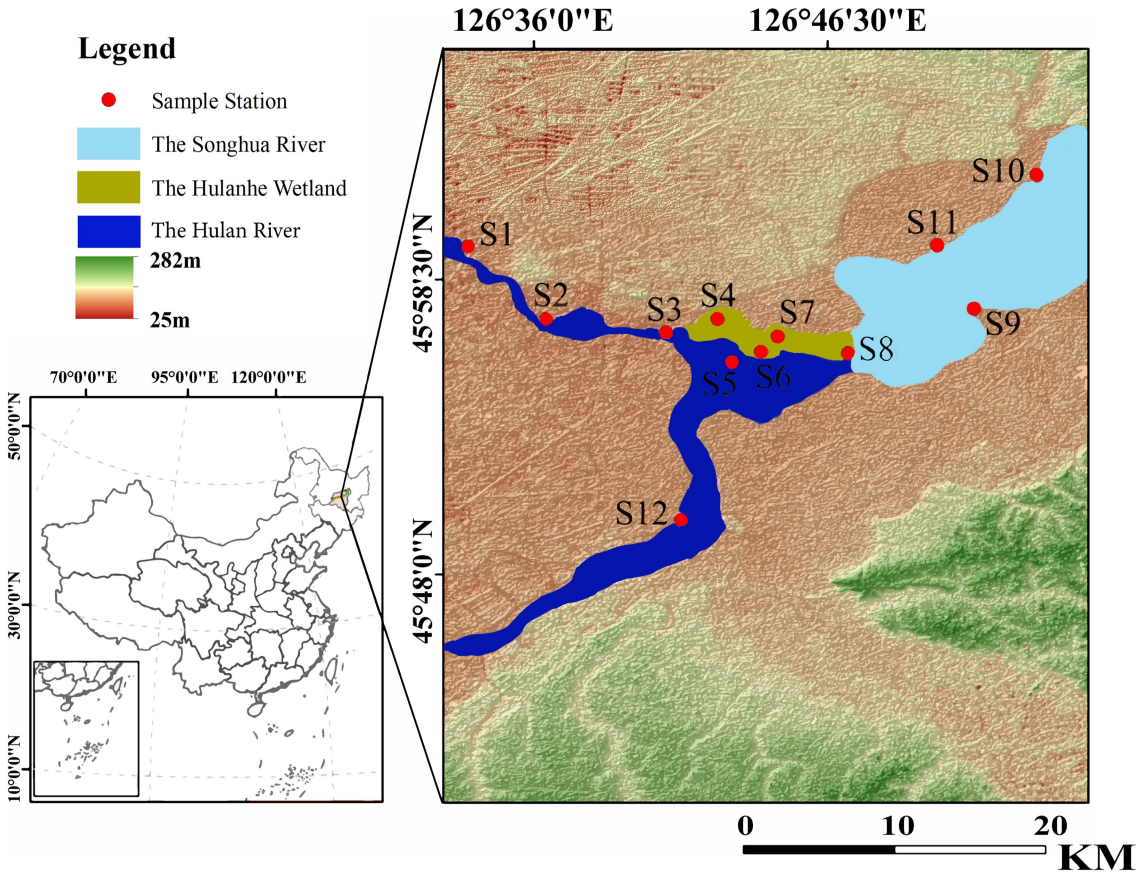

FIGURE 1
Sampling site map of Hulanhe in Harbin, Heilongjiang Province.

2.2.2. Plankton sampling

Plankton samples and water samples were collected simultaneously in the Hulanhe Wetland. Phytoplankton (5 L) and zooplankton (5 L) samples were collected at 1 m depth from each sampling site. Phytoplankton samples were stored in acidified Lugol's solution, and zooplankton samples were stored in formaldehyde (4%). All samples were stored for 24 h before analysis and concentrated to 50 mL (Zhang and Hang, 1991).

Phytoplankton and protozoa were examined at ×400 magnification (×10 eyepiece and ×40 objective) using an Olympus microscope (Optec B302, Chongqing, China) with a 0.1 mL plankton counting chamber. Rotifera, cladocera, and copepods were examined at ×200 magnification (×10 eyepiece and ×20 objective) using an Olympus microscope with a 1 mL plankton counting chamber. Majority of the phytoplankton samples were identified at the species level, and their abundance was expressed as cells L^{-1} (Zhang and Hang, 1991).

Enumerating plankton cells, usually requires settling of samples in order to concentrate the cells (Claessens and Prast, 2007). Precipitation and concentration are carried out in a cylindrical funnel. Fix the funnel on a shelf and place it on a stable table. The water sample was poured into the funnel, and the plankton was naturally precipitated for 60 h. The supernatant was sucked with a siphon and the sample was concentrated to 50 mL (Zhang and Hang, 1991).

The publications 'Freshwater algae in China: systems, classification and ecology' (Hu and Wei, 2006), 'Freshwater Microorganisms and Benthic Animals Atlas' (Zhou and Chen, 2011), 'China Freshwater Rotifer' (Wang, 1961), the Rotifer World Catalog[1], International Commission on Zoological Nomenclature[2], and 'Chinese Fauna Freshwater Cladocera' (Board, 1979) were used to identify the plankton organisms.

2.3. Statistical analysis

The dominant species of plankton were determined based on the dominance value Y for each species, and plankton diversity was represented by the Shannon–Wiener (H′) (Magnussen and Boyle, 1995), Margalef (H) (Margalef, 1969), Pielou evenness (J) (Pielou, 1966), and Simpson indices(D) (Simpson, 1949), as follows:

$$Y = \left(\frac{n_i}{N}\right) \times f_i$$

1 http://www.rotifera.hausdernatur.at/
2 http://iczn.org/lan/rotifer

Shannon–Wiener index:

$$H' = -\sum_{i=1}^{s} P_i \times \ln P_i$$

Margalef index:

$$H = (S-1) / \ln N$$

Pielou evenness index:

$$J = H' / \ln S$$

Simpson index:

$$D = 1 - \sum_{i=1}^{s} P_i^2$$

where n_i and N are the number of individuals of species i and the total number of individuals of all species within a given area in the whole year, respectively; P_i is the relative proportion of species i, which is calculated by n_i / N; S is the number of species within a given sample; and f_i is the occurrence frequency of species i, which is calculated by the ratio of the number of samples with species i to the total number of samples within the given area in the whole year. If the dominance value Y of a species was greater than 0.02, it was considered dominant.

2.4. Plankton RUE

In this experiment, the mass per unit volume was used to represent the biomass of plankton, and the calculation formula was: biomass = density×volume×abundance×10^{-6}. It is assumed that the density of plankton is 1 g/L, the volume unit is μm^3, the abundance unit is cells/L, and the biomass unit is μg/L.

RUE represents the amount of standing stock biomass per unit resource. We evaluated the RUE of phytoplankton (RUE_{pp}) and zooplankton (RUE_{zp}) communities, which quantifies the ratio of realized to potential productivity. RUE_{pp} was calculated as phytoplankton biomass per unit TP (Davidson and Howarth, 2007; Filstrup et al., 2014). RUE_{zp} was calculated as zooplankton biomass per unit of phytoplankton biomass. As we were interested in calculating community biomass per unit resource directly available to each trophic level, RUE_{zp} was calculated in relation to phytoplankton biomass, whereas RUE_{pp} was calculated in relation to TP (Filstrup et al., 2014).

$$RUE_{pp} = \frac{BIO(Phyto)}{TP}$$

$$RUE_{zp} = \frac{Bio(Zoo)}{Bio(Phyto)}$$

Here, $BIO(Phyto)$ is phytoplankton biomass; $BIO(Zoo)$ is zooplankton biomass; and TP is total phosphorus.

Plankton community turnover was determined by Bray–Curtis dissimilarity index between the two samples; the smaller the community turnover, the stronger the community stability (Jeppesen et al., 2011; Filstrup et al., 2014). Bray–Curtis dissimilarity index was calculated as:

$$BC = \frac{\sum_{i=1}^{n} |y_{i1} - y_{i2}|}{\sum_{i=1}^{n} |y_{i1} + y_{i2}|}$$

Here, BC is the Bray–Curtis dissimilarity index between samples 1 and 2; y_{i1} and y_{i2} are the biomasses of plankton species i in the two samples, respectively; and n is the total number of plankton species in both the samples.

2.5. Data analysis

Analysis of variance (ANOVA) and *Post-hoc* test were conducted to evaluate differences in environmental data and was performed using SPSS 22.0 for Windows. Pearson correlation coefficient between community stability and RUE, biodiversity, and water environment factors were determined using SPSS 22.0 for Windows. Then, Origin 2022 was used for ordinary least squares regression analysis. The 'vegan', 'ggpubr', 'ggplot2', and 'corrplot' packages in R 4.0.3 were used for the difference tests and heat maps.

3. Results

3.1. Physicochemical characteristics of water samples

There were significant differences in WT (ANOVA, $p < 0.001$), pH (ANOVA, $p < 0.001$) and TN (ANOVA, $p < 0.001$) (Tables 1, 2). The variation range of WT was 8.10–27.80°C and an average of 18.07°C. The variation pattern of Tur, DO, and BOD_5 was to increase gradually with the change of season, with a variation range of 1.70–186.80 NTU (Tur), 4.47–14.11 mg/L (DO), and 0.05–10.04 mg/L (BOD_5), The mean values were 54.65 NTU (Tur), 9.96 mg/L (DO), and 5.53 mg/L (BOD_5). TN decreased gradually with the change of spring, summer, and autumn, with a variation range of 0.15–0.78 mg/L and an average of 0.46 mg/L. The pH, COD_{Mn}, TP, and Cond. values were the greatest in summer, followed by in spring, and the lowest in autumn, ranging from 6.47–9.06 (pH), 2.47–15.80 mg/L (COD_{Mn}), 0.03–1.03 mg/L (TP), and 160.90–1123.00 μS/cm (Cond.), with an average of 7.72 (pH), 6.46 mg/L (COD_{Mn}), 0.30 mg/L (TP), and 359.03 μS/cm (Cond.).

TABLE 1 Environmental characteristics of the Hulanhe Wetland.

Mental variables	Unit	Spring	Summer	Autumn	ANOVA		
					Eta-Squared	*p*-value	*q*-value
Tur.	NTU	49.90 ± 71.90	51.45 ± 94.25	53.30 ± 51.45	0.051	0.186	0.233
pH	–	7.94 ± 7.76	8.02 ± 7.89	6.64 ± 6.58	0.552	0.001**	0.001
WT	°C	16.30 ± 16.75	21.95 ± 21.65	9.05 ± 10.30	0.463	0.001**	0.001
DO	mg/L	9.37 ± 9.29	9.46 ± 12.44	12.21 ± 11.77	0.081	0.059	0.132
BOD_5	mg/L	4.26 ± 5.05	5.17 ± 8.76	7.60 ± 7.19	0.068	0.096	0.144
TN	mg/L	0.51 ± 0.59	0.45 ± 0.42	0.42 ± 0.47	0.004	0.884	0.884
TP	mg/L	0.17 ± 0.26	0.30 ± 0.53	0.25 ± 0.42	0.179	0.001**	0.004
COD_{Mn}	mg/L	6.17 ± 6.20	6.45 ± 9.51	4.82 ± 7.61	0.021	0.502	0.565
Cond.	μS/cm	310.75 ± 597.90	323.85 ± 641.95	241.15 ± 380.65	0.075	0.073	0.132

** Represents $p < 0.01$ (extremely significant correlation).

TABLE 2 *Post-hoc* test of environmental characteristics in Hulanhe Wetland.

	Spring × Summer	Summer × Autumn	Spring × Autumn
WT	0.929	0.001**	0.001**
pH	0.382	0.001**	0.001**
TP	0.001**	0.211	0.451

** Represents $p < 0.01$ (extremely significant correlation).

3.2. Plankton community structure

3.2.1. Composition of plankton community

The species composition and dominant species of the plankton community in the Hulanhe Wetland are shown in Figures 2, 3 and Tables 3, 4. The identified phytoplankton in the Hulanhe Wetland belonged to eight phyla, 11 classes, 22 orders, 42 families, 91 genera, and 209 species. Among them, Bacillariophyta had the most number of species (74 species), followed by Chlorophycophyta (73 species), Cyanophyta (32 species), Euglenophyta (16 species), Pyrrophyta (6 species), Cryptophyta (4 species), Chrysophyta (3 species), and Xanthophyta (1 species), respectively.

A total of four categories and 90 species of zooplankton were identified in the Hulanhe Wetland, including 43 species of rotifers, 36 species of protozoa, 5 species of copepods, and 6 species of cladocerans. There were 18 dominant species of zooplankton. The dominant species of zooplankton in spring and summer were mainly protozoa and rotifers. The dominant species in autumn were less, mainly copepods. Figure 3 shows the spatio-temporal distribution of plankton species in the Hulanhe Wetland. In terms of time distribution, the number of phytoplankton species was in the order of summer>autumn>spring and the number of zooplankton species was in the order of summer>spring>autumn.

There were 39 dominant species of phytoplankton, with a significant seasonal distribution. In spring, the dominant species were mainly Bacillariophyta and Cryptophyta, such as *Cyclotella meneghiniana* and *Chroomonas acuta*. The dominant species in summer were Chlorophyta, Cyanophyta, and Chrysophyta, among which *Ankistrodesmus angustus*, *Arthrospira platensis*, and *Dinobryon cylindricum* were the most dominant. Bacillariophyta and some cyanobacteria were the dominant species in autumn, and *Cyclotella meneghiniana* and *Chroomonas acuta* were the dominant species in spring. The spatial distribution also had certain differences. The proportions of the dominant species (cyanobacteria) in the water outlet areas were higher than those in the water inlet areas, while the proportions of other categories were lower than those in the water inlet areas. The dominant species in the wetland protection area were evenly distributed and much higher than those in the water inlet and outlet areas. *Melosira granulata* had the highest dominance in the Hulanhe Wetland. There were eight dominant species of protozoa, among which *Strombidium viride* had the highest dominance in spring, while *Difflugia acuminate* had absolute dominance in summer. There were seven dominant species of rotifers, *Polyarthra euryptera* in spring and *Polyarthra euryptera* and *Keratella valga* in summer. There were three dominant species of copepods. *Nauplius* was mainly dominant in summer, and the dominance of *Neutrodiaptomus incongruens* was the highest in autumn. Cladocera was the least dominant with only one species. From the perspective of spatial variation, the dominant species in the water inlet areas were mainly rotifers (such as *Anuiaeopsis fissa* and *Polyarthra euryptera*), while that at the water outlet areas were protozoa (such as *Difflugia acuminate*). The dominant species in the wetland reserve were generally higher than those in the water inlet and outlet areas. Rotifers, protozoa, copepods, and cladocera were mainly distributed, among which *Neutrodiaptomus incongruens* and *Polyarthra euryptera* had the highest dominance in the entire region.

3.2.2. Plankton abundance

The variation range of phytoplankton abundance in the three seasons in 2021 was $0.53–16.61 \times 10^6$ cells/L. The average abundance of phytoplankton in the time scale was in the order summer>autumn>spring, and the variation range was $0.99–16.61 \times 10^6$ cells/L (summer), $0.85–14.96 \times 10^6$ cells/L (autumn), and $0.53–13.55 \times 10^6$ cells/L (spring) (Figure 4A). The zooplankton

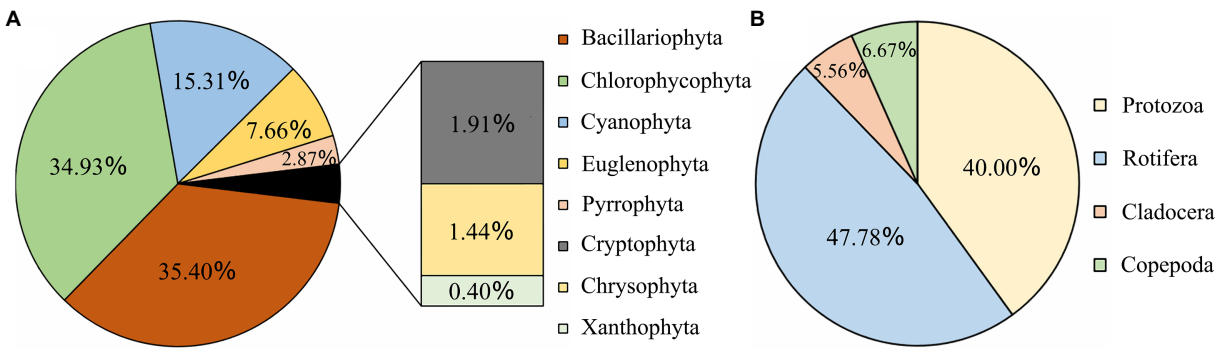

FIGURE 2
Schematic diagram of plankton species distribution in Hulanhe Wetland. **(A)** Phytoplankton. **(B)** Zooplankton.

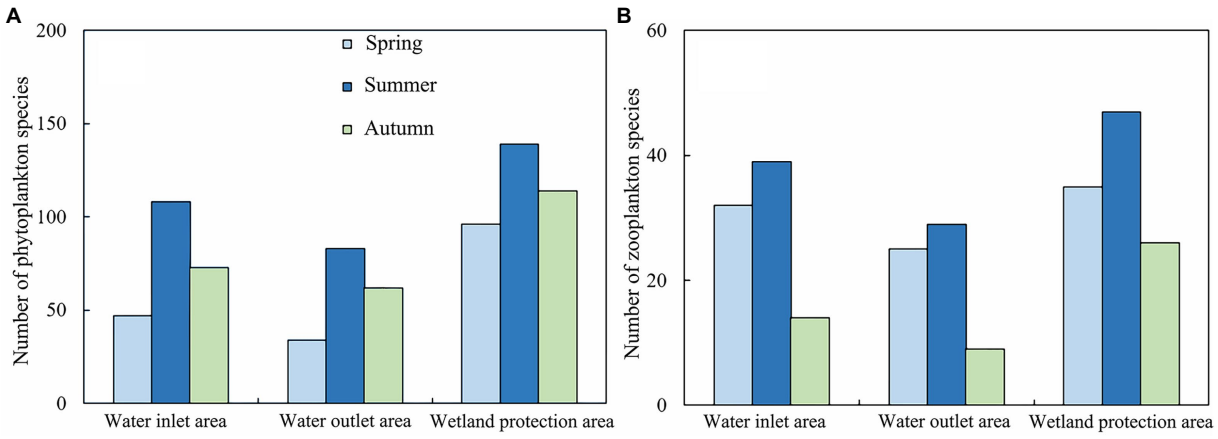

FIGURE 3
Schematic diagram of plankton species distribution in Hulanhe Wetland. **(A)** Phytoplankton. **(B)** Zooplankton.

community structure also showed temporal distribution differences, and the community abundance was mainly dominated by protozoa and rotifers. The abundance of zooplankton in the three seasons in 2021 was in the range 0.15–8.60 × 10^4 cells/L, and the abundance of zooplankton species was in the order summer>autumn>spring, with a range of 0.20–8.60 × 10^4 cells/L (summer), 0.15–3.25 × 10^4 cells/L (autumn), and 0.20–4.08 × 10^4 cells/L (spring) (Figure 4C).

The variation in phytoplankton abundance on a spatial scale was in the order wetland protection area > water inlet area > water outlet area > agriculture-affected area > fisheries-affected area. The wetland protection area had the highest abundance, with a range of 0.53–15.75 × 10^6 cells/L; the abundance in the water inlet area was the second, with a range of 0.85–8.67 × 10^6 cells/L; the abundance of the water outlet area ranged from 1.92–9.43 × 10^6 cells/L; the abundance was the lowest in the agriculture-affected area and fisheries-affected area, with a variation range of 0.05–4.28 × 10^6 cells/L and 0.22–5.61 × 10^6 cells/L, respectively (Figure 4B). The overall spatial variation of zooplankton was in the order wetland protection area > water inlet area > water outlet area > agriculture-affected area > fisheries-affected area. The wetland protection area had the highest abundance, with a range of 2.25–8.60 × 10^4 cells/L; the abundance in the water inlet area was second, with a range of 0.20–7.25 × 10^4 cells/L; the variation ranges were 0.20–2.25 × 10^4 cells/L, 0.35–3.00 × 10^4 cells/L, and 0.20–0.95 × 10^4 cells/L for water outlet area, agriculture-affected area, and fisheries-affected area, respectively (Figure 4D).

3.2.3. Correlation between phytoplankton and zooplankton

Predation and competition are the main driving forces for regulating the structure of plankton communities in freshwater ecosystems. Plankton can be classified into phytoplankton and zooplankton according to the trophic relationship (Bottom-up/Top-down effect) of the food web, and there is a long-term predation and predation relationship between them. In this study, the correlations between phytoplankton (eight phyla) and zooplankton (four categories) were analyzed by correlation heatmap (Figure 5). As shown in the diagram, rotifers showed a

10.3389/fevo.2023.1148580

TABLE 3 Dominant species of phytoplankton in Hulanhe Wetland.

		Dominant species	Season			Area		
			Spring	Summer	Autumn	Wetland	Water inlet	Water outlet
Phytoplankton	Bacillariophyta	*Cyclotella meneghiniana*	0.257	0.130	0.051	0.143	0.128	0.113
		Melosira granulata	0.195	–	0.421	0.476	–	–
		Melosira varians	0.165	–	0.101	0.101	–	0.165
		Asterionella formosa	0.121	–	–	0.096	–	–
		Ulnaria ulna	0.082	0.194	0.285	0.206	0.022	0.241
		Nitzschia palea	0.054	0.052	0.069	0.053	0.046	0.091
		Navicula radiosa	0.052	–	–	0.034	0.069	–
		Aulacoseira pusilla	0.048	0.079	0.057	0.056	0.072	0.062
		Ulnaria acus	0.037	–	–	0.037	–	–
		Melosira granulata var. *angustissima*	0.033	0.085	0.203	0.186	0.128	0.119
	Chlorophycophyta	*Ankistrodesmus falcatus*	–	0.158	–	0.158	–	–
		Tetraëdron minimum	–	0.084	–	0.084	–	–
		Scenedesmus quadricauda	–	0.082	0.069	–	0.076	–
		Crucigenia tetrapedia	–	0.026	–	–	–	0.026
		Chlamydomonas globosa	0.099	0.069	0.057	0.196	0.080	0.134
		Ankistrodesmus angustus	0.076	0.269	0.120	0.180	0.152	0.022
		Scenedesmus dimorphus	0.056	0.101	0.164	0.133	0.056	–
		Schroederia setigera	0.049	0.039	–	0.044	–	–
		Chodatella quadriseta	0.024	–	–	0.024	–	–
	Cyanophyta	*Arthrospira platensis*	–	0.389	0.068	0.319	–	–
		Anabaenopsis circularis	–	0.156	0.032	0.156	–	–
		Merismopedia minima	–	0.088	–	0.088	–	–
		Chroococcus minor	–	0.069	–	–	–	0.069
		Anabaena azotica	–	0.066	0.078	0.110	–	0.022
		Merismopedia convoluta	–	0.054	–	0.054	–	–
		Oscillatoria chlorina	0.082	0.146	0.027	0.098	–	–
		Anabaena circinalis	0.042	0.156	–	0.099	–	–
		Pseudanabaena limnetica	0.022	0.100	0.215	0.127	–	–
	Euglenophyta	*Strombomonas fluviatilis*	–	0.025	–	–	0.027	0.022
		Trachelomonas planctonica	0.040	0.071	0.038	0.119	0.047	–
		Euglena geniculata	0.036	–	–	–	0.036	–
		Euglena viridis	0.026	0.044	0.137	0.139	0.036	–
	Pyrrophyta	*Peridinium umbonatum*	–	0.094	–	–	0.094	–
		Gymnodinium aeruginosum	–	0.027	–	–	0.027	–
	Chrysophyta	*Dinobryon cylindricum*	0.123	0.251	0.196	0.215	0.132	–
	Cryptophyta	*Chroomonas acuta*	0.251	0.028	–	0.202	0.099	0.144
		Cryptomonas erosa	0.109	–	–	0.109	–	–
		Cryptomonas ovata	0.048	0.062	0.044	0.053	0.063	0.040

"–" means not involved; "Wetland" is wetland protection areas (S4–S8); "Water inlet" is water inlet areas (S1–S3, S12); "Water outlet" is water outlet areas (S9–S11).

significant correlation between Chlorophyta and Cryptophyta ($p < 0.01$); there was a significant correlation between Protozoa and Bacillariophyta ($p < 0.05$). However, compared with Chlorophyta, Cyanophyta was not significantly correlated with zooplankton although it was the dominant phylum. It may be because Cyanophyta clusters often have gum sheaths and cyanobacterial toxins, resulting in discomfort and rarely preyed by zooplankton.

TABLE 4 Dominant species of zooplankton in Hulanhe Wetland.

		Dominant species	Season			Area		
			Spring	Summer	Autumn	Wetland	Water inlet	Water outlet
Zooplankton	Protozoa	*Centropyxis aculeata*	–	0.136	–	0.132	–	0.094
		Tintinnidium fluviatile	–	0.036	–	0.032	–	–
		Strombidium virid	0.258	0.09	0.099	0.177	0.056	0.081
		Difflugia urceolata	0.097	0.025	–	0.097	–	0.025
		Vorticella micostoma	0.072	–	–	0.072	–	–
		Arcella rotundata	0.045	–	–	0.045	–	–
		Difflugia acuminate	0.031	0.454	–	0.025	–	0.246
		Tintinnopsis wangi	0.025	0.174	–	0.168	0.026	–
	Rotifera	*Lecane signifera*	–	–	–	–	–	–
		Anuiaeopsis fissa	–	0.074	–	0.072	0.066	–
		Polyarthra trigla	–	0.053	–	0.049	0.027	–
		Brachionus angularis	–	0.039	–	0.039	0.021	–
		Trichocerca cylindrica	–	0.036	–	0.034	–	–
		Polyarthra euryptera	0.073	0.335	–	0.213	0.054	–
		Keratella valga	0.046	0.086	–	0.066	–	0.023
	Copepoda	*Neutrodiaptomus incongruens*	–	–	0.208	0.294	–	0.089
		Nauplius	–	0.132	–	0.126	0.047	–
	Cladocera	*Moina rectirostris*	–	–	0.032	0.028	0.024	–

"–" means not involved; "Wetland" is wetland protection areas (S4–S8); "Water inlet" is water inlet areas (S1–S3, S12); "Water outlet" is water outlet areas (S9–S11).

3.3. Factors affecting plankton community stability

3.3.1. Resource utilization and plankton community stability

As shown in Figures 6A,B the utilization rate of phytoplankton resources (RUE_{pp}) and zooplankton resources (RUE_{zp}) in the Hulanhe Wetland showed that they were much larger in summer than those in autumn and spring. As shown in Figures 6C,D, both RUE_{pp} and RUE_{zp} showed that they much larger in the wetland protected areas (S4–S8) than those in other regional samples, while RUE_{pp} and $RUE_{zp,}$ in the agriculture-affected area (S2) and fisheries-affected area (S10) were the lowest. The community turnover (BC) of the plankton community showed an opposite trend to the community stability. The larger the BC, the easier the community to produce species turnover (that is, the worse the community stability). The ordinary least squares regression curve between plankton community stability and RUE in Hulanhe Wetland is shown in Figure 6E. There was a significant correlation between stability and RUE ($p < 0.01$), indicating that plankton communities with high resource utilization often have higher stability.

3.3.2. Species diversity and plankton community stability

As shown in Figure 7, the Margalef diversity (H), Pielou evenness (J), Shannon-Wiener diversity (H'), and Simpson ecological dominance indices (D) of plankton in the Hulanhe Wetland in three seasons were calculated. The variation ranges were 1.36–3.89 (H), 0.39–0.81 (J), 1.43–3.54 (H'), and 0.43–0.88 (D). The diversity of plankton communities was generally higher in summer than that in spring and autumn. The diversity of sampling sites (S4–S8) in wetland reserves was higher than that in other sites, and the areas affected by agriculture and fishery (S2, S10) were generally lower than other sites. The linear relationship between plankton community stability and species diversity is shown in Figure 8. BC had a significant positive correlation with H and J, and there was no significant linear relationship with H' and D. This shows that with the increase in species diversity and evenness, the community structure of plankton in the Hulanhe Wetland tended to be stable.

3.3.3. Environmental factors and plankton community stability

The ordinary least squares equation of the stability of the plankton community and environmental factors in the Hulanhe Wetland is shown in Figures 9, 10. There was a significant negative correlation between the stability of the phytoplankton community and WT and pH ($p < 0.01$), and there was a significant negative correlation between the stability of the zooplankton community and WT, pH, and TN ($p < 0.01$). There was no significant linear relationship between other environmental factors, indicating that only some water environmental factors can increase the stability of the plankton community.

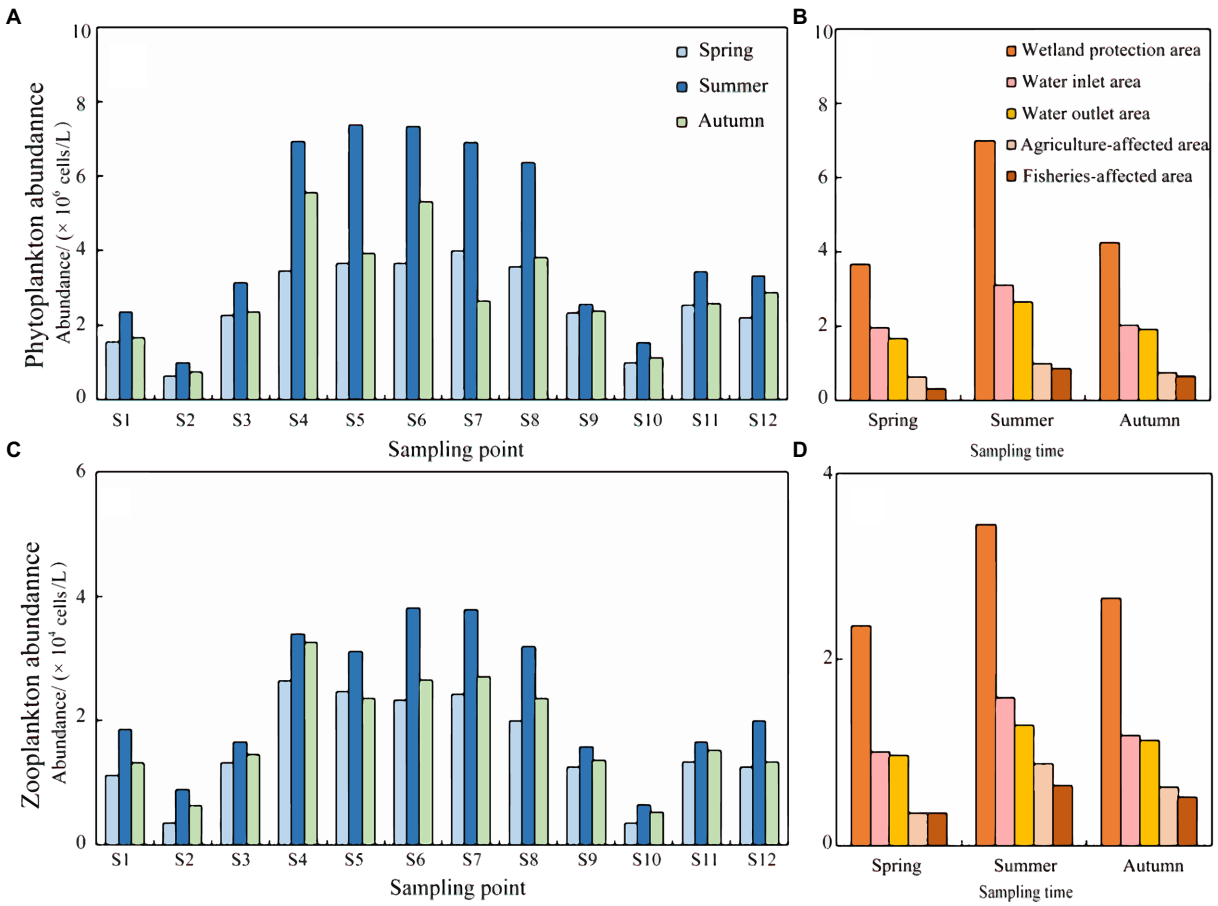

FIGURE 4
Schematic diagram of plankton abundance in Hulanhe Wetland. **(A)** Temporal distribution of phytoplankton abundance. **(B)** Spatial distribution map of phytoplankton abundance. **(C)** Time distribution map of zooplankton abundance. **(D)** Spatial distribution of zooplankton abundance.

4. Discussion

4.1. Plankton community structure

4.1.1. Spatio-temporal distribution characteristics of plankton community

During the study period, the plankton community structure in the Hulanhe Wetland showed some heterogeneity at the spatial and temporal scales (Tables 2, 3 and Figures 3, 4). The Hulanhe Wetland was affected by the temperate monsoon climate, and the physicochemical factors of the waterbody changed between seasons. In particular, the change in WT can directly affect the community composition and succession direction of phytoplankton in the Hulanhe Wetland. In spring and autumn, when the Hulanhe Wetland was just released or was about to enter the frozen period, the WT was low, and the dominant species of phytoplankton were mostly cold-tolerant Bacillariophyta, such as *Melosira varians*, *Cyclotella meneghiniana*. However, after entering summer, the WT and light intensity increased rapidly, and cyanobacteria and Chlorophycophyta that prefer warm water began to multiply and gradually occupy a dominant position (Zhu et al., 2022), such as *Arthrospira platensis*, *Anabaenopsis circularis*, and *Ankistrodesmus falcatus*. The results of this experiment are similar to the results of phytoplankton community characteristics and succession rules of Hui et al. (2011), Lu et al. (2014), and Jia et al. (2021)

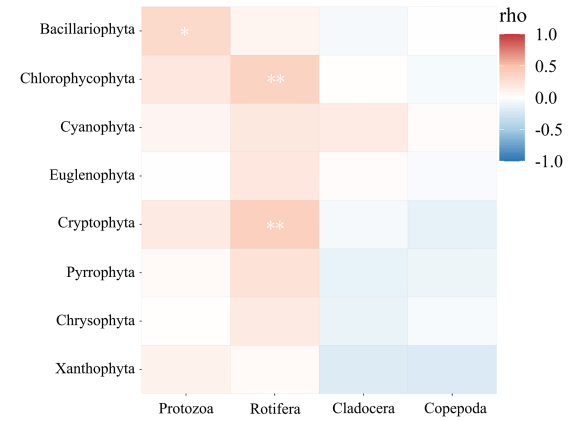

FIGURE 5
Heat map of correlation between phytoplankton and zooplankton in Hulanhe Wetland. **represents extremely significant correlation between groups (p<0.01); *Significant correlation between representative groups (p<0.05).

in 2013, 2018 and 2019, respectively. WT is an important environmental factor affecting the phytoplankton community, which further indicates that the composition and succession direction of phytoplankton

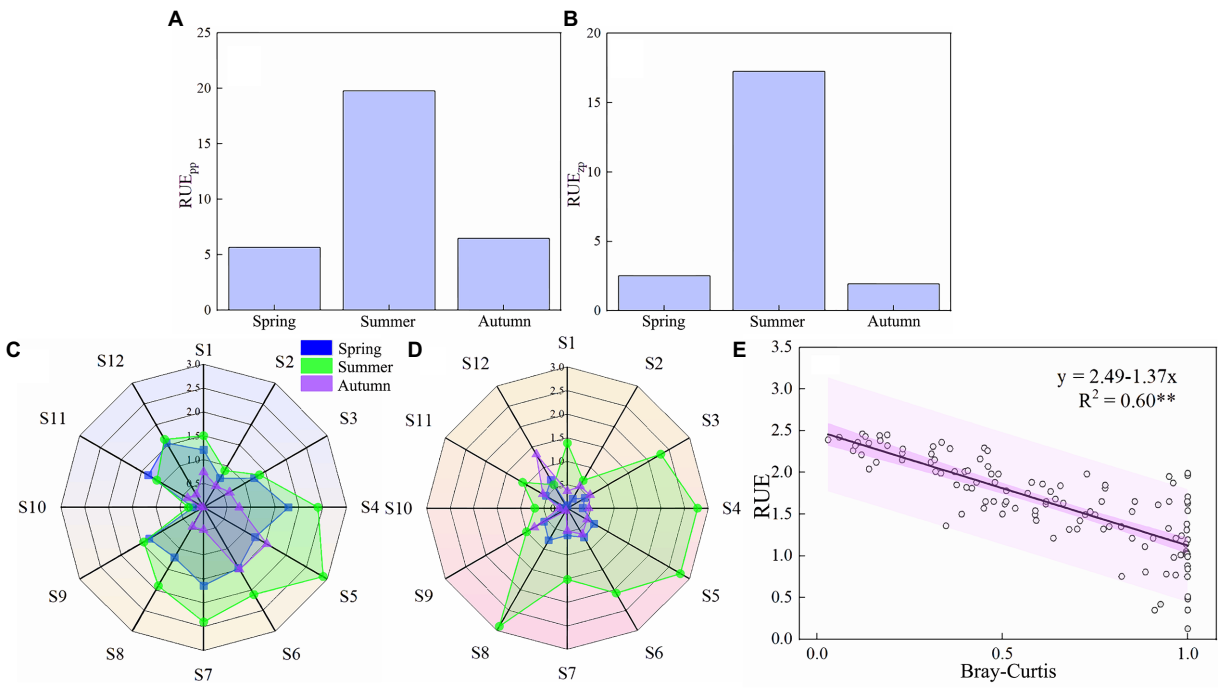

FIGURE 6
Relationship between the utilization rate of plankton community resources and community turnover in Hulanhe Wetland. **(A)** Average RUEpp in different seasons. **(B)** Average RUEzp in different seasons. **(C)** Radar map of sample points of RUEpp. **(D)** Radar map of RUEzp. **(E)** Ordinary least regression curve between RUE and community turnover.

community in the Hulanhe Wetland were relatively stable in the past 10 years.

From the perspective of the zooplankton community structure, high similarity in species composition for three seasons in 2021 and the temporal variation was not obvious. The proportion of species and abundance of small zooplankton (protozoa, rotifers) was higher than that of large zooplankton (cladocerans, copepods). The community structure of zooplankton showed a trend of miniaturization, such as *Centorpyxis aculeata*, *Tintinnidium fluviatile*, and *Polyarthra trigla*, which was similar to the results of other wetland studies on the distribution of zooplankton (Chen et al., 2014; An et al., 2017; Wang et al., 2017). The reason may be that protozoa and rotifers have small size, short cycle, and rapid development (Arndt, 1993; Li et al., 2017). They can quickly adapt to changes in hydrological conditions and physicochemical environment in the water body; therefore, they often occupy a dominant position in wetland habitats. This result is consistent with the research results of Zhang et al. (2018) showing a trend of miniaturization of zooplankton community structure.

Anthropogenic activities and urban sewage are the reasons behind the nutrient content of the Hulan River being at a relatively high-level (Xing, 2016), and wetlands can restore the water quality of polluted rivers (Zheng et al., 2014). As the largest urban wetland in China, Hulanhe Wetland has achieved great results in ecological restoration in recent years. From the spatial scale analysis, phytoplankton and zooplankton species abundance changes are consistent. The species number and average abundance of plankton in the Hulanhe Wetland protection area were much larger than those in the Hulanhe Wetland water outlet and inlet areas, which may be because the wetland had the function of purifying water and depositing nutrients, and the slow water flow rate in the wetland caused the deposition of nutrients (Kobayashi et al., 2014), which was also conducive to the growth and reproduction of plankton, such as *Cyclotella meneghiniana*, *Arthrospira platensis*, and *Tintinnidium fluviatile*. Compared with the area outside the wetland, the species number and abundance of plankton in the water inlet area were larger than those in the water outlet area. The richness and abundance of plankton in the water inlet area were higher than those in the water outlet area. Water outlet area through the wetland sediment filtration and biological filtration effect resulted in reduced nutrients (Aziz and Van Cappellen, 2021). The richness and abundance of plankton in the water outlet area decreased with the decrease in nutrients. Most of the plankton were *Anabaena circinalis*, *Ankistrodesmus angustus*, and *Polyarthra euryptera*, indicating that the Hulanhe Wetland had a certain effect of nutrient salt deposition. This led to certain spatial differences in plankton communities.

The composition of the plankton community is a strong indicator of the water environment (Jagadeesan et al., 2019). As one of the key wetlands in Harbin, the Hulanhe Wetland has achieved great results in ecological restoration in recent years. During the investigation period, the dominant species of plankton communities in the Hulanhe Wetland in the three seasons were mainly pollution-indicator organism species of clean water and oligo-sewage bodies. Zooplankton, such as *Polyarthra euryptera* (Chen et al., 2011), *Strombidium virid* (Ju et al., 2017), and *Difflugia acuminate* (Ju et al., 2017) were dominant. Phytoplankton, such as *Asterionella formosa* (Shan et al., 2022), *Dinobryon cylindricum* (Zhang and Li, 2016), *Ulnaria ulna* (Zhu et al., 2017), and *Navicula radiosa* (Zhang N. et al., 2016), which prefer clean water, also appeared as dominant communities, which are highly similar to the results of plankton

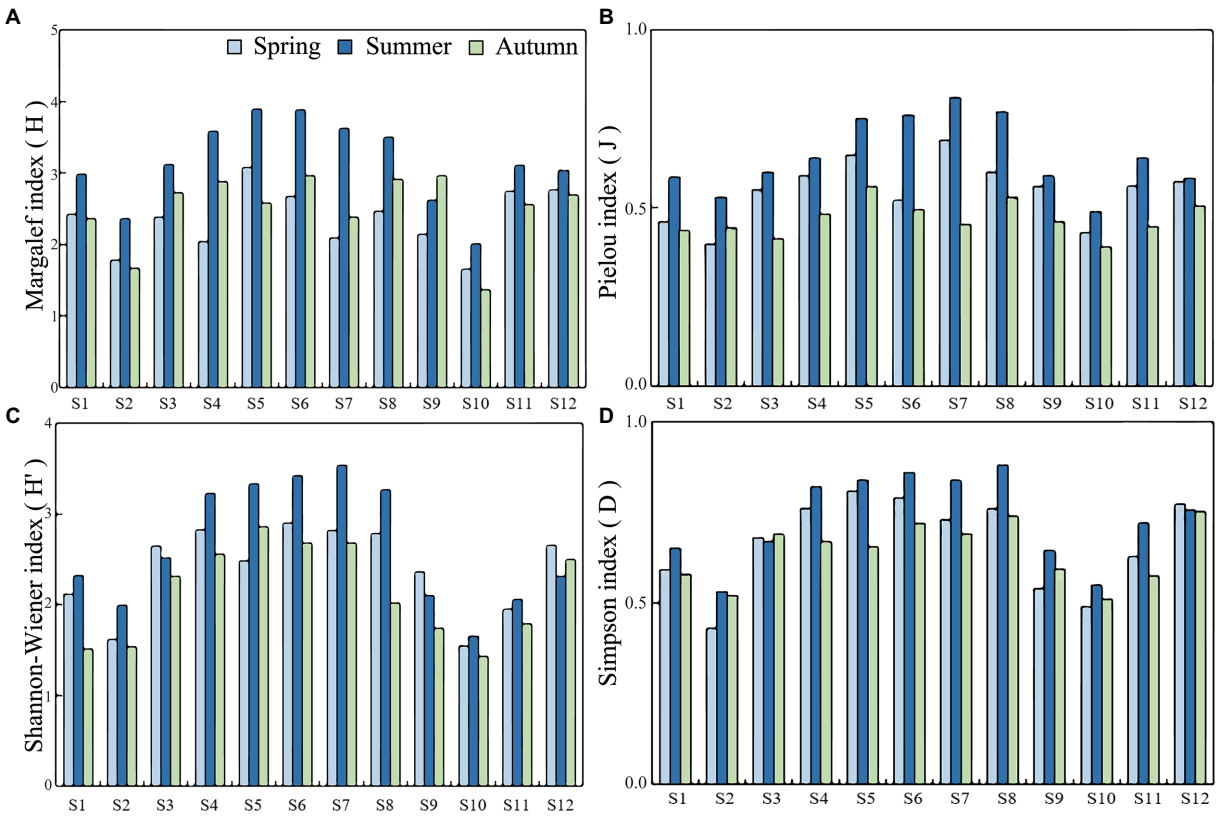

FIGURE 7
Species diversity index of plankton at various site of Hulanhe Wetland in different seasons. **(A)** Margalef diversity index. **(B)** Pielou evenness index. **(C)** Shannon-Wiener index. **(D)** Simpson's index.

surveys in the Macquarie wetland (Chaparro et al., 2018), which is also a temperate area and has been ecologically restored. The results show that in recent years, with the restoration of the Hulanhe Wetland, the ecological function gradually improved, the water quality was cleaner, and the damage to water ecosystem health was reduced to a controllable range (Hui et al., 2011).

4.1.2. Correlation between phytoplankton and zooplankton

Phytoplankton and zooplankton are important components of the food web in aquatic ecosystems, and there is a very close competition between them and the relationship between predation and predation (Mcqueen et al., 1989). Some studies have confirmed that the predatory grazing behavior of zooplankton is the main reason for the change in the phytoplankton communities (Mcqueen et al., 1989; Vanni and Temte, 1990; Figure 5).

In this study, protozoa and diatoms showed a significant correlation. Protozoa are eukaryotic unicellular animals that belong to heterotrophic organisms and are preyed by large zooplankton (such as copepods and cladocerans) (Burns and Schallenberg, 2001; Turner et al., 2001). Protozoa constitute a complete food chain by preying on diatoms (Min et al., 2019). Many experiments have shown that (Liu and Dagg, 2003; Stelfox-Widdicombe et al., 2004; Kim et al., 2007; Hu et al., 2015) large zooplankton cannot directly ingest diatoms, probably because of the shell of diatoms or because diatoms release harmful substances (such as unsaturated aldehydes) when they reach a certain high concentration to inhibit the growth and reproduction of large zooplankton. Therefore, large zooplankton will directly choose to feed on protozoa and then transfer the primary productivity of diatom sources upwards in the food chain, thus playing a role in the transmission of diatoms in the food chain.

During the study period, rotifers had a strong correlation with Chlorophycophyta, Euglenophyta, and cryptophytes. Rotifer is a small filter-feeding zooplankton. The efficiency of filtering phytoplankton is determined by the size of the phytoplankton. The palatable food range of most filter-feeding rotifers is between 1 and 15 μm (Zhang and Hang, 1991). Chlorophyta and some Cryptophyta (such as *Chroomonas acuta*), as the dominant species in the Hulanhe Wetland, have a fast reproduction rate and a palatable volume. They mostly exist in the filter-feeding range of Rotifers and are easy for rotifers to prey on. Some previous studies have shown that cryptophytes are often used as high-quality bait for zooplankton because of their cell wall digestibility, non-toxicity and suitable biochemical composition (Porter, 1973). Chlorophycophyta and cryptophytes can be successfully ingested by rotifers and can meet the corresponding nutritional needs; therefore, rotifers tend to prey on Chlorophyta and Cryptophyta (Wang et al., 2012). The predation of rotifers on green algae is also one of the reasons that affect the phytoplankton community structure, with Chlorophycophyta as the main dominant species (Yang, l., 2012).

Cyanophyta, Bacillariophyta, and Chlorophyta were the dominant species of phytoplankton in the Hulanhe Wetland, but there was no significant correlation between Cyanophyta and zooplankton. The

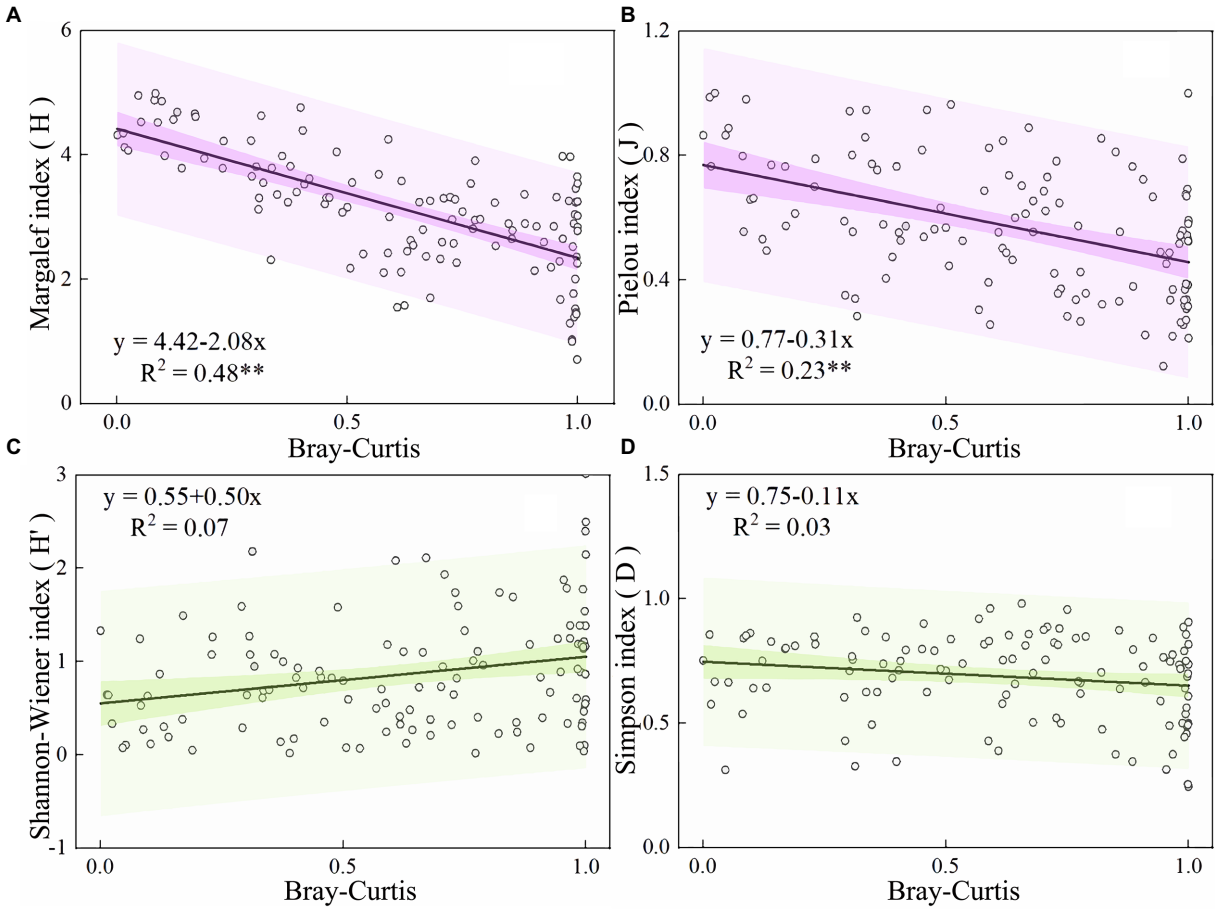

FIGURE 8
Relationship between biodiversity index and community turnover of phytoplankton community in Hulanhe Wetland. **(A)** Ordinary least squares regression curve between Margelef diversity index and community turnover. **(B)** Pielou evenness index. **(C)** Shannon-Wiener index. **(D)** Simpson's index.

reason may be that zooplankton does not prefer ingesting cyanobacteria. Studies have shown that cyanobacteria do not have zooplankton palatability, and the lack of highly unsaturated fatty acids has a negative impact on the growth rate of zooplankton (Juliana et al., 2016); simultaneously, the life form of cyanobacteria is mostly gathered into filaments or surrounded by gelatinous sheaths, which are too large and not easy to be fed (Tan and Ransangan, 2017); some species of zooplankton may also be sensitive to toxins produced by cyanobacteria (De Silva and Jang, 2017).

In conclusion, we found that the abundance of phytoplankton in water was closely related to the growth and reproduction of zooplankton. Phytoplankton is an important food source for zooplankton. High-density phytoplankton ensures the supply of zooplankton food and promotes the reproduction and growth of zooplankton. However, the feeding of zooplankton on phytoplankton is also selective. Zooplankton is more inclined to be easily ingested and palatable than phytoplankton, such as Chlorophyta and Cryptophyta.

4.2. Driving factors of plankton stability

4.2.1. RUE

RUE can reflect the nutrient cycle and transfer process of the ecosystem (He et al., 2021). Communities with high abundance of plankton often have higher RUE, and species in high-abundance communities have a high occupancy rate of trophic niches, increasing the overall RUE (Tian, 2017). In this study, the spatio-temporal differences in RUE and plankton abundance showed the same pattern (Figures 6A,B). The WT of the Hulanhe Wetland increased gradually with the increase of months, which was conducive to the growth and reproduction of plankton. Summer was the season with the most plankton species. At the same time, studies have shown that communities with diatoms, Chlorophycophyta, and protozoa as dominant species can use resources more efficiently (Tillmanns, 2006; Filstrup et al., 2014). Cyanobacteria, Chlorophycophyta, and Protozoa were the dominant phyla of plankton in the Hulanhe Wetland in summer. They have a wide ecological range and strong adaptability to the environment, which improves the RUE of plankton in summer; therefore, the RUE in summer was much greater than that in other seasons.

Some studies have found that the increase in biodiversity will increase RUE and community stability (Filstrup et al., 2014; Zhang et al., 2021), which is similar to the results of this study (Figure 6E). This study found that the gradually abundant plankton species community can use resources more effectively in the ecosystem, and the species community with high diversity has a large number of species and uniform distribution, which makes the community more stable. The abundance and diversity of plankton in the Hulanhe

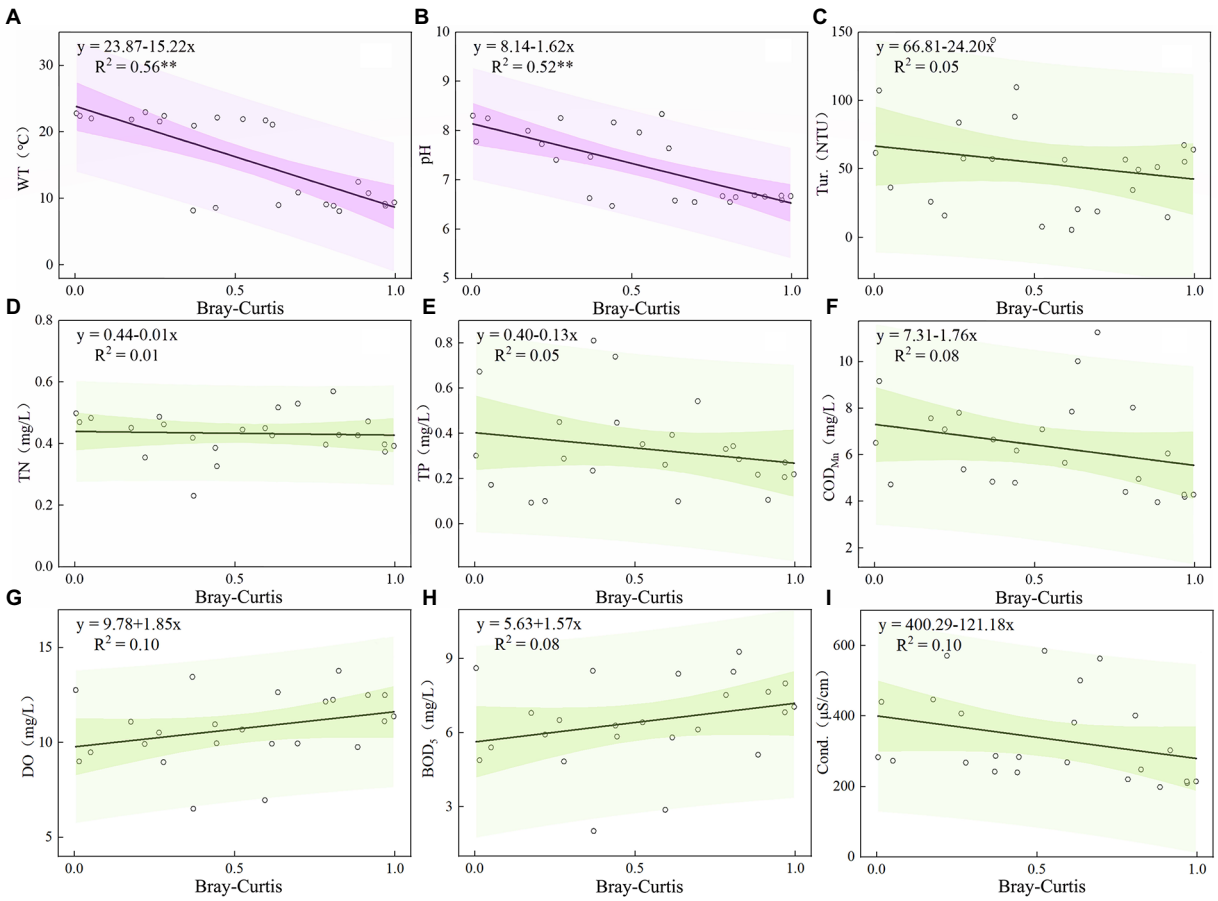

FIGURE 9
Relationship between Environmental Factors and Community Turnover of Phytoplankton Community in Hulanhe Wetland. **(A)** Water temperature and community turnover. **(B)** pH. **(C)** Turbidity. **(D)** Total nitrogen. **(E)** Total phosphorus. **(F)** Permanganate index. **(G)** Dissolved oxygen. **(H)** Bio-chemical oxygen demand. **(I)** Conductivity.

Wetland showed the same pattern (Figures 4, 7). The level of biodiversity increased with the increase in abundance, which enhanced the niche complementarity of plankton in the aquatic ecosystem to a certain extent. The ecological complementarity effect will cause overproduction (Hillebrand et al., 2008), which will promote the utilization efficiency of ecosystem resources.

High concentrations of nutrients are also one of the reasons for the correlation between RUE and the stability of plankton communities (Zhang et al., 2021). Higher concentrations of nutrients can promote the rapid growth and reproduction of plankton. The wetland ecosystem deposits nutrients and purifies water, which is one of the reasons for the high abundance of plankton in the Hulanhe Wetland protection area. Therefore, the RUE in the reserve was much higher than that in other areas (Figures 6C,D). In this study, the RUE in the agriculture-affected area (S2) and fisheries-affected area (S10) was the lowest of all samples (Figures 6C,D). The long-term effects of field herbicides on macrophytes may result in delayed, indirect responses to zooplankton and phytoplankton communities, and pollution may result in single species and a low abundance of plankton (Relyea, 2005). Due to the obvious agricultural disturbance, the RUE of the agriculture-affected area (S2) of the Hulan River inlet was low, indicating that anthropogenic disturbance destroyed the ecological function systems, resulting in low resource utilization (Wang et al., 2019). S10 was an area greatly affected by the fishery. The disturbance caused by the fishing process inhibited the growth of plankton. At the same time, the fish school carries out a large number of downward effect control on plankton, resulting in low species number and abundance (Shen and Wang, 1991), which leads to a low RUE. Therefore, to maintain the stability and sustainability of the regional ecological security pattern, the regional ecological function system affected by anthropogenic disturbance needs further restoration.

4.2.2. Species diversity

Species diversity is an important measure of community stability. There is a certain coupling relationship between plankton species diversity and community stability (Tilman, 1999). Exploring the correlation between plankton diversity and community stability is of great significance for explaining plankton community structure and diversity. In aquatic ecosystems, the increase in plankton species diversity makes the community more stable (Ptacnik et al., 2007), which is the same as the results of this study (Figure 8A).

In this study, with the increase in plankton community diversity, the community became more stable. It is speculated that the food chain and food web of communities with high diversity tend to be more complex, and there are more ways for energy flow within the

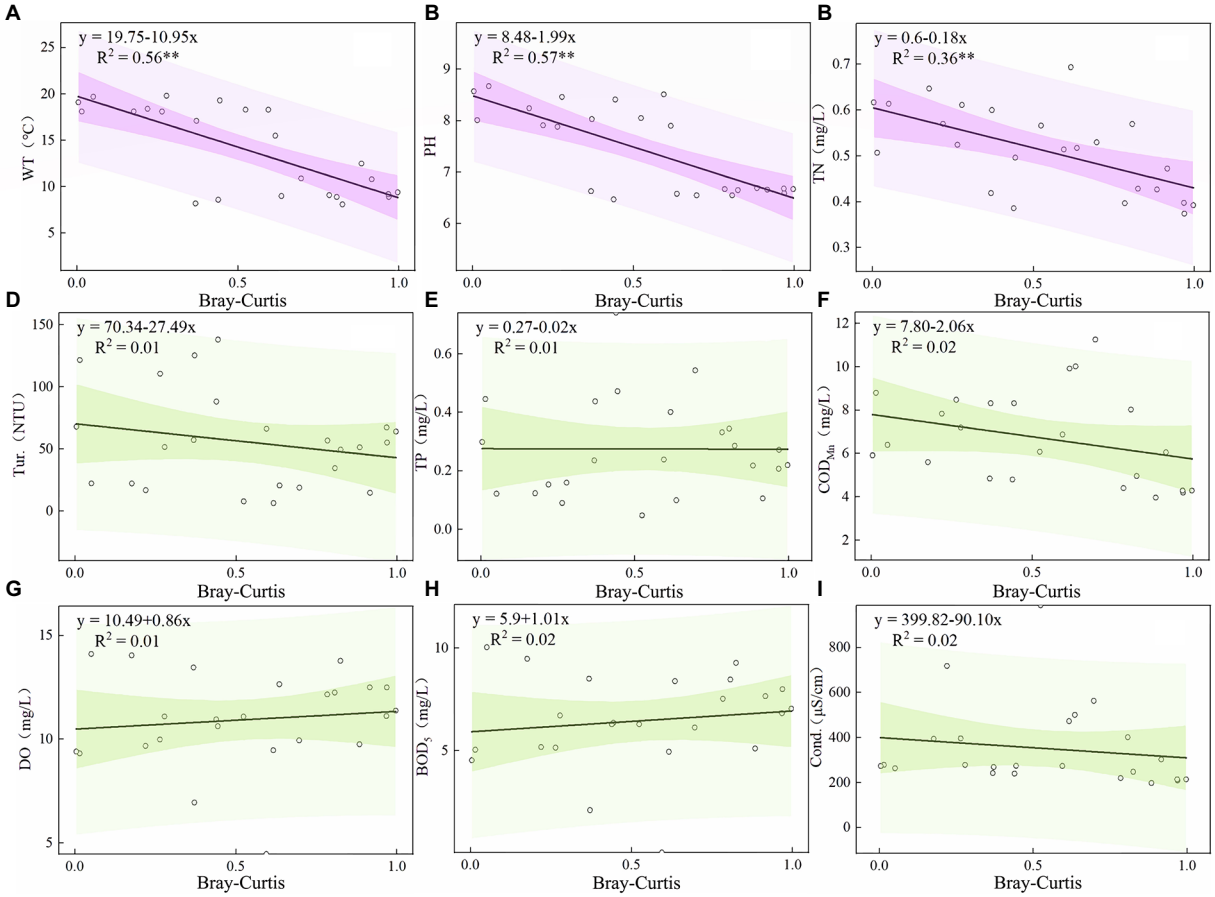

FIGURE 10
Relationship between Environmental Factors and Community Turnover of Zooplankton Community in Hulanhe Wetland. **(A)** Water temperature and community turnover. **(B)** pH. **(C)** Total nitrogen. **(D)** Turbidity. **(E)** Total phosphorus. **(F)** Permanganate index. **(G)** Dissolved oxygen. **(H)** Bio-chemical oxygen demand. **(I)** Conductivity.

community. If a certain way is blocked by interference, there may be other routes to compensate (Cao and Zhan, 2015). Therefore, a community with high diversity has less fluctuation among species, which makes the community more stable. A structurally stable plankton community has a strong feedback system, which can buffer environmental changes or fluctuations in the population from within the community and is less susceptible to external disturbances (MacArthur, 1955; Cao and Zhan, 2015).

The evenness index reflects the uniformity of the individual number distribution of each species. The higher the evenness, the more uniform the species distribution. This study showed high Pielou evenness, which implies high community stability (Figure 8B). Many studies have shown that the higher the species' evenness, the stronger the ecosystem function conversion, making the plankton community more stable (Wittebolle et al., 2009; Allan et al., 2011; Filstrup et al., 2014). The results of this study also reached the same conclusion. The community with high plankton evenness had a more uniform distribution of species resources, and the anti-interference ability of the community also increased, which is conducive for the better adaptation of the plankton community to the aquatic ecological environment (Tian, 2017; Zheng, 2019).

4.2.3. Environmental factors

Through ordinary least squares analysis, it was found that the physical and chemical environmental factors of the waterbody had a certain driving effect on the stability of the phytoplankton community, and the environmental factors affecting phytoplankton and zooplankton were similar. WT ($p < 0.01$, $p < 0.01$) and pH ($p < 0.01$, $p < 0.01$) were both the driving factors of phytoplankton and zooplankton community stability, while TN ($p < 0.01$) was only the driving factor of zooplankton community stability.

Plankton community stability will increase with the increase of WT (Figures 9A, 10A). WT can affect the metabolic intensity, growth and development, and reproduction cycle of plankton, and then affect its abundance and biomass changes and the distribution of community structure, and ultimately affect the material circulation and energy flow of the ecosystem. The average temperature of the Hulanhe Wetland in summer is 22.0°C, while cyanobacteria, Chlorophycophyta, and rotifers are more suitable for growing in warm water. The average temperature in spring and autumn is slightly lower than 16.3°C and 9.1°C, which is more suitable for the growth and reproduction of diatoms, Chrysophyta, and Protozoa, and is more dominant in the plankton community. In addition, the predation rate of zooplankton

is similar to the growth rate of zooplankton, which increases the grazing frequency and achieves rapid reproduction of zooplankton as the water temperature increases (Pulsifer and Laws, 2021). This further proves that the stability of plankton community will be more stable with the increase of WT.

pH is an important water environmental factor driving the stability of phytoplankton and zooplankton communities. The results showed that there was a significant negative correlation between pH and the turnover of zooplankton and phytoplankton communities (Figures 9B, 10B). Phytoplankton communities were more stable in alkaline water. The pH affects the absorption of nutrients by affecting the activity of some enzymes in plankton cells or transmembrane proton gradient. In the season with high WT, the dissolved CO_2 in water decreases, increasing the pH value, and the Hulanhe Wetland is weakly alkaline (7.51 ± 0.38), which promotes the growth and reproduction of plankton, thus affecting its community structure (Zhang et al., 2021). The alkaline environment is conducive to phytoplankton absorbing CO_2 for photosynthesis. In alkaline water, phytoplankton has high primary productivity, which ensures the food source of zooplankton. The abundance of zooplankton also increases, and the phytoplankton community gradually stabilizes (Jakobsen et al., 2015).

TN is an essential element for the synthesis and energy transfer of aquatic organisms and also an important nutrient source for zooplankton. The variation in TN concentration can affect the food source of zooplankton and the dynamic pattern of community (Shen et al., 2021). TN indirectly affects the composition of zooplankton by affecting the community structure of phytoplankton (Guo et al., 2017). At the same time, changes in the ratio of nitrogen to phosphorus in the water affects the competition between zooplankton with different growth characteristics and the change in population structure (Yang et al., 2021). During the study period, the average nitrogen-phosphorus ratio of the Hulanhe Wetland was 1.52 ($N/p < 16{:}1$), which was a nitrogen limitation. The average TN of the Hulanhe Wetland in spring, summer, and autumn was at a relatively high level (0.46 mg/L). High concentrations of TN made the zooplankton community more stable (Figure 10C). Bhavya et al. (2020)have shown that the total uptake of nitrogen by phytoplankton is in the range of 10.24–59.36% and 30.21–68.55%. Therefore, high concentration of TN promotes the reproduction of phytoplankton (Liu et al., 2022). Phytoplankton photosynthesis in water not only provides sufficient food for zooplankton but also creates an oxygen-rich environment for zooplankton, which makes zooplankton species more abundant and increases community stability.

Overall, the stability of the plankton community is a very complex problem. The stability of the plankton community is not only affected by the single factor of community structure characteristics but also has a certain correlation with RUE, biodiversity, and water environment factors.

For future studies, we suggest observing the effects of microorganisms on plankton (Pearce and Butler, 2002; Rana et al., 2021), the predation of plankton by fish (Villéger et al., 2019; Xia et al., 2020), and the variation in plankton stability under special conditions (e.g., heavy rain, freezing, and advection; Manna et al., 2019; Liu et al., 2021; Lu et al., 2022), which will help to improve our mechanistic understanding of the maintenance and stability of plankton community structure.

5. Conclusion

Specific predation relationship was observed between phytoplankton and zooplankton in the Hulanhe Wetland. Protozoa tend to prey on diatoms, rotifers prefer to ingest Chlorophycophyta and cryptophytes, but cyanobacteria are rarely preyed on by zooplankton because of their own cyanobacterial toxins and mismatched caliber. The stability of plankton community in the Hulanhe Wetland is controlled by biotic and abiotic factors. The stability of the plankton community had a significant linear relationship with the Margalef diversity index, Pielou evenness index, and RUE. The key factors affecting phytoplankton community stability in the Hulanhe Wetland were WT and pH, while zooplankton community stability was mainly driven by WT, pH, and TN.

Data availability statement

The raw data supporting the conclusions of this article will be made available by the authors, without undue reservation.

Author contributions

XL conceived the original concept. XL and YF developed experimental strategies and sampling design. TT carried out the collection of plankton samples and the determination of water physic-chemical indicators under the guidance of XL. TT and HW carried out the counting and identification of plankton specimens and contributed in sampling collection, data analysis, and manuscript writing. TT, HW, and XN performed all data analysis and integration with help from XL and YF. TT prepared the manuscript with significant input from HW, XN, NZ, XL, YL, and YF. All authors contributed experimental assistance and intellectual input to this study.

Acknowledgments

We thank Yimin Zhu, Zhenxiang Li, Tao Shan, Tian Lou, Chao Ma, Anlong Yuan, Hongying Xin, Jinyan Liang, and Xiaoyi Chen for sample collection.

Conflict of interest

The authors declare that the research was conducted in the absence of any commercial or financial relationships that could be construed as a potential conflict of interest.

Publisher's note

References

Allan, E., Weisser, W., Weigelt, A., Roscher, C., Fischer, M., and Hillebrand, H. (2011). More diverse plant communities have higher functioning over time due to turnover in complementary dominant species. *Proc. Natl. Acad. Sci. U. S. A.* 108, 17034–17039. doi: 10.1073/pnas.1104015108

Amorim, C. A., and Moura, A. D. N. (2021). Ecological impacts of freshwater algal blooms on water quality, plankton biodiversity, structure, and ecosystem functioning. *Sci. Total Environ.* 758:143605. doi: 10.1016/j.scitotenv.2020.143605

An, R., Wang, F. Y., Yu, H. X., and Ma, C. X. (2017). Seasonal dynamics of zooplankton functional groups and their relationships with environmental factors in the Sanhuanpao wetland reserve. *Acta Ecol. Sin.* 37, 1851–1860. doi: 10.5846/stxb201510292184

Arndt, H. (1993). Rotifers as predators on components of the microbial web (bacteria, heterotrophic flagellates, ciliates) - a review. *Hydrobiologia* 255-256, 231–246. doi: 10.1007/bf00025844

Aziz, T., and Van Cappellen, P. (2021). Economic valuation of suspended sediment and phosphorus filtration services by four different wetland types: A preliminary assessment for southern Ontario, Canada. *Hydrol. Process.* 35, 1–15. doi: 10.1002/hyp.14442

Bhavya, P. S., Kang, J. J., Jang, H. K., Joo, H., Lee, J. H., Lee, J. H., et al. (2020). The contribution of small phytoplankton communities to the total dissolved inorganic nitrogen assimilation rates in the east/Japan Sea: An experimental evaluation. *J. Mar. Sci. Eng.* 8:854. doi: 10.3390/jmse8110854

Board, F.S.E. (1979). *Chinese Fauna freshwater Cladocera*. Beijing, China: Science Press.

Boucot, A. J. (1985). The complexity and stability of ecosystems. *Nature* 315, 635–636. doi: 10.1038/315635c0

Burns, C. W., and Schallenberg, M. (2001). Calanoid copepods versus cladocerans: Consumer effects on protozoa in lakes of different trophic status. *Limnol. Oceanogr.* 46, 1558–1565. doi: 10.4319/lo.2001.46.6.1558

Cao, Z., and Zhan, M. (2015). *An introduction to ecology.* Bejing, China: Higher Education Press.

Chaparro, G., Horvath, Z., O'Farrell, I., Ptacnik, R., and Hein, T. (2018). Plankton metacommunities in floodplain wetlands under contrasting hydrological conditions. *Freshw. Biol.* 63, 380–391. doi: 10.1111/fwb.13076

Chen, Q., He, W., Liu, Y., and Huang, J. (2014). Characteristics of the Zooplankton communities in four typical wetlands of Macao. *J. Hydroecol.* 35, 24–30. doi: 10.15928/j.1674-3075.2014.06.004

Chen, L., Liu, Q., Peng, Z., Hu, Z., Xue, J., and Wang, W. (2011). The variation and analysis of rotifer community structure in and out of crab-net-pen closing in the Yangcheng Lake. *J. Fish. China* 35, 1247–1257. doi: 10.3724/SP.J.1231.2011.17365

Cheng, X. (2013). Flora of Hulan estuary wetlands nature reserve. *Prot. For. Sci. Technol.* 8, 14–17+19. doi: 10.13601/j.issn.1005-5215.2013.08.002

Claessens, M., and Prast, M. (2007). Concentration of fixed plankton samples via settling: How long is long enough? *J. Plankton Res.* 30, 57–64. doi: 10.1093/plankt/fbm095

Davidson, E. A., and Howarth, R. W. (2007). Environmental science: Nutrients in synergy. *Ecol. Lett.* 10, 1135–1142. doi: 10.1111/j.1461-0248.2007.01113.x

De Silva, M., and Jang, S. R. J. (2017). Dynamical behavior of systems of two phytoplankton and one zooplankton populations with toxin producing phytoplankton. *Math. Methods Appl. Sci.* 40, 4295–4309. doi: 10.1002/mma.4305

Easson, C. G., and Lopez, J. V. (2019). Depth-dependent environmental drivers of microbial plankton community structure in the Northern Gulf of Mexico. *Front. Microbiol.* 9:3175. doi: 10.3389/fmicb.2018.03175

Elton, C. S. (2020). *The ecology of invasions by animals and plants. Berlin*. Germany: Springer Nature.

Filstrup, C. T., Hillebrand, H., Heathcote, A. J., Harpole, W. S., and Downing, J. A. (2014). Cyanobacteria dominance influences resource use efficiency and community turnover in phytoplankton and zooplankton communities. *Ecol. Lett.* 17, 464–474. doi: 10.1111/ele.12246

Gao, Z., Xiao, R., Ren, A., and Zhao, W. (2015). Community structure and diversity of summer birds in Hulan River estuary wetland nature reserve, Heilongjiang Province. *Sichuan J. Zool.* 34, 285–289. doi: 10.3969/j.issn.1000-7083.2015.02.021

Guo, K., Peng, T., Luo, J., Yang, D., He, Y., and Chai, Y. (2017). Community structure of zooplankton and the driving physicochemical factors in Changhu Lake. *Oceanol. Limnol. Sin.* 48, 40–49. doi: 10.11693/hyhz20160700152

He, S., Ouyang, T., Zhao, L., Ji, L., Yang, S., Shi, J., et al. (2021). Analysis of phytoplankton community stability and influencing factors in a tributary of the three gorges reservoir. *Environ. Sci.* 42, 3242–3252. doi: 10.13227/j.hjkx.202012096

Hillebrand, H., Bennett, D. M., and Cadotte, M. W. (2008). Consequences of dominance: A review of evenness effects on local and regional ecosystem processes. *Ecology* 89, 1510–1520. doi: 10.1890/07-1053.1

Holling, S. C. (1973). Resilience and stability of ecological systems. *Annu. Rev. Ecol. Syst.* 4, 1–23. doi: 10.2307/2096802

Hu, S., Guo, Z., Li, T., Xu, C., Huang, H., Liu, S., et al. (2015). Molecular analysis of in situ diets of coral reef copepods: Evidence of terrestrial plant detritus as a food source in Sanya Bay, China. *J. Plankton Res.* 37, 363–371. doi: 10.1093/plankt/fbv014

Hu, H., and Wei, Y. (2006). *Freshwater Algae in China—System, Classification and Ecology*. Beijing, China: Science Press.

Hui, H., Ma, Y., and Fan, Y. (2011). Algae community structure and distribution in Hulanhe Wetland, Heilongjiang Province. *J. Lake Sci.* 23, 949–954. doi: 10.18307/2011.0618

Jagadeesan, L., Kumar, G. S., Rao, D. N., Babu, N. S., and And Srinivas, T. N. R. (2019). Role of eddies in structuring the mesozooplankton composition in coastal waters of the western Bay of Bengal. *Ecol. Indic.* 105, 137–155. doi: 10.1016/j.ecolind.2019.05.068

Jakobsen, H. H., Blanda, E., Staehr, P. A., Højgård, J. K., Rayner, T. A., Pedersen, M. F., et al. (2015). Development of phytoplankton communities: Implications of nutrient injections on phytoplankton composition, pH and ecosystem production. *J. Exp. Mar. Biol. Ecol.* 473, 81–89. doi: 10.1016/j.jembe.2015.08.011

Jeppesen, E., Nõges, P., Davidson, T. A., Haberman, J., Nõges, T., Blank, K., et al. (2011). Zooplankton as indicators in lakes: A scientific-based plea for including zooplankton in the ecological quality assessment of lakes according to the European Water Framework Directive (WFD). *Hydrobiologia* 676, 279–297. doi: 10.1007/s10750-011-0831-0

Jia, P., Fan, Y., and Lu, X. (2021). Analysis of phytoplankton structure based on different functional groups in Hulanhe Wetland. *Acta Ecol. Sin.* 41, 1042–1054. doi: 10.5846/stxb201911152444

Jonkers, L., Hillebrand, H., and Kucera, M. (2019). Global change drives modern plankton communities away from the pre-industrial state. *Nature* 570, 372–375. doi: 10.1038/s41586-019-1230-3

Ju, Y., Yu, H., Yu, T., Chai, F., Yao, Y., and Yu, P. (2017). Zooplankton community structure characters and water quality assessment in Harbin section of Songhua River. *J. Lake Sci.* 29, 646–653. doi: 10.18307/2017.0313

Juliana, D. S. S., Lúcia, D. S. A.-M. V., Enaide, M. D. M.-M., Maria, D. C. B.-O., and And Ariadne, D. N. M. (2016). Effects of zooplankton and nutrients on phytoplankton: An experimental analysis in a eutrophic tropical reservoir. *Mar. Freshw. Res.* 68, 1061–1069. doi: 10.1071/mf15393

Kim, S., Park, M. G., Moon, C., Shin, K., and Chang, M. (2007). Seasonal variations in phytoplankton growth and microzooplankton grazing in a temperate coastal embayment, Korea. *Estuar. Coast. Shelf Sci.* 71, 159–169. doi: 10.1016/j.ecss.2006.07.011

Kobayashi, T., Ralph, T. J., Ryder, D. S., Hunter, S. J., Shiel, R. J., and Segers, H. (2014). Spatial dissimilarities in plankton structure and function during flood pulses in a semi-arid floodplain wetland system. *Hydrobiologia* 747, 19–31. doi: 10.1007/s10750-014-2119-7

Li, Y., Chen, Y., Wang, L., Yao, L., Pan, X., and Lee, D. (2017). Pollution tolerant protozoa in polluted wetland. *Bioresour. Technol.* 240, 115–122. doi: 10.1016/j.biortech.2017.02.051

Liu, M. (2012). *The ecological monitoring and health assessment based on aquatic animals in Hulan estuary natural reserves and the surrounding waters*. Harbin: Northeast Forestry University.

Liu, H., and Dagg, M. (2003). Interactions between nutrients, phytoplankton growth, and micro- and mesozooplankton grazing in the plume of the Mississippi River. *Mar. Ecol. Prog. Ser.* 258, 31–42. doi: 10.3354/meps258031

Liu, Z., Liu, S., Tian, D., and Wang, D. (2021). Stability analysis of the plankton community with advection. *Chaos Solitons Fractals* 146:110836. doi: 10.1016/j.chaos.2021.110836

Liu, Q., Liu, Z., Wang, J., Liao, C., Li, J., Guo, C., et al. (2022). Spatial-temporal characteristics of zooplankton community structure and analysis for the impact factors in the Shanmei Reservoir, Fujian Province. *J. Lake Sci.* 34, 1–22. doi: 10.18307/2022.0619

Lu, X., Liu, Y., and Fan, Y. (2014). Relationships between environmental variables and seasonal succession in phytoplankton functional groups in the Hulan River Wetland. *Acta Ecol. Sin.* 34, 1264–1273. doi: 10.5846/stxb201306061369

Lu, X., Zhang, Y., Liu, Y., and Fan, Y. (2022). Differences in planktonic and benthic diatoms reflect water quality during a rainstorm event in the Songhua River Basin of Northeast China. *Ecol. Indic.* 144:109547. doi: 10.1016/j.ecolind.2022.109547

MacArthur, R. (1955). Fluctuations of animal populations and a measure of community stability. *Ecology* 36, 533–536. doi: 10.2307/1929601

Magnussen, S., and Boyle, T. (1995). Estimating sample size for inference about the Shannon-weaver and the Simpson indices of species diversity. *For. Ecol. Manag.* 78, 71–84. doi: 10.1016/0378-1127(95)03596-1

Manna, V., Fabbro, C., Cerino, F., Bazzaro, M., Del Negro, P., and Celussi, M. (2019). Effect of an extreme cold event on the metabolism of planktonic microbes in the northernmost basin of the Mediterranean Sea. *Estuar. Coast. Shelf Sci.* 225:106252. doi: 10.1016/j.ecss.2019.106252

Margalef, R. (1969). Abnormal expression of normal transferrin alleles in cattle. *Biochem. Genet.* 2, 371–382. doi: 10.1007/BF01458497

Matchett, E. L., and Fleskes, J. P. (2017). Projected impacts of climate, urbanization, water management, and wetland restoration on Waterbird habitat in California's Central Valley. *PLoS One* 12:e0169780. doi: 10.1371/journal.pone.0169780

Mcqueen, D. J., Johannes, M. R. S., and Post, J. R. (1989). Bottom-up and top-down impacts on freshwater pelagic community structure. *Ecology* 59, 289–309. doi: 10.2307/1942603

Min, W., Xiang, Y., Wang, X., Wang, W., Wang, X., Zeng, S., et al. (2019). Community structure and diversity of plankton in Wujiang River basin in autumn. *Guizhou Agric. Sci.* 47, 70–74. doi: 10.3969/j.issn.1001-3601.2019.07.016

Mougi, A. (2022). Predator interference and complexity-stability in food webs. *Sci. Rep.* 12:2464. doi: 10.1038/s41598-022-06524-w

Norberg, J., Swaney, D. P., Dushoff, J., Lin, J., Casagrandi, R., Levin, S. A., et al. (2001). Phenotypic diversity and ecosystem functioning in changing environments: A theoretical framework. *Proc. Natl. Acad. Sci. U. S. A.* 98, 11376–11381. doi: 10.1073/pnas.171315998

Pearce, D., and Butler, H. (2002). Short-term stability of the microbial community structure in a maritime Antarctic lake. *Polar Biol.* 25, 479–487. doi: 10.1007/s00300-002-0370-2

Pennekamp, F., Pontarp, M., Tabi, A., Altermatt, F., Alther, R., Choffat, Y., et al. (2018). Biodiversity increases and decreases ecosystem stability. *Nature* 563, 109–112. doi: 10.1038/s41586-018-0627-8

Pielou, E. C. (1966). The measurement of diversity in different types of biological collections. *J. Theor. Biol.* 13, 131–144. doi: 10.1016/0022-5193(66)90013-0

Porter, K. R. R. (1973). Selective grazing and differential digestion of algae by zooplankton. *Nature* 244, 179–180. doi: 10.1038/244179a0

Ptacnik, R., Solimini, A. G., Andersen, T., Tamminen, T., Brettum, P., Lepistö, L., et al. (2007). Diversity predicts stability and resource use efficiency in natural phytoplankton communities. *Proc. Natl. Acad. Sci. U. S. A.* 105, 5134–5138. doi: 10.1073/pnas.0708328105

Pulsifer, J., and Laws, E. (2021). Temperature dependence of freshwater phytoplankton growth rates and zooplankton grazing rates. *Water* 13:1591. doi: 10.3390/w13111591

Rana, A., Kobayashi, T., and Ralph, T. J. (2021). Planktonic metabolism and microbial carbon substrate utilization in response to inundation in semi-arid floodplain wetlands. *J. Geophys. Res. Biogeosci.* 126:e2019JG005571. doi: 10.1029/2019jg005571

Relyea, R. A. (2005). The impact of insecticides and herbicides on the biodiversity and productivity of aquatic communities. *Ecol. Appl.* 15, 618–627. doi: 10.1890/03-5342

Schaum, C. E., Rost, B., and Collins, S. (2016). Environmental stability affects phenotypic evolution in a globally distributed marine picoplankton. *ISME J.* 10, 75–84. doi: 10.1038/ismej.2015.102

Seilheimer, T. S., Mahoney, T. P., and Chow-Fraser, P. (2009). Comparative study of ecological indices for assessing human-induced disturbance in coastal wetlands of the Laurentian Great Lakes. *Ecol. Indic.* 9, 81–91. doi: 10.1016/j.ecolind.2008.02.001

Sennhauser, E. B. (1991). The concept of stability in connection with thegallery forests of the Chaco region. *Vegetatio* 94, 1–13. doi: 10.1007/bf00044911

Shan, T., Yuan, A., Huang, Z., Zhou, J., Lu, X., and Fan, Y. (2022). Characteristics of benthic diatom community structure and water ecological health evaluation in the Lalin River basin. *Environ. Sci.* 44, 266–275. doi: 10.13227/j.hjkx.202205168

Shen, J., Qin, G., Yu, R., Zhao, Y., Yang, J., An, S., et al. (2021). Urbanization has changed the distribution pattern of zooplankton species diversity and the structure of functional groups. *Ecol. Indic.* 120:106944. doi: 10.1016/j.ecolind.2020.106944

Shen, B., and Wang, S. (1991). A model of catching food in fishery ecology. *J. Dalian Ocean Univ.* 6s, 66–70. doi: 10.16535/j.cnki.dlhyxb.1991.01.011

Simpson, E. H. (1949). Measurement of diversity. *Nature* 163:688. doi: 10.1136/thx.27.2.261

Stelfox-Widdicombe, C. E., Archer, S. D., Burkill, P. H., and Stefels, J. (2004). Microzooplankton grazing in Phaeocystis and diatom-dominated waters in the southern North Sea in spring. *J. Sea Res.* 51, 37–51. doi: 10.1016/j.seares.2003.04.004

Tan, K. S., and Ransangan, J. (2017). Effects of nutrients and zooplankton on the phytoplankton community structure in Marudu Bay. *Estuar. Coast. Shelf Sci.* 194, 16–29. doi: 10.1016/j.ecss.2017.05.008

Tian, W. (2017). *Response mechanisms of Lake plankton community to environment and biodiversity*. Beijing, China: North China Electric Power University.

Tian, W., Zhang, H., Zhang, J., Zhao, L., Miao, M., and Huang, H. (2017). Biodiversity effects on resource use efficiency and community turnover of plankton in Lake Nansihu, China. *Environ. Sci. Pollut. Res. Int.* 24, 11279–11288. doi: 10.1007/s11356-017-8758-2

Tian, W., Zhang, H., Zhao, L., Xiong, Y., and Huang, H. (2016). Effects of environmental factors on the temporal stability of phytoplankton biomass in a eutrophic man-made Lake. *Water* 8:582. doi: 10.3390/w8120582

Tillmanns, A. E. W. O. S. A. R. (2006). Effects of cyanobacterial toxicity and morphology on the population growth of freshwater zooplankton: Meta-analyses of laboratory experiments. *Limnol. Oceanogr.* 51, 1915–1924. doi: 10.4319/lo.2006.51.4.1915

Tilman, D. (1999). The ecological consequences of changes in biodiversity: A search for general principles. *Ecology* 80, 1455–1474. doi: 10.1890/0012-9658(1999)080[1455:tecoci]2.0.co;2

Turner, J. T., Levinsen, H., Nielsen, T. G., and Hansen, B. (2001). Zooplankton feeding ecology: Grazing on phytoplankton and predation on protozoans by copepod and barnacle nauplii in Disko Bay, West Greenland. *Mar. Ecol. Prog. Ser.* 221, 209–219. doi: 10.3354/meps221209

Vanni, M. J., and Temte, J. (1990). Seasonal patterns of grazing and nutrient limitation of phytoplankton in a eutrophic lake. *Limnol. Oceanogr.* 35, 697–709. doi: 10.4319/lo.1990.35.3.0697

Villéger, S., Fouilland, E., Argenty, J., Bouvier, C., Carré, C., and Bouvier, T. (2019). Interspecific differences in the effect of fish on marine microbial plankton. *Aquat. Microb. Ecol.* 82, 289–298. doi: 10.3354/ame01897

Wang, J. (1961). *China freshwater rotifer*. Beijing, China: Science Press.

Wang, H., Hou, W., Ma, C., Yu, H., Gao, J., Bai, R., et al. (2017). Distribution of Zooplankton in Genheyuan National Wetland Park. *Wetland Sci.* 15, 99–106. doi: 10.13248/j.cnki.wetlandsci.2017.01.015

Wang, H., Huang, X., Wu, J., Du, X., Wang, Q., Song, D., et al. (2019). Effect of agricultural non-point source pollution on plankton and Zoobenthos communities in a reservoir in Morin Dawa Daur autonomous banner. *Chinese J. Fish.* 32, 55–62.

Wang, Y., Qiu, G., Chen, S., and Hu, S. (2012). Research on plankton community in three gorges reservoir during its trial impoundment. *Yangtze River* 43, 4–9. doi: 10.16232/j.cnki.1001-4179.2012.12.027

Wittebolle, L., Marzorati, M., Clement, L., Balloi, A., Daffonchio, D., Heylen, K., et al. (2009). Initial community evenness favours functionality under selective stress. *Nature* 458, 623–626. doi: 10.1038/nature07840

Xia, Y. P., Zhou, W. S., and Yang, Z. C. (2020). Global analysis and optimal harvesting for a hybrid stochastic phytoplankton-zooplankton-fish model with distributed delays. *Math. Biosci. Eng.* 17, 6149–6180. doi: 10.3934/mbe.2020326

Xing, C. (2016). Protection strategy of Hulan Estuary National Wetland Park in Harbin. *J. Green Sci. Technol.* 2, 33–34. doi: 10.16663/j.cnki.lskj.2016.02.013

Yang, L. (2012). *Zooplankton community structure and its relation to environment factors in Qiandao Lake*. Shanghai: Shanghai Ocean University.

Yang, X., Ma, J., Zhang, H., and Zhou, Q. (2021). Community structure and the water quality during different hydrological periods in poyang lake. *Acta Hydrobiol. Sin.* 45, 1093–1103. doi: 10.7541/2021.2020.148

Zhang, Z., and Hang, X. (1991). *Freshwater plankton research methods*. Beijing, China: Science Press.

Zhang, Y., Jin, R., Zhu, W., Zhang, D., and Zhang, X. (2020). Impacts of land use changes on wetland ecosystem services in the Tumen River Basin. *Sustainability* 12:9821. doi: 10.3390/su12239821

Zhang, X., and Li, C. (2016). Analysis of phytoplankton community characteristics and its influencing factors in Tanghe reservoir. *Environ. Sci. Technol.* 39, 394–401. doi: 10.3969/j.issn.1003-6504.2016.S2.078

Zhang, X., Liu, K., Wan, A., Chen, M., Liu, Z., Lian, Y., et al. (2018). Community structure of zooplankton and its relationship with survivability of the yangtze finless porpoise in xijiang oxbow, Anqing city. *Acta Hydrobiol. Sin.* 42, 392–399. doi: 10.7541/2018.050

Zhang, N., Liu, Y., and Zang, S. (2016). Relationships between phytoplankton community in different functional regions and environmental factors in Zhalong Wetland, Heilongjiang Province. *J. Lake Sci.* 28, 554–565. doi: 10.18307/2016.0311

Zhang, M., Shi, X., Chen, F., Yang, Z., and Yu, Y. (2021). The underlying causes and effects of phytoplankton seasonal turnover on resource use efficiency in freshwater lakes. *Ecol. Evol.* 11, 8897–8909. doi: 10.1002/ece3.7724

Zhang, H., Zhao, L., Tian, W., and Huang, H. (2016). Stability of food webs to biodiversity loss: Comparing the roles of biomass and node degree. *Ecol. Indic.* 67, 723–729. doi: 10.1016/j.ecolind.2016.03.045

Zheng, Y. (2019). *Research on the effects of plankton species diversity on community productivity and stability*. Beijing, China: North China Electric Power University.

Zheng, B., Chen, Z., Li, Y., Fohrer, N., Zhang, Y., Wu, D., et al. (2020). Structural characteristics and driving factors of the planktonic eukaryotic community in the Danjiangkou Reservoir, China. *Water* 12:3499. doi: 10.3390/w12123499

Zheng, Y., Wang, X., Xiong, J., Liu, Y., and Zhao, Y. (2014). Hybrid constructed wetlands for highly polluted river water treatment and comparison of surface- and subsurface-flow cells. *J. Environ. Sci.* 26, 749–756. doi: 10.1016/s1001-0742(13)60482-9

Zhou, F., and Chen, J. (2011). *Freshwater microorganisms and Zoobenthos atlas. 2nd Edn*. Beijing, China: Chemical Industry Publishing House.

Zhu, W., Pang, W., You, Q., and Wang, Q. (2017). Phytoplankton community structure and the evaluation of water quality in spring, Huaihe River Basin. *J. Lake Sci.* 29, 637–645. doi: 10.18307/2017.0312

Zhu, Y., Xu, H., Zhang, S., Liang, C., Li, M., Yu, Z., et al. (2022). Spatio-temporal changes of phytoplankton communities and their correlation with environmental factors in Kulipao Lake, Daqing City. *Environ. Monit. China* 38, 104–117. doi: 10.19316/j.issn.1002-6002.2022.04.11

frontiers | Frontiers in Ecology and Evolution

TYPE Original Research
PUBLISHED 30 March 2023
DOI 10.3389/fevo.2023.1123645

OPEN ACCESS

EDITED BY
Xiaodong Zhang,
Chinese Academy of Forestry, China

REVIEWED BY
Meng Li,
Nantong University, China
Ming Jiang,
Northeast Institute of Geography and Agroecology (CAS), China
Liang Yan,
Institute of Ecological Conservation and Restoration, Chinese Academy of Forestry, China

*CORRESPONDENCE
Zhizhong Zhao
✉ 1989990003@qhu.edu.cn

SPECIALTY SECTION
This article was submitted to Population, Community, and Ecosystem Dynamics, a section of the journal Frontiers in Ecology and Evolution

RECEIVED 14 December 2022
ACCEPTED 14 March 2023
PUBLISHED 30 March 2023

CITATION
Feng X, Zhao Z, Ma T and Hu B (2023) A study of the effects of climate change and human activities on NPP of marsh wetland vegetation in the Yellow River source region between 2000 and 2020.
Front. Ecol. Evol. 11:1123645.
doi: 10.3389/fevo.2023.1123645

A study of the effects of climate change and human activities on NPP of marsh wetland vegetation in the Yellow River source region between 2000 and 2020

Xueke Feng[1], Zhizhong Zhao[1,2]*, Tao Ma[1] and Bixia Hu[1]

[1]College of Agriculture and Animal Husbandry, Qinghai University, Xining, China, [2]College of Ecological and Environment Science, Xining University, Xining, China

Quantitative assessment of the impacts of climate change and human activities on marsh wetland is essential for the sustainable development of marsh wetland ecosystem. This study takes the marsh wetland in the Yellow River source region (YRSR) as the research object, using the method of residual analysis, the potential net primary productivity (NPPp) of marsh wetland vegetation in the YRSR between 2000 and 2020 was stimulated using the Zhou Guangsheng model, and the actual primary productivity (NPPa) of marsh wetland vegetation was download from MOD17A3HGF product, and the difference between them was employed to calculate the NPP affected by human activities, the relative contribution of climate change and human activities to the change of NPPa of marsh wetland vegetation was quantitatively evaluated. The results revealed that between 2000 and 2020, NPPa of marsh wetland vegetation increased in the YRSR by 95.76%, among which climate-dominated and human-dominated NPP change occupied by 66.29% and 29.47% of study areas, respectively. The Zoige Plateau in the southeast accounted for the majority of the 4.24% decline in the NPPa of the marsh wetland vegetation, almost all of which were affected by human activities. It is found that the warming and humidifying of climate, as well as human protective construction activities, are the important reasons for the increase of NPPa of marsh wetland vegetation in the YRSR. Although climate change remains an important cause of the increase in NPPa of marsh wetland vegetation, the contribution of human activities to the increase in NPPa of marsh wetland vegetation is increasing.

KEYWORDS

marsh wetland, climate variation, human activities, quantitative assessment, vegetation NPP

1. Introduction

Typical alpine marsh wetland with the highest altitude in the world are distributed in the YRSR (Xue et al., 2018; Hou et al., 2020; Wang et al., 2020). These wetlands perform a variety of ecological functions, including carbon fixation and oxygen release, water conservation, climate regulation, and biodiversity maintenance (Yan et al., 2017); they have a significant impact on the sustainable development of society, economy, ecology, and water resources in the whole Yellow River basin (Dong et al., 2020; Qiu et al., 2021). However, the ecological environment in this region is fragile and sensitive to climate change (Tang and Lin, 2021). Since 1950, the Qinghai-Tibet Plateau has experienced significantly warming, which has led to the accelerated degradation of permafrost, reduced solid water reserves, and increased precipitation (Zhao et al., 2020; Zhang Q. et al., 2022), which makes the stability of the marsh wetland ecosystem in the YRSR worse; simultaneously, human activities, such as overgrazing, expansion of construction land, and peat mining have intensified (Liu et al., 2019; Pan et al., 2020); the marsh wetland in the YRSR have been degraded to varying degrees, with serious landscape fragmentation and decreased species diversity, posing a serious threat to the aquatic ecological function, frozen soil, and ecological environment in this area (Xiang et al., 2009; Li et al., 2018). With the strengthening of ecological environment protection and the regulation of relevant policies, the Chinese government has implemented a series of ecological protection and restoration projects since 2000, including turning grazing land back to green and establishing the Sanjiangyuan National Ecological Protection Area, especially the construction of the Yellow River Source National Park, which has improved the ecological environment in the YRSR (Du et al., 2015; Shao et al., 2017; Ma et al., 2022). However, the exact mechanism of the change in marsh wetland in the YRSR is still unknown because of the mutual interference and interaction between climate change and human activities. Therefore, it is necessary to quantitatively analyze the underlying mechanisms of marsh wetland change in the YRSR, quantify the relative contributions of climate change and human activities to marsh wetland change, and further guide the scientific protection and sustainable development of marsh wetland in the YRSR.

Net primary productivity, a crucial representation of ecosystem functioning, is the difference between the total quantity of organic matter that vegetation accumulates through photosynthesis over time and the cumulative respiration per unit of time (Yan, 2022). The NPP of vegetation also reveals obvious variability owing to the influence of climate change and human activities (Cloern et al., 2021). Numerous studies have estimated the difference between NPPp and NPPa of vegetation to represent the influence of human activities on vegetation change (NPPh), quantitatively evaluated the relative contributions of climate change and human activities to various changes in land cover (Yin et al., 2020). For instance, Xie et al. (2022) explained the relative contribution of climate change and human activities to desertification reversal in Mu Us Sandy Land in northern China by employing meteorological data and MODIS NPP products whose results revealed that human activities were the leading factors of desertification reversal in different periods; Zhang F. et al. (2022) quantitatively assessed the relative contributions of climate change and human activities to grassland NPP based on the changes of grassland NPP in the YRSR, and revealed that the contribution of human activities to the restoration of grassland is increasing; Li et al. (2021) examined the relative effects of climate change and human activities on the productivity of various vegetation in Northeast China, and found that human activities resulted in 53.84% reduced NPP in deciduous coniferous forests. Although there are lots of studies have quantified the impacts of climate change and human activities on vegetation changes on the Tibetan Plateau, most of them focus on grassland or forest ecosystems (Shen et al., 2022; Wang Y. F. et al., 2022). Until recently, the research on wetland ecosystems is scarce (Mao et al., 2014; Yan et al., 2022). The marsh ecosystem has unique environmental conditions, which may lead to obvious differences in the response of marsh wetland vegetation to climate change and human activities compared with other ecosystems (Shen et al., 2022). Climate change and human activities, as well as the degradation of marsh wetland habitat quality and the changes in marsh wetland plant communities, exhibit significant effects on the NPP of marsh wetland vegetation; therefore, the relative effects of climate change and human activities on marsh wetland vegetation could be quantitatively assessed by quantifying NPP of marsh wetland vegetation (Mao et al., 2014). It is crucial for the protection and management of alpine marsh wetland and even for global marsh changes.

In this process, the key to quantifying the NPP of marsh wetland vegetation is the accurate estimation of NPPp. NPPp reflects the effects of light, temperature, and water on the productivity of vegetation. NPPp is generally estimated by employing a climate-driven model. One of the reasonable models to estimate the global distribution of vegetation NPPp is the Miami model, which is a fitting model based on the correlation between measured data at stations and annual precipitation and annual average temperature (Lieth, 1975). However, vegetation NPPp is influenced by other climatic variables in addition to temperature and precipitation, Therefore, based on Miami model, Thornthwaite Memorial model considers actual evapotranspiration, while Chikugo model considers plant physiology and ecology, and uses parameters such as net radiation and radiation dryness, which is a semi-empirical and semi-theoretical NPP estimation model (Wang J. Y. et al., 2015). However, the climate-related models such as Miami model and Thornthwaite Memorial model were originally established by statistical regression between climate conditions and measured NPP, and the model parameters may need to be adjusted when applied to specific areas (Sun et al., 2017). Zhou Guangsheng model is based on the water utilization efficiency of vegetation which is determined by the ratio of the carbon dioxide flux equation (equivalent to NPP) to the water vapor flux equation (equivalent to evapotranspiration) on the surface of vegetation. According to the precipitation in China and the net radiation data obtained from the physical process of the influence of energy and water on evaporation, a regional evapotranspiration model corresponding to the energy balance equation and water balance equation has been derived, and a net primary productivity model of natural vegetation based on plant physiological and ecological characteristics has been established, which could help better represent the characteristics of vegetation in China (Zhou and Zhang, 1996; Chen et al., 2015).

Therefore, this study uses the marsh wetland in the YRSR as the research object, the NPPp of marsh wetland vegetation in the YRSR between 2000 and 2020 was stimulated using the Zhou

Guangsheng model, and the NPPa of marsh wetland vegetation was download from MOD17A3HGF product, and to estimate the NPPh of marsh wetland vegetation by the difference between NPPp and NPPa. The main purpose of this study is to: (1) estimate and analyze the temporal and spatial distribution trends of NPPp, NPPa, and NPPh of marsh wetland vegetation in the YRSR between 2000 and 2020; (2) discuss the response of NPP of marsh wetland vegetation to climate change and human activities based on the temporal and spatial changes of climate factors and human factors of marsh wetland in the YRSR between 2000 and 2020; and (3) evaluate quantitatively the relative contribution of climate change and human activities to NPP change of marsh wetland vegetation in the YRSR between 2000 and 2020. The results of this research could serve as a theoretical and methodological foundation for the formulation of wetland management policies in this region and have various implications for further guiding the scientific protection and sustainable development of wetland resources in the YRSR.

2. Materials and methods

2.1. Study area

The YRSR is located on the eastern edge of the Qinghai-Tibet Plateau, which is defined as the basin above the Tangnaihai Hydrological Station. It comprises a total area of 12.21 km^2 (95.9°E∼103.4°E, 32.2°N∼36.1°N) (**Figure 1**), accounting for 16.29% of the Yellow River basin area (Tang and Lin, 2021; Mo et al., 2022). According to the Köppen climate classification, the YRSR has a subarctic climate that is influenced by the monsoon and tundra climate with extreme seasonal precipitation, strong evaporation, and strong solar radiation. The YRSR is rainy, accompanied by short-term strong convection between July and September every year during the summer season, which is affected by the southwest monsoon in South Asia and Southeast Asia, and gradually becomes dry and cold between October and December during the winter season which is affected by the cold and high pressure of the Qinghai-Tibet Plateau (Yuan et al., 2020). The YRSR possesses complex landforms and diverse landscapes. The terrain is typically high in the central and western regions and low in the northeast and southeast, with an altitude drop of approximately 3800 m and an average altitude of over 4000 m. The western part is separated from the Jinsha River by the Bayan Har Mountains, while the northern part is the Animaqing Mountain, covered with glacier snow the majority of the year. Wetland is one of the primary ecosystems in the YRSR, including river, lake, marsh, and artificial wetland, in which the marsh wetland accounts for 82.36% of the total wetland area in the YRSR. The vegetation dominated by herbaceous marsh vegetation and aquatic vegetation, and the main species of marsh plants are *Carex pseudosupina*, *Poa attenuata*, and *Kobresia tibetica*, etc. (Liu et al., 2021).

2.2. Data

The data employed in this study include marsh wetland distribution data, NPPa remote sensing data, and temperature and precipitation data. The marsh distribution data is the 2015 China marsh wetland spatial distribution dataset obtained from the National Science and Technology Basic Platform-National Earth System Science Data Center.[1] The data were classified using Landsat-8 OLI remote sensing images with a spatial resolution of 30 m. The decision tree method was used to classify the wetland objects step by step, and the classification results were checked and corrected by merging them with a large number of field survey samples. The classification accuracy was 95% (Mao et al., 2020).

The remote sensing image data of NPPa was obtained from the MOD17A3HGF product, which was a MODIS image with a spatial resolution of 500 m. The NPP was synthesized by calculating the net photosynthesis (PSN) every 8 days, which was the difference between the total primary productivity and the respiratory maintenance value. The annual total as the NPPa data between 2000 and 2020 was calculated using Google Earth Engine (GEE) platform to calculate,[2] which finally covers the marsh wetland in the YRSR.

The meteorological data, including temperature and precipitation data, were obtained from the National Earth System Science Data Center, National Science and Technology Infrastructure of China (see text footnote 1). This dataset was based on the Global 0.5° climate data released by Climatic Research Unit (CRU) and the global high-resolution climate data released by WorldClim. It was obtained through delta spatial downscaling and verified by 496 independent meteorological observation points, with a spatial resolution of 1 km (Peng et al., 2019). ArcGIS V10.8 (developed by Environmental Systems Research Institute, Inc., Redlands, CA, USA) was employed to calculate the average annual temperature and annual precipitation of the marsh wetland in the YRSR between 2000 and 2020.

The data of human activities are mainly the statistics of the number of livestock and population at the county level in the study area from 2000 to 2020, which comes from the Statistical Yearbook[3] of each county. In order to unify the expression, the conversion coefficient is used to convert different livestock into standard sheep units, and the conversion coefficient refers to the Calculation of Proper Carrying Capacity of Rangelands in the Agricultural Industry Standard of China.

To facilitate the unified data processing, ArcMap V10.8 software was used to reprogram the aforementioned data to the WGS-84 coordinate system, and the spatial resolution was resampled to 30 m.

2.3. Methods

2.3.1. Mann-Kendall (MK) test

Mann-Kendall test, as a non-parametric statistical method to detect the trend of variables, has been widely used to study the abrupt change and trend change characteristics of time series of climatic and hydrological elements, such as temperature, precipitation, and runoff, as well as their grid-scale spatio-temporal

1 http://www.geodata.cn (accessed October 2, 2022).

2 https://developers.google.cn/earth-engine/datasets/catalog/MODIS_006_MOD17A3HGF (accessed October 2, 2022).

3 https://data.cnki.net/ (accessed October 2, 2022).

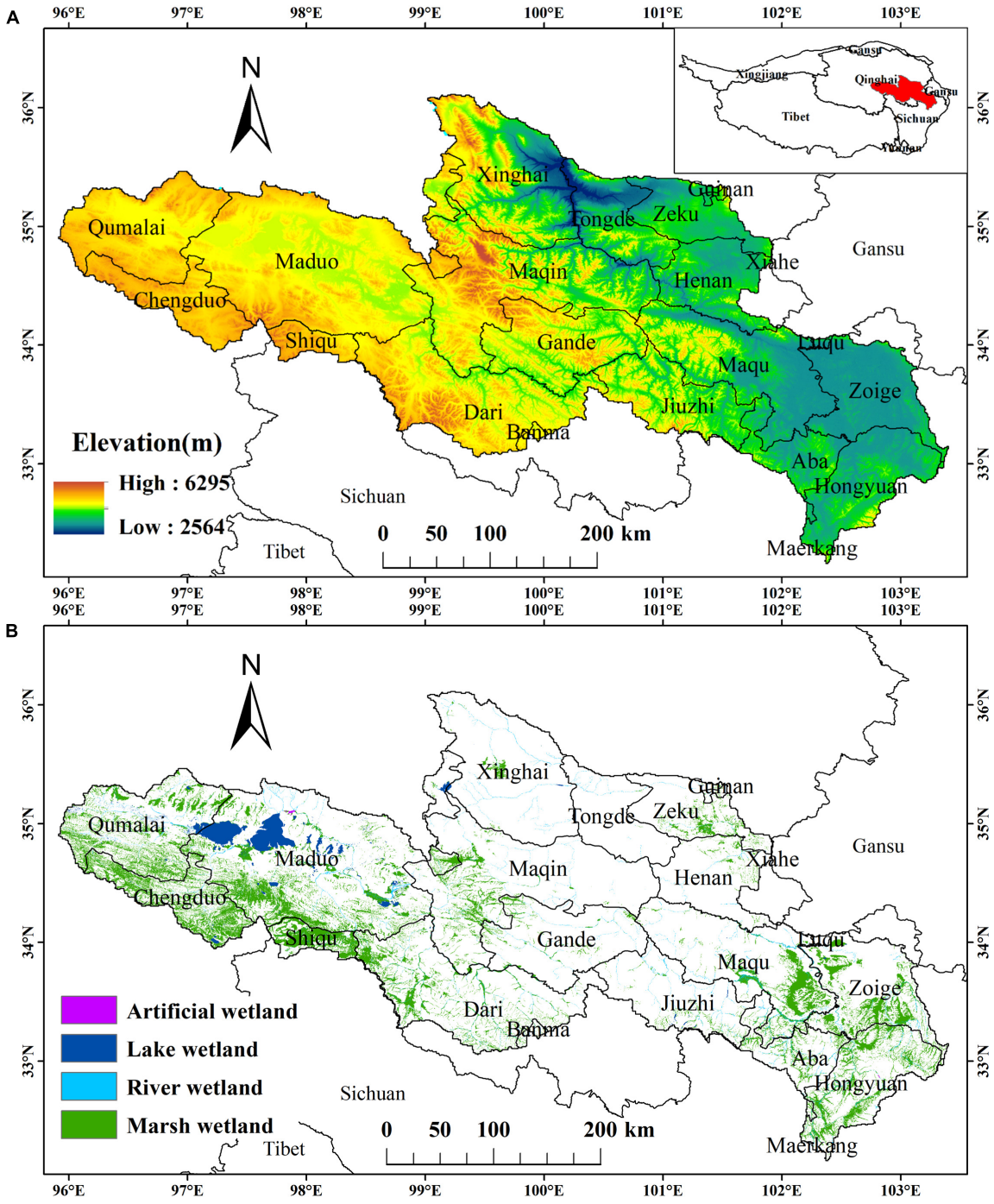

FIGURE 1
(A) The location and elevation of the YRSR. **(B)** Spatial distribution of wetland in the YRSR.

TABLE 1 Different categories of driving factors for NPPa changes.

Categories	Driving factors for NPPa changes
Slope NPPa $\geq$ 0 and Slope NPPp > Slope NPPh	NPPa increased owing to climate factors
Slope NPPa $\geq$ 0 and Slope NPPp < Slope NPPh	NPPa increased owing to anthropogenic activities
Slope NPPa < 0 and Slope NPPp > Slope NPPh	NPPa decreased owing to climate factors
Slope NPPa < 0 and Slope NPPp < Slope NPPh	NPPa decreased owing to anthropogenic activities

The contribution rate analysis of this research was realized by ArcMap V10.8.

data. Its advantage is that it does not require samples to follow a certain distribution, and it is unaffected by a few outliers. It is more suitable for type and order variables. In this study, it is used to estimate the changing trend of climate factors and NPP of marsh wetland in the YRSR between 2000 and 2020. The following formula was used to calculate the MK test (Gao and Jin, 2022; Ogunsola and Dilau, 2022):

$$Z_s = \begin{cases} \frac{S-1}{\sqrt{Var(S)}}, if\ S > 0 \\ 0, if\ S = 0 \\ \frac{S+1}{\sqrt{Var(S)}}, if\ S < 0 \end{cases} \quad (1)$$

$$S = \sum_{i=1}^{n-1} \sum_{j=i+1}^{n} sgn\left(X_j - X_i\right) \quad (2)$$

$$Var\left(S\right) = \frac{n\left(n-1\right)\left(2n+5\right)}{18} \quad (3)$$

$$sgn\left(X_j - X_i\right) = \begin{cases} 1, X_j - X_i > 0 \\ 0, X_j - X_i = 0 \\ -1, X_j - X_i < 0 \end{cases} \quad (4)$$

where n represents the length of the time series, and i is 2000, 2001,..., 2020, and S is the test statistic, and Var(S) is the variance of S, and sgn (X_j-X_i) is a symbolic function, the value is 1, 0 or −1. Zs is MK test statistics, Under a given significance level α, when | Zs| > $u_{1-\alpha/2}$, the time series data of the study were at α level. Significant changes were generally taken as α = 0.05. When | Zs| > 1.96, the time series had a significance α < 0.05, and | Zs| < 1.96 denotes significance α > 0.05. The MK text of this study was implemented by Rstudio-2022.07.2−576 (developed by Delaware Public Benefit Corporation, Boston, MA, USA).

2.3.2. Estimating NPP

In this study, the NPPp of wetland vegetation in the YRSR was calculated employing the Zhou Guangsheng model, and the difference between NPPp and NPPa was estimated to represent NPPh. Zhou Guangsheng's model is as follows (Zhou and Zhang, 1996):

$$NPPp = RDI^2 \times \frac{P \times (1+RDI+RDI^2)}{(1+RDI)(1+RDI^2)} \times Exp\left(-\sqrt{9.87+6.25RDI}\right) \quad (5)$$

$$RDI = \left(0.629+0.237PER-0.00313PER^2\right)^2 \quad (6)$$

$$PER = \frac{BT \times 58.93}{P} \quad (7)$$

$$BT = \frac{\sum T}{12} \quad (8)$$

Where NPPp represents the potential net primary productivity and RDI the radiation index of dryness. P denotes the annual precipitation (mm), PER the potential evapotranspiration rate, BT the annual average temperature (°C), and T the monthly mean temperature (°C).

The formula for calculating NPPh is as follows:

$$NPP_h = NPP_p - NPP_a \quad (9)$$

Where NPPh represents the net primary productivity affected by human activities, with NPPh > 0 indicating that NPP is decreased by human activities; NPPp is the potential net primary productivity, calculated by the formula (5); NPPa is the actual net primary productivity obtained from the annual synthetic data of MOD17A3HGF. Estimation of NPP was performed using ArcMap V10.8 and Envi V5.3 (produced by Exelis Visual Information Solutions).

2.3.3. Slope of marsh wetland NPP and climate factors

In each marsh wetland pixel in the study area, slope trend analysis was employed to determine the changing trend of vegetation NPP and climate factors between 2000 and 2020. The calculation formula is as follows (Ma et al., 2022; Yan et al., 2022):

$$Slope = \frac{n \times \sum_{i=1}^{n}(X \times i) - \sum_{i=1}^{n} X \sum_{i=1}^{n} i}{n \times \sum_{i=1}^{n} i^2 - \left(\sum_{i=1}^{n} i\right)^2} \quad (10)$$

Where Slope is the changing trend between 2000 and 2020, X is the vegetation NPP (NPPp, NPPa, and NPPh) or climate factors (temperature and precipitation) in the i-th year, and i = 1, 2, 3, . . ., 20. n represents the time between 2000 and 2020. Slope > 0 denotes an increasing trend, while Slope0 denotes a decreasing trend. The slope analysis of this study was based on ArcMap V10.8.

2.3.4. Correlation analysis

To further analyze the relationship between climate change and NPP change in wetland vegetation, this study measured the correlation between climate factors and NPP change in wetland vegetation based on the correlation coefficient, which was calculated as follows (Shen et al., 2019):

$$r = \frac{\sum_{i=1}^{n}\left(x_i - \overline{x}\right)\left(y_i - \overline{y}\right)}{\sqrt{\sum_{i=1}^{n}\left(x_i - \overline{x}\right)^2 \sum_{i=1}^{n}\left(y_i - \overline{y}\right)^2}} \quad (11)$$

Where r is the correlation coefficient; n = 21, representing the time span between 2000 and 2020; x_i is the NPP value of the i-th year, y_i is the climate value (temperature or precipitation) of the i-th year, and $\overline{x}$ is the average annual NPP value, $\overline{y}$ is the multi-year climatic average. The Correlation analysis of this research is realized by Matlab R2016b (developed by the Mathworks, Inc., Natick, MA, USA).

2.3.5. Contribution rate analysis

The contribution rate analysis was employed to clarify the relative contributions of climate factors and human activities to NPP changes of marsh wetland vegetation in the YRSR. The reasons for NPP changes were examined in accordance with the slope changes of NPPp, NPPa, and NPPh of marsh wetland vegetation, as depicted in the following **Table 1** (Xu et al., 2010).

3. Results

3.1. Climate change in the YRSR between 2000 and 2020

According to the change analysis of climatic factors of marsh wetland in the YRSR between 2000 and 2020 (**Figure 2**), the

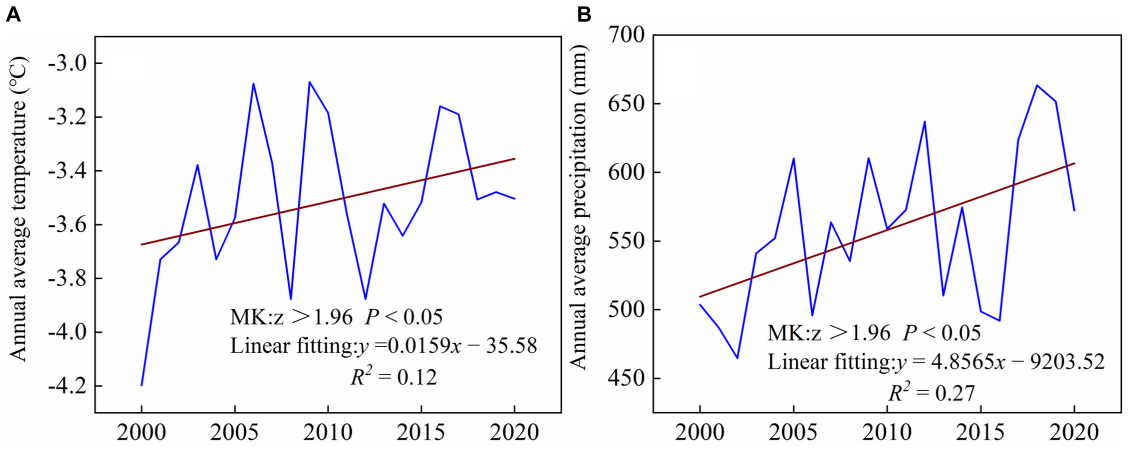

FIGURE 2
Variations in climate factors of marsh wetland in the YRSR between 2000 and 2020. **(A)** The annual variation in average annual average temperature. **(B)** The interannual variation in annual precipitation.

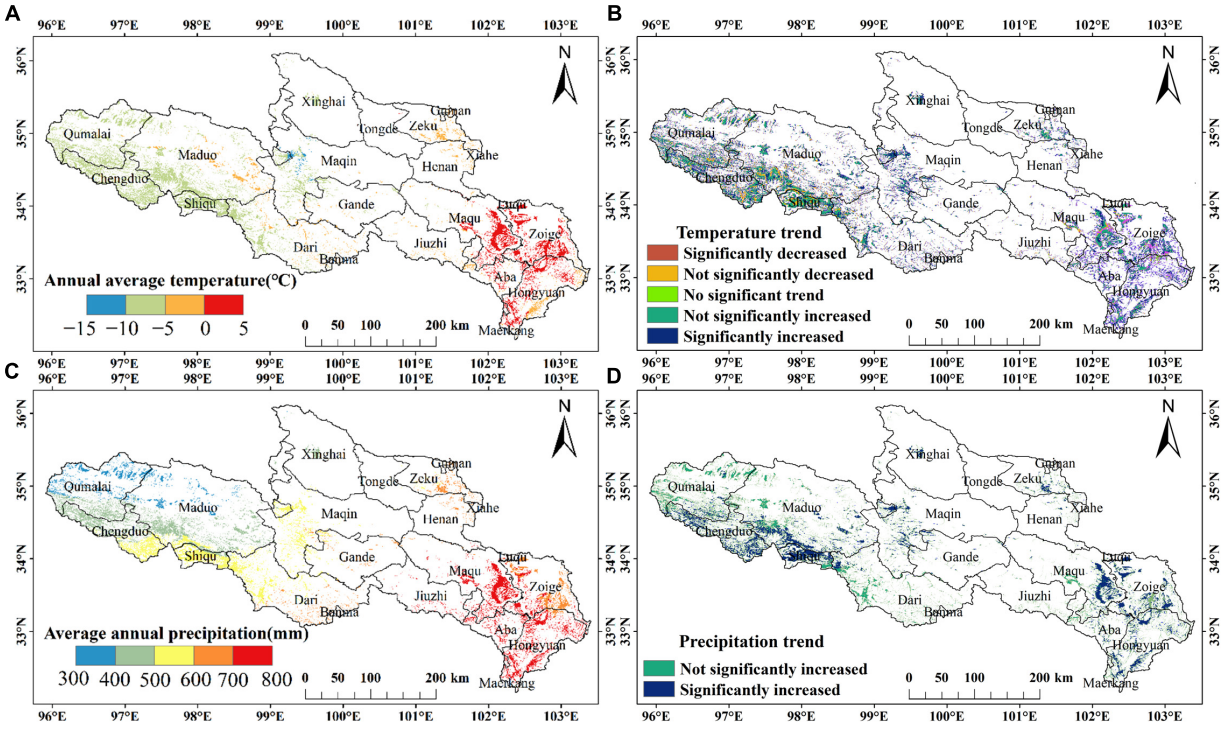

FIGURE 3
Spatial distribution in climate factors of marsh wetland in the YRSR between 2000 and 2020. **(A)** Average annual temperature. **(B)** Average annual temperature changing trend. **(C)** Average annual precipitation. **(D)** Average annual precipitation changing trend.

average annual temperature of marsh wetland in the YRSR was −3.51°C, with a minimum temperature of −4.20°C (in 2000) and a maximum temperature of −3.07°C (in 2009). The overall fluctuation of the annual average temperature displayed an insignificant upward trend (z-score > 1.96, *P*-value < 0.05). The average temperature increase rate in 21 years was 0.16°C/10a in accordance with the linear fitting equation. Between 2000 and 2020, the average annual precipitation of marsh wetland in the YRSR was 558.03 mm, with a minimum precipitation of 464.73 mm (in 2002) and a maximum precipitation of 663.35 mm (in 2018). The overall fluctuation of the average annual precipitation displayed an insignificant upward trend (z-score > 1.96, *P*-value < 0.05). The average precipitation increase rate in 21 years was 48.57 mm/10a in accordance with the linear fitting equation.

The average annual temperature of marsh wetland in the YRSR exhibited apparent spatial heterogeneity over the last 21 years according to the spatial distribution (Figure 3). The temperature centered on Mount Animaqing in the central region and increased to the periphery. The temperature revealed a decreasing trend from southeast to northwest, with higher temperatures in the

north and southeast regions and lower temperatures in the central and western regions. Overall, 83.64% of the regional temperatures exhibited an increasing trend. The spatial heterogeneity of the average annual precipitation of marsh wetland in the YRSR was apparent, exhibiting a decreasing trend from east to west. In contrast to the southeast, the precipitation in the northwest was lower. The variation trend of precipitation was consistent with the spatial distribution of precipitation, and the increment of precipitation decreased from east to west. Overall, between 2000 and 2020, the marsh wetland in the YRSR exhibited a warming and humidifying trend.

3.2. Human activities in the YRSR between 2000 and 2020

The population in the YRSR increased from 42.40×10^4 in 2000 to 56.94×10^4 in 2020, with an increase of 34.29%. The number of livestock increased from 1297.50×10^4 in 2000 to 1392.90×10^4 in 2020, with an increase of 7.35% (Figure 4). The number of livestock units per person decreased from 30.60 to 24.46, with a decrease of 25.10%. From 2000 to 2020, the population of the counties in the YRSR generally showed an increasing trend, among which Maqin County, Maqu County and Gande County increased the most; 52.87% of the areas in the YRSR have increased the number of livestock, mainly distributed in the Zoige Plateau in the southeast of the YRSR, while the decreased areas were mainly distributed in Maqin County, Gande county and Maduo county in the middle and west of the YRSR; 76.01% of the areas in the YRSR have decreased the number of livestock units per person, mainly distributed in Maqin County, Gande County and Maduo County in the middle and south of the YRSR, while the number of livestock units per person in Aba County, Hongyuan County and Zoige County in the southeast of the YRSR has increased.

3.3. NPP changes of marsh wetland vegetation in the YRSR between 2000 and 2020

Between 2000 and 2020, NPPp and NPPa of marsh wetland vegetation in the YRSR exhibited a consistently increasing trend, while NPPh exhibited a decreasing trend (negative value indicates that human activities have a positive impact on NPP increase) (Figure 5). Among them, NPPp was the lowest in 2002, at 63.21 gC/m^2, and the highest in 2018, at 101.93 gC/m^2, with a multi-year average of 82.23 gC/m^2; the NPPa was the lowest in 2003, at 201.75 gC/m^2, and the highest in 2006 at 252.71 gC/m^2, with a multi-year average of 224.53 gC/m^2; the NPPh was the lowest in 2006, at −178.00 gC/m^2, and the highest in 2003, at −120.86 gC/m^2, with a multi-year average of −143.36 gC/m^2. Overall, between 2000 and 2020, the NPPp of marsh wetland vegetation in the YRSR was smaller in comparison to NPPa, and the NPP of marsh wetland vegetation in the YRSR was supplemented by human activities and exhibited an increasing trend, which demonstrated that human activities had a positive effect on the NPP of marsh wetland vegetation in the YRSR.

According to the spatial distribution (Figure 6), between 2000 and 2020, NPPp of the marsh wetland vegetation in the YRSR had the same spatial heterogeneity as NPPa, exhibiting the spatial characteristics of the decreasing trend from southeast to northwest, while NPPh exhibiting the spatial characteristics of the increasing trend from southeast to northwest. According to slope analysis, the average NPPp of marsh wetland vegetation in the YRSR increased by 1.05 gC/m^{2}a between 2000 and 2020, accounting for 100% of the increased area, and the increase rate in the southeast region of the YRSR was significantly higher in comparison to that in the northwest region. NPPa increased by 1.21 gC/m^{2}a on average, accounting for 95.79% of the increased area, and the decreased area was primarily distributed in the Zoige Plateau. The average decrease of NPPh was 0.25 gC/m^{2}a, and the decreased area accounted for 67.18%; the increased area was concentrated in the Zoige Plateau, located in the southeast of the YRSR. In general, the NPP of marsh wetland vegetation in the YRSR was increasing, and NPPp exhibited a similar spatial distribution pattern to NPPa but was considerably different from NPPh. In comparison to the changing trend of NPP of marsh wetland vegetation in the YRSR, the increase of NPPa was greater than NPPp, which demonstrated that human activities have a positive impact on the NPP of marsh wetland vegetation. However, the area where NPPa decreases was approximately the same as where NPPh increases, primarily distributed in the Zoige Plateau located in the southeast of the YRSR, which indicated that there is an adverse impact of human activities in this region on the NPP of marsh wetland vegetation.

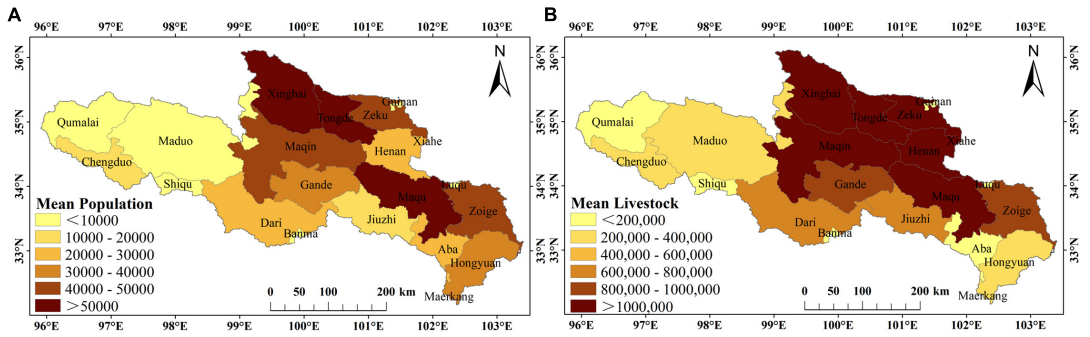

FIGURE 4
Spatial distribution of population and livestock in YRSR from 2000 to 2020. **(A)** Population from 2000 to 2020. **(B)** Livestock from 2000 to 2020.

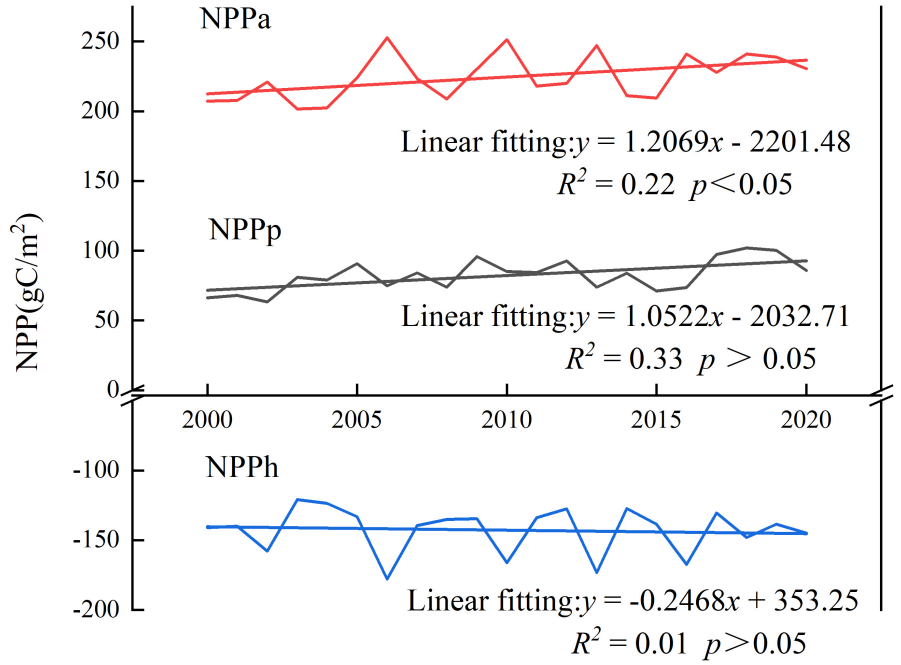

FIGURE 5
Variations of NPP of wetland vegetation in the YRSR between 2000 and 2020.

3.4. Correlation between climate factors, human activities, and NPP

3.4.1. Correlation analysis between climate factors and NPP

According to the correlation analysis between the NPP of marsh wetland vegetation and climate factors in the YRSR from 2000 to 2020 (Figure 7), the correlation coefficient between NPPa and temperature was between −0.82 and 0.79, with an average correlation coefficient being 0.01, and 50.85% of NPPa was positively correlated with temperature; the average correlation coefficient between NPPa and precipitation was between −0.83 and 0.78, with an average correlation coefficient being 0.11, and 41.93% of NPPa was positively correlated with precipitation. The correlation coefficient between NPPh and temperature was between −0.79 and 0.79, with an average correlation coefficient being 0.11, and 49.76% of NPPh was positively correlated with temperature; the correlation coefficient between NPPh and precipitation was between −0.79 and 1, with an average correlation coefficient being 0.32, and 75.62% of NPPh was positively correlated with precipitation. Overall, the correlation between NPP and precipitation of marsh wetland vegetation in the YRSR was higher in comparison to that between NPP and temperature, but the degree of correlation was relatively low.

3.4.2. Correlation analysis between human activities and NPP

The change of human activities was expressed by the number of livestock units per person in the YRSR from 2000 to 2020. The results of correlation analysis with NPP show that the number of livestock units per person was negatively correlated with NPPh ($P < 0.01$, $r = -0.773$), but no significant positive correlation with NPPa ($P < 0.05$, $r = 0.226$).

3.5. Relative contribution of climate change and human activities to NPP changes of marsh wetland vegetation

The relative contribution of climate-dominated and human-dominated to NPPa change was quantitatively assessed by superimposing the changing trends of NPPp, NPPa, and NPPh of marsh wetland vegetation in the YRSR between 2000 and 2020 (Figure 8). A total of 95.76% of NPPa of the wetland vegetation in the YRSR was increasing, of which 66.29% was influenced by climate change; it was primarily distributed in the southeast and central areas, which was also the area with the largest increase of the marsh wetland precipitation in the YRSR. A total of 29.47% of NPPa of the marsh wetland vegetation was influenced by human activities, primarily distributed in the northwest of the YRSR. The regions with reduced NPPa of marsh wetland vegetation were mainly distributed in sporadic areas of Zoige, Hongyuan, and Maqu counties in the southeast of the YRSR, accounting for 4.24%, almost all of them being influenced by human activities. Overall, the NPPa of marsh wetland vegetation in the YRSR exhibited an increasing trend between 2000 and 2020, with climate change being the dominate factor for the increase of NPPa. In the northwest of the YRSR, the contribution of human activities to the restoration of marsh wetland increased annually, while in the Zoige Plateau in the southeast of the YRSR, the NPPa of marsh wetland vegetation decreased as a result of human activities.

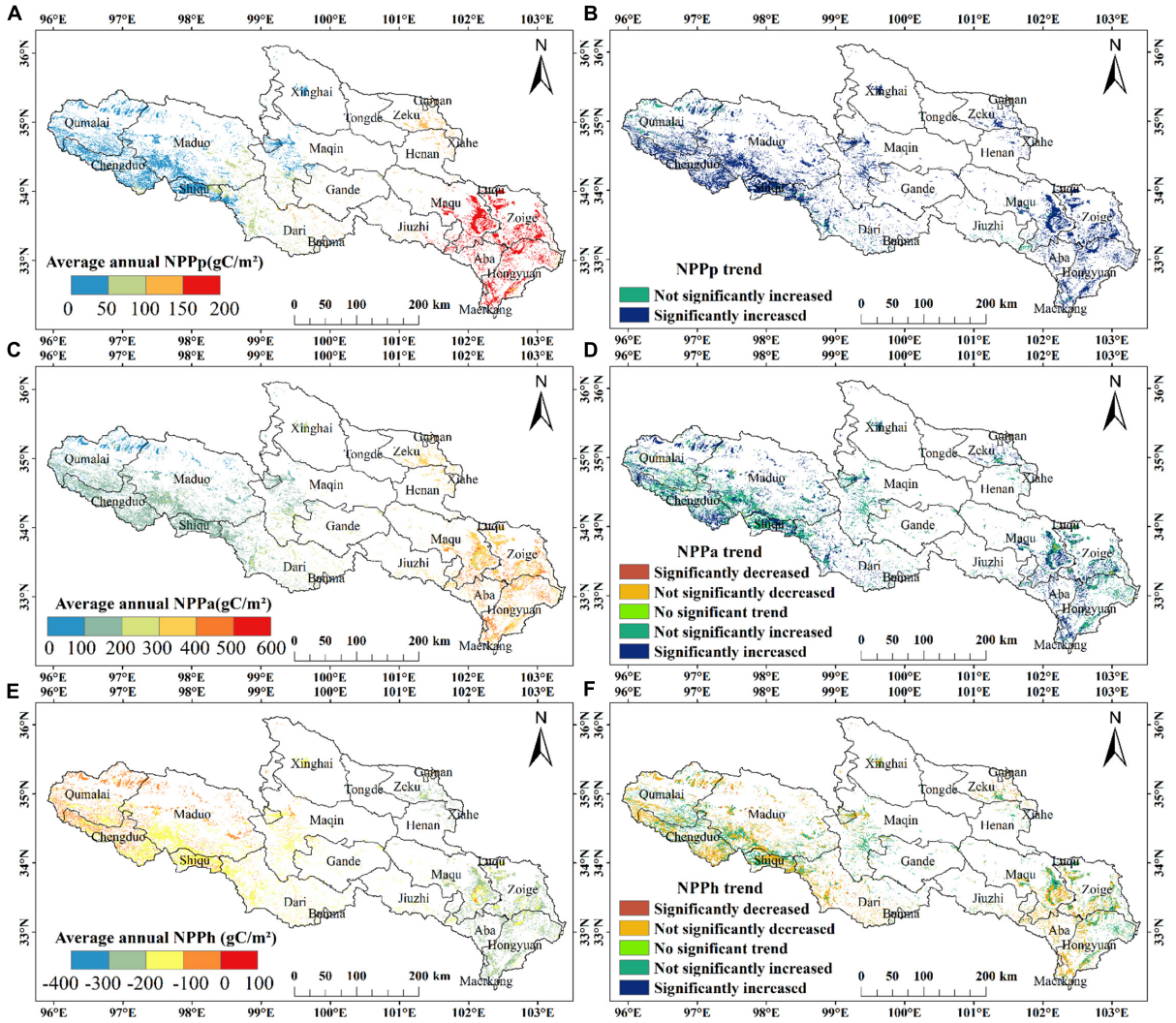

FIGURE 6
Spatial distribution of NPP of marsh wetland vegetation in the YRSR between 2000 and 2020. **(A)** NPPp between 2000 and 2020. **(B)** NPPp changing trend. **(C)** NPPa between 2000 and 2020. **(D)** NPPa changing trend. **(E)** NPPh between 2000 and 2020. **(F)** NPPh changing trend.

4. Discussion

4.1. NPP changes

In this study, the NPPp of marsh wetland vegetation in the YRSR between 2000 and 2020 was stimulated using the Zhou Guangsheng model, and the NPPa of marsh wetland vegetation was download from MOD17A3 product, and the NPPh of marsh wetland vegetation was calculated by the difference between them, which simplified the complex change mechanism of marsh wetland (Cloern et al., 2021) and allowed for quantitative evaluation of the driving mechanism of marsh wetland change. However, NPP estimation results might vary owing to the limitations of data sources, research area, and model methods. In this study, between 2000 and 2020, the NPPp of marsh wetland vegetation in the YRSR ranged between 63.21 and 101.93 gC/m^2, with an average value of 82.23 gC/m^2 and an average increase of 1.05 gC/m^{2}a; The range of NPPa was between 201.75 and 252.71 gC/m^2, with an average value of 224.53 gC/m^2 and an average increase of 1.21 gC/m^{2}a; The range of NPPh was between −120.86 and −178.00 gC/m^2, with an average value of −143.36 gC/m^2 and an average decrease of 0.25 gC/m^{2}a. The estimated NPP values of marsh wetland in similar research were different, but the spatial distribution trend of decreasing from southeast to northwest was approximately the same. For example, using MODIS17A3 NPP data, Shen et al. obtained that the average NPP of marshes on the Qinghai-Tibet Plateau from 2000 to 2020 was about 184.37 ± 11.12 gC/m^{2}a, and shows a trend of increasing gradually from northwest to southeast (Shen et al., 2022). The YRSR is located in the eastern part of the Qinghai-Tibet Plateau, the average NPPa of marsh vegetation in this study (224.53 gC/m^2) is higher than the average NPP of marshes on the Qinghai-Tibet Plateau, meanwhile, the distribution trend of NPPa in marsh vegetation of this study is also gradually increasing from northwest to southeast. Besides, Yan et al. (2022) used CASA model to estimate the NPP of zoige plateau marsh wetland in the southeast of the YRSR from 2000 to 2015, ranging from 206.04 to 250.23 gC/m^2, it is almost consistent with the NPPa

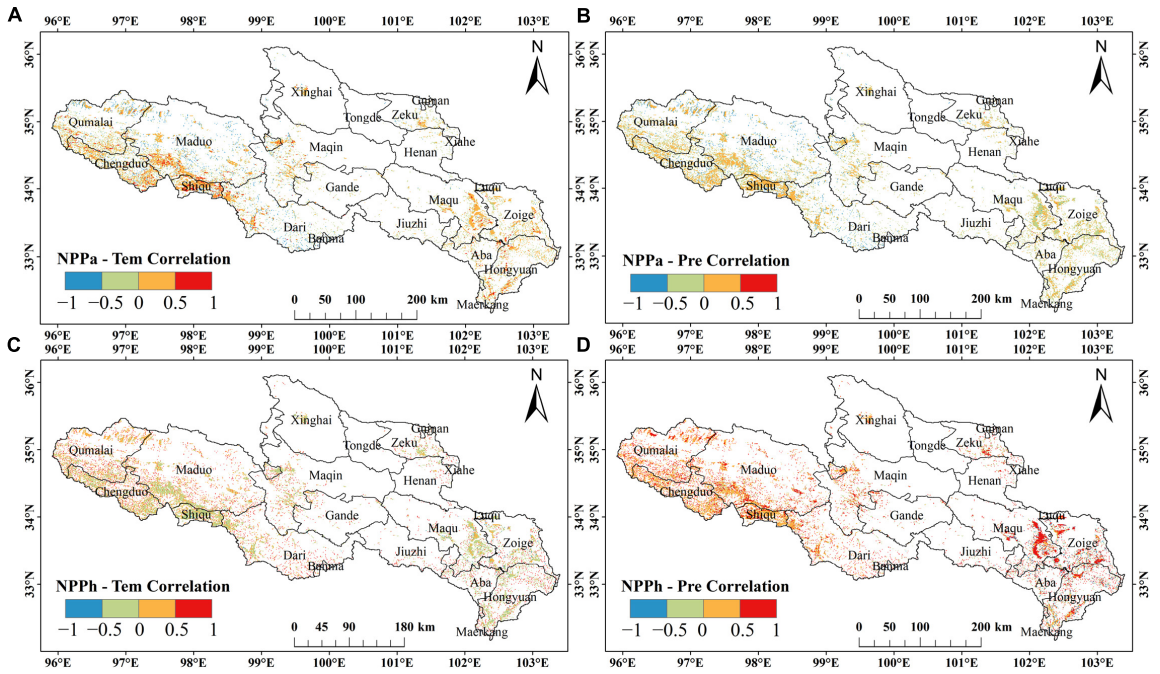

FIGURE 7
Spatial distribution of correlation analysis between NPP and climate factors of marsh wetland vegetation in the YRSR between 2000 and 2020. **(A)** NPPa and temperature. **(B)** NPPa and precipitation. **(C)** NPPh and temperature. **(D)** NPPh and precipitation.

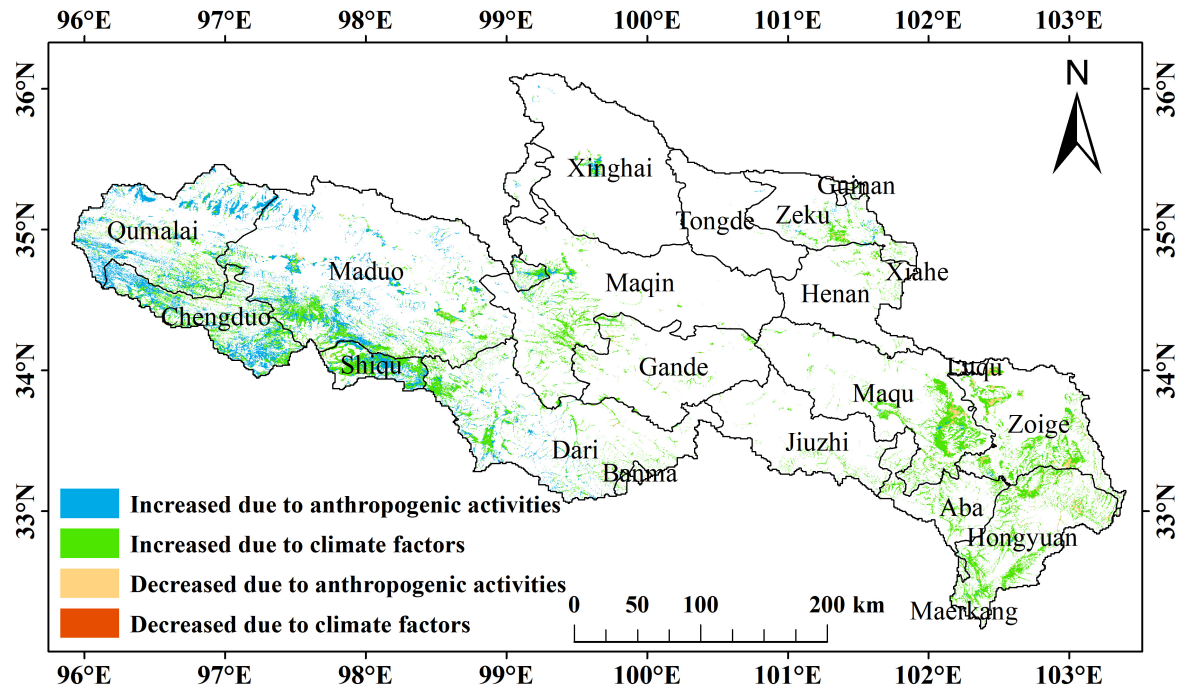

FIGURE 8
Spatial distribution of driving factors of NPPa change of marsh wetland vegetation in the YRSR between 2000 and 2020.

of marsh vegetation in the YRSR obtained by using MOD17A3 product (201.75~252.71 gC/m^2). Tang et al. used CASA model to estimate the change of NPP in the YRSR from 2000 to 2017. The average NPP was 301.6 gC/m^2, and the distribution trend was decreasing from southeast to northwest (Tang and Lin, 2021). It is higher than the NPP (224.53 gC/m^2) of marsh wetland vegetation in our study, because grassland is the main vegetation type in the YRSR., accounting for about 89.75%, so the estimated value of NPP is higher, but the spatial distribution trend of NPP is consistent with our study. Compared with the above research, it can be proved

that the NPP of marsh vegetation in the YRSR obtained by using MODIS17A3 product in this study is accurate. The northwest of the YRSR located in the inland hinterland was weakly affected by the warm and humid air current in the Pacific Ocean. Less precipitation and the lower temperature limited the growth and development of marsh wetland vegetation in the northwest of the YRSR, resulting in the lower NPP of marsh wetland vegetation in the northwest of the YRSR in comparison to that in the southeast (Tang and Lin, 2021). In this study, the NPPh was obtained by Formula (9), which was negative because NPPp was lower than NPPa in some areas. This shows that the ecological restoration measures affected by human activities have supplemented the NPP of marsh wetland vegetation, that is, human activities have promoted the restoration of marsh wetland vegetation in the YRSR. This is similar to the quantitative research results of vegetation NPP changes in Qinghai-Tibet Plateau in recent years. Since 2000, the vegetation in Qinghai-Tibet Plateau has changed from over-utilization to moderate protection, Under the influence of human activities, the area where vegetation NPP increases is expanding (Chen et al., 2020; Zhang et al., 2021). The NPPa of marsh wetland vegetation in the YRSR was increasing, indicating that the NPPa of marsh wetland vegetation was in a recovery state as a whole, while NPPh exhibited a decreasing trend, indicating that the overall impact of human activities was positive. In some regions of the Zoige Plateau in the southeast of the YRSR, NPPa exhibited a decreasing trend, and NPPh exhibited a negative effect, indicating that the NPPa of marsh wetland vegetation in this region was primarily reduced by human activities. The results obtained were consistent with those of similar studies (Guo et al., 2020; Ma et al., 2022; Yan et al., 2022), proving the accuracy and reliability of the NPP estimation result of this study.

4.2. Impacts of climate change and human activities on NPP

Between 2000 and 2020, the annual average temperature of the marsh wetland in the YRSR ranged from −4.20 to −3.07°C. The average temperature in 21 years was −3.51°C, with an average temperature increase rate being 0.16°C/10a. The annual precipitation of marsh wetland ranged from 464.73 to 663.35 mm; the average precipitation in 21 years was 558.03 mm, with an average water increase rate being 48.57 mm/10a. The spatial distribution pattern was decreasing from southeast to northwest, the temperature and precipitation exhibited an increasing trend, and the increasing trend from northwest to southeast was progressively obvious, which was consistent with the climate change trend distribution of earlier research results (Wang et al., 2015; Zhang, 2015; Wang et al., 2020), that is, the climate of the whole Qinghai-Tibet Plateau was warm and humid as a result of global warming. According to the correlation analysis between climate factors and NPP of marsh wetland vegetation, there was a positive correlation between NPP and precipitation in most regions of the YRSR, which was higher in comparison to the positive correlation with temperature. The spatial distribution and changing trend of precipitation were basically consistent with the NPP of marsh wetland vegetation, indicating that the overall increase of precipitation was the important factor affecting the increase of NPP of marsh wetland vegetation in the YRSR. However, there was a strong correlation between the temperature and the changes in the NPP of marsh wetland vegetation in some regions of Shiqu and Chengduo counties in the northwest of the YRSR, indicating that the influences of precipitation and temperature on the NPP of marsh wetland vegetation were complex and interactive (Guo et al., 2020). Glaciers and frozen soil melt as a result of increased precipitation and temperature, enriching the water supply of marsh wetland and increasing the NPP of marsh wetland vegetation in the YRSR which was approximately the same as the results of earlier studies (Ke et al., 2017; Hong et al., 2022; Zhang B. et al., 2022). Although the population and livestock in the YRSR have increased to varying degrees, the decrease of the number of livestock units per person shows that the overgrazing situation in this area has been controlled, which is one of the important reasons for the increase of NPP of marsh wetland vegetation in the YRSR from 2000 to 2020. The number of livestock units per person in the northwest of the YRSR has decreased especially obviously, therefore, affected by human activities, more NPP has been added in this region. However, in the southeast of the YRSR, the number of livestock units per person increased, which made the NPP in this area decrease due to human activities (Yan et al., 2022). The results of correlation analysis show that human activities are negatively correlated with NPPh, also demonstrates the NPP of marsh wetland vegetation in the YRSR has been effectively supplemented by human activities.

4.3. Relative contribution of climate change and human activities on marsh dynamics

According to the contribution rate analysis of this study, between 2000 and 2020, 66.29% of NPPa of the marsh wetland vegetation increased under the influence of climate change, which was primarily distributed in the southeast and central regions of the YRSR; 29.47% of NPPa of the marsh wetland vegetation increased under the influence of human activities, which was primarily distributed in the northwest part of the YRSR. The decrease in NPPa of wetland vegetation was primarily distributed in the sporadic areas of Zoige, Hongyuan, and Maqu counties in the southeast of the YRSR, accounting for 4.24%; almost all of them being influenced by human activities. This was similar to the studies by Yan et al. (2022) on NPP in the Zoige plateau wetland and Zhang F. et al. (2022) on NPP in grassland at the YRSR. That is, some areas in the northwest of the YRSR, such as Maduo, Qumalai, Chengduo, and Shiqu counties, were affected by the environmental protection project of the Three Rivers source, the construction of the Yellow River source national park, and other protection measures. The NPPa of the marsh wetland vegetation in this region was increased as a result of human activities. Although environmental protection projects mitigated some negative impacts of human activities in the Zoige plateau area in the southeast of the YRSR, the adverse human activities, such as the privatization of pastures, construction expansion, and drainage channel laying, have resulted in more fragmentation of marsh wetland (Yan and Wu, 2005; Li et al., 2020); consequently, the NPPa of marsh wetland vegetation decreased. Overall, even though climate-dominated change continues to play

a major role in the increase of NPPa in marsh wetland vegetation in the YRSR, we could observe that the positive effects of human-dominated NPP change are becoming progressively obvious, which are approximately related to the environmental protection policy implemented by the government of China since 2000. For instance, in 2003, the ecological environment of the YRSR was enhanced by the environmental protection project of the Three Rivers source with an investment of 750 million renminbi (RMB) (Shao et al., 2017; Zhao et al., 2018). The wetlands in the YRSR would be further preserved and restored with the 14th Conference of Contracting Parties to the Convention on Wetlands held in China in 2022, and human activities would play a significant role in promoting the restoration of wetlands.

5. Conclusion

In this study, the marsh wetland in the YRSR was used as the object. By the quantitative analysis of NPPp, NPPa, and NPPh of the marsh wetland vegetation, the relative contributions of climate change and human activities to the NPPa change of the marsh wetland vegetation were quantitatively assessed. The results revealed that the ecological environment of marsh wetland in the YRSR was improved between 2000 and 2020 with increased NPP. The warming and humidifying climate, particularly the increase in precipitation, is the leading factor of marsh wetland restoration, but the contribution of human activities to wetland restoration is also increasing. In the process of marsh wetland restoration, scientific policy management and engineering measures have produced excellent results and are becoming progressively remarkable. The area of marsh wetland restoration influenced by human activities would be further enlarged in the future with the implementation of several environmental protection engineering measures. In general, this study adopted a simple but reliable method to analyze the spatial distribution of the relative contributions of climate change and human activities to the NPP change of marsh wetland vegetation and quantitatively assessed the change mechanism of marsh wetland. The research results not only assisted policymakers in understanding the degradation and restoration status of marsh wetland in the YRSR but also helped in formulating future environmental protection policies and had important guiding significance for the sustainable development of marsh wetland.

Data availability statement

Publicly available datasets were analyzed in this study. This data can be found here: http://www.geodata.cn, http://developers.google.cn, and https://data.cnki.net.

Author contributions

ZZ conceived the study, supervised the writing, revised the manuscript, and provided funding support. XF led the writing. TM and BH contributed sections to the manuscript. All authors read and approved the final submission.

Funding

This work was supported by the Key Research and Development and Translational Program of Qinghai Province (No. 2022-QY-225).

Conflict of interest

The authors declare that the research was conducted in the absence of any commercial or financial relationships that could be construed as a potential conflict of interest.

Publisher's note

All claims expressed in this article are solely those of the authors and do not necessarily represent those of their affiliated organizations, or those of the publisher, the editors and the reviewers. Any product that may be evaluated in this article, or claim that may be made by its manufacturer, is not guaranteed or endorsed by the publisher.

References

Chen, A. F., Li, R. Y., Wang, H. L., and He, B. (2015). Quantitative assessment of human appropriation of aboveground net primary production in China. *Ecol. Modelling* 312, 54–60. doi: 10.1016/j.ecolmodel.2015.05.017

Chen, H., Ju, P. J., Zhang, J., Wang, Y. Y., Zhu, Q. A., Yan, L., et al. (2020). Attribution analyses of changes in alpine grasslands on the Qinghai-Tibetan Plateau. *Chin. Sci. Bull.* 65, 2406–2418. doi: 10.1360/TB-2019-0619

Cloern, J. E., Safran, S. M., Vaughn, L. S., Robinson, A., Whipple, A. A., Boyer, K. E., et al. (2021). On the human appropriation of wetland primary production. *Sci. Total Environ.* 785:9. doi: 10.1016/j.scitotenv.2021.147097

Dong, L. Q., Yang, W., Zhang, K., Zhen, S., Cheng, X. P., and Wu, L. H. (2020). Study of marsh wetland landscape pattern evolution on the Zoige Plateau due to natural/human dual-effects. *Peerj* 8:e9904. doi: 10.7717/peerj.9904

Du, J. Z., Wang, G. X., Yang, Y., Zhang, T., and Mao, T. X. (2015). Temporal and spatial variation of the distributive patterns and driving force analysis in the Yangtze River and Yellow River source regions wetland. *Acta Ecol. Sin.* 35, 6173–6182. doi: 10.5846/stxb201401260196

Gao, H., and Jin, J. X. (2022). Analysis of water yield changes from 1981 to 2018 using an improved Mann-Kendall test. *Remote Sens.* 14:17. doi: 10.3390/rs14092009

Guo, B., Wang, S., and Wang, M. T. (2020). Spatio-temporal variation of NPP from 1999 to 2015 in Zoige grassland wetland, China. *J. Appl. Ecol.* 31, 424–432. doi: 10.13287/j.1001-9332.202002.018

Hong, Z. D., Ding, S. Y., Zhao, Q. H., Geng, Z. H., Qiu, P. W., Zhang, J., et al. (2022). Relative contribution of multi-source water recharge to riparian wetlands along the lower Yellow River. *J. Environ. Manage.* 321:12. doi: 10.1016/j.jenvman.2022.115804

Hou, M. J., Gao, J. L., Ge, J., Li, Y. C., Liu, J., Yin, J. P., et al. (2020). An analysis of dynamic changes and their driving factors in marsh wetlands in the eastern Qinghai-Tibet Plateau. *Acta Pratacult. Sin.* 29, 13–27. doi:10.1168/cyxb 20191

Ke, L. H., Ding, X. L., Li, W. K., and Qiu, B. (2017). Remote sensing of glacier change in the central Qinghai- Tibet plateau and the relationship with changing climate. *Remote Sens.* 9:19. doi: 10.3390/rs9020114

Li, H., Zhang, H. Y., Li, Q. X., Zhao, J. J., Guo, X. Y., Ying, H., et al. (2021). Vegetation productivity dynamics in response to climate change and human activities under different topography and land cover in northeast China. *Remote Sens.* 13:18. doi: 10.3390/rs13050975

Li, Q. J., Zhang, Y., Fu, L., Li, Y. G., Li, F. C., Li, S. T., et al. (2018). Degradation mechanism of mires and recovery technology for them in the source regions of the yellow river. *Wetland Sci.* 16, 466–471. doi: 10.13248/j.cnki.wetlandsci.2018.04.003

Li, W. L., Xue, P. F., Liu, C. L., Yan, H. P., Zhu, G. F., and Cao, Y. P. (2020). Monitoring and landscape dynamic analysis of alpine wetland area based on multiple algorithms: A case study of Zoige Plateau. *Sensors* 20:19. doi: 10.3390/s20247315

Lieth, H. (1975). Modeling the primary productivity of the world. *Prim. Product. Biosph.* 14, 237–263. doi: 10.1007/978-3-642-80913-2_12

Liu, M., Fu, B. L., Xie, S. Y., He, H. C., Lan, F. W., Li, Y. Y., et al. (2021). Comparison of multi-source satellite images for classifying marsh vegetation using DeepLabV3 Plus deep learning algorithm. *Ecol. Indic.* 125:107562. doi: 10.1016/j.ecolind.2021.107562

Liu, Z. W., Li, S. N., Wei, W., and Song, X. J. (2019). Research progress on alpine wetland changes and driving forces in Qinghai-Tibet Plateau during the last three decades. *Chin. J. Ecol.* 38, 856–862. doi: 10.13292/j.1000-4890.201903.002

Ma, T., She, Y. D., Zhao, L., Hu, B. X., Feng, X. K., Zhao, J., et al. (2022). Alpine wetland evolution and their response to climate change in the yellow-river-source national park from 2000 to 2020. *Water* 14:17. doi: 10.3390/w14152351

Mao, D. H., Wang, Z. M., Du, B. J., Li, L., Tian, Y. L., Jia, M. M., et al. (2020). National wetland mapping in China: A new product resulting from object-based and hierarchical classification of Landsat 8 OLI images. *ISPRS J. Photogramm. Remote Sens.* 164, 11–25. doi: 10.1016/j.isprsjprs.2020.03.020

Mao, D. H., Wang, Z. M., Li, L., Song, K. S., and Jia, M. M. (2014). Quantitative assessment of human-induced impacts on marshes in Northeast China from 2000 to 2011. *Ecol. Eng.* 68, 97–104. doi: 10.1016/j.ecoleng.2014.03.010

Mo, X. G., Liu, S. X., and Hu, S. (2022). Co-evolution of climate-vegetation-hydrology and its mechanisms in the source region of Yellow River. *Acta Geograph. Sin.* 77, 1730–1744. doi: 10.11821/dlxb202207011

Ogunsola, O., and Dilau, K. A. (2022). Temperature variability comparison using mann-kendall test. *J. Sci. Technol.* 14, 29–36. doi: 10.30880/jst.2022.14.01.003

Pan, T., Hou, S., Liu, Y. J., Tan, Q. H., Liu, Y. H., and Gao, X. F. (2020). In fluence of degradation on soil water availability in an alpine swamp meadow on the eastern edge of the Tibetan Plateau. *Sci. Total Environ.* 722:13. doi: 10.1016/j.scitotenv.2020.137677

Peng, S. Z., Ding, Y. X., Liu, W. Z., and Li, Z. (2019). 1 km monthly temperature and precipitation dataset for China from 1901 to 2017. *Earth Syst. Sci. Data* 11, 1931–1946. doi: 10.5194/essd-11-1931-2019

Qiu, Z. Q., Mao, D. H., Xiang, H. X., Du, B. J., and Wang, Z. M. (2021). Patterns and changes of wetlands in the yellow river basin for 5 periods. *Wetland Sci.* 19, 518–526. doi: 10.13248/j.cnki.wetlandsci.2021.04.017

Shao, Q. Q., Cao, W., Fan, J. W., Huang, L., and Xu, X. L. (2017). Effects of an ecological conservation and restoration project in the Three-River Source Region, China. *J. Geogr. Sci.* 27, 183–204. doi: 10.1007/s11442-017-1371-y

Shen, X. J., Liu, Y. W., Zhang, J. Q., Wang, Y. J., Ma, R., Liu, B. H., et al. (2022). Asymmetric impacts of diurnal warming on vegetation carbon sequestration of marshes in the Qinghai Tibet Plateau. *Glob. Biogeochem. Cycles* 36:e2022GB007396. doi: 10.1029/2022gb007396

Shen, X. J., Xue, Z. S., Jiang, M., and Lu, X. G. (2019). Spatiotemporal change of vegetation coverage and its relationship with climate change in freshwater marshes of northeast China. *Wetlands* 39, 429–439. doi: 10.1007/s13157-018-1072-z

Sun, Q. L., Li, B. L., Zhou, C. H., Li, F., Zhang, Z. J., Ding, L. L., et al. (2017). A systematic review of research studies on the estimation of net primary productivity in the Three-River Headwater Region, China. *J. Geograph. Sci.* 27, 161–182. doi: 10.1007/s11442-017-1370-z

Tang, R., and Lin, H. L. (2021). Quantitative assessment of NPP changes in the Yellow River Source Area from 2001 to 2017. *IOP Conf. Ser.* 687:012002. doi: 10.1088/1755-1315/687/1/012002

Wang, J. Y., Li, A. N., and Jin, H. A. (2015). A review on research advances in estimation models for net primary production of vegetation in wetlands. *Wetland Sci.* 13, 636–644. doi: 10.13248/j.cnki.wetlandsci.2015.05.018

Wang, R., He, M., and Niu, Z. G. (2020). Responses of alpine wetlands to climate changes on the Qinghai-Tibetan Plateau based on remote sensing. *Chin. Geograph. Sci.* 30, 189–201. doi: 10.1007/s11769-020-1107-2

Wang, Y. F., Lv, W. W., Xue, K., Wang, S. P., Zhang, L. R., Hu, R. H., et al. (2022). Grassland changes and adaptive management on the Qinghai-Tibetan Plateau. *Nat. Rev. Earth Environ.* 3, 668–683. doi: 10.1038/s43017-022-00330-8

Wang, Y. L., Wang, X., Li, C. H., Wu, F. F., and Yang, Z. F. (2015). Spatiotemporal analysis of temperature trends under climate change in the source region of the Yellow River, China. *Theor. Appl. Climatol.* 119, 123–133. doi: 10.1007/s00704-014-1112-4

Xiang, S. A., Guo, R. Q., Wu, N., and Sun, S. C. (2009). Current status and future prospects of zoige marsh in eastern Qinghai-Tibet Plateau. *Ecol. Eng.* 35, 553–562. doi: 10.1016/j.ecoleng.2008.02.016

Xie, J. L., Lu, Z. X., and Feng, K. (2022). Effects of climate change and human activities on aeolian desertification reversal in Mu US Sandy Land, China. *Sustainability* 14:12. doi: 10.3390/su14031669

Xu, D. Y., Kang, X. W., Zhuang, D. F., and Pan, J. J. (2010). Multi-scale quantitative assessment of the relative roles of climate change and human activities in desertification–A case study of the Ordos Plateau, China. *J. Arid Environ.* 74, 498–507. doi: 10.1016/j.jaridenv.2009.09.030

Xue, Z. S., Lyu, X. G., Chen, Z. K., Zhang, Z. S., Jiang, M., Zhang, K., et al. (2018). Spatial and temporal changes of wetlands on the Qinghai-Tibetan Plateau from the 1970s to 2010s. *Chin. Geograph. Sci.* 28, 935–945. doi: 10.1007/s11769-018-1003-1

Yan, F. Q. (2022). Effects of climate changes on net primary productivity variation in the marsh area of the Sanjiang Plain. *Front. Ecol. Evol.* 10:11. doi: 10.3389/fevo.2022.1002397

Yan, F. Q., Zhang, S. W., Liu, X. T., Yu, L. X., Chen, D., Yang, J. C., et al. (2017). Monitoring spatiotemporal changes of marshes in the Sanjiang Plain, China. *Ecol. Eng.* 104, 184–194. doi: 10.1016/j.ecoleng.2017.04.032

Yan, W. C., Wang, Y. Y., Chaudhary, P., Ju, P. J., Zhu, Q. A., Kang, X. M., et al. (2022). Effects of climate change and human activities on net primary production of wetlands on the Zoige Plateau from 1990 to 2015. *Glob. Ecol. Conserv.* 35:13. doi: 10.1016/j.gecco.2022.e02052

Yan, Z. L., and Wu, N. (2005). Rangeland privatization and its impacts on the Zoige wetlands on the Eastern Tibetan Plateau. *J. Mt. Sci.* 2, 105–115. doi: 10.1007/bf02918326

Yin, L., Dai, E. F., Zheng, D., Wang, Y. H., Ma, L., and Tong, M. (2020). What drives the vegetation dynamics in the Hengduan Mountain region, southwest China: Climate change or human activity? *Ecol. Indic.* 112:12. doi: 10.1016/j.ecolind.2019.106013

Yuan, F. F., Liu, J. H., Berndtsson, R., Hao, Z. C., Cao, Q., Wang, H. M., et al. (2020). Changes in precipitation extremes over the source region of the yellow river and its relationship with teleconnection patterns. *Water* 12:15. doi: 10.3390/w12040978

Zhang, B., Niu, Z. G., Zhang, D. Q., and Huo, X. L. (2022). Dynamic changes and driving forces of alpine wetlands on the Qinghai-Tibetan Plateau based on long-term time series satellite data: A case study in the Gansu Maqu Wetlands. *Remote Sens.* 14:21. doi: 10.3390/rs14174147

Zhang, F., Hu, X. S., Zhang, J., Li, C. Y., Zhang, Y. P., and Li, X. L. (2022). Change in alpine grassland NPP in response to climate variation and human activities in the Yellow River source zone from 2000 to 2020. *Sustainability* 14:15. doi: 10.3390/su14148790

Zhang, Q., Yuan, R. Y., Singh, V. P., Xu, C. Y., Fan, K. K., Shen, Z. X., et al. (2022). Dynamic vulnerability of ecological systems to climate changes across the Qinghai-Tibet Plateau, China. *Ecol. Indic.* 134:11. doi: 10.1016/j.ecolind.2021.108483

Zhang, X. Q. (2015). Climate change impacts on wetlands of the yellow river headwaters. *Nat. Environ. Pollut. Technol.* 14:217.

Zhang, Y., Hu, Q. W., and Zou, F. L. (2021). Spatio-temporal changes of vegetation net primary productivity and its driving factors on the Qinghai-Tibetan plateau from 2001 to 2017. *Remote Sens.* 13:1566. doi: 10.3390/rs13081566

Zhao, D. D., He, H. S., Wang, W. J., Wang, L., Du, H. B., Liu, K., et al. (2018). Predicting wetland distribution changes under climate change and human activities in a mid- and high-latitude region. *Sustainability* 10:14. doi: 10.3390/su10030863

Zhao, L., Zou, D. F., Hu, G. J., Du, E. J., Pang, Q. Q., Xiao, Y., et al. (2020). Changing climate and the permafrost environment on the Qinghai-Tibet (Xizang) plateau. *Permafr. Periglac. Process.* 31, 396–405. doi: 10.1002/ppp.2056

Zhou, G. S., and Zhang, X. S. (1996). Study on NPP of natural vegetation in China under global climate change. *Acta Phytoecol. Sin.* 20, 11–19.

frontiers | Frontiers in Ecology and Evolution

TYPE Original Research
PUBLISHED 06 April 2023
DOI 10.3389/fevo.2023.1171688

OPEN ACCESS

EDITED BY
Zhongqing Yan,
Chinese Academy of Forestry,
China

REVIEWED BY
Meng Wang,
Northeast Normal University,
China
Minna Maria Väliranta,
University of Helsinki,
Finland

*CORRESPONDENCE
Chuanyu Gao
✉ gaochuanyu@iga.ac.cn
Guoping Wang
✉ wangguoping@iga.ac.cn

SPECIALTY SECTION
This article was submitted to Population, Community, and Ecosystem Dynamics, a section of the journal Frontiers in Ecology and Evolution

RECEIVED 22 February 2023
ACCEPTED 20 March 2023
PUBLISHED 06 April 2023

CITATION
Cong J, Gao C, Zhao H, Han D, Meng F and Wang G (2023) Chemical stability of carbon pool in peatlands dominated by different plant types in Jilin province (China) and its potential influencing factors.
Front. Ecol. Evol. 11:1171688.
doi: 10.3389/fevo.2023.1171688

Chemical stability of carbon pool in peatlands dominated by different plant types in Jilin province (China) and its potential influencing factors

Jinxin Cong[1], Chuanyu Gao[1]*, Haiyang Zhao[1], Dongxue Han[1], Fang Meng[2] and Guoping Wang[1]*

[1]Key Laboratory of Wetland Ecology and Environment, Northeast Institute of Geography and Agroecology, Chinese Academy of Sciences, Changchun, China, [2]School of Economics and Management, Qiqihar University, Qiqihar, China

Introduction: The peat carbon pool stores 30% of the total global soil carbon accounting for 3–4% of the global land surface. The stability of the peatland carbon pool is a key factor affecting global carbon cycling that is seriously disturbed by climate change and regional human activities. However, the impact of these factors on carbon pool stability remains poorly understood.

Methods: Based on the physicochemical properties and carbon compounds of 973 peat samples from Jilin Province (China), which are widely distributed in different altitude regions of the Changbai Mountains, we investigated the stability of the carbon pool in different dominant plants and degradation types of peatlands and assessed the effects of regional environmental factors on the peatland carbon pool.

Results and Discussion: Our results showed that the carbohydrate content of peat soils in different peatland types ranged from 33.2±6.9% to 40.5±4.8%, and the aromatic content ranged from 19.8±1.2% to 22.7±2.3%. Bulk density is the most important physicochemical factor, and annual average temperature is the most important environmental factor that influences carbon stability. The effects of selected environmental factors on the peatland carbon pool covered by different plants were different, and the carbon stability in shrub peatlands is more sensitive to climate characteristics than in peatlands dominated by the other two plant types. Peatland degradation decreases the carbon stability in herb and herb/shrub peatlands and increases the carbon stability in shrub peatlands, leading the peatland carbon pool to be more easily influenced by regional human activities than natural peatlands.

KEYWORDS

peatland, carbohydrate, aromatic, carbon stability, FTIR, Changbai Mountain

1. Introduction

Peatlands store approximately 500 ± 100 Pg of carbon, which accounts for 30% of the global soil carbon pool and only 3% of the total global land area (Yu et al., 2010; Loisel et al., 2014). Water-saturated and low-pH environments are the major causes of carbon storage in peatlands, which is much higher than that in other ecosystems (Ye et al., 2012; Wu and Roulet, 2014; Loisel et al., 2017). Peatlands are mainly distributed across mid- and high-latitude regions, which are more sensitive to climate change than other regions, and the peatland carbon pool has become vulnerable

to climate change in recent years (Solomon et al., 2007; Xu et al., 2018; Loisel et al., 2020). The stability of the peatland carbon pool acts as a key factor that affects its response to climate change and must be evaluated (Leifeld and Menichetti, 2018; Qiu et al., 2020; Cong et al., 2022).

Organic matter chemistry is widely used as a key factor for evaluating the decomposition process and chemical stability of peatland carbon pools (Sjögersten et al., 2016), and several typical chemical compounds of organic matter have been widely selected as indicators (Wilson et al., 2016; Cong et al., 2020). As the carbohydrate content in peat soils increases, organic matter is more easily decomposed, and more CO_2 is released through microbial activities under aerobic environment, which means that an increase in carbohydrate content decreases the stability of the peatland carbon pool (Leifeld et al., 2012). Phenolic acid acts as an important factor that inhibits microbial activities and decreases the decomposition rate of organic matter (Fenner and Freeman, 2020). Thus, the release of phenolic compounds from shrubs has been widely hypothesized to be a key factor that increases carbon stability and protects the peatland carbon pool in warm and dry environments (Wang et al., 2015). The aromatic contents in peat soils in low-latitude peatlands with warm environments are significantly higher than those in high-latitude peatlands with cold environments, and the chemical stability of the carbon pool in low-latitude peatlands is significantly higher than that in high-latitude peatlands (Hodgkins et al., 2018). Furthermore, as the mean July temperature increased and the annual precipitation increased, the carbohydrate content in peat soils decreased and the aromatic content increased markedly, indicating an increase in the stability of the peatland carbon pool (Cong et al., 2020). These results indicate that peatland carbon pools with high aromatic contents and low carbohydrate contents are more stable than others, and these special carbon chemical compounds are majorly influenced by regional climate factors (Verbeke et al., 2022).

In addition to climatic factors, chemical compounds of organic matter are mainly influenced by their sources and the storage environment (Heller et al., 2015). Considering the dominant plant community and plant biomass in peatlands, plant litter from herbs and shrubs acts as the major organic matter (OM) source, and the carbon compounds of OM in the surface soils of these two types of plant communities are significantly different (Normand et al., 2017). In general, more lignin content is available in shrub stems than in herb plant litter, which causes the aromatic contents and the stability of the carbon pool in shrub peatlands to be higher than that in herb peatlands (Wang et al., 2015). In recent years, the increase in human activities has also become an important disturbance factor that has serious effects on peatlands, such as decreasing the water table and accumulating more nutrient/pollution elements (Gao et al., 2018). For example, the increase in atmospheric nitrogen deposition not only increases gross ecosystem production but also increases the decomposition rates of the soil carbon pool (Bragazza et al., 2006; Wu et al., 2015), which accelerates the carbon cycling rates in peatlands and may also cause serious changes in the stability of the peatland carbon pool. Serious environmental disturbances may also cause peatland degradation, such as a decrease in the water table through drained or climate drying and an increase in pH values through the accumulation of more nutrients (Dohong et al., 2017; Šimanauskienė et al., 2019). The degradation of peatlands has serious effects on peat soil accumulation and promotes peat decomposition (Drollinger et al., 2020). Liable carbon compounds are more easily decomposed in degraded peatland carbon pools and increase the residual carbon recalcitrance to environmental changes, which may also cause the chemical stability of residual carbon compounds to be higher than that in natural peatland carbon pools (Leifeld et al., 2020). Thus, the dominant plant types, degradation, climate characteristics, and regional human activities not only cause serious changes in the peatland environment but also have potential effects on the chemical compounds of organic matter and the stability of the peatland carbon pool. However, these effects remain uncertain.

Peatlands in Jilin Province (China) are mainly covered by herb and shrub plants and are located in the Changbai Mountains, which are widely distributed in different altitudes from 17 to 1,550 m (Xing et al., 2015). The different altitudes caused the peatlands in this region to develop under different climatic characteristics and regional environmental disturbances. In addition, the increasing population in Northeast China during the 20th century caused serious effects on peatlands in the Changbai Mountains and more serious effects on low-altitude peatlands than those located at high altitudes (Gao et al., 2016). The marked differences in climatic factors and anthropogenic disturbances may also have serious effects on the stability of peatland carbon pools in different altitude regions; however, these are still unclear.

To address these knowledge gaps, the goals of this study were to assess the stability of the peatland carbon pool in Jilin Province based on detailed physiochemical properties and carbon chemistry analysis of peat soils in different peatland types. Second, we wanted to identify the differences in peatland carbon pools under the different dominant plant types and evaluate whether peatland degradation causes serious effects on the peatland carbon pool. Finally, by comparing the natural and anthropogenic factors with the peatland carbon pool stability, we aimed to clarify the effects of climate characters and human activities on the stability of the peatland carbon pool in Jilin Province.

2. Materials and methods

2.1. Site description and sampling

The peatlands studied in Jilin Province are mainly located in the middle part of the Changbai Mountains in Northeast China. In this study, we collected 973 peat samples from typical peatlands in Jilin Province, which cover the different dominant plants in natural and degraded peatlands and are widely distributed in different altitude regions (Figure 1). Based on the dominant plants, the peatlands were divided into herb peatland (i.e., the dominant plants are *Carex* sp., *Typha orientalis Presl*), herb/shrub peatland (i.e., the dominant plants are *Betula platyphylla Suk.*, *Spiraea salicifolia* L., Carex sp.), and shrub peatland (i.e., the dominant plants are *Betula platyphylla Suk.*, *Spiraea salicifolia* L., *Sphagnum palustre* L.). Unlike natural peatlands, the degraded peatlands are threatened by regional human activities (e.g., graze, drainage, and reclamation) or extreme climate change (e.g., drought). Most of degraded peatlands are distributed in the middle and south of Jilin Province and the natural peatlands are distributed in the eastern of Jilin Province. The sampling sites were randomly selected in 2013 and were widely distributed in the middle of the Changbai Mountains to reflect the regional peatland carbon pool. The studied peatlands have a temperate continental monsoon climate with mean annual temperatures of −0.5–6°C and a mean annual precipitation of 500–900 mm (Fick and Hijmans, 2017). The regional

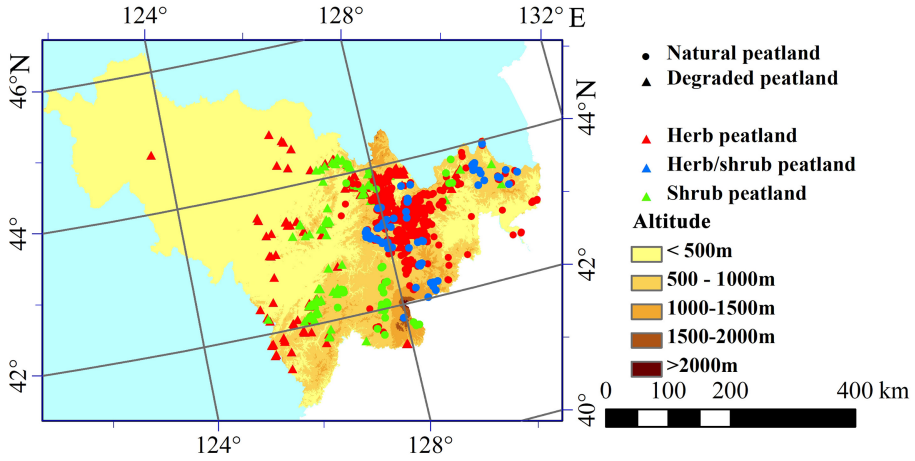

FIGURE 1
Locations of peatland sampling in Jilin Province, China.

human influence index (HII) of selected peatlands ranged from 10 to 41 (WCS and CIESIN, 2005), and the altitudes ranged from 17 to 1,550 m. Considering the number of peat samples and peat sites, one samples from each site would be better than several samples from different depth in several selected typical peatlands for evaluating the chemical stability of peatland carbon pool in Jilin Province. The peat samples for each site were a mixture of the whole peat layer to ensure that the samples reflected the average carbon content and stability of the peatland carbon pool at selected sites. The location of each site was determined using a portable global positioning system (GPS; Figure 1). The samples were stored in polyethylene plastic bags and brought to the laboratory for analysis. The samples were loosely disaggregated to facilitate air-drying at 20°C.

2.2. Physical and chemical analysis

The bulk density of peat soils was obtained from the weight of peat soils with known volumes dried in an oven at 105°C for 12 h. The pH of the peat soils was measured directly using a pH meter, and the weight ratio of peat soils to water was 0.1. The sources of residual fiber in peat samples were mainly from the undecomposed plant litters, and the percentage of fiber content was used to define the peat decomposition level. With the fiber proportion increasing, more undecomposed plant litters and the peat decomposition degree decreasing. The fiber content was determined from the dry weight of fibers retained on a 0.15 mm sieve as a percentage of oven-dried mass, and the ratio of the weight loss of peat to total peat was regarded as the decomposition degree of peat samples (Abd Rahman and Ming, 2015). Soil organic carbon was determined by external heating potassium dichromate oxidation method, and details of this method was described in Zhao et al. (2012).

2.3. Carbohydrate and aromatic contents

The carbohydrate and aromatic contents of peat soils were estimated based on FTIR spectra and selected peat heights, which were area-normalized and baseline corrected (Cong et al., 2020). The FTIR spectra of the peat soils were obtained using a Spectrum Two FTIR spectrometer (PerkinElmer, United States) using KBr pellets (150 mg dried KBr and 1 mg peat soil). Measurements were recorded from 4,000 to 300 cm^{-1} using a resolution of 1 cm^{-1}. The carbohydrate content was estimated based on the regression equations of the heights of the FTIR carb (1,030 cm^{-1}), and the aromatic content were estimated based on the height of the FTIR arom15 (1,510 cm^{-1}) and arom16 (1,615 cm^{-1}; Hodgkins et al., 2018).

2.4. Statistical method

2.4.1. Two-Way analysis of variance

The physicochemical and carbon properties of peat soils (i.e., bulk density, decomposition degree, pH, carbon content, carbohydrate content, and aromatic content) were analyzed using a two-way analysis of variance (ANOVA, SPSS 22.0, IBM, Armonk, United States). For peatlands in Jilin Province, the peatlands were classified by dominant plant types and divided into herb peatlands, herb/shrub peatlands, and shrub peatlands. Thus, peatland-dominant plant types (i.e., herbs, herb/shrub, and shrub) and degradation (i.e., degraded or natural) were regarded as two distinct factors, and their effects on the tested variables were evaluated through two-way ANOVA. Significant differences are reported at a probability level of 0.05, unless otherwise stated.

2.4.2. Random forest

The importance of the selected environmental factors on peat physicochemical properties was calculated using a random forest (RF) model. The RF classification was conducted using the "randomForest" package in R software. The selected soil physicochemical properties (bulk density, decomposition degree, and pH) and environmental factors (altitude, annual precipitation, annual average temperature, degradation, HII, and dominant plant type) were considered as explanatory variables, and the carbon properties were considered as the response variables. Seventy percent of the selected data were regarded as the training dataset, and the RF then searched for the

predictor that best partitioned the response variable in the training dataset. The relative importance of the selected environmental factors for each physicochemical property of peat soils was calculated based on the increase in the mean squared error (%IncMSE).

3. Results

3.1. Physicochemical properties of peat soils in Jilin Province

The average values with standard error of the bulk density, pH, and decomposition degree of peat soils in Jilin Province are shown in Table 1, and box plots of these properties are shown in Figure 2. The bulk density of peat soils in Jilin Province ranged from 0.23 ± 0.10 g.cm^{-3} to 0.40 ± 0.10 g.cm^{-3}. In herb/shrub peatlands, the bulk density were 0.23 ± 0.10 g.cm^{-3} in natural peatlands and 0.29 ± 0.12 g.cm^{-3} in degraded peatlands, which were markedly lower than those in other peatland types. The decomposition degree of peat soils ranged from 62.5 ± 17.6% to 81.6 ± 10.4%, and the decomposition degree in degraded peatlands was markedly higher than that in natural peatlands, especially for peatlands covered by shrubs, which was 62.5 ± 17.6% in natural peatlands and 81.6 ± 10.4% in degraded peatlands. The pH of peat soils ranged from 4.91 ± 0.34 to 5.09 ± 0.30. Based on the two-way ANOVA results, both the dominant plant types and degradation had significant effects on the bulk density and decomposition degree of peat soils (Table 2). However, only the dominant plant types had significant effects on the pH of peat soils, and the effects of degradation on the pH of peat soils were not significant.

3.2. Carbon contents and chemical stability of peat soils in Jilin Province

The carbon content of peat soils in Jilin Province in different peatland types ranged from 14.4 ± 7.5% to 31.9 ± 9.0%, and the lowest carbon contents were observed in degraded shrub peatlands (Table 1; Figure 2). The carbon content of peat soils in degraded peatlands was significantly lower than that of natural peatlands, and the effects of dominant plant types on carbon content were also significant. Carbohydrate contents of peat soils in Jilin province ranged from 33.2 ± 6.9% to 40.5 ± 4.8%, and the average carbohydrate contents in different peatland types (i.e., dominant plant types and degradation) were significant different. Compared to natural peatlands, carbohydrate content in degraded peatlands were significantly higher than those in natural peatlands. Conversely, the aromatic content in degraded peatlands were slightly lower than those in natural peatlands. However, the effects of degradation on the aromatic content were not significant. In shrub peatlands, the average aromatic content in degraded peatlands was 19.8 ± 1.2%, which was markedly lower than that in natural peatlands which was 22.4 ± 2.9%. In others, the aromatic contents were approximately 22% and ranged from 21.0 ± 3.0% to 22.7 ± 2.3%. Interestingly, the effects of the interaction between dominant plant types and degradation on both these variables were not significant.

3.3. Importance of typical factors on peatland carbon pool

The importance of the selected environmental factors, dominant plant types, and physicochemical properties of peat soils on peatland carbon pools is shown in Figure 3. The IncMSE results shown that the importance of physicochemical properties for the peatland carbon pool are stronger than the selected environmental factors and the dominant plant types. Bulk density was listed as the most important factor for all four indicators of the peatland carbon pool, ranging from 35.30 to 89.36%. The importance of bulk density on carbon content was 89.36%, which is obviously higher than that of other factors, in which the IncMSE values only ranged from 0.95 to 21.53%. The degree of decomposition was the second most important factor (21.53%) for the carbon content. Compared with the bulk density and decomposition degree, the impact of pH on the peatland carbon pool

TABLE 1 Basic information of selected peat soils in different dominated plant types of natural and degraded peatland.

	Herb peatland				Herb/shrub peatland				Shrub peatland			
	Natural *N* =497		Degraded *N* =260		Natural *N* =40		Degraded *N* =101		Natural *N* =72		Degraded *N* =3	
	mean	S.D.	mean	S.D.	mean	S.D.	mean	S.D.	mean	S.D.	mean	S.D.
Annual precipitation (mm)	630.79	30.31	662.68	82.94	730.83	68.83	734.01	93.55	657.53	39.08	648.67	28.15
Annual average temperature (°C)	3.22	0.51	3.67	0.63	2.82	0.84	3.91	0.61	2.83	0.60	3.18	0.14
Altitude (m)	544	138	458	108	746	232	455	122	646	164	545	5
Human influence index	21.21	6.35	22.35	6.24	17.73	4.64	17.78	3.58	20.93	6.10	20.67	8.33
Bulk density (g/cm^3)	0.32	0.16	0.37	0.20	0.23	0.10	0.29	0.12	0.26	0.15	0.40	0.10
Decomposition degree (%)	70.9	15.4	72.4	15.0	63.9	14.4	70.5	13.6	62.5	17.6	81.6	10.4
pH	5.02	0.30	5.09	0.42	4.91	0.34	5.01	0.34	5.09	0.30	5.05	0.17
Carbon contents (%)	25.0	10.3	22.7	10.5	31.9	9.0	27.1	9.9	26.9	9.0	14.4	7.5
Carbohydrate contents (%)	35.5	7.5	36.4	7.1	33.5	6.9	35.2	6.4	33.6	7.7	40.5	4.8
Aromatic contents (%)	21.6	2.8	21.0	3.0	22.7	2.3	22.5	2.6	22.4	2.9	19.8	1.2
Aromatic/carbohydrate ratio	0.65	0.21	0.61	0.19	0.73	0.21	0.67	0.20	0.72	0.26	0.50	0.09

10.3389/fevo.2023.1171688

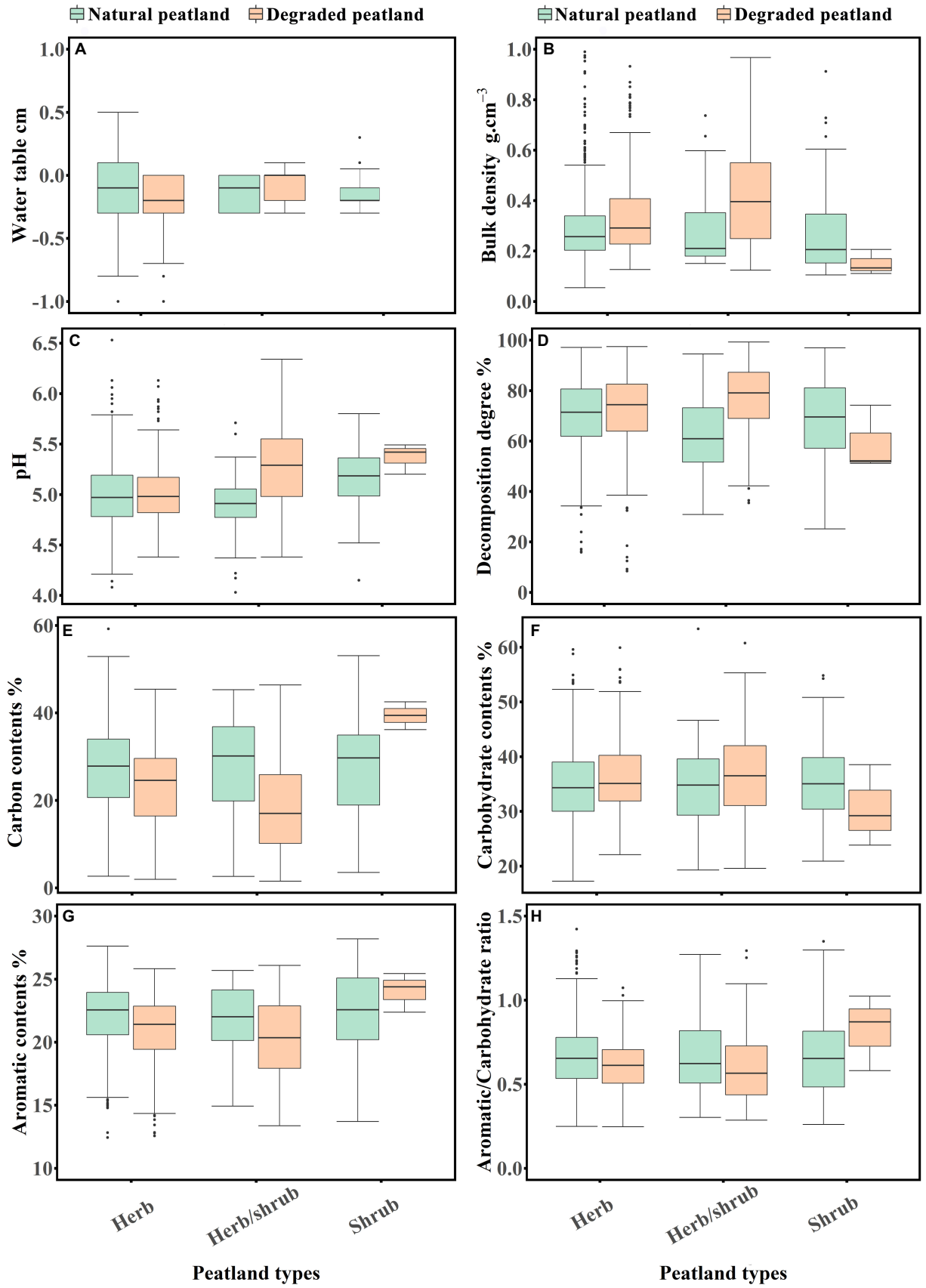

FIGURE 2
Boxplot of water table **(A)**, bulk density **(B)**, pH **(C)**, decomposition degree **(D)**, carbon contents **(E)**, carbohydrate contents **(F)**, aromatic contents **(G)**, and the ratio of aromatic/carbohydrate **(H)** of peat soils in different dominated plant types of natural and degraded peatland.

TABLE 2 Two-way ANOVA for typical physicochemical properties, carbon contents, and carbon compounds in peat soils.

	Plant types		Degradation		Plant types*degradation	
	F	*p*	*F*	*p*	*F*	*p*
Bulk density	11.789	0.000	5.545	0.019	0.509	0.601
Decomposition degree	4.103	0.017	8.175	0.004	3.118	0.045
pH	4.141	0.016	0.303	0.582	0.258	0.773
Carbon contents	16.016	0.000	9.578	0.002	2.044	0.130
Carbohydrate contents	3.063	0.047	4.664	0.031	1.184	0.307
Aromatic contents	10.249	0.000	3.607	0.058	0.939	0.391
Aromatic/carbohydrate ratio	5.497	0.004	5.925	0.015	1.175	0.309

The dominant plant types and natural/degradation were considered as two independent variables.

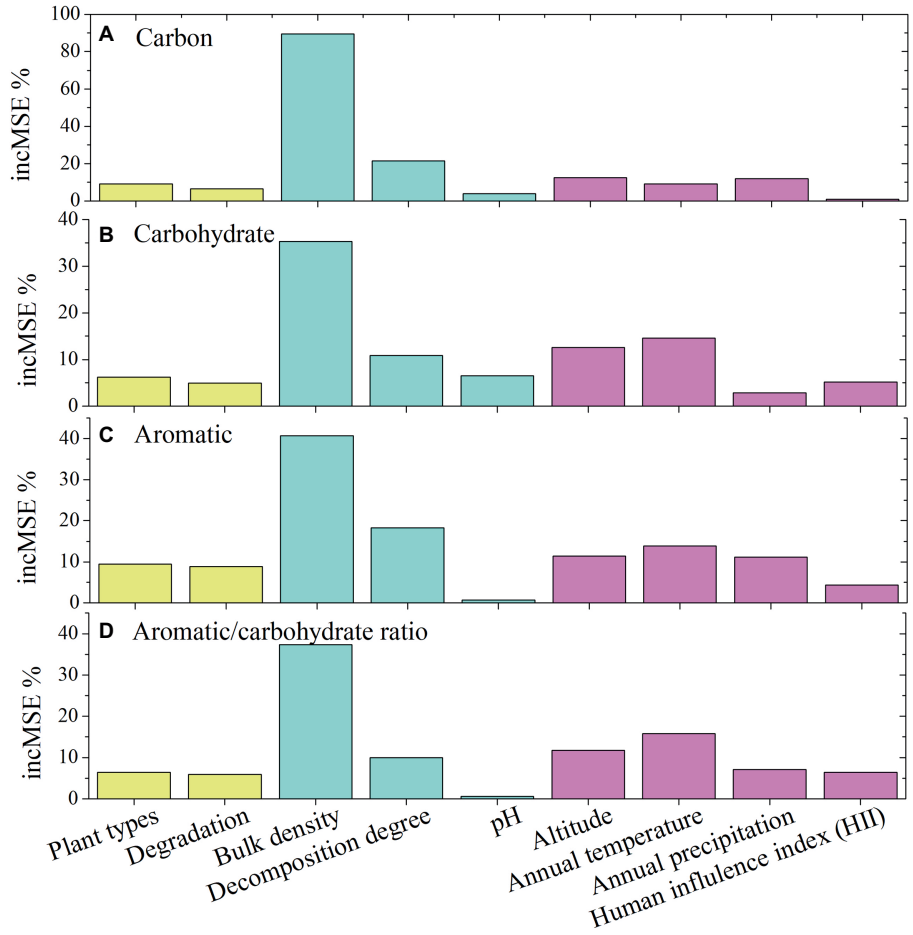

FIGURE 3
Based on random forest analysis, the increase in mean squared error (%IncMSE) of selected environmental factors to carbon contents **(A)**, carbohydrate contents **(B)**, aromatic contents **(C)**, and the ratio of aromatic/carbohydrate **(D)**.

was markedly lower, ranging from 0.57 to 6.56%. Among the environmental factors, altitude was the most important factor (12.47%) for carbon content, and the annual average temperature was the most important factor for carbon chemical stability. Compared to climate factors, the importance of the HII for peatland carbon pools was markedly lower, ranging from 0.95 to 6.43%. The importance of plant types on the peatland carbon pool was slightly higher than that of degradation and ranged from 6.26 to 9.49%.

4. Discussion

4.1. Effects of dominant plant types and degradation on peat soil properties

The chemical properties of OM in peatland carbon pools are affected by the natural conditions of formation, land use, and drainage (Heller et al., 2015; Negassa et al., 2019; Leifeld et al., 2020). Because

local plants are a major source of OM in peatlands, the dominant plant community acts as one of the major factors influencing the chemical properties of OM in the peatland carbon pool (Paul, 2016). The effects of the dominant plant types on natural and degraded peat soil properties and carbon pools are shown in Figure 2.

In shrub peatlands, the pH of peat soils was higher and the bulk density was lower than those in peatlands covered by the other two plant types. The decomposition degree in herb/shrub peatlands was lower than that in the others. The pH of peat soils in peatlands, which are influenced by surface water (i.e., fen), are higher than those only influenced by rain water (i.e., bog; Rydin and Jeglum, 2013). Due to the high pH in shrub peatlands, we speculated that more shrub peatlands in Jilin province are influenced by surface water than herb peatlands. Additionally, the water table of peatlands are also important that affect the plants, and the water table in shrub peatlands is lower than that in herb peatlands (Keddy, 2010; Rydin and Jeglum, 2013). Thus, changes in the water table also act as another factor that influences the physicochemical properties of peat soils. In natural peatlands, many studies have reported that the decomposition of peat soils always increases with decreasing water table (Clarkson et al., 2013; Munir et al., 2014). The decomposition of peat soils in herb and shrub peatlands was similar in our study and obviously higher than that in herb/shrub peatlands, where the water table should be at the middle level of these three peatland types. However, because herb plant litter contains more carbohydrates and less aromatics than shrub plant litter (Wang et al., 2021a), herb plant litter is more easily decomposed than shrub plants. Thus, the decomposition degree of peat soils in herb and shrub peatlands was similar. We also speculated that the reason that the low decomposition degree of peat soils in herb/shrub peatlands is that the plant litter sources in herb/shrub peatlands are contain more stable compounds than herb peatlands and the decomposition environment are more restrictive under higher water tables than in shrub peatlands.

Compared to peat physicochemical properties, the effects of peatland-dominant plant types on carbon content, carbohydrate content, and aromatic content were lower, and the differences in the carbon pool in peatlands covered by different plants were weak. Although the aromatic content in shrub plants was higher than that in herb plants, there was no obvious difference in aromatic content between shrub and herb peatlands. Compared to carbohydrate compounds, aromatic compounds are recalcitrant and limiting the decomposition of peatland carbon pool (Fenner and Freeman, 2020). The major reason for the similar contents of residual aromatics and carbohydrates in herb peatlands and shrub peatlands is speculated to be that the decomposition processes of peat soils cause less aromatic compounds and more carbohydrate compounds from the herb plant to decompose, which cause the aromatic compounds contents increasing in residual herb peatland carbon pool.

Interestingly, the effects of degradation on peat physicochemical properties and carbon pools in peatlands covered by different plant types varied (Figure 3). The bulk density and decomposition degree in the degraded herb and herb/shrub peatlands were markedly higher than those in natural peatlands. These two properties in degraded shrub peatlands were markedly lower than those in natural peatlands. A similar trend was also found in carbohydrate content and the effects of degradation on the carbon and aromatic contents of peatlands covered by different plant types. The most important characteristic of peatland degradation is the decreasing in the water table (Guo et al., 2013; Han et al., 2021). Due to there was no clear water table for measuring the degradation of herb/shrub peatlands and shrub peatlands, especially for dry degraded peatlands. The available water table data for these two peatland types could not be used to reflect the real water level conditions. For herb peatlands, the water table could be measured in most of the degraded herb peatlands, and the results showed that the water table in degraded peatlands was clearly lower, and the decomposition degree of peat soils was markedly higher than that in natural peatlands (Figure 2). Decreasing the water table also decreases the biomass of herb plants and increases the biomass of shrub plants (Lou et al., 2018), which may be the major factor for plant litter residuals in degraded herb and herb/shrub peatlands.

The increase in the degree of decomposition and changes in plant litter sources also cause changes in the stability of the peatland carbon pool (Leifeld et al., 2012). More carbohydrate and less aromatic contents in degraded peatlands means the chemical stability in degradation herb and herb/shrub peatlands was slightly lower than that in natural peatlands (Hodgkins et al., 2018). In the present study, increasing the degree of decomposition increased the bulk density and decreased the carbon content, which was clearly found in herb peatlands and herb/shrub peatlands. However, the effects of degradation on shrub peatlands were opposite to those of the other peatland types. Unlike herb plants, decreasing the water table in degraded peatlands is beneficial for shrub plant growth, and the aboveground biomass of shrub plants increases under low water table environments (Lou et al., 2015). With more plant litter from the shrub plant residue, more carbon with high aromatic contents in shrub plant litter accumulated in the peatland carbon pool, which increased the stability of the peatland carbon pool and decreased the decomposition degree of peat soils in degraded shrub peatlands (Straková et al., 2012; Cong et al., 2022). Thus, the different effects of degradation on dominant plant communities are the major factors that cause the degradation decreases the carbon content and carbon chemical stability in herb and herb/shrub peatlands and causes opposite effects on shrub peatlands.

4.2. Effects of peat physicochemical properties on peatland carbon pool

The bulk density, decomposition degree, and pH of peat soils were selected as physicochemical property indicators to evaluate the effects of peat physicochemical properties on carbon content and stability in the peatland carbon pool, and the results are shown in Figure 4. The results of the RF analysis showed that the importance of the bulk density on the peatland carbon pool was markedly higher than that of the other two factors (Figure 3). The effects of bulk density on carbon content in peat soils were negative for all peatland types, and the slope for natural herb/shrub peatlands was the highest. Carbon decomposition and mineral element accumulation in peatlands are the major reasons for the increase in the bulk density of peat soils (Bao et al., 2012; Kareksela et al., 2015; Wang et al., 2021b). With the bulk density of peat soils increasing, more carbon decomposed and less carbon residual in peat soils which is the major factor that explain the negative correlation between bulk density and carbon contents. While, as the bulk density increased, the carbohydrate content increased and the aromatic content decreased, which caused a marked decrease in the aromatic/carbohydrate ratios.

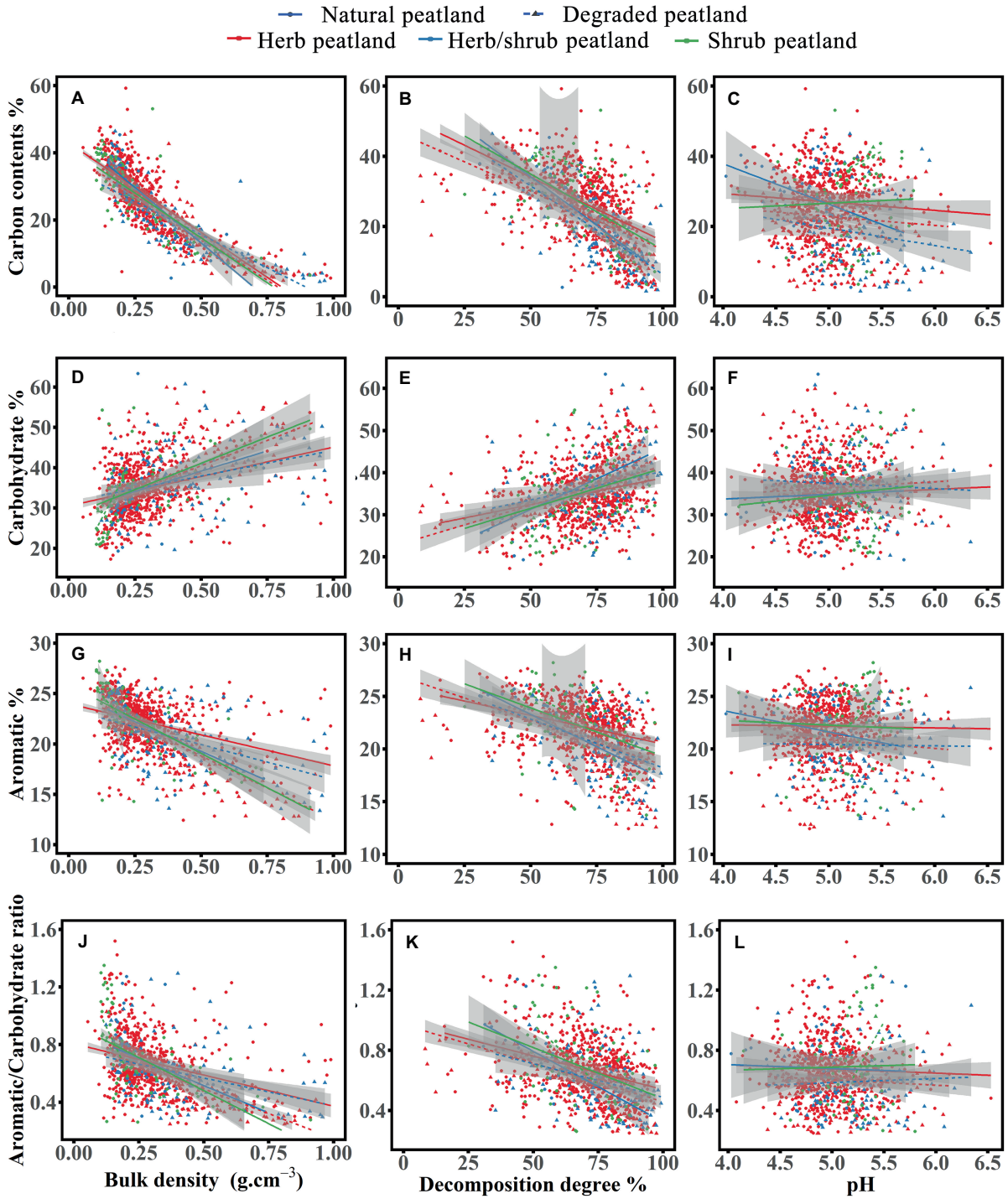

FIGURE 4
Relation between carbon contents **(A–C)**, carbohydrate contents **(D–F)**, aromatic contents **(G–I)**, and aromatic/carbohydrate ratio **(J–L)** with bulk density, degree of decomposition, and pH in different dominated plant types of natural and degraded peatland. The trend lines were fitted with a linear model, and the grey shadows indicate 95% confidence interval of fitted lines.

More mineral elements available in peat soils with high bulk density was speculate to support more nutrients for plant growth, and more leaves with high carbohydrate contents in surface plant under sufficient nutrition environment (Poorter et al., 2012; Wang et al., 2015). More leaves with high carbohydrate contents as organic matter sources under high nutrients environment is speculated as a potential reason that cause the stability of the peatland carbon pool decreased with increasing bulk density.

As the bulk density increases, a marked decreasing trend in natural peatlands indicates that the carbon content in natural peatlands is more sensitive to decomposition and mineral accumulation than that in degraded peatlands. However, the effects of

bulk density on carbohydrate and aromatic contents in natural/degraded peatlands covered by different plants were different. For herb and shrub peatlands, the carbohydrate and aromatic contents in natural peatlands were less sensitive than those in degraded peatlands. This result indicates that the stability of the natural peatland carbon pool is less sensitive to bulk density than that of degraded peatlands. However, the opposite trend for herb/shrub peatlands showed that the increase in bulk density decreased the stability of the carbon pool in natural herb/shrub peatlands. The decreasing trend of the fitted line also showed that the effects of bulk density on carbon content in natural herb/shrub peatlands were more marked than in others, and the effects of bulk density on carbon stability (i.e., aromatic/carbohydrate ratio) in degraded shrub peatlands were more marked than in other peatland types.

The high degree of decomposition in our selected method indicates that high amount of undecomposed plant litter (i.e., fibers) is decomposed and converted to organic matter in peat soils (Abd Rahman and Ming, 2015). Similar to bulk density, the effects of decomposition degree on carbon, aromatic content, and the aromatic/carbohydrate ratio in all peatland types were the same and negative, with opposite effects on carbohydrate content. Due to the carbohydrate compounds are more easily decomposed than aromatic compounds (Leifeld et al., 2012), residual plant litters with high aromatic and low carbohydrate contents in peat soils were not easy decomposed and converted to organic matter. And more undecomposed plant litters with high aromatic compounds contents was speculated as an important reason that cause high aromatic and low carbohydrate available in low decomposition degree of peat soils. What is more, high amount of available aromatics in weakly decomposed plant litter may also act as a major reason that inhibit the organic matter decomposition and increase carbon stability (Fenner and Freeman, 2020; Wilson et al., 2022). As the decomposition degree of peat soils increased, most of plant litter converted to organic matter, and the decrease in carbon content and aromatic/carbohydrate ratios showed that the decomposition processes not only caused carbon loss also decreased the stability of the peatland carbon pool.

Unlike bulk density and decomposition, the effects of pH on the selected carbon properties of different peatland types were different. For example, the effects of pH on carbon content in degraded and natural shrub peatlands were positive, whereas the effects on other peatland types were negative. The effects of pH on carbohydrate and aromatic contents in degraded shrub peatlands were more marked than in others. In degraded shrub peatlands, as the pH increased, the aromatic content increased and the carbohydrate content decreased markedly, and the aromatic/carbohydrate ratio also increased more markedly than in the others. The pH of peatlands is significantly influenced by water sources and nutrients availability, and peat soils with low pH are mainly found in peatlands, where the only water source is rainwater and low available nutrients (Rydin and Jeglum, 2013). As the pH increases, more nutrients are available in peat soils and cause organic matter to decompose more easily under high microbial metabolic activities (Ye et al., 2012; Zhao et al., 2022). For natural peatlands, the effects of pH on herb/shrub peatlands were more marked than in others, which indicates that the effects of water and nutrient sources in herb/shrub peatlands were also more marked than in others. However, except for degraded shrub peatlands, the weak effects of pH on the aromatic/carbohydrate ratios in all peatland types indicate that the effects of water sources and available nutrients on carbon stability were weak. Thus, the influence of increasing pH on the peatland carbon pool mainly decreased the carbon content in peat soils and had weak effects on the stability of peatland carbon pools.

4.3. Effects of environmental factors on peatland carbon pool

To assess the effects of environmental factors on the carbon content and stability of the peatland carbon pool, the altitude, annual average temperature, annual precipitation, and HII were selected as regional climate and human factors, and the correlation between these factors and carbon properties is shown in Figure 5. The importance of altitude for carbon content was highest in three of the four selected potential factors, and for carbon stability, it was slightly lower than the annual average temperature (Figure 3). With increasing altitude, the carbon and aromatic contents in herb-peatlands and herb/shrub peatlands increased, and the carbohydrate content decreased. Opposite trends were observed in shrub peatlands, and the contents of carbon and aromatics decreased markedly in high-altitude peatlands. Based on global peat samples, a previous study found that carbohydrate content was greater and aromatic content was lower at higher altitudes in similar latitudes (Verbeke et al., 2022), which was similar to the effects on shrub peatlands in our study. Thus, the response of the carbon pool in peatlands covered by different plant types to altitude increase is different and should be considered individually. Furthermore, the effects of altitude on carbohydrate and aromatic content in natural peatlands were more marked than those in degraded peatlands. Additionally, no obvious changes were observed for carbohydrate and aromatic contents in degraded peatlands in different altitude regions, and only carbon contents were increased slightly with an increase in altitude. The increase in altitude also markedly increased the aromatic/carbohydrate ratio in the natural peatlands and was more obvious in herb/shrub peatlands. The increase in the aromatic/carbohydrate ratio indicates that the chemical stability of the peatland carbon pool increased, which indicates that the peatland carbon pool in the high-altitude region was more stable than that in the low-altitude region.

Temperature and precipitation also act as two important climatic factors that have serious effects on the peatland carbon pool (Figure 5). Similar to altitude, the effects of temperature and precipitation on the carbon pool in different peatland types were also different. With an increase in the annual average temperature, the carbon and aromatic contents in the shrub peatlands increased markedly, and the carbohydrate content decreased. The shrub peatland carbon pool in the high-temperature region was more stable than that in the low-temperature region, which is similar to that observed in previous studies at the global scale (Hodgkins et al., 2018; Verbeke et al., 2022). However, the effects of annual average temperature on herb and herb/shrub peatlands were the opposite, and high aromatic/carbohydrate ratios occurred in those located in the low annual average temperature region. The increase in annual precipitation decreased carbon stability in shrub peatlands and increased carbon stability in others. The high slope of the trend line between carbon properties and annual precipitation in shrub peatlands indicates that shrub peatland carbon pools are more easily influenced by precipitation than in

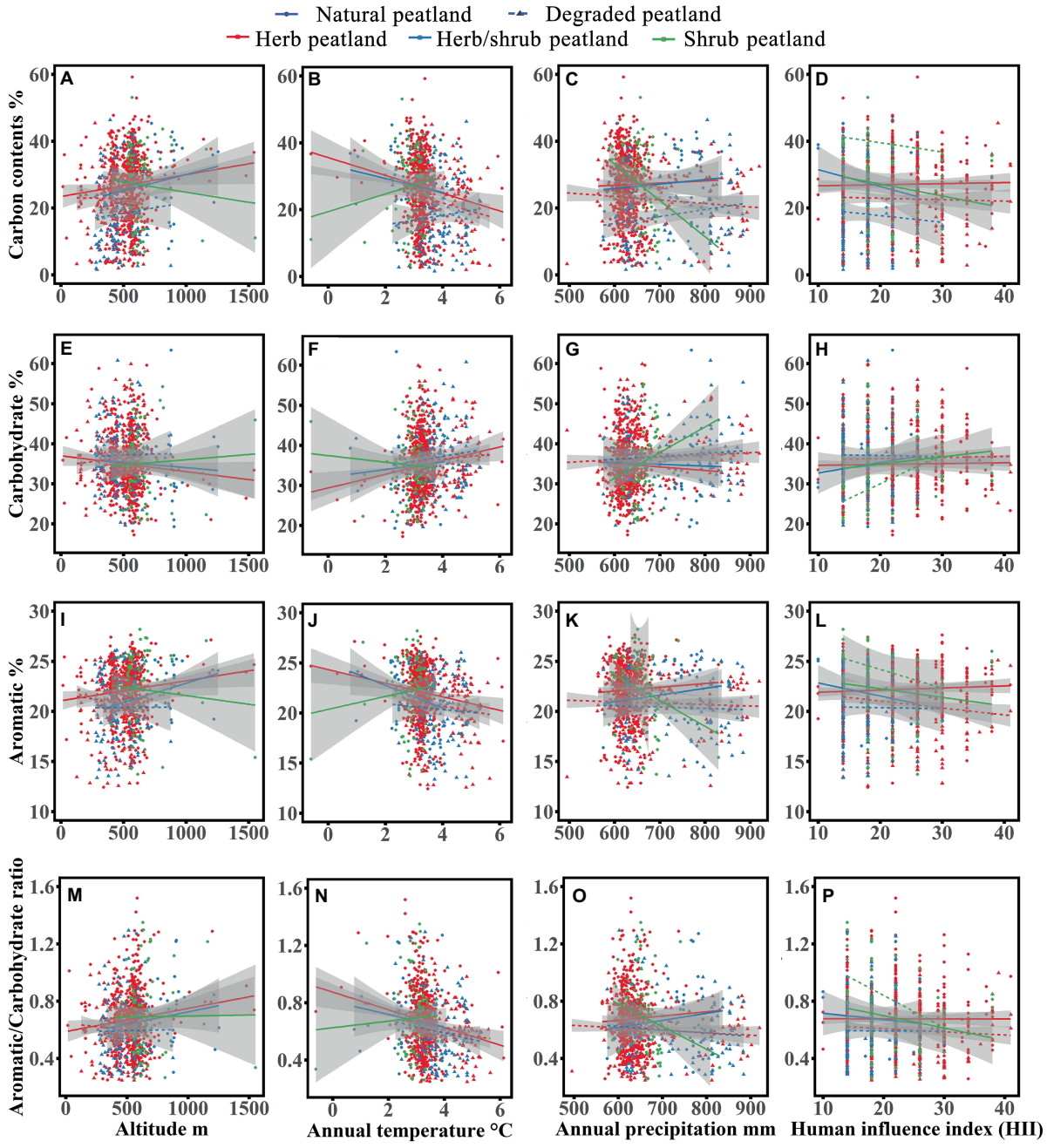

FIGURE 5
Relation between carbon contents (**A–D**), carbohydrate contents **(E–H)**, aromatic contents **(I–L)**, and aromatic/carbohydrate ratio **(M–P)** with altitude, mean annual temperature, annual precipitation, and human influence index (HII) in different dominated plant types of natural and degraded peatland. The trend lines were fitted with linear model, and the grey shadows indicate 95% confidence interval of fitted lines.

other peatland types. Because the water tables in shrub peatlands are lower than in others (Rydin and Jeglum, 2013), the importance of precipitation for shrub peatland water sources is stronger, and the changes in precipitation more easily cause water table fluctuations in shrub peatlands, which ultimately causes the dominate plant and the decomposition degree in the peatland carbon pool to change. The increase in precipitation increased the water table and biomass of herbs or mosses in shrub peatlands, which was speculated to be the major reason for the decrease in shrub peatlands.

Except for carbohydrate content, the importance of HII in the peatland carbon pool was the lowest among the four selected factors. With HII increasing, the carbon content in shrub and herb/shrub peatlands decreased and the carbohydrate content slightly increased. The effects of HII on aromatic content in the peatland carbon pool were more marked than those of the aromatic content of degraded

shrub peatlands. Similar to the aromatic contents, the effects of HII on the carbohydrate content and aromatic/carbohydrate ratio in degraded shrub peatlands were also the strongest, and the stability of the peatland carbon pool decreased with increasing HII. Although the effects of HII on natural shrub peatlands were slightly lower than those of degraded shrub peatlands, the increase in HII also decreased the stability of natural shrub peatlands more than that of natural herb and herb/shrub peatlands. The increase in the HII mainly caused more nutrients and pollution elements to accumulate in natural peatlands and decreased the surface water table due to regional agricultural water consumption (Gao et al., 2018). Thus, our results show that the carbon pool in shrub peatlands was more sensitive to regional human activities and climate change than in other peatland types. Compared with natural peatlands, degradation caused the shrub peatland carbon pool to be more easily influenced by regional human activities.

5. Conclusion

In this study, we identified the stability of the peatland carbon pool dominated by different peatland types and evaluated the effects of climate factors and human activities on the carbon pool in natural and degraded peatlands. Physicochemical factors of peat soils are the most important factors (especially bulk density) for the stability of the peatland carbon pool, and the annual average temperature is the most important environmental factor. The effects of environmental factors on carbon stability in peatlands covered by different plant types varied, and even the trend lines were opposite for some specific factors (e.g., annual average temperature and HII). Owing to the low water table and high frequency of aerobic/anaerobic changes in shrub peatlands, the stability of the carbon pool in shrub peatlands is more sensitive to climate change than in other peatland types. Compared to natural peatlands, the carbon stability in degraded herb peatlands and degraded herb/shrub peatlands was lower. Although the degradation process significantly increased the carbon stability in shrub peatlands, the degradation process also caused the shrub peatland carbon pool to be more easily influenced by regional human activities than in natural peatlands.

Data availability statement

The raw data supporting the conclusions of this article will be made available by the authors, without undue reservation.

Author contributions

JC, CG, and GW designed the research and provided the funding. JC and HZ ran the experiment, JC, DH, and FM analyze the data. JC and CG wrote the manuscript with input from HZ, DH, FM, and GW. All authors contributed to the article and approved the submitted version.

Funding

Financial support was provided by the National Natural Science Foundation of China (No. 42101108, 42171103), the Education Department of Heilongjiang Province (No. 135509145), the Youth Innovation Promotion Association CAS (No. 2020235), the Young Scientist Group Project of Northeast Institute of Geography and Agroecology, Chinese Academy of Sciences (2022QNXZ01), the Jilin Association for Science and Technology (QT202126), and the China Postdoctoral Science Foundation (2020M681059).

Acknowledgments

The authors gratefully acknowledge the assistance of the Analysis and Test Center of Northeast Institute of Geography and Agroecology, Chinese Academy of Sciences. The authors thank Prof. Hongwen Yu and Dr. Na Guo for FTIR analysis.

Conflict of interest

The authors declare that the research was conducted in the absence of any commercial or financial relationships that could be construed as a potential conflict of interest.

Publisher's note

All claims expressed in this article are solely those of the authors and do not necessarily represent those of their affiliated organizations, or those of the publisher, the editors and the reviewers. Any product that may be evaluated in this article, or claim that may be made by its manufacturer, is not guaranteed or endorsed by the publisher.

References

Abd Rahman, J., and Ming, C. C. (2015). Physico-chemical characterization of peat at different decomposition levels. *Electron. J. Geotech. Eng.* 20, 4011–4019.

Bao, K., Xing, W., Yu, X., Zhao, H., McLaughlin, N., Lu, X., et al. (2012). Recent atmospheric dust deposition in an ombrotrophic peat bog in great Hinggan Mountain, Northeast China. *Sci. Total Environ.* 431, 33–45. doi: 10.1016/j.scitotenv.2012.05.014

Bragazza, L., Freeman, C., Jones, T., Rydin, H., Limpens, J., Fenner, N., et al. (2006). Atmospheric nitrogen deposition promotes carbon loss from peat bogs. *Proc. Natl. Acad. Sci. U. S. A.* 103, 19386–19389. doi: 10.1073/pnas.0606629104

Clarkson, B. R., Moore, T. R., Fitzgerald, N. B., Thornburrow, D., Watts, C. H., and Miller, S. (2013). Water table regime regulates litter decomposition in Restiad Peatlands, New Zealand. *Ecosystems* 17, 317–326. doi: 10.1007/s10021-013-9726-4

Cong, J., Gao, C., Han, D., Li, Y., and Wang, G. (2020). Stability of the permafrost peatlands carbon pool under climate change and wildfires during the last 150 years in the northern great Khingan Mountains. *China. Sci. Total Environ.* 712:136476. doi: 10.1016/j.scitotenv.2019.136476

Cong, J., Gao, C., Xing, W., Han, D., Li, Y., and Wang, G. (2022). Historical chemical stability of carbon pool in permafrost peatlands in northern great Khingan Mountains (China) during the last millennium, and its paleoenvironmental implications. *Catena* 209:105853. doi: 10.1016/j.catena.2021.105853

Dohong, A., Aziz, A. A., and Dargusch, P. (2017). A review of the drivers of tropical peatland degradation in South-East Asia. *Land Use Policy* 69, 349–360. doi: 10.1016/j.landusepol.2017.09.035

Drollinger, S., Knorr, K.-H., Knierzinger, W., and Glatzel, S. (2020). Peat decomposition proxies of alpine bogs along a degradation gradient. *Geoderma* 369:114331. doi: 10.1016/j.geoderma.2020.114331

Fenner, N., and Freeman, C. (2020). Woody litter protects peat carbon stocks during drought. *Nat. Clim. Chang.* 10, 363–369. doi: 10.1038/s41558-020-0727-y

Fick, S. E., and Hijmans, R. J. (2017). WorldClim 2: new 1-km spatial resolution climate surfaces for global land areas. *Int. J. Climatol.* 37, 4302–4315. doi: 10.1002/joc.5086

Gao, C., Knorr, K.-H., Yu, Z., He, J., Zhang, S., Lu, X., et al. (2016). Black carbon deposition and storage in peat soils of the Changbai Mountain, China. *Geoderma* 273, 98–105. doi: 10.1016/j.geoderma.2016.03.021

Gao, C., Zhang, S., Liu, H., Cong, J., Li, Y., and Wang, G. (2018). The impacts of land reclamation on the accumulation of key elements in wetland ecosystems in the Sanjiang plain, Northeast China. *Environ. Pollut.* 237, 487–498. doi: 10.1016/j.envpol.2018.02.075

Guo, X., Du, W., Wang, X., and Yang, Z. (2013). Degradation and structure change of humic acids corresponding to water decline in Zoige peatland, Qinghai-Tibet Plateau. *Sci. Total Environ.* 445–446, 231–236. doi: 10.1016/j.scitotenv.2012.12.048

Han, D., Gao, C., Liu, H., Li, Y., Cong, J., Yu, X., et al. (2021). Anthropogenic and climatic driven peatland degradation during the past 150 years in greater Khingan Mountains, NE China. *Land Degrad. Dev.* 32, 4845–4857. doi: 10.1002/ldr.4036

Heller, C., Ellerbrock, R. H., Roßkopf, N., Klingenfuß, C., and Zeitz, J. (2015). Soil organic matter characterization of temperate peatland soil with FTIR-spectroscopy: effects of mire type and drainage intensity. *Eur. J. Soil Sci.* 66, 847–858. doi: 10.1111/ejss.12279

Hodgkins, S. B., Richardson, C. J., Dommain, R., Wang, H., Glaser, P. H., Verbeke, B., et al. (2018). Tropical peatland carbon storage linked to global latitudinal trends in peat recalcitrance. *Nat. Commun.* 9:3640. doi: 10.1038/s41467-018-06050-2

Kareksela, S., Haapalehto, T., Juutinen, R., Matilainen, R., Tahvanainen, T., and Kotiaho, J. S. (2015). Fighting carbon loss of degraded peatlands by jump-starting ecosystem functioning with ecological restoration. *Sci. Total Environ.* 537, 268–276. doi: 10.1016/j.scitotenv.2015.07.094

Keddy, P. A. (2010). *Wetland Ecology: Principles and Conservation*. Cambridge, United Kingdom: Cambridge University Press.

Leifeld, J., Klein, K., and Wust-Galley, C. (2020). Soil organic matter stoichiometry as indicator for peatland degradation. *Sci. Rep-UK* 10:7634. doi: 10.1038/s41598-020-64275-y

Leifeld, J., and Menichetti, L. (2018). The underappreciated potential of peatlands in global climate change mitigation strategies. *Nat. Commun.* 9:1071. doi: 10.1038/s41467-018-03406-6

Leifeld, J., Steffens, M., and Galego-Sala, A. (2012). Sensitivity of peatland carbon loss to organic matter quality. *Geophys. Res. Lett.* 39, 1–6. doi: 10.1029/2012gl051856

Loisel, J., Gallego-Sala, A. V., Amesbury, M. J., Magnan, G., Anshari, G., Beilman, D. W., et al. (2020). Expert assessment of future vulnerability of the global peatland carbon sink. *Nat. Clim. Chang.* 11, 70–77. doi: 10.1038/s41558-020-00944-0

Loisel, J., van Bellen, S., Pelletier, L., Talbot, J., Hugelius, G., Karran, D., et al. (2017). Insights and issues with estimating northern peatland carbon stocks and fluxes since the last glacial maximum. *Earth-Sci. Rev.* 165, 59–80. doi: 10.1016/j.earscirev.2016.12.001

Loisel, J., Yu, Z., Beilman, D. W., Camill, P., Alm, J., Amesbury, M. J., et al. (2014). A database and synthesis of northern peatland soil properties and Holocene carbon and nitrogen accumulation. *Holocene* 24, 1028–1042. doi: 10.1177/0959683614538073

Lou, Y., Gao, C., Pan, Y., Xue, Z., Liu, Y., Tang, Z., et al. (2018). Niche modelling of marsh plants based on occurrence and abundance data. *Sci. Total Environ.* 616-617, 198–207. doi: 10.1016/j.scitotenv.2017.10.300

Lou, Y., Zhao, K., Wang, G., Jiang, M., Lu, X., and Rydin, H. (2015). Long-term changes in marsh vegetation in Sanjiang plain, Northeast China. *J. Veg. Sci.* 26, 643–650. doi: 10.1111/jvs.12270

Munir, T. M., Xu, B., Perkins, M., and Strack, M. (2014). Responses of carbon dioxide flux and plant biomass to water table drawdown in a treed peatland in northern Alberta: a climate change perspective. *Biogeosciences* 11, 807–820. doi: 10.5194/bg-11-807-2014

Negassa, W., Acksel, A., Eckhardt, K.-U., Regier, T., and Leinweber, P. (2019). Soil organic matter characteristics in drained and rewetted peatlands of northern Germany: chemical and spectroscopic analyses. *Geoderma* 353, 468–481. doi: 10.1016/j.geoderma.2019.07.002

Normand, A. E., Smith, A. N., Clark, M. W., Long, J. R., and Reddy, K. R. (2017). Chemical composition of soil organic matter in a subarctic Peatland: influence of shifting vegetation communities. *Soil Sci. Soc. Am. J.* 81, 41–49. doi: 10.2136/sssaj2016.05.0148

Paul, E. A. (2016). The nature and dynamics of soil organic matter: plant inputs, microbial transformations, and organic matter stabilization. *Soil Biol. Biochem.* 98, 109–126. doi: 10.1016/j.soilbio.2016.04.001

Poorter, H., Niklas, K. J., Reich, P. B., Oleksyn, J., Poot, P., and Mommer, L. (2012). Biomass allocation to leaves, stems and roots: meta-analyses of interspecific variation and environmental control. *New Phytol.* 193, 30–50. doi: 10.1111/j.1469-8137.2011.03952.x

Qiu, C., Zhu, D., Ciais, P., Guenet, B., Peng, S., and Xu, X. (2020). The role of northern peatlands in the global carbon cycle for the 21st century. *Glob. Ecol. Biogeogr.* 29, 956–973. doi: 10.1111/geb.13081

Rydin, H., and Jeglum, J. K. (2013). *The Biology of Peatlands, 2e*. Oxford, United Kingdom: Oxford University Press.

Šimanauskienė, R., Linkevičienė, R., Bartold, M., Dąbrowska-Zielińska, K., Slavinskienė, G., Veteikis, D., et al. (2019). Peatland degradation: the relationship between raised bog hydrology and normalized difference vegetation index. *Ecohydrology* 12:e2159. doi: 10.1002/eco.2159

Sjögersten, S., Caul, S., Daniell, T. J., Jurd, A. P. S., O'Sullivan, O. S., Stapleton, C. S., et al. (2016). Organic matter chemistry controls greenhouse gas emissions from permafrost peatlands. *Soil Biol. Biochem.* 98, 42–53. doi: 10.1016/j.soilbio.2016.03.016

Solomon, S., Qin, D., Manning, M., Averyt, K., and Marquis, M. (2007). *Climate Change 2007-the Physical Science Basis: Working Group I Contribution to the Fourth Assessment Report of the IPCC*. Cambridge, United Kingdom: Cambridge University Press.

Straková, P., Penttilä, T., Laine, J., and Laiho, R. (2012). Disentangling direct and indirect effects of water table drawdown on above- and belowground plant litter decomposition: consequences for accumulation of organic matter in boreal peatlands. *Glob. Chang. Biol.* 18, 322–335. doi: 10.1111/j.1365-2486.2011.02503.x

Verbeke, B. A., Lamit, L. J., Lilleskov, E. A., Hodgkins, S. B., Basiliko, N., Kane, E. S., et al. (2022). Latitude, elevation, and mean annual temperature predict peat organic matter chemistry at a global scale. *Global Biogeochem. Cy.* 36:e2021GB007057. doi: 10.1029/2021gb007057

Wang, Y., Paul, S. M., Jocher, M., Espic, C., Alewell, C., Szidat, S., et al. (2021b). Soil carbon loss from drained agricultural peatland after coverage with mineral soil. *Sci. Total Environ.* 800:149498. doi: 10.1016/j.scitotenv.2021.149498

Wang, H., Richardson, C. J., and Ho, M. (2015). Dual controls on carbon loss during drought in peatlands. *Nat. Clim. Chang.* 5, 584–587. doi: 10.1038/nclimate2643

Wang, H., Tian, J., Chen, H., Ho, M., Vilgalys, R., Bu, Z.-J., et al. (2021a). Vegetation and microbes interact to preserve carbon in many wooded peatlands. *Commun. Earth Environ.* 2, 1–8. doi: 10.1038/s43247-021-00136-4

WCS and CIESIN (2005). Last of the Wild Project, Version 2 (LWP-2): Last of the wild dataset (geographic). NASA Socioeconomic Data and Applications Center (SEDAC), Palisades, NY, 2005.

Wilson, R. M., Hopple, A. M., Tfaily, M. M., Sebestyen, S. D., Schadt, C. W., Pfeifer-Meister, L., et al. (2016). Stability of peatland carbon to rising temperatures. *Nat. Commun.* 7:13723. doi: 10.1038/ncomms13723

Wilson, R. M., Hough, M. A., Verbeke, B. A., Hodgkins, S. B., IsoGenie, C., Chanton, J. P., et al. (2022). Plant organic matter inputs exert a strong control on soil organic matter decomposition in a thawing permafrost peatland. *Sci. Total Environ.* 820:152757. doi: 10.1016/j.scitotenv.2021.152757

Wu, Y., Blodau, C., Moore, T. R., Bubier, J., Juutinen, S., and Larmola, T. (2015). Effects of experimental nitrogen deposition on peatland carbon pools and fluxes: a modelling analysis. *Biogeosciences* 12, 79–101. doi: 10.5194/bg-12-79-2015

Wu, J., and Roulet, N. T. (2014). Climate change reduces the capacity of northern peatlands to absorb the atmospheric carbon dioxide: the different responses of bogs and fens. *Global Biogeochem. Cy.* 28, 1005–1024. doi: 10.1002/2014GB004845

Xing, W., Bao, K., Gallego-Sala, A. V., Charman, D. J., Zhang, Z., Gao, C., et al. (2015). Climate controls on carbon accumulation in peatlands of Northeast China. *Quaternary Sci. Rev.* 115, 78–88. doi: 10.1016/j.quascirev.2015.03.005

Xu, J., Morris, P. J., Liu, J., and Holden, J. (2018). PEATMAP: refining estimates of global peatland distribution based on a meta-analysis. *Catena* 160, 134–140. doi: 10.1016/j.catena.2017.09.010

Ye, R., Jin, Q., Bohannan, B., Keller, J. K., McAllister, S. A., and Bridgham, S. D. (2012). pH controls over anaerobic carbon mineralization, the efficiency of methane production, and methanogenic pathways in peatlands across an ombrotrophic–minerotrophic gradient. *Soil Biol. Biochem.* 54, 36–47. doi: 10.1016/j.soilbio.2012.05.015

Yu, Z., Loisel, J., Brosseau, D. P., Beilman, D. W., and Hunt, S. J. (2010). Global peatland dynamics since the last glacial maximum. *Geophys. Res. Lett.* 37, 1–5. doi: 10.1029/2010gl043584

Zhao, X., Chen, J., Guo, M., Li, C., Hou, N., and Bai, S. (2022). Constructed wetlands treating synthetic wastewater in response to day-night alterations: performance and mechanisms. *Chem. Eng. J.* 446:137460. doi: 10.1016/j.cej.2022.137460

Zhao, H., Tong, D. Q., Lin, Q., Lu, X., and Wang, G. (2012). Effect of fires on soil organic carbon pool and mineralization in a northeastern China wetland. *Geoderma* 189–190, 532–539. doi: 10.1016/j.geoderma.2012.05.013

frontiers | Frontiers in Ecology and Evolution

TYPE Original Research
PUBLISHED 24 April 2023
DOI 10.3389/fevo.2023.1126651

OPEN ACCESS

EDITED BY
Zhongqing Yan,
Chinese Academy of Forestry, China

REVIEWED BY
Linfeng Li,
University of Chinese Academy of Sciences, China
Chitra Bahadur Baniya,
Tribhuvan University, Nepal

*CORRESPONDENCE
Gang Fu
✉ fugang@igsnrr.ac.cn;
✉ fugang09@126.com
†These authors have contributed equally to this work

RECEIVED 18 December 2022
ACCEPTED 03 April 2023
PUBLISHED 24 April 2023

CITATION
Han F, Yu C and Fu G (2023) Asymmetric warming among elevations may homogenize plant α-diversity and aboveground net primary production of alpine grasslands.
Front. Ecol. Evol. 11:1126651.
doi: 10.3389/fevo.2023.1126651

Asymmetric warming among elevations may homogenize plant α-diversity and aboveground net primary production of alpine grasslands

Fusong Han[1,2†], Chengqun Yu[1†] and Gang Fu[1*]

[1]Lhasa Plateau Ecosystem Research Station, Key Laboratory of Ecosystem Network Observation and Modeling, Institute of Geographic Sciences and Natural Resources Research, Chinese Academy of Sciences, Beijing, China, [2]School of Resource and Environment and Safety Engineering, Hunan University of Science and Technology, Xiangtan, Hunan, China

It is well known that asymmetric warming among elevations (i.e., warming magnitude increases with increasing elevation) will weaken the difference of air temperature among elevations. However, it remains controversial on whether asymmetric warming among elevations can homogenize plant α-diversity and above-ground net primary production (ANPP) in alpine regions. In the present study, we conducted an experiment of asymmetric warming among elevations in alpine grasslands, Northern Tibet since 2010. There were four experiment treatments, including a treatment under natural conditions at elevation 4,313m (C4313), a treatment under natural conditions at elevation 4,513m (C4513), a treatment under warming conditions at elevation 4,513m (W4513) and a treatment under warming conditions at elevation 4,693m (W4693). We investigated ANPP, taxonomic α-diversity (i.e., species richness, Shannon, Simpson and Pielou) and phylogenetic α-diversity (mean nearest taxon distance, MNTD; phylogenetic diversity, PD) in 2011–2019. There were no significant differences of mean air temperature between C4313 and W4513, or between C4513 and W4693 in 2011–2019, indicating the differences of air temperature were eliminated among elevations. Then we found that the differences of plant α-diversity and ANPP were also eliminated among elevations: (1) there were no significant differences of ANPP, Pielou and MNTD between C4313 and W4513, or between C4513 and W4693 in 2011–2019. (2) There were also no significant differences of mean species richness, Shannon and Simpson between C4513 and W4693 in 2011–2019. (3) There were also no significant differences of ANPP, species richness, Shannon, Simpson, Pielou, PD and MNTD between C4313 and W4513, or C4513 and W4693 in 2019. Therefore, asymmetric warming among elevations may homogenize plant α-diversity and aboveground net primary production in alpine grasslands, at least in Northern Tibet.

KEYWORDS

biodiversity, symmetrical warming, phylogenetic diversity, Tibetan Plateau, asymmetric warming

1. Introduction

Climate warming is an accepted fact, and the warming magnitudes vary by region (Tian and Fu, 2022). The asymmetric warming among elevations, as a case of spatial asymmetric warming, can generally refer to warming magnitude increases with increasing elevation for some special regions, especially in some highland areas (Yao et al., 2000; Rangwala and Miller, 2012). However, there is still argument on how such asymmetric warming among elevations can influence terrestrial ecosystems, which can be mainly due to the following facts. First, previous studies have focused on the phenomenon itself of asymmetric warming among elevations and possible driving mechanisms (Rangwala and Miller, 2012) rather than the effects of asymmetric warming among elevations on ecosystem structure and function. Second, asymmetric warming generally includes daily asymmetric warming (Zhong and Fu, 2022), seasonal asymmetric warming (Fu et al., 2019; Fu and Shen, 2022; Han et al., 2023) and spatial asymmetric warming (Wang et al., 2021b, 2022; Fu et al., 2022). Previous studies have primarily explored the impacts of daily and seasonal asymmetric warming on terrestrial ecosystems (Bokhorst et al., 2011; Tozzi et al., 2014; Ji et al., 2017; Yang et al., 2017; Fu et al., 2019; Fu and Shen, 2022; Zhong and Fu, 2022), but only a small number of studies have tried to probe the responses of terrestrial ecosystems to asymmetric warming among elevations (Wang et al., 2021b). Symmetric warming among elevations may overestimate the impact of asymmetric warming among elevations on plant species and phylogenetic composition (Wang et al., 2021a,b; Fu and Sun, 2022), which implies that some related conclusions from previous studies may exaggerate the impacts of climate warming on ecosystem structure and function. There is still a great deal of uncertainty about the effects of climate warming on various ecosystems, because asymmetric warming among elevations has not received enough attention. Third, warming magnitude is one of the core problems for spatial and temporal asymmetric warming, and thus many previous studies have tried to investigate how warming magnitude can alter the impacts of climate warming on terrestrial ecosystems and found that temperature sensitivities of ecosystem structure and function can generally change with warming magnitude (Fu et al., 2015b, 2018, 2022; Yu et al., 2019b; Fu and Sun, 2022). Such studies may indirectly support that the effects of asymmetric warming among elevations on various ecosystems are different from those of symmetric warming among elevations, but can hardly obtain the impacts of asymmetric warming among elevations on terrestrial ecosystems directly. Therefore, further investigation on the impacts of asymmetric warming among elevations on terrestrial ecosystems will be necessary.

Grasslands, as an important vegetation type in global ecosystems, are key resources for high-quality development of livestock industry and an important place for wildlife protection (Fu et al., 2022; Zha et al., 2022; Han et al., 2022a; Wang and Fu, 2023). Alpine grasslands are important sections of global grasslands, and may be the most sensitive and fragile grassland types to global change (Zhang et al., 2015, 2022; Fu and Sun, 2022). Alpine meadows and alpine steppes on the Qinghai-Tibet Plateau are not only two of the most typical alpine grasslands on the world, but also the grassland types closest to the sky on the earth (Zhang et al., 2015; Zong and Fu, 2021; Han et al., 2022b). Aboveground net primary production (ANPP) determines the largest carrying capacity of grazing livestock and wild animals in grasslands (Wang et al., 2022). A certain size of plant α-diversity and relatively rational plant community composition are the basis for sustaining large ANPP in grasslands (Wang et al., 2021a; Fu and Sun, 2022). The ANPP and plant diversity of alpine grasslands are survival basis for maintaining yaks and other specific plateau grazing livestock and wild animals, which can ensure the livelihood of Tibetan people's on the Qinghai-Tibet Plateau (Fu et al., 2022; Wang et al., 2022). Alpine grasslands of the Qinghai-Tibet Plateau are not only the typical regions with asymmetric warming among elevations (Qin et al., 2009; Du et al., 2019), but also the perfect areas to trace alterations in ANPP and biodiversity under external disturbance conditions (Trisos et al., 2020; Tian and Fu, 2022; Zhang et al., 2022). However, as we refer to the best knowledge, only one study has tried to explore the effects of asymmetric warming among elevations on plant species and phylogenetic composition in alpine grasslands on the Tibetan Plateau (Wang et al., 2021b) and no reports have investigated the impacts of asymmetric warming among elevations on ANPP and plant α-diversity in alpine grasslands of the Tibetan Plateau. This limits our ability to accurately predict plant productivity and diversity in alpine grassland ecosystems under future scenes of asymmetric warming among elevations, which in turn may limit our abilities to fully use grassland forages for scientific and high-quality livestock development, as well as biodiversity conservation. Therefore, investigating the impacts of asymmetric warming among elevations on plant α-diversity and ANPP in alpine grasslands of the Tibetan Plateau will undisputablly broaden our mind.

Here, since May 2010, we performed an experiment of asymmetric warming among elevations in alpine grasslands of the Tibet, and measured ANPP, plant phylogenetic and species α-diversity in 2011–2019. The main goal of the present study was to explore whether asymmetric warming among elevations may homogenize ANPP, plant phylogenetic and species α-diversity. Previous studies found that asymmetric warming among elevations may homogenize plant phylogenetic and species composition in alpine grasslands of the Qinghai-Tibet Plateau (Wang et al., 2021b). Previous studies also found that the temperature sensitivity of plant production were mainly related to temperature itself (Fu and Sun, 2022) and asymmetric warming among elevations can result in homogeneous temperature among elevations in alpine grasslands (Wang et al., 2021b). Therefore, we hypothesized that asymmetric warming among elevations may homogenize ANPP, plant phylogenetic and species α-diversity in alpine grasslands.

2. Materials and methods

2.1. Study area and experimental design

The detailed information about the study area and experiment design have been published in our previous studies (Zhang et al., 2021; Wang et al., 2021b; Fu and Sun, 2022). Since May 2010, we chose three alpine grassland sites with elevation about 4,313, 4,513, and 4,693 m in the Northern Tibet Plateau, respectively. Four open top chambers (top with 1.00 m in diameter, bottom with 1.45 m in diameter, and height with 0.40 m) were established at elevation 4,513 m (W4513) and 4,693 m (W4693), and four control plots (no open top chambers) were established at elevation 4,313 m (C4313) and 4,513 m (C4513), respectively.

2.2. Microclimate observations, soil sampling, and analyses

The detailed information about the monitoring and observations of soil temperature (T_s, 0.05 m), air temperature (T_a, 0.15 m), soil moisture (SM, 0.10 m), and relative humidity (RH, 0.15 m), and a derived microclimate variable (i.e., vapor pressure deficit, VPD), could be discovered by our prior reports (Zhang et al., 2021; Wang et al., 2021b). The HOBO microclimate observation stations were used to monitor T_s, T_a, SM and RH, and the original sampling frequency of these climate data was 1 min (Zhang et al., 2021; Fu and Sun, 2022). The VPD was calculated from T_a and RH (Yu et al., 2019b; Fu and Shen, 2022). The T_s, T_a, SM, and VPD during the period from June to September in 2011–2019 were used in the present study. The topsoil (0–0.10 m) samples were gathered in August, 2013 and 2015–2019, and then used to measure soil nitrate nitrogen (NO_3^--N), ammonium nitrogen (NH_4^+-N), pH and available phosphorus (AP; Yu et al., 2019a). The comparisons of T_s, T_a, SM, VPD, NO_3^--N, NH_4^+-N, AP, and pH between C4313 and W4513, C4313 and W4693, or C4513 and W4693 were published by our a previous study (Wang et al., 2021b).

2.3. Community investigation and ANPP simulations

The detailed information about plant community investigation could be discovered by our prior reports (Wang et al., 2021a,b). We used measured species height and coverage to obtain the important value for each species. Important values were used to obtain species α-diversity, including species richness, Shannon, Simpson and Pielou (Sun et al., 2021). We obtained plant phylogenetic tree from taxonomic information for each species (Sun et al., 2021). Then we calculated phylogenetic α-diversity (Faith's phylogenetic diversity, PD; mean nearest taxon distance, MNTD) using important values matrix of all species and phylogenetic tree (Sun et al., 2021). All the detected species in our experimental plots were categorized into sedge, graminoid and forb function groups. Aboveground net primary production of sedge ($ANPP_{sedge}$), graminoid ($ANPP_{graminoid}$), and forb ($ANPP_{forb}$) were estimated from measured sedge, graminoid and forb coverage and height, respectively (Wang et al., 2021a). Community aboveground net primary production (ANPP) was obtained from the following equation.

$$ANPP = \mathrm{ANPP}_{sedge} + ANPP_{graminold} + \mathrm{ANPP}_{forb} \quad (1)$$

2.4. Statistical analyses

The temperature difference among elevations can be decreased and even approached zero under the asymmetric warming among elevations conditions (Wang et al., 2021b). If there were no significant differences of plant productivity and α-diversity among elevations, asymmetric warming among elevations were supposed to homogenize ANPP and plant α-diversity. We calculated geographic distance among the three elevations. For each year, we used *t*-test to compare the differences of ANPP, species richness, Shannon, Simpson, Pielou, PD and MNTD between C4313 and W4513, between C4513 and W4693, or between C4313 and W4693. Then we used repeated measure analysis of variance to test the differences of ANPP, species richness, Shannon, Simpson, Pielou, PD, and MNTD between C4313 and W4513, between C4513 and W4693, or between C4313 and W4693 based on all the nine-year measured data. We used environment variables to partition the variations of plant α-diversity and ANPP into four parts. All the tests of significance referred to $p < 0.05$ and performed in R 4.1.2. The package used in the present study included the SPAA, vegan, Plantlist and Picante.

3. Results

3.1. Comparisons of plant α-diversity and aboveground plant production between the C4313 versus W4513, C4313 versus W4693, and C4513 versus W4693

Significant dissimilarities for the multi-year average ANPP of the C4313 versus W4513, C4313 versus W4693, and C4513 versus W4693 in 2011–2019 were not detected (Table 1). Significant

TABLE 1 Comparison of average ANPP, $ANPP_{graminoid}$, $ANPP_{sedge}$, $ANPP_{forb}$, SR, Shannon, Simpson, Pielou, PD, and MNTD in 2011–2019 of the C4313 versus W4513, C4313 versus W4693, and C4513 versus W4693 based on a repeated ANOVA.

Variable	C4313 versus W4513		C4313 versus W4693		C4513 versus W4693	
	C4313	W4513	C4313	W4693	C4513	W4693
ANPP	34.37 ± 2.06	31.17 ± 3.28	34.37 ± 2.06	49.85 ± 11.13	39.94 ± 7.77	49.85 ± 11.13
$ANPP_{graminoid}$	15.40 ± 7.02	18.45 ± 4.80	15.40 ± 7.02 a	1.34 ± 0.82 b	23.55 ± 5.36 a	1.34 ± 0.82 b
$ANPP_{sedge}$	6.89 ± 3.05	8.35 ± 4.34	6.89 ± 3.05 b	37.78 ± 10.40 a	10.12 ± 2.33 b	37.78 ± 10.40 a
$ANPP_{forb}$	12.07 ± 2.82 a	4.37 ± 0.48 b	12.07 ± 2.82	10.73 ± 1.60	6.26 ± 0.76 b	10.73 ± 1.60 a
SR	8.72 ± 0.88 a	6.44 ± 0.79 b	8.72 ± 0.88	7.97 ± 0.60	6.94 ± 0.61	7.97 ± 0.60
Shannon	1.75 ± 0.15 a	1.45 ± 0.12 b	1.75 ± 0.15	1.65 ± 0.06	1.57 ± 0.03	1.65 ± 0.06
Simpson	0.77 ± 0.04 a	0.69 ± 0.04 b	0.77 ± 0.04	0.74 ± 0.02	0.73 ± 0.01	0.74 ± 0.02
Pielou	0.82 ± 0.04	0.79 ± 0.04	0.82 ± 0.04	0.82 ± 0.02	0.83 ± 0.03	0.82 ± 0.02
PD	908.14 ± 55.99 a	692.23 ± 49.16 b	908.14 ± 55.99	859.59 ± 48.78	748.51 ± 47.26 b	859.59 ± 48.78 a
MNTD	138.57 ± 6.95	121.94 ± 27.96	138.57 ± 6.95	122.26 ± 25.88	136.25 ± 5.49	122.26 ± 25.88

ANPP, aboveground net primary production of plant community; $ANPP_{graminoid}$, aboveground net primary production of graminoid; $ANPP_{sedge}$, aboveground net primary production of sedge; $ANPP_{forb}$, aboveground net primary production of forb; SR, species richness; PD, Faith's phylogenetic diversity; MNTD, mean nearest taxon distance. Different letters indicate significant dissimilarity.

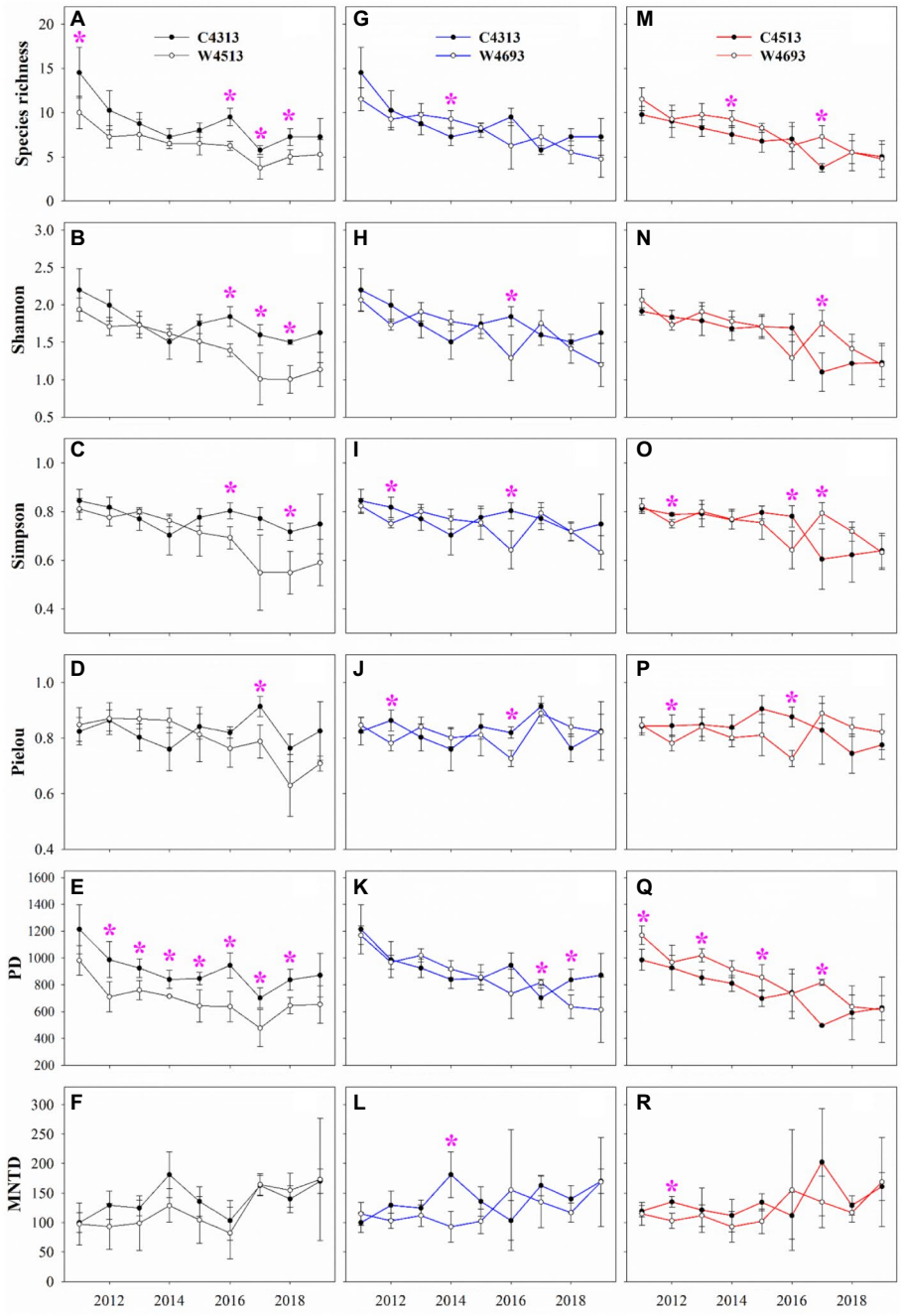

FIGURE 1
Comparison of species richness (SR), Shannon, Simpson, Pielou, Faith's phylogenetic diversity (PD) and mean nearest taxon distance (MNTD) of plant community **(A–F)** between the non-warming plots at elevation 4,313 m (C4313) and warming plots at elevation 4,513 m (W4513), **(G–L)** between the C4313 and warming plots at elevation 4,693 m (W4693), and **(M–R)** between the non-warming plots at elevation 4,513 m (C4513) and the W4693.

dissimilarities for multi-year average $ANPP_{sedge}$ and $ANPP_{graminoid}$ of the C4313 versus W4513, and significant dissimilarity for multi-year average $ANPP_{forb}$ of the C4313 versus W4693 in 2011–2019 were not detected (Table 1). The multi-year average $ANPP_{sedge}$ of the W4693 was larger than that of the C4313 and C4513, while the multi-year average $ANPP_{graminoid}$ of the W4693 was lower than that of the C4313 and C4513 in 2011–2019 (Table 1). A significant dissimilarity of multi-year average $ANPP_{forb}$ was also detected between the C4313 versus W4513, and the C4513 versus W4693 in 2011–2019 (Table 1). Two of the six variables of plant α-diversity (i.e., Pielou and MNTD) between the C4313 versus W4513 were not significant dissimilar in 2011–2019 (Table 1). None of the six variables of plant α-diversity between the C4313 versus W4693 was significant dissimilar in 2011–2019 (Table 1). Only one of the six variables of plant α-diversity (i.e., PD) between the C4513 versus W4693 was significant dissimilar in 2011–2019 (Table 1). The dissimilarities of the ANPP, $ANPP_{sedge}$, $ANPP_{graminoid}$, $ANPP_{forb}$, and the six variables of plant α-diversity between the C4313 versus W4513, the C4313 versus W4693, and the C4513 versus W4693 varied with year (Figures 1, 2).

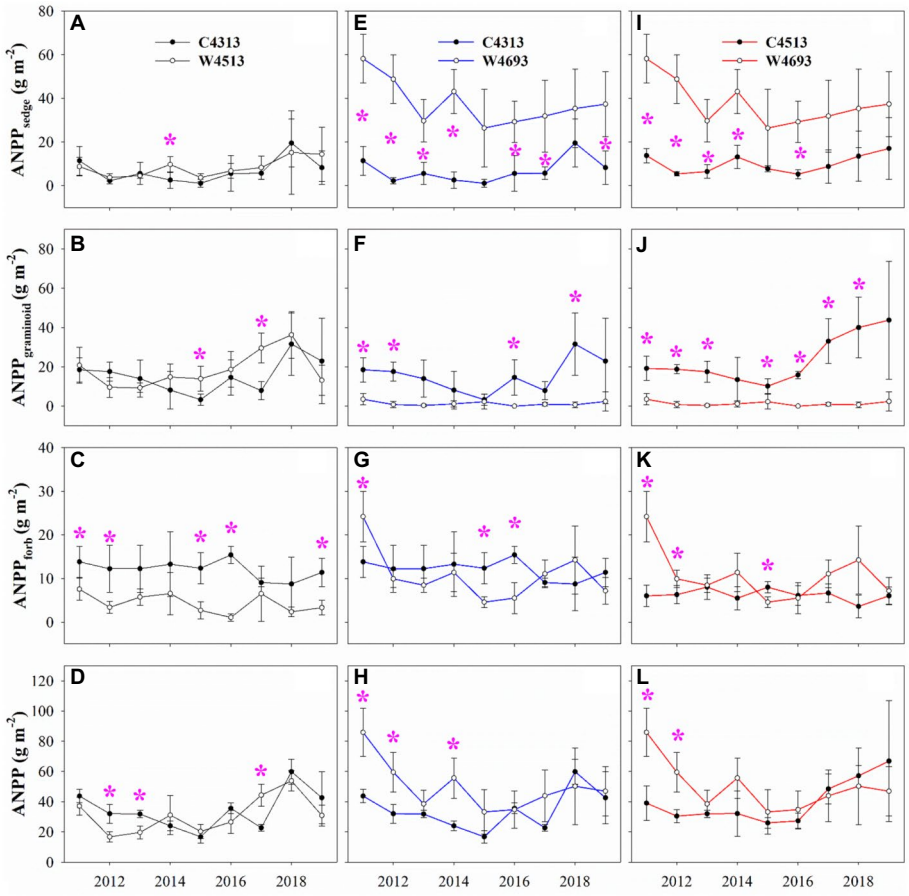

FIGURE 2
Comparison of aboveground net primary production of plant community (ANPP), aboveground net primary production of sedge (ANPP$_{sedge}$), aboveground net primary production of graminoid (ANPP$_{graminoid}$), and aboveground net primary production of forb (ANPP$_{forb}$; **A–D**) between the non-warming plots at elevation 4,313 m (C4313) and warming plots at elevation 4,513 m (W4513), **(E–H)** between the C4313 and warming plots at elevation 4,693 m (W4693), and **(I–L)** between the non-warming plots at elevation 4,513 m (C4513) and the W4693.

3.2. Correlations between ANPP, ANPPgraminoid, ANPPsedge, ANPPforb, and α-diversity versus environmental variables, and ANPP versus α-diversity

The ANPP dissimilarities of C4313 versus W4513, C4313 versus W4693, and C4513 versus W4693 decreased with warming duration, but that of Shannon, Simpson and Pielou increased with warming duration (Supplementary Table S1). The ANPP dissimilarity increased with phylogenetic composition dissimilarity of C4313 versus W4513, C4313 versus W4693, and C4513 versus W4693 (Supplementary Table S1). The ANPP$_{sedge}$ dissimilarity increased with the dissimilarity of T_s and pH of C4313 versus W4513, C4313 versus W4693, and C4513 versus W4693 (Supplementary Table S1). The Pielou dissimilarity decreased with the NO_3^--N dissimilarity of C4313 versus W4513, C4313 versus W4693, and C4513 versus W4693 (Supplementary Table S1).

All the four explained parts had excluded impacts on Shannon, Simpson, PD, ANPP$_{sedge}$ and ANPP$_{forb}$ (Figure 3; Supplementary Figure S1). Only one of the four explained parts (i.e., soil pH) had a no excluded impact on species richness (Figure 3). Two of the four explained parts (i.e., "GeoDist.Dur." and "Soil nutrition") had excluded impacts on Pielou, but they did not have excluded impacts on MNTD (Figure 3). Two of the four explained parts (i.e., "Temp.Water" and "Soil nutrition") had excluded impacts on ANPP (Supplementary Figure S1). Only one of the four explained parts (i.e., Temp.Water) had a no excluded impact on ANPP$_{graminoid}$ (Supplementary Figure S1). Only one of the four explained parts (i.e., species β-diversity) had a no excluded impact on ANPP (Figure 4). Only the "Env." had an excluded impact on ANPP (Figure 5). Besides the impact of the "Env.", the β-diversity had interactive impacts with "GeoDist.Dur." and α-diversity on ANPP (Figure 5).

4. Discussion

Concordant with the hypothesis, asymmetric warming among elevations might homogenize plant phylogenetic and species α-diversity. This phenomenon might be consequent to at least one of the subsequent mechanisms. First, each species has its special niche width of temperature, water, nitrogen and phosphorus availability (Thuiller et al., 2005; Brathen et al., 2018). Elevated temperature, water, nitrogen and phosphorus availability can alter plant α-diversity (Klein et al., 2004; Fu and Shen, 2016; Wang et al., 2021a).

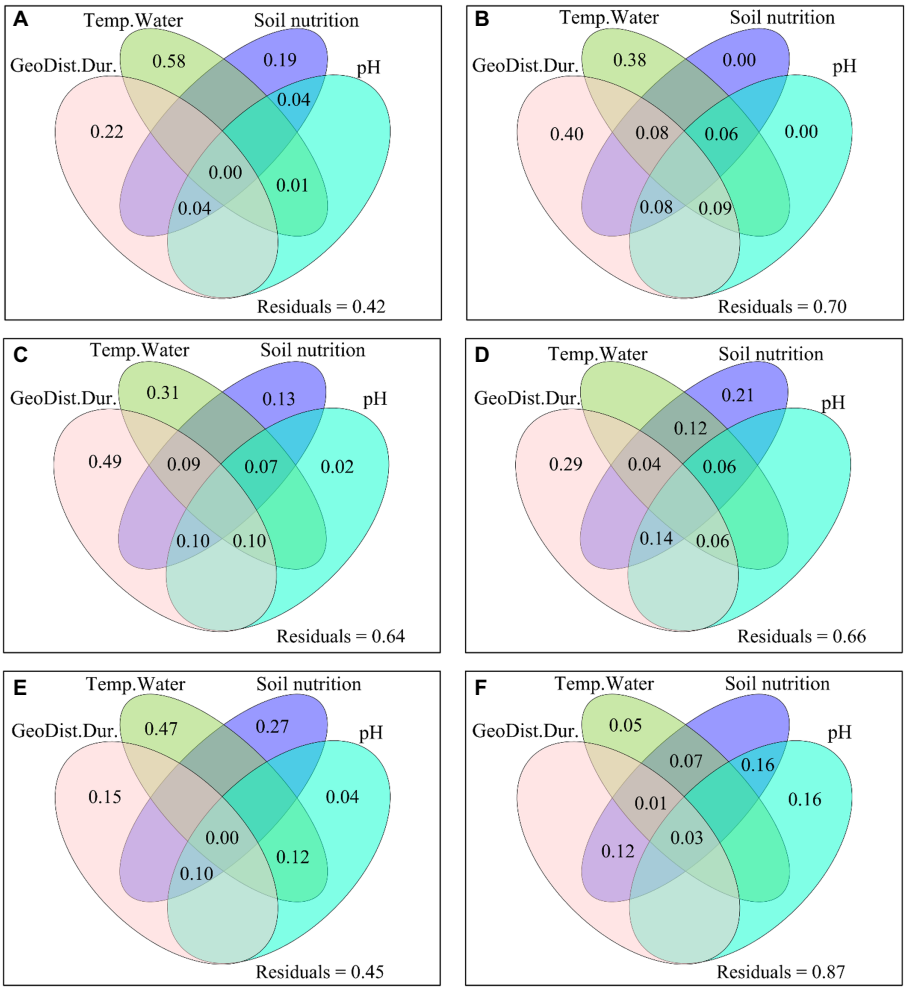

FIGURE 3
The excluded and interactive impacts of GeoDist.Dur., the dissimilarity of Temp.Water, soil nutrition and pH on the dissimilarity of **(A)** species richness, **(B)** Shannon, **(C)** Simpson, **(D)** Pielou, **(E)** PD, and **(F)** MNTD between C4313 versus W4513, C4313 versus W4693, and C4513 versus W4693. PD: phylogenetic diversity; MNTD: mean nearest taxon distance; GeoDist.Dur.: geographic distance and warming duration; Temp.Water: soil and air temperatures, vapor pressure deficit and/or soil moisture; soil nutrition: available phosphorus, nitrate and ammonium nitrogen. C4313: non-warming plots at elevation 4,313 m; C4513: non-warming plots at elevation 4,513 m; W4513: warming plots at elevation 4,513 m; W4693: warming plots at elevation 4,693 m.

Asymmetric warming among elevations may homogenize temperature, water, nitrogen and phosphorus availability among elevations, which in turn may result in similar niche width of temperature, water, nitrogen and phosphorus availability among elevation. Second, wind may also impact plant diversity (Wang et al., 2021b), and warming may result in the declines in gale days and wind speed (Xiaomei et al., 2012; Yao and Li, 2019). Asymmetric warming among elevations may homogenize gale days and wind speed among elevations, which in turn may increase dispersal limitation of anemophilae plants among elevations. Third, radiation is an important limit variable of plant species α-diversity (Tian and Fu, 2022), and generally closely correlated with precipitation (Fu et al., 2022; Han et al., 2022a). Homogenization of wind among elevations may lead to homogenization of precipitation among elevation, which in turn may weaken the difference of radiation among elevations. Fourth, asymmetric warming among elevations may homogenize species composition in alpine grasslands (Wang et al., 2021a).

Concordant with the hypothesis, asymmetric warming among elevations might also homogenize ANPP. This phenomenon might be consequent to at least one of the subsequent mechanisms. First, our previous study (Wang et al., 2021a) and this study showed that asymmetric warming among elevations can homogenize plant α- and β-diversity. As is well known, both plant α- and β-diversity can be closely correlated with ANPP (Wu et al., 2014; Wang et al., 2021a). This phenomenon was strengthened by this study (Figures 2, 3). Second, climate change can significantly affect soil moisture (Wang and Fu, 2023) and asymmetric warming among elevations can homogenize temperature and water availability among elevations (Wang et al., 2021b). Ambient temperature and humidity conditions can influence plant phenology (Han et al., 2023), which are closely correlated with ANPP in alpine grasslands of the "Third Pole of the Earth" (Fu and Shen, 2022; Wang et al., 2022). Ambient temperature and humidity conditions can also impact plant net photosynthesis rate of the "Third Pole of the Earth" (Fu et al., 2015a). Temperature can also impact the allocation of photosynthetic products between plant

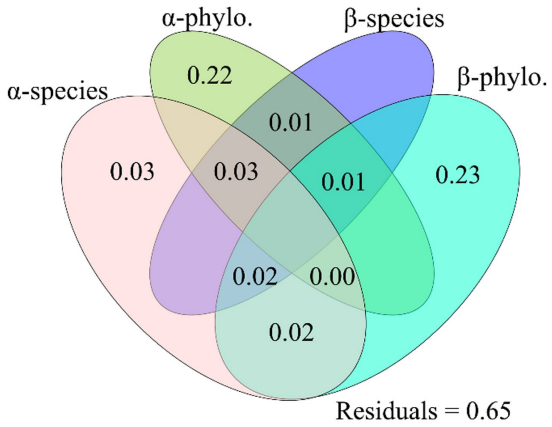

FIGURE 4
The excluded and interactive impacts of the dissimilarity of α-species and α-phylo., β-species and β-phylo. on the dissimilarity of plant community aboveground net primary production between C4313 versus W4513, C4313 versus W4693, and C4513 versus W4693. The α-phylo. and α-species indicated phylogenetic and species α-diversity, and β-phylo,. and β-species indicated phylogenetic and species β-diversity between C4313 versus W4513, C4313 versus W4693, and C4513 versus W4693, respectively. C4313: non-warming plots at elevation 4,313 m; C4513: non-warming plots at elevation 4,513 m; W4513: warming plots at elevation 4,513 m; W4693: warming plots at elevation 4,693m. Species and phylogenetic β-diversity data were obtained from Wang et al. (2021a,b), Frontiers in Ecology and Evolution.

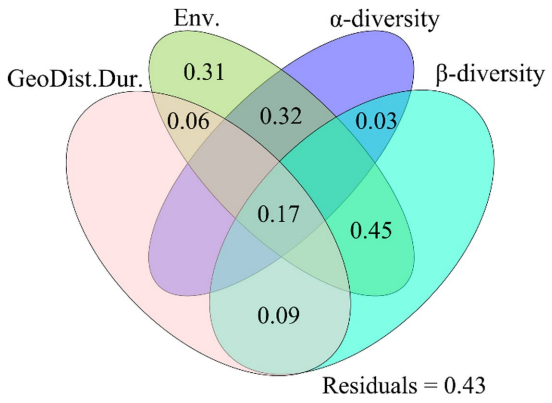

FIGURE 5
The excluded and interactive impacts of GeoDist.Dur., the dissimilarity of Env. and α-diversity, and β-diversity on the dissimilarity of plant community aboveground net primary production between C4313 versus W4513, C4313 versus W4693, and C4513 versus W4693. GeoDist.Dur.: geographic distance and warming duration; Env.: soil and air temperatures, soil moisture, vapor pressure deficit, available phosphorus, nitrate and ammonium nitrogen, and/or pH; C4313: non-warming plots at elevation 4,313m; C4513: non-warming plots at elevation 4,513m; W4513: warming plots at elevation 4,513m; W4693: warming plots at elevation 4,693m. Species and phylogenetic β-diversity data were obtained from Wang et al. (2021a,b), Frontiers in Ecology and Evolution.

aboveground and belowground parts (Friend and Woodward, 1990; Weih and Karlsson, 2001). Temperature sensitivities and precipitation sensitivities of plant production can be closely related to ranges of temperature and precipitation in alpine grasslands of the "Third Pole of the Earth" (Fu et al., 2018; Fu and Sun, 2022). Temperature sensitivities of plant production may decline with warming magnitude and may not be significantly correlated with elevation in alpine grasslands (Fu et al., 2018; Fu and Sun, 2022), which in turn may further imply that asymmetric warming among elevations may homogenize the temperature sensitivities of plant production in alpine grasslands. Third, asymmetric warming among elevations may homogenize soil nitrogen and phosphorus availability among elevations (Wang et al., 2021b), and nitrogen input can generally increase plant biomass of the "Third Pole of the Earth" (Fu and Shen, 2016; Fu et al., 2019).

This study and our previous study (Wang et al., 2021a) exhibited that symmetric warming among elevations may overestimate the impact of asymmetric warming among elevations on ANPP. Moreover, the reaction of plant α-diversity to asymmetric warming among elevations was different from that to symmetric warming among elevations (Wang et al., 2021a). This phenomenon might be consequent to at least one of the subsequent mechanisms. First, each plant species may have its own elevation range and optimum elevation, and climate change can result in the upward of the optimum elevation for a specific plant species (Lenoir et al., 2008). However, asymmetric warming and symmetric warming among elevations may cause different potentials of elevation upward. Second, asymmetric warming and symmetric warming among elevations may have different impacts on gale days and wind speed (Xiaomei et al., 2012; Yao and Li, 2019), and in turn the dispersal ability for wind-pollination plants (Wang et al., 2022). Third, asymmetric warming but not symmetric warming among elevations may homogenize environmental conditions among elevations (Wang et al., 2021a,b). Fourth, the reaction of plant β-diversity to asymmetric warming among elevations may underestimate that to symmetric warming in the identical alpine grasslands (Wang et al., 2021a,b).

Some previous studies found that the warming effects on plant production and α-diversity varied with years in alpine grasslands on the Tibetan Plateau (Wang et al., 2012; Zhang et al., 2021). Similar with these some previous studies, the effects of asymmetric warming among elevations on plant ANPP, species and phylogenetic α-diversity can vary with years. This phenomenon might be consequent to the fact that the effects of asymmetric warming among elevations on water availability, plant species and phylogenetic β-diversity, soil nitrogen and phosphorus availability, and soil pH varied with years (Wang et al., 2021b). Moreover, the effects of warming on plant production and α-diversity can be related to the background values of climatic conditions (Zhang et al., 2021; Fu and Sun, 2022), and climate conditions generally change with years (Wang et al., 2022; Han et al., 2022a; Wang and Fu, 2023). Third, the effects of warming on plant production and α-diversity can be also related to warming duration, and warming may have lagging effects on plant production and α-diversity (Fu et al., 2019; Wang et al., 2021a; Fu and Shen, 2022; Han et al., 2023). Fourthly, the effects of warming on plant production can be also related to its effects on plant precipitation use efficiency, which varied with years (Han et al., 2023). Fifthly, the effects of warming on plant production and α-diversity can be also related to its effects on soil microbial community structure, which also varied with years (Yu et al., 2019a; Zhang et al., 2021; Zhang and Fu, 2021).

Indeed, there may be some flaws in our study. For example, only two grassland types and only a relatively narrow elevation range

(about 4,313–4,693 m) were included in our study (Wang et al., 2021b). These uncertainties implied that when the findings observed by this current study were extrapolated to the regions outside our study area, it needed to be careful. Therefore, we need to further carry out related studies in regions outside our study area to explore these uncertainties. However, our findings demonstrated that asymmetric warming among elevations can homogenize ANPP and plant α-diversity among elevations, at least in our study area.

5. Conclusion

Dependent on a decade experiment of asymmetric warming among elevations, this study discovered that asymmetric warming among elevations homogenized aboveground net primary production, plant phylogenetic and species α-diversity among elevations.

Data availability statement

The original contributions presented in the study are included in the article/Supplementary material, further inquiries can be directed to the corresponding author.

Author contributions

GF and FH: conceptualization, formal analysis, writing – original draft preparation, and writing – review and editing. GF: methodology, validation, investigation, and data curation. CY: software, resources, project administration, and funding acquisition. FH: visualization and supervision. All authors contributed to the article and approved the submitted version.

Funding

This research was funded by the Youth Innovation Promotion Association of the Chinese Academy of Sciences (2020054), Pilot project of Chinese Academy of Sciences (XDA26050501), the National Natural Science Foundation of China (31600432), the Bingwei Outstanding Young Talents Program of the Institute of Geographic Sciences and Natural Resources Research, Chinese Academy of Sciences (2018RC202), the Science and Technology Project of the Tibet Autonomous Region (XZ202101ZD0003N, XZ202101ZD0007G, XZ202201ZY0003N, XZ202202YD0009C, and XZ202301YD0012C), the construction of the fixed Observation and Experimental Station of the first Support System for Agricultural Green Development in Zhongba County, and the Study on the Path of Agricultural Green Development and Carbon Reduction and Sequestration in Typical Counties of Yarlung Zangbo River Basin.

Acknowledgments

We would like to thank the reviewers and editors for their valuable suggestions.

Conflict of interest

The authors declare that the research was conducted in the absence of any commercial or financial relationships that could be construed as a potential conflict of interest.

Publisher's note

Supplementary material

The Supplementary material for this article can be found online at: https://www.frontiersin.org/articles/10.3389/fevo.2023.1126651/full#supplementary-material

References

Bokhorst, S., Bjerke, J. W., Street, L. E., Callaghan, T. V., and Phoenix, G. K. (2011). Impacts of multiple extreme winter warming events on sub-Arctic heathland: phenology, reproduction, growth, and CO_2 flux responses. *Glob. Chang. Biol.* 17, 2817–2830. doi: 10.1111/j.1365-2486.2011.02424.x

Brathen, K. A., Gonzalez, V. T., and Yoccoz, N. G. (2018). Gatekeepers to the effects of climate warming? Niche construction restricts plant community changes along a temperature gradient. *Perspect. Plant Ecol. Evol. Syst.* 30, 71–81. doi: 10.1016/j.ppees.2017.06.005

Du, M. Y., Liu, J., Li, Y., Zhang, F., Zhao, L., Niu, B., et al. (2019). Are high altitudinal regions warming faster than lower elevations on the Tibetan plateau? *Int. J. Glob. Warm.* 18, 363–384. doi: 10.1504/IJGW.2019.101094

Friend, A., and Woodward, F. (1990). Evolutionary and ecophysiological responses of mountain plants to the growing season environment. *Adv. Ecol. Res.* 20, 59–124. doi: 10.1016/S0065-2504(08)60053-7

Fu, G., and Shen, Z. X. (2016). Response of alpine plants to nitrogen addition on the Tibetan plateau: a meta-analysis. *J. Plant Growth Regul.* 35, 974–979. doi: 10.1007/s00344-016-9595-0

Fu, G., and Shen, Z. (2022). Asymmetrical warming of growing/non-growing season increases soil respiration during growing season in an alpine meadow. *Sci. Total Environ.* 812:152591. doi: 10.1016/j.scitotenv.2021.152591

Fu, G., Shen, Z. X., Sun, W., Zhong, Z. M., Zhang, X. Z., and Zhou, Y. T. (2015a). A meta-analysis of the effects of experimental warming on plant physiology and growth on the Tibetan plateau. *J. Plant Growth Regul.* 34, 57–65. doi: 10.1007/s00344-014-9442-0

Fu, G., Shen, Z. X., and Zhang, X. Z. (2018). Increased precipitation has stronger effects on plant production of an alpine meadow than does experimental warming in the Northern Tibetan plateau. *Agric. For. Meteorol.* 249, 11–21. doi: 10.1016/j.agrformet.2017.11.017

Fu, G., and Sun, W. (2022). Temperature sensitivities of vegetation indices and aboveground biomass are primarily linked with warming magnitude in high-cold grasslands. *Sci. Total Environ.* 843:157002. doi: 10.1016/j.scitotenv.2022.157002

Fu, G., Sun, W., Yu, C. Q., Zhang, X. Z., Shen, Z. X., Li, Y. L., et al. (2015b). Clipping alters the response of biomass production to experimental warming: a case study in an alpine meadow on the Tibetan plateau, China. *J. Mt. Sci.* 12, 935–942. doi: 10.1007/s11629-014-3035-z

Fu, G., Wang, J., and Li, S. (2022). Response of forage nutritional quality to climate change and human activities in alpine grasslands. *Sci. Total Environ.* 845:157552. doi: 10.1016/j.scitotenv.2022.157552

Fu, G., Zhang, H. R., and Sun, W. (2019). Response of plant production to growing/non-growing season asymmetric warming in an alpine meadow of the Northern Tibetan plateau. *Sci. Total Environ.* 650, 2666–2673. doi: 10.1016/j.scitotenv.2018.09.384

Han, F., Fu, G., Yu, C., and Wang, S. (2022a). Modeling nutrition quality and storage of forage using climate data and normalized-difference vegetation index in alpine grasslands. *Remote Sens.* 14. doi: 10.3390/rs14143410

Han, F. S., Yu, C. Q., and Fu, G. (2022b). Warming alters elevation distributions of soil bacterial and fungal communities in alpine grasslands. *Glob. Ecol. Conserv.* 39:e02306. doi: 10.1016/j.gecco.2022.e02306

Han, F., Yu, C., and Fu, G. (2023). Non-growing/growing season non-uniform-warming increases precipitation use efficiency but reduces its temporal stability in an alpine meadow. *Front. Plant Sci.* 14:1090204. doi: 10.3389/fpls.2023.1090204

Ji, S. N., Classen, A. T., Zhang, Z. H., and He, J. S. (2017). Asymmetric winter warming advanced plant phenology to a greater extent than symmetric warming in an alpine meadow. *Funct. Ecol.* 31, 2147–2156. doi: 10.1111/1365-2435.12909

Klein, J. A., Harte, J., and Zhao, X. Q. (2004). Experimental warming causes large and rapid species loss, dampened by simulated grazing, on the Tibetan plateau. *Ecol. Lett.* 7, 1170–1179. doi: 10.1111/j.1461-0248.2004.00677.x

Lenoir, J., Gegout, J. C., Marquet, P. A., de Ruffray, P., and Brisse, H. (2008). A significant upward shift in plant species optimum elevation during the 20th century. *Science* 320, 1768–1771. doi: 10.1126/science.1156831

Qin, J., Yang, K., Liang, S. L., and Guo, X. F. (2009). The altitudinal dependence of recent rapid warming over the Tibetan plateau. *Clim. Chang.* 97, 321–327. doi: 10.1007/s10584-009-9733-9

Rangwala, I., and Miller, J. R. (2012). Climate change in mountains: a review of elevation-dependent warming and its possible causes. *Clim. Chang.* 114, 527–547. doi: 10.1007/s10584-012-0419-3

Sun, W., Li, S., Wang, J., and Fu, G. (2021). Effects of grazing on plant species and phylogenetic diversity in alpine grasslands, Northern Tibet. *Ecol. Eng.* 170:106331. doi: 10.1016/j.ecoleng.2021.106331

Thuiller, W., Lavorel, S., and Araujo, M. B. (2005). Niche properties and geographical extent as predictors of species sensitivity to climate change. *Glob. Ecol. Biogeogr.* 14, 347–357. doi: 10.1111/j.1466-822X.2005.00162.x

Tian, Y., and Fu, G. (2022). Quantifying plant species α-diversity using normalized difference vegetation index and climate data in alpine grasslands. *Remote Sens.* 14. doi: 10.3390/rs14195007

Tozzi, E., Lyons, E. M., and Van Acker, R. C. (2014). The effect of simulated winter warming spells on Canada fleabane [*Conyza canadensis* (L.) Cronq. var.canadensis] seeds and plants. *Can. J. Plant Sci.* 94, 963–969. doi: 10.4141/cjps2013-302

Trisos, C. H., Merow, C., and Pigot, A. L. (2020). The projected timing of abrupt ecological disruption from climate change. *Nature* 580, 496–501. doi: 10.1038/s41586-020-2189-9

Wang, S. P., Duan, J., Xu, G., Wang, Y., Zhang, Z., Rui, Y., et al. (2012). Effects of warming and grazing on soil N availability, species composition, and ANPP in an alpine meadow. *Ecology* 93, 2365–2376. doi: 10.1890/11-1408.1

Wang, S., and Fu, G. (2023). Modelling soil moisture using climate data and normalized difference vegetation index based on nine algorithms in alpine grasslands. *Front. Environ. Sci.* 11:1130448. doi: 10.3389/fenvs.2023.1130448

Wang, J., Li, M., Yu, C., and Fu, G. (2022). The change in environmental variables linked to climate change has a stronger effect on aboveground net primary productivity than does phenological change in alpine grasslands. *Front. Plant Sci.* 12:798633. doi: 10.3389/fpls.2021.798633

Wang, J., Yu, C., and Fu, G. (2021a). Warming reconstructs the elevation distributions of aboveground net primary production, plant species and phylogenetic diversity in alpine grasslands. *Ecol. Indic.* 133:108355. doi: 10.1016/j.ecolind.2021.108355

Wang, J. W., Yu, C. Q., and Fu, G. (2021b). Asymmetrical warming between elevations may result in similar plant community composition between elevations in alpine grasslands. *Front. Ecol. Evol.* 9:757943. doi: 10.3389/fevo.2021.757943

Weih, M., and Karlsson, P. S. (2001). Growth response of mountain birch to air and soil temperature: is increasing leaf-nitrogen content an acclimation to lower air temperature? *New Phytol.* 150, 147–155. doi: 10.1046/j.1469-8137.2001.00078.x

Wu, J. S., Shen, Z. X., and Zhang, X. Z. (2014). Precipitation and species composition primarily determine the diversity-productivity relationship of alpine grasslands on the northern Tibetan plateau. *Alp. Bot.* 124, 13–25. doi: 10.1007/s00035-014-0125-z

Xiaomei, Y., Zongxing, L., Qi, F., Yuanqing, H., Wenlin, A., Wei, Z., et al. (2012). The decreasing wind speed in southwestern China during 1969-2009, and possible causes. *Quat. Int.* 263, 71–84. doi: 10.1016/j.quaint.2012.02.020

Yang, Z. L., Zhang, Q., Su, F., Zhang, C., Pu, Z., Xia, J., et al. (2017). Daytime warming lowers community temporal stability by reducing the abundance of dominant, stable species. *Glob. Chang. Biol.* 23, 154–163. doi: 10.1111/gcb.13391

Yao, H. R., and Li, D. L. (2019). The gale concentration period and degree over the Tibetan plateau and related atmospheric circulation during the windy period. *J. Desert Res.* 39, 122–133.

Yao, T. D., Liu, X. D., Wang, N. L., and Shi, Y. F. (2000). Amplitude of climatic changes in Qinghai-Tibetan plateau. *Chin. Sci. Bull.* 45, 1236–1243. doi: 10.1007/BF02886087

Yu, C. Q., Han, F. S., and Fu, G. (2019a). Effects of 7 years experimental warming on soil bacterial and fungal community structure in the northern Tibet alpine meadow at three elevations. *Sci. Total Environ.* 655, 814–822. doi: 10.1016/j.scitotenv.2018.11.309

Yu, C. Q., Wang, J. W., Shen, Z. X., and Fu, G. (2019b). Effects of experimental warming and increased precipitation on soil respiration in an alpine meadow in the Northern Tibetan plateau. *Sci. Total Environ.* 647, 1490–1497. doi: 10.1016/j.scitotenv.2018.08.111

Zha, X. J., Tian, Y., Ouzhu, and Fu, G. (2022). Response of forage nutrient storages to grazing in alpine grasslands. *Front. Plant Sci.* 13:991287. doi: 10.3389/fpls.2022.991287

Zhang, H., and Fu, G. (2021). Responses of plant, soil bacterial and fungal communities to grazing vary with pasture seasons and grassland types, northern Tibet. *Land Degrad. Dev.* 32, 1821–1832. doi: 10.1002/ldr.3835

Zhang, X. Z., Shen, Z. X., and Fu, G. (2015). A meta-analysis of the effects of experimental warming on soil carbon and nitrogen dynamics on the Tibetan plateau. *Appl. Soil Ecol.* 87, 32–38. doi: 10.1016/j.apsoil.2014.11.012

Zhang, G., Shen, Z., and Fu, G. (2021). Function diversity of soil fungal community has little exclusive effects on the response of aboveground plant production to experimental warming in alpine grasslands. *Appl. Soil Ecol.* 168:104153. doi: 10.1016/j.apsoil.2021.104153

Zhang, G., Shen, Z., and Fu, G. (2022). Geo-distribution patterns of soil fungal community of *Pennisetum flaccidum* in Tibet. *J. Fungi* 8. doi: 10.3390/jof8111230

Zhong, Z., and Fu, G. (2022). Response of soil fungal species, phylogenetic and functional diversity to diurnal asymmetric warming in an alpine agricultural ecosystem. *Agric. Ecosyst. Environ.* 335:107993. doi: 10.1016/j.agee.2022.107993

Zong, N., and Fu, G. (2021). Variations in species and function diversity of soil fungal community along a desertification gradient in an alpine steppe. *Ecol. Indic.* 131:108197. doi: 10.1016/j.ecolind.2021.108197

frontiers | Frontiers in Ecology and Evolution

TYPE Original Research
PUBLISHED 09 May 2023
DOI 10.3389/fevo.2023.1169297

OPEN ACCESS

EDITED BY
Zhongqing Yan,
Chinese Academy of Forestry, China

REVIEWED BY
Qinghai Song,
Xishuangbanna Tropical Botanical Garden (CAS), China
Bing Song,
Ludong University, China
Xiaodong Zhang,
Chinese Academy of Forestry, China

*CORRESPONDENCE
Li Zhou
✉ zhouli@cma.gov.cn
Guangsheng Zhou
✉ zhougs@cma.gov.cn

RECEIVED 19 February 2023
ACCEPTED 20 April 2023
PUBLISHED 09 May 2023

CITATION
Song J, Zhou L, Zhou G, Wang Y, Zhang S and Yan Y (2023) Hydrometeorological controls on net carbon dioxide exchange over a temperate desert steppe in Inner Mongolia, China. *Front. Ecol. Evol.* 11:1169297. doi: 10.3389/fevo.2023.1169297

Hydrometeorological controls on net carbon dioxide exchange over a temperate desert steppe in Inner Mongolia, China

Jiaxin Song[1], Li Zhou[2,3]*, Guangsheng Zhou[2,3]*, Yu Wang[4], Sen Zhang[1] and Yujie Yan[1]

[1]School of Geo-Science and Technology, Zhengzhou University, Zhengzhou, China, [2]State Key Laboratory of Severe Weather, Chinese Academy of Meteorological Sciences, Beijing, China, [3]Joint Laboratory of Eco-Meteorology, Chinese Academy of Meteorological Sciences, Zhengzhou University, Zhengzhou, China, [4]College of Horticulture and Plant Protection, Henan University of Science and Technology, Luoyang, China

Understanding the effect of environmental factors on the net ecosystem CO_2 exchange (NEE) and the response of NEE to rainfall events is of great significance for an accurate understanding of the carbon cycle for desert steppe ecosystems. Based on the long-term (2011–2018) eddy covariance flux data of a temperate desert steppe in Inner Mongolia, China, this study used path analysis to analyze the combined impact of the environmental factors on NEE. The results showed that during the growing season, vapor pressure deficit (VPD) and soil water content (SWC) was the most prominent environmental factor for the daytime NEE and nighttime NEE, respectively. NEE responds differently to individual environmental factors among multi-year climatic conditions. The size of rainfall event has significant impacts on NEE, it can effectively promote the CO_2 uptake of the desert steppe ecosystem when rainfall event size is greater than 5mm, and the NEE response increased with the rainfall event size. Moreover, NEE peaked approximately 1–3 days after a 5–10mm rainfall event, while the rainfall event size >10mm, it would take 3–5 days for NEE to reach a peak value; and yet, small rainfall events (< 5mm) slightly increased CO_2 emissions. During the growing season, carbon uptake increased with monthly rainfall, except in May. Our results are important for understanding the carbon cycle and its control mechanisms in the temperate desert steppe of Inner Mongolia.

KEYWORDS

desert steppe, net ecosystem CO_2 exchange, rainfall events, eddy covariance, environmental controls

1. Introduction

Over half of the carbon emitted by human activities is absorbed through nature's carbon cycle, which has become one of the core problems of global change research (Gong et al., 2018; Zhou et al., 2020). Arid and semi-arid regions account for approximately 30% of the global carbon sequestration (Adams et al., 1990; Chen et al., 2021), and the ecosystems in these regions are highly sensitive to climate change because of low precipitation, strong sunlight, and high evaporation rates (Gu et al., 2018). Previous studies have revealed that climate change causes changes in meteorological and other environmental factors that affect both ecosystem

photosynthesis and respiration and, as a result, the ecosystem carbon balance (Li et al., 2015; Nyantakyi-Frimpong and Bezner-Kerr, 2015). Grassland is the dominant ecosystem type in arid and semi-arid areas, covering approximately one-third of the global natural vegetation (Parton et al., 1995). Among terrestrial ecosystems, grasslands have a large carbon storage capacity, second only to forest ecosystems, and are critical to the global carbon balance (Yang and Zhou, 2013; Li et al., 2021).

Carbon flux is regulated by both environmental and biological factors, and the study of its driving factors has been a major research topic regarding the global carbon cycle, particularly under the premise of climate change (Fang et al., 2018). Water availability is the primary driver of plant growth (Zhang et al., 2020), and previous studies have shown that carbon flux over grassland ecosystems is closely related to the vapor pressure deficit (VPD) and soil moisture (Chen et al., 2018). In semi-arid grassland ecosystems, high carbon uptake usually occurs under humid conditions, whereas high carbon release is associated with warm and dry conditions (Ahlström et al., 2015). Meanwhile, it was proposed that the effects of environmental factors on NEE might differ among different climatic years, and the variation of NEE may even have different dominant factors for different climatic years (Aguilos et al., 2018; Wang et al., 2019). However, to date, few such studies have been conducted on the desert steppe.

Desert steppe is water-limited, and the carbon cycle in grassland ecosystems is sensitive to changes in rainfall (Zhang et al., 2020). Precipitation occurs in the form of discrete, intermittent, and unpredictable pulse events (Rey et al., 2017), the size of a single rainfall event can have a large impact on grassland carbon flux (Huxman et al., 2004). A previous study showed that small-pulse rainfall events (e.g., 2.1 mm) slightly increased CO_2 emissions by stimulating microbial respiration, whereas large-pulse rainfall events (e.g., 19.7 mm) promoted CO_2 uptake by affecting plant photosynthesis (Schwinning et al., 2004; Fa et al., 2015). A study of a *Stipa* grassland in Inner Mongolia, China showed that the CO_2 uptake increased when the rainfall event size >10 mm (Peng et al., 2013), but another study of a *Leymus chinensis* grassland in Inner Mongolia showed that the CO_2 uptake increased when the rainfall event size >5 mm (Hao et al., 2017). This suggests that the size of effective rainfall event may vary among different climate and vegetation types.

Herein, this study aims to investigate the impact of environmental factors on the net ecosystem CO_2 exchange (NEE) and the response of NEE to rainfall events, based on eddy covariance flux data from 2011 to 2018 of a temperate desert steppe in Inner Mongolia, China. The long-term measurement campaign provided a broad range of conditions to thoroughly investigate the environmental regulations of NEE in the desert steppe ecosystem. The specific objectives are (1) to analyze the combined impact of the environmental factors on NEE, and compare the controlling factors of NEE between years with different climatic conditions; and (2) to determine the NEE response to rainfall events of different magnitudes.

2. Materials and methods

2.1. Site description

The research site is located in Damao Banner of Baotou city in Inner Mongolia (41°38.6′ N, 110°19.9′ E, 1409 m a.s.l.). Desert steppe vegetation covers the area including subregions with a temperate, continental, and semiarid climate. The Information and Research Institute of Meteorology, Hydrology, and Environment of Inner Mongolia reports that from 1990 to 2019, the site's mean annual air temperature was 5.22°C and its mean annual precipitation was 247.4 mm. Most of the rainfall occurs during the growing season (May–September). The vegetation is dominated by a degraded *Stipa klemenzii* community. The soil was brown and calcified, with a calcified layer at 20–50 cm. The total K, total P, and organic carbon contents are 23.29 g kg^{-1}, 0.31 g kg^{-1}, and 12.67 g kg^{-1}, respectively, and the average bulk density was 1.23 g cm^{-3}, with a pH of 7.4.

2.2. Fluxes and meteorological measurements

From 2011 to 2018, the turbulence fluxes were monitored at a height of 4 m using an open-path eddy covariance system. An infrared gas analyzer (Li-7500, LICOR, Inc., Lincoln, NE, United States) and a 3D sonic anemometer (CSAT-3, Campbell Scientific, Inc., Logan, UT, United States) were employed to calculate the variations in the densities of gaseous CO_2 and H_2O at 10 Hz and three wind speed components, respectively. The original data were recorded and stored automatically at 10 Hz and 0.5 h online flux data were provided by a datalogger (CR5000, Campbell Scientific Inc., Logan, UT, United States).

During the research project (2011–2018), a shielded sensor (model HMP45C, Vaisala, Helsinki, Finland) was used to measure the air temperature (Ta) and relative humidity (RH) at levels of 1.5 and 3.5 m. From Ta and RH, the VPD was computed. Precipitation was measured at a height of 1.2 m using a tipping-bucket rain gauge (model 52203, RM Young Inc., Traverse City, MI, United States). Using a quantum sensor, photosynthetically active radiation (PAR) was recorded (4 m; LI190SB, LI-COR, Lincoln, United States). The soil temperature sensor comprised a thermistor (107 L, Campbell Scientific Inc., Logan, UT, United States) (5, 10, 15, 20, 40, and 80 cm) that was used to measure soil temperature (Ts). The soil temperature recorded at a depth of 10 cm was used in this study, defined as Ts. The volumetric water content of the soil at depths of 10 cm (SWC10), 20 cm (SWC20), 30 cm (SWC30), and 40 cm (SWC40) were monitored using time-domain reflectometry probes (Easy AG; Campbell Scientific Inc., Logan, UT, United States). Data loggers (CR23X, Campbell Scientific Inc., Logan, UT, United States) were used to collect all data, and 30 min mean values were automatically recorded and stored.

2.3. Flux calculations and data processing

Eddy covariance data were processed by EddyPro7.0.6 (LI-COR), including double rotation, Webb–Pearman–Leuning correction, potential temporal lags correction, frequency response correction etc. (Webb et al., 1980; Moncrieff et al., 1997; Reichstein et al., 2005). In this study, positive NEE values denoted a source of atmospheric CO_2 at the location, whereas negative values denoted a carbon sink. During the observation period, the power supply may have been interrupted by abnormal weather or instruments. Half-hourly fluxes were filtered for: (1) incomplete measurements taken every half-hourly, (2) outliers,

(3) low turbulence situations, and (4) rain events (Papale et al., 2006). A cutoff friction velocity (u*) was employed, and nocturnal fluxes below the threshold were eliminated (Zhu et al., 2006). Subsequently, the gaps in the flux data were filled using a marginal distribution sampling (MDS) technique (Reichstein et al., 2005). The flux data for 2013 were not obtained because of instrument failure.

2.4. Characterization of rainfall events

Rainfall events can be described as discontinuous, highly varied, and usually comprise unpredictable pulses of rainfall (Li et al., 2013). The division of rainfall events is based on the absence of rainfall within 24 h after a certain rainfall time. Rainfall events were classified into six levels, according to their size (Table 1). Rainfall events of <10 mm were regarded as a small rainfall event, 10–25 mm as moderate rainfall event, and rainfall >25 mm as a heavy rainfall event.

Response of NEE to rainfall event ($NEE_{response}$) was determined as the difference between mean daily NEE post-event (NEE_{after}) and mean daily NEE pre-event (NEE_{before}) (Wang et al., 2017),

$$NEE_{response} = NEE_{after} - NEE_{before}$$

where, NEE is the daily NEE average (g C m^{-2} day^{-1}).

The relative response effect of NEE to rainfall event ($NEE_{response,\,r}$) was calculated as the following equation:

$$NEE_{response,r} = \left(NEE_{after} - NEE_{before}\right) / NEE_{before}$$

2.5. Path analysis

Earlier studies suggested that the combined effects of the various environmental factors should receive more attention because the independent effect of any one factor alone is insufficient to explain the variations in NEE (Wang et al., 2016). To examine the combined impact of the environmental factors on NEE, and the relative importance of these factors, the path analysis method was used in this study. Path analysis is an extension of multiple regression and can be used to understand the causal structure of data (Kozak and Kang, 2006). The path analysis method reveals the relationships between dependent and independent variables using the direct and indirect path coefficients as well as the determinative coefficient (Yuan et al., 2001; Jiang et al., 2014). Based on the determinative coefficient, the sequence of the synthetic action of every independent variable to the response variable can be decided, and which variable is the principal decision variable can be identified (Yuan et al., 2001). Path analysis were applied using IBM SPSS Statistics 26.0.

TABLE 1 The classification of rain events based on the size of rainfall.

Rainfall level	Rainfall
Level 1	< 1 mm
Level 2	1 ~ 3 mm
Level 3	3 ~ 5 mm
Level 4	5 ~ 10 mm
Level 5	10 ~ 25 mm
Level 6	> 25 mm

3. Results

3.1. Environmental conditions

Seasonal fluctuations in air temperature (Ta), soil temperature (Ts), precipitation (Prec), photosynthetically active radiation (PAR), vapor pressure deficit (VPD), and volumetric soil water content (SWC) are shown in Figure 1. During the measurement campaign (2011–2018), Ta and Ts showed similar seasonal dynamics with a single-peak curve (Figures 1A,D). The highest monthly mean Ta was 22.39°C, which typically occurs in July, and the lowest monthly mean Ta was −13.92°C, which was observed in January. The monthly mean Ts ranged from −10.5 to −24.27°C, with January and July recording the lowest and highest values, respectively. During the study period (2011–2018), the annual precipitation ranged from 229.8 mm (in 2015) to 513.2 mm (in 2018), with the growth season (May–September) accounting for roughly 92.3% of the total. Seasonal variations in SWC matched well with the seasonal distribution of precipitation (Figures 1B,E), and the daily SWC ranged from 10% to 57%. PAR and VPD exhibited relatively large day-to-day fluctuations and their seasonal variations generally showed unimodal curves (Figures 1C,F). The peak PAR values usually occurred in May, and the average PAR in May was 44.62 mol m^{-2} day^{-1}. The VPD typically peaks between May and July. The highest VPD (3.17 kPa) was observed in mid-July 2017.

In this study, the differences between the growing season temperature and precipitation and the respective multi-year averages were used to define the annual climate types (Figure 2). Mean Ta for the growing season ranged from 17.42°C (2012) to 19.61°C (2017). Growing-season precipitation was highest in 2018 (474.9 mm, 112.1% higher than the multi-year (1990–2019) average of 223.9 mm) and lowest in 2015 (174.6 mm, 22.0% lower than the multi-year average). Accordingly, 2016 was selected to represent a normal year (normal climatic conditions), 2017 was classified as a warm year, and 2018 was classified as a warm and moist year (Figure 2).

3.2. Environmental controls on NEE

Path analysis method was used to examine the combined impact of the environmental factors on NEE (Figure 3), and the determinative coefficient generated by path analysis was used to determine the relative importance of environmental factors in NEE fluctuations (Table 2). As seen in Table 2, moisture-related environmental factors (e.g., VPD and SWC) had greater effects on NEE in the desert steppe ecosystems than heat-related environmental factors (e.g., Ta and Ts).

During the growing season, VPD was the most prominent environmental factor affecting the daytime NEE, followed by SWC, Ta, and PAR. Daytime NEE increased (i.e., carbon uptake reduced) with an increase in VPD and declined (i.e., carbon uptake increased) with an increase in Ta, SWC, and PAR. From the absolute values of path coefficient, there was little difference between the direct and

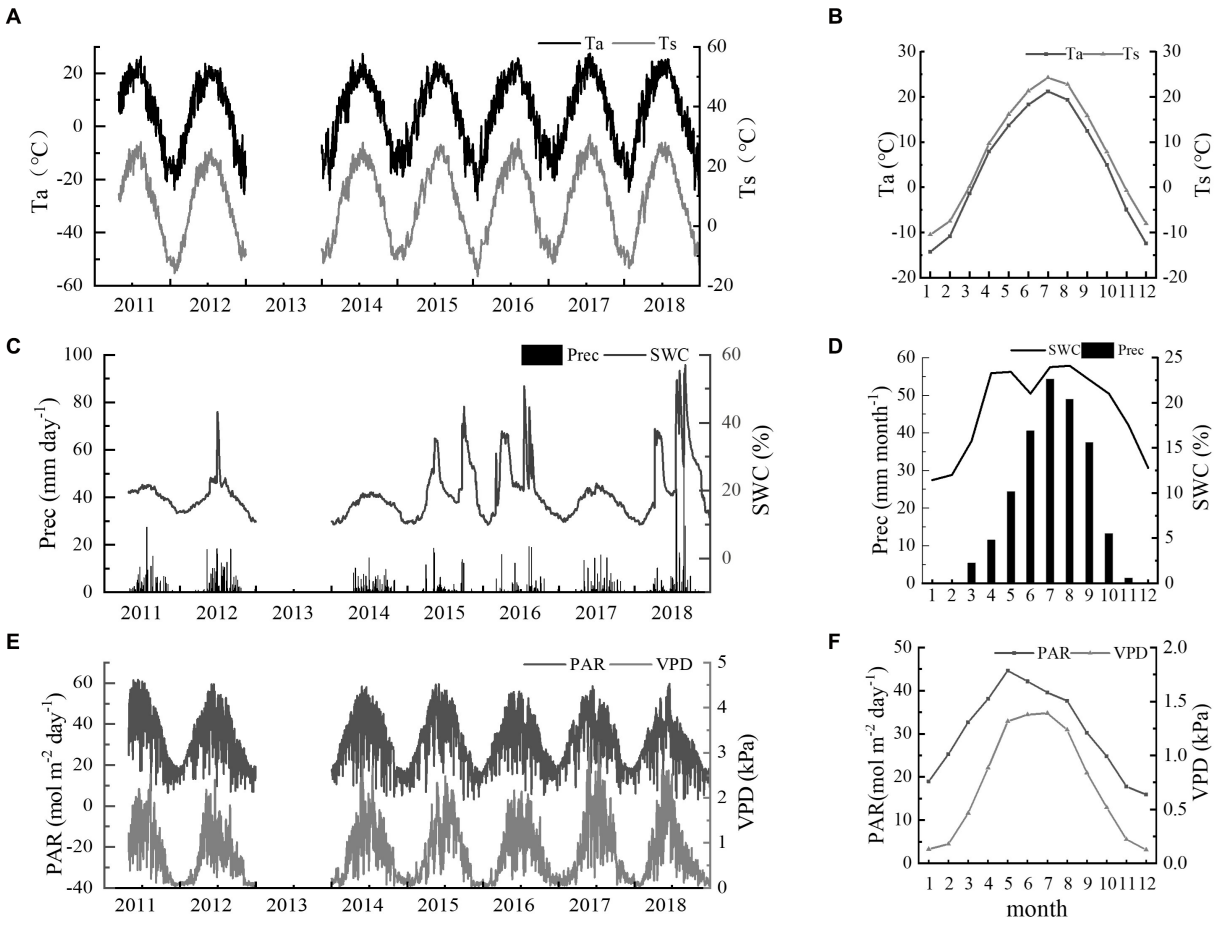

FIGURE 1
(A) Seasonal variations of daily mean air temperature (Ta) and soil temperature (Ts); **(B)** daily sum of precipitation (Prec) and daily average of volumetric soil water content (SWC) at 10cm depth; **(C)** photosynthetically active radiation (PAR) and daily mean vapor pressure deficit (VPD). Seasonal variations in monthly mean values of **(D)** Ta and Ts; **(E)** Prec and SWC; and **(F)** PAR and VPD.

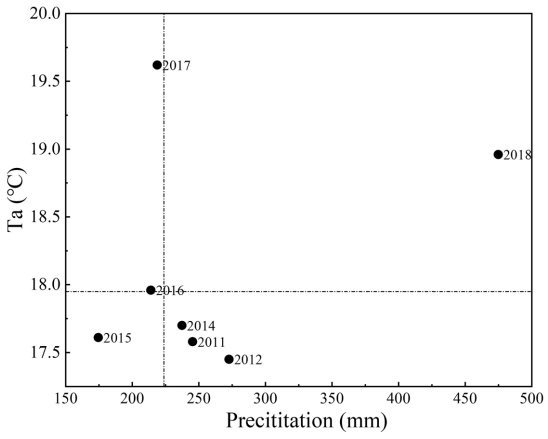

FIGURE 2
Average air temperature and cumulative precipitation during each growing season from 2011 to 2018. The growing season precipitation average over the long term (1990–2019) is shown by the horizontal dashed line (223.9mm); the long-term average air temperature for the growing season is illustrated by the vertical dashed line (17.95°C).

indirect effects of VPD and Ta, whereas SWC and PAR mainly had direct effects on daytime NEE. For night-time NEE, SWC had the strongest effect, followed by VPD, Ts, and Ta. Among these, SWC, VPD, and Ta mainly had direct effects on nighttime NEE.

During the non-growing season, VPD was the most important factor controlling NEE, followed by Ts, SWC, and Ta. In contrast to the growing season, the influence of environmental factors on NEE during the non-growing season was mainly attributed to direct effects.

Moreover, the effects of environmental factors on NEE may vary under different climatic conditions (Aguilos et al., 2018; Wang et al., 2019). In this study, we considered three types of climatic conditions: normal, warm, warm and moist, which were classified according to the average air temperature and cumulative precipitation during the growing season (see Section 3.1 and Figure 2). Path diagrams illustrating the effects of environmental factors on daytime net ecosystem CO_2 exchange for different climatic conditions (Figure 4). The results showed that in a normal year or warm year, moisture (SWC or VPD) was the primary factor controlling daytime NEE during the growing season, followed by Ta and PAR; in comparison, PAR proved to be the most important controlling factor for NEE in a warm and moist year (Table 3).

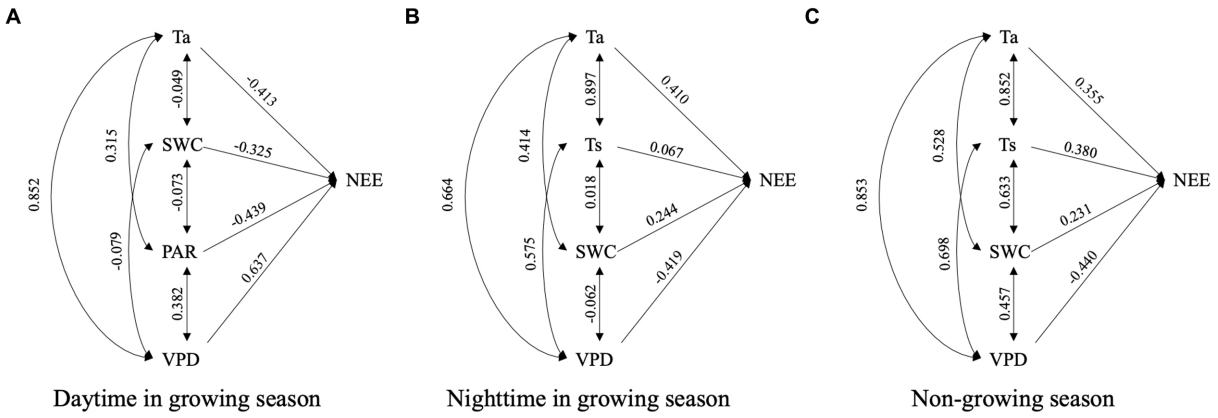

FIGURE 3
Path diagrams illustrating the effects of environmental factors on **(A)** daytime net ecosystem CO_2 exchange (NEE) during the growing season, **(B)** nighttime NEE during the growing season, and **(C)** NEE during the non-growing season.

TABLE 2 Direct and indirect path coefficients of environmental factors on the variation of NEE.

Period	Factors	Related coefficient	Direct path coefficient	Sum of indirect path coefficient	Determinative coefficient
Daytime in growing season	Ta	−0.065**	−0.413	0.348	0.117
	SWC	−0.372**	−0.325	−0.047	0.136
	PAR	−0.287**	−0.439	0.151	0.060
	VPD	0.122**	0.673	−0.551	0.288
Nighttime in growing season	Ta	0.190**	0.410	−0.221	0.013
	Ts	0.178**	0.067	0.111	0.019
	SWC	0.296**	0.244	0.052	0.085
	VPD	−0.147**	−0.419	0.272	0.053
Non-growing season	Ta	0.284**	0.355	−0.071	0.046
	Ts	0.217**	0.380	−0.163	0.097
	SWC	0.285**	0.231	0.054	0.078
	VPD	−0.369**	−0.440	0.070	0.131

The growing season generally lasts from May to September. October to April is referred to as the non-growing season. Ta, air temperature; Ts, soil temperature; SWC, soil water content; PAR, photosynthetically active radiation; VPD, vapor pressure deficit. ** indicates an extremely significant correlation between the factor and NEE ($p < 0.01$).

3.3. Effects of rainfall events on NEE

The NEE at this site was primarily water-limited according to the results of the aforementioned environmental controls. The effects of rainfall events on NEE are further explored in this section. From 2011 to 2018 (excluding 2013), 258 rainfall events were recorded in the study area, of which 196 (75% of all rainfall events) occurred during the growing season. A total of 196 events from this seven-growing-season study were used for statistical analysis (Figure 5). Most rainfall events were small in the size, with the majority (61%) being <5 mm. However, despite the low proportion of large rainfall events (> 5 mm), the total rainfall from them was greater than that of small rainfall events (80% vs. 20%).

By comparing the daily average NEE in a sliding window of 3 days after rainfall with the daily average NEE including the 3 days before rainfall, the impact of the rainfall event on NEE was evaluated (Figure 6). The results showed that the CO_2 uptake increased (negative $NEE_{response}$ in Figure 6) when the rainfall event was >5 mm, and the response increased with the size of the rainfall event. The relative response effect of NEE to rainfall event ($NEE_{response,\ r}$) represented a different trend; that is, the CO_2 uptake increased 10-, 8-, and 5-fold, respectively, compared to the uptake level before a rainfall event of 5–10 mm, 10–25 mm, and > 25 mm. Moreover, CO_2 uptake peaked approximately 1–3 days after a 5–10 mm rainfall event. However, it took 3–5 days to reach the highest carbon uptake after a rainfall event of >10 mm; On the other hand, small rainfall events (< 5 mm) slightly increased CO_2 emissions (positive $NEE_{response}$ in Figure 6).

As there were differences in the size of rainfall events that occurred in different months. For example, May is dominated by small rainfall events (rainfall events of <5 mm account for 74.3% of the total), while July and August are dominated by large rainfall events. The frequency of rainfall events of >5 mm in July and August was 45.0% and 40.5%, respectively, and the rainfall percentage of rainfall events of >5 mm in July and August was 87.1% and 88.0%, respectively. Therefore, a correlation analysis was conducted between monthly

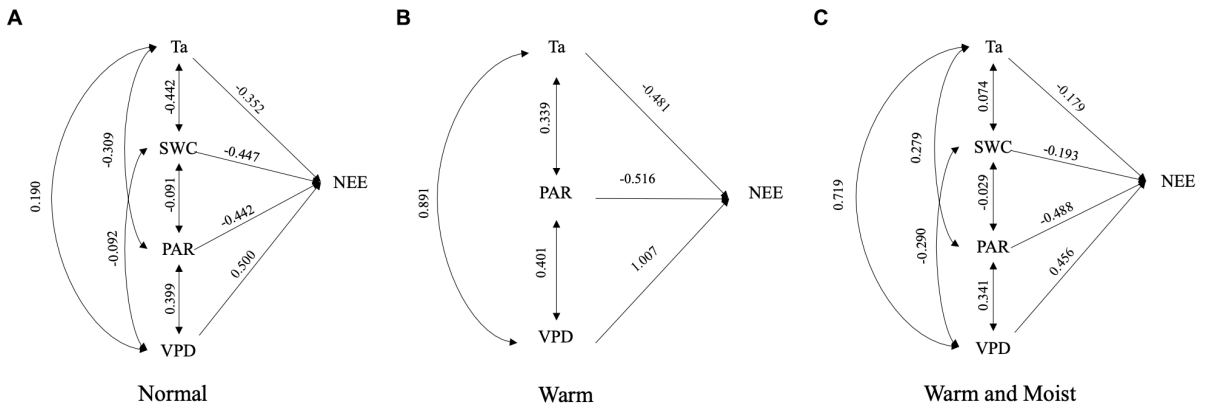

FIGURE 4
Path diagrams illustrating the effects of environmental factors on daytime net ecosystem CO_2 exchange (NEE) for **(A)** normal year, **(B)** warm year, and **(C)** warm and moist year.

TABLE 3 Direct and indirect path coefficients of environmental factors on daytime NEE changes in the growing season under different climatic conditions.

Climatic conditions	Factors	Related coefficient	Direct path coefficient	Sum of indirect path coefficient	Determinative coefficient
Normal	Ta	0.084**	−0.352	0.436	0.183
	SWC	−0.442**	−0.447	0.005	0.195
	PAR	−0.309**	−0.442	0.133	0.078
	VPD	0.190**	0.500	−0.310	0.060
Warm	Ta	0.078**	−0.481	0.559	0.306
	SWC	−0.014	–	–	–
	PAR	−0.247**	−0.516	0.269	0.011
	VPD	0.242**	1.007	−0.765	0.527
Warm and Moist	Ta	−0.098**	−0.179	0.081	0.003
	SWC	−0.363**	−0.193	−0.170	0.103
	PAR	−0.378**	−0.488	0.110	0.131
	VPD	0.162**	0.456	−0.294	0.060

The growing season was from May to September each year. Ta, air temperature; Ts, soil temperature; SWC, soil water content; PAR, photosynthetically active radiation; VPD, vapor pressure deficit. ** indicates an extremely significant correlation between the factor and NEE ($p < 0.01$).

precipitation and NEE during the growing season (Figure 7). The results showed that an increase in rainfall in May increased CO_2 emissions from the desert steppe ecosystem, whereas an increase in rainfall from June–September increased the CO_2 uptake. It supports the findings of previous related studies that seasonal distribution patterns of rainfall have important effects on the annual carbon balance (Dong, 2011). From the perspective of the entire growing season, NEE was greatly influenced by rainfall, and with an increase in rainfall, NEE decreased; that is, carbon uptake was enhanced.

4. Discussion

4.1. Constraints on NEE

It is generally agreed that in most ecosystems, radiation acts as the main regulating factor for NEE on a half-hourly scale (Baldocchi, 2014; Wang et al., 2019; Yan et al., 2023). However, certain studies have suggested that the two most important factors controlling carbon exchange in grassland ecosystems are temperature and water (Kim and Verma, 1990; Xue et al., 2014). This study showed that VPD (a function of temperature and humidity) had the largest effect on daytime NEE during the growing season, and that ecosystem carbon uptake decreased with increasing VPD, which is consistent with an earlier study in a desert steppe in Xilamuren (Li, 2020). VPD has a strong effect on stomatal conductance and can, therefore, modulate CO_2 exchange between the canopy and the atmosphere (Novick et al., 2016; Umair et al., 2020; Xie et al., 2020). Lower VPD stimulates stomatal opening, which is thought to increase CO_2 uptake (Wu et al., 2017). However, when VPD is higher than a certain threshold, plants may partially close their stomata to prevent excessive water loss; thus, ecosystem carbon uptake is constrained (Wang, 2015; Novick et al., 2016).

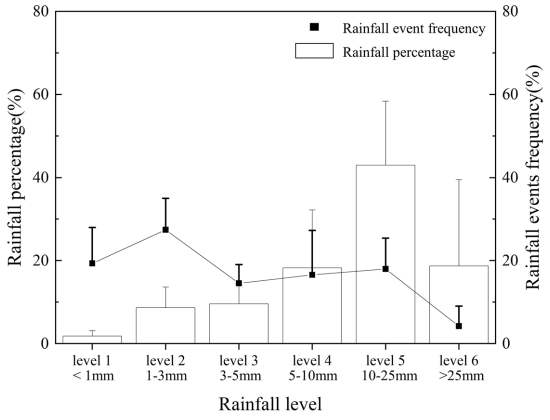

FIGURE 5
Frequency distributions of rainfall events and rainfall amounts from May to September between 2011 and 2018 (excluding 2013).

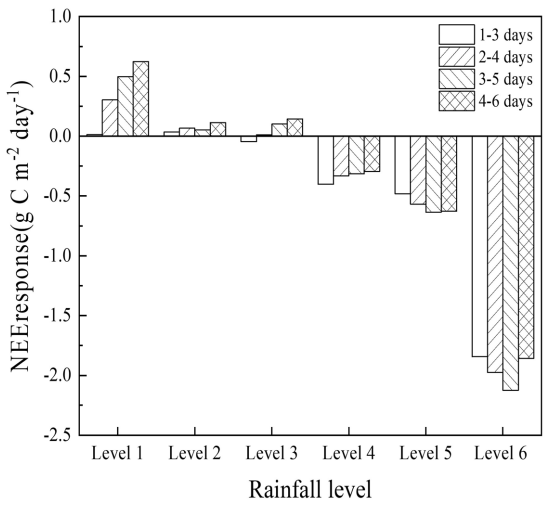

FIGURE 6
Variation of NEE before and after rainfall with different rainfall levels. The figure shows the difference between the daily average of the sliding window NEE for 3 days after a rainfall event and the daily average of the NEE for the 3 days before the rainfall event.

Our findings also revealed that SWC played a significant role in explaining nighttime variation NEE (i.e., ecosystem respiration), as reported in other previous studies (Balogh et al., 2011; Vicca et al., 2014; Meena et al., 2020). This implies that soil moisture should be considered when simulating ecosystem respiration, especially in water-limited ecosystems. Ecosystem respiration is the sum of the plant (autotrophic) and heterotrophic microbial respiration. Water availability is one of the most significant constraints on plant and microbial growth and changes in soil moisture can significantly affect ecosystem respiration (Piao et al., 2019). Reduced SWC in water-limited ecosystems such as at our study site leads to restricted plant growth and decreased microbial decomposition; thus, ecosystem respiration also shows a downward trend.

Path analysis suggested that temperature played a subordinate role in influencing half-hourly NEE changes at this site, which is consistent with previous studies in semiarid grasslands; that is, soil moisture availability is more important than soil temperature in regulating respiration in water-limited ecosystems (Vargas et al., 2010; Thomey et al., 2011; Wang et al., 2015). In this desert steppe, during the daytime of the growing season, an increase in temperature promoted ecosystem CO_2 uptake, while during the nighttime of the growing and non-growing seasons, an increase in temperature promoted ecosystem respiration and increased CO_2 emissions.

The effects of environmental factors on NEE may vary under different climatic conditions (Aguilos et al., 2018; Wang et al., 2019). Take daytime NEE during the growing season, for example, in the normal year, SWC was the primary factor controlling NEE, and the significant impact of SWC on NEE is mainly attributed to its direct impact. A previous study also showed that SWC has a strong direct impact on the eco-physiological processes of desert steppe plants (Aguilos et al., 2018); in the warm year, VPD became the most prominent environmental factor influencing NEE since variations in VPD are closely correlated with changes in temperature, which in turn influences plant stomatal conductance and modifies NEE; In the warm and moist year, water restriction for carbon uptake was lessened along with increased rainfall, and the significant impact of PAR on NEE emerged, because PAR directly promotes plant photosynthesis and increases ecosystem carbon absorption (Yue et al., 2010). The significant effects of SWC and PAR were mainly attributed to their direct effects; regarding Ta, its effects on NEE were dominated by direct effects in a warm and moist year, whereas they were primarily indirect in a normal year or a warm year, which is consistent with previous research (Jia et al., 2014; Ouyang et al., 2014; Aguilos et al., 2018).

4.2. Responses of NEE to rainfall events

Studies have shown that in grassland ecosystems with limited water resources, the ecosystem carbon flux is closely related to annual precipitation at different locations and in different years (Huxman et al., 2004; Gemechu Legesse et al., 2021). Small rainfall events predominate in arid and semi-arid ecosystems, and the results showed that small-scale rainfall events can enhance the carbon emissions of the ecosystem (Tang et al., 2018); whereas rainfall events of >5 mm can effectively increase soil water content, which enhances the carbon uptake capacity of the ecosystem and leads to a longer duration of ecosystem changes (Chen and Wang, 2009; Wang et al., 2018). This is in line with our analysis results, rainfall events of <5 mm slightly increased CO_2 emissions in the desert steppe, and rainfall events of >5 mm increased the CO_2 uptake in the desert steppe. Hence it can be inferred that a rainfall event of 5 mm is considered ecologically significant for NEE responses in desert steppe ecosystems (Li et al., 2013).

The carbon uptake peak was delayed by 1–5 days after rainfall, which was due to the faster response of ecosystem respiration to rainfall than to photosynthesis (Delgado-Balbuena et al., 2022). In addition, this pattern may be influenced by the dry period after rainfall, which offsets the soil water deficit and decreases the photosynthetic rate (Harper et al., 2005). The relationship between rainfall, infiltration depth, and the response of ecosystem carbon exchange to rainfall patterns depends on the position of soil microflora

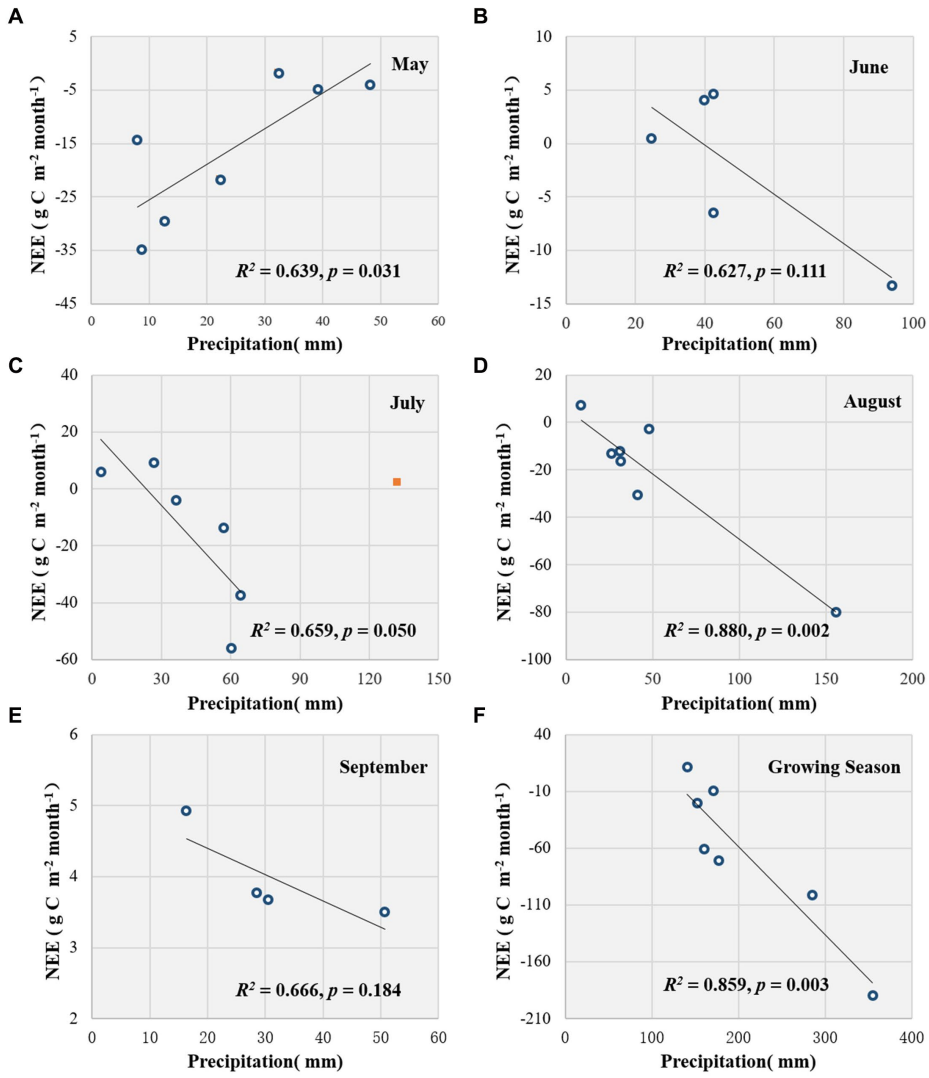

FIGURE 7
Relationship between NEE and corresponding rainfall. The relationship between NEE and rainfall in May **(A)**, June **(B)**, July **(C)**, August **(D)**, September **(E)**, and the growing season (May–September) **(F)**, respectively. The orange square in Plot C represented a singular point, and it was excluded from the regression; all the variables used in the analyses were monthly values, and if the effective observed data for a given month is less than 80%, that month's value is excluded from the analysis.

and plant roots in the soil as well as temporal changes in microbial and plant responses to wetting episodes (Huxman et al., 2004). Larger rainfall events may penetrate deep into the soil, whereas smaller rainfall events are intercepted by the canopy or directly replenished to the top soil layer, where water evaporates and cannot reach the root system (Hao et al., 2010).

This study showed that seasonal distribution patterns of rainfall have a large impact on desert steppe NEE. The CO_2 uptake increased with monthly rainfall from June to September, whereas it decreased with monthly rainfall in May. The main reason might be that small rainfall events (<5 mm) dominated in May, which are not expected to stimulate ecosystem productivity by altering the soil water content effectively, but instead increase ecosystem respiration and carbon emissions (Fay et al., 2008; Tang et al., 2018). It can be inferred that summer rainfall is more favorable for carbon sequestration than spring rainfall for desert steppe (Peng et al., 2013; Wang et al., 2018).

5. Conclusion

NEE of the studied desert steppe was primarily water-limited. Moisture-related environmental factors, VPD and SWC was the most prominent environmental factor for the daytime NEE and nighttime NEE during the growing season, respectively. But the interannual differences in climatic conditions can lead to changes in the controlling factor of NEE, e.g., PAR became the main controlling factor of NEE under climatic conditions of warm and moist.

The size of rainfall events has significant impacts on the NEE of the desert steppe. Small rainfall events (< 5 mm) slightly increased CO_2 emissions; Rainfall events of >5 mm increased the CO_2 uptake, and the NEE response increased with the rainfall event size. Moreover, NEE had a longer response time to rainfall events with a larger size, e.g., NEE peaked approximately 1–3 days after a 5–10 mm rainfall event, while the rainfall event size >10 mm, it would take 3–5 days for

NEE to reach a peak value. During the growing season, carbon uptake increased with monthly rainfall, except in May. These findings are important for predicting the carbon balance trends in desert steppe ecosystems under various climate change scenarios.

Data availability statement

The original contributions presented in the study are included in the article/supplementary material, further inquiries can be directed to the corresponding authors.

Author contributions

LZ and GZ: conceptualization and funding acquisition. JS and LZ: methodology and writing—original draft preparation. JS, YY, and SZ: investigation. JS and YW: data curation. All authors contributed to the article and approved the submitted version.

Funding

This research is funded by the National Key Research and Development Program of China (grant number 2018YFA0606103), National Natural Science Foundation of China (grant number 42130514), National Science and Technology Basic Resources Survey Program of China (grant number 2019FY101302), and China Meteorological Administration Innovation Development Special Project, (grant number CXFZ2023P052).

Acknowledgments

The authors wish to acknowledge Feng Zhang and Deng Ao for the fieldwork.

Conflict of interest

The authors declare that the research was conducted in the absence of any commercial or financial relationships that could be construed as a potential conflict of interest.

Publisher's note

References

Adams, J. M., Faure, H., Faure-Denard, L., Mcglade, J. M., and Woodward, F. I. (1990). Increases in terrestrial carbon storage from the last glacial maximum to the present. *Science* 348, 711–714. doi: 10.1038/348711a0

Aguilos, M., Herault, B., Burban, B., Wagner, F., and Bonal, D. (2018). What drives long-term variations in carbon flux and balance in a tropical rainforest in French Guiana? *Agric. For. Meteorol.* 253-254, 114–123. doi: 10.1016/j.agrformet.2018.02.009

Ahlström, A., Raupach, M. R., Schurgers, G., Smith, B., Arneth, A., Jung, M., et al. (2015). The dominant role of semi-arid ecosystems in the trend and variability of the land CO_2 sink. *Science* 348, 895–899. doi: 10.1126/science.aaa1668

Baldocchi, D. (2014). Measuring fluxes of trace gases and energy between ecosystems and the atmosphere - the state and future of the eddy covariance method. *Glob. Chang. Biol.* 20, 3600–3609. doi: 10.1111/gcb.12649

Balogh, J., Pinter, K., Foti, S., Cserhalmi, D., Papp, M., and Nagy, Z. (2011). Dependence of soil respiration on soil moisture, clay content, soil organic matter, and CO_2 uptake in dry grasslands. *Soil Biol. Biochem.* 43, 1006–1013. doi: 10.1016/j.soilbio.2011.01.017

Chen, C., Jing, C. Q., Xing, W. Y., Deng, X. J., Fu, H. Y., and Guo, W. (2021). Desert grassland dynamics in the last 20 years and its response to climate change in Xinjiang. *Acta Pratacul. Sin.* 30, 1–14. doi: 10.11686/cyxb2020143

Chen, X. P., Liu, T. X., Wang, G. L., Duan, L. M., Lei, H. M., and Wang, D. (2018). Effects of temperature and moisture on net ecosystem CO_2 exchange over a meadow wetland in the Horqin, China. *Chin. J. Appl. Ecol.* 29, 1523–1534. doi: 10.13287/j.1001-9332.201805.003

Chen, X. Q., and Wang, L. H. (2009). Progress in remote sensing Phenological research. *Prog. Geogr.* 28, 33–40. doi: 10.11820/dlkxjz.2009.01.005

Delgado-Balbuena, J., Loescher, H. W., Aguirre-Gutiérrez, C. A., Alfaro-Reyna, T., Pineda-Martínez, L. F., Vargaset, R., et al. (2022). Dynamics of short-term ecosystem carbon fluxes induced by precipitation events in a semiarid grassland. *Biogeosci. Discuss.* 1–29. doi: 10.5194/bg-2022-231

Dong, G. (2011). Carbon and water fluxes and water Ilse efficiency of the Svngnen meadow steppe in Northeast China. Master's thesis. JL: Northeast Normal University.

Fa, K. Y., Liu, J. B., Zhang, Y. Q., Wu, B., Qin, S. G., Feng, W., et al. (2015). CO_2 absorption of sandy soil induced by rainfall pulses in a desert ecosystem. *Hydrol. Process.* 29, 2043–2051. doi: 10.1002/hyp.10350

Fang, Q. Q., Wang, G. Q., Xue, B. L., Liu, T. X., and Kiem, A. (2018). How and to what extent does precipitation on multi-temporal scales and soil moisture at different depths determine carbon flux responses in a water-limited grassland ecosystem? *Sci. Total Environ.* 635, 1255–1266. doi: 10.1016/j.scitotenv.2018.04.225

Fay, P. A., Kaufman, D. M., Nippert, J. B., Carlisle, J. D., and Harper, C. W. (2008). Changes in grassland ecosystem function due to extreme rainfall events: implications for responses to climate change. *Glob. Chang. Biol.* 14, 1600–1608. doi: 10.1111/j.1365-2486.2008.01605.x

Gemechu Legesse, T., Dong, G., Jiang, S. C., Chen, J. Y., Dong, X. B., Alemu Daba, N., et al. (2021). Small precipitation events enhance the Eurasian grassland carbon sink. *Ecol. Indic.* 131:108242. doi: 10.1016/j.ecolind.2021.108242

Gong, T. T., Lei, H. M., Yang, D. W., Yang, H. B., Liu, T. X., and Duan, L. M. (2018). Assessing impacts of extreme water and temperature conditions on carbon fluxes in two desert shrublands. *J. Hydroelectr. Eng.* 37, 32–46. doi: 10.11660/slfdxb.20180204

Gu, Q., Wei, J., Luo, S. C., Ma, M. G., and Tang, X. G. (2018). Potential and environmental control of carbon sequestration in major ecosystems across arid and semi-arid regions in China. *Sci. Total Environ.* 645, 796–805. doi: 10.1016/j.scitotenv.2018.07.139

Hao, Y., Wang, Y., Mei, X., and Cui, X. (2010). The response of ecosystem CO_2 exchange to small precipitation pulses over a temperate steppe. *Plant Ecol.* 209, 335–347. doi: 10.1007/s11258-010-9766-1

Hao, Y. B., Zhou, C. T., Liu, W. J., Li, L. F., Kang, X. M., Jiang, L. L., et al. (2017). Aboveground net primary productivity and carbon balance remain stable under extreme precipitation events in a semiarid steppe ecosystem. *Agric. For. Meteorol.* 240-241, 1–9. doi: 10.1016/j.agrformet.2017.03.006

Harper, C. W., Blair, J. M., and Fay, P. A. (2005). Increased rainfall variability and reduced rainfall amount decreases soil CO_2 flux in a grassland ecosystem. *Glob. Chang. Biol.* 11, 322–334. doi: 10.1111/j.1365-2486.2005.00899.x

Huxman, T. E., Snyder, K. A., Tissue, D., Leffler, A. J., Ogle, K., Pockman, W. T., et al. (2004). Precipitation pulses and carbon fluxes in semiarid and arid ecosystems. *Oecologia* 141, 254–268. doi: 10.1007/s00442-004-1682-4

Jia, X., Zha, T. S., Wu, B., Zhang, Y. Q, Gong, J. N., Qin, S. G., et al. (2014). Biophysical controls on net ecosystem CO2 exchange over a semiarid shrubland in northwest China. *Biogeosci.* 11, 4679–4693. doi: 10.5194/bg-11-4679-2014

Jiang, Y., Wang, P., Xu, X., and Zhang, J. (2014). Dynamics of carbon fluxes with responses to vegetation, meteorological and terrain factors in the south-eastern Tibetan plateau. *Environ. Earth Sci.* 72, 4551–4565. doi: 10.1007/s12524-0

Kim, J., and Verma, S. B. (1990). Carbon dioxide exchange in a temperate grassland ecosystem. *Bound.-Layer Meteorol.* 52, 135–149. doi: 10.1007/bf00123181

Kozak, M., and Kang, M. S. (2006). Note on modern path analysis in application to crop science. *Commun. Biometry Crop Sci.* 1, 32–34.

Li, Q. Q. (2020). Application of eddy covariance theory in carbon flux observation of Xilamuren Desert steppe. Master's thesis. NM: Inner Mongolia Agricultural University.

Li, B. W., Wang, Q., Lu, W. W., Zhou, Y., Jiang, L. L., Liu, P. P., et al. (2021). The effects of warming and added water on key processes of grassland carbon cycle. *Acta Ecol. Sin.* 41, 1668–1679. doi: 10.5846/stxb201901010006

Li, C. F., Zhang, C., Luo, G. P., Chen, X., Maisupova, B., Madaminov, A. A., et al. (2015). Carbon stock and its responses to climate change in Central Asia. *Glob. Chang. Biol.* 21, 1951–1967. doi: 10.1111/gcb.12846

Li, F., Zhao, W. Z., and Liu, H. (2013). The response of aboveground net primary productivity of desert vegetation to rainfall pulse in the temperate desert region of Northwest China. *PLoS One* 8:e73003. doi: 10.1371/journal.pone.0073003

Meena, A., Hanief, M., Dinakaran, J., and Rao, K. S. (2020). Soil moisture controls the spatio-temporal pattern of soil respiration under different land use systems in a semi-arid ecosystem of Delhi, India. *Ecol. Process.* 9, 1–13. doi: 10.1186/s13717-020-0218-0

Moncrieff, J. B., Massheder, J. M., Debruin, H., Elbers, J., Friborg, T., Heusinkveld, B., et al. (1997). A system to measure surface fluxes of momentum, sensible heat, water vapour and carbon dioxide. *J. Hydrol.* 188-189, 589–611. doi: 10.1016/S0022-1694(96)03194-0

Novick, K. A., Ficklin, D. L., Stoy, P. C., Williams, C. A., Bohrer, G., Oishi, A. C., et al. (2016). The increasing importance of atmospheric demand for ecosystem water and carbon fluxes. *Nat. Clim. Chang.* 6, 1023–1027. doi: 10.1038/nclimate3114

Nyantakyi-Frimpong, H., and Bezner-Kerr, R. (2015). The relative importance of climate change in the context of multiple stressors in semi-arid Ghana. *Glob. Environ. Change* 32, 40–56. doi: 10.1016/j.gloenvcha.2015.03.003

Ouyang, Z., Chen, J., Becker, R., Chu, H., Xie, J., Shao, C., et al. (2014). Disentangling the confounding effects of PAR and air temperature on net ecosystem exchange at multiple time scales. *Ecol. Complex.* 19, 46–58. doi: 10.1016/j.ecocom.2014.04.005

Papale, D., Reichstein, M., Aubinet, M., Canfora, E., Bernhofer, C., Kutsch, W., et al. (2006). Towards a standardized processing of net ecosystem exchange measured with eddy covariance technique: algorithms and uncertainty estimation. *Biogeosciences* 3, 571–583. doi: 10.5194/bg-3-571-2006

Parton, W. J., Scurlock, J. M. O., Ojima, D. S., Schimel, D. S., Hall, D. O., Coughenour, M. B., et al. (1995). Impact of climate-change on grassland production and soil carbon worldwide. *Glob. Chang. Biol.* 1, 13–22. doi: 10.1111/j.1365-2486.1995.tb00002.x

Peng, S. S., Piao, S. L., Shen, Z. H., Ciais, P., Sun, Z. Z., Chen, S. P., et al. (2013). Precipitation amount, seasonality and frequency regulate carbon cycling of a semi-arid grassland ecosystem in Inner Mongolia, China: a modeling analysis. *Agric. For. Meteorol.* 178-179, 46–55. doi: 10.1016/j.agrformet.2013.02.002

Piao, S. L., Zhang, X. P., Chen, A. P., Liu, Q., Lian, X., Wang, X. H., et al. (2019). The impacts of climate extremes on the terrestrial carbon cycle: a review. *Sci. China Earth Sci.* 62, 1551–1563. doi: 10.1007/s11430-018-9363-5

Reichstein, M., Falge, E., Baldocchi, D., Papale, D., Aubinet, M., Berbigier, P., et al. (2005). On the separation of net ecosystem exchange into assimilation and ecosystem respiration: review and improved algorithm. *Glob. Chang. Biol.* 11, 1424–1439. doi: 10.1111/j.1365-2486.2005.001002.x

Rey, A., Oyonarte, C., Moran-Lopez, T., Raimundo, J., and Pegoraro, E. (2017). Changes in soil moisture predict soil carbon losses upon rewetting in a perennial semiarid steppe in SE Spain. *Geoderma* 287, 135–146. doi: 10.1016/j.geoderma.2016.06.025

Schwinning, S., Sala, O. E., Loik, M. E., and Ehleringer, J. R. (2004). Thresholds, memory, and seasonality: understanding pulse dynamics in arid/semi-arid ecosystems. *Oecologia* 141, 191–193. doi: 10.1007/s00442-004-1683-3

Tang, Y. K., Jiang, J., Chen, C., Chen, Y. M., and Wu, X. (2018). Rainfall pulse response of carbon fluxes in a temperate grass ecosystem in the semiarid loess plateau. *Ecol. Evol.* 8, 11179–11189. doi: 10.1002/ece3.4587

Thomey, M. L., Collins, S. L., Vargas, R., Johnson, J. E., Brown, R. F., Natvig, D. O., et al. (2011). Effect of precipitation variability on net primary production and soil respiration in a Chihuahuan Desert grassland. *Glob. Chang. Biol.* 17, 1505–1515. doi: 10.1111/j.1365-2486.2010.02363.x

Umair, M., Kim, D., Ray, R. L., and Choi, M. (2020). Evaluation of atmospheric and terrestrial effects in the carbon cycle for forest and grassland ecosystems using a remote sensing and modeling approach. *Agric. For. Meteorol.* 295:108187. doi: 10.1016/j.agrformet.2020.108187

Vargas, R., Baldocchi, D. D., Allen, M. F., Bahn, M., Black, T. A., Collins, S. L., et al. (2010). Looking deeper into the soil: biophysical controls and seasonal lags of soil CO_2 production and efflux. *Ecol. Appl.* 20, 1569–1582. doi: 10.1890/09-0693.1

Vicca, S., Bahn, M., Estiarte, M., Van Loon, E. E., Vargas, R., Alberti, G., et al. (2014). Can current moisture responses predict soil CO_2 efflux under altered precipitation regimes? A synthesis of manipulation experiments (vol 11, pg 2991, 2014). *Biogeosciences* 11, 3307–3308. doi: 10.5194/bg-11-3307-2014

Wang, J. (2015). Study on flux observation and characteristic of cycle of carbon and water in Horqin dune-meadow landscape using Eddy covariance method. Master's thesis. NM: Inner Mongolia Agricultural University.

Wang, Y., Chen, J. Q., Zhou, G. S., Shao, C. L., Chen, J., Wang, Y., et al. (2018). Predominance of precipitation event controls ecosystem CO_2 exchange in an inner Mongolian desert grassland, China. *J. Clean. Prod.* 197, 781–793. doi: 10.1016/j.jclepro.2018.06.107

Wang, W. Y., Guo, J. X., Wang, Y. S., and Wu, K. (2015). Observing characteristics of CO_2 flux and its influencing factors over Xilinhot grassland. *J. Meteorol. Sci.* 35, 100–107. doi: 10.3969/2013jms.0065

Wang, H., Tetzlaff, D., Dick, J. J., and Soulsby, C. (2017). Assessing the environmental controls on scots pine transpiration and the implications for water partitioning in a boreal headwater catchment. *Agric. For. Meteorol.* 240-241, 58–66. doi: 10.1016/j.agrformet.2017.04.002

Wang, S., Zhang, Y., Lü, S., Su, P., Shang, L., and Li, Z. (2016). Biophysical regulation of carbon fluxes over an alpine meadow ecosystem in the eastern Tibetan plateau. *Int. J. Biometeorol.* 60, 801–812. doi: 10.1007/s00484-015-1074-y

Wang, Y., Zhou, L., Jia, Q. Y., and Ping, X. Y. (2019). Direct and indirect effects of environmental factors on daily CO_2 exchange in a rainfed maize cropland-a SEM analysis with 10 year observations. *Field Crop Res.* 242:107591. doi: 10.1016/j.fcr.2019.107591

Webb, E. K., Pearman, G. I., and Leuning, R. (1980). Correction of flux measurements for density effects due to heat and water vapour transfer. *Q. J. R. Meteorol. Soc.* 106, 85–100. doi: 10.1002/qj.49710644707

Wu, J., Guan, K., Hayek, M., Restrepo-Coupe, N., Wiedemann, K. T., Xu, X., et al. (2017). Partitioning controls on Amazon forest photosynthesis between environmental and biotic factors at hourly to interannual timescales. *Glob. Chang. Biol.* 23, 1240–1257. doi: 10.1111/gcb.13509

Xie, X. D., Wang, T. J., Yue, X., Li, S., Zhuang, B. L., and Wang, M. H. (2020). Effects of atmospheric aerosols on terrestrial carbon fluxes and CO_2 concentrations in China. *Atmos. Res.* 237:104859. doi: 10.1016/j.atmosres.2020.104859

Xue, H. X., Li, Q., Huang, Y., Wang, Y. L., and Wu, D. L. (2014). The effect of soil environmental factors on the carbon flux over *Stipa krylovii* ecosystem. *Sci. Geogr. Sin.* 34, 1385–1392. doi: 10.13249/j.cnki.sgs.2014.011.1385

Yan, Y. J., Zhou, L., Zhou, G. S., Wang, Y., Song, J. X., Zhang, S., et al. (2023). Extreme temperature events reduced carbon uptake of a boreal forest ecosystem in Northeast China: evidence from an 11-year eddy covariance observation. *Front. Plant Sci.* 14:1119670. doi: 10.3389/fpls.2023.1119670

Yang, F. L., and Zhou, G. S. (2013). Sensitivity of temperate desert steppe carbon exchange to seasonal droughts and precipitation variations in Inner Mongolia. *Plos One* 8:e55418. doi: 10.1371/journal.pone.0055418

Yuan, Z. F., Zhou, J. Y., Guo, M. C., Lei, X. Q., and Xie, X. L. (2001). Decision coefficient-the decision index of path analysis. *J. Northwest Sci. Tech. Univ. Agric. For* 29, 133–135. doi: 10.13207/j.cnki.jnwafu.2001.05.035

Yue, G. Y., Zhao, L., Zhao, Y. H., and Li, Y. S. (2010). Research advances of grassland ecosystem CO_2 flux on Qinghai-Tibetan plateau. *J. Glaciol. Geocryol.* 25, 1263–1267. doi: 10.3724/SP.J.1077.2010.01263

Zhang, R., Zhao, X. Y., Zuo, X. A., Degen, A. A., Li, Y. L., Liu, X. P., et al. (2020). Drought-induced shift from a carbon sink to a carbon source in the grasslands of Inner Mongolia. *China. Catena* 195:104845. doi: 10.1016/j.catena.2020.104845

Zhou, Y. Y., Li, X. R., Gao, Y. H., He, M. Z., Wang, M. M., Wang, Y. L., et al. (2020). Carbon fluxes response of an artificial sand-binding vegetation system to rainfall variation during the growing season in the Tengger Desert. *J. Environ. Manag.* 266:110556. doi: 10.1016/j.jenvman.2020.110556

Zhu, Z. L., Sun, X. M., Wen, X. F., Zhou, Y. L., Tian, J., and Yuan, G. F. (2006). Study on the processing method of nighttime CO_2 eddy covariance flux data in ChinaFLUX. *Sci. China. Ser. D Earth Sci.* 49, 36–46. doi: 10.1007/s11430-006-8036-5

frontiers | Frontiers in Ecology and Evolution

TYPE Original Research
PUBLISHED 15 May 2023
DOI 10.3389/fevo.2023.1097817

OPEN ACCESS

EDITED BY
Chao Chen,
Zhejiang Ocean University, China

REVIEWED BY
Zhongqing Yan,
Chinese Academy of Forestry, China
Gang Fu,
Chinese Academy of Sciences (CAS), China
Xiangjin Shen,
Chinese Academy of Sciences (CAS), China

*CORRESPONDENCE
Cheng-Zhang Zhao
✉ zhaocz1710@163.com

RECEIVED 14 November 2022
ACCEPTED 17 April 2023
PUBLISHED 15 May 2023

CITATION
Kang M-P, Zhao C-Z, Li X-Y, Ma M and Zhao X-W (2023) Temporal and spatial characteristics of vegetation coverage and their influencing factors in the Sugan Lake wetland on the northern margin of the Qinghai–Tibet Plateau. *Front. Ecol. Evol.* 11:1097817. doi: 10.3389/fevo.2023.1097817

Temporal and spatial characteristics of vegetation coverage and their influencing factors in the Sugan Lake wetland on the northern margin of the Qinghai–Tibet Plateau

Man-Ping Kang[1], Cheng-Zhang Zhao[1,2]*, Xiao-Ya Li[1], Min Ma[1] and Xia-Wei Zhao[3]

[1]College of Geography and Environmental Science, Northwest Normal University, Lanzhou, China, [2]College of Geography and Environmental Science, Northwest Normal University, Research Center of Wetland Resources Protection and Industrial Development Engineering of Gansu Province, Lanzhou, China, [3]School of Life Sciences, Lanzhou University, Lanzhou, China

Fractional vegetation cover (FVC) is an important indicator of the development or reversal of salt marsh due to its absence in arid desert areas. Many studies have emphasized the differences in factors that affect fractional vegetation cover (FVC) in different temporal and spatial scales. However, few studies have reported on the temporal and spatial variations in vegetation coverage and their response to climate and also on the hydrological environment in inland salt marsh wetlands. Accordingly, based on a wetland community survey, different types of data, such as meteorological data, hydrological data, and Landsat remote sensing image data, recorded during the period from 1990 to 2020 were collected. The characteristics of the spatial and temporal distribution of vegetation coverage in the Sugan Lake wetland over the past 30 years were analyzed using a binary pixel model. Furthermore, a quantitative analysis on the response of vegetation coverage to hydrological and meteorological factors was undertaken. The results of the present study showed that the dimidiate pixel model had a high simulation accuracy in retrieving the vegetation coverage in inland salt marsh wetlands. The vegetation coverage of the Sugan Lake wetland increased with each year from 1990 to 2020, and its annual average was 19.34%. The spatial distribution of vegetation coverage was patchy and decreased from the center to the edge of the wetland. Within the same period, the vegetation coverage showed an increasing trend in Quan-shui and He-hong areas and a decreasing trend in the Shan-hong area. Vegetation coverage was mainly affected by various factors, such as precipitation, lake area, surface runoff, groundwater depth, and residential density, respectively. It was significantly positively correlated with precipitation ($R^2 = 0.56$, $P < 0.01$), lake area ($R^2 = 0.50$, $P < 0.01$), air temperature ($R^2 = 0.46$, $P < 0.01$), and river system density ($R^2 = 0.52$, $P < 0.01$) and negatively correlated with groundwater depth ($R^2 = -0.57$, $P < 0.01$) and residential density ($R^2 = -0.38$, $P < 0.05$). Implicit in these findings are complex mechanisms of change in vegetation coverage that help prevent the degradation of vegetation in fragile ecosystems.

KEYWORDS

salt marsh wetland, vegetation coverage, spatial characteristics, climate, hydrology

1. Introduction

A wetland is a groundwater-dependent ecosystem that is formed by the interaction between land and water. The inland salt marsh is a type of wetland ecosystem that is endowed with a distinct eco-hydrological process and a highly heterogeneous environment. The wetland ecosystem is controlled by hydrological processes. Spatial and temporal differences between water supply and static water directly affect the growth, development, reproduction, and spatial distribution pattern of wetland plants (Herring et al., 2013; Yao et al., 2019). Vegetation is an important part of the wetland ecosystem and plays a crucial role in material and energy exchange, atmospheric homeostasis, hydrological processes, carbon cycle, and stability of ecosystem (Shen et al., 2018; Zhang et al., 2018). Fractional vegetation cover (FVC) is an important parameter that reflects the growth distribution characteristics and structural density of surface vegetation, while it also serves as a sensitive index for the response of ecosystems to climate change and hydrological disturbance (Derakhshannia et al., 2020). The spatiotemporal heterogeneity of vegetation coverage in inland salt marshes is the key contributing factor to the stability of fragile wetland ecosystems in arid desert areas and is important for understanding the formation of the distribution patterns of the plant community in salt marshes.

Fractional vegetation cover refers to the proportion of the vertical projection area of above-ground vegetation (including leaves, stems, and branches) on the ground in a whole study area (Feng et al., 2019). Vegetation coverage not only reflects the appearance and nature of the plant community but is also important for maintaining the stability of wetland vegetation's community structure and function and, consequently, wetland landscape diversity and habitat environmental security (Li et al., 2016). Preferred methods for calculating FVC are ground verification and remote sensing estimation (Tang et al., 2020). Validation methods primarily include visual estimation in the field, sampling investigation, and photogrammetry; however, these methods can be influenced by individual differences as well as by the weather, time, and terrain (Okin et al., 2013). Vegetation coverage is characterized by the continuity of time and space, and the traditional methods of vegetation community investigation have limitations on the spatiotemporal scale. Remote sensing inversion is a preferred and feasible method for estimating vegetation coverage. Satellite remote sensing has several advantages, such as low requirements, speed of acquisition, and ability to cover a large area, compared with traditional ground-based verification. Many methods, such as empirical models (Gitelson, 2013), spectral mixing analysis (Okin, 2007), dimidiate pixel models, artificial neural networks (Atzberger and Rembold, 2013), and regression trees (Tottrup et al., 2007), are available to perform the inversion of vegetation coverage based on remotely sensed data. The normalized vegetation index (NDVI) is an important indicator of the effective radiation absorbed by vegetation during photosynthesis. This index is very sensitive to the growth potential and biomass variability of vegetation and has been successfully used to monitor vegetation conditions and their growth status. The dimidiate pixel model can largely eliminate the influence of background factors such as soil; accurately extract pure vegetation pixels in arid areas; and objectively and effectively reflect vegetation canopy conditions. With the continuous development of remote sensing science and technology, the inversion of vegetation coverage based on multisource remote sensing data is an essential means to obtain a large range of long-time series data. Remote sensing technology can overcome the limitations of a traditional community survey in temporal and spatial scales and complete the estimation of regional vegetation coverage. Most of the existing studies are based on different resolution and remote sensing imaging mechanisms, such as Landsat and MODIS (Okin et al., 2013; Cheng et al., 2017), GF-1 (Tao et al., 2019), radar (Liu L. et al., 2019), and other satellite data, to make estimates. However, few studies have combined wetland field surveys with remote sensing technology to describe patchy and spatial heterogeneity of vegetation coverage. In this study, the combination of wetland field survey and remote sensing technology can better describe the evolution of spatial–temporal heterogeneity of vegetation coverage in salt marsh wetlands. It is of great significance for understanding the formation mechanism of the spatial distribution pattern of plant communities in salt marsh wetlands.

Vegetation coverage is an important ecological indicator of wetland plant growth as well as ecological and environmental changes. The spatiotemporal dynamics of vegetation coverage in salt marsh wetlands is influenced by both human disturbances and natural environmental factors (Meixler et al., 2018; Zheng et al., 2019). Natural environmental factors comprise climatic factors, including precipitation (Mo et al., 2019; Meng et al., 2020), temperature (Lamchin et al., 2018; Liu L. et al., 2019), and extreme weather events (Wang et al., 2015; Jiang et al., 2017), terrain (Peng et al., 2012), topography (Liu et al., 2010), hydrology (Li et al., 2019), soil type, and moisture conditions (Liu S. et al., 2019; Peng et al., 2019). Climate change, especially any change that affects temperature and precipitation, influences the ecology of plant communities and plant growth cycles (Chen et al., 2019; Ding et al., 2020). Hydrological factors (groundwater depth and surface water runoff) are the main driving forces of succession of wetland vegetation through their effects on the soil environment, which, in turn, impact vegetation growth and distribution and shape the composition and structure of vegetation communities. In the short term, human disturbance is the main factor affecting vegetation coverage (Shen et al., 2018; Wu et al., 2022); ultimately, however, vegetation coverage is determined by both natural and human factors (Wang et al., 2019). Exploring vegetation coverage and its responses to different natural and anthropogenic factors is crucial for understanding ecosystem processes in the context of global climate change.

Suganhu Wetland is located in the Huahaizi Plateau Basin between Mount Taishan in the Altun mountain range, Mount Nanshan in the Danghe mountain range, and Saishiteng Mountain. The study area is a typical saline-marsh wetland ecosystem with the distribution of saline soil, and the wetland ecological series keeps the original state, which has a special eco-hydrological process. It has a typical, representative, and special protection and scientific research value in the northwest desert area. To date, studies on the vegetation coverage of wetlands have mainly focused on marsh wetlands in the Qinghai–Tibet Plateau (Peng et al., 2012; Zhang et al., 2018; Zhou et al., 2019), Lake Wetlands

(Mao et al., 2022), Coastal Wetlands (Hao et al., 2020), and Yellow River Delta Wetland (He et al., 2018). Studies investigating the Sugan Lake wetland have mainly focused on the relationship between vegetation root morphology and biomass allocation (Li et al., 2021) and the influence of groundwater chemistry on the distribution of wetland vegetation (Zhou et al., 2019). However, relatively few studies have addressed the spatial distribution pattern of plant coverage and its response to climatic and hydrological factors in inland salt marshes, and the question of how the functional stability of plant communities in inland salt marshes is maintained remains unexplained. Accordingly, in this study, based on a wetland community survey, different types of data, such as meteorological data, hydrological data, and Landsat remote sensing image data, recorded during the period from 1990 to 2020 were collected. The characteristics of the spatial and temporal distribution of vegetation coverage in the Sugan Lake wetland over the past 30 years were analyzed using a dimidiate pixel model. Furthermore, a quantitative analysis of the responses of the vegetation coverage to hydrological and meteorological factors was undertaken. We sought to clarify (1) the spatiotemporal variation in vegetation coverage in the Sugan Lake wetland from 1990 to 2020; (2) the characteristics of the changes in vegetation coverage in different hydrological zones; and (3) the main factors influencing changes in vegetation coverage in the hydrological zone of the salt marsh. This study aimed to provide a theoretical basis for revealing the mechanism involved in the synergistic adaptation between wetland plant growth and the hydrological environment under climate change.

2. Materials and methods

2.1. Study sites

The Sugan Lake wetland is located in the Sugan Lake Provincial Migratory Bird Nature Reserve, Aksai County, Jiuquan City, Gansu Province, China. The study area is located in the Huahaizi Plateau Basin on the northern margin of Qaidam Basin on the Qinghai–Tibet Plateau (39.22°—39.35° N, 94.45°—94.59° E) (Figure 1) at an altitude ranging from 2,795 to 2,808 m. The area is characterized by an inland alpine semi-arid climate, windy weather, frequent sandstorms, an average annual temperature of 2°C, an average annual precipitation of 77.6 mm, an average annual evaporation capacity of 1,964.8 mm, an average frost-free period of 90 days, and a dry air temperature of 30°C (Li et al., 2021).

The Sugan Lake wetland is an independent water system at the central and northwest end of the Qaidam inner water system. The Large and Small Harteng Rivers originating from the South Mountain of Danghe River flow underground through the mountain pass into the Large and Small Sugan Lakes of the Haizi Basin and then into the Large and Small Sugan Lakes. Finally, they are consumed by lake evaporation and evapotranspiration in the spring overflow zone. According to the classification criteria of the Chinese Soil Classification System of 1992, the main soil types in the study area are meadow soil, meadow marsh soil, and saline–alkali soil. The dominant plant species are *Saussurea salsa*, *Leymus secalinus*, *Phragmites australis*, *Glaux maritima*, *Triglochin palustre*, *Triglochin maritimum*, *Suaeda glauca*, *Blysmus sinocompressus*, and *Salicornia europaea* (Li et al., 2021).

2.2. Division of the Sugan Lake wetland ecological function zone

Sugan Lake is a plateau basin that is located at the end of the Large and Small Harteng River flow system, which is composed of lakes, rivers, freshwater springs, and various wetlands. The soil hydrological process is complex. The said complexity makes it necessary to further characterize the vegetation distribution pattern and the heterogeneity of wetland eco-hydrological processes in Sugan Lake. A survey was undertaken on the vegetation based on soil. The results of the aforementioned survey were combined with the results of the surrounding area of the hydrogeological survey conducted by the Geological Environmental Monitoring Institute in the Sugan Lake basin in Gansu Province. Based on the study of the changes in elevation, the trend of the river, freshwater springs in the distribution, and surface water source will facilitate Sugan Lake area topography, vegetation map, soil map, and land utilization to present situation chart datum's superposition (Gou et al., 2021). The Sugan Lake wetland is divided into three ecological function zones—Shan-hong area, Quan-shui area, and He-hong area (Table 1). The Shan-hong area, with relatively high terrain, is mainly distributed in the wet geographical zone at the periphery of the wetland and at the end of the diluvial fan. It is composed of two terrain units—micro-highland and low-lying land—and is divided into two parts in the north and south. Shan-hong area is dominated by a Gobi-like bare land with a large exposed surface area, limited conditions for vegetation growth, short and sparsely distributed plants, and low-density rhizomatous plants, mainly *Leymus secalinus* and *Saussurea runcinata*. The Quan-shui area is located in the south of the small Sugan Lake, east of the Dasugan Lake wetland center, low-lying, slow due to terrain and sediment particles, and aquifer permeability decreases, the underground water level rises gradually, and eventually overflows the surface to form a linear or a planar overflow, which develops to form a freshwater spring or a spring river, apart from the formation of surface water in rivers and springs. In this area, there is abundant vegetation. The vegetation is typical of a freshwater spring, herbaceous marsh, and marsh meadow, such as *Carex reptabunda*, *Triglochin maritimum*, and *Polygonum sibiricum*. The He Hong area lies on the east side of the Sugan Lake wetland. Every summer, the small Harteng flood of the river flows through the 215 national roads and forms small alluvial fans, thereby developing the advantage for *Leymus secalinus* inland salt marsh wetland, the scouring and silting of the flooding process, the influence of the area formed by east–west silt erosion gully and terrace landscape. In the erosion gullies and low-lying areas with seasonal surface water, river wetland plants, such as *Phragmites australis* and *Triglochin maritimum*, can be found. With increasing elevation, vegetation, such as *Leymus secalinus*, distributed in the silt platform area, is short and sparsely distributed due to the action of water and salt stress, and the vegetation coverage is low.

2.3. Wetland community investigation and remote sensing data acquisition

Based on the field investigation, a total of 146 sampling sites with a relatively flat terrain in the study area were selected

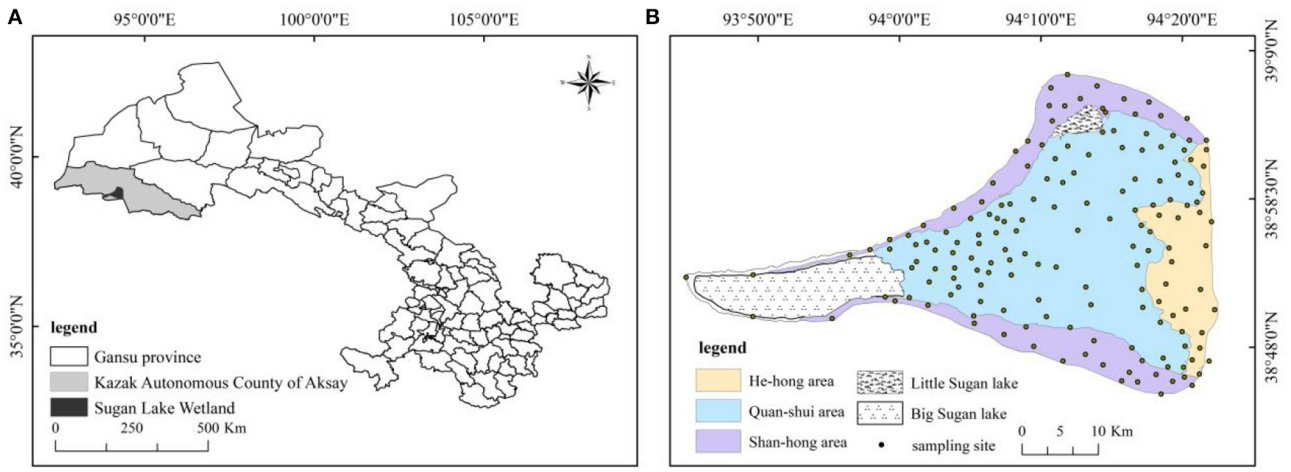

FIGURE 1
Sampling points of field survey data for the Sugan Lake wetland. **(A)** The study area is located in Aksai Kazak Autonomous County, Jiuquan City, Gansu Province, China. **(B)** Functional partition and sampling point of the study area.

TABLE 1 The trend and level of significance of θ_{slope}.

Class	θ_{slope}	P	R	Classification
1	<0	$P > 0.01$	(−0.92, −0.5)	More significant negative correlation
2	<0	$0.01 < P < 0.05$	(−0.5, −0.25)	Significant negative correlation
3	<0	$0.05 < P < 0.1$	(−0.25, 0)	No significant negative correlation
4	>0	$P > 0.10$	(0, 0.5)	No significant positive correlation
5	>0	$0.05 < P < 0.10$	(0.5, 0.8)	Significant positive correlation
6	>0	$0.00 < P < 0.05$	(0.8, 1)	More significant positive correlation

From: Analysis of spatial and temporal changes of vegetation cover and its driving forces in the Sugan Lake wetland.

(Figure 1), and 1 m × 1 m quadrates were set. From 15 August to 27 August 2020, a wetland community survey was conducted; the names of the members of the vegetation community were recorded; and the coverage, height, and density of the plant community were measured and repeated three times.

Remote sensing data from the geospatial cloud (https://earthexplorer.usgs.gov/) and Landsat (Landsat-5 TM/ETM and Landsat-8 OLI) satellite remote sensing were used in this study. To better identify wetland vegetation cover, imaging data from the vegetation growing season (July to September) were selected as much as possible, and the cloud cover of remote sensing images in the study area was 10%. The satellite revisit period was 16 days and the row number of the study area was 137, with a total of 30 scenes (Gauss–Kruger projection is universally used in image projection systems and World Geodetic System 1984 (WGS84) was the reference ellipsoid). The NDVI was calculated based on radiometric calibration, atmospheric correction, and band fusion of Landsat data under the ENVI5.1 software platform. The vegetation coverage of each period was calculated using a binary pixel model.

2.4. Data acquisition of meteorological and hydrological elements

The existing cold lake meteorological stations housed in the area surrounding Sugan Lake were selected to obtain information on temperature, precipitation, and average humidity data recorded from 1990 to 2020 *via* the China Meteorological Science Data Sharing Service network (http://cdc.cma.gov.cn/). Based on the Landsat remote sensing images, the water area of the Sugan Lake wetland was monitored from 1990 to 2020. The information pertaining to the areas of Da and Xiao Sugan Lakes over the last 30 years was extracted by combining supervised classification and visual interpretation, while the density of the water system was extracted by the index calculation. Groundwater and surface runoff data recorded from 1990 to 2020 in the Akesesu Dry Lake Basin were used for gathering information on ecological background verification and eco-hydrological monitoring research report (unpublished).

2.5. Research methods

2.5.1. Calculation of the NDVI

The normalized vegetation index was calculated as the ratio of the difference between the values of the red spectral band (R) and the near-infrared spectral band (NIR) to the sum of the values of the two bands, as follows:

$$NDVI = (NIR - R)/(NIR + R) \quad (1)$$

Image data from 1990 to 2012 were obtained from band 3 (R region) and band 4 (NIR region) of Landsat-5 TM/ETM images.

Image data from 2013 to 2020 were obtained from Landsat-8 OLI images in band 4 (R region) and band 5 (NIR region) and were utilized for NDVI calculation (Mao et al., 2020).

2.5.2. Fractional vegetation cover

The FVC is an important variable for describing the quality of vegetation and the changes in the ecosystem (Jiapaer et al., 2011). In this study, the dimidiate pixel model was used to calculate vegetation coverage using the following formula (Tong et al., 2016):

$$FVC = [(NDVI - NDVI_{soil})/(NDVIveg - NDVI_{soil})], \quad (2)$$

where $NDVI_{soil}$ and $NDVI_{veg}$ are the NDVI values of the pixels completely covered by bare soil and vegetation and represent the minimum and maximum NDVI values of a region, respectively. NDVI values with cumulative frequencies of 2 and 98% were selected as $NDVI_{soil}$ and $NDVI_{veg}$, respectively (Hao et al., 2020).

This study was conducted according to the technical regulations stipulated for the investigation of land use *status quo* and the technical regulations stipulated for the investigation of wetland resources (2008). The vegetation coverage standard of Sugan Lake wetland was formulated based on the wetland community coverage, wetland type, wetland plant composition, and other field wetland survey data. The studies were divided into the following five coverage groups: very low vegetation coverage (≤10%), low vegetation coverage (10%−30%), medium vegetation coverage (30%−50%), high vegetation coverage (50%−70%), and very high vegetation coverage (≥70%).

2.5.3. Calculation of the trend of vegetation coverage change over time

A one-dimensional (1D) linear regression model was used to analyze the interannual changes in vegetation cover in the Suganhu Lake wetland from 1990 to 2020. The spatiotemporal characteristics of vegetation coverage were displayed by comparing the differences between individual image elements (Li et al., 2019). The *t*-test was used to examine the correlation and significance level between the two variables. Unary linear regression $\theta slope$ was calculated as follows:

$$\theta_{\text{slope}} = \frac{\text{n} \times \sum_{i=1}^{n} i \times FVC_i - \sum_{i=1}^{n} i \sum_{i=1}^{n} FVC_i}{\text{n} \times \sum_{i=1}^{n} i^2 - \left(\sum_{i=1}^{n} i\right)^2} \quad (3)$$

$$R = \sqrt{\frac{\sum_{\text{i}=1}^{\text{n}} t_i^2 - \frac{1}{n}\left(\sum_{i=1}^{n} t_i\right)^2}{\sum_{\text{i}=1}^{\text{n}} X_i^2 - \frac{1}{n}\left(\sum_{i=1}^{n} X_i\right)^2}}, \quad (4)$$

where θ_{slope} is the θ_{slope} of the image element regression equation; *FVCi* is the mean value of FVC_i in the year *i*; *n* is the monitoring time, and *n*=30. When θ_{slope} *was* =0, the FVC_i of the image element is unchanged. When θ_{slope} *was* >0, the FVC_i of the image element tends to increase; and when it is <0, the image element tends to decrease. The correlation coefficient (*R*) was used to determine the significance of the changing trend. When *R* was <0, the vegetation cover tended to decrease, and when *R* was >0, the vegetation cover tended to increase. A *t*-distribution was used to test whether the variables were truly correlated with each other and to determine the level of significance of their correlation (Zhang et al., 2016). The θ_{slope} of the meta-regression line was obtained based on Eq. (1) and the trend and significance were classified into six levels based on the fitted correlation coefficient that corresponded to the results of a *t*-test (Hao et al., 2020; Yang et al., 2021) (Table 1).

2.5.4. The Pearson correlation coefficient and principal component analysis (PCA)

The correlation between vegetation coverage and climatic and hydrological factors was calculated based on Pearson's correlation coefficient, as follows: If the joint distribution of the random variables *x* and *y* is a two-dimensional (2D) normal distribution, (x_1, y_1), (x_2, y_2),…, (x_n, y_n) is the *n*th independent observation value, *r* represents Pearson's correlation coefficient, and the calculation formula is:

$$r = \frac{\sum_{i=1}^{n}(x_i - \bar{x})(y_i - \bar{y})}{\sqrt{\sum_{i=1}^{n}(x_i - \bar{x})^2 \sum_{i=1}^{n}(y_i - \bar{y})^2}} \quad (5)$$

where $\bar{x} = \frac{1}{n}\sum_{i=1}^{n} x_i$, $\bar{y} = \frac{1}{\text{n}}\sum_{\text{i}=1}^{\text{n}} y_i$, the range of the correlation coefficient *r* is [1, −1], and the larger the value of *r*, the stronger the correlation between variables.

Principal component analysis mainly analyzes the features of the covariance matrix to minimize the data dimension while maintaining the maximum contribution of the variance of the data set. The specific calculation process is as follows:

1) Calculate the matrix *X* of the standardized data index, set the number of relevant indicators as *n* and the number of sampling sites as *m*, and then calculate the matrix as follows:

$$X = \begin{vmatrix} X_{11} & \cdots & X_{1n} \\ \cdots & \cdots & \cdots \\ X_{m1} & \cdots & X_{mn} \end{vmatrix} \quad (6)$$

2) Calculate the correlation coefficient matrix and obtain the principal component:

$$\text{r}_{\text{ij}} = \frac{\sum_{k=1}^{\text{n}} \left|(x_{ki} - \bar{x_i})\right| \left|(x_{kj} - \bar{x_j})\right|}{\sqrt{\sum_{k=1}^{n}(x_{ki} - \bar{x_i})^2 \sum_{k=1}^{n}(x_{kj} - \bar{x_j})^2}}, \quad (7)$$

where r_{ij} is the correlation coefficient between the *i*th index and the *j*th index of the standardized data, and the correlation coefficient matrix can be obtained.

3) Principal components with an eigenvalue >1 and a cumulative variance contribution rate >85% were extracted.

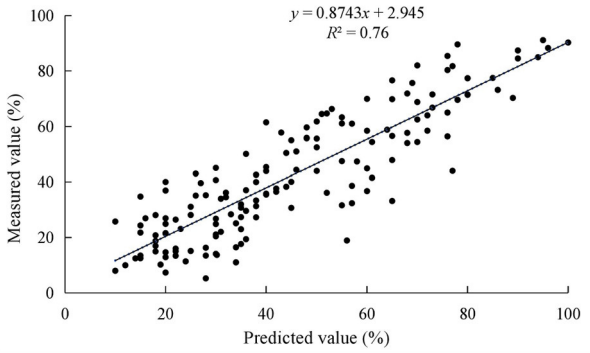

FIGURE 2
Measured and predicted vegetation coverage in 2020.

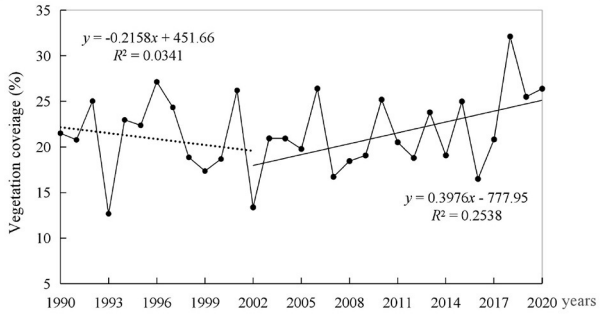

FIGURE 3
The interannual variation in vegetation coverage in the Sugan Lake wetland from 1990 to 2020.

3. Results

3.1. Test of the degree of fitting of the vegetation coverage

The linear regression model of vegetation coverage was established based on the Landsat remote sensing data and the measured values of vegetation coverage from the community survey, and the pixel binary model was tested by the degree of fitting. As shown in Figure 2, the estimated values of remote sensing inversion and the measured values of the community survey tended to be $y = 0.8743x + 2.945$ ($R^2 = 0.76$, $P \leq 0.01$). The correlation degree was satisfactory and the fitting degree of the linear model was high. The results showed that the vegetation coverage simulated by a pixel dichotomous model based on remote sensing data NDVI has high simulation accuracy and reliability in the Sugan Lake inland salt marsh wetland.

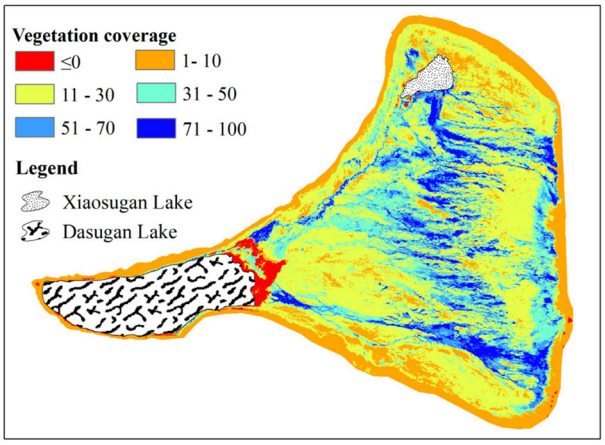

FIGURE 4
Spatial distribution of vegetation coverage in the Sugan Lake wetland in 2020.

3.2. Analysis of the temporal and spatial variation in wetland vegetation coverage in the Sugan Lake

3.2.1. Analysis of the interannual variation in vegetation coverage

The interannual variation in vegetation coverage in the Sugan Lake wetland from 1990 to 2020 is shown in Figure 3. Overall, vegetation coverage exhibited a significant upward trend in this wetland during this period. The maximum vegetation coverage occurred in 2018 (32.12%) and the minimum in 1993 (12.8%). The interannual variation in vegetation coverage in the Sugan Lake wetland can be divided into two stages. From 1990 to 2002, vegetation coverage showed a fluctuating but decreasing trend, and from 2003 onward, vegetation coverage showed a fluctuating but increasing trend, especially between 2016 and 2018.

3.2.2. Analysis of the spatial change in vegetation coverage

Figure 4 shows the spatial distribution of vegetation coverage in the Sugan Lake wetland in 2020. Vegetation coverage was very low (<10%) at the edge of the wetland; low (10–30%) in the east of the Dasugan Lake, Huahaizi, and the area surrounding Saishiteng Village; medium (31–50%) mainly around the Da and Xiao Sugan Lakes, the river beach in the south of Shuiyazi River, and the waterlogged depression in the middle of the wetland; and high (50–70%) or very high (71–100%) primarily in the center of the wetland. Vegetation coverage was also high in a strip located in the freshwater area south of the Xiao Sugan Lake, the spring outcrop zone of the wetland, and the beach downstream of the Shuiyazi River. In the eastern part of Dasugan Lake, the lake water is trapped in low-lying areas due to flooding; here, the vegetation coverage was ≤0.

3.2.3. The trend in vegetation coverage variation

The θ_{slope} and the corresponding correlation coefficient R were calculated, and the ArcGIS 10.3 superposition analysis function was used to obtain the spatial trend in vegetation coverage change in the study area (Figure 5, Table 2). The trend in vegetation coverage variation showed an increase overall, and the positive area was larger than the negative area, indicative of an improving

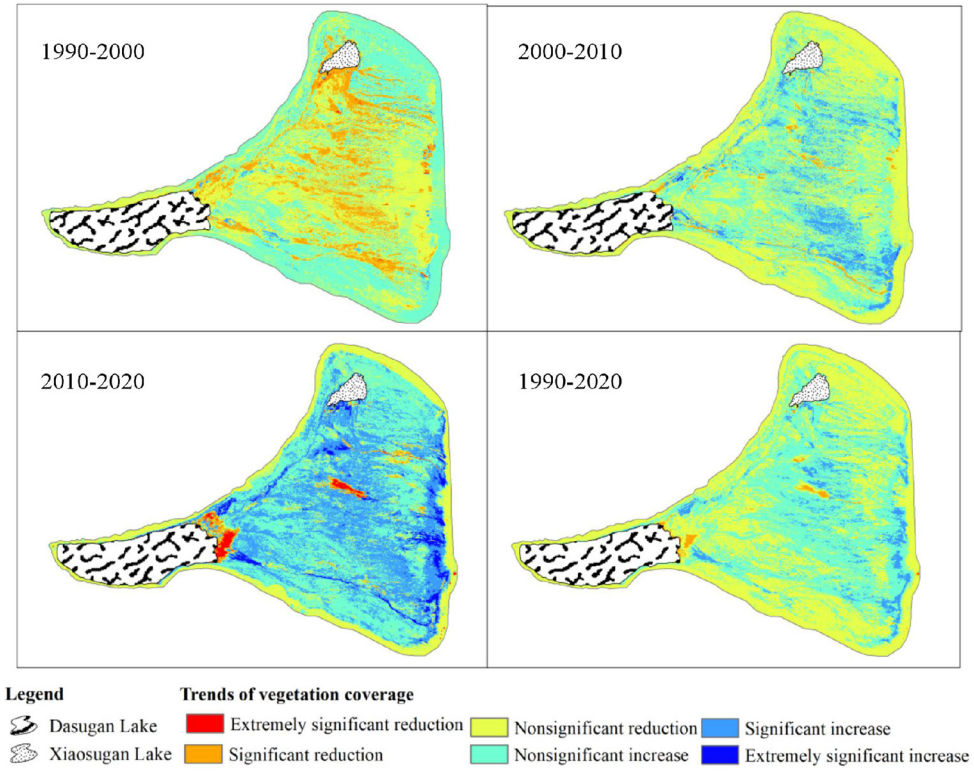

FIGURE 5
The trend in vegetation cover variation in the Sugan Lake wetland from 1990 to 2020.

trend in the wetland vegetation of Sugan Lake from 1990 to 2020. The proportion of area where the vegetation coverage did not increase significantly was 40.06%, which was mainly distributed in the center of the wetland and the river area. The proportion of area with no significant decrease in vegetation coverage was 52.04%. It is distributed primarily on the edge of the Sugan Lake wetland and the area east of the Dasugan Lake. However, in the area east of the Dasugan Lake, the proportion of area showing an extremely significant decrease in vegetation coverage was relatively small. The proportion of area in the Sugan Lake wetland in which vegetation coverage increased significantly was 5.87% and was mainly distributed in the area surrounding Huahaizi.

Differences in the trend toward vegetation coverage change were observed in different periods. The area showing a significant decrease in vegetation coverage was the largest from 1990 to 2000, accounting for 0.26% of the total area. The area with a non-significant decrease in FVC was the largest from 1990 to 2000 and from 2001 to 2010, accounting for 39.93% and 55.06% of the total area, respectively. The area with a non-significant decrease in vegetation coverage was 23.48% between 2011 and 2020. The maximum proportion of the area with a non-significant increase in vegetation coverage was 48.26% and 39.46% of the total area between 1990 and 2000 and between 2011 and 2020, respectively, while the area with a non-significant increase in vegetation coverage was 35.82% from 2001 to 2010 (Figure 5, Table 2).

3.3. Characteristics of the variation in vegetation coverage in different eco-hydrological zones

3.3.1. Change in vegetation coverage in the ecological function zone of the Sugan Lake wetland

Overall, the interannual change in vegetation coverage in Quan-shui and He-hong areas showed an increasing trend (Figure 6), with annual average values of 30.12 and 15.12%, respectively. The maximum values of vegetation coverage in Quan-shui and He-hong areas (44.08 and 27.58%, respectively) were reached in 2018. The minimum values of vegetation coverage in Quan-shui and He-hong areas were reached in 2002 and 2008 (18.97 and 6.18%, respectively). The average annual value of vegetation coverage in the Shan-hong area was 8.75% and the annual rate of change was −0.1187%. The maximum and minimum values of vegetation coverage were recorded in 1997 and 1993 (24.92 and 4.2%, respectively).

3.3.2. The trend in vegetation coverage variation in the ecological function zone of Sugan Lake wetland

Differences were found in the trends in vegetation coverage among the regions. From 1990 to 2020, the area

TABLE 2 The trend in vegetation coverage variation in various subareas of the Sugan Lake wetland from 1990 to 2020.

	1990–2000	2001–2010	2011–2020	1990–2020	1990–2000	2001–2010	2011–2020	1990–2020
Slope	Quan-shui area				He-hong area			
Extremely significant reduction	1.51	0.10	1.46	0.36	1.95	0.27	0.18	3.24
Significant reduction	19.71	2.98	2.88	1.25	3.88	1.28	1.26	0.26
Non-significant reduction	43.11	33.18	5.95	37.01	48.08	60.00	25.55	42.11
Non-significant increase	32.61	49.75	44.13	54.93	44.93	33.01	26.36	43.63
Significant increase	2.42	13.26	42.99	6.26	0.77	4.71	35.65	10.72
Extremely significant increase	0.64	0.74	2.58	0.18	0.49	0.73	10.99	0.04
Slope	Shan-hong area				Mean			
Extremely significant reduction	0.43	0.13	0.09	0.65	1.29	0.17	0.58	1.42
Significant reduction	2.16	0.80	0.27	0.09	8.58	1.68	1.47	0.53
Non-significant reduction	28.59	72.01	38.93	77.00	39.93	55.06	23.48	52.04
Non-significant increase	67.25	24.70	47.88	21.61	48.26	35.82	39.46	40.06
Significant increase	1.22	2.15	12.63	0.61	1.47	6.71	30.42	5.87
Extremely significant increase	0.36	0.21	0.20	0.03	0.50	0.56	4.59	0.09

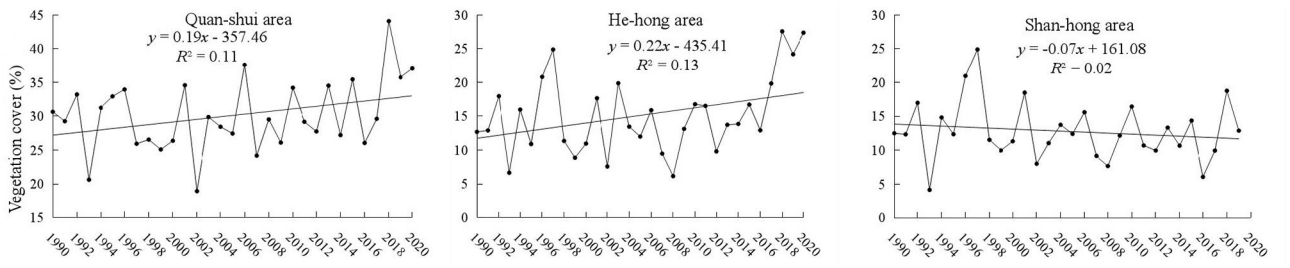

FIGURE 6
The interannual change in FVC in different regions from 1990 to 2020.

with a non-significant increase in vegetation coverage in Quan-shui accounted for 54.93% of the total area (Table 2), while the area with an extremely significant increase and an extremely significant decrease accounted for 0.18 and 0.36% of the total area, respectively. The area in He-hong with a non-significant increase and a non-significant decrease in vegetation coverage accounted for 42.11 and 43.63% of the total area, respectively, while the area with a significant decrease and an extremely significant increase in vegetation coverage accounted for 0.26 and 0.04% of the total area, respectively. In the Shan-hong region, the area with a non-significant increase in vegetation coverage accounted for 77% of the total area, while the area with a significant decrease and an extremely significant increase accounted for 0.09% and 0.03% of the total area, respectively. During the last 30 years, the area with a non-significant increase in vegetation coverage in Quan-shui accounted for 49.75% of the total area from 2001 to 2010 (Table 2). The areas in He-hong and Shan-hong with a non-significant decrease in vegetation coverage accounted for 60 and 72.01% of the total area, respectively.

3.4. Analysis of the factors influencing vegetation coverage in the Sugan Lake wetland

3.4.1. Interannual variation in climate elements in the Sugan Lake wetland

From 1990 to 2017, the temperature, precipitation, and humidity of the Sugan Lake wetland showed an increasing trend. The annual average temperature is 3.49°C, the lowest mean annual temperature was 2.65°C in 1992, and the highest was 4.4°C in 2017 (Figure 7). The annual average precipitation is 18.28 mm, the lowest average annual precipitation was 5.2 mm in 2000, and the highest was 35.8 mm in 2019. The annual average relative humidity is 30%, with a minimum of 23.46% in 1991 and a maximum of 37.63% in 2007 (Figure 7).

3.4.2. Interannual variation in hydrological elements in the Sugan Lake wetland

The interannual variation in the average lake area and groundwater depth of the Sugan Lake wetland from 1990 to 2020

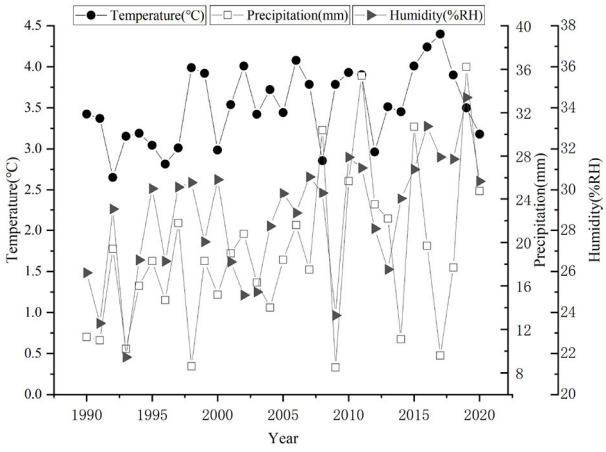

FIGURE 7
Interannual variation in air temperature, precipitation, and humidity in the Sugan Lake wetland.

is shown in Figure 8A. Over the past 30 years, the interannual variation in the lake area of Dasugan Lake has increased, and the average annual lake area was ∼107.42 m^2. From 1990 to 2020, the groundwater depth of the Sugan Lake wetland showed a decreasing trend, and the average groundwater depth was 2.49 m.

Figure 8B shows the interannual variation in surface runoff and drainage density in hydrological elements in the Sugan Lake wetland from 1990 to 2020. Over the last 30 years, the average annual surface runoff was 10.97 m^3/s, and the maximum surface runoff was 13.26 m^3/s, which was recorded in 2020. The drainage density of the Sugan Lake wetland showed an increasing trend over the last 30 years, with an average value of 18.34%. The lowest water system density was 13.76% in 1993 and the highest was 27.6% in 2018.

3.4.3. Analysis of the relationship between vegetation coverage and climatic and hydrological factors in the Sugan Lake wetland

We next explored the effects of climatic and hydrological factors on the spatial distribution of vegetation coverage in the Sugan Lake wetland. PCA and the Pearson correlation coefficient were used to comprehensively analyze the influence of climate (temperature, precipitation, and humidity), hydrology (groundwater depth, surface runoff, lake area, and water density), human activities (residential density), and other environmental factors on vegetation coverage in the Sugan Lake wetland.

The results of the PCA showed that the variance contribution rates of the first, second, and third principal components were 53.38, 13.82, and 12.63%, respectively, and their cumulative contribution rates reached 79.82%, indicating that they had fully summarized most of the indicators (Tables 3, 4). The index coefficient of the first principal component can reflect the contribution of the index to each principal component. Among them, the first principal component contains the maximum information and has the greatest influence on vegetation coverage. From the perspective of the loading of the principal component, the absolute values of correlation coefficients of groundwater depth, residential density, surface runoff, precipitation, and lake area in the first principal component are all >0.80. The results showed that the vegetation coverage was mainly affected by precipitation, lake area, surface runoff, groundwater depth, and residential density. The second principal component shows that the temperature phase relation value is 0.70, indicating that this component further reflects the influence of temperature on vegetation coverage to a certain extent based on the first principal component. In the third principal component, the correlation coefficient of humidity was 0.84, indicating that the influence of humidity on vegetation coverage was further reflected based on the first principal component and the second principal component.

The results of the Pearson correlation analysis showed that there was a significant positive correlation between vegetation coverage and precipitation, air temperature, lake surface area, and water system density ($P < 0.01$) (Figure 9). Meanwhile, there was a significant negative correlation between vegetation coverage and groundwater depth ($P < 0.01$) and between vegetation coverage and residential density ($P < 0.05$) (Figure 9).

The impacts of hydrological factors on FVC were different in different regions. In the Quan-shui area, there was a significant negative correlation between vegetation coverage and groundwater depth ($R^2 = -0.54$, $P < 0.01$). Vegetation coverage was significantly positively correlated with surface runoff ($R^2 = 0.58$, $P < 0.01$) and precipitation ($R^2 = 0.56$, $P < 0.01$), respectively. In the He-hong area, vegetation coverage was significantly positively correlated with surface runoff ($R^2 = 0.53$, $P < 0.01$) but negatively correlated with groundwater depth ($R^2 = -0.45$, $P < 0.05$). In the Shan-hong area, vegetation coverage was significantly positively correlated with precipitation ($R^2 = 0.45$, $P < 0.05$) and water system density ($R^2 = 0.48$, $P < 0.01$) but not significantly correlated with hydrological factors (groundwater depth, surface runoff, and lake surface area), and the correlation coefficient was low.

4. Discussion

Hydrological and climatic change characteristics are key abiotic factors that affect salt marsh zonation. Temperature and precipitation are the main abiotic determinants of the spatial distribution of vegetation and affect the ecological processes of plant communities and the growth cycle of plants (Liang et al., 2015; Zhang et al., 2019). In this study, we found that vegetation coverage in the Sugan Lake salt marsh showed an increasing trend from 1990 to 2020, as did air temperature, precipitation, and humidity. Vegetation coverage was positively correlated with precipitation ($R^2 = 0.56$, $P < 0.01$) and air temperature ($R^2 = 0.4$, $P < 0.05$). Precipitation is the main factor that affects the ecological environment in arid desert areas and determines the growth and development of wetland vegetation and the distribution of the dominant population. The reason attributed to precipitation is as follows: first, in the Sugan Lake wetland in the arid desert, precipitation is vital for the growth of vegetation, with the increase in average annual precipitation. On the one hand, it reduces drought stress and provides the much-needed water for the growth of vegetation. On the other hand, from both sides of the mountain, flood and rain gather in a closed basin, and for

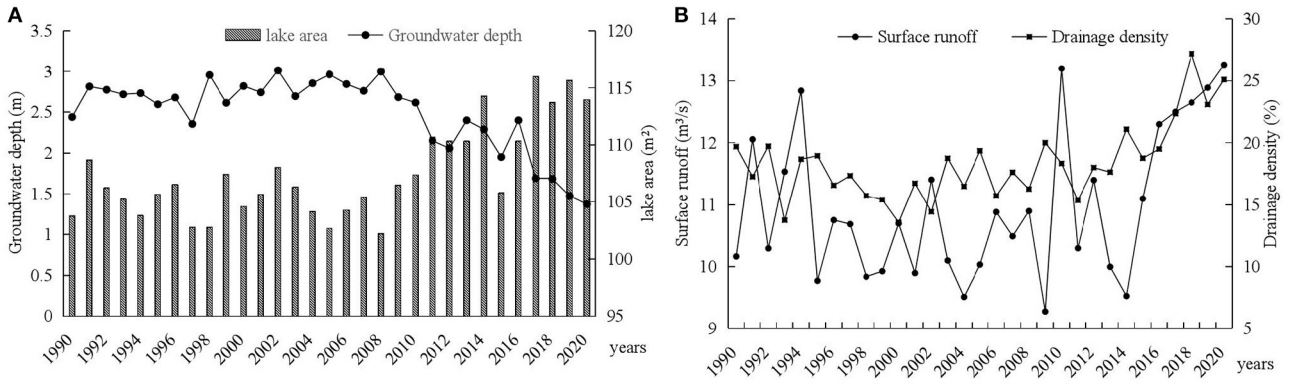

FIGURE 8
Interannual variation in hydrological elements in the Sugan Lake wetland. **(A)** Lake area and groundwater depth of Dasugan Lake. **(B)** Interannual variation in surface runoff and drainage density.

the development of marsh wetland, this pool of water provides abundant water resources and promotes the growth of wet raw halophytes. The vegetation coverage of the wetland was improved. Second, the research area has an inland alpine climate, and the temperature is relatively low. In this study, there was a significant positive correlation between vegetation coverage and temperature ($R^2 = 0.6$, $P < 0.05$). An increase in temperature can enhance the rate of photosynthesis, promote the synthesis and transport of carbohydrates, promote water absorption and conductance through the roots, and accelerate plant growth and development, thereby increasing vegetation coverage (Yan et al., 2012; Coldren et al., 2018). Climate warming and humidification are crucial to the ecology and hydrology of high-altitude areas. Ougahi found that, in high-altitude areas, with the rise of temperature, due to the melting of snow, soil moisture increases and vegetation growth becomes vigorous (Ougahi et al., 2022). Over the last 30 years, vegetation coverage in the Sugan Lake wetland was positively correlated with both air temperature and precipitation; however, the correlation between vegetation coverage and precipitation was greater than that between vegetation coverage and air temperature. This suggests that the vegetation coverage of the Sugan Lake wetland is more sensitive to precipitation than to air temperature, which is consistent with that reported by Simpson (Simpson et al., 2017). Solar radiation, as the main source of surface energy, is also the most direct and important meteorological factor to affect vegetation growth and development (Jiang et al., 2020). Some scholars have found that, in high-altitude areas, a low solar radiation limits vegetation growth, whereas an increase in radiation enhances the net photosynthesis of vegetation and thereby promotes vegetation growth, thus affecting vegetation coverage (Fu and Shen, 2017, 2022; Han et al., 2022).

Hydrology is an important driving force of wetland ecosystems. Under a constant climate, changes in hydrological parameters affect the type and structure of wetland vegetation, which, in turn, influence wetland ecosystem's productivity (He et al., 2018). The results of the present study showed that vegetation coverage was positively correlated with surface area, surface runoff, and drainage density and negatively correlated with groundwater depth ($P < 0.01$, $R^2 = -0.55$) in Sugan Lake. The correlation between

TABLE 3 The eigenvalues and the contribution rate of the principal components.

Principal component analysis	Characteristic value	Contribution rate (%)	Cumulative contribution rate (%)
Z1	4.804	53.38	53.38
Z2	1.244	13.82	67.20
Z3	1.136	12.63	79.82

vegetation coverage and hydrological factors differed according to the zone assessed. First, there was a very significant positive correlation between vegetation coverage and water system density, and lake area ($R^2 = 0.5$, $P < 0.05$) in the Quan-shui area. The main reason for this correlation is that the region is low-lying and the groundwater outcrops gather into large waters and rivers. Surface water has diluted the salinization of the surface soil of the tidal flat and salt marsh wetland around the river, which provides favorable environmental conditions for the growth and development of wetland vegetation such as *Carex reptabunda*, *Triglochin maritimum*, and *Polygonum sibiricum*. With the increase in precipitation and temperature, snow and ice melts in the surrounding mountains, seasonal flood, and surface runoff increase and converge in the low-lying wetland center, resulting in an increase of surface runoff and water system density in this region (Dar et al., 2022). The surface water flows to Dasugan Lake, thus increasing the surface area of the lake. The lake water flooding diluted the soil salinization on the lake shore and provided conditions for the growth of wet xerophytic vegetation such as *Phragmites australis* and *Saussurea salsa*. Therefore, vegetation coverage in the spring area increased significantly and extremely significantly. Second, there was a significant positive correlation between vegetation coverage and surface runoff ($R^2 = 0.53$, $P < 0.05$) in the He-hong area. This development takes place mainly because, when both precipitation and temperature increase, mountain ice and snow melt more, which intensifies the runoff of the Large and Small Harteng rivers. The waters of the Large and Small Harteng rivers converge on the area after passing

TABLE 4 The factor loading matrix of the four principal components.

Principal component	T	*P*	H	LA	GWD	SR	WD	DS
Z1	0.19	0.82	0.06	0.95	−0.89	0.84	0.73	−0.84
Z2	0.70	0.08	−0.47	−0.18	0.07	0.05	−0.15	0.33
Z3	0.61	−0.13	0.84	0.00	0.05	−0.05	−0.12	−0.13

T, temperature; P, precipitation; H, humidity; LA, lake area; GWD, groundwater depth; SR, surface runoff; WD, river system density; DS, residential density.

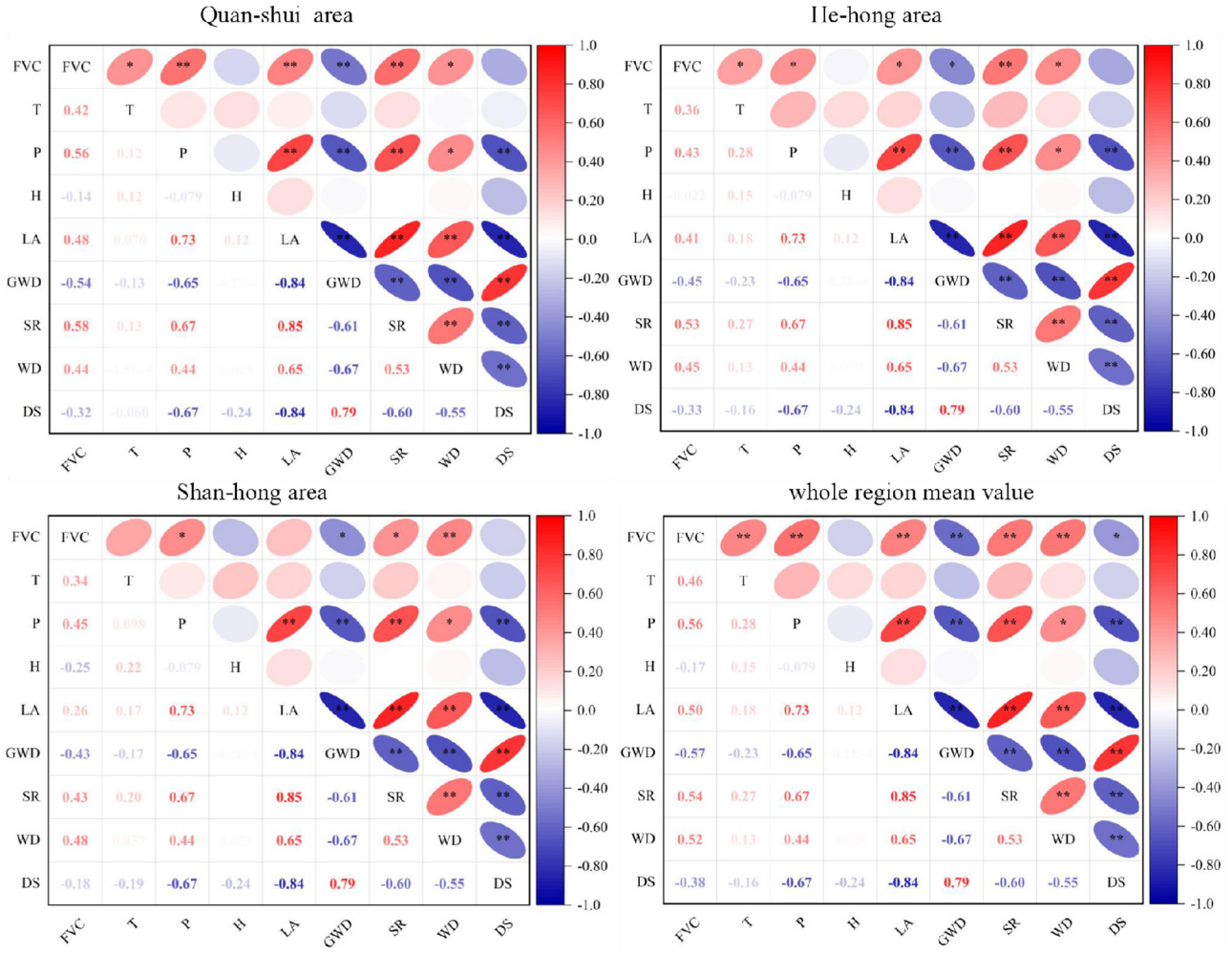

FIGURE 9
Analysis of factors influencing vegetation coverage in different subareas of the Sugan Lake wetland. FVC, vegetation coverage; T, temperature; P, precipitation; H, humidity; LA, lake area; GWD, groundwater depth; SR, surface runoff; WD, river system density; DS, residential density.

through National Highway 215, eroding gullies and low-lying areas and creating seasonal water on the surface to provide water for vegetation growth. Finally, the Shan-hong area is mainly located on the northern and southern edges of the Sugan Lake wetland. This area is dominated by a Gobi-like bare land, with a large exposed surface area and deep underground water burial depth, which makes it difficult for plant roots to absorb underground water, limited vegetation growth conditions, and short and sparse plants. With the increase in precipitation and temperature, snow and ice melting to water, seasonal floods, and precipitation in the mountains on both sides provide the vegetation in this region with the water needed for growth (Azmat et al., 2017). Vegetation coverage is affected by precipitation and stream density but has no significant correlation with groundwater depth, surface runoff, the lake area, and other hydrological factors. It was found that there was a significant negative correlation between vegetation coverage and groundwater depth. The main reason for this negative correlation is that, in the past 30 years, the surface runoff and the area of the Great Sugan Lake increased, while the groundwater depth decreased, which provided water resources for the growth of vegetation in this area. In addition, human disturbance (grazing) was weakened, the wetland eco-hydrological

environment improved, and consequently, the vegetation coverage gradually increased. There was a significant negative correlation between vegetation coverage and residential density ($R^2 = -0.47$, $P < 0.01$), which was consistent with Cheng's research conclusion (Cheng et al., 2017).

With the continuous advancement in remote sensing science and technology, satellite remote sensing image has become an important data source for earth observation. The inversion of vegetation coverage based on multisource remote sensing data is an important means to obtain a large range of long-time series data. We should note that there may be limitations or uncertainties in the data and methods used in this study. First, the data of Landsat-5 TM/ETM and Landsat-8 OLI were used in this study to retrieve vegetation coverage. On the one hand, NDVI data may have certain uncertainties in reflecting the actual vegetation status of salt marsh wetlands within 30 × 30 m (Liu et al., 2022). On the other hand, some scholars proposed that, when FVC reaches 80–90%, NDVI is nearly close to saturation, considering that the supersaturation of NDVI may have a certain impact on the inversion of vegetation coverage (Shen et al., 2020, 2022). This uncertainty may affect the result of the fitting test between predicted and measured vegetation coverage. Therefore, high-resolution remote sensing images, such as GF-2 image data, are considered for later research. Second, this study only considered the effects of climate (temperature, precipitation, and humidity) and hydrological factors on the vegetation coverage of each zone, but the conditions affecting the vegetation coverage of salt marsh wetlands are far more complex. In our previous studies, we found that the spatial distribution of vegetation coverage in the Sugan Lake wetland was patchy, which was influenced by the depth of groundwater and the spatial heterogeneity of soil as well as the total salt content in the soil. Some previous studies have shown that solar radiation, as the main source of surface energy, is also the most direct and important meteorological factor that affects vegetation growth and development. In addition, plant phenology, grazing, and human activities also affect vegetation growth and vegetation coverage (Chen et al., 2014; Fu et al., 2022; Wang et al., 2022; Zha et al., 2022). In the future, it is necessary to comprehensively consider the effects of solar radiation, plant phenology, grazing, nitrogen input, soil environment, and other factors on the zoning of vegetation communities and the spatial pattern of vegetation coverage, which have an important practical significance in the evaluation of the future ecological environment of the Sugan Lake wetland.

5. Conclusion

In conclusion, based on the combination of a wetland community survey and a remote sensing technology, the characteristics of the spatial and temporal distribution of vegetation coverage in the Sugan Lake wetland over the past 30 years were analyzed using a binary pixel model. The results of the present study showed that the dimidiate pixel model displayed a high simulation accuracy in retrieving the vegetation coverage in inland salt marsh wetlands. Over the past 30 years, vegetation coverage of the Sugan Lake wetland showed an increasing trend, and the trend in vegetation coverage variation differed according to the region evaluated. Spatially, the high and low values of vegetation coverage were distributed in patches. Vegetation coverage was mainly affected by precipitation, lake area, surface runoff, groundwater depth, and residential density. There was a significant positive correlation between vegetation coverage and precipitation ($R^2 = 0.56$, $P < 0.01$) and lake area ($R^2 = 0.50$, $P < 0.01$) and between vegetation coverage and air temperature ($R^2 = 0.46$, $P < 0.01$) and river system density ($R^2 = 0.52$, $P < 0.01$). Vegetation coverage was negatively correlated with groundwater depth ($R^2 = -0.57$, $P < 0.01$) and resident density ($R^2 = -0.38$, $P < 0.05$). The correlation between FVC and environmental factors also differed in a region-dependent manner. We were able to draw the conclusions that, in a cold climate background, a temperature rise is beneficial for vegetation growth and development but precipitation has a greater impact on vegetation.

Data availability statement

The raw data supporting the conclusions of this article will be made available by the authors, without undue reservation.

Author contributions

M-PK, C-ZZ, MM, X-YL, and X-WZ conceived and designed the experiments. M-PK performed the experiments, analyzed the data, and drafted the manuscript. C-ZZ supported in the funding acquisition, resources, and critical revision of the article. M-PK, MM, X-YL, and X-WZ undertook the investigation and contributed the methodology. All authors reviewed and approved the final manuscript.

Funding

This work was supported, in part, by the National Natural Science Foundation of China (Grant Nos. 41461013 and 41861009).

Acknowledgments

We acknowledge Charlesworth Author Services (https://dashboard.cwauthors.com.cn) for editing the English text of a draft of this manuscript. In addition, we are very grateful to Zhiwei Zhang, Xuqian Bai, XL, and DaWei Wang for their assistance in the field and laboratory work.

Conflict of interest

The authors declare that the research was conducted in the absence of any commercial or financial relationships that could be construed as a potential conflict of interest.

Publisher's note

References

Atzberger, C., and Rembold, F. (2013). Mapping the spatial distribution of winter crops at sub-pixel level using AVHRR NDVI time series and neural nets. *Remote Sens.* 5, 1335–1354. doi: 10.3390/rs5031335

Azmat, M., Liaqat, U. W., Qamar, M. U., and Awan, U. K. (2017). Impacts of changing climate and snow cover on the flow regime of Jhelum River, Western Himalayas. *Reg. Environ. Change* 17, 813–825. doi: 10.1007/s10113-016-1072-6

Chen, B. X., Zhang, X. Z., Tao, J., Wu, J. S., Wang, J. S., Shi, P. L., et al. (2014). The impact of climate change and anthropogenic activities on alpine grassland over the Qinghai-Tibet Plateau. *Agric. For. Meteorol.* 189, 11–18. doi: 10.1016/j.agrformet.2014.01.002

Chen, X. Y., Fu, B. H., Shi, P. L., et al. (2019). Vegetation dynamics in response to climate change in Tianshan, Central Asia from 2000 to 2016. *Arid Land Geogr.* 42, 162–171. doi: 10.12118 /j.issn.1000-6060

Cheng, F. Y., Liu, S. L., Yin, Y. J., Lü, Y. H., An, N. N., and Liu, X. M. (2017). The dynamics and main driving factors of coastal vegetation in Guangxi based on MODIS NDVI. *Acta Ecol. Sin.* 37, 788–797. doi: 10.5846/stxb201509091866

Coldren, G. A., Langley, J. A., Feller, I. C., and Chapman, S. K. (2018). Warming accelerates mangrove expansion and surface elevation gain in a subtropical wetland. *J. Ecol.*107, 79–90. doi: 10.1111/1365-2745.13049

Dar, T., Rai, N., Kumar, S., and Bhat, M. A. (2022). Climate change impact on cryosphere and streamflow in the Upper Jhelum River Basin (UJRB) of north-western Himalayas. *Environ. Monit. Assess.* 194, 140(2022). doi: 10.1007/s10661-022-09766-3

Derakhshannia, M., Dalvand, S., Asakereh, B., and Ostad Ali Askari, K. (2020). Corrosion and deposition in Karoon River, Iran, based on hydrometric stations. *Int. J. Hydrol. Sci. Technol.* 10, 334. doi: 10.1504/IJHST.2020.108264

Ding, Y., Halike, A., Chen, X. Y., and Abdirahman, M. (2020). Spatialtemporal changes in vegetation characteristics and climate in Hotan prefecture. *Acta Ecol. Sin.* 40, 1258–1268. doi: 10.5846/stxb201811292600

Feng, L. L., Jia, Z. Q., Li, Q. X., Zhao, A. Z., Zhao, Y. L., and Zhang, Z. J. (2019). Spatiotemporal change of sparse vegetation coverage in northern China. *J. Indian Soc. Remote Sens.* 47, 359–366. doi: 10.1007/s12524-018-0912-x

Fu, G., and Shen, Z. X. (2017). Effects of enhanced UV-B radiation on plant physiology and growth on the Tibetan Plateau: a meta-analysis. *Acta Physiol. Plant* 39, 85. doi: 10.1007/s11738-017-2387-8

Fu, G., and Shen, Z. X. (2022). Asymmetrical warming of growing/non-growing season increases soil respiration during growing season in an alpine meadow. *Sci. Total Environ.* 812, 152591. doi: 10.1016/j.scitotenv.2021.152591

Fu, G., Wang, J. H., and Li, S. W. (2022). Response of forage nutritional quality to climate change and human activities in alpine grasslands. *Sci. Total Environ.* 845, 157552. doi: 10.1016/j.scitotenv.2022.157552

Gitelson, A. A. (2013). Remote estimation of crop fractional vegetation cover: the use of noise equivalent as an indicator of performance of vegetation indices. *Int. J. Remote Sens.* 34, 6054–6066. doi: 10.1080/01431161.2013.793868

Gou, F. Z., Zhao, C. Z., Yang, J. C., Ren, J., Ma, J. Y., and Li, Z. Q. (2021). Spatial heterogeneity of above-ground biomass in sugan lake wetland vegetation. *Acta Ecol. Sin.* 41, 7774–7784. doi: 10.5846/stxb201909161918

Han, F., Fu, G., Yu, C., and Wang, S. (2022). Modeling nutrition quality and storage of forage using climate data and normalized-difference vegetation index in alpine grasslands. *Remote Sens.* 14, 3410. doi: 10.3390/rs14143410

Hao, J., Xu, G., Luo, L., i., Zhang, Z., Yang, H., et al. (2020). Quantifying the relative contribution of natural and human factors to vegetation coverage variation in coastal wetlands in China. *Catena* 188, 104429. doi: 10.1016/j.catena.2019.104429

He, W. J., Han, G. X., Xu, Y. N., Zhang, X. T., Wang, A. D., Che, C. G., et al. (2018). Effects of tidal dry-wet alternation on CO_2 exchange in the net ecosystem of salt marsh in the Yellow River Delta. *Chin. J. Appl. Ecol.* 29, 269–277. doi: 10.13287/j.1001 - 9332. 201801.035

Herring, G., Eagles-Smith, C. A., Ackerman, J. T., Gawlik, D. E., and Beerens, J. M. (2013). Landscape factors and hydrology influence mercury concentrations in wading birds breeding in the Florida Everglades, USA. *Sci. Total Environ.* 458, 637–646. doi: 10.1016/j.scitotenv.2013.04.036

Jiang, H. L., Xu, X., Guan, M. X., Wang, L. F., Huang, Y. M., and Jiang, Y. (2020). Determining the contributions of climate change and human activities to vegetation dynamics in agro-pastural transitional zone of northern China. *Sci. Total Environ.* 718, 134871. doi: 10.1016/j.scitotenv.2019.134871

Jiang, L., Jiapaer, G., Bao, A., Guo, H., and Ndayisaba, F. (2017). Vegetation dynamics and responses to climate change and human activities in Central Asia. *Sci. Total Environ.* 599–600, 967–980. doi: 10.1016/j.scitotenv.2017.05.012

Jiapaer, G., Chen, X., and i., Bao, A. (2011). A comparison of methods for estimating fractional vegetation cover in arid regions. *Agric. For. Meteorol.* 151, 1698–1710. doi: 10.1016/j.agrformet.2011.07.004

Lamchin, M., Lee, W. K., Jeon, S. W., Wang, S. W., Lim, C. H., Song, C., et al. (2018). Long-term trend and correlation between vegetation greenness and climate variables in Asia based on satellite data. *Sci. Total Environ.* 618, 1089–1095. doi: 10.1016/j.scitotenv.2017.09.145

Li, N., Li, L. W., Lu, D. S., Zhang, Y. L., and Wu,. M. (2019). Detection of coastal wetland change in China: a case study in Hangzhou Bay. *Wetlands Ecol. Manag.* 27, 103–124. doi: 10.1007/s11273-018-9646-3

Li, Q., Zhao, C. Z., Kang, M. P., and Li, X. Y. (2021). The relationship of the main root-shoot morphological characteristics and biomass allocation of Saussurea salsa under different habitat conditions in Sugan lake wetland on the northern margin of the Qinghai-Tibet Plateau. *Ecol. Indicat.* 128, 107836. doi: 10.1016/j.ecolind.2021.107836

Li, X. R., Sun, L., and Zhu, J.S. (2016). Vegetation coverage extraction in arid regions based on multi-scale remote sensing data. *Chinese J. Ecol.* 35, 1394-1402. (in Chinese). doi: 10.13292/J.1000-4890.201605.029

Liang, S. Z., Yu, D. F., Wang, M., and Shi, P. (2015). Application of remote sensing time-series data to investigate the relationship between vegetation change and climatic factors: A case study of Circum-Bohai Sea area. *Remote Sens.* 27, 114–121. doi: 10.6046/gtzyyg. 2015.03.19

Liu, L., Wang, Y., Wang, Z., Li, D., Zhang, Y., Qin, D., et al. (2019). Elevation-dependent decline in vegetation greening rate driven by increasing dryness based on three satellite NDVI datasets on the Tibetan Plateau. *Ecol. Indic.* 107, 105569. doi: 10.1016/j.ecolind.2019.105569

Liu, R. J., Zhang, W. C., and Pei, H. Q. (2010). Relationship between soil erosion and influencing factors in Huaihe River Basin. *Soil Water Conserv.* 2010, 29–32. (in Chinese). doi: 10.3969/j.issn.1000-0941.2010.05.012

Liu, S., Huang, S., Xie, Y., Wang, H., Huang, Q., Leng, G., et al. (2019). Spatial temporal change in vegetation cover in a typical semi-humid and semi-arid region in China: changing patterns, causes and implications. *Ecol. Indic.* 98, 462–475. doi: 10.1016/j.ecolind.2018.11.037

Liu, Y. C., Li, Z., Chen, Y. N., Li, Y. P., Li, H. W., Xia, Q. Q., et al. (2022). Evaluation of consistency among three NDVI products applied to High Mountain Asia in 2000-2015. *Remote Sens. Environ.* 269, 112821, doi: 10.1016/j.rse,0.2021.112821

Mao, D. H., Wang, Z. M., Du, B. J., Li, L., Tian, Y. L., Jia, M. M., et al. (2020). National wetland mapping in China: A new product resulting from object-based and hierarchical classification of Landsat 8 OLI images. *ISPRS J. Photogramm. Remot. Sens.* 164, 11–25. doi: 10.1016/j.isprsjprs.2020.03.020

Mao, P. P., Zhang, J., Li, M., Liu, Y. L., Wang, X., Yan, R. R., et al. (2022). Spatial and temporal variations in fractional vegetation cover and its driving factors in the Hulun Lake region. *Ecol. Indic.* 108490. doi: 10.1016/j.ecolind.2021.108490

Meixler, M. S., Kennish, M. J., and Crowley, K. F. (2018). Assessment of plant community characteristics in natural and human-altered coastal marsh ecosystems. *Estuar. Coasts* 41, 52–64. doi: 10.1007/s12237-017-0296-0

Meng, X., Gao, X., Li, S., and Lei, J. (2020). Spatial and temporal characteristics of vegetation NDVI change and the driving forces in Mongolia during 1982–2015. *Remote Sens.* 2, 603. doi: 10.3390/rs12040603

Mo, K., Chen, Q., Chen, C., Zhang, J., Wang, L., and Bao, Z. (2019). Spatiotemporal variation of correlation between vegetation cover and precipitation in an arid mountain-oasis river basin in northwest China. *J. Hydrol.* 574, 138–147. doi: 10.1016/j.jhydrol.2019.04.044

Okin, G. S. (2007). Relative spectral mixture analysis—a multitemporal index of total vegetation cover. *Remote Sens. Environ.* 106, 467–479. doi: 10.1016/j.rse.2006.09.018

Okin, G. S., Clarke, K. D., and Lewis, M. M. (2013). Comparison of methods for estimation of absolute vegetation and soil fractional cover using MODIS normalized BRDF-adjusted reflectance data. *Remote Sens. Environ.* 130, 266–279. doi: 10.1016/j.rse.2012.11.021

Ougahi, J. H., Cutler, M. J., and Cook, S. (2022). Assessment of climate change effects on vegetation and river hydrology in a semi-arid river basin. *PLoS ONE* 17, e0271991. doi: 10.1371/journal.pone.0271991

Peng, J., Liu, Z., Liu, Y., Wu, J., and Han, Y. (2012). Trend analysis of vegetation dynamics in Qinghai-Tibet Plateau using Hurst Exponent. *Ecol. Indic.* 14:28–39. doi: 10.1016/j.ecolind.2011.08.011

Peng, W., Kuang, T., and Tao, S. (2019). Quantifying influences of natural factors on vegetation NDVI change based on geographical detector in Sichuan, western China. *J. Clean. Prod.* 233, 353–367. doi: 10.1016/j.jclepro.2019.05.355

Shen, Q., Gao, G., Han, F., Xiao, F., Ma, Y., Wang, S., et al. (2018). Quantifying the effects of human activities and climate variability on vegetation cover change in a hyperarid endorheic basin. *Land Degrad. Dev.* 29, 3294–3304. doi: 10.1002/ldr.3085

Shen, X., Liu, B., Jiang, M., and Lu, X. (2020). Marshland loss warms local land surface temperature in China. *Geophys. Res. Lett.* 47, e2020GL087648. doi: 10.1029/2020GL087648

Shen, X., Liu, Y., Zhang, J., Wang, Y., Ma, R., and Liu, B. (2022). Asymmetric impacts of diurnal warming on vegetation carbon sequestration of marshes in the Qinghai Tibet Plateau. *Glob. Biogeochem. Cycles* 36, e2022GB007396. doi: 10.1029/2022GB007396

Simpson, L. T., Osborne, T. Z., and Duckett, L. J., I.C. (2017). Feller Carbon storages along a climate induced coastal wetland gradient. *Wetlands* 37, 1023–1035, doi: 10.1007/s13157-017-0937-x

Tang, L., He, M., and Li, X. (2020). Verification of fractional vegetation coverage and NDVI of desert vegetation via UAVRS technology. *Remote Sens.* 12, 1742. doi: 10.3390/rs12111742

Tao, G., Jia, K., Zhao, X., Wei, X., Xie, X., Zhang, X., et al. (2019). Generating High Spatio-Temporal Resolution Fractional Vegetation Cover by Fusing GF-1 WFV and MODIS Data. *Remote Sens.* 11, 2324. doi: 10.3390/rs11192324

Tong, X., Wang, K., Brandt, M., Yue, Y., Liao, C., and Fensholt, R. (2016). Assessing future vegetation trends and restoration prospects in the karst regions of Southwest China. *Remote Sens.* 8, 357. doi: 10.3390/rs8050357

Tottrup, C., Rasmussen, M. S., Eklundh, L., and Jonsson, P. (2007). Mapping fractional forest cover across the highlands of mainland Southeast Asia using MODIS data and regression tree modelling. *Int. J. Remote Sens.* 28, 23–46. doi: 10.1080/01431160600784218

Wang, J., Wang, K., Zhang, M., and Zhang, C. (2015). Impacts of climate change and human activities on vegetation cover in hilly southern China. *Ecol. Eng.* 81, 451–461. doi: 10.1016/j.ecoleng.2015.04.022

Wang, J. W., Li, M., Yu, C., and Fu, G. (2022). The change in environmental variables linked to climate change has a stronger effect on aboveground net primary productivity than does phenological change in alpine grasslands. *Front. Plant Sci.* 12, 798633. doi: 10.3389/fpls.2021.798633

Wang, X., Tan, K., Xu, K., Chen, Y., and Ding, J. (2019). Quantitative evaluation of the eco-environment in a coalfield based on multi-temporal remote sensing imagery: A case study of Yuxian, China. *Int. J. Environ. Res. Public Health.* 16, 511. doi: 10.3390/ijerph16030511

Wu, D., Liu, Q. X., Xia, R. L., and Li, T. (2022). Study on the changes in vegetation structural coverage and its response mechanism to hydrology. *Open Geosci.* 14, 79–88. doi: 10.1515/geo-2020-0322

Yan, S. F., Lu, Q., Zhang, J. C., Zhang, Z. X., Bai, S. Y., and Wang, L. (2012). The spatio-temporal evolution characteristics and response of regional climate change of NDVI at Jiangsu coastal areas. *J. Nanjing For. Univ.* 36, 43–47. doi: 10.3969/j.issn.1000-2006.2012.01.009

Yang, L., Shen, F., Zhang, L., Cai, Y., Yi, F., and Zhou, C. (2021). Quantifying influences of natural and anthropogenic factors on vegetation change using structural equation modeling: a case study in Jiangsu Province. *China J. Clean. Prod.* 280, 124330. doi: 10.1016/j.jclepro.2020.124330

Yao, S., Li, X., Liu, C., Yuan, D., Zhu, L., Ma, X., et al. (2019). Quantitative assessment of impact of the proposed Poyang Lake Hydraulic Project (China) on the habitat suitability of migratory birds. *Water* 11, 1639. doi: 10.3390/w11081639

Zha, X. J., Tian, Y., and Ouzhu., Fu,. G. (2022). Response of forage nutrient storages to grazing in alpine grasslands. *Front. Plant Sci.*13, 991287. doi: 10.3389/fpls.2022.991287

Zhang, S., Li, Z., Lin, X., and Zhang, C. (2019). Assessment of climate change and associated vegetation cover change on watershed-scale runoff and sediment yield. *Water* 11, 1373. doi: 10.3390/w11071373

Zhang, S. W., Ning, H. R., Xu, D. L., Ye, H. C., Zheng, Y., Zhang, H. Y., et al. (2016). Analysis of spatio-temporal evolution and driving factors of vegetation fraction for opencast coal mine in grassland area. *Trans. Chin. Soc. Agri. Eng.* 32, 233–241. doi: 10.11975/j.issn.1002-6819.2016.17.031

Zhang, Z., Chang, J., Xu, C., Zhou, Y., Wu, Y., Chen, X., et al. (2018). The response of lake area and vegetation cover variations to climate change over the Qinghai-Tibetan Plateau during the past 30 years. *Science of the Total Environment.* 635, 443–451. doi: 10.1016/j.scitotenv.2018.04.113

Zheng,. K., Wei, J. Z., Pei, J. Y., Cheng,.H., Zhang,. X. L., Huang, F. Q., et al. (2019). Impacts of climate change and human activities on grassland vegetation variation in the Chinese Loess Plateau. *Sci. Total Environ.* 660:236–244, doi: 10.1016/j.scitotenv.2019.01.022

Zhou, J., Xiang, J., Wang, L., Zhong, G., Zhu, G., Liu, C., et al. (2019). The impacts of groundwater chemistry on wetland vegetation distribution in the Northern Qinghai–Tibet Plateau. *Sustainability* 11, 5022. doi: 10.3390/su11185022

frontiers | Frontiers in Ecology and Evolution

TYPE Original Research
PUBLISHED 07 July 2023
DOI 10.3389/fevo.2023.1193939

OPEN ACCESS

EDITED BY
Kerou Zhang,
Chinese Academy of Forestry, China

REVIEWED BY
Yulong Yan,
Inner Mongolia University, China
Weiwei Chen,
Chinese Academy of Sciences (CAS), China
Xianglan Li,
Beijing Normal University, China

*CORRESPONDENCE
Zhiqiang Wan
wanzhiqiang@imnu.edu.cn

RECEIVED 26 March 2023
ACCEPTED 21 June 2023
PUBLISHED 07 July 2023

CITATION
Chen X, Wan Z, Gu R, Ganjurjav H, Hu G, Gao Q, Chun X, Zhou H and Hai C (2023) Warming promoted CH_4 absorption compared with precipitation addition in typical steppe in Inner Mongolia. *Front. Ecol. Evol.* 11:1193939. doi: 10.3389/fevo.2023.1193939

Warming promoted CH_4 absorption compared with precipitation addition in typical steppe in Inner Mongolia

Xuemeng Chen[1], Zhiqiang Wan[1,2]*, Rui Gu[3], Hasbagan Ganjurjav[2], Guozheng Hu[2], Qingzhu Gao[2], Xi Chun[1], Haijun Zhou[1] and Chunxing Hai[1]

[1]College of Geographical Science / Provincial Key Laboratory of Mongolian Plateau's Climate System, Inner Mongolia Normal University, Hohhot, China, [2]Institute of Environment and Sustainable Development in Agriculture, Chinese Academy of Agricultural Sciences, Beijing, China, [3]College of Grassland, Resources and Environment, Inner Mongolia Agricultural University, Hohhot, China

Introduction: Climate change, characterized by rising temperatures and changing precipitation patterns, has emerged as a significant global concern. Particularly, the warming potential of CH_4 is 28 times greater than that of CO_2, leading to an increased focus on its impact. Among various ecosystems, grasslands exhibit a high vulnerability to climate change. Grassland in Inner Mongolia is an important component of the typical grassland in Eurasian, and there was evidence that warmer and more precipitation in this area in future.

Methods: In this study, we utilized an open-top chamber (OTC) to conduct warming and precipitation experiments on a representative steppe located in Inner Mongolia in 2011. From 2017 to 2019, we monitored various factors, including soil temperature, moisture, CH_4 flux, community characteristics, soil carbon nitrogen content. Subsequently, we analyzed the response of CH_4 flux and its influencing factors to warming and precipitation in this typical steppe.

Results: The soil in the typical steppe acted as a CH_4 sink. In 2018, CH_4 flux during the growing season and t during the non-growing season were –59.31 and –21.21 under C, –56.55 and –31.17 under T, –41.34 and –24.93 under P, –50.09 and –26.51 ug $C{\cdot}m^{-2}{\cdot}h^{-1}$ under TP respectively. Warming stimulated absorption of CH_4 during the non-growing season (25.8%), while the addition of precipitation hindered CH_4 absorption during the growing season (76.37%). Warming and precipitation addition decreased the percentage of CH_4 absorbed in growing season and increased that in non-growing season which account 67.66% and 32.34% under C, 59.81% and 40.19% under T, 62.71% and 37.29% under P, 62.03% and 37.97% under TP respectively. Soil temperature exhibited a positive correlation with CH_4 flux (P<0.001), while the dominance of *Leymus chinensis* (IV-L.c.) exhibited a negative correlation with CH_4 flux (P<0.01). Moreover, NH_4^+-N displayed a positive correlation with CH_4 flux (P<0.05).

Conclusion: The findings suggest that CH_4 absorption in a typical steppe may increase in a warmer future, and warming is conducive to the absorption of CH_4 in the non-growing season. Not only abiotic factors had an impact on CH_4 absorption, but also changes in community composition. Consequently, further exploration of the underlying mechanisms is warranted.

KEYWORDS

climate change, typical grassland, CH4, growing season, non-growing season

1 Introduction

Global warming has garnered considerable attention worldwide, with the increasing concentration of carbon dioxide (CO_2), methane (CH_4), and nitrous oxide (N_2O) being significant contributors to climate change (IPCC, 2021). CH_4 the second-largest greenhouse gas after CO_2, possesses a potent warming potential and can raise surface temperatures by absorbing long-wave radiation emitted by the Earth's surface. Grasslands represent crucial terrestrial ecosystems, and the Inner Mongolian grassland, situated at the eastern edge of Eurasia, serves as a vital ecological barrier in northern China, making it highly susceptible to climate change. Investigating the variations and influencing factors of greenhouse gas fluxes in typical grasslands and understanding the feedback and response of grassland ecosystems in the context of climate change are of utmost importance.

Scholars have explored CH_4 fluxes during both the growing and non-growing seasons. For instance, CH_4 absorption rates in alpine meadows on the Qinghai-Tibet Plateau are higher in summer and lower in winter (Chen W. et al., 2019). CH_4 oxidative absorption occurs in temperate semi-arid grasslands during winter with a low absorption rate (Wang et al., 2011). Meadows exhibit net CH_4 absorption throughout the year, primarily during the growing season, while the non-growing season weakens the sink's ability to emit CH_4 (Li et al., 2022). Warming affects CH_4-producing and oxidising bacteria by altering environmental factors such as soil temperature, moisture, permeability, and nutrient levels within the ecosystem (Dijkstra et al., 2011; Dijkstra et al., 2013; Lin et al., 2015), consequently affecting soil CH_4 flux. The results showed that the methane oxidation rate was $0.14 \pm 0.04 mg \cdot cm^{-2} \cdot d^{-1}$ in grasslands with an annual average temperature of −7.8°C (Li et al., 2020). In alpine grasslands with an annual average temperature of 0.08°C, the methane oxidation rate significantly increased with a 1°C temperature rises (Li et al., 2020). In the range of −10 to 30°C, the amount of methane oxidation increases with the increase of temperature (Chen et al., 2010). Furthermore, when the soil temperature rises from 18°C to 28°C, the activity of methanotrophs increases (Ma et al., 2016). Changes in precipitation affect the production or oxidation processes of soil CH_4 and regulate its emission or absorption (Xu et al., 2015a). For example, reduced precipitation promotes CH_4 oxidation in tropical and temperate forest soils, thereby enhancing CH_4 uptake (Savi et al., 2016; Yan et al., 2019; Wu et al., 2020a; Wu et al., 2021). As the temperature and precipitation vary across different grassland ecosystems, the effects of temperature rise and precipitation fluctuations on CH_4 flux also differ among various grassland types. Furthermore, limited continuous observations of CH_4 fluxes in different seasons in previous studies have resulted in gaps in understanding the influence of temperature and precipitation changes on CH_4 dynamics.

Climate change also affects soil carbon and nitrogen pools (Zhang et al., 2018; Wei et al., 2020; Xie et al., 2020; Wang et al., 2022) leading changes in methane flux. Soil soluble carbon and nitrogen act as nutrient sources that influence the activity of methanotrophs and control soil CH_4 oxidation processes (Shukla et al., 2013). For instance, changes in soil dissolved organic carbon content can affect soil CH_4 flux by limiting the carbon mineralization process of methane-oxidizing bacteria, and indirectly impact the soil CH_4 oxidation process by affecting other soil characteristics such as water content and soil inorganic nitrogen content (Tate, 2015). Inorganic nitrogen has long been considered an important factor in regulating soil CH_4 oxidation capacity. The addition of NH_4^+ may inhibit, promote, or even have no significant effect on the soil CH_4 oxidation process (Bodelier, 2011; Shukla et al., 2013; Tate, 2015). Additionally, variations in biomass, nutrient uptake, and photosynthetic characteristics among different plant species contribute to differences in ecosystem nitrogen and carbon cycles, as well as greenhouse gas fluxes (Han and Chen, 2020). Alterations in plant species composition significantly reduce CH_4 flux, primarily due to a decrease in soil active carbon content (such as microbial biomass carbon) and soil enzyme activity (Luan et al., 2016). The effects of grassland species richness and functional group presence on CH_4 production found that the emission flux of species mixtures can be significantly higher than that of the species monoculture because of the significant increase in biomass (Khalsa et al., 2014). Moreover, plant species richness can significantly increase CH_4 flux (Zhang et al., 2012). However, few studies have examined how simulated climate change affects CH_4 flux through vegetation. While abiotic factors are often considered when explaining the influencing factors of CH_4, the response of biological factors, particularly vegetation community composition, to climate change is intuitively significant. Thus, understanding the impact of climate change on CH_4 flux should not neglect the role of vegetation.

To obtain more accurate observations of the feedback on the CH_4 flux and climate change, long-term monitoring is essential. Therefore, the aim of this study was to conduct warming and precipitation addition experiments in Inner Mongolia, China, in 2011, based on the climate change trend in temperate steppes. The study sought to elucidate (1) how warming and precipitation addition affect CH_4 emission fluxes in temperate steppes, particularly during the growing and non-growing seasons, and (2) the main factors influencing CH_4 fluxes. By monitoring vegetation and soil nutrient changes and analysing their relationship with greenhouse gas fluxes, we aimed to reveal the response of greenhouse gas fluxes to climate change in a typical steppe, providing further insights into the temporal dynamics and influencing factors of CH_4 flux in grassland ecosystems.

2 Research method

2.1 Study site

The study site is located at the Grassland Ecology Research Base of Inner Mongolia University in Mauden Pasture (44°09'N, 116° 29'" E, 1102 m above sea level), 40 km east of XilinHot (Figure 1). The region experiences a temperate continental climate characterised by cold and dry winters and hot and humid summers. The average annual temperature is 2.6°C, with the lowest temperature occurring in January (−23.8°C) and the highest temperature in July (24.9°C). The average annual precipitation is 271.42 mm, concentrated between May and September, which accounts for 87.3% of the total annual precipitation. The annual evaporation ranges from 1600 to 1800 mm. The soil in the study area is chestnut soil, and the vegetation type is typical steppe dominated by *Stipa krylovii* and *Leymus chinensis*.

2.2 Experimental design

The simulated warming and precipitation addition experiment commenced in July 2011 using open-top chamber (OTC). The OTC were fixed in the plots throughout the year to avoid disturbance. The warming treatment in this experiment was set at 2°C based on the IPCC Fourth Assessment Report. The OTC is a cone-shaped device made of polycarbonate (PC board) with a fan for temperature control. The upper bottom surface diameter of the OTC was 0.7 m, the lower bottom surface diameter was 1.2 m, and the height was 0.4 m. Precipitation addition was conducted twice each month during the growing season, equivalent to 20% of the average monthly precipitation from 1961 to 2010 (Wan et al., 2018). Precipitation was added after 18:00 to avoid damage to plants during high daytime temperatures. Four treatments were applied: control (CK), warming (T), warming and precipitation (TP), and precipitation (P). Each treatment had 4 replicates, resulting in a total of 16 experimental plots (Figure 1).

The greenhouse gas collection in this experiment used the platform of warming and precipitation addition experiment to collect and measure greenhouse gases in 2017–2018 after 6 years of continuous warming and precipitation addition and continued the warming and precipitation addition experiment.

2.3 Determination method

2.3.1 Determination of soil temperature and moisture

Temperature and moisture measurements were measured using a data collector with a (temperature probe model: DS18B20; humidity probe model: EC-5). Soil temperature and humidity were recorded at 10 cm intervals, and data were automatically recorded every 30 min.

2.3.2 Determination of greenhouse gas concentration

Static chamber gas chromatography was used to measure greenhouse gas concentration. The static chamber material was a PVC cylinder with a diameter of 0.4 m and a height of 0.3 m, were. The static chamber was placed at the base to collect the gas. Gas samples were collected at 0, 10, 20, and 30 minutes and injected into sealed glass gas cylinders. The sampling time was from May 2017 to February 2019, with measurements taken every 7 days during the growing season (May to early September) was measured every 7 days. During the spring freeze–thaw period (March to April), it was measured every 4 days, in late September to October every 15 days, and once a month from November to February of the following year. The collected samples were analyzed for CH_4 concentration using gas chromatography (HP6890N, Agilent Company). The CH_4 flux was calculated based on the difference in gas concentration within the time range of the static chamber (70).

2.3.3 Investigation of community characteristics

The community characteristics and biomass were determined using quadrat surveys. Monthly surveys were conducted during the growing season (May to August) in each plot, with a sampling area of $1\times1m^2$. The surveys included assessments of community species composition, density, and height.

At the end of August, the growing season, the quadrat was selected outside the sample plot, and the plants in the quadrat were cut off on the ground and seeded into envelopes. They were then oven-dried at 65°C for 48 h to determine peak above-ground biomass (Xu et al., 2015b). A regression equation was used to calculate the biomass in the plot (Table S1).

2.3.4 Determination of soil carbon and nitrogen

Soil samples were collected at the end of August in 2017 and 2018, with the top 10 cm of soil collected using a 3 cm diameter soil drill. Fresh soil samples were partially air-dried and passed through a 0.15 mm sieve. The sieved soil was placed in tin cups for sample packaging. The total carbon and nitrogen content of the soil were determined using an elemental analyzer (Thermo Fisher, Thermo Fisher Scientific, USA). The microbial biomass, carbon, and nitrogen were determined using the chloroform fumigation

method. After sieving the fresh soil through a 2 mm sieve, three portions of fresh soil (20 g each) were weighed. One portion was placed in an aluminum box and dried in an oven at 70°C to determine dry weight. The remaining two soil samples were placed in a 50 ml beaker. One of the beakers was placed into a vacuum pumping vessel and, at the same time, placed in a beaker containing 25 ml of chloroform. The chloroform was vacuum boiled for 5 min, and the piston and air pump were closed. The beaker was covered with black cloth, fumigated in the dark. for 24 h, removed, vacuumed three times for 5 min each time, and vacuum chloroform was added. Another beaker was used as a control without the fumigation treatment; the other treatments were consistent and placed under the same conditions. After 24 h, the treated soil samples were transferred to centrifuge tubes, and each bottle was injected with 50 ml 0.5 mol/L K_2SO_4 solution, shocked for 30 min, centrifuged, and filtered, and the filtrate was analyzed using a Multi N/C 3000 DOC analyzer (German Jena company). The extractable carbon and nitrogen were converted to MBC and MBN using conversion factors (Kec and Ken) of 0.45 both (Xu et al., 2010). NH_4^+-N and NO_3^-–N were determined by a continuous flow analyzer with 2 mol·L^{-1} KCL solution and water–soil ratio of 5:1. The soil samples (10 g) were weighed, and distilled water was added according to the ratio of water to soil (2:1). The soil samples were shaken at 25°C for 30 min and filtered with 0.45 μm filter membrane. The DOC and DON in the filtrate were determined using a Multi N/C 3000 DOC analyzer (Jena, Germany).

2.4 Data calculation and analysis

2.4.1 Greenhouse gas flux calculation

$$F = \rho \times h \times \frac{\Delta C}{\Delta t} \times \frac{273.15}{273.15 + T} \qquad \text{Formula 1}$$

In the formula, F is the greenhouse gas flux, CH_4 flux unit is (ug·m^{-2}·h^{-1}). A positive value represents emissions, and a negative value represents absorption. ρ is the density of a greenhouse gas under standard conditions, h is the height of the sampling static chamber (m), $\frac{\Delta C}{\Delta t}$ is the rate of change of a gas concentration with time, and T is the air temperature (°C) at the time of sampling.

2.4.2 Data analysis method

Microsoft Excel 2016 and IBM SPSS Statistics 24.0 (SPSS Inc., Chicago, IL, USA) were utilized for data processing and analysis. One-way analysis of variance (ANOVA) was employed to analyze the significance of differences between different treatments, and multiple comparisons were conducted using Duncan's method. Correlation analysis was performed to analyze the relationship between greenhouse gas fluxes, environmental factors, and nutrients (results of soil carbon and nitrogen used in correlation heat map analysis in Table S2; results of community characteristics used in correlation heat map analysis in Tables S3 and S4). We used piecewise structural equation modelling (SEM) with AMOS 21.0 (Amos Development Co., Armonk, New York, USA) to evaluate the effects of temperature and moisture changes on CH4 emissions by affecting vegetation and soil carbon and nitrogen pools. Before establishing SEM, we conducted a stepwise regression analysis of CH4 flux and its influencing factors, and established formulas, CH4= −337.40 + 146.27 IV-L.c + 3.03 MBN ($F = 10.92$, $P = 0.001$). Finally, we verify the feasibility of the model through $P > 0.05$.

3 Results and analysis

3.1 Effects of warming and precipitation addition on CH_4 flux in typical steppe

Typical steppe soil acts as a sink for CH_4, with higher CH_4 absorption during the growing season compared to the non-growing season (the percentage of CH_4 absorption during the growing season to the non-growing season ranges from 1.27 to 2.47) (Figures 2, 3, 4B). The average CH_4 flux during the growing season accounted for 55.80% to 69.71% of the entire year under different treatments (Figure 4A), while the non-growing season contributed 30.29% to 44.2% of the annual CH_4 flux (Figure 4A). Warming and precipitation addition decreased the percentage of

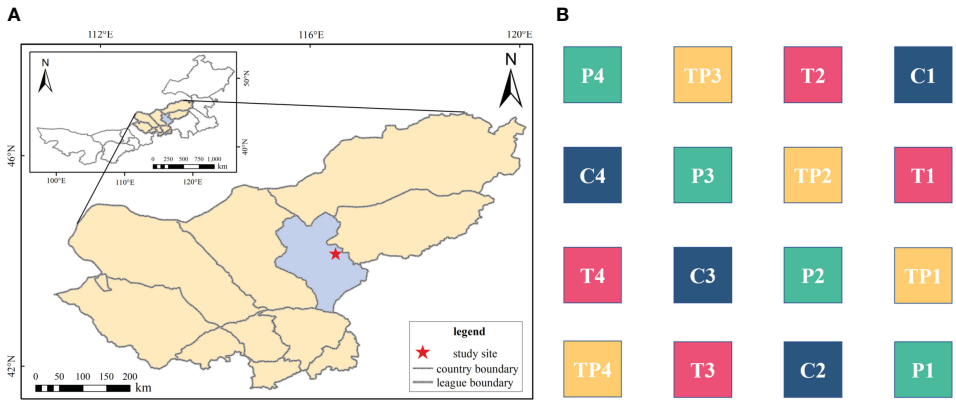

FIGURE 1
Study site **(A)** and the schematic diagram of experimental warming design **(B)**. Control (C), warming (T, warming 2 °C), warming plus precipitation addition (TP, warming 2 °C plus precipitation addition 20%), and precipitation (P, precipitation addition 20%).

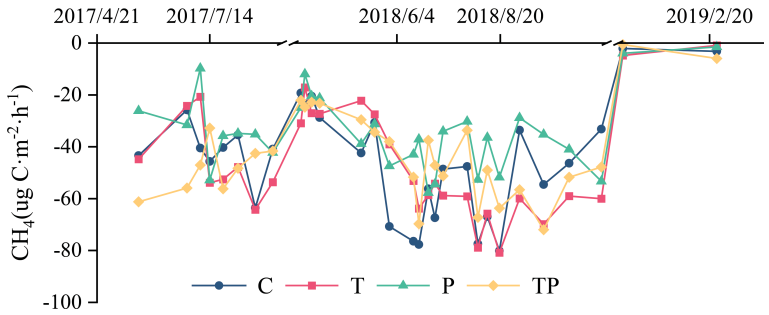

FIGURE 2
Effect of warming and precipitation addition on CH_4 flux.

CH_4 absorbed in growing season and increased that in non-growing season which account 67.66% and 32.34% under C, 59.81% and 40.19% under T, 62.71% and 37.29% under P, 62.03% and 37.97% under TP respectively. The addition of precipitation (P treatment) reduced the absorption of CH_4 by the soil, likely due to decreased soil permeability caused by increased precipitation, which hinders the diffusion of CH_4 into the soil. On the other hand, warming promoted the absorption of CH_4 in typical steppe ecosystems.

3.2 Relationships between CH_4 and environmental factors

Warming and precipitation addition significantly affected soil temperature and moisture. Warming increased soil temperature and decreased soil moisture, while precipitation addition decreased soil temperature and increased soil moisture. Combined warming and precipitation addition can alleviate the adverse effects of individual warming on the soil environment (Wan et al., 2018). Soil temperature showed a significant positive correlation with CH_4 flux (P<0.001). In this study, the variation in soil surface temperature explained the variation in CH_4 flux well (R2=0.52) (Figure 5). With seasonal changes, the decrease in soil moisture caused by warming leaded to increased soil permeability (Juc´a and Maciel, 2006; Lu et al., 2023), promoting the diffusion of CH_4 from the atmosphere into the deep soil and thereby enhancing CH_4 absorption. In a typical steppe in semiarid areas, the increase in water may not reach the threshold level that affects methanotrophs, hence no significant correlation between CH_4 flux and soil surface moisture was noted.

3.3 Relationships between CH_4 flux with soil factors and community factors

Community species diversity decreased, *Leymus chinensis* biomass increased, and *Stipa krylovii* biomass decreased due to warming and precipitation addition (community factors, soil carbon, and nitrogen under warming and precipitation are shown in Tables S2–S4).

The correlation heat map of CH_4 flux, which used negative values (higher absolute value indicating higher absorption), revealed that IV-L. c. is positively correlated with CH_4 flux (P<0.01). The Simpson and Shannon indices were negatively correlated with CH_4 flux (P<0.05). NH_4^+-N was negatively correlated with CH_4 flux (P<0.05). The increase in the dominance of *Leymus chinensis* hampered CH_4 absorption, whereas an increase in species diversity and NH_4^+ content promoted CH_4 absorption. CH_4 flux was not only affected by soil carbon and nitrogen but also by vegetation species diversity and dominant species dominance (Figure 6).

Warming mainly affected CH_4 flux by influencing IV-L. c. Precipitation addition precipitation addition primarily affected CH_4 flux through its influence on soil nitrogen (Figure 7).

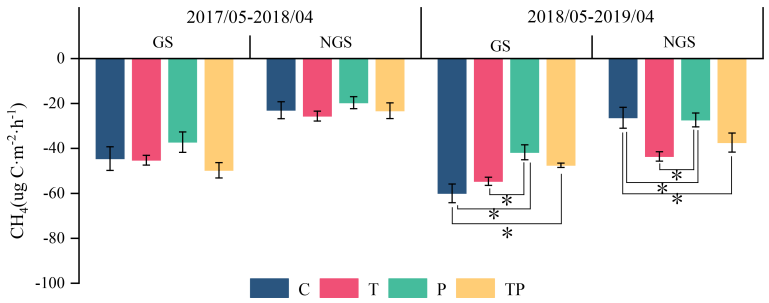

FIGURE 3
Effects of warming and precipitation addition on CH_4 flux in growing and non-growing seasons.

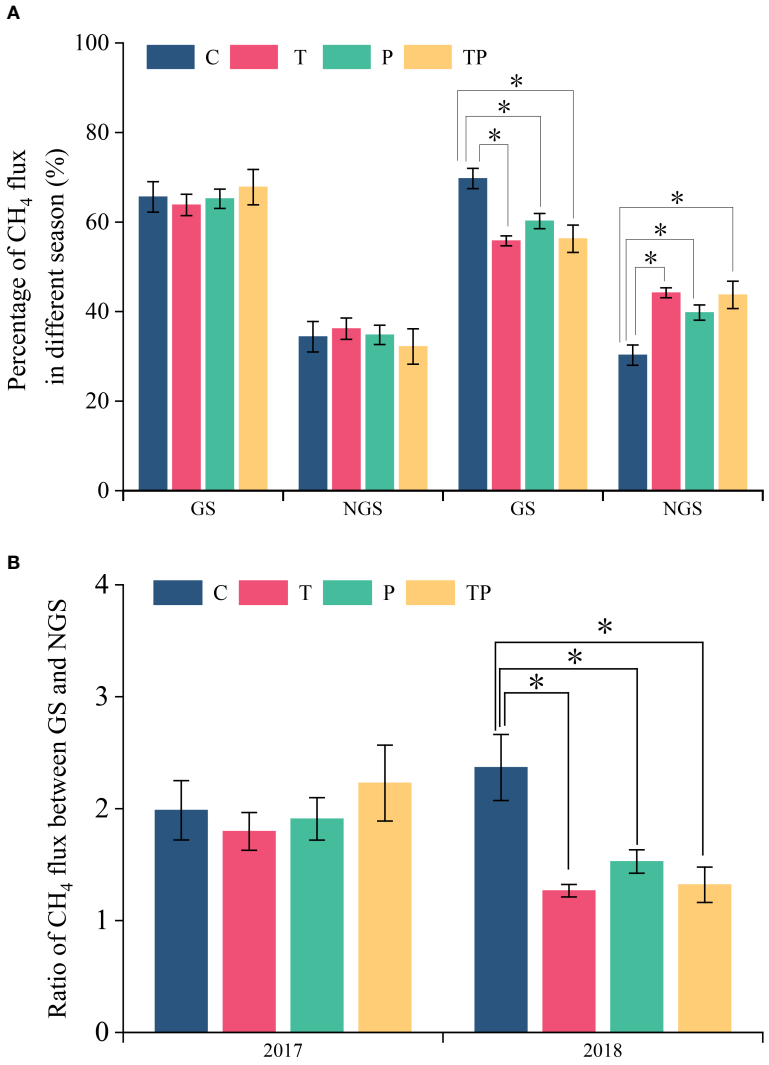

FIGURE 4
Percentage of CH_4 flux in growing season and non-growing season in the whole year and CH_4 emission of GS to NGS. C, Control, no warming and no precipitation addition; W, warming; P, precipitation addition; WP, warming plus precipitation addition; GS, growing season; NGS, non-growing season; * significant at P<0.05.

4 Discussion

4.1 Effects of warming and precipitation addition on greenhouse gas flux in typical steppe

Grassland ecosystems act as sinks for CH_4. Air temperature is an important factor that affects soil CH_4 uptake, it can affect the activity of methanotrophs in the soil. Within a certain temperature range, the oxidation rate of CH_4 in the soil increases with rising temperature. Additionally, warming leads to reduced soil water content through increased evaporation (Bokhorst et al., 2008), and soil water can exert physiological pressure on methanotrophs, which in turn affects the diffusion of CH_4 in the soil (Luo et al., 2013; Li et al., 2015). In addition to soil temperature, soil moisture is also an important factor influencing CH_4 flux. Decreased water content results in thinner plant roots, increased soil nitrogen cycling rates, enhanced methanotrophic community, reduced methanogen community, and increased CH_4 uptake (Konda et al., 2010; Lawrence et al., 2015; Liu et al., 2015). Water addition, on the other hand, reduces soil permeability, hinders CH_4 transmission from the atmosphere to the soil, and decreases CH_4 absorption (Conrad, 2007). However, an increase in soil water content creates an anaerobic environment favorable for CH_4-producing bacteria, resulting in reduced CH_4 absorption and increased CH_4 emissions (Dijkstra et al., 2013). In dry years, the increase in soil moisture caused by the addition of precipitation did not reach the threshold level to affect methanotrophs, thus having no significant impact on CH_4 uptake (Zhang et al., 2017). However, other studies have suggested that net methane uptake increases with humidity under drought conditions (Von et al., 2009). The results differed in 2017, which was a more drought-prone year with higher temperatures and lower precipitation

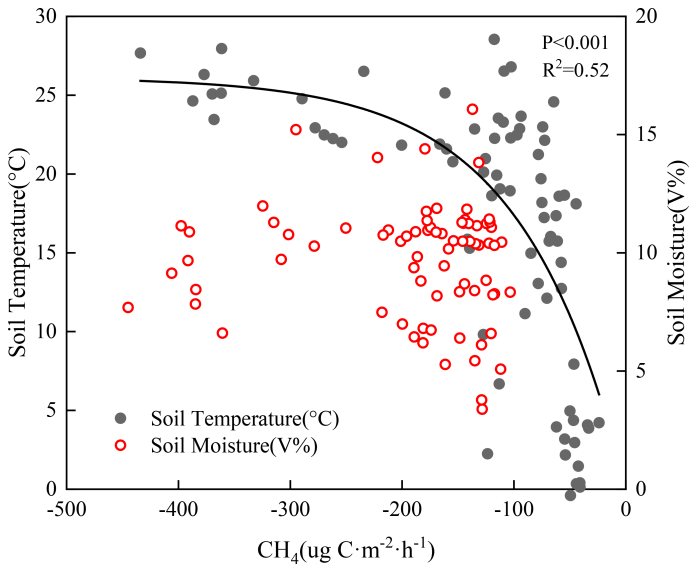

FIGURE 5
Correlation between soil temperature, soil moisture, and CH_4 flux under warming and precipitation addition conditions.

compared to the period of 2012–2022. Additionally, warming can promote CH_4 absorption, while precipitation had an inhibitory effect on CH_4 absorption, which is consistent with the results of Zhu et al. (2015) and Xu et al. (2015a). This indicates that temperature and water jointly regulate CH_4 fluxes in typical steppes in arid and semi-arid regions, with increasing temperature strengthening CH_4 absorption in the area. Warming increased CH_4 absorption was closely correlated with soil temperature and soil moisture (Wang et al., 2021a). Warming-induced increase in soil temperature directly enhances methanotrophic and decreases methanogen abundance (Zheng et al., 2012; Peltoniemi et al., 2016), thus resulting in an enhancement of soil CH_4 absorption. Furthermore, a lower soil water content was found under warming, which could have decreased anaerobic conditions by increasing air permeability and O_2 diffusion in the soil (Chen et al., 2017), favoring microbial oxidation of CH_4 (Dijkstra et al., 2013).

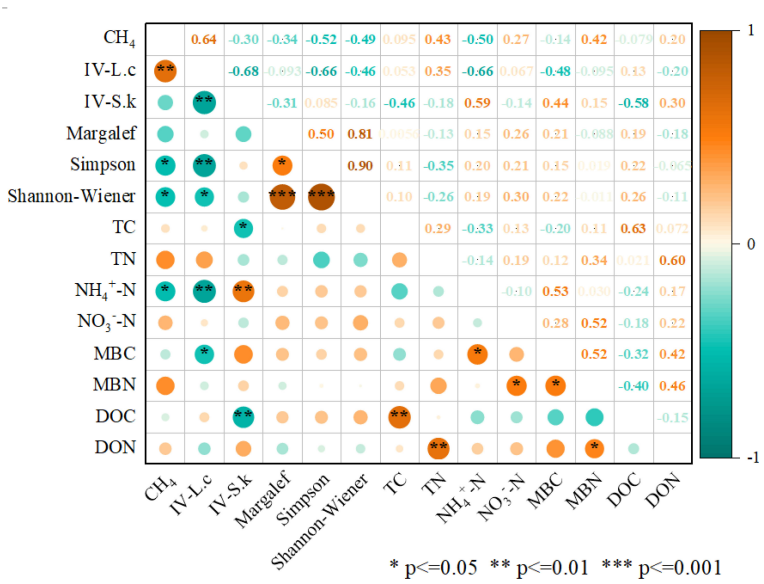

FIGURE 6
Correlation heat map of CH_4 flux with soil factors and community factors. Significant differences shown at * P<0.05; ** P<=0.01; ***P<=0.001. IV-L.c, important value of *Leymus chinensis*; IV-S.k, important value of *Stipa krylovii*; Margalef, Margalef richness index; Simpson, Simpson's diversity; TC, Total carbon; TN, Total nitrogen; NH_4^+-N, Ammonniacal nitrogen; NO_3^-N, Nitrate nitrogen; MBC, Microbial carbon; MBN, Microbial nitrogen; DOC, Dissolved organic carboon; DON, Soluble organic nitrogen.

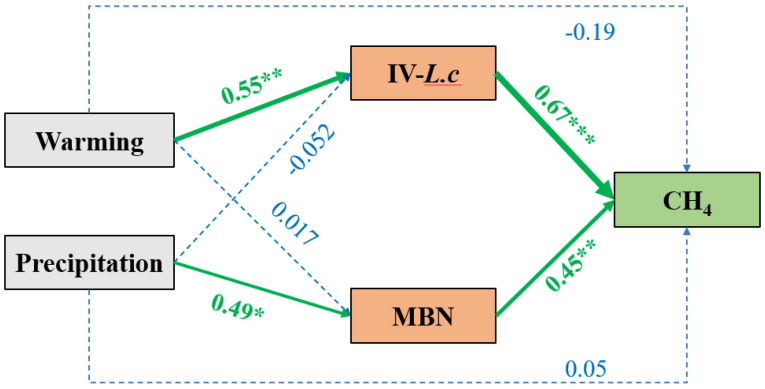

FIGURE 7
SEM model analysis of the influence mechanism of warming and precipitation on CH_4 emission. Chi-square = 0.034; Probability level = 0.854. Significant differences shown at * P<0.05; ** P<=0.01; ***P<=0.001. IV-L.c, important value of *Leyms chinensis*; MBN, microbial biomass nitrogen. The thickness of the lines indicated the strength of the correlation. Green lines represent a significant positive correlation; red line represents a significant negative correlation; blue lines indicate that the correlation is not significant.

4.2 Effects of vegetation and soil carbon and nitrogen on greenhouse gas fluxes under warming and precipitation addition conditions

Simulated warming and precipitation have significant effects on soil carbon and nitrogen pools (Zhang et al., 2018; Wei et al., 2020; Wang et al., 2022), and greenhouse gas emissions are closely related to the stability of these pools (Wu et al., 2020b). Grasslands act as sinks for CH_4, and therefore, increased soil nitrogen can inhibit CH_4 oxidation by raising NH_4^+ concentration, resulting in reduced CH_4 absorption. However, more soil nitrogen can alleviate the nitrogen limitation in grassland soil microorganisms, enhance microbial activity, and promote CH_4 absorption. Thus, the effect of soil nitrogen on grassland CH_4 flux is complex and depends on multiple factors. Previous studies have yielded different conclusions, with some reporting that in Inner Mongolian grasslands, nitrogen addition reduces soil CH_4 uptake (Zhang et al., 2017). In the Tianshan grassland, nitrogen addition promotes CH_4 uptake in (Li et al., 2012). Furthermore, the addition had no significant effect on CH_4 emissions (Zhao et al., 2017). In the present study, soil NH_4^+ promoted CH_4 absorption, while soil NO_3^- inhibited it. Soil NO_3^- increases soil redox potential, exerting osmotic pressure on methanotrophs and exhibiting toxic effects on them. Long-term nitrogen addition leads to changes in the methanotroph community and reduced abundance, ultimately inhibiting CH_4 absorption (Treseder, 2008; Li et al., 2020). Thus, high concentrations of NO_3^- in soil can suppress methanotroph activity (Yue et al., 2016; Chen S. et al., 2019; Zhang et al., 2019; Pan et al., 2022), affecting their abundance and reducing CH_4 absorption. Warming and precipitation affected CH_4 flux by influencing soil nitrogen. Direct and indirect positive correlations were observed between precipitation enhancement and soil N and CH_4 fluxes. However, increased temperature did not facilitate the effect of soil nitrogen or promote greenhouse gas emissions. Considering the warming and drying trends expected under future climate change, increasing CH_4 absorption in the typical steppe area of Inner Mongolia would be beneficial.

Soil temperature and moisture explain most of the seasonal variations in CH_4 fluxes, but the effects of environmental factors on greenhouse gas emissions and uptake are not only direct but also indirect through their influence on soil nutrients and vegetation growth (Shaver et al., 2000; Sampson et al., 2007; Aires et al., 2008; Xu and Wan, 2008; Kuzyakov and Gavrichkova, 2010; Nakano and Shinoda, 2010; Potthast et al., 2010; Phillips et al., 2012). Warming can impact species richness by altering soil nutrient content and plant interspecific relationships (Nogueira et al., 2017), while increased water availability improves soil water availability, alleviating the inhibitory effects of water deficit on plant growth (Xu et al., 2014), thereby affecting species diversity. Higher species diversity can promote biomass growth and significantly increase CH_4 flux (Zhang et al., 2012). Plant phenology, which influences plant growth (Fu and Shen, 2022; Jiang et al., 2022; Han et al., 2023a), also indirectly affects CH_4 flux. Although this study did not consider the impact of plant phenology on productivity and CH_4 flux, it examined productivity and community structure under relatively stable plant growth conditions, which can still reflect community changes in response to environmental changes. Warming increased the Simpson, Shannon–Wiener, and Pielou indices (Table S3), and both the Simpson and Shannon indices were negatively correlated with CH_4 flux ($P<0.05$). Community composition may also be related to plant production (Li et al., 2014; Wang et al., 2021b; Wang et al., 2021c; Han et al., 2023b), and changes in community composition and productivity have a significant impact on CH_4 flux (Zhang et al., 2012; Khalsa et al., 2014). In this study, warming and precipitation addition significantly increased the dominance of the *Leymus chinensis* population and decreased the dominance of *Stipa krylovii* population (Table S4), and IV-L.c was significantly positively correlated with the CH_4 flux ($P<0.01$). Warming primarily affected CH_4 flux through changes in species dominance. As a dominant species, the increased biomass of *Leymus chinensis* in the

community and its inhibitory effect on CH_4 absorption was stronger. This showed that the dominance of *Leymus chinensis* increases and the species diversity index decreases, which aggravates the inhibition of CH_4 absorption and weakens the function of the CH_4 sink under a warmer future in typical grasslands.

It is well known that soil CH_4 fluxes are determined by the balance between CH_4 production from methanogens and CH_4 oxidation from methanotrophs (Prabhu et al., 2013; Christiansen et al., 2015). Multiple studies have shown that soil microbial community structure was influenced by warming and precipitation changes (Yu et al., 2019; Zhang et al., 2021; Han et al., 2022; Zhong and Fu, 2022). Methanogenic bacteria typically exist in anaerobic environments, and long periods of soil water deficiency, increase contact with soil oxygen, making it difficult to establish low oxidation reduction potential for CH_4 absorption through anaerobic respiration (Yang et al., 2017). The lower soil moisture under warming could lead to higher potential redox conditions, in which microbes degraded SOC by gradually using electron acceptors with higher redox potentials, leading to conditions less suitable for methanogenesis (Johnston et al., 2019; Tano et al., 2020). Meanwhile, soil oxygen content could increase with the decline of soil moisture, resulting in more favorable conditions for methane oxidation (Li et al., 2020). While this study mainly considered the impact of environmental factors and plant community characteristics on CH_4, future research could improve our ability for projecting future CH_4 absorption changes via a better understanding of microbial mechanisms in response to climate changes (Cavicchioli et al., 2019; Guo et al., 2020).

5 Conclusion

1) The typical grassland soil was sink of CH_4. CH_4 flux during non-growing seasons accounted for a large proportion of whole year, which account for 30.29% ~ 44.20% under different treatments and was an indispensable part of CH_4 flux. Warming promoted the CH_4 absorption flux during the non-growing seasons, while precipitation addition inhibited that during the growing seasons compared with C. Warming and precipitation addition both reduced the proportion of CH_4 flux in the growing season to the whole year, and increased the proportion in the non-growing season, and the effect of warming was stronger than that of precipitation addition on that. Warming and precipitation addition increased the percentage of CH_4 absorbed in non-growing season which account 32.34% under C, 40.19% under T, 37.29% under P, 37.97% under TP respectively.

2) Increase of soil temperature, soil NH_4^+-N content and species diversity were conducive to CH_4 absorption, but the increase of *Leymus chinensis* dominance was not conducive to that. Under future climate warming, the increase in *Leymus chinensis* population dominance and decrease in the species diversity index will further inhibit the absorption of CH_4 and weaken the function of the CH_4 sink in a typical steppe. However, there are many other ways in which warming affects CH_4 absorption, and the results showed that warming promoted CH_4 absorption. Therefore, we need to explore the mechanisms by which different factors affect CH_4 flux in the future.

Data availability statement

The raw data supporting the conclusions of this article will be made available by the authors, without undue reservation.

Author contributions

HG and QG designed the research; ZW and RG performed the experiments; ZW and XMC analyzed the data and wrote the draft; ZW, XMC, HZ, XC, and CH revised the manuscript.

Funding

We gratefully acknowledge the financial support from the National Natural Science Foundation of China (32260278), Fundamental Research Funds for the Inner Mongolia Normal University (2022JBQN095), and Natural Science Foundation of Inner Mongolia (2021BS03024).

Conflict of interest

The authors declare that the research was conducted in the absence of any commercial or financial relationships that could be construed as a potential conflict of interest.

The reviewer YY declared a past co-authorship with the author ZW to the handling editor.

Publisher's note

Supplementary material

The Supplementary Material for this article can be found online at: https://www.frontiersin.org/articles/10.3389/fevo.2023.1193939/full#supplementary-material

References

Aires, L. M. I., Pio, C. A., and Pereira, J. S. (2008). Carbon dioxide exchange above a Mediterranean C3/C4 grassland during two climatologically contrasting years. *Global Change Biol.* 14 (3), 539–555. doi: 10.1111/j.1365-2486.2007.01507.x

Bodelier, P. L. E. (2011). Interactions between nitrogenous fertilizers and methane cycling in wetland and upland soils. *Curr. Opin. Environ. Sustainability* 3 (5), 379–388. doi: 10.1016/j.cosust.2011.06.002

Bokhorst, S., Huiskes, A., Convey, P., Bodegom, P. V., and Aerts, R. (2008). Climate change effects on soil arthropod communities from the Falkland islands and the maritime Antarctic. *Soil Biol. Biochem.* 40 (7), 1547–1556. doi: 10.1016/j.soilbio.2008.01.017

Cavicchioli, R., Ripple, W. J., Timmis, K. N., Azam, F., Bakken, L. R., Baylis, M., et al. (2019). Scientists' warning to humanity: microorganisms and climate change. *Nat. Rev. Microbiol.* 17, 569–586. doi: 10.1038/s41579-019-0222-5

Chen, S., Hao, T., Goulding, K., Misselbrook, T. H., and Liu, X. J. (2019). Impact of 13-years of nitrogen addition on nitrous oxide and methane fluxes and ecosystem respiration in a temperate grassland. *Environ. Pollut.* 252, 675–681. doi: 10.1016/j.envpol.2019.03.069

Chen, X. P., Wang, G. X., Zhang, T., Mao, T. X., Wei, D., Song, C. L., et al. (2017). Effects of warming and nitrogen fertilization on GHG flux in an alpine swamp meadow of a permafrost region. *Sci. Total Environment.* 601–602, 1389–1399. doi: 10.1016/j.scitotenv.2017.06.028

Chen, W., Wolf, B., Yao, Z., Brüggemann, N., Butterbach-Bahl, K., Liu, C. Y., et al. (2010). Annual methane uptake by typical semiarid steppe in inner Mongolia. *J. Geophysical Research-Atmospheres* 115. doi: 10.1029/2009JD013783

Chen, W., Zhang, F., Wang, B., Wang, J. S., Tian, D. S., Han, G. X., et al. (2019). Diel and seasonal dynamics of ecosystem-scale methane flux and their determinants in an alpine meadow. *J. Geophysical Research-Biogeosciences* 124 (6), 1731–1745. doi: 10.1029/2019JG005011

Christiansen, J. R., Romero, A. J. B., Jørgensen, N. O. G., Glaring, M. A., Jørgensen, C. J., Berg, L. K., et al. (2015). Methane fluxes and the functional groups of methanotrophs and methanogens in a young Arctic landscape on disko island, West Greenland. *Biogeochemistry* 122, 15–33. doi: 10.1007/s10533-014-0026-7

Conrad, R. (2007). Microbial ecology of methanogens and methanotrophs. *Adv. Agron.* 96, 1–63. doi: 10.1016/S0065-2113(07)96005-8

Dijkstra, F. A., Morgan, J. A., Follett, R., and Lecain, D. (2013). Climate change reduces the net sink of CH_4 and N_2O in a semiarid grassland. *Global Change Biol.* 19 (6), 1816–1826. doi: 10.1111/gcb.12182

Dijkstra, F. A., Morgan, J. A., Von, F. J. C., and Follett, R. (2011). Elevated CO_2 and warming effects on CH_4 uptake in a semiarid grassland below optimum soil moisture. *J. Geophysical Research-Biogeosciences* 116, G01007. doi: 10.1029/2010JG001288

Fu, G., and Shen, Z. (2022). Asymmetrical warming of growing/non-growing season increases soil respiration during growing season in an alpine meadow. *Sci. Total Environ.* 812, G01007. doi: 10.1016/j.scitotenv.2021.152591

Guo, X., Gao, Q., Yuan, M., Wang, G., Zhou, X., Feng, J., et al. (2020). Gene-informed decomposition model predicts lower soil carbon loss due to persistent microbial adaptation to warming. *Nat. Commun.* 11, 4897. doi: 10.1038/s41467-020-18706-z

Han, X., and Chen, B. M. (2020). Progress in the effects of warming on soil N_2O and CH4emission and the underlying micro-bial mechanisms. *Chin. J. Appl. Ecol.* 31 (11), 3906–3914. doi: 10.13287/j.1001-9332.202011.026

Han, F., Yu, C., and Fu, G. (2022). Warming alters elevation distributions of soil bacterial and fungal communities in alpine grasslands. *Global Ecol. Conserv.* 39, e02306. doi: 10.1016/j.gecco.2022.e02306

Han, F., Yu, C., and Fu, G. (2023a). Asymmetric warming among elevations may homogenize plant α-diversity and aboveground net primary production of alpine grasslands. *Front. Ecol. Evol.* 11, 1126651. doi: 10.3389/fevo.2023.1126651

Han, F., Yu, C., and Fu, G. (2023b). Non-growing/growing season non-uniform-warming increases precipitation use efficiency but reduces its temporal stability in an alpine meadow. *Front. Plant Sci.* 14. doi: 10.3389/fpls.2023.1090204

IPCC. (2021). Climate change 2021–the physical science basis. *Chem. Int.* 43 (4), 22–23. doi: 10.1017/9781009157896

Jiang, W. W., Meng, L., Cheng, Q. Y., and Fu, G. (2022). The change in environmental variables linked to climate change has a stronger effect on aboveground net primary productivity than does phenological change in alpine grasslands. *Front. Plant Sci.* 12. doi: 10.3389/fpls.2021.798633

Johnston, E. R., Hatt, J. K., He, Z., Wu, L., Guo, X., Luo, Y., et al. (2019). Responses of tundra soil microbial communities to half a decade of experimental warming at two critical depths. *Proc. Natl. Acad. Sci. U. S. A.* 116, 15096–15105. doi: 10.1073/pnas.1901307116

Juc´a, J. F. T., and Maciel, F. J. (2006). Gas permeability of a compacted soil used in a landfill cover layer. *Unsaturated Soils* 2006, 1535–1546. doi: 10.1061/40802(189)128

Khalsa, J., Fricke, T., Weigelt, A., and Wachendorf, M. (2014). Effects of species richness and functional groups on chemical constituents relevant for methane yields from anaerobic digestion: results from a grassland diversity experiment. *Grass Forage Sci.* 69 (1), 49–63. doi: 10.1111/gfs.12028

Konda, R., Ohta, S., Ishizuka, S., Heriyanto, J., and Wicaksono, A. (2010). Seasonal changes in the spatial structures of N_2O, CO_2, and CH_4 fluxes from acacia mangium plantation soils in Indonesia. *Soil Biol. Biochem.* 42 (9), 1512–1522. doi: 10.1016/j.soilbio.2010.05.022

Kuzyakov, Y., and Gavrichkova, O. (2010). REVIEW: time lag between photosynthesis and carbon dioxide efflux from soil: a review of mechanisms and controls. *Global Change Biol.* 16 (12), 3386–3406. doi: 10.1111/j.1365-2486.2010.02179.x

Lawrence, D. M., Koven, C. D., Swenson, S. C., Riley, W., and Slater, A. G. (2015). Permafrost thaw and resulting soil moisture changes regulate projected high-latitude CO_2 and CH_4 emissions. *Environ. Res. Lett.* 10 (9), 094011. doi: 10.1088/1748-9326/10/9/094011

Li, Y., Dong, S., Liu, S., Zhou, H. K., Gao, Q. Z., Cao, G. M., et al. (2015). Seasonal changes of CO_2, CH_4 and N_2O fluxes in different types of alpine grassland in the qinghai-Tibetan plateau of China. *Soil Biol. Biochem.* 80, 306–314. doi: 10.1016/j.soilbio.2014.10.026

Li, K., Gong, Y., Song, W., He, G. X., Hu, Y. K., Tian, C. Y., et al. (2012). Responses of CH_4, CO_2 and N_2O fluxes to increasing nitrogen deposition in alpine grassland of the tianshan mountains. *Chemosphere* 88 (1), 140–143. doi: 10.1016/j.chemosphere.2012.02.077

Li, Z., Lin, J., Zhang, T., Zhang, N., Mu, C., and Wang, J. (2014). Effects of summer nocturnal warming on biomass production of leymus chinensis in the songnen grassland of China: from bud bank and photosynthetic compensation. *J. Agron. Crop Sci.* 200 (1), 66–76. doi: 10.1111/jac.12041

Li, F., Yang, G., Peng, Y., Wang, G. Q., Qin, S. Q., Song, Y. T., et al. (2020). Warming effects on methane fluxes differ between two alpine grasslands with contrasting soil water status. *Agric. For. Meteorology* 290. doi: 10.1016/j.agrformet.2020.107988

Li, H., Zhu, J., Zhang, F., Qin, G., Li, Y. K., Wang, J. B., et al. (2022). The predominance of nongrowing season emissions to the annual methane budget of a semiarid alpine meadow on the northeastern qinghai-Tibetan plateau. *Ecosystems* 25 (3), 526–536. doi: 10.1007/s10021-021-00669-x

Lin, X., Wang, S., Hu, Y., Luo, C. Y., Zhang, Z. H., Niu, H. S., et al. (2015). Experimental warming increases seasonal methane uptake in an alpine meadow on the Tibetan plateau. *Ecosystems* 18 (2), 274–286. doi: 10.1007/s10021-014-9828-7

Liu, M., Jin, H., Luo, D., Wang, Q. F., Jin, X. Y., Li, X. Y., et al. (2015). Progress in studies of carbon emission from soil on the qinghai-Tibetan plateau. *J. Glaciology Geocryology* 37 (6), 1544–1554. doi: 10.7522/.issn.1000-0240.2015.0171

Lu, S. F., Han, Z. J., Lu, L., Lan, T. G., Wei, X., and Zhao, T. Y. (2023). On measuring methods and influencing factors of air permeability of soils: an overview and a preliminary database. *Geoderma* 435, 116509. doi: 10.1016/j.geoderma.2023.116509

Luan, J., Song, H., Xiang, C., Zhu, D., and Duoerji, S. (2016). Soil moisture, species composition interact to regulate CO_2 and CH_4 fluxes in dry meadows on the Tibetan plateau. *Ecol. Eng.* 91, 101–112. doi: 10.1016/j.ecoleng.2016.02.012

Luo, G. J., Kiese, R., Wolf, B., and Butterbach-Bahl, K. (2013). Effects of soil temperature and moisture on methane uptake and nitrous oxide emissions across three different ecosystem types. *Biogeosciences* 10 (5), 3205–3219. doi: 10.5194/bg-10-3205-2013

Ma, T., Chen, H., Kang, X., and Wang, Y. F. (2016). Effects of enclosure time on the activity of methanotrophs in soils of the inner Mongolia grassland. *Chin. J. Appl. Ecol.* 22 (1), 0008–0012. doi: 10.3724/SP.J.1145.2015.05024

Nakano, T., and Shinoda, M. (2010). Response of ecosystem respiration to soil water and plant biomass in a semiarid grassland. *Soil Sci. Plant Nutr.* 56 (5), 773–781. doi: 10.1111/j.1747-0765.2010.00502.x

Nogueira, C., Bugalho, M. N., Pereira, J. S., and Caldeira, M. C. (2017). Extended autumn drought, but not nitrogen deposition, affects the diversity and productivity of a Mediterranean grassland. *Environ. Exp. Bot.* 138, 99–108. doi: 10.1016/j.envexpbot.2017.03.005

Pan, H., Li, Y., Meng, C., Zheng, Y., Liu, X. M., Zhuge, Y. P., et al. (2022). Effects of nitrogen levels on interactions between active methanotrophs and nitrifiers. *Acta Pedologica Sin.* 59 (2), 557–567. doi: 10.11766/trxb202101050577

Peltoniemi, K., Laiho, R., Juottonen, H., Bodrossy, L., Kell, D. K., Minkkinen, K., et al. (2016). Responses of methanogenic and methanotrophic communities to warming in varying moisture regimes of two boreal fens. *Soil Biol. Biochem.* 97, 144–156. doi: 10.1016/j.soilbio.2016.03.007

Phillips, R. P., Meier, I. C., Bernhardt, E. S., Grandy, S., Wickings, K., and Finzi, A. C. (2012). Roots and fungi accelerate carbon and nitrogen cycling in forests exposed to elevated CO_2. *Ecol. Lett.* 15 (9), 1042–1049. doi: 10.1111/j.1461-0248.2012.01827.x

Potthast, K., Hamer, U., and Makeschin, F. (2010). Impact of litter quality on mineralization processes in managed and abandoned pasture soils in southern Ecuador. *Soil Biol. Biochem.* 42 (1), 56–64. doi: 10.1016/j.soilbio.2009.09.025

Prabhu, N. S., Kapil, D. P., and Virendra, M. (2013). Environmental determinants of soil methane oxidation and methanotrophs. *Crit. Rev. Environ. Sci. Technol.* 43 (18), 1945–2011. doi: 10.1080/10643389.2012.672053

Sampson, D. A., Janssens, I. A., Yuste, J. C., and Ceulemans, R. (2007). Basal rates of soil respiration are correlated with photosynthesis in a mixed temperate forest. *Global Change Biol.* 13 (9), 2008–2017. doi: 10.1111/j.1365-2486.2007.01414.x

Savi, F., Di, B. C., Canfora., L., Mondini, C., and Fares, S. (2016). Environmental and biological controls on CH_4 exchange over an evergreen Mediterranean forest. *Agric. For. Meteorol.* 226, 67–79. doi: 10.1016/j.agrformet.2016.05.014

Shaver, G. R., Canadell, J., Chapin, F. S., Gurevitch, J., Harte, J. H. R., Henry, G., et al. (2000). Global warming and terrestrial ecosystems: a conceptual framework for analysis. *Bioscience* 50 (10), 871–882. doi: 10.1641/0006-3568(2000)050[0871:GWATEA]2.0.CO;2

Shukla, P. N., Pandey, K. D., and Mishra, V. K. (2013). Environmental determinants of soil methane oxidation and methanotrophs. *Crit. Rev. Environ. Sci. Technol.* 43 (18), 1945–2011. doi: 10.1080/10643389.2012.672053

Tano, B. F., Brou, C. Y., Dossou-Yovo, E. R., Saito, K., Futakuchi, K., Wopereis, M. C. S., et al. (2020). Spatial and temporal variability of soil redox potential, pH and electrical conductivity across a toposequence in the savanna of West Africa. *Agronomy* 10, 1787. doi: 10.3390/agronomy10111787

Tate, K. R. (2015). Soil methane oxidation and land-use change - from process to mitigation. *Soil Biol. Biochem.* 80, 260–272. doi: 10.1016/j.soilbio.2014.10.010

Treseder, K. K. (2008). Nitrogen additions and microbial biomass: a meta-analysis of ecosystem studies. *Ecol. Lett.* 11 (10), 1111–1120. doi: 10.1111/j.1461-0248.2008.01230.x

Von, F. J. C., Butters, G., Duchateau, P. C., Thelwell, R. J., and Siller, R. (2009). *In situ* measures of methanotroph activity in upland soils: a reaction-diffusion model and field observation of water stress. *J. Geophysical Research-Biogeosciences* 114, G01015. doi: 10.1029/2008JG000731

Wan, Z. Q., Hu, G. Z., Chen, Y. L., Chao, L. M., and Gao, Q. Z. (2018). Ecological responses of stipa steppe in inner mongolia to experimentally increased temperature and precipitation 1: background and experimental design. *Rangeland J.* 40 (2), 143–146. doi: 10.1071/RJ16081

Wang, Z., Hao, X., Shan, D., Han, G. D., Zhao, M. L., Willms, W. D., et al. (2011). Influence of increasing temperature and nitrogen input on greenhouse gas emissions from a desert steppe soil in inner Mongolia. *Soil Sci. Plant Nutr.* 57 (4), 508–518. doi: 10.1080/00380768.2011.591283

Wang, J. S., Quan, Q., Chen, W. N., Tian, D. S., Ciais, P., W. Crowther, T., et al. (2021a). Increased CO_2 emissions surpass reductions of non-CO_2 emissions more under higher experimental warming in an alpine meadow. *Sci. Total Environment*. 769 (11), 144559. doi: 10.1016/j.scitotenv.2020.144559

Wang, J. W., Yu, C., and Fu, G. (2021b). Warming reconstructs the elevation distributions of aboveground net primary production, plant species and phylogenetic diversity in alpine grasslands. *Ecol. Indic.* 133, 108355. doi: 10.1016/j.ecolind.2021.108355

Wang, J., Yu, C., and Fu, G. (2021c). Asymmetrical warming between elevations may result in similar plant community composition between elevations in alpine grasslands. *Front. Ecol Evol.* 9, 757943. doi: 10.3389/fevo.2021.757943

Wang, X., Zhong, Z., Wang, J. Y., Jian, J. N., Yang, G. H., Ren, C. J., et al. (2022). Responses of soil carbon pool of abandoned grassland on the loess plateau to two-years warming and increased precipitation. *Acta Pedologica Sinica*. 43 (05), 2812–2821. doi: 10.13227/j.hjkx.202109219

Wei, Y., Wu, X., Zeng, R., Cai, C. F., and Guo, Z. L. (2020). Spatial variations of aggregate-associated humic substance in heavy-textured soils along a climatic gradient. *Soil Tillage Res.* 197 (1), 104497. doi: 10.1016/j.still.2019.104497

Wu, H., Wang, X., Ganjurjav, H., Hu, G. Z., Qin, X. B., and Gao, Q. Z. (2020a). Effects of increased precipitation combined with nitrogen addition and increased temperature on methane fluxes in alpine meadows of the Tibetan plateau. *Sci. Total Environ.* 705 (2), 135818. doi: 10.1016/j.scitotenv.2019.135818

Wu, X., Wang, F., Li, T., Fu, B. J., Lv, Y. H., and Liu, G. H. (2020b). Nitrogen additions increase N_2O emissions but reduce soil respiration and CH4 uptake during freeze-thaw cycles in an alpine meadow. *Geoderma* 363, 114157. doi: 10.1016/j.geoderma.2019.114157

Wu, J., Wang, H., Li, G., Wu, J. H., Gong, Y., Wei, X. X., et al. (2021). Responses of CH_4 flux and microbial diversity to changes in rainfall amount and frequencies in a wet meadow in the Tibetan plateau. *Catena* 202 (3), 105253. doi: 10.1016/j.catena.2021.105253

Xie, M., Zhao, L., Wu, X., Tian, L. M., Yue, G. Y., Zhou, H. Y., et al. (2020). Seasonal variations of nitrogen in permafrost-affected soils of the qinghai-Tibetan plateau. *Catena* 195. doi: 10.1016/j.catena.2020.104793

Xu, X., Elias, D. A., Graham, D. E., Phelps, T. J., Carroll, S. L., Wullschleger, S. D., et al. (2015a). A microbial functional group-based module for simulating methane production and consumption: application to an incubated permafrost soil. *J. Geophysical Research-Biogeosciences* 120 (7), 1315–1333. doi: 10.1002/2015JG002935

Xu, Z. F., Hu, R., Xiong, P., Wan, C. A., Cao, G., and Liu, Q. (2010). Initial soil responses to experimental warming in two contrasting forest ecosystems, Eastern Tibetan plateau, China: nutrient availabilities, microbial properties and enzyme activities. *Appl. Soil Ecol.* 46, 291–299. doi: 10.1016/j.apsoil.2010.07.005

Xu, Z. W., Ren, H. Y., Cai, J., Wang, R. Z., Li, M. H., Wan, S. Q., et al. (2014). Effects of experimentally-enhanced precipitation and nitrogen on resistance, recovery and resilience of a semi-arid grassland after drought. *Oecologia* 176 (4), 1187–1197. doi: 10.1007/s00442-014-3081-9

Xu, Z. W., Ren, H. Y., Li, M. H., Ruijven, J. V., Han, X. G., Wan, S. Q., et al. (2015b). Environmental changes drive the temporal stability of semi-arid natural grasslands through altering species asynchrony. *J. Ecol.* 103 (5), 1308–1316. doi: 10.1111/1365-2745.12441

Xu, W., and Wan, S. (2008). Water- and plant-mediated responses of soil respiration to topography, fire, and nitrogen fertilization in a semiarid grassland in northern China. *Soil Biol. Biochem.* 40 (3), 679–687. doi: 10.1016/j.soilbio.2007.10.003

Yan, G., Xing, Y., Lü, X.-T., Xu, L. J., Zhang, J. H., Dai, G. H., et al. (2019). Effects of artificial nitrogen addition and reduction in precipitation on soil CO_2 and CH_4 effluxes and composition of the microbial biomass in a temperate forest. *Eur. J. Soil Sci.* 70 (6), 1197–1211. doi: 10.1111/ejss.12812

Yang, G., Peng, Y., Olefeldt, D., Chen, Y. L., Wang, G. Q., Li, F., et al. (2017). Changes in methane flux along a permafrost thaw sequence on the Tibetan plateau. *Environ. Sci. Technol.* 52, 1244–1252. doi: 10.1021/acs.est.7b04979

Yu, C., Han, F., and Fu, G. (2019). Effects of 7 years experimental warming on soil bacterial and fungal community structure in the northern Tibet alpine meadow at three elevations. *Sci. Total Environ.* 655, 814–822. doi: 10.1016/j.scitotenv.2018.11.309

Yue, P., Li, K., Gong, Y., Hu, Y. K., Mohammat, A., Christie, P., et al. (2016). A five-year study of the impact of nitrogen addition on methane uptake in alpine grassland. *Sci. Rep.* 6. doi: 10.1038/srep32064

Zhang, G.Y., Shen, Z., and Fu, G. (2021). Function diversity of soil fungal community has little exclusive effects on the response of aboveground plant production to experimental warming in alpine grasslands. *Appl. Soil Ecol.* 168C. doi: 10.1016/j.apsoil.2021.104153

Zhang, L., Hou, L., Guo, D., Li, L. H., and Xu, X. F. (2017). Interactive impacts of nitrogen input and water amendment on growing season fluxes of CO_2, CH_4, and N_2O in a semiarid grassland, northern China. *Sci. Total Environ.* 578 (feb.1), 523–534. doi: 10.1016/j.scitotenv.2016.10.219

Zhang, Q., Shao, M. A., Jia, X., and Zhang, C. C. (2018). Understory vegetation and drought effects on soil aggregate stability and aggregate-associated carbon on the loess plateau in China. *Soil Sci. Soc. America J.* 82 (1), 106–114. doi: 10.2136/sssaj2017.05.0145

Zhang, C.-B., Sun, H.-Y., Ge, Y., Gu, B. J., Wang, H., and Chang, J. (2012). Plant species richness enhanced the methane emission in experimental microcosms. *Atmospheric Environ.* 62, 180–183. doi: 10.1016/j.atmosenv.2012.08.034

Zhang, J. Z., Zhou, D., Guo, X. D., Guo, Y., Wang, H., Cheng, J. W., et al. (2019). Moderate grazing increases the abundance of soil methane-oxidizing bacteria and CH4 uptake rate in a typical steppe of inner Mongolia, China. *J. Appl. Ecol.* 06 (6), 1–11. doi: 10.13287/j.1001-9332.201906.035

Zhao, Z., Dong, S., Jiang, X., Liu, S. L., Ji, H. Z., Li, Y., et al. (2017). Effects of warming and nitrogen deposition on CH_4, CO_2 and N_2O emissions in alpine grassland ecosystems of the qinghai-Tibetan plateau. *Sci. Total Environ.* 592, 565–572. doi: 10.1016/j.scitotenv.2017.03.082

Zheng, Y., Yang, W., Sun, X., Wang, S. P., Rui, Y. C., Luo, C. Y., et al. (2012). Methanotrophic community structure and activity under warming and grazing of alpine meadow on the Tibetan plateau. *Appl. Microbiol. Biotechnol.* 93, 2193–2203. doi: 10.1007/s00253-011-3535-5

Zhong, Z., and Fu, G. (2022). Response of soil fungal species, phylogenetic and functional diversity to diurnal asymmetric warming in an alpine agricultural ecosystem. *Agric. Ecosyst. Environ.* 335. doi: 10.1016/j.agee.2022.107993

Zhu, X., Luo, C., Wang, S., Zhang, Z. H., Cui, S. J., Bao, X. Y., et al. (2015). Effects of warming, grazing/cutting and nitrogen fertilization on greenhouse gas fluxes during growing seasons in an alpine meadow on the Tibetan plateau. *Agric. For. Meteorol.* 214, 506–514. doi: 10.1016/j.agrformet.2015.09.008

frontiers | Frontiers in Ecology and Evolution

TYPE Original Research
PUBLISHED 20 July 2023
DOI 10.3389/fevo.2023.1125775

OPEN ACCESS

EDITED BY
Zhongqing Yan,
Chinese Academy of Forestry, China

REVIEWED BY
Michael Alister Reid,
University of New England, Australia
Shahid Ahmad Dar,
University of Kashmir, India

*CORRESPONDENCE
Wenfeng Gong
994206@hainanu.edu.cn
Tao Liu
daliu_1978@126.com
Tiedong Liu
liu@hainanu.edu.cn

†These authors have contributed equally to this work

RECEIVED 16 December 2022
ACCEPTED 03 July 2023
PUBLISHED 20 July 2023

CITATION
Sun Y, Wu G, Mao M, Duan X, Hu J, Zhang Y, Xie Y, Qiu X, Gong W, Liu T and Liu T (2023) Remote sensing and environmental assessment of wetland ecological degradation in the Small Sanjiang Plain, Northeast China. *Front. Ecol. Evol.* 11:1125775. doi: 10.3389/fevo.2023.1125775

Remote sensing and environmental assessment of wetland ecological degradation in the Small Sanjiang Plain, Northeast China

Yuxin Sun[1,2†], Genghong Wu[1,2†], Mingjiang Mao[1,2], Xuanyu Duan[1,2], Jihan Hu[1,2], Yangyang Zhang[1,2], Yidan Xie[1,2], Xincai Qiu[1,2], Wenfeng Gong[1,2*], Tao Liu[3*] and Tiedong Liu[1,2*]

[1]Intelligent Forestry Key Laboratory, School of Forestry, Hainan University, Haikou, China, [2]Key Laboratory of Genetics and Germplasm Innovation of Tropical Special Forest Trees and Ornamental Plants, Ministry of Education, School of Forestry, Hainan University, Haikou, China, [3]College of Hydraulic and Electrical Engineering, Heilongjiang University, Harbin, China

Introduction: The plain marsh wetland ecosystems are sensitive to changes in the natural environment and the intensity of human activities. The Sanjiang Plain is China's largest area of concentrated marsh wetland, the Small Sanjiang Plain is the most important component of the Sanjiang Plain. However, with the acceleration of the urbanization and development of large-scale agricultural reclamation activities in the Small Sanjiang Plain in Northeast China, the wetland has been seriously damaged. In light of this degradation this study examines the Small Sanjiang Plain.

Methods: From the four aspects of area, structure, function, and human activities, we try to construct a wetland degradation comprehensive index (WDCI) in cold region with expert scoring methods and analytic hierarchy process (AHP), coupled with network and administrative unit. The objective was to reveal the degradation of wetlands in Northeast China over three decades at a regional scale.

Results: The results showed that (1) the overall wetland area decreased between 1990 and 2020 by 39.26×10^3 hm^2. Within this period a significant decrease of 336.56×10^3 hm^2 occurred between 1990 and 200 and a significant increase of 214.62×10^3 hm^2 occurred between 2010 and 2020. (2) In terms of structural changes, the fractal dimension (FRAC) has the same trend as the Landscape Fragmentation Index (LFI) with little change. (3) In terms of functional changes, the average above-ground biomass (AGB) increased from 1029.73 kg/hm^2 to 1405.38 kg/hm^2 between 1990 and 2020 in the study area. (4) In terms of human activities, the average human disturbance was 0.52, 0.46, 0.57 and 0.53 in 1990, 2000, 2010 and 2020, with the highest in 2010. (5) The composite wetland degradation index shows that the most severe wetland degradation was 49.61% in 2010 occurred between 1990 and 2020. (6) Among the severely deteriorated trajectory types in 2010–2020, mild degradation → serious degradation accounted for the largest area of 240.23×10^3 hm^2, and the significant improvement trajectory type in 1990–2000 accounted for the largest area of 238.50×10^3 hm^2.

Discussion: In brief, we conclude that the degradation of the Small Sanjiang Plain wetland was caused mainly by construction, overgrazing, deforestation, and farmland reclamation. This study can also provide new views for monitoring and managing wetland degradation by remote sensing in cold regions.

KEYWORDS

wetland, ecological degradation assessment, remote sensing, land use, Small Sanjiang Plain, Northeast China

1 Introduction

Wetlands are among the most important and valuable ecosystems on Earth (Dar et al., 2020). They play a critical role in protecting rare species and biodiversity, maintaining ecological balance, protecting water sources, regulating climate, and controlling soil erosion (Erwin, 2009; Myers et al., 2013). Moreover wetlands are one of the most important carbon reservoirs on Earth, absorbing huge amounts of atmospheric carbon dioxide and regulating regional climate (Sileshi et al., 2020; Slagter et al., 2020). However, studies have shown that up to 54% of the global wetland area has been lost since 1900 (Jie et al., 2021), and the severe situation of wetland degradation and area shrinkage has become globally recognized, with the natural environment and human activities often cited as the main drivers of wetland degradation (Rashid et al., 2022). In particular, the combined effects of human activities such as rapid urbanization and agricultural intensification have accelerated the shrinkage of natural wetland areas and the degradation of wetland ecological functions, seriously disturbing regional wetland ecosystems and increasing the vulnerability of wetlands (Liu et al., 2013; Dar et al., 2021). Therefore, it is of great importance for the sustainable development of the regional economy and environment to strengthen research on the characteristics of regional wetland degradation and its spatiotemporal patterns of change.

Wetland degradation assessment occupies an important position in the study of wetland restoration ecology, and is a fundamental work to carry out restoration and management of degraded wetlands. Initially, evaluation indicators were mainly focused on chemical and biological aspects (Van Dam et al., 1998), and as the understanding of ecosystem structure and function continued to improve, wetland degradation evaluation methods based on a variety of biological indicators, hydrogeomorphology, socioculture and policy factors gradually emerged (Miller and Wardrop, 2006; Gianopulos, 2018; Zekarias et al., 2021; Zhao et al., 2021) Currently, international studies on wetland degradation have mostly focused on the functional aspects of wetlands, mainly emphasizing the destruction of wetland functions and values by the impacts of human activities (Van Dam et al., 1998). Studies of wetland degradation in China have mostly focused on the dynamic processes of wetland degradation in time and space (Shen et al., 2019; Hu et al., 2020). However, most studies have neglected to combine the effects of human disturbance on the spatial and temporal patterns of regional wetland ecological degradation, ecosystem function and structure (Kotze et al., 2012; Behn et al., 2018; Niu et al., 2022). Therefore, under the background of human activity interference, it is particularly important to construct the unit, which combines the geographic grid with administrative division, to analyze the spatiotemporal differentiation of regional wetland degradation.

Multiband, multispectral, and high-resolution remote sensing technology and GIS have been widely used in monitoring wetland dynamics and to research the patterns and causes of wetland degradation (Held et al., 2003; Lhermitte et al., 2011; Houborg et al., 2015; Zhu et al., 2022). Some scholars have extracted the Land-Use/Land-Cover (LULC) databases based on remote sensing data and constructed remote sensing models to quantitatively and qualitatively explore and evaluate the spatial and temporal patterns of regional wetland shrinkage and degradation (Jiang et al., 2017; Lin et al., 2021; Cui et al., 2022). Cui et al. (2015) established a comprehensive model of wetland ecological degradation based on regional habitat succession and, combined with remote sensing images, proved that human disturbance and species invasion were the main causes of coastal wetland degradation in Jiangsu Province, China. Zhu et al. (2022) extracted the lake area, vegetation cover, and soil degradation from multitemporal remote sensing (TM, ETM and OLI) and constructed a new wetland degradation index to assess the degree of lake wetland degradation in the Bashang Plateau. Yang et al. (2021) used remote sensing and point of interest (POI) data to assess the ecological status of a wetland in Suzhou, China. It has been found that 3S technology (Geographic Information System, GIS; Global Positioning System, GPS; and Remote Sensing, RS) can accurately reveal the spatiotemporal variation in wetland ecological degradation across scales (Yin and Cheng, 2019). However, most studies have focused mainly on coastal wetlands from near-tropical to tropical regions. Due to the impact of different natural conditions and human activities, there is no unified evaluation index system to assess the dynamics and degradation of wetlands in cold areas, and there are relatively few studies on the spatiotemporal trends of wetland ecological degradation in cold areas.

Northeast China has the largest area of inland marshes in China, and thus, it represents a globally significant wetland region, particularly in relation to cold climate wetlands. The Sanjiang Plain in Northeast China is the largest and most concentrated, marsh wetland of its type in China (Luo et al.,

2022). The wetlands of the Sanjiang Plain function to purify water, conserve soil, control pollution and provide habitat for wild animals and plants. The wetlands provide climate regulation, water conservation and flood disaster control in Northeast China, supporting industrial and agricultural production and people's livelihoods. The region is also an important commodity grain base in China. Since the middle of the 20th century, under the dual influence of large-scale agricultural reclamation activities and regional natural environment changes in China (Yan, 2020). Natural landscapes such as grasslands, lakes, forests, and complex natural marshes were gradually transformed into single-structure sites, such as cultivated land (Liu and Ma, 2000). The reclamation of natural wetlands into paddy fields or dry fields leads to a significant decline in evaporation, an increase in the runoff coefficient, a downward trend in groundwater level in some areas, a weakening or loss of the "carbon sink" function and a transition into a "carbon source", a decrease in CH_4 flux and other negative effects. In the process of transforming from the "Northern Wilderness" to the "Northern Warehouse", the wetland ecosystem has been severely damaged by wetland atrophy and degradation, and the plant community structure and function of degraded wetland have obviously changed, weakening the ecological function of the wetland (Chen et al., 2020).

The Small Sanjiang Plain is the most prominent area experiencing wetland ecological degradation within the Sanjiang Plain region. The regional natural ecosystem dominated by wetlands and grassland was gradually transformed into an agricultural ecosystem mainly consisting of farmland, and this change has resulted in a sharp shrinkage of the regional wetland area, land salinization, a decline in the area of landscape patches, and an increase in fragmentation (Wan et al., 2015). Furthermore, regional ecosystem stability and national food ecological security will be affected. Most current studies have focused on land use and landscape pattern change (Wan et al., 2015), the loss of ecosystem services (Chen et al., 2020) and biodiversity changes (Qu et al., 2022). However, there have been few comprehensive assessments of degraded wetlands in terms of wetland area, structure, and function in combination with human activity. Currently, there is no international standard methods or comprehensive index used to assess the degradation status of wetlands in the cold areas of Northeast China (Shen and Liu, 2021). Therefore, based on the wetland changes and human disturbance in the study area, this paper analyzes the spatiotemporal variation in long-term wetland degradation as well as the main causes of and the response mechanism to human disturbance activities. In so doing, the study provides a scientific basis for the ecological restoration of degraded wetlands and the promotion of the regional ecological security.

Based on the aforementioned background, this study focuses on the Small Sanjiang Plain and attempts to construct a wetland degradation comprehensive index (WDCI) for cold region wetlands based on four components of wetland character: area, structure, function, and human activities, to reveal spatial and temporal patterns in relation to the degradation status of the wetlands in the cold region of Northeast China at a regional scale. The specific research objectives were: 1) study the changes in the spatial distribution pattern of wetlands in the Small Sanjiang Plain and the mechanisms driving the observed spatiotemporal patterns; 2) construct a comprehensive index to assess the degree of wetland degradation due to human disturbance; 3) use the geo-atlas to develop a conceptual model describing spatiotemporal variation in wetland degradation; 4) explore the mechanisms linking wetland response to human activity and disturbance intensity over time; and 5) provide a technical reference and theoretical basis for the protection, restoration, and development and utilization of regional wetlands.

2 Materials and methods

2.1 Study area

The Small Sanjiang Plain is located in the Sanjiang Plain north of the Wanda Mountains in Heilongjiang Province, China (nd) (46°20′40″~ 48°27′40″N, 129°11′20″~ 135°05′26″E). The total area is 4.55×10^4 km^2, with 78.4% plain region and 21.6% mountainous region. The overall topography is high in the southwest and low in the northeast (Figure 1). The Small Sanjiang Plain is an alluvial plain formed by the alluvial deposits of the Heilongjiang, Ussuri and Songhua Rivers. It is rich in freshwater marshes and wetlands. Its annual precipitation ranges from 500 to 600 mm. The soil air permeability is between 0.0013 and 0.00066 cm s^{-1}. Due to abundant rainfall and special soil characteristics, a large area of wetlands has formed in this area (Liu et al., 2016). The Small Sanjiang Plain is also listed as a major wetland reserve in Asia and China, with several nature reserves, such as the Sanjiang Nature Reserve and Honghe Nature Reserve (Luo et al., 2022).

2.2 Data sources and processing

2.2.1 Data source

In this study, the satellite remote sensing data of Landsat 5 (1990, 2000 and 2010) and Landsat TM8 (2020) were used as the main data source (30 m×30 m), and both were from the geospatial data Cloud platform (https://www.gscloud.cn/). Remote sensing data were selected from mid-May to mid-September. Remote sensing images in this period have high quality, zero or very few clouds, and meet the requirements of reflecting surface information to the maximum extent (Wang, 2021).

Other data mainly included 1:50,000 topographic maps, drainage maps, hydrogeological maps, some soil distribution maps, geomorphological maps, some field survey data, some land use maps, and administrative division maps of state farms in the study area, which were obtained from local government databases. Various statistical yearbook data (socioeconomic) and historical information were also collected (http://tjj.hlj.gov.cn/tjsj/).

2.2.2 Data processing

Complete pre-processing was conducted using the image processing software ENVI5.4 (Exelis Visual Information Solutions, Inc.), e.g., radiometric correction, geometric correction,

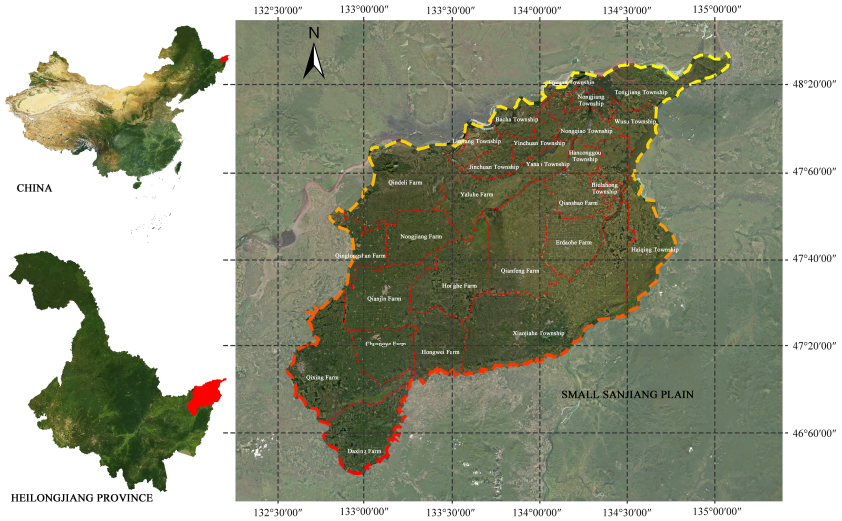

FIGURE 1
Location of the Small Sanjiang Plain Region in Heilongjiang Province.

image enhancement, mosaicking and image cropping of remote sensing images in different periods. Based on China's land classification system and the actual land use situation in the Small Sanjiang Plain, the land use types in the study area were classified into cropland, forestland, grassland, water area, built-up land and wetland. With the help of field survey data and collected land use data, the land use interpretation of the study area was completed based on maximum likelihood classification (MLC) and human–computer interaction. With reference to Google Earth (Google, Inc.) and field survey data, the accuracy of the image classification was evaluated using the statistical accuracy verification method of sampling, and the overall classification accuracy was guaranteed to be greater than 85%; data were stored in ArcGIS10.8 (Environmental Systems Research Institute) in GRID format.

In addition, the quantitative extraction of the normalized difference vegetation index (NDVI), difference vegetation index (DVI) and ratio vegetation index (RVI) was achieved by ENVI 5.4. This study also extracted quantitative remote sensing information variables such as individual principal components (PC1, PC2, PC3) and individual components of tassel hat transformation (BRIGHT, GREEN, WET), based on which the aboveground biomass model was constructed.

2.3 Analysis of ecological degradation processes in wetlands

To investigate the spatial heterogeneity of wetland degradation in the Small Sanjiang Plain (Li et al., 2021; Wu et al., 2021), this study used a 5 km×5 km grid for equally spaced sampling of the study area. The study area was divided into 732 sampling grid cells, and a comprehensive model of wetland degradation based on the characteristics of wetland attributes such as area, structure, function, and human activities was constructed. The spatial interpolation of wetland degradation was carried out based on kriging interpolation, and the grid was used to analyze the regional wetland degradation status and its spatial and temporal differentiation patterns.

2.3.1 Area

The reduction in wetland area is the most direct embodiment and an important indicator of wetland ecosystem degradation. In this paper, the rate of change in wetland area (RAC) was used to reveal the change in wetlands (Shen et al., 2019). The formula is as follows:

$$RAC = \frac{EA - IA}{IA} \times 100\%$$

where EA is the wetland area at the end of the study period, and IA is the initial wetland area in the study period.

2.3.2 Structure

The quantitative analysis of wetland landscape pattern dynamics is helpful for grasping the characteristics of regional wetland resources and provides a basis for effective wetland planning, protection and management (Wang et al., 2000; Gong et al., 2020). Therefore, the fractal dimension (FRAC) and landscape fragmentation index (LFI) were selected to characterize the degradation of wetland landscape structure in this study. The FRAC is described quantitatively in terms of the core area landscape, patch size, and study area boundary line curvature, expressed by the mean patch fractional dimension (MPFD), as shown in the formula:

$$MPFD = \left(\sum_{i=1}^{m}\sum_{j=1}^{n}\left[\frac{2\ln(0.25P_{ij})}{\ln a_{ij}}\right]\right)/N$$

where P_{ij} is the perimeter (m) of computing unit ij, a_{ij} is the area (m^2) of computing unit ij, N is the number of patches in the landscape, m is the number of landscape types, and n is the number of patches of a certain type of landscape.

The LFI reflects the complexity of landscape spatial structure and the degree of landscape fragmentation, as shown in the formula:

$$LFI=\sum[NP_{t+1}(i,j)-NP_t(i,j)]/\sum A(i,j)$$

where t is the start time of the study period, t+1 is the end time of the study period, NP_t is the number of plaques at the beginning of the study period in the calculation unit, NP_{t+1} is the number of plaques at the end of the study period in the calculation unit, A is the total area (m^2) of the calculation unit, and (i,j) is the location of the calculation unit.

2.3.3 Function

The wetland ecosystem provides a range of ecosystem services in relation to water conservation, biodiversity maintenance, and climate regulation, and wetland vegetation is important to these wetland ecosystem functions and an important component of wetland ecosystems generally. The aboveground biomass (AGB) and vegetation cover density (VCD) of wetland vegetation are not only essential indicators that can be used to reflect the function of the wetland ecosystem but also key elements that can be used to scientifically evaluate degradation and reveal the mechanisms driving this degradation. Moreover, AGB and VCD can reflect the proportion of vegetation in a certain area from a macroscopic perspective, which can more intuitively show the extent of the role of wetland ecosystem function and the degree of restoration. With reference to relevant research (Han et al., 2014), this study used a regression model best suited to the inverse model of the AGB of vegetation in the Small Sanjiang wetland, with the following formula:

$$\begin{aligned}AGB=&7943.815TM1-64609.656TM2\\&-26919.853TM3+9985.581TM5\\&-6399.439TM7-21527.197WET\\&-649.473NDVI-352.876RVI\\&+23116.377PC2+7397.939\ (R2=0.813)\end{aligned}$$

where *TM1-3*, *TM5* and *TM7* are band reflectances, and *WET* is the humidity component of the tasseled cap transformation. *NDVI* and *RVI* are the normalized difference vegetation index and ratio vegetation index, respectively; *PC2* is the second principal component.

The NDVI is the best indicator of vegetation growth status and VCD (Pu et al., 2008). The pixel dichotomous model is widely used in the remote sensing estimation of vegetation coverage, and the NDVI data are mostly used in estimation, as shown in the formula:

$$VCD_i=(NDVI_i-NDVI_{soil})/(NDVI_{veg}-NDVI_{soil})$$

where VCD_i is the vegetation coverage of the ith period, $NDVI_i$ is the normalized difference vegetation index of the i period, $NDVI_{soil}$ is the normalized difference vegetation index of a bare ground (or bare sand) observation pixel, and $NDVI_{veg}$ is the normalized difference vegetation index of a pixel completely covered by vegetation.

2.3.4 Human activity

Human disturbance to wetlands caused by rapid urbanization and excessive industrial and agricultural development is visually reflected by the structure and composition of wetland ecosystems (Zeng and Liu, 1999). Negative human disturbances have led to a drastic reduction in the area of natural wetlands and significant changes in the type of wetland and the distribution of wetlands in the landscape. In this study, the extent of human activity was mainly realized using the Hemeroby index (HI) and the human disturbance index (HD), which have been widely used in a range of settings, including wetlands, towns and mountains (Zhou et al., 2018). Based on existing research results (Hill et al., 2002; Chen et al., 2010; Liu et al., 2016), to reveal the extent of regional human disturbance activities on the wetland ecosystems of the Small Sanjiang Plain or the impact of damaged ecosystems and their composition, this study coupled regional administrative units and sampling grids and combined them with the landscape types and actual conditions of wetland ecosystems in the cold region of China (Table 1) (Liu et al., 2004a; Wang Z. et al., 2011; Song et al., 2014). The human disturbance index was assigned to six landscape types in the study area, and a comprehensive degree of human disturbance model based on the weight of the surface coverage area was used to calculate and assess the intensity of human activities (HD′) within different evaluation units.

The following formulas were used to calculate the degree of human disturbance in grid cells and human activities in grid cells:

$$HD=\frac{\sum_{i=1}^{m}HI_i\cdot S_i}{S}$$

TABLE 1 Landscape type considered interference degree assignment table (Liu et al., 2016).

Interference type	Landscape types	Index of interference
No-interference	Wetland	0.10
	Waters	0.23
Semi-interference	Forestland	0.55
	Grassland	0.58
	Cropland	0.67
Full-interference	Built-up land	0.95

No-interference: almost no interference; Semi-interference: combined man-made and natural effects, mainly for agriculture and aquaculture and other ecosystems; Full-interference: man-made features, such as highways, etc.

$$HI=\sum_{i=1}^{m} a\left(\frac{A_i}{A}\right)\cdot C_i$$

where HD is the degree of human interference, HI_i is the interference index of the class i landscape type, S_i is the area of the class i landscape type, S is the total area of grid cells, m is the number of landscape types in the calculation unit, A_i is the area of the ith type of landscape type in the calculation unit, A is the total area of the calculation unit, and C_i is the disturbance index corresponding to the ith type of landscape type.

$$HD'=1-HD_i$$

where HD_i is the normalized index of the human interference degree in period i.

2.4 Wetland ecological degradation evaluation model

The Small Sanjiang Plain wetlands belong to the mid-latitude cold region in Northeast China and have a fragile ecological environment. Moreover, there is no unified evaluation index system for wetland degradation risk assessment in cold regions. This study was based on the actual condition of wetlands in cold areas, and the relevant wetland degradation assessment studies were conducted in concert with the "Technical Specification of Ecological Effects Assessment of Ecosystem Protection and Recovery in San Jiang Yuan Region" (DB 63/T1342-2015,2015) (Shen et al., 2019) from the perspective of natural and human coercion and wetland area, ecosystem structure, function, stress coercion and degradation. After expert identification and screening of four characterization wetland degradation evaluation systems, wetland area degradation, structural degradation, functional degradation and human activities, the weights of the evaluation systems were determined based on the analytic hierarchy process (AHP) and expert evaluation method, and the resulting values were 0.3019, 0.2250, 0.3240 and 0.1490, respectively. Based on this, wetland area degradation (area change rate), structural degradation (landscape fractal dimension, landscape fragmentation), functional degradation (vegetation aboveground biomass, vegetation cover) and human activities (human disturbance degree) were the six indicators, and their indicator weights were determined (Malekmohammadi and Blouchi, 2014; Fang et al., 2021; Sun et al., 2021) as 0.3019, 0.1575, 0.0675, 0.2430, 0.0810 and 0.1490, respectively. These values were used to construct a regional WDCI to carry out a quantitative assessment of wetland degradation in cold regions.

$$f_{WDCI}=0.3019f_{area}+0.2250f_{structure}+0.3240f_{function}+0.1490f_{human\ activity}$$

$$WDCI=0.3019RAC+0.1575FRAC+0.0675LFI+0.2430VAB+0.0810VCD+0.1490(1-HD)$$

where $WDCI$ is the wetland degradation composite index, RAC is the area change rate, $FRAC$ is the landscape fractal dimension, LFI is the landscape fragmentation index, VAB is the vegetation aboveground biomass, VCD is the vegetation cover, and HD is the human disturbance.

2.5 Geological information mapping method

The geological information mapping method is a comprehensive spatiotemporal composite analysis method supported by RS, GIS, computer mapping and spatial information technology (Wang D. et al., 2011). While the mapping unit was constructed by superimposing different periods of land use at different spatiotemporal scales, the ecogeographic processes and spatiotemporal variation of regional land use cover could be revealed in time series. In this paper, with the support of ArcGIS 10.8, the land use data of the region from 1990 to 2000, 2000 to 2010, and 2010 to 2020 were analyzed by spatial overlay, and the land use information maps of the three periods were finally synthesized (Gong et al., 2015). The spatial and temporal trends in land use, and their driving mechanisms, were established quantitatively so as to explore their impact on ecosystems over the past 30 years. The calculation formula of the atlas is as follows:

$$C=10A+B$$

where C is the atlas element grid of the land use succession model in the research stage, and A and B are the raster attribute values of the land use atlas at the beginning and end of the study. Then, based on ArcGIS, according to the difference in degradation levels in different periods, the situation of increasing levels was defined as improvement, such as 1→2, 2→3, and 3→4; adding two or more levels was defined as a significant improvement, for example, 1→3, 1→4, and 2→4. However, a reduction in rank was defined as deterioration, such as 4→3, 3→2, and 2→1; a reduction of two or more grades was defined as serious deterioration, such as 4→1, 4→2, and 3→1. Stable indicates that the level does not change.

3 Results

3.1 Analysis of changes in land use characteristics of the Small Sanjiang Plain in the last 30 years

From 1990 to 2020, land use in the study area underwent significant changes (Table 2). The area of forest land decreased most, which was 147.2×10^3 hm^2, and the area of wetland decreased 39.26×10^3 hm^2. The areas of cropland, grassland, built-up land and water area increased by 145×10^3 hm^2, 27.16×10^3 hm^2, 8.87×10^3 hm^2 and 6.57×10^3 hm^2, respectively. The areas of grassland and built-up land increased significantly, with area percentage changes of 646.76% and 79.5%, respectively.

During the 30-year period, cropland showed an initial decreasing trend followed by a significant increase and slight decline, with decreases of 211.83×10^3 hm^2 and 54.48×10^3 hm^2 in

TABLE 2 Area of land use types in the study area from 1990 to 2020 (hm^2).

	1990	2000	2010	2020
Cropland	1037.69×10^3	825.86×10^3	1237.18×10^3	1182.70×10^3
Wetland	318.06×10^3	400.74×10^3	64.18×10^3	278.80×10^3
Grassland	4.20×10^3	17.64×10^3	0.15×10^3	31.36×10^3
Forest	199.83×10^3	312.27×10^3	150.69×10^3	52.62×10^3
Built-up land	11.16×10^3	8.24×10^3	18.46×10^3	20.04×10^3
Water	34.41×10^3	40.51×10^3	36.66×10^3	40.97×10^3

1990–2000 (first phase) and 2010–2020 (third phase), respectively, and an increase of 411.32×10^3 hm^2 in 2000–2010 (second phase). The dynamic attitude of the three periods was −20.41%, 49.81% and −4.40%, respectively. Grassland and wetland showed a change trend of first increasing, then significantly decreasing, and finally increasing again, with increases of 82.68×10^3 hm^2 and 13.44×10^3 hm^2, respectively, from 1990 to 2000. Cropland was the main source of the increase in wetlands, which was due to the ecological protection by the state, which actively promoted the return of cropland to wetlands and grassland. The reduction in wetlands and grasslands from second phase reached 236.56×10^3 hm^2 and 17.49×10^3 hm^2, with dynamic trends of −59.03% and −99.18%, respectively. As a consequence of the development of agricultural mechanization, the dramatic increase in population and the combined effect of agricultural reclamation activities, many wetlands, grasslands and wastelands that were previously not easily exploitable have been continuously reclaimed into cropland. A total of 63.25% of wetlands and 59.23% of grasslands were converted into cropland (Figure 2), and wetlands were the main source of increases in cropland. From 2010 to 2020, the areas of wetlands and grasslands increased by 114.62×10^3 hm^2 and 31.22×10^3 hm^2, respectively, of which 21.48% and 13% of cropland was transformed into wetlands and grasslands, respectively. The increase in wetland area was related to the continuous improvement of the national policy of returning farmland to wetlands, and the establishment of wetland parks and nature reserves has effectively curbed the reclamation and encroachment of wetlands. The area of forestland expanded by 112.44×10^3 hm^2 in the first phase, and cropland was the main source of forestland increase, with 92.55×10^3 hm^2 of cropland changing to forestland. However, the forestland decreased in area by 161.58×10^3 hm^2 and 98.07×10^3 hm^2 in the second and third phases, respectively, with 48.73% and 28.25% of forestland being converted to cropland, and unsustainable land use such as deforestation in some areas still exists. The built-up land showed a trend of continuous increase, with the largest increase from 2000 to 2010, reaching 10.21×10^3 hm^2. The overall area of the water did not change much.

3.2 Analysis and evaluation of ecological degradation characteristics in the Small Sanjiang Plain in the last 30 years

3.2.1 Characteristics of wetland area degradation in the Small Sanjiang Plain

The changes in the overall wetland area in the three stages were (+) 82.68×10^3 hm^2, (−) 336.56×10^3 hm^2 and (+) 214.62×10^3 hm^2,

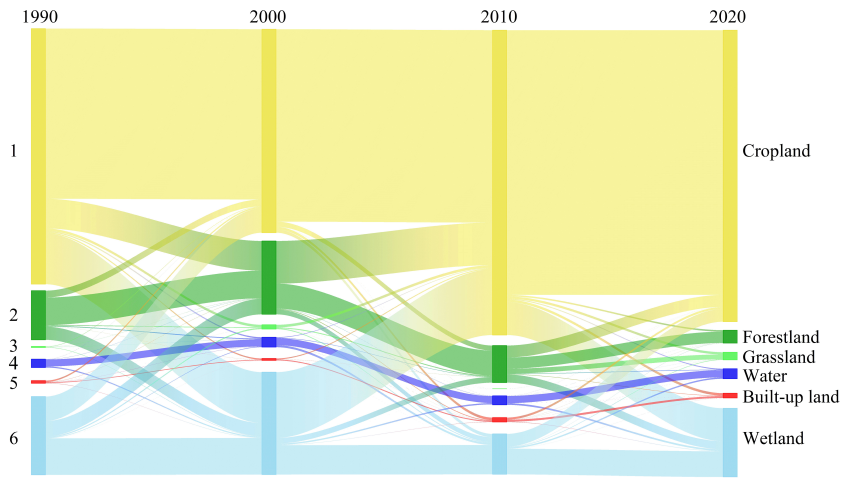

FIGURE 2
Land use type area conversion sankey map for the study area from 1990 to 2020.

respectively. The area of increased wetland area in the first phase was distributed mainly in the eastern and central parts of Haiqing Township, Qianfeng Farm and Erdaohe Farm and concentrated in the townships of Linjiang, Bacha, Jinchuan, Yinchuan and Fuyuan in the northwest region in the third phase (Figure 3), which was largely due to the implementation of the national wetland ecological protection policy. The most serious degradation of the wetland area in the second phase stemmed from 2000, when the government encouraged a fourth investment in the development of wetlands, especially in the renovation and use of remaining wetlands after previous development. Moreover, several water conservancy facilities, such as drainage ditches and reservoirs, were constructed during the development of wetlands, with 422.4 km of main river channels dug throughout the Sanjiang Plain, as well as 2,800 km of drainage canals, 362 drainage structures, 25 large and medium-sized reservoirs, and 138 small reservoirs (Liu et al., 2014). These hydraulic facilities disrupted the natural hydrological pattern of the region, isolated the connection between natural rivers and wetlands such as lakes and marshes, accelerated wetland desiccation, led to changes in wetland hydrology, and eventually resulted in the loss of wetlands (Wang and Li, 2015). The interplay of natural factors and human disturbances was the main factor affecting the ecological degradation of wetlands during this period.

In conclusion, the wetlands in the study area were mainly growing and stable from 1990 to 2000 (Figure 3), with area proportions of 37.14% and 30.04%, respectively. During, 2000–2010 and 2010–2020, the wetlands were mainly degraded and stable, with area proportions of 41.2% and 42.81%, respectively, and the wetland areas with significant growth were 14.84%, 8.44%, and 13.71% in the three phases, respectively, indicating that the degradation of wetlands has been reduced in the last decade.

3.2.2 Changes in structural geometric features of the Small Sanjiang Plain

As shown in Figure 4, the FRAC values in 1990, 2000, 2010, and 2020 were distributed between 1.00 and 1.13, which indicated that the study area was subjected to different degrees of human disturbance. The lowest overall FRAC occurred in 1990 and was in the range of 1.04–1.06 for all years, while 2000 had the highest FRAC in the range of 1.06–1.13 overall. The overall FRAC in the study area slowed between 2000 and 2020. In this period, the human disturbance to wetlands decreased, and the wetland environment improved in stages due to the active promotion of national ecological policies.

The FRAC values were relatively high in the river valley areas in the northwest and east of the study area and relatively low in the central and southern parts. Due to the low and flat topography, favorable reclamation conditions and fertile soil in the river valley area, these areas are the preferred places for the residents distributed in the nearby area. The residual wetlands were reclaimed on a large scale, and a large number of farming activities caused the natural vegetation to be replaced by artificial landscapes. Fragmentation of the natural landscape was exacerbated by the impact of human activities, making the shape of the regional patches more irregular, with a high number of subdimensions in some areas. The southern and central parts were concentrated in large areas of cropland, which constituted a local regional matrix landscape with a relatively regular shape and decreasing landscape fragmentation, making the FRAC relatively low.

Overall, the number of landscape patches was the largest in 1990, and the LFI was the largest; the LFI was smaller in 2000 and 2010, and the distribution of landscape patches was more concentrated; from 2010 to 2020, the LFI showed an increasing trend (Figure 5).

3.2.3 Analysis of functional degradation characteristics of the Small Sanjiang Plain

The results of vegetation AGB and VCD in the study area are shown in Table 3. The average AGB in the study area increased from 1029.73 kg/hm^2 to 1405.38 kg/hm^2, with an overall increase of 375.65 kg/hm^2 and a growth rate of 36.48%. The overall biomass growth increased in some townships in the northern part of the study area, while some areas in the central part showed negative biomass growth, and the AGB in farm areas was higher than that in township areas.

In 1990, the average biomass yield was 1029.73 kg/hm^2, which was significantly higher in the southwest than in the northeast, and

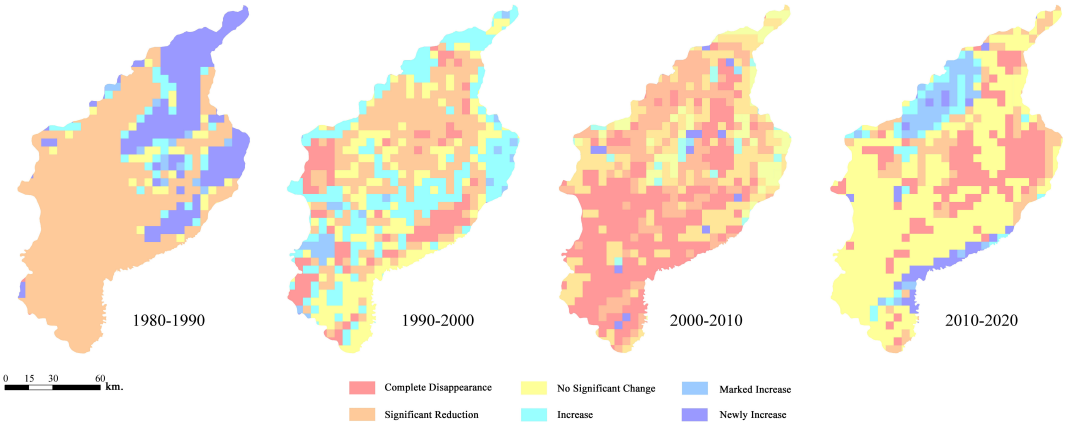

FIGURE 3
The change rate of wetland area in the study area.

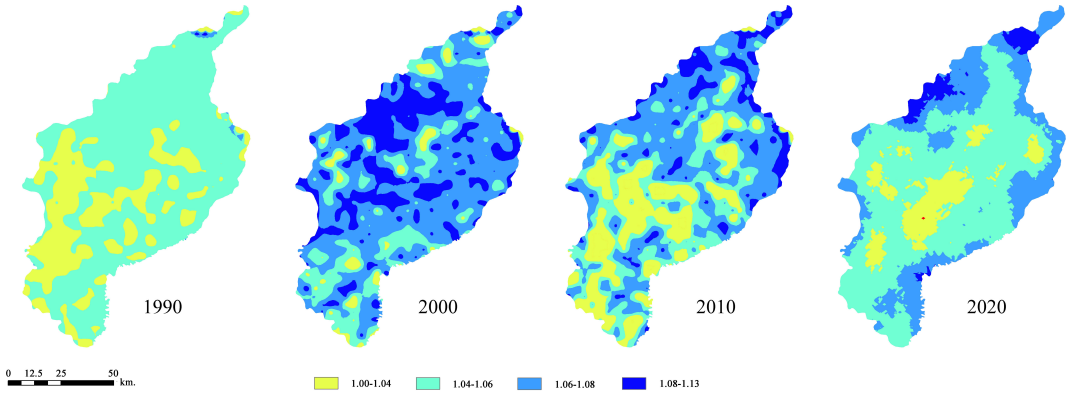

FIGURE 4
The distribution of wetland FRAC in the study area.

the highest yield was in Chuangye Farm and the lowest was in Haiqing Township, at 2346.42 kg/hm^2 and 214.73 kg/hm^2, respectively. The average biomass yield reached 1683.58 kg/hm^2 in 2000, with a growth rate of 63.5% over the decade, and the largest growth rate of 2359.92 kg/hm^2 was in Yanan Township. In 2010, the average aboveground biomass yield was 1045.18 kg/hm^2, and it was higher in the central area, lower in the surrounding areas, and higher in the southwestern area than in the northeastern area. From 2010 to 2020, the average biomass yield increased by 350.2 kg/hm^2 to 1405.38 kg/hm^2. The overall biomass was relatively high, but the biomass in some areas (Erdaohe Farm, Qianshao Farm, Beilahong Township, Hanconggou Township and Yainan Township) was much lower than the average biomass per unit area.

The average VCD in 1990, 2000, 2010 and 2020 was 0.72, 0.75, 0.82 and 0.81, respectively. In general, the VCD was high and stable in the four periods. It had an overall increasing trend from 1990 to 2010, with relatively small changes in 2010 and 2020.

3.2.4 Characteristics of human activity in the Small Sanjiang Plain

The ArcGIS natural break method was used to classify the degree of human interference in the study area into five types: slight interference [0.1,0.2], mild interference [0.2,0.4], moderate interference [0.4,0.5], severe interference [0.5,0.6], and extremely heavy interference [0.6,0.7] (Figure 6).

The average human interference in 1990, 2000, 2010 and 2020 resulted in HD values of 0.52, 0.46, 0.57 and 0.53, respectively. Human interference decreased in the first phase, and the average HD decreased by 12.61%. The HD underwent a large increase from 2000 to 2020, and the average HD increased by 19.16% in the 10 years. The areas of slight interference in the study area fluctuated greatly, showing a pattern of a large increase, followed by a small decline and ending with a considerable increase, with the area expanding 2300% during the first phase, shrinking by two-thirds to 52.76×10^3 hm^2 during the second phase, and then growing by 300% during the third phase. The areas of Mild interference remained relatively consistent. The areas of moderate interference and severe interference showed an overall downward annual trend. The proportion of extremely heavy interference areas was the highest, with 39.82%, 32.00%, 70.88% and 69.58% in 1990, 2000, 2010 and 2020 (Table 4). Although the country has introduced ecological protection projects such as returning farmland to forest and grassland, the large fraction of extremely heavy interference areas indicates that human interference with

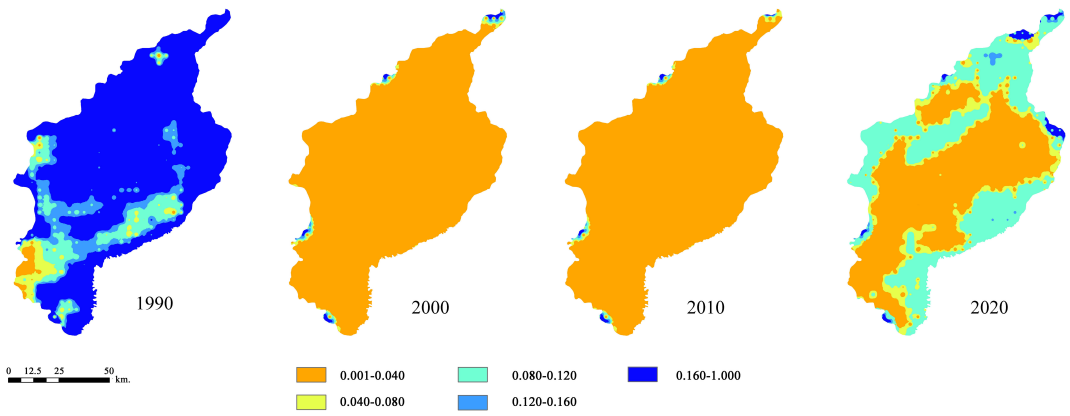

FIGURE 5
The distribution of wetland LFI in the study area.

TABLE 3 Vegetation above-ground biomass (kg/hm^2) and vegetation coverage results in 1990–2020.

Region		1990		2000		2010		2020	
		Biomass	Coverage	Biomass	Coverage	Biomass	Coverage	Biomass	Coverage
Farm	Qindeli Farm	1089.24	0.72	1234.96	0.76	1383.65	0.79	1422.62	0.81
	Qinglongshan Farm	1565.9	0.74	1272.47	0.77	857.64	0.84	1559.5	0.87
	Qianjin Farm	1792.37	0.72	1090.27	0.78	1458.87	0.81	1378.2	0.88
	Honghe Farm	1585.2	0.71	1240.66	0.78	1211.02	0.83	1532.14	0.88
	Yaluhe Farm	1213.63	0.72	1472.67	0.77	1082.75	0.81	1256.34	0.86
	Nongjiang Farm	1580.07	0.71	1557.65	0.77	1672.53	0.81	1434.66	0.88
	Qixing Farm	1835.17	0.7	1592.62	0.77	1036.99	0.84	1846.93	0.88
	Daxing Farm	946.73	0.75	1246.92	0.78	793.38	0.86	1765.78	0.86
	Chuangye Farm	2346.42	0.69	868.22	0.78	953.49	0.83	2040.68	0.91
	Qianshao Farm	575.99	0.74	2354.63	0.72	1046.04	0.84	560.61	0.77
	Qianfeng Farm	995.99	0.73	1889.32	0.74	1406.53	0.82	1084.47	0.84
	Erdaohe Farm	805.88	0.71	2968.44	0.69	1102.72	0.8	541.92	0.77
	Hongwei Farm	1157.19	0.75	898.84	0.8	882.53	0.83	1546.87	0.87
Township	Linjiang Township	609.35	0.76	1377.42	0.78	920.98	0.87	1537.06	0.76
	Bacha Township	761.61	0.67	2454.56	0.66	1121.17	0.72	1295.95	0.7
	Jinchuan Township	234.91	0.79	1602.62	0.78	865.15	0.88	1840.96	0.82
	Yinchuan Township	224.61	0.76	2330.01	0.71	1261.64	0.84	1841.01	0.79
	Fuyuan Township	1456.72	0.62	1276.14	0.73	918.41	0.71	1123.14	0.7
	Hanconggou Township	539.42	0.74	2313.7	0.74	897.83	0.84	717.22	0.76
	Nongqiao Township	500.45	0.75	2127.63	0.74	1033.61	0.85	1471.19	0.78
	Wusu Township	622.29	0.69	2073.57	0.7	977.69	0.74	1518	0.78
	Tongjiang Township	544.48	0.69	1637.77	0.73	840.79	0.76	1665.2	0.76
	Nongjiang Township	684.81	0.68	1362.98	0.78	785.2	0.84	1744.69	0.78
	Haiqing Township	214.73	0.76	1976.01	0.71	780.91	0.83	1223.31	0.79
	Bielahong Township	652.95	0.73	2160.26	0.75	851.67	0.85	431.65	0.76
	Yanan Township	476.91	0.75	2836.83	0.7	608.77	0.85	745.86	0.76
	Xiaojiahe Township	568.85	0.76	1995.53	0.75	728.4	0.86	1409.52	0.82
Average		947.48	0.72	1748.62	0.75	1017.79	0.82	1353.17	0.81
Total Accounts		25581.87		47212.70		27480.36		36535.48	

regional land has been intensifying, and unsustainable activities such as land reclamation and deforestation have not been effectively curbed. Some root causes of this phenomenon include the combined influence of certain interests, increasing population pressure and intensifying human activities. As a result, the quality of the regional ecological environment has tended to deteriorate. The interference areas were mainly concentrated in the west and south, including Deli Farm, Qinglongshan Farm, Qixing Farm, Qianjin Farm, Chuangye Farm, Hongwei Farm, Xiaojiahe Town and Qianshao Farm, and the intensity of disturbance gradually increased from southwest to northeast, with the center of gravity gradually shifting northward.

3.3 Evaluation of ecological degradation characteristics in the Small Sanjiang Plain in the last 30 years

3.3.1 Characterization of wetland degradation

Based on the "Evaluation Specification of Wetland Ecosystem in Heilongjiang Province" (DB 23/T 2378-2019, 2019), the equal interval method was used to divide the calculated results of the WDCI into four degradation levels (Uyan, 2014; Glanville and Chang, 2015; Lobatskaya and Strelchenko, 2016; Patriche et al., 2016), which were as follows: severe degradation (WDCI ≤ 0.335), moderate degradation (0.335 < WDCI ≤ 0.470), mild degradation (0.470 < WDCI ≤ 0.605),

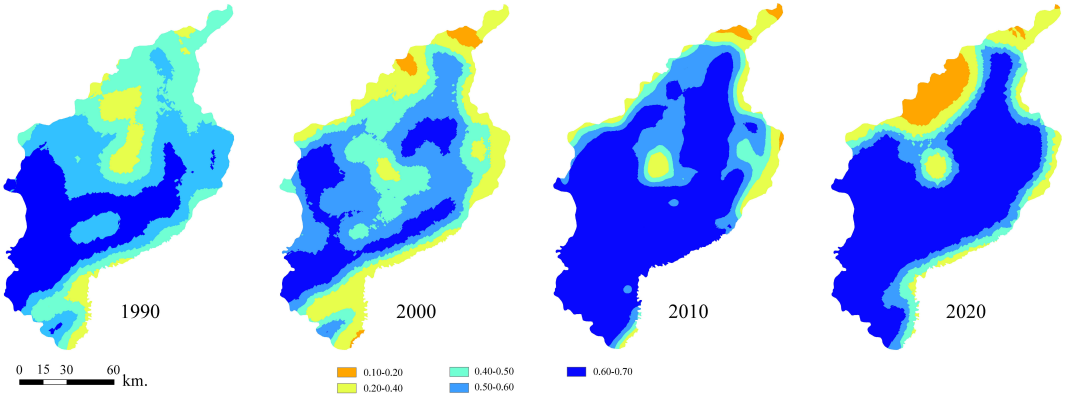

FIGURE 6
The distribution of human interference in the study area.

and no degradation (0.605 < WDCI ≤ 0.740), and the corresponding degradation grades were assigned 1, 2, 3 and 4, respectively.

The severely degraded areas in 1990, 2000, 2010 and 2020 accounted for 42.50%, 20.52%, 49.61% and 41.14% of the total area, respectively (Figure 7). The severely degraded areas in 1990, 2010 and 2020 accounted for a large proportion, and the overall degradation was the most serious in 2010. In the first stage, the severely degraded area decreased by approximately 50%, while in the second stage, the severely degraded area increased by 140%. The severely degraded area was mainly distributed in the southwest of the study area, including the Gendeli Farm, Qinglongshan Farm, Qixing Farm, Qianjin Farm, Honghe Farm, Chungye Farm and Hongwei Farm. Qinglongshan Farm, Qianjin Farm and Qixing Farm were the most representative, and the severely degraded areas in the four periods accounted for 85.52%, 40.28%, 94% and 52.33% of the whole area, respectively. The moderately and mildly degraded areas accounted for 75.74%, 87.12%, 74% and 69.42% of the total area in the four periods, respectively. The proportion of moderately degraded areas was the largest in 2000 and the smallest in 2020. The moderately degraded areas were distributed mainly in the southeastern part of the study area, and the overall area showed a downward trend, with a large decline from 2000 to 2010. The slightly degraded area showed an overall upward trend, and the area of slightly degraded area accounted for the largest proportion of the total area, which was 40.43%. The area change of the nondegraded area was relatively stable and concentrated in the central region, which was due to the distribution of a certain number of wetland nature reserves (Table 5).

3.3.2 Characterization of wetland degradation mapping

To better visually reveal the spatial and temporal variation of wetland ecological degradation in the Small Sanjiang Plain from 1990 to 2020, a spatial overlay analysis of wetland degradation in different periods was completed using ArcGIS, and three stages of wetland degradation mapping were generated from 1990–2000, 2000–2010 and 2010–2020 (Table 6).

The areas of significant improvement in the three periods were 238.50×10^3 hm^2, 135.70×10^3 hm^2 and 220.44×10^3 hm^2, respectively. The severe degradation → mild degradation (Code13) transition was the largest area change mapped in the first period, and the transformation area reached 165.19×10^3 hm^2, mainly concentrated in Yaluhe Farm and Honghe Farm, which was largely attributed to the promotion of the Heilongjiang Honghe Nature Reserve from the provincial to national level in 1996. Under the implementation of the national wetland protection policy, some regional wetlands have been effectively protected, and degradation has been alleviated to some extent. Change over the second period was mainly concentrated in the northern area of Qianqiang Farm and Qianfeng Farm, and the maximum area mapped was still heavily degraded → lightly degraded (Code13) 57.47×10^3 hm^2, which was mainly attributed to the establishment of the Naoli River and Qixing River Nature Reserve in the central part of the area, which has preserved a large number of marsh wetlands. Change over the third period was mainly concentrated in Bacha Township, Linjiang Township, Jinchuan Township, Yinchuan Township and the southern area of Xiaojiahe Township. The largest area mapped

TABLE 4 Area of human interference degree type in the study area from 1990 to 2020 (hm^2).

	1990	2000	2010	2020
Slight interference	6.60×10^3	160.97×10^3	52.76×10^3	222.35×10^3
Mild interference	236.02×10^3	252.07×10^3	105.21×10^3	149.73×10^3
Moderate interference	310.56×10^3	249.82×10^3	99.02×10^3	59.38×10^3
Heavy interference	414.10×10^3	430.09×10^3	211.13×10^3	116.93×10^3
Extremely heavy interference	640.05×10^3	514.37×10^3	1139.21×10^3	1118.32×10^3

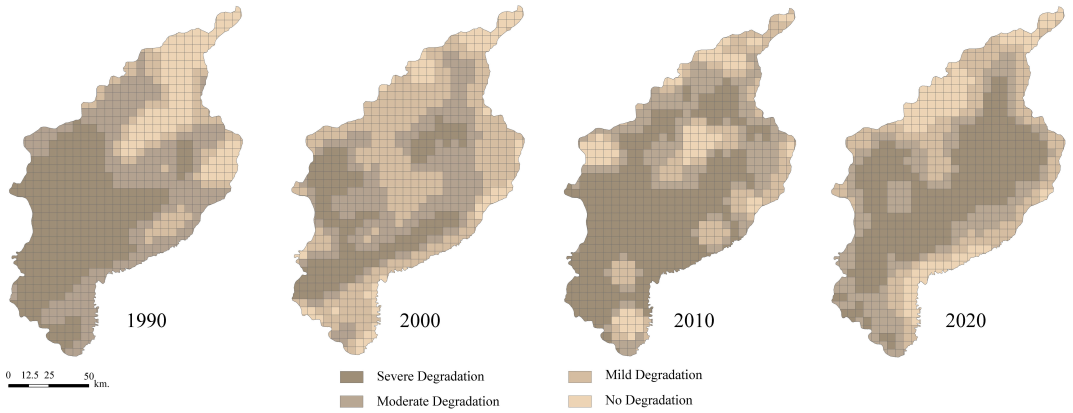

FIGURE 7
The distribution of wetland degradation characteristics in the study area.

was severe degradation → no degradation (Code14), which covered an area of 79.14×10^3 hm^2. The region's wetlands were mostly river mudflat wetlands distributed on both sides of the Yalu River. After 2010, the local government began to pay attention to wetland protection and implemented scientific wetland protection policy, actively implemented the project of returning farmland to wetlands and grass, and strictly restricted human interference activities of regional cropland and built-up land encroaching on the wetland. The wetland has been well protected, and its ecological condition has been improved to a great extent, which is also directly related to the establishment of the Bacha Island Nature Reserve in the area. A total of 97.32% of the heavily degraded wetland area in 1990 was restored to 88.32% of the nondegraded state in 2020. The areas with improvement were 597.02× 10^3 hm^2, 147.82×10^3 hm^2 and 339.99×10^3 hm^2, with a more dispersed overall distribution. Change over the first period was concentrated mainly in some areas in the central and southern parts of the country and in the areas of Linjiang Township, Jinchuan Township and Yinchuan Township in the northwest, with the largest area mapped as moderate degradation → mild degradation (Code23), and the area was 311.03×10^3 hm^2. Change over the third period with the largest area mapped was severe degradation → moderate degradation (Code12). This change was directly related to the local government's protection of wetlands and farmers' increased awareness of the ecological value of wetlands (Figure 8).

The stable areas of the three periods were 482.90×10^3 hm^2, 365.42×10^3 hm^2 and 688.12×10^3 hm^2, respectively. The area proportions of continuous severe degradation (Code11) were 49.45%, 55.33% and 66.65%, respectively, accounting for the highest proportion in the past 30 years, concentrated mainly in the areas of Qindeli Farm, Qinglongshan Farm, Qixing Farm, Qianjin Farm, Honghe Farm, Chuangye Farm and Hongwei Farm. The main land types in this area were cultivated land. The enhancement of the degree of human interference increased the disturbance to wetlands, resulting in the transformation of wetland into cultivated land, and the serious degradation of the regional wetland was aggravated while the area of cultivated land increased. Mild degradation and no degradation areas were concentrated mainly in Honghe Farm, Qianfeng Farm and Yaluhe Farm of the central region and in Tongjiang township of the north, near the Honghe wetland nature reserve and Heixiazi Island Wetland Park, China. The overall ecological condition was stable under mild degradation and no degradation conditions.

The deteriorated areas of the three stages were 141.37×10^3 hm^2, 662.15×10^3 hm^2 and 213.01×10^3 hm^2, respectively. In the second stage, the areas of mild degradation → moderate degradation (Code32) and moderate degradation → severe degradation (Code21) were relatively large, concentrated mainly in Nongjiang Farm, Honghe Farm, Xianfeng Farm, Erdaohe Farm, Qianshao Farm, Hanconggou town and Haiqing township in the central and northern parts of the country. The areas of serious deterioration were 147.52×10^3 hm^2, 296.22×10^3 hm^2 and 145.76×10^3 hm^2, respectively, and the proportions of no deterioration → serious deterioration (Code 41) areas were 16.94%, 8.86% and 29.14%, respectively. In the third stage, which was mild degradation → serious degradation (Code31), the area ratios were 22.03%, 81.10%

TABLE 5 Area of wetland degradation comprehensive index from 1990 to 2020 in the study area (hm^2).

	1990	2000	2010	2020
Severe degradation	683.05×10^3	329.90×10^3	797.46×10^3	661.20×10^3
Moderate degradation	501.68×10^3	485.42×10^3	386.59×10^3	396.77×10^3
Mild degradation	181.59×10^3	649.79×10^3	263.06×10^3	338.65×10^3
No degradation	241.00×10^3	142.22×10^3	160.21×10^3	210.70×10^3
Extremely heavy interference	640.05×10^3	514.37×10^3	1139.21×10^3	1118.32×10^3

TABLE 6 Proportional distribution of degraded wetland areas in townships and farms of the study area(hm^2).

Type		1990–2000	2000–2010	2010–2020
Significant Improvement	1–3	165.19×10^3	57.47×10^3	73.51×10^3
	1–4	11.24×10^3	43.25×10^3	79.14×10^3
	2–4	62.07×10^3	34.97×10^3	67.79×10^3
	Total	238.50×10^3	135.70×10^3	220.44×10^3
Improvement	1–2	267.83×10^3	26.92×10^3	186.24×10^3
	2–3	311.03×10^3	62.59×10^3	106.76×10^3
	3–4	18.16×10^3	58.31×10^3	46.99×10^3
	Total	597.02×10^3	147.82×10^3	339.99×10^3
Stable	1–1	238.81×10^3	202.20×10^3	458.61×10^3
	2–2	94.99×10^3	59.10×10^3	104.50×10^3
	3–3	98.36×10^3	80.51×10^3	108.27×10^3
	4–4	50.74×10^3	23.61×10^3	16.74×10^3
	Total	482.90×10^3	365.42×10^3	688.12×10^3
Deteriorate	4–3	75.19×10^3	62.60×10^3	50.20×10^3
	3–2	32.63×10^3	270.73×10^3	55.36×10^3
	2–1	33.5×10^3	328.8×10^3	107.4×10^3
	Total	141.37×10^3	662.15×10^3	213.01×10^3
Seriously Deteriorate	4–1	24.99×10^3	26.25×10^3	42.47×10^3
	4–2	90.03×10^3	29.75×10^3	50.74×10^3
	3–1	32.50×10^3	240.23×10^3	52.54×10^3
	Total	147.52×10^3	296.22×10^3	145.76×10^3

and 36.05%, respectively, and a maximum was reached in the second stage. Seriously deteriorated areas radiated mainly from the northern part of Qianshao Farm. The second and third stages of marsh wetland transitioning into cultivated land were still the main regional land process, and wetland protection policy played a role; however, human activities and the drive for economic benefits caused farmland reclamation activity to intensify, and the transition of wetlands to farmland continued, the center of gravity of the cultivated land expansion constantly moved north, and natural landscape fragmentation continued.

4 Discussion

4.1 Driving force of wetland degradation

The protection and restoration of degraded wetlands have become important issues at present, and exploring the root causes of wetland degradation can provide a more scientific and targeted basis for wetland conservation policies and actions.

In the late 1980s, continuous agricultural modernization and rapid increases in population drove increased development activities in the wetlands in this area, including unsustainable human activities such as grassland and wetland reclamation (Zhou et al., 2009). As a result, the natural landscape, which was mainly composed of wetlands and grassland, was replaced by an artificial landscape (farmland), and the natural ecosystem gradually transformed into an agricultural ecosystem, and the natural landscape became fragmented. Especially after 1983, the government intensified the construction of farmland water conservancy projects such as the water intake project and the project supporting field drainage and diversion in the Small Sanjiang Plain so that irrigation water for farmland was fully guaranteed. Under large-scale agricultural development activities (Liu et al., 2004b), paddy field areas increased rapidly, a large amount of natural vegetation was replaced by paddy fields, and some regional natural ecosystems gradually transformed into agricultural ecosystems. According to statistics, during the decade from 1980 to 1990, the rapid expansion of agriculture and the rapid development of cities and towns resulted in a reduction of 340.32×10^3 hm^2 of wetland. In parallel, the increased population generated domestic sewage that entered the wetland ecosystem, which resulted in an intensification of regional ecological environment pollution, a change in vegetation type, a reduction in biomass and the fragmentation of large-scale wetland landscapes (Sun et al., 2014). Regional marshe wetlands changed from carbon

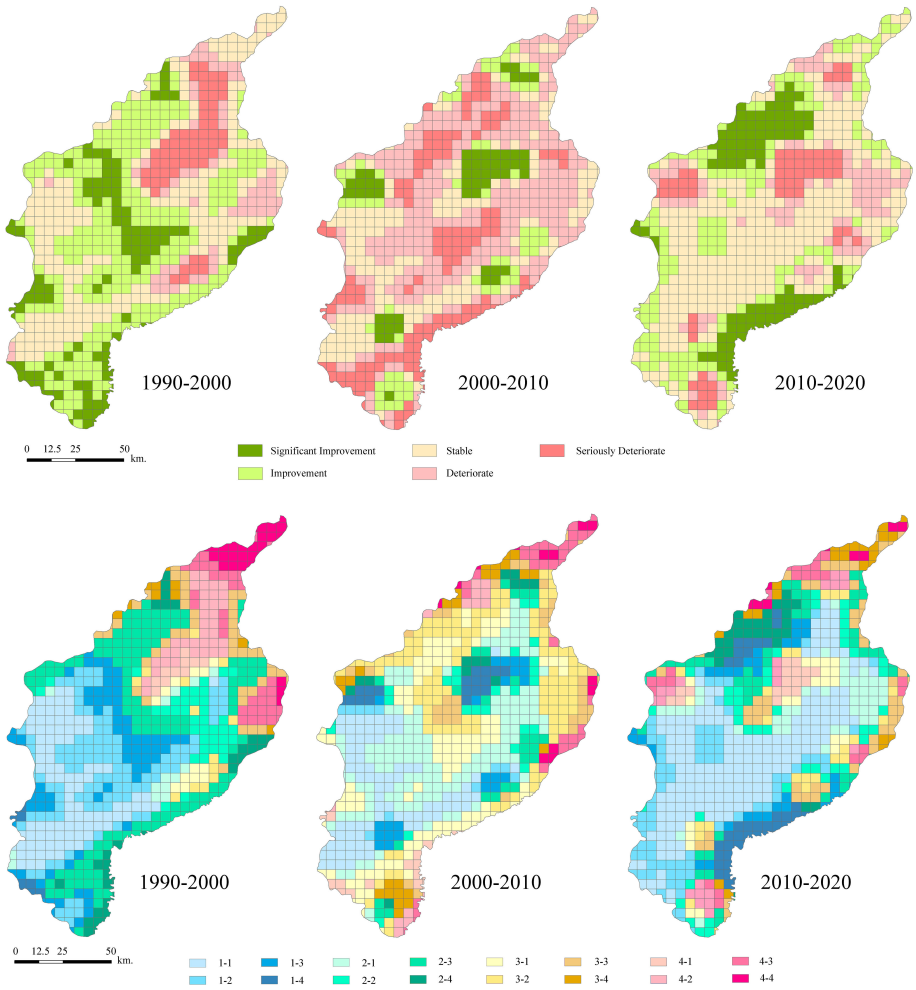

FIGURE 8
Degradation transform classification in the study area.

sinks to carbon sources (Song et al., 2008). The transformation of wetland to cropland can produce huge economic benefits in a short period of time, but it has degraded natural ecosystems. Therefore, agricultural policy changes and wetland ecological are necessary for sustainable development in China (Lai et al., 2020; Ma et al., 2020).

In the late 1990s, the trend of wetland area reduction in the study area was somewhat curbed with the introduction of the national policy of restoring wetlands such as returning farmland to wetlands and the establishment of ecological reserves, especially the establishment of the Honghe Protected Area and Sanjiang Protected Area (Du et al., 2023). From 1990 to 2000, the wetland area of the study area increased by 82.68×10^3 hm^2, and the average biomass per unit area increased by 653.85 kg/hm^2, indicating that wetland degradation was alleviated to a certain extent during this period. However, the encroachment of some regional wetlands occurred, and there was still encroachment of wetlands in the northeastern part of the study area. This condition showed the demand for farmland expansion and was a direct reflection of human interference activities on wetland resources (Li et al., 2023).

In 2003, the "*Heilongjiang Wetland Protection Regulations*" strengthened the protection of wetland resources. However, from 2000 to 2010, the wetland area of the Small Sanjiang Plain decreased by 236.56×10^3 hm^2, and the average biomass per unit area decreased by 638.4 kg/hm^2. In the national agricultural policy adjustment, various investments and changes in climate, the government encouraged people to increase the drainage network and construct road systems, artificially increasing the development and utilization of the last remaining marsh wetland area, which not only caused vast areas of wetlands to gradually become atrophic and for fragmentation to increase but also accelerated the degeneration of the remaining wetland ecosystems (Du et al., 2018). As a result, some of the marshes-wetlands degraded into marshy meadows and dry meadows (Liu et al., 2017), the forest swamps in some areas almost disappeared, and the mixed landscape dominated by farmland and wetland gradually transformed into a landscape based on farmland.

Compared with 2010, the wetland area in 2020 increased by 114.62×10^3 hm^2, and the average biomass per unit area increased by 360.20 kg/hm^2. This was due to a range of factors, including the adjustment of national agricultural policies, the implementation of ecological measures such as returning farmland to forests and wetlands, the introduction of the national ecological protection

red line by the government and rationalization of land use in the study area. The study area has curbed wetland degradation to varying degrees by establishing Bacha Island National Nature Reserve in 1999, Heilongjiang Naoli River National Nature Reserve in 2002 and Heixizi Island National Wetland Park in 2012. In the future, the "*14th Five-Year Plan for Ecological and Environmental Protection of Heilongjiang Province*" released in 2021 will comprehensively promote the protection and restoration of wetland habitats and improve the quality of wetland ecosystems. In the same year, the "*Construction Plan of Major Projects for Ecological Protection and Restoration of the Northeast Forest Belt (2021–2035)*" was implemented, which established five ecological restoration zones of "three Rivers and two original fields" and clearly stipulated the restoration of natural wetlands in the Sanjiang Plain. The "*Wetland Protection Law of the People's Republic of China*", implemented in 2022, emphasized the protection of wetland functions, sustainable use and the integration of ecological, social and economic benefits. Therefore, the decreasing trend of wetland area in the study area was curtailed to a certain extent and policy settings have been put in place in an attempt to continue this trend.

In summary, human activities and national policy adjustments are important causes of wetland degradation in the Small Sanjiang Plain, revealing a positive correlation between the degradation status of wetlands and the degree of human interference in the study area. Although the current wetland protection and restoration work has been largely effective, the protection of wetlands requires reduced unsustainable agricultural development, strict compliance with the national ecological protection red line, improvements and enhancements of ecological service functions to promote high-quality socioecological and social development to build a sustainable development pattern in the Sanjiang Plain.

4.2 Reliability of evaluation model for wetland ecological degradation

Wetlands are one of the most important environments for human beings, so it is important to assess the status and degradation trend in wetland resources to evaluate the effectiveness of wetland management (Song et al., 2014). Small Sanjiang Plain is a concentrated area of marsh wetland in China, which is also one of the richest and most critical areas of wetland resources and biodiversity. The studies of Li et al. (2020) and Yan (2020) on the dynamic changes in the core wetlands in the Small Sanjiang Plain showed that the wetlands were degraded and fragmentation was intensified. The studies of Chen et al. (2014) and Yan and Zhang (2019) also showed that the expansion of agricultural activities in the Small Sanjiang Plain in the past 30 years has reduced the value of ecosystem services provided by the wetlands. Therefore, the model constructed in this study provides an important new method for the quantitative evaluation of wetland ecosystems, that can be used to effectively explore the response mechanisms of wetlands to human activity and disturbance intensity over time and provide a scientific reference and theoretical guidance for the task of achieving balance between the sustainable development of wetlands and land development and utilization.

Moreover, compared with most of the documents with the unit as the research unit at the county level (Shen et al., 2019), this study combines the advantages of the geographic grid with administrative division to complete a longtime series of the wetland degradation variation law and human interference on the response mechanism of wetland degradation research (Yin et al., 2022; Chai et al., 2023). It makes the research results more accurate and reliable, and can provide a certain basis for the government in wetland conservation and restoration decisions.

The evaluation method employed in this study has certain limitations. First, this study uniformly used medium-resolution remote sensing data (30m resolution), so the classification accuracy of the land use data obtained was limited to some extent, and there are some uncertainties. Second, the primary land use classification adopted in this study is not able to explore the impact of secondary land use classifications, such as paddy fields and dry fields, in more detail. Finally, although the aboveground biomass of the Small Sanjiang Plain was calculated based on the relevant model, the process was proven to be feasible, and the results were credible, long-term positioning experimental data are still lacking, and it was impossible to verify the model more accurately, so estimation error still occurred. In summary, future research will continue to accumulate experimental data, continue to monitor the changes in wetlands in the Small Sanjiang Plain through remote sensing, and strive for a more accurate evaluation in the direction of a multidimensional and comprehensive assessment. Remote sensing images with a higher spatial resolution will be added to investigate wetland shrinkage and spatiotemporal pattern changes in the Small Sanjiang Plain, and more attention will be given to the transformation between wetlands and other land classes, as well as to further explore wetland changes outside the protected area.

5 Conclusions

This study combined the structure, function and changes in human activities of the Small Sanjiang Plain wetland ecosystem and set up the WDCI model in the study area to comprehensively and quantitatively assess wetland degradation from 1990 to 2020. Through a wetland degradation assessment, we provide a database for the recovery of degraded wetlands and related follow-up work. The results showed that the overall wetland degradation trend in the study area was severe in 1990 and 2010, and the degradation trend was alleviated in 2020. Moreover, the wetland degradation index in the southwest was significantly higher than that in the northeast, which was confirmed by the development trend of the overall ecological status of the study area. Therefore, the method was reasonable. In addition, the Small Sanjiang Plain is a typical marsh wetland in cold area in China that is subject to intense human disturbance. In this study, the WDCI model was optimized and the parameters were revised to construct the wetland degradation comprehensive index based on the characteristics of wetland ecosystems such as area, structure, function and human activities, and the index of human disturbance degree was

added on the basis of retaining the original area, structure and function. And the applicability and reliability of WDCI on wetlands in cold areas are confirmed. Therefore, this study can also provide a new perspective for the selection of indicators and model construction for the comprehensive evaluation of wetland degradation in other cold regions.

Data availability statement

The original contributions presented in the study are included in the article/supplementary material. Further inquiries can be directed to the corresponding authors.

Author contributions

WG conceived the research route; WG, YS, XD, MM, JH, GW, YZ, YX, XQ, TL, and TDL designed, and performed the experiments; WG, YS, and XD analyzed the data and wrote the main manuscript. All authors contributed to the article and approved the submitted version.

Funding

This research was supported by Hainan Provincial Natural Science Foundation of China, grant number 621RC507 and 421MS013; Hainan Ecological Environment Monitoring Project of China Meteorological Administration, grant number ZQC-J20142; the Science and Technology Project of Haikou City, China, grant number 2020-057; and the Natural Science Foundation of Hainan University, grant numbers KYQD (ZR) 20058, 1863 and 20057.

Acknowledgments

We appreciate the staff of the 3S laboratory of Hainan University, the Key Laboratory of Germplasm Resources of Tropical Special Ornamental Plants of Hainan Province, and the Haikou Urban Forestry Engineering Technology Development and Research Center. We also want to express our respect and thanks to the anonymous reviewers and the editors for their helpful comments in improving the quality of this paper.

Conflict of interest

The authors declare that the research was conducted in the absence of any commercial or financial relationships that could be construed as a potential conflict of interest.

Publisher's note

References

Behn, K., Becker, M., Burghof, S., Möseler, B. M., Willy, D. K., and Alvarez, M. (2018). Using vegetation attributes to rapidly assess degradation of East African wetlands. *Ecol. Indic.* 89, 250–259. doi: 10.1016/j.ecolind.2018.02.017

Chai, C., Zhang, B., Li, Y., Niu, W., Zheng, W., Kong, X., et al. (2023). A new multi-dimensional framework considering environmental impacts to assess green development level of cultivated land during 1990 to 2018 in China. *Environ. Impact Assess. Rev.* 98, 106927. doi: 10.1016/j.eiar.2022.106927

Chen, J., Sun, B.-M., Chen, D., Wu, X., Guo, L.-Z., and Wang, G. (2014). Land use changes and their effects on the value of ecosystem services in the Small Sanjiang Plain in China. *Sci. World J.* 2014, 752846. doi: 10.1155/2014/752846

Chen, J., Yu, L., Yan, F., and Zhang, S. (2020). Ecosystem service loss in response to agricultural expansion in the small sanjiang plain, northeast China: process, driver and management. *Sustainability* 12, 2430. doi: 10.3390/su12062430

Chen, A., Zhu, B., Chen, L., Wu, Y., and Sun, R. (2010). Dynamic changes of landscape pattern and eco-disturbance degree in Shuangtai estuary wetland of Liaoning Province, China. *Chin. J. Appl. Ecolog.* 21, 1120–1128. doi: 10.13287/j.1001-9332.2010.0191

Cui, L., Li, G., Liao, H., Ouyang, N., Li, X., and Liu, D. (2022). Remote sensing of coastal wetland degradation using the landscape directional succession model. *Remote Sens.* 14, 5273. doi: 10.3390/rs14205273

Cui, L., Li, G., Liao, H., Ouyang, N., and Zhang, Y. (2015). Integrated approach based on a regional habitat succession model to assess wetland landscape ecological degradation. *Wetlands* 35, 281–289. doi: 10.1007/s13157-014-0617-z

Dar, S. A., Bhat, S. U., Rashid, I., and Dar, S. A. (2020). Current status of wetlands in srinagar city: threats, management strategies, and future perspectives. *Front. Environ. Sci.* 7. doi: 10.3389/fenvs.2019.00199

Dar, S. A., Rashid, I., and Bhat, S. U. (2021). Land system transformations govern the trophic status of an urban wetland ecosystem: perspectives from remote sensing and water quality analysis. *Land Degradation Dev.* 32, 4087–4104. doi: 10.1002/ldr.3924

Du, C., Gong, L., Zhang, Z., Zhao, H., Wu, S., Tian, B., et al. (2018). Characteristics and effects on crop production of heat resources changes in heilongjiang province. *Chin. J. Ecol. Agric. (in English Chinese)* 26, 242–252. doi: 10.13930/j.cnki.cjea.170621

Du, G., Xie, J., Hou, D., and Yu, F. (2023). Regional differences in the green use level of cultivated land in the heilongjiang reclamation area. *Front. Environ. Sci.* 11. doi: 10.3389/fenvs.2023.1134271

Erwin, K. L. (2009). Wetlands and global climate change: the role of wetland restoration in a changing world. *Wetlands Ecol. Manage.* 17, 71–84. doi: 10.1007/s11273-008-9119-1

Fang, X.-S., Liu, S., Chen, W.-Z., and Wu, R.-Z. (2021). An effective method for wetland park health assessment: a case study of the guangdong xinhui national wetland park in the pearl river delta, China. *Wetlands* 41, 1–16. doi: 10.1007/s13157-021-01418-5

Gianopulos, K. (2018). Performance of rapid floristic quality assessment indices for increasing cost-effectiveness of wetland condition evaluation. *Ecol. Indic.* 95, 502–508. doi: 10.1016/j.ecolind.2018.08.003

Glanville, K., and Chang, H.-C. (2015). Mapping illegal domestic waste disposal potential to support waste management efforts in Queensland, Australia. *Int. J. Geographical Inf. Sci.* 29, 1042–1058. doi: 10.1080/13658816.2015.1008002

Gong, M., Wen, W., Zhang, W., Zhao, Q., Wang, J., Li, H., et al. (2020). A study of patterns of wetland landscapes in fangshan district of Beijing. *WETLAND Sci. Manage.* 16, 41–44. doi: 10.3969/j.issn.1673-3290.2020.04.10

Gong, W., Yuan, L., Fan, W., and Stott, P. (2015). Analysis and simulation of land use spatial pattern in Harbin prefecture based on trajectories and cellular automata–

Markov modelling. *Int. J. Appl. Earth Observation Geoinformation* 34, 207–216. doi: 10.1016/j.jag.2014.07.005

Han, Y., Pei, L., and Du, J. (2014). Remote sensing inversion of aboveground biomass over the honghe wetland. *Remote Sens. Technol. Appl.* 29, 224–231. doi: 10.11873/j.issn.1004-0323.2014.2.0224

Held, A., Ticehurst, C., Lymburner, L., and Williams, N. (2003). High resolution mapping of tropical mangrove ecosystems using hyperspectral and radar remote sensing. *Int. J. Remote Sens.* 24, 2739–2759. doi: 10.1080/0143116031000066323

Hill, M. O., Roy, D. B., and Thompson, K. (2002). Hemeroby, urbanity and ruderality: bioindicators of disturbance and human impact. *J. Appl. Ecol.* 39, 708–720. doi: 10.1046/j.1365-2664.2002.00746.x

Houborg, R., Fisher, J. B., and Skidmore, A. K. (2015). Advances in remote sensing of vegetation function and traits. *Int. J. Appl. Earth Obs. Geoinf.* 43, 1–6. doi: 10.1016/j.jag.2015.06.001

Hu, T., Liu, J., Zheng, G., Zhang, D., and Huang, K. (2020). Evaluation of historical and future wetland degradation using remote sensing imagery and land use modeling. *Land Degradation Dev.* 31, 65–80. doi: 10.1002/ldr.3429

Jiang, W., Lv, J., Wang, C., Chen, Z., and Liu, Y. (2017). Marsh wetland degradation risk assessment and change analysis: a case study in the zoige plateau, China. *Ecol. Indic.* 82, 316–326. doi: 10.1016/j.ecolind.2017.06.059

Jie, W.-H., Xiao, C.-L., Zhang, C., Zhang, E., Li, J.-Y., Wang, B., et al. (2021). Remote sensing-based dynamic monitoring and environmental change of wetlands in southern Mongolian plateau in 2000–2018. *China Geology* 4, 353–363. doi: 10.31035/cg2021032

Kotze, D., Ellery, W., Macfarlane, D., and Jewitt, G. (2012). A rapid assessment method for coupling anthropogenic stressors and wetland ecological condition. *Ecol. Indic.* 13, 284–293. doi: 10.1016/j.ecolind.2011.06.023

Lai, Z., Chen, M., and Liu, T. (2020). Changes in and prospects for cultivated land use since the reform and opening up in China. *Land Use Policy* 97, 104781. doi: 10.1016/j.landusepol.2020.104781

Lhermitte, S., Verbesselt, J., Verstraeten, W. W., and Coppin, P. (2011). A comparison of time series similarity measures for classification and change detection of ecosystem dynamics. *Remote Sens. Environ.* 115, 3129–3152. doi: 10.1016/j.rse.2011.06.020

Li, G., Fang, C., and Qi, W. (2021). Different effects of human settlements changes on landscape fragmentation in China: evidence from grid cell. *Ecol. Indic.* 129, 107927. doi: 10.1016/j.ecolind.2021.107927

Li, Z., Liu, M., Hu, Y., Xue, Z., and Sui, J. (2020). The spatiotemporal changes of marshland and the driving forces in the sanjiang plain, northeast China from 1980 to 2016. *Ecol. processes* 9, 1–13. doi: 10.1186/s13717-020-00226-9

Li, X., Wu, K., Yang, Q., Hao, S., Feng, Z., and Ma, J. (2023). Quantitative assessment of cultivated land use intensity in Heilongjiang Province, China 2001 -2015. *Land Use Policy* 125, 106505. doi: 10.1016/j.landusepol.2022.106505

Lin, S., Li, X., Yang, B., Ma, Y., Jiang, C., Xue, L., et al. (2021). Systematic assessments of tidal wetlands loss and degradation in shanghai, China: from the perspectives of area, composition and quality. *Global Ecol. Conserv.* 25, e01450. doi: 10.1016/j.gecco.2020.e01450

Liu, J., Dong, C., Sheng, L., and Liu, Y. (2016). Landscape pattern change of the marsh and its response to human disturbance in the Small Sanjiang Plain 1955-2010. *Scientia Geographica Sin.* 36, 879–887. doi: 10.13249/j.cnki.sgs.2016.06.010

Liu, J., Du, B., Sheng, L., and Tian, X. (2017). Dynamic patterns of change in marshes in the sanjiang plain and their influential factors. *Adv. Water Sci.* 28, 22–31. doi: 10.14042/j.cnki.32.1309.2017.01.003

Liu, W., Liu, G., Liu, H., Song, Y., and Zhang, Q. (2013). Subtropical reservoir shorelines have reduced plant species and functional richness compared with adjacent riparian wetlands. *Environ. Res. Lett.* 8, 44007. doi: 10.1088/1748-9326/8/4/044007

Liu, X., and Ma, X. (2000). Influence of Large-scale reclamation on natural environment and regional environmental protection in the sanjiang plain. *SCIENTIA GEOGRAPHICA Sin.* 20, 14–19. doi: 10.3969/j.issn.1000-0690.2000.01.003

Liu, H., Zhang, S., Li, Z., Lu, X., and Yang, Q. (2004a). Impacts on wetlands of large-scale land-use changes by agricultural development: the Small Sanjiang Plain, China. *AMBIO: A J. Hum. Plain Environ.* 33, 306–310. doi: 10.1579/0044-7447-33.6.306

Liu, H., Zhang, S., and Lu, X. (2004b). Wetland landscape structure and the spatial-temporal changes in 50 years in the Sanjiang Plain. *Acta Geographica Sin.* 59, 391–400. doi: 10.3321/j.issn:0375-5444.2004.03.009

Liu, J., Zhao, D., Tian, X., Zhao, L., and Liu, J. (2014). Landscape pattern dynamics and driving forces analysis in the Sanjiang Plain from 1954 to 2010. *Acta Ecologica Sin.* 34, 3234–3244. doi: 10.5846/stxb201306101639

Lobatskaya, R., and Strelchenko, I. (2016). GIS-based analysis of fault patterns in urban areas: a case study of Irkutsk city, Russia. *Geosci. Front.* 7, 287–294. doi: 10.1016/j.gsf.2015.07.004

Luo, C., Fu, X., Zeng, X., Cao, H., Wang, J., Ni, H., et al. (2022). Responses of remnant wetlands in the Sanjiang Plain to farming-landscape patterns. *Ecol. Indic.* 135, 108542. doi: 10.1016/j.ecolind.2022.108542

Ma, L., Long, H., Tu, S., Zhang, Y., and Zheng, Y. (2020). Farmland transition in China and its policy implications. *Land Use Policy* 92, 104470. doi: 10.1016/j.landusepol.2020.104470

Malekmohammadi, B., and Blouchi, L. R. (2014). Ecological risk assessment of wetland ecosystems using multi criteria decision making and geographic information system. *Ecol. Indic.* 41, 133–144. doi: 10.1016/j.ecolind.2014.01.038

Miller, S. J., and Wardrop, D. H. (2006). Adapting the floristic quality assessment index to indicate anthropogenic disturbance in central Pennsylvania wetlands. *Ecol. Indic.* 6, 313–326. doi: 10.1016/j.ecolind.2005.03.012

Myers, S., Clarkson, B. R., Reeves, P., and Clarkson, B. D. (2013). Wetland management in new Zealand: are current approaches and policies sustaining wetland ecosystems in agricultural landscapes? *Ecol. Eng.* 56, 107–120. doi: 10.1016/j.ecoleng.2012.12.097

Niu, L., Zou, G., Guo, Y., Li, Y., Wang, C., Hu, Q., et al. (2022). Eutrophication dangers the ecological status of coastal wetlands: a quantitative assessment by composite microbial index of biotic integrity. *Sci. Total Environ.* 816, 151620. doi: 10.1016/j.scitotenv.2021.151620

Patriche, C. V., Pirnau, R., Grozavu, A., and Rosca, B. (2016). A comparative analysis of binary logistic regression and analytical hierarchy process for landslide susceptibility assessment in the dobrov river basin, Romania. *Pedosphere* 26, 335–350. doi: 10.1016/s1002-0160(15)60047-9

Pu, R., Gong, P., Tian, Y., Miao, X., Carruthers, R. I., and Anderson, G. L. (2008). Using classification and NDVI differencing methods for monitoring sparse vegetation coverage: a case study of saltcedar in Nevada, USA. *Int. J. Remote Sens.* 29, 3987–4011. doi: 10.1080/01431160801908095

Qu, Y., Zheng, Y., Gong, P., Shi, J., Li, L., Wang, S., et al. (2022). Estimation of wetland biodiversity based on the hydrological patterns and connectivity and its potential application in change detection and monitoring: a case study of the sanjiang plain, China. *Sci. Total Environ.* 805, 150291. doi: 10.1016/j.scitotenv.2021.150291

Rashid, I., Dar, S. A., and Bhat, S. U. (2022). Modelling the hydrological response to urban land-use changes in three wetland catchments of the Western Himalayan region. *Wetlands* 42, 64. doi: 10.1007/s13157-022-01593-z

Shen, M., and Liu, X. (2021). Assessing the effects of lateral hydrological connectivity alteration on freshwater ecosystems: a meta-analysis. *Ecol. Indic.* 125, 107572. doi: 10.1016/j.ecolind.2021.107572

Shen, G., Yang, X., Jin, Y., Xu, B., and Zhou, Q. (2019). Remote sensing and evaluation of the wetland ecological degradation process of the zoige plateau wetland in China. *Ecol. Indic.* 104, 48–58. doi: 10.1016/j.ecolind.2019.04.063

Sileshi, A., Awoke, A., Beyene, A., Stiers, I., and Triest, L. (2020). Water purifying capacity of natural riverine wetlands in relation to their ecological quality. *Front. Environ. Sci.* 8. doi: 10.3389/fenvs.2020.00039

Slagter, B., Tsendbazar, N.-E., Vollrath, A., and Reiche, J. (2020). Mapping wetland characteristics using temporally dense sentinel-1 and sentinel-2 data: a case study in the st. Lucia wetlands, south Africa. *Int. J. Appl. Earth Observation Geoinformation* 86, 102009. doi: 10.1016/j.jag.2019.102009

Song, K., Liu, D., Wang, Z., Zhang, B., Jin, C., Li, F., et al. (2008). Land use change in Sanjiang Plain and its driving forces analysis since 1954. *Acta Geographica Sin.* 01, 93–104. doi: 10.3321/j.issn:0375-5444.2008.01.010

Song, K., Wang, Z., Du, J., Liu, L., Zeng, L., and Ren, C. (2014). Wetland degradation: its driving forces and environmental impacts in the sanjiang plain, China. *Environ. Manage.* 54, 255–271. doi: 10.1007/s00267-014-0278-y

Sun, B., Chen, Q., Wu, X., Chen, D., Zhang, Y., and Guo, L. (2014). Ecosystem services value based on land-use changes in the small sanjiang plain. *J. Irrigation Drainage* 33, 261–265. doi: 10.13522/j.cnki.ggps.2014.04/05.057

Sun, J., Han, Y., Li, Y., Zhang, P., Liu, L., Cai, Y., et al. (2021). Construction of a near-natural estuarine wetland evaluation index system based on analytical hierarchy process and its application. *Water* 13, 2116. doi: 10.3390/w13152116

Uyan, M. (2014). MSW landfill site selection by combining AHP with GIS for konya, Turkey. *Environ. Earth Sci.* 71, 1629–1639. doi: 10.1007/s12665-013-2567-9

Van Dam, R., Camilleri, C., and Finlayson, C. (1998). The potential of rapid assessment techniques as early warning indicators of wetland degradation: a review. *Environ. Toxicol. Water Quality: Int. J.* 13, 297–312. doi: 10.1002/(sici)1098-2256(1998)13:4<297::aid-tox3>3.0.co;2-2

Wan, L., Zhang, Y., Zhang, X., Qi, S., and Na, X. (2015). Comparison of land use/land cover change and landscape patterns in honghe national nature reserve and the surrounding jiansanjiang region, China. *Ecol. Indic.* 51, 205–214. doi: 10.1016/j.ecolind.2014.11.025

Wang, Y. (2021). Evaluation of lake wetland ecotourism resources based on remote sensing ecological index. *Arabian J. Geosciences* 14, 1–8. doi: 10.1007/s12517-021-06892-z

Wang, D., Gong, J., and Zhang, L. (2011). "Joint rectification of image series classification results based on trajectory analysis", in *Remote Sensing of the Environment: The 17th China Conference on Remote Sensing*. (Zhejiang, China: SPIE) 59–66. doi: 10.1117/12.910366

Wang, S., and Li, S. (2015). Wetland ecosystem health and disturbance factors analysis on the sanjiang plain based on SEM theory. *J. Northeast Forestry Univ.* 43, 101–101. doi: 10.3969/j.issn.1000-5382.2015.02.024

Wang, Z., Song, K., Ma, W., Ren, C., Zhang, B., Liu, D., et al. (2011). Loss and fragmentation of marshes in the sanjiang plain, northeast chin–2005. *Wetlands* 31, 945–954. doi: 10.1007/s13157-011-0209-0

Wang, R., Wang, Y., Yang, Q., Yang, G., Zhang, G., and Liu, B. (2000). The current situation, problems and countermeasures of wetland resources in China. *Resour. Sci.* 22, 9–13. doi: 10.3321/j.issn:1007-7588.2000.01.003

Wu, T., Zha, P., Yu, M., Jiang, G., Zhang, J., You, Q., et al. (2021). Landscape pattern evolution and its response to human disturbance in a newly metropolitan area: a case study in jin-yi metropolitan area. *Land* 10, 767. doi: 10.3390/land10080767

Yan, F. (2020). Large-Scale marsh loss reconstructed from satellite data in the small sanjiang plain since 1965: process, pattern and driving force. *Sensors* 20, 1036. doi: 10.3390/s20041036

Yan, F., and Zhang, S. (2019). Ecosystem service decline in response to wetland loss in the sanjiang plain, northeast China. *Ecol. Eng.* 130, 117–121. doi: 10.1016/j.ecoleng.2019.02.009

Yang, Z., Bai, J., and Zhang, W. (2021). Mapping and assessment of wetland conditions by using remote sensing images and POI data. *Ecol. Indic.* 127, 107485. doi: 10.1016/j.ecolind.2021.107485

Yin, L., and Cheng, Z. (2019). "Study on 3S technology applied in law enforcement of satellite image", in *Proceedings of the 2019 2nd International Conference on Geoinformatics and Data Analysis, NY, America*. 104–109. doi: 10.1145/3318236.3318244

Yin, T., Feng, Y., Liang, S., Wang, G., Yuan, N., Yan, D., et al. (2022). A suitable method for alpine wetland delineation: an example for the headwater area of the yellow river, Tibetan plateau front. *Environ. Sci.* doi: 10.3389/fenvs.2022.1062954

Zekarias, T., Govindu, V., Kebede, Y., and Gelaw, A. (2021). Degradation of wetlands and livelihood benefits of Lake Abaya-Chamo wetland, southern Ethiopia. *Curr. Res. Environ. Sustainability* 3, 100060. doi: 10.21203/rs.3.rs-165097/v1

Zeng, H., and Liu, G. (1999). Analysis of regional ecological risk based on landscape structure. *China Environ. Sci.* 19, 454–457. doi: 10.3321/j.issn:1000-6923.1999.05.017

Zhao, Y., Liao, J., Bao, X., and Ma, M. (2021). Soil seed bank dynamics are regulated by bird diversity and soil moisture during alpine wetland degradation. *Biol. Conserv.* 263, 109360. doi: 10.1016/j.biocon.2021.109360

Zhou, D., Gong, H., Wang, Y., Khan, S., and Zhao, K. (2009). Driving forces for the marsh wetland degradation in the honghe national nature reserve in sanjiang plain, northeast China. *Environ. modeling Assess.* 14, 101–111. doi: 10.1007/s10666-007-9135-1

Zhou, Y., Ning, L., and Bai, X. (2018). Spatial and temporal changes of human disturbances and their effects on landscape patterns in the jiangsu coastal zone, China. *Ecol. Indic.* 93, 111–122. doi: 10.1016/j.ecolind.2018.04.076

Zhu, L., Ke, Y., Hong, J., Zhang, Y., and Pan, Y. (2022). Assessing degradation of lake wetlands in bashang plateau, China based on long-term time series landsat images using wetland degradation index. *Ecol. Indic.* 139, 108903. doi: 10.1016/j.ecolind.2022.108903

Frontiers in
Ecology and Evolution

Ecological and evolutionary research into our natural and anthropogenic world

This multidisciplinary journal covers the spectrum of ecological and evolutionary inquiry. It provides insights into our natural and anthropogenic world, and how it can best be managed.

Discover the latest Research Topics

See more →

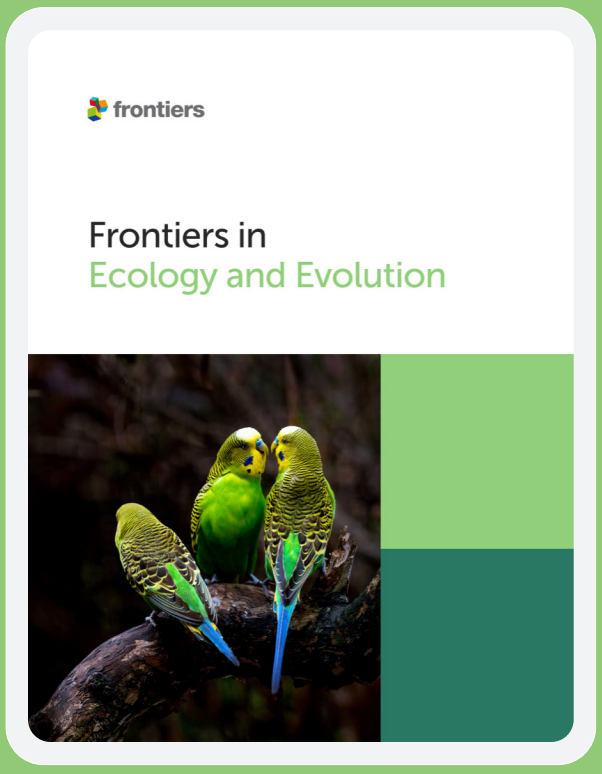

Frontiers

Avenue du Tribunal-Fédéral 34
1005 Lausanne, Switzerland
frontiersin.org

Contact us

+41 (0)21 510 17 00
frontiersin.org/about/contact